

**UNIVERSITY OF NATAL
DURBAN**

**HIGH PRESSURE PHASE EQUILIBRIUM
STUDIES**

D. RAMJUGERNATH

HIGH PRESSURE PHASE EQUILIBRIUM STUDIES

Deresh Ramjugernath

A thesis submitted
in the
School of Chemical Engineering
University of Natal
Durban

In fulfillment of the requirements for
the degree
Doctor of Philosophy

October 2000

To
My Parents

DECLARATION

All work that is submitted in this thesis is my own, except as otherwise specifically acknowledged in the text. This work has not been submitted in part, or in whole to any other University.

This project was undertaken in the School of Chemical Engineering at the University of Natal under the supervision of Prof. J.D. Raal. The project was undertaken so as to further the expertise of the institution as a centre of excellence in the field of high-pressure vapour-liquid equilibria.

D. Ramjugernath

ACKNOWLEDGEMENTS

I am in debt to my supervisor, Professor J.D. Raal, for all his advice and assistance during the entire project.

I would also like to express my appreciation and thanks to the following persons:-

To my parents, for being supportive and an endless source of encouragement and motivation.

To Professor S.I. Sandler, University of Delaware, USA, for providing some computer software and advice on high-pressure vapour liquid equilibrium computations.

To Professor M. Starzak, for his assistance in the use of MATLAB and with computations for critical properties.

To the workshop staff in the School of Chemical Engineering at the University of Natal, especially Mr L.C. Clarence and Mr M. Dietz.

To the electronics technician in the School of Chemical Engineering at the University of Natal, Mr D. Naidoo.

To Mrs D. Harrison, former senior chemical technician in the School of Chemical Engineering at the University of Natal, for all her assistance with gas chromatography analysis.

To the Foundation for Research and Development (FRD) and the University of Natal Research Fund (URF) for their financial assistance.

SUMMARY

This project involved the design, construction and commissioning of a new isothermal multipurpose high-pressure vapour-liquid equilibrium (HPVLE) apparatus of the static type. The equilibrium cell was approximately 200 cm³ in volume, and by use of a stepper motor and piston, was also variable in volume. The equipment had a combined pressure and temperature operating limit of 175 bar and 175 °C respectively. The equilibrium cell contents could be viewed through two pairs of illuminated sapphire windows.

The equilibrium cell was mounted in an air-bath, which provided the isothermal environment. The air-bath was constructed of mild steel and was copper-lined with a Fibrefrax sandwich that provided more than adequate insulation to ensure that there were no temperature gradients induced by conduction and heat element radiation.

The sampling method and procedures utilized in this project caused no disturbance to the equilibrium condition. The liquid and vapour phases were sampled by a novel means of circulating representative equilibrium samples through the sample loop of a VALCO six-port two-position sampling valve. The sample loop contained approximately 300 µl of sample, which was homogenized in jet-mixers. Analysis of the equilibrium sample was by gas chromatography.

Experimental measurements of isothermal HPVLE were undertaken for the systems, carbon dioxide + toluene, carbon dioxide + methanol and propane + 1-propanol. In addition, to show the versatility of the apparatus, P-V-T measurements were undertaken for the nitrogen, propane and the propane + nitrogen binary system.

Isothermal measurements were undertaken for carbon dioxide + toluene at 38 °C, 80 °C and 118.3 °C. There was excellent agreement between literature and the data measured.

For the carbon dioxide + methanol system, measurements were undertaken at 40 °C, 90 °C and 100 °C. The 90 °C isotherm had not previously been measured.

The propane + 1-propanol system was measured at 105.1 °C and 120 °C. It was compared to the experimental data of Mühlbauer [1990]. There was a slight difference in the vapour compositions between literature and the data measured in this project. Experimental data of Mühlbauer [1990] showed a higher mole fraction of the volatile component (propane).

Modeling of all the systems for the various isotherms measured were undertaken using both the direct and combined methods. The direct method involved the use of the Soave and Peng-Robinson equations of state with various mixing rules e.g. van der Waals, Wong and Sandler, Huron-Vidal and modifications thereof. The combined method, based on a liquid phase model and an equation of state model for the corresponding activity and fugacity coefficients was used as discussed in Prausnitz et al. [1980].

A new combined method model was proposed that incorporated the Peng-Robinson-Stryjek-Vera equation of state with the Wong-Sandler mixing rule together with the NRTL activity coefficient model. The model modeled all systems measured as well or at times better than current models in literature.

P-V-T measurements undertaken for propane, nitrogen and the propane + nitrogen binary system illustrated the versatility of the experimental apparatus. From the measured P-V-T data, second virial coefficients were computed for propane and nitrogen. Second virial cross coefficients for the binary system, propane + nitrogen, were also calculated.

Critical property computations were undertaken for the three binary systems measured using the method cited by Deiters and Schneider [1976]. The critical properties were computed by the Soave, Peng-Robinson and Peng-Robinson-Stryjek-Vera equations of state.

Vapour-liquid equilibrium data measured were tested for thermodynamic consistency using the test suggested by Chueh et al. [1965] and residual plots. The consistency tests indicated that the data measured were not inconsistent. This was the findings for the carbon dioxide + toluene, carbon dioxide + methanol and propane +1-propanol systems for all the isotherms measured.

TABLE OF CONTENTS

CHAPTER ONE : INTRODUCTION	1
CHAPTER TWO : LITERATURE SURVEY OF HIGH PRESSURE VLE EXPERIMENTAL EQUIPMENT	3
2.1. PRESENTATION OF HPVLE DATA	3
2.2. CLASSIFICATION OF EXPERIMENTAL EQUIPMENT	3
2.3. ANALYTICAL METHODS	5
2.3.1. Primary features of the analytical method	5
2.3.2. Experimental difficulties associated with analytical methods	7
2.4. DYNAMIC METHODS	11
2.4.1. Single Vapour Pass Method	11
2.4.1.1. Description of the single vapour pass method	11
2.4.1.2. Selected examples from literature for the single vapour pass method	12
2.4.1.3. Difficulties associated with the single vapour pass method	14
2.4.2. Phase Recirculation Methods	14
2.4.2.1. Description of the phase recirculation method	14
2.4.2.2. Selected examples from literature for the single phase recirculation method	17
2.4.2.2.1. Liquid phase recirculation	17
2.4.2.2.2. Vapour phase recirculation	18
2.4.2.3. Selected examples from literature for the two phase recirculation method	25
2.4.2.4. Difficulties associated with the phase recirculation methods	34
2.4.3. Single vapour and liquid pass method	37
2.4.3.1. Description of the single vapour and liquid pass method	37
2.4.3.2. Selected examples from literature of the single vapour and pass method	38

2.4.3.3. Difficulties associated with the single vapour and liquid pass method	41
2.5. STATIC METHODS	43
2.5.1. The Static Analytical Method	43
2.5.1.1. Description of the static analytical method	43
2.5.1.2. Selected examples from literature of the static analytical method	44
2.5.2. The Static Non-analytical Method	58
2.5.2.1. Description of the static non-analytical method	58
2.5.2.2. Selected examples from literature of the static non-analytical method	58
2.5.2.3. Advantages of the static non-analytical method	61
2.5.2.4. Disadvantages of the static non-analytical method	61
2.5.3. The Static Combined Method	61
2.5.3.1. Description of the static combined method	61
2.5.3.2. Selected examples from literature of the static combined method	62
CHAPTER THREE : REVIEW OF THE COMPUTATION AND THERMODYNAMICS INTERPRETATION OF HPVLE	68
3.1. CRITERION FOR PHASE EQUILIBRIA	69
3.2. THEORETICAL METHODS IN HPVLE	70
3.2.1. The Direct Method	71
3.2.1.1. Difficulties associated with the application of the direct method	72
3.2.2. The Combined Method	74
3.2.2.1. Standard states	75
3.2.2.2. Activity coefficients	76
3.2.2.3. Difficulties associated with the application of the combined method ..	77
3.3. SURVEY OF EQUATIONS OF STATE	82
3.3.1. Brief history of Equations of State	82
3.3.2. Virial Equation of State	84
3.3.3. van der Waals Family of Cubic Equations	86
3.4. ACTIVITY COEFFICIENTS	101
3.4.1. Margules Equation	102

3.4.2. van Laar Equation	104
3.4.3. Wilson Equation	104
3.4.4. NRTL Equation (Non-Random Two-Liquid Model)	106
3.4.5. UNIQUAC Model (Universal Quasi-Chemical Theory)	107
3.4.6. Group contribution liquid-phase models	110
3.5. CRITICAL PROPERTIES	112
3.5. CONSISTENCY TESTS FOR HPVLE	116
3.6. DETERMINATION OF SECOND VIRIAL COEFFICIENTS	117

**CHAPTER FOUR : EXPERIMENTAL APPARATUS: DESIGN,
CONSTRUCTION AND DEVELOPMENT..... 118**

4.1. HISTORY OF HPVLE STUDIES IN THE DEPARTMENT	118
4.2. EXPERIMENTAL APPARATUS: DESCRIPTION AND CONSTRUCTION	120
4.2.1. The equilibrium cell and piston assembly	120
4.2.2. Method of agitation of the equilibrium cell contents	128
4.2.3. Method of sampling vapour and liquid phases	131
4.2.4. Jet-mixers	132
4.2.5. Air-bath	135
4.2.5.1. Insulation	135
4.2.5.2. Interior copper lining	135
4.2.5.3. Air agitation	137
4.2.5.4. Temperature control	137
4.2.5.5. Minimizing all possible thermal leaks, conductive paths and thermal disturbances	138
4.2.5.6. Temperature profiles	139
4.2.6. Temperature and Pressure Measurement	140
4.2.6.1. Temperature measurement	140
4.2.6.2. Pressure measurement	141
4.2.7. Composition measurement	142
4.2.8. Safety features	143

CHAPTER FIVE : EXPERIMENTAL PROCEDURE 144

5.1. THE PREPARATION STAGE	144
5.1.1. Preparation of the equilibrium cell	144
5.1.2. Preparation of the liquid component for experimentation	145
5.1.3. Verification of gas chromatograph detector calibration factors	145
5.1.4. Calibration of the pressure transducers	145
5.2. THE START-UP PROCEDURE	146
5.2.1. The Carbon dioxide + Toluene and Carbon dioxide + Methanol systems	146
5.2.2. The Propane + 1-Propanol system	147
5.2.3. Positioning of the liquid-level	149
5.4. THE SAMPLING PROCEDURE	149
5.4.1. Sampling of the liquid phase	150
5.4.2. Sampling of the vapour phase	152
5.4.3. Some important notes on experimental procedure	152
5.5. PROCEDURE FOR P-V-T MEASUREMENTS	154
5.6. GC CALIBRATION PROCEDURE	155

CHAPTER SIX : SYSTEMS CHOSEN FOR EXPERIMENTATION 157

A 6.1. THE CARBON DIOXIDE + TOLUENE SYSTEM	157
6.2. THE CARBON DIOXIDE + METHANOL SYSTEM	159
6.3. THE PROPANE + 1-PROPANOL SYSTEM	159
6.4. P-V-T MEASUREMENTS	161

CHAPTER SEVEN : EXPERIMENTAL RESULTS 162

7.1. PURITY OF CHEMICALS	162
7.1.1. Gaseous materials	162
7.1.1.1. Carbon Dioxide	162
7.1.1.2. Nitrogen	162
7.1.1.3. Helium	163
7.1.1.4. Propane	163
7.1.2. Liquid materials	163
7.1.2.1. Toluene	163

7.1.2.2. Methanol	163
7.1.2.3. 1-Propanol	164
7.2. ACCURACY OF MEASURED PROPERTIES	164
7.2.1. Temperature	164
7.2.2. Pressure	165
7.2.3. Composition	165
7.3. GC CALIBRATION CURVES	165
7.4. VAPOUR-LIQUID EQUILIBRIUM MEASUREMENTS	171
7.4.1. Carbon Dioxide + Toluene	171
7.4.1.1. Carbon Dioxide + Toluene – 38 °C isotherm	171
7.4.1.2. Carbon Dioxide + Toluene – 80 °C isotherm	171
7.4.1.3. Carbon Dioxide + Toluene – 118.3 °C isotherm	172
7.4.2. Carbon Dioxide + Methanol System	180
7.4.2.1. Carbon Dioxide + Methanol – 40 °C isotherm	180
7.4.2.2. Carbon Dioxide + Methanol – 90 °C isotherm	180
7.4.2.3. Carbon Dioxide + Methanol – 100 °C isotherm	181
7.4.3. Propane + 1-Propanol	187
7.4.3.1. Propane + 1-Propanol – 105.1 °C isotherm	187
7.4.3.2. Propane + 1-Propanol – 120 °C isotherm	187
7.5. P-V-T MEASUREMENTS	192
7.5.1. Nitrogen	192
7.5.2. Propane	193
7.5.3. Propane + Nitrogen Binary	195
7.6. GC OPERATING CONDITIONS	195
7.7. TEMPERATURE PROFILES	196

CHAPTER EIGHT : DISCUSSION OF EXPERIMENTAL RESULTS 197

8.1. COMPARISON OF EXPERIMENTAL HPVLE DATA	198
8.1.1. Carbon Dioxide + Toluene	198
8.1.2. Carbon Dioxide + Methanol	198
8.1.3. Propane + 1-Propanol	198
8.2. THE DIRECT METHOD	199
8.2.1. EOS Models and mixing rules used	199

8.2.2. Data fitting/correlation	200
8.2.3. Fitted parameters	202
8.2.3.1. Carbon Dioxide + Toluene System	202
8.2.3.2. Carbon Dioxide + Methanol System	205
8.2.3.3. Propane + 1-Propanol System	216
8.3. THE COMBINED METHOD	227
8.3.1. Model combinations for the combined method	234
8.3.2. Data fitting/correlation	234
8.3.3. Fitted parameters	239
8.3.3.1. Carbon Dioxide + Toluene System	239
8.3.3.2. Carbon Dioxide + Methanol System	247
8.3.3.3. Propane + 1-Propanol System	248
8.4. ANALYSIS OF THE MODELING	256
8.4.1. Carbon Dioxide + Toluene System	261
8.4.2. Carbon Dioxide + Methanol System	263
8.4.3. Propane + 1-Propanol System	267
8.4.4. Direct versus Combined Methods	271
8.5. EXTRAPOLATION AND PREDICTION OF HPVLE DATA	271
8.5.1. Extrapolation Methods	271
8.5.2. Predictive Methods	275
8.6. CRITICAL PROPERTIES	280
8.7. THERMODYNAMIC CONSISTENCY TESTING	285
8.7.1. Carbon Dioxide + Toluene System	286
8.7.2. Carbon Dioxide + Methanol System	290
8.7.3. Propane + 1-Propanol System	294
8.8. DETERMINATION OF SECOND VIRIAL COEFFICIENTS	297
CHAPTER NINE : CONCLUSIONS	298
CHAPTER TEN : RECOMMENDATIONS	300
10.1. LARGER JET MIXERS	300
10.2. MODIFICATION FOR LARGER OPERATING TEMPERATURE RANGE	300

10.3. MODIFICATION OF EQUIPMENT FOR DATA LOGGING AND CONTROL ...	301
10.4. GREATER COMPRESSION RATIO	301
10.5. INSERTION OF A CATALYST BASKET	302
10.6. FUTURE WORK	302
CHAPTER ELEVEN : REFERENCES	303
APPENDIX A	349
A.1. INTERPRETATION OF PHASE DIAGRAMS	349
A.2. DYNAMIC METHODS : SELECTED EXAMPLES OF APPARATUS FROM LITERATURE	351
A.2.1. Single vapour pass	351
A.2.2. Liquid phase recirculation	352
A.2.3. Vapour phase recirculation	355
A.2.4. Two phase recirculation	362
A.2.5. Single liquid and vapour pass	372
A.2.6. Static methods	378
A.2.6.1. Static analytical methods	378
A.2.6.2. Static non-analytical methods	384
A.3. DEW- AND BUBBLE POINT METHOD FOR DETERMINATION OF VLE	384
A.4. P-V-T APPARATUS	385
APPENDIX B	399
B.1. DEVELOPMENT OF THE CRITERION FOR PHASE EQUILIBRIUM	399
B.2. STANDARD STATES: SYMMETRIC/UNSYMMETRIC NORMALISATION OF ACTIVITY COEFFICIENTS	402
B.3. CONDENSABLE AND NON-CONDENSABLE COMPONENT ACTIVITY COEFFICIENTS	403
B.4. COMBINED METHODS IN LITERATURE	405
B.5. RATING OF THE COMPUTATIONAL METHODS FOR HPVLE	408
B.6. CORRELATIONS FOR THE VIRIAL COEFFICIENTS	410

B.7. DETERMINATION OF PARAMETERS (<i>A</i> AND <i>B</i>) FOR CUBIC EOS	416
B.8. METHODS FOR APPLICATION OF CUBIC EOS TO MIXTURES	417
B.9. FORMULATION OF THE WONG-SANDLER MIXING RULE	417
B.10. TWO PARAMETER VAN DER WAALS ONE-FLUID MODEL (2PVDW)	420
B.11. HURON-VIDAL MIXING RULE (HVO) (Huron and Vidal [1979])	421
B.12. MODIFIED HURON-VIDAL FIRST ORDER MIXING RULE (MHV1) (Michelsen [1990(b)])	422
B.13. MODIFIED HURON-VIDAL SECOND ORDER MIXING RULE (MHV2) (Dahl and Michelsen [1990])	422
B.14. LINEAR COMBINATION OF HURON-VIDAL AND MICHELSEN MODELS (LCVM) (Boukourvalas et al. [1994])	423
B.15. ORBEY-SANDLER MODIFICATION OF HURON-VIDAL MIXING RULE (HVOS) (Orbey and Sandler [1995(b)])	424
B.16. THE CORRESPONDING STATES PRINCIPLE	424
B.17. MODIFIED CUBIC EQUATIONS OF STATE	425
B.18. MODIFICATIONS TO THE CUBIC EOS CLASSICAL MIXING RULE	427
B.18.1. van der Waals one-fluid classical mixing rule	427
B.18.2. Local Composition Mixing Rules (LCMR)	428
B.18.3. Density-dependent mixing rules (DDMR)	430
B.18.4. Density-dependent local composition mixing rules	431
B.18.4.1. The GC EOS	431
B.18.4.2. The UNIWAALS EOS	432
B.18.5. Composition-dependent mixing rules (CDMR)	433
B.18.6. Composition and density-dependent mixing rules	433
B.18.7. Density-independent mixing rules (DIMR)	434
B.19. EQUATIONS OF STATE FROM THEORY AND COMPUTER SIMULATION	435
B.19.1. Integral Equation Theory	435
B.19.2. Perturbation Theory	435
B.19.3. Computer Simulations	436
B.20. APPLICATION OF THE DEITERS AND SCHNIEDER METHOD [1976] TO THE PENG-ROBINSON EOS	436
B.21. HPVLE CONSISTENCY TESTS	437
B.21.1. Chueh et al. [1965] Area Test	437
B.21.2. Won and Prausnitz [1973] Consistency Test	439

B.21.3. Christiansen and Fredenslund [1975] Consistency Test	441
B.21.4. Mühlbauer Consistency Test based on vapour compositions	443
B.22. SOME INTERESTING PUBLICATIONS NOT DIRECTLY REFERENCED ...	444
APPENDIX C	447
C.1. DESCRIPTION OF ANCILLARY EQUIPMENT	447
C.1.1. The degassing apparatus	447
C.1.2. The propane compression device	448
C.2. DETAILS FOR THE STEPPER MOTOR	449
C.3. LIQUID-LEVEL DETERMINATION DEVICES	450
C.3.1. Direct Methods	450
C.3.1.1. Viewing windows	450
C.3.1.2. Fibre Optics	450
C.3.2. Indirect Methods	450
C.3.2.1. Capacitance Measurement	450
C.3.2.2. Solid-state sensors	451
C.3.2.3. Float sensors	451
C.4. PRESSURE EQUALIZATION CIRCUIT	451
C.5. UPPER STIRRER DESIGN	453
C.6. JET-MIXER DESIGN	454
C.7. PROPERTIES OF INSULATION MATERIAL	455
C.8. CALIBRATION OF TEMPERATURE SENSORS AND TUNING OF TEMPERATURE CONTROLLERS	456
C.8.1. Calibration of temperature sensors	456
C.8.2. Tuning of temperature sensors	456
C.9. CALIBRATION OF PRESSURE TRANSDUCERS	457
APPENDIX D	458
D.1. EXPERIMENTAL PROCEDURE FOR AUXILIARY EQUIPMENT	458
D.1.1. Degassing Apparatus	458
D.1.2. Propane Compressor	459

D.2. GC CALIBRATION	461
D.2.1. Calibration Methods	461
D.2.1.1. Internal standardisation	461
D.2.1.2. Direct injection	462
D.2.2. Quantitative and Qualitative Aspects	462
D.2.3. GC Calibration Method utilised in this project	463
D.2.3.1. Liquid component calibration	463
D.2.3.2. Gas component calibration	463
D.2.3.3. Precautions taken during calibration	464
D.3. DETERMINATION OF JET-MIXER OPERATING TEMPERATURE	465
APPENDIX E	467
E.1. LITERATURE DATA FOR SYSTEMS STUDIED.....	467
E.1.1. Carbon Dioxide + Toluene System	467
E.1.1.1. Data at approximately 311.15 K	467
E.1.1.2. Data at approximately 353.15 K	468
E.1.1.3. Data at approximately 391.45 K	470
E.1.2. Carbon Dioxide + Methanol System	471
E.1.2.1. Data at approximately 313.15 K	471
E.1.2.2. Data at approximately 373.15 K	473
E.1.3. Propane + 1-Propanol System	474
E.1.3.1. Data at approximately 378.25 K	474
E.1.3.2. Data at approximately 393.15 K	475
E.2. REFERENCES TO SYSTEMS REVIEWED WHICH CONTAINED COMPONENTS INVESTIGATED IN THIS PROJECT	476
E.2.1. Systems containing Carbon Dioxide	476
E.2.2. Systems containing Toluene	476
E.2.3. Systems containing Methanol	477
E.2.4. Systems containing Propane	477
E.3. LITERATURE DATA FOR SECOND VIRIAL COEFFICIENTS	478
E.3.1. Second Virial coefficients for Nitrogen	478
E.3.1.1. Second virial coefficients at 323.15 K	478
E.3.1.2. Second virial coefficients at 348.15 K	478

E.3.1.3. Second virial coefficients at 373.15 K	478
E.3.2. Second Virial coefficients for Propane	479
E.3.2.1. Second virial coefficients at 323.15 K	479
E.3.2.2. Second virial coefficients at 348.15 K	479
E.3.2.3. Second virial coefficients at 373.15 K	480
E.3.3. Second Virial coefficients for Propane + Nitrogen binary system	480
APPENDIX F	481
F.1. PROPERTIES FOR COMPONENTS INVESTIGATED	481
F.2. ACTIVITY COEFFICIENT PLOTS	483
F.2.1. Carbon Dioxide + Toluene System	483
F.2.2. Carbon Dioxide + Methanol System	483
F.2.3. Propane + 1-Propanol System	483
F.3. CRITICAL PROPERTIES	492
F.3.1. Carbon Dioxide + Toluene System	492
F.3.2. Carbon Dioxide + Methanol System	492
F.3.3. Propane + 1-Propanol System	492
F.4. THERMODYNAMIC CONSISTENCY	505
F.5. P-V-T COMPUTATIONS – DETERMINATION OF VOLUME	538

LIST OF FIGURES

Figure 2-1: Classification of experimental equipment for HPVLE (extracted from Raal and Muhlbauer [1994])	5
Figure 2-2: Schematic illustrating the features of a typical analytical method (extracted from Raal and Muhlbauer [1994])	6
Figure 2-3: Schematic illustrating typical features of a single vapour pass method (extracted from Raal and Muhlbauer [1994])	12
Figure 2-4: Flowsheet of the experimental apparatus of Wan and Dodge [1940]	13
Figure 2-5: Schematic illustrating the features of the phase recirculation method (extracted from Raal and Muhlbauer [1994])	15
Figure 2-6: Schematic of the experimental apparatus of Kim et al. [1986]	17
Figure 2-7: Illustration of the liquid sampling unit of Fredenslund et al. [1973]	20
Figure 2-8: The high pressure equilibrium cell of Weber et al. [1984]	21
Figure 2-9: Schematic of the vapour-liquid equilibrium apparatus of Weber et al. [1984] with internal recycle	22
Figure 2-10: Schematic of the vapour-liquid equilibrium apparatus of Weber et al. [1984] with external recycle	22
Figure 2-11: Cross-sectional view of microcell of Chou et al. [1990]	24
Figure 2-12: Schematic of the sample-analysis system of Chou et al. [1990]	24
Figure 2-13: Flow diagram of equilibrium system of Muirbrook and Prausnitz [1965] ...	28

Figure 2-14: Longitudinal section through the equilibrium cell (extracted from Muirbrook and Prausnitz [1965])	28
Figure 2-15: Sections through the vane pumps designed by Muirbrook and Prausnitz [1965]	29
Figure 2-16: Equilibrium cell of Kubota et al. [1983]	30
Figure 2-17: Illustration of the layout of the experimental apparatus of Kubota et al. [1983]	31
Figure 2-18: Mixing and separation sections of apparatus of Radosz [1984]	32
Figure 2-19: Apparatus of Adams et al. [1988]	33
Figure 2-20: Schematic illustrating the single vapour and liquid pass method (extracted from Raal and Mühlbauer [1994])	37
Figure 2-21: Equilibrium cell of Lin et al. [1985]	38
Figure 2-22: Sapphire window housing of Chen et al. [1994]	39
Figure 2-23: Machine drawing of the sapphire window housing (extracted from Chen et al. [1994])	40
Figure 2-24: Schematic illustrating the typical features of the static analytical method (extracted from Raal and Mühlbauer [1994])	43
Figure 2-25: Schematic of the equilibrium cell and sampling system of Rogers and Prausnitz [1970]	44
Figure 2-26: Thermostat system for the equilibrium cell of Rogers and Prausnitz [1970]	45
Figure 2-27: Equilibrium cell of Besserer and Robinson [1971]	47

Figure 2-28: Schematic of the carrier gas circulation through the cell to carry off the samples (Figuiere et al. [1980])	48
Figure 2-29: Equilibrium cell assembly of Figuiere et al. [1980]	49
Figure 2-30: Sampling microcell of Legret et al. [1981]	50
Figure 2-31: Schematic of the apparatus of Konrad et al. [1983]	51
Figure 2-32: Equilibrium cell of Ashcroft et al. [1983]	53
Figure 2-33: Schematic of the overall layout of Ashcroft et al. [1983]	53
Figure 2-34: Sampling apparatus of Ashcroft et al. [1983]	54
Figure 2-35: Experimental apparatus of Occhiogrosso et al. [1986]	55
Figure 2-36: Flow diagram of the experimental apparatus of Laugier and Richon [1986]	56
Figure 2-37: Equilibrium cell and air-bath arrangement of Mühlbauer [1990]	57
Figure 2-38: Total volume measuring device of Fontalba et al. [1984]	60
Figure 2-39: Interface level measuring device of Fontalba et al. [1984]	60
Figure 2-40: High pressure equipment of Japas and Franck [1985]	62
Figure 3-1: Computational procedure for the bubble pressure calculation using the direct method [Mühlbauer and Raal, 1995]	73
Figure 3-2: Computational procedure for the bubble pressure calculation using the combined method [Mühlbauer and Raal, 1995]	79

Figure 3-3: The excess Gibbs energy and Helmholtz energies of mixing for the methanol + benzene system at 1 bar and 1000 bar calculated from the Stryjek-Vera modification of the Peng-Robinson equation of state and the Wong and Sandler mixing rules (extracted from Sandler et al. [1994])	97
Figure 3-4: Classification of the various classes of mixing rules according to Mühlbauer and Raal [1995]	100
Figure 4-1: Schematic of the equilibrium cell assembly	121
Figure 4-2: Stainless-steel housing for the sapphire windows	124
Figure 4-3: Housing for the sapphire windows that was made from gasket-type material..	125
Figure 4-4: Illustration of the piston with the liquid level manipulation attachment	126
Figure 4-5: Schematic of the composite stirrer	129
Figure 4-6: Schematic of the bottom stirrer	130
Figure 4-7: Schematic showing the two modes of operation of the six-port GC valves ...	132
Figure 4-8: Cross-section through the jet-mixer	134
Figure 4-9: Location of the temperature sensors in the air-bath and on the equilibrium cell body (1-8 denotes the number on the Eurotherm selector and C denotes the air-bath temperature controller sensor)	140
Figure 5-1: Equipment arrangement for the carbon dioxide + toluene and carbon dioxide + methanol systems	146
Figure 5-2: Equipment arrangement for the propane + 1-propanol system	148

Figure 5-3: Layout of the sampling lines for the apparatus	153
Figure 7-1: GC calibration for Toluene	166
Figure 7-2: GC calibration for Methanol	167
Figure 7-3: GC calibration for 1-Propanol	168
Figure 7-4: GC calibration for Carbon Dioxide	169
Figure 7-5: GC calibration for Propane	170
Figure 7-6: Experimental HPVLE data for the Carbon Dioxide + Toluene System at 38 °C	173
Figure 7-7: HPVLE data for the Carbon Dioxide + Toluene System at 38 °C (Comparison with literature)	174
Figure 7-8: Experimental HPVLE data for the Carbon Dioxide + Toluene System at 80 °C	175
Figure 7-9: HPVLE data for the Carbon Dioxide + Toluene System at 80 °C (Comparison with literature).....	176
Figure 7-10: HPVLE data for the Carbon Dioxide + Toluene System at 80 °C (Comparison with literature)	177
Figure 7-11: Experimental HPVLE data for the Carbon Dioxide + Toluene System at 118.3 °C	178
Figure 7-12: HPVLE data for the Carbon Dioxide + Toluene System at 118.3 °C (Comparison with literature)	179

Figure 7-13: Experimental HPVLE data for the Carbon Dioxide + Methanol System at 40 °C	182
Figure 7-14: HPVLE data for the Carbon Dioxide + Toluene System at 40 °C (Comparison with literature)	183
Figure 7-15: Experimental HPVLE data for the Carbon Dioxide + Methanol System at 90 °C	184
Figure 7-16: Experimental HPVLE data for the Carbon Dioxide + Methanol System at 100 °C	185
Figure 7-17: HPVLE data for the Carbon Dioxide + Toluene System at 100 °C (Comparison with literature)	186
Figure 7-18: Experimental HPVLE data for the Propane + 1-Propanol System at 105.1 °C	188
Figure 7-19: HPVLE data for the Propane + 1-Propanol System at 105.1 °C (Comparison with literature)	189
Figure 7-20: Experimental HPVLE data for the Propane + 1-Propanol System at 120 °C	190
Figure 7-21: HPVLE data for the Propane + 1-Propanol System at 120 °C (Comparison with literature)	191
Figure 8-1: Flowchart for the bubble P computation via the direct method	203
Figure 8-2: Comparison between the predicted and experimental VLE for the Carbon Dioxide + Toluene System at 38 °C	206
Figure 8-3: Comparison between the predicted and experimental VLE for the Carbon Dioxide + Toluene System at 38 °C	207

Figure 8-4: Comparison between the predicted and experimental VLE for the Carbon Dioxide + Toluene System at 38 °C	208
Figure 8-5: Comparison between the predicted and experimental VLE for the Carbon Dioxide + Toluene System at 80 °C	209
Figure 8-6: Comparison between the predicted and experimental VLE for the Carbon Dioxide + Toluene System at 80 °C	210
Figure 8-7: Comparison between the predicted and experimental VLE for the Carbon Dioxide + Toluene System at 80 °C	211
Figure 8-8: Comparison between the predicted and experimental VLE for the Carbon Dioxide + Toluene System at 118.3 °C	212
Figure 8-9: Comparison between the predicted and experimental VLE for the Carbon Dioxide + Toluene System at 118.3 °C	213
Figure 8-10: Comparison between the predicted and experimental VLE for the Carbon Dioxide + Toluene System at 118.3 °C	214
Figure 8-11: Comparison between the predicted and experimental VLE for the Carbon Dioxide + Methanol System at 40 °C	217
Figure 8-12: Comparison between the predicted and experimental VLE for the Carbon Dioxide + Methanol System at 40 °C	218
Figure 8-13: Comparison between the predicted and experimental VLE for the Carbon Dioxide + Methanol System at 40 °C	219
Figure 8-14: Comparison between the predicted and experimental VLE for the Carbon Dioxide + Methanol System at 90 °C	220

Figure 8-15: Comparison between the predicted and experimental VLE for the Carbon Dioxide + Methanol System at 90 °C	221
Figure 8-16: Comparison between the predicted and experimental VLE for the Carbon Dioxide + Methanol System at 90 °C	222
Figure 8-17: Comparison between the predicted and experimental VLE for the Carbon Dioxide + Methanol System at 100 °C	223
Figure 8-18: Comparison between the predicted and experimental VLE for the Carbon Dioxide + Methanol System at 100 °C	224
Figure 8-19: Comparison between the predicted and experimental VLE for the Carbon Dioxide + Methanol System at 100 °C	225
Figure 8-20: Comparison between the predicted and experimental VLE for the Propane + 1-Propanol System at 105.1 °C	228
Figure 8-21: Comparison between the predicted and experimental VLE for the Propane + 1-Propanol System at 105.1 °C	229
Figure 8-22: Comparison between the predicted and experimental VLE for the Propane + 1-Propanol System at 105.1 °C	230
Figure 8-23: Comparison between the predicted and experimental VLE for the Propane + 1-Propanol System at 120 °C	231
Figure 8-24: Comparison between the predicted and experimental VLE for the Propane + 1-Propanol System at 120 °C	232
Figure 8-25: Comparison between the predicted and experimental VLE for the Propane + 1-Propanol System at 120 °C	233
Figure 8-26: Flowchart for the bubble P computation via the combined method	235

Figure 8-27: Comparison between the predicted and experimental VLE data for the Carbon dioxide + Toluene system at 38 °C	241
Figure 8-28: Comparison between the predicted and experimental VLE data for the Carbon dioxide + Toluene system at 38 °C	242
Figure 8-29: Comparison between the predicted and experimental VLE data for the Carbon dioxide + Toluene system at 80 °C	243
Figure 8-30: Comparison between the predicted and experimental VLE data for the Carbon dioxide + Toluene system at 80 °C	244
Figure 8-31: Comparison between the predicted and experimental VLE data for the Carbon dioxide + Toluene system at 118.3 °C	245
Figure 8-32: Comparison between the predicted and experimental VLE data for the Carbon dioxide + Toluene system at 118.3 °C	246
Figure 8-33: Comparison between the predicted and experimental VLE data for the Carbon dioxide + Methanol system at 40 °C	249
Figure 8-34: Comparison between the predicted and experimental VLE data for the Carbon dioxide + Methanol system at 40 °C	250
Figure 8-35: Comparison between the predicted and experimental VLE data for the Carbon dioxide + Methanol system at 90 °C	251
Figure 8-36: Comparison between the predicted and experimental VLE data for the Carbon dioxide + Methanol system at 90 °C	252
Figure 8-37: Comparison between the predicted and experimental VLE data for the Carbon dioxide + Methanol system at 100 °C	253

Figure 8-38: Comparison between the predicted and experimental VLE data for the Carbon dioxide + Methanol system at 100 °C	254
Figure 8-39: Comparison between the predicted and experimental VLE data for the Propane + 1-Propanol system at 105.1 °C	257
Figure 8-40: Comparison between the predicted and experimental VLE data for the Propane + 1-Propanol system at 105.1 °C	258
Figure 8-41: Comparison between the predicted and experimental VLE data for the Propane + 1-Propanol system at 120 °C	259
Figure 8-42: Comparison between the predicted and experimental VLE data for the Propane + 1-Propanol system at 120 °C	260
Figure 8-43: Plot of G^E/RT versus liquid mole fraction CO_2 for the Carbon dioxide + Toluene system	264
Figure 8-44: Plot of G^E/RT versus liquid mole fraction CO_2 for the Carbon dioxide + Methanol system	266
Figure 8-45: Plot of G^E/RT versus liquid mole fraction Propane for the Propane + 1-Propanol system	270
Figure 8-46: Comparison between extrapolated and literature data for the Carbon dioxide + Methanol system at 200 °C	273
Figure 8-47: Comparison between extrapolated and literature data for the Carbon dioxide + Methanol system at 40 °C	274
Figure 8-48: Comparison between experimental and predicted HPVLE data for the Carbon dioxide + Methanol system at 40 °C	276
Figure 8-49: Comparison between experimental and predicted HPVLE data for the Propane + 1-Propanol system at 120 °C	278

Figure 8-50: Comparison between experimental and predicted HPVLE data for the Propane + 1-Propanol system at 120 °C	279
Figure 8-51: Plot of ln P versus temperature for the Carbon dioxide + Toluene binary system	281
Figure 8-52: Plot of ln P versus temperature for the Carbon dioxide + Methanol binary system	282
Figure 8-53: Plot of ln P versus temperature for the Propane + 1-Propanol binary system	283
Figure 8-54: Residual plot of vapour composition for the Carbon dioxide + Toluene system at 38 °C isotherm	287
Figure 8-55: Residual plot of vapour composition for the Carbon dioxide + Toluene system at 80 °C	288
Figure 8-56: Residual plot of vapour composition for the Carbon dioxide + Toluene system at 118.3 °C	289
Figure 8-57: Residual plot of vapour composition for the Carbon dioxide + Methanol system at 40 °C	291
Figure 8-58: Residual plot of vapour composition for the Carbon dioxide + Methanol system at 90 °C	292
Figure 8-59: Residual plot of vapour composition for the Carbon dioxide + Methanol system at 100 °C	293
Figure 8-60: Residual plot of vapour composition for the Propane + 1-Propanol system at 105.1 °C	295
Figure 8-61: Residual plot of vapour composition for the Propane + 1-Propanol system at 120 °C	296

Figure A-1: Phase diagram for a simple system (extracted from Streett [1983])	350
Figure A-2: Experimental apparatus of Duncan and Hiza [1970]	351
Figure A-3: Experimental apparatus of Mohamed and Holder [1987]	352
Figure A-4: Flow diagram of the experimental apparatus of Toyama et al. [1962]	357
Figure A-5: Flowsheet of the experimental apparatus of Fredenslund and Sather [1970]	358
Figure A-6: Schematic of the experimental apparatus of Katayama et al. [1975]	359
Figure A-7: Diagram of the experimental apparatus of Streett and Calado [1978]	360
Figure A-8: Schematic of the high pressure vapour-liquid apparatus of Shah et al. [1990]	361
Figure A-9: Schematic illustrating details of the sapphire tube pressure vessel of Shah et al. [1990]	362
Figure A-10: Illustration of the electromagnetic pump of Behrens and Sandler [1983] ...	368
Figure A-11: Vapour-liquid equilibrium apparatus of Behrens and Sandler [1983]	369
Figure A-12: Phase equilibria measurement apparatus of Hsu et al. [1985]	370
Figure A-13: Probe guide assembly of Kneisl et al. [1988]	371
Figure A-14: Equilibrium cell assembly of Kneisl et al. [1988]	371
Figure A-15: Experimental apparatus of Simnick et al. [1977]	378

Figure A-16: Experimental apparatus of Ohgaki and Katayama [1975]	382
Figure A-17: The sampling chamber of Reiff et al. [1987]	383
Figure A-18: Pressure-composition and pressure-volume diagrams for the method of dew and bubble point determination of VLE (Raal and Mühlbauer [1998])	385
Figure A-19: P-V-T apparatus of Kay [1936]	386
Figure C-1: Schematic of the degassing apparatus	447
Figure C-2: The propane compression device	449
Figure C-3: Schematic of the valving arrangement for the pressure equalization	
mechanism	452
Figure C-4: Cross-section through the equilibrium cell body and the upper stirrer	453
Figure C-5: Illustration of the solenoid coil designed	354
Figure D-1: Schematic of the degassing apparatus	459
Figure D-2: Schematic of the propane compression device arrangement	460
Figure D-3: Plot of jet-mixer pressure versus saturation pressure to determine the operating temperature for the jet-mixer	466
Figure F-1: Plot of activity coefficient versus liquid mole fraction for the Carbon dioxide (1) + Toluene (2) system for the 38 °C isotherm	484

Figure F-2: Plot of activity coefficient versus liquid mole fraction for the Carbon dioxide (1) + Toluene (2) system for the 80 °C isotherm	485
Figure F-3: Plot of activity coefficient versus liquid mole fraction for the Carbon dioxide (1) + Toluene (2) system for the 118.3 °C isotherm	486
Figure F-4: Plot of activity coefficient versus liquid mole fraction for the Carbon dioxide (1) + Methanol (2) system for the 40 °C isotherm	487
Figure F-5: Plot of activity coefficient versus liquid mole fraction for the Carbon dioxide (1) + Methanol (2) system for the 90 °C isotherm	488
Figure F-6: Plot of activity coefficient versus liquid mole fraction for the Carbon dioxide (1) + Methanol (2) system for the 100 °C isotherm	489
Figure F-7: Plot of activity coefficient versus liquid mole fraction for the Propane (1) + 1-Propanol (2) system for the 105.1 °C isotherm	490
Figure F-8: Plot of activity coefficient versus liquid mole fraction for the Propane (1) + 1-Propanol (2) system for the 120 °C isotherm	491
Figure F-9: Plot of critical temperature versus composition for the Carbon dioxide + Toluene binary system	493
Figure F-10: Plot of critical pressure versus composition for the Carbon dioxide + Toluene binary system	494
Figure F-11: Plot of critical volume versus composition for the Carbon dioxide + Toluene binary system	495
Figure F-12: Plot of critical compressibility factor versus composition for the Carbon dioxide + Toluene binary system	496
Figure F-13: Plot of critical temperature versus composition for the Carbon dioxide + Methanol binary system	497

Figure F-14: Plot of critical pressure versus composition for the Carbon dioxide + Methanol binary system	498
Figure F-15: Plot of critical volume versus composition for the Carbon dioxide + Methanol binary system	499
Figure F-16: Plot of critical compressibility factor versus composition for the Carbon dioxide + Methanol binary system	500
Figure F-17: Plot of critical temperature versus composition for the Propane + 1-Propanol binary system	501
Figure F-18: Plot of critical pressure versus composition for the Propane + 1-Propanol binary system	502
Figure F-19: Plot of critical volume versus composition for the Propane + 1-Propanol binary system	503
Figure F-20: Plot of critical compressibility factor versus composition for the Propane + 1-Propanol binary system	504
Figure F-21: Plot of $\ln(K_2/K_1)$ versus liquid mole fraction CO_2 for the Carbon dioxide (2) + Toluene (1) system at 38 °C	506
Figure F-22: Plot of $\ln\left(\frac{\hat{\phi}_2}{\hat{\phi}_1}\right)$ versus liquid mole fraction CO_2 for the Carbon dioxide (2) + Toluene (1) system at 38 °C	507
Figure F-23: Plot of liquid molar volume versus pressure for the Carbon dioxide + Toluene system at 38 °C	508
Figure F-24: Plot of $\ln(K_2/K_1)$ versus liquid mole fraction CO_2 for the Carbon dioxide (2) + Toluene (1) system at 80 °C	509

Figure F-25: Plot of $\ln\left(\frac{\hat{\phi}_2}{\hat{\phi}_1}\right)$ versus liquid mole fraction CO ₂ for the Carbon dioxide (2) + Toluene (1) system at 80 °C	510
Figure F-26: Plot of liquid molar volume versus pressure for the Carbon dioxide + Toluene system at 80 °C	511
Figure F-27: Plot of $\ln(K_2/K_1)$ versus liquid mole fraction CO ₂ for the Carbon dioxide (2) + Toluene (1) system at 118.3 °C	512
Figure F-28: Plot of $\ln\left(\frac{\hat{\phi}_2}{\hat{\phi}_1}\right)$ versus liquid mole fraction CO ₂ for the Carbon dioxide (2) + Toluene (1) system at 118.3 °C	513
Figure F-29: Plot of liquid molar volume versus pressure for the Carbon dioxide + Toluene system at 118.3 °C	514
Figure F-30: Plot of $\ln(K_2/K_1)$ versus liquid mole fraction CO ₂ for the Carbon dioxide (2) + Methanol (1) system at 40 °C	515
Figure F-31: Plot of $\ln\left(\frac{\hat{\phi}_2}{\hat{\phi}_1}\right)$ versus liquid mole fraction CO ₂ for the Carbon dioxide (2) + Methanol (1) system at 40 °C	516
Figure F-32: Plot of liquid molar volume versus pressure for the Carbon dioxide + Methanol system at 40 °C	517
Figure F-33: Plot of $\ln(K_2/K_1)$ versus liquid mole fraction CO ₂ for the Carbon dioxide (2) + Methanol (1) system at 90 °C	518
Figure F-34: Plot of $\ln\left(\frac{\hat{\phi}_2}{\hat{\phi}_1}\right)$ versus liquid mole fraction CO ₂ for the Carbon dioxide (2) + Methanol (1) system at 90 °C	519

Figure F-35: Plot of liquid molar volume versus pressure for the Carbon dioxide + Methanol system at 90 °C	520
Figure F-36: Plot of $\ln(K_2/K_1)$ versus liquid mole fraction CO ₂ for the Carbon dioxide (2) + Methanol (1) system at 100 °C	521
Figure F-37: Plot of $\ln\left(\frac{\hat{\phi}_2}{\hat{\phi}_1}\right)$ versus liquid mole fraction CO ₂ for the Carbon dioxide (2) + Methanol (1) system at 100 °C	522
Figure F-38: Plot of liquid molar volume versus pressure for the Carbon dioxide + Methanol system at 100 °C	523
Figure F-39: Plot of $\ln(K_2/K_1)$ versus liquid mole fraction Propane for the Propane (2) + 1-Propanol (1) system at 105.1 °C	524
Figure F-40: Plot of $\ln\left(\frac{\hat{\phi}_2}{\hat{\phi}_1}\right)$ versus liquid mole fraction Propane for the Propane (2) + 1-Propanol (1) system at 105.1 °C	525
Figure F-41: Plot of liquid molar volume versus pressure for the Propane for the Propane (2) + 1-Propanol (1) system at 105.1 °C	526
Figure F-42: Plot of $\ln(K_2/K_1)$ versus liquid mole fraction Propane for the Propane (2) + 1-Propanol (1) system at 120 °C	527
Figure F-43: Plot of $\ln\left(\frac{\hat{\phi}_2}{\hat{\phi}_1}\right)$ versus liquid mole fraction Propane for the Propane (2) + 1-Propanol (1) system at 120 °C	528
Figure F-44: Plot of liquid molar volume versus pressure for the Propane for the Propane (2) + 1-Propanol (1) system at 120 °C	529

Figure F-45: Residual plot of pressure for the Carbon dioxide + Toluene system at 38 °C isotherm	530
Figure F-46: Residual plot of pressure for the Carbon dioxide + Toluene system at 80 °C isotherm	531
Figure F-47: Residual plot of pressure for the Carbon dioxide + Toluene system at 118.3 °C isotherm	532
Figure F-48: Residual plot of pressure for the Carbon dioxide + Methanol system at 40 °C isotherm	533
Figure F-49: Residual plot of pressure for the Carbon dioxide + Methanol system at 90 °C isotherm	534
Figure F-50: Residual plot of pressure for the Carbon dioxide + Methanol system at 100 °C isotherm	535
Figure F-51: Residual plot of pressure for the Propane + 1-Propanol system at 105.1 °C isotherm	536
Figure F-52: Residual plot of pressure for the Propane + 1-Propanol system at 120 °C isotherm	537

LIST OF TABLES

Table 2-1: Single vapour pass apparatus surveyed	16
Table 2-2: Liquid phase recirculation apparatus surveyed	19
Table 2-3: Vapour phase recirculation apparatus surveyed	26
Table 2-4: Two phase recirculation apparatus surveyed	35
Table 2-5: Single liquid and vapour pass apparatus surveyed	42
Table 2-6: Static apparatus surveyed	64
Table 3-1: Standard states available as listed by Mühlbauer and Raal [1995]	76
Table 3-2: Comparison of the Direct and Combined Methods	80
Table 3-3: List of α functions surveyed	91
Table 3-4: Some of the combining rules surveyed	95
Table 6-1: Survey of measured data for the Carbon Dioxide + Toluene System	158
Table 6-2: Survey of measured data for the Carbon Dioxide + Methanol System	160
Table 6-3: Survey of measured data for the Propane + 1-Propanol System	161
Table 7-1: Purity of the liquid materials verified by refractive index measurement (20 °C) and GC analysis	164
Table 7-2: Experimental data for the Carbon Dioxide + Toluene System at 38 °C	171

Table 7-3: Experimental data for the Carbon Dioxide + Toluene System at 80 °C	172
Table 7-4: Experimental data for the Carbon Dioxide + Toluene System at 118.3 °C	172
Table 7-5: Experimental data for the Carbon Dioxide + Methanol System at 40 °C	180
Table 7-6: Experimental data for the Carbon Dioxide + Methanol System at 90 °C	181
Table 7-7: Experimental data for the Carbon Dioxide + Methanol System at 100 °C	181
Table 7-8: Experimental data for the Propane + 1-Propanol System at 105.1 °C	187
Table 7-9: Experimental data for the Propane + 1-Propanol System at 120 °C	192
Table 7-10: P-V data for nitrogen at the 50 °C isotherm	192
Table 7-11: P-V data for nitrogen at the 75 °C isotherm	193
Table 7-12: P-V data for nitrogen at the 100 °C isotherm	193
Table 7-13: Second Virial coefficients for nitrogen	193
Table 7-14: P-V data for propane at the 50 °C isotherm	194
Table 7-15: P-V data for propane at the 75 °C isotherm	194
Table 7-16: P-V data for propane at the 100 °C isotherm	194
Table 7-17: Second Virial coefficients for propane	194
Table 7-18: P-V data for propane (1) + nitrogen (2) binary at the 75 °C isotherm for y ₁ = 0.78 mole fraction	195
Table 7-19: Operating conditions for the Chrompack CP 9000 with Poropak N column ...	195

Table 7-20: Temperature profiles for three operating temperatures for the experimental apparatus	196
Table 8-1: Interaction parameters obtained for various EOS's, from the fitting of experimental data measured in this project, using the direct method for the Carbon Dioxide + Toluene System	202
Table 8-2: Interaction parameters obtained for the PRSV EOS with 2-parameter van der Waals mixing rules, from the fitting of experimental data measured in this project, using the direct method for the Carbon Dioxide + Toluene system	204
Table 8-3: Literature values for the binary interaction parameters for the Carbon dioxide + Toluene System	204
Table 8-4: Interaction parameters obtained for the PRSV EOS with Huron-Vidal (and modifications thereof) mixing rules, from the fitting of experimental data measured in this project, using the direct method for the Carbon Dioxide + Toluene System	205
Table 8-5: Interaction parameters obtained for the PRSV EOS with Wong-Sandler mixing rules, from the fitting of experimental data measured in this project, using the direct method for the Carbon Dioxide + Toluene System	205
Table 8-6: Interaction parameters obtained for various EOS's, from the fitting of experimental data measured in this project, using the direct method for the Carbon Dioxide + Methanol System	205
Table 8-7: Interaction parameters obtained for the PRSV EOS with 2-parameter van der Waals mixing rules, from the fitting of experimental data measured in this project, using the direct method for the Carbon Dioxide + Methanol System	215

Table 8-8: Literature values for the binary interaction parameters for the Carbon dioxide + Methanol System	215
Table 8-9: Interaction parameters obtained for the PRSV EOS with Huron-Vidal (and modifications thereof) mixing rules, from the fitting of experimental data measured in this project, using the direct method for the Carbon Dioxide + Methanol System	216
Table 8-10: Interaction parameters obtained for the PRSV EOS with Wong-Sandler mixing rules, from the fitting of experimental data measured in this project, using the direct method for the Carbon Dioxide + Methanol System	216
Table 8-11: Interaction parameters obtained for various EOS's, from the fitting of experimental data measured in this project, using the direct method for the Propane + 1-Propanol System	216
Table 8-12: Interaction parameters obtained for the PRSV EOS with 2-parameter van der Waals mixing rules, from the fitting of experimental data measured in this project, using the direct method for the Propane + 1-Propanol System ...	226
Table 8-13: Literature values for the binary interaction parameters for the Propane + 1-Propanol System	226
Table 8-14: Interaction parameters obtained for the PRSV EOS with Huron-Vidal (and Modifications thereof) mixing rules, from the fitting of experimental data measured in this project, using the direct method for the Propane + 1-Propanol system	226
Table 8-15: Interaction parameters obtained for the PRSV EOS with Wong-Sandler mixing rules, from the fitting of experimental data measured in this project, using the direct method for the Propane + 1-Propanol System	227
Table 8-16: Interaction parameters obtained for various activity coefficient models with the virial EOS, from fitting of experimental data measured in this project, using the combined method for the Carbon dioxide + Toluene system	239

Table 8-17: Interaction parameters obtained for various activity coefficient models with the PRSV EOS, from fitting of experimental data measured in this project, using the combined method for the Carbon dioxide + Toluene system	239
Table 8-18: Interaction parameters obtained for the NRTL activity coefficient model with the PRSV EOS with Wong-Sandler mixing rules (NRTL activity coefficient model), from fitting of experimental data measured in this project, using the modified combined method for the Carbon dioxide + Toluene system	240
Table 8-19: Interaction parameters obtained for the virial EOS with the UNIQUAC model using the combined method for the Carbon dioxide + Toluene system by Mühlbauer and Raal [1991]	240
Table 8-20: Interaction parameters obtained for the PR EOS with the UNIQUAC model using the combined method for the Carbon dioxide + Toluene system by Mühlbauer and Raal [1991]	240
Table 8-21: Interaction parameters obtained for various activity coefficient models with the virial EOS, from fitting of experimental data measured in this project, using the combined method for the Carbon dioxide + Methanol system	247
Table 8-22: Interaction parameters obtained for various activity coefficient models with the PRSV EOS, from fitting of experimental data measured in this project, using the combined method for the Carbon dioxide + Methanol system	247
Table 8-23: Interaction parameters obtained for the NRTL activity coefficient model with the PRSV EOS with Wong-Sandler mixing rules (NRTL activity coefficient model), from fitting of experimental data measured in this project, using the modified combined method for the Carbon dioxide + Methanol system	248

Table 8-24: Interaction parameters obtained for various activity coefficient models with the virial EOS, from fitting of experimental data measured in this project, using the combined method for the Propane + 1-Propanol system	255
Table 8-25: Interaction parameters obtained for various activity coefficient models with the PRSV EOS, from fitting of experimental data measured in this project, using the combined method for the Propane + 1-Propanol system	255
Table 8-26: Interaction parameters obtained for the NRTL activity coefficient model with the PRSV EOS with Wong-Sandler mixing rules (NRTL activity coefficient model), from fitting of experimental data measured in this project, using the modified combined method for the Propane + 1-Propanol system	255
Table 8-27: Interaction parameters obtained for the virial EOS with the UNIQUAC model using the combined method for the Propane + 1-Propanol system by Mühlbauer and Raal [1993]	256
Table 8-28: Interaction parameters obtained for the PR EOS with the UNIQUAC model using the combined method for the Propane + 1-Propanol system by Mühlbauer and Raal [1993]	256
Table 8-29: Absolute average errors for the Carbon dioxide + Toluene system	261
Table 8-30: Absolute average errors for the Carbon dioxide + Methanol system	265
Table 8-31: Absolute average errors for the Propane + 1-Propanol system	269
Table 8-32: Computed critical properties for the Carbon dioxide + Toluene binary system using the PRSV EOS	284
Table 8-33: Computed critical properties for the Carbon dioxide + Methanol binary system using the PRSV EOS	284

Table 8-34: Computed critical properties for the Propane + 1-Propanol binary system using the PRSV EOS	284
Table 8-35: Summary of Chueh et al. [1965] consistency test for the Carbon dioxide + Toluene system at 38 °C	286
Table 8-36: Summary of Chueh et al. [1965] consistency test for the Carbon dioxide + Toluene system at 80 °C	286
Table 8-37: Summary of Chueh et al. [1965] consistency test for the Carbon dioxide + Toluene system at 118.3 °C	286
Table 8-38: Summary of Chueh et al. [1965] consistency test for the Carbon dioxide + Methanol system at 40 °C	290
Table 8-39: Summary of Chueh et al. [1965] consistency test for the Carbon dioxide + Methanol system at 90 °C	290
Table 8-40: Summary of Chueh et al. [1965] consistency test for the Carbon dioxide + Methanol system at 100 °C	290
Table 8-41: Summary of Chueh et al. [1965] consistency test for the Propane + 1-Propanol system at 105.1 °C	294
Table 8-42: Summary of Chueh et al. [1965] consistency test for the Propane + 1-Propanol system at 120 °C	294
Table A-1: Single vapour pass apparatus surveyed	353
Table A-2: Single phase liquid recirculation apparatus surveyed	356
Table A-3: Vapour phase recirculation apparatus surveyed	363
Table A-4: Two phase recirculation apparatus surveyed	373

Table A-5: Single liquid and vapour pass apparatus surveyed	379
Table A-6: Static apparatus surveyed	387
Table B-1: Number of parameters required for the Prausnitz-Chueh Method [Wichterle, 1978(b)]	408
Table B-2: Rating of the computational methods for HPVLE [Raal and Mühlbauer, 1998]	408
Table B-3: Capabilities of the various classes of equations of state [Raal and Mühlbauer, 1998]	409
Table B-4: Comparison of the Direct and Combined Methods [Wichterle, 1978(b)]	409
Table B-5: Modifications to the attractive term (equation (3-35)) as reproduced from Mühlbauer and Raal [1995]	426
Table C-1: Typical physical properties of Fibrefrax Duraback [Carborundum Company Catalogue, 1995]	456
Table E-1: Experimental VLE data of Ng and Robinson [1978] for the system Carbon Dioxide + Toluene at 311.26 K	467
Table E-2: Experimental VLE data of Fink and Hershey [1998] for the system Carbon Dioxide + Toluene at 308.16 K	467
Table E-3: Experimental VLE data of Ng and Robinson [1978] for the system Carbon Dioxide + Toluene at 352.59 K	468
Table E-4: Experimental VLE data of Morris and Donohue [1985] for the system Carbon Dioxide + Toluene at 353.15 K	468

Table E-5: Experimental VLE data of Kim et al. [1986] for the system Carbon Dioxide + Toluene at 353.4 K	468
Table E-6: Experimental VLE data of Fink and Hershey [1990] for the system Carbon Dioxide + Toluene at 353.18 K	469
Table E-7: Experimental VLE data of Mühlbauer and Raal [1990] for the system Carbon Dioxide + Toluene at 352.15 K	469
Table E-8: Experimental VLE data of Ng and Robinson [1978] for the system Carbon Dioxide + Toluene at 393.71 K	470
Table E-9: Experimental VLE data of Sebastian et al. [1980] for the system Carbon Dioxide + Toluene at 393.25 K	470
Table E-10: Experimental VLE data of Kim et al. [1986] for the system Carbon Dioxide + Toluene at 311.26 K	470
Table E-11: Experimental VLE data of Ohgaki and Katayama [1976] for the system Carbon Dioxide + Methanol at 313.15 K	471
Table E-12: Experimental VLE data of Suzuki et al. [1990] for the system Carbon Dioxide + Methanol at 313.4 K	471
Table E-13: Experimental VLE data of Chang et al. [1997] for the system Carbon Dioxide + Methanol at 313.14 K	472
Table E-14: Experimental VLE data of Brunner et al. [1987] for the system Carbon Dioxide + Methanol at 373.15 K	473
Table E-15: Experimental VLE data of Mühlbauer and Raal [1993] for the system Propane + 1-Propanol at 378.15 K	474

Table E-16: Experimental VLE data of Mühlbauer and Raal [1993] for the system Propane + 1-Propanol at 393.15 K	475
Table E-17: Second Virial coefficients for Nitrogen at 323.15 K (Dymond and Smith [1980])	478
Table E-18: Second Virial coefficients for Nitrogen at 348.15 K (Dymond and Smith [1980])	478
Table E-19: Second Virial coefficients for Nitrogen at 373.15 K (Dymond and Smith [1980])	479
Table E-20: Second Virial coefficients for Propane at 323.15 K (Dymond and Smith [1980])	479
Table E-21: Second Virial coefficients for Propane at 348.15 K (Dymond and Smith [1980])	479
Table E-22: Second Virial coefficients for Propane at 373.15 K (Dymond and Smith [1980])	480
Table E-23: Cross-term second virial coefficients for the system Propane + Nitrogen as measured by Wormald et al. [1996]	480
Table F-1: Properties for components studied	481
Table F-2: Antoine constants for the components studied	481
Table F-3: Correlation constants for vapour pressure	482
Table F-4: UNIQUAC parameters for the components investigated	482
Table F-5: Constants for the standard-state zero pressure fugacity as given by Equation (8-6)	482

Table F-6: Association and solvation parameters for the systems investigated	483
--	-----

LIST OF PHOTOGRAPHS

Photograph 4-1: Front-view of the main assembly of the apparatus	122
Photograph 4-2: Side-view of the main assembly of the apparatus	123
Photograph 4-3: The removable base supporting the composite impeller	127
Photograph 4-4: The HPVLE apparatus designed in this project with its ancillary equipment	136
Photograph 4-5: The interior of the air-bath showing the copper jacket, insulation, equilibrium cell and plumbing	136
Photograph 4-6: The control/display panel for the apparatus with display units for temperature and pressure measurement	141
Photograph 4-7: Arrangement of the high-pressure apparatus and the GC facilitating online analysis of the equilibrium phase compositions	142

NOMENCLATURE

LIST OF SYMBOLS

a, b	EOS parameters
A	Second virial coefficient / Helmholtz free energy
C	Third virial coefficient
f	Fugacity
G	Gibbs excess free energy
H	Enthalpy
K	Equilibrium ratio
k	EOS interaction parameter
l	EOS interaction parameter
n	Number of moles
P	Pressure
R	Universal gas constant
T	Temperature
V	Volume
x	Liquid phase mole fraction
y	Vapour phase mole fraction
Z	Compressibility factor
z	Co-ordination number

GREEK LETTERS

α	NRTL interaction parameter / EOS temperature dependent parameter
ϕ	Fugacity coefficient
γ	Activity coefficient
κ	EOS parameter
μ	Chemical potential
Δ	Change of mixing
ω	Accentric factor

SUPERSCRIPTS

<i>E</i>	Excess property
<i>L</i>	Liquid phase
<i>o</i>	Standard-state
<i>V</i>	Vapour phase
<i>r</i>	Reference state
\wedge	In solution property
-	Partial property

SUBSCRIPTS

<i>c</i>	critical point
<i>i,j</i>	Molecular species
<i>mix</i>	Mixture
<i>T</i>	Total
<i>v</i>	Vapour phase
<i>x</i>	Liquid phase

ABBREVIATIONS

EOS	Equation of state
FID	Flame ionized detector
GC	Gas chromatograph
G-C	Group-Contribution
HPVLE	High pressure vapour-liquid equilibrium
HPVLLE	High pressure vapour-liquid-liquid equilibrium
LLE	Liquid-liquid equilibrium
PR	Peng-Robinson
PRSV	Peng-Robinson-Stryjek-Vera
P-V-T	Pressure-Volume-Temperature
SRK	Soave-Redlich-Kwong (Soave)
TCD	Thermal conductivity detector
VLE	Vapour-liquid equilibrium
VLLE	Vapour-liquid-liquid equilibrium

CHAPTER ONE

INTRODUCTION

Separation and purification processes are a core component of the chemical industry. They are seen as the unit operations that generate the most capital, however, they are also the ones that consume the major portion of both the design and operating costs of chemical plants. It is these unit operations where the most efficient design and optimal performance can vastly increase the profitability of a process. The main separation processes in use today such as distillation, gas absorption and extraction to name a few, are based to a large extent, on the knowledge of phase equilibrium between coexisting phases. Consequently, the thermodynamic modeling and measurement of phase equilibrium is crucial in the chemical process design, e.g. the occurrence of an azeotrope or a liquid-liquid phase split may require major modification and this may decrease the feasibility of a proposed process scheme.

Engineers are continually striving to obtain more economical separation methods and conditions as products get more complex in nature and begin to push the envelope of proven current separation technology. The rapidly developing technology of supercritical technology is testament to this. Supercritical extraction is currently being used in the food and petrochemical industry and is fast finding many more applications. This has led to considerable interest in high pressure vapour-liquid equilibrium data, initially for systems containing carbon dioxide and light hydrocarbons, but has now spread to a wide range of hydrocarbons.

The measurement of high-pressure vapour-liquid equilibrium is an extremely demanding task and requires considerable skill and expertise. Design of equipment for the measurement of HPVLE must rate as one of the most difficult tasks that can be undertaken by a researcher. It is time consuming and expensive and requires tremendous dedication and attention to detail. The demanding nature of HPVLE is not only restricted to measurement, but also extends to theoretical analysis of the measured experimental data.

The theoretical reduction of HPVLE data is complex and is extremely tedious and time consuming. It prohibited a number of researchers from performing rigorous computation for the reduction of HPVLE data. With the advent of the personal computer however and with the ever-increasing speed of processors, researcher can venture to correlate and even predict HPVLE data by complex theoretical and/or empirically derived equations. Their only limitation on accuracy of the results is the validity of the equations employed and reliability of the

thermodynamic information. As a result, over the last two decades the number of proposed thermodynamic equations, especially in the area of VLE has snowballed.

This project serves to further strengthen and enhance research into the area of HPVLE in the Thermodynamics Research Group in the School of Chemical Engineering at the University of Natal. The Group has some 20 years of expertise in this area. The equipment design detailed in this project is as a result of years of modification and improvement over previous equipment designs. The predecessors to the current apparatus were HPVLE designs by Bradshaw [1985] and Mühlbauer [1990]. The type of apparatus remains the same, i.e. it is of the static type, but there have been vast improvements in terms of accuracy of measurements, compactness and versatility, as well as being able to visually detect the equilibrium phases and having capabilities for measurement of vapour-liquid-liquid equilibrium.

The theoretical aspects of HPVLE are also tackled in this project. Different methods (direct and combined) for the reduction of HPVLE are discussed and undertaken for the systems measured. A host of activity coefficient models, equations of state and mixing rules are discussed and applied to the modeling of the systems measured. Consistency testing of the measured HPVLE is undertaken so as to infer the quality of the measured data.

One could say that in addition to the development of a new versatile HPVLE apparatus, this project also served to increase the knowledge base in the field of HPVLE in terms of the latest experimental and theoretical developments.

CHAPTER TWO

LITERATURE SURVEY OF HIGH PRESSURE VLE EXPERIMENTAL EQUIPMENT

2.1. PRESENTATION OF HPVLE DATA

To fully understand why VLE equipment is designed in various fashions, one has to have knowledge of the forms in which measured two-phase binary HPVLE data are normally presented. In most instances, the way in which the data are presented indicates the method by which the data were measured. The forms in which the data are normally presented graphically are as follows:-

- a) Isobaric, T - x - y
- b) Isothermal, P - x - y
- c) Isopleth, P - T data (phase boundaries at constant composition).

The x - y graphical representation that is common in low pressure VLE is infrequently seen in HPVLE.

Schneider [1978], Streett [1983], de Swan Arons and de Loos [1994] and Bolz et al. [1998] give excellent reviews on the underlying principles involved in the construction and interpretation of phase diagrams. A brief introduction of binary phase diagrams is given in Appendix A.1.

2.2. CLASSIFICATION OF EXPERIMENTAL EQUIPMENT

An experimental method chosen for the measurement of HPVLE is generally based on the requirements of the researcher and the properties of the material or system being investigated. By requirements of the researcher one refers to either, the operating conditions; the type of data required; experience; or financial means.

In dealing with the thermodynamics of mixtures, Deiters and Schneider [1986] refer to *density* and *field* variables. *Field* variables are variables that have the same value in coexisting phases (e.g. temperature and pressure), whereas *densities* are usually different (e.g. mole fractions and molar volumes). Usually the *field* variables are easier to determine experimentally. The determination of *density* variables experimentally, however, has always posed a major problem. Deiters and Schneider [1986] based their classification of different experimental methods according to the *densities* that are primarily observed. They have come up with the so-called *synthetic* and *analytic* methods.

In the *synthetic* method a mixture of known composition is prepared and its behaviour observed as a function of temperature and pressure. This replaces the problem of analysing the fluid mixture by the problem of synthesising it. The typical results of synthetic experiments are sets of isopleths. The traditional P - x and T - x diagrams can then be obtained from the primary data through cross plotting.

The *analytic* method does not rely on a precise knowledge of the overall composition. Phase separation is brought about by adjustment of temperature and pressure, and then samples are taken of the phases and analysed by appropriate methods. The major problem with the analytical method though is not the determination of the composition of a sample, but the handling of the sample. This is as a result of the equilibrium state being very different from the *input* state (in HPVLE) of the analytical device being used and the slightest change in temperature or pressure may lead to a partial separation of the components.

HPVLE equipment has been simply and elegantly classified by Raal and Mühlbauer [1994] as shown in Figure 2-1. According to Raal and Mühlbauer [1994] classification is dependent on whether one, both, or neither of the phases are circulated through the equilibrium cell. If there is circulation, then it is known as a *dynamic* or *flow* method, else it is known as a *static* method. The Raal and Mühlbauer [1994] method of classification was adopted in this project. Another scheme for classification of experimental methods is described by Richon [1996].

To give one greater insight into the experimental methods for HPVLE, each of the methods will now be outlined. Since the equipment designed for this research project was an analytical cell, emphasis will be placed on the analytical method. Examples from literature will be presented under each of the methods. As it would not be feasible to cover all of the various apparatus reported in literature, only selected examples will be presented. Examples presented were chosen

according to aspects of equipment design incorporated into this project and also according to novelty and interest. For more detailed descriptions of experimental apparatus, excellent reviews by Tsiklis [1968], Schneider [1975], Young [1978], Eubank et al. [1980], and Malanowski [1982(b)] cover the earlier period, while the period up to 1990 is excellently reviewed by Marsh [1989] and Raal and Mühlbauer [1994]. It is interesting to note that in the period from 1991 to date, relatively few papers have been published on new equipment in this area of research.

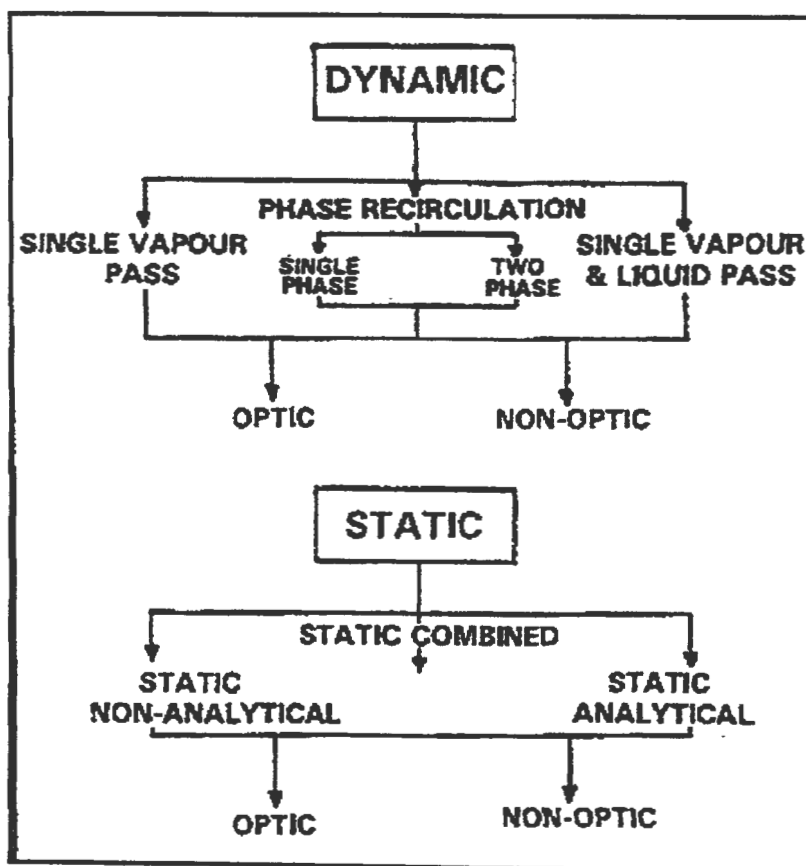


Figure 2-1: Classification of experimental equipment for HPVLE (extracted from Raal and Mühlbauer [1994])

2.3. ANALYTICAL METHODS

2.3.1. Primary features of the analytical method

The main features of the analytical method, be it static or dynamic, are as follows (Figure 2-2 illustrates the primary features of the analytical method):-

- (a) An equilibrium cell in which the vapour and liquid phases are in equilibrium.

- (b) A temperature controlled environment in which the equilibrium cell is housed. Typical environments are air-baths [Mühlbauer, 1990], oil [Kim et al., 1986(a)] or water baths, copper [Konrad et al., 1983] or aluminium [Ng and Robinson, 1978] jackets, and cryostats [Duncan and Hiza, 1970].
- (c) A mechanism for agitating and mixing the cell contents. In dynamic methods this is normally achieved by circulation of one or more of the phases, whereas in static methods it is normally achieved with an internal stirrer. Dynamic methods have been known to have internal stirring in addition to phase re-circulation [Suzuki et al., 1990(a)]. More unorthodox ways of producing agitation of cell contents include some equilibrium cell assemblies being rocked mechanically [Ashcroft et al., 1983, and Huang et al., 1985] and piston action has also been used to mix cell contents [Gomez-Nieto and Thodos, 1978].
- (d) A method to sample the vapour and liquid phases. Static methods require a sampling device for both the liquid and vapour phases. In the two-phase recirculation and single-pass vapour and liquid methods this may be eliminated since a representative portion of the flow can very readily be diverted for sampling. However, for the vapour recirculation method, a sampling device is still needed for the liquid phase.
- (e) A means of accurately analysing the withdrawn samples.
- (f) An instrument to measure pressure and temperature.

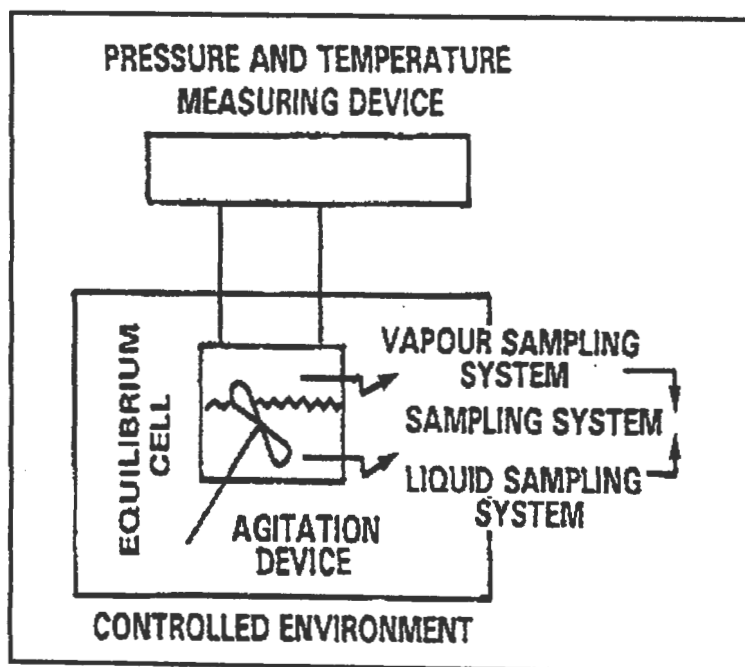


Figure 2-2: Schematic illustrating the features of a typical analytical method (extracted from Raal and Mühlbauer [1994])

2.3.2. Experimental difficulties associated with analytical methods

The following are problems commonly encountered in the accurate measurement of isothermal HPVLE:-

a) Obtaining truly isothermal conditions

Raal and Mühlbauer [1994] state that even very small vertical temperature gradients in the equilibrium chamber of a static or dynamic cell can cause considerable error in measurement. The problem is particularly acute when measuring volatile/non-volatile systems. They recommend that several temperature sensors be installed in the walls of the equilibrium cell to test temperature homogeneity. A value of 0.2K in temperature deviation is quoted as being acceptable. It is also stated that there should be no conductive paths to or from the cell through fittings or attachments, and that there should be no direct radiative energy exchange between the cell and the bath heaters. Measurements of bath and cell temperature profiles have also been reported by many other researchers, e.g. Rogers and Prausnitz [1970], and Konrad et al. [1983]. It is quite interesting to note that most of the researchers who mentioned measurement of temperature profiles made use of static cells.

b) The attainment of equilibrium

In phase equilibria the term *equilibrium* implies a state of no change of material with time on the macroscopic level. A state of *true equilibrium* is probably never achieved as there are always small changes in the surroundings and also due to retarding resistances. The rate at which equilibrium is reached decreases as equilibrium is attained. Therefore, in phase equilibrium studies, high stirring rates are desired so as to speed up the attainment of equilibrium. This mechanical stirring produces fluid friction and as a result of dissipation of energy to the surroundings, this must result in some temperature gradient being produced in the fluid.

Property variables that are used to judge whether equilibrium has been reached are temperature, pressure, vapour and liquid compositions [Wan and Dodge, 1940], and in some cases stability of refractive indices [Besserer and Robinson, 1971]. Fluctuations in the measured temperature and pressure within a specified tolerance over a period of time has also been used by various researchers as an indication of phase equilibrium having been achieved. Fredenslund et al. [1973] used a change in pressure of less than 0.05% of the total pressure in 30 minutes as their criterion in judging whether equilibrium had been reached. By the way of composition as a criterion,

repeated vapour and liquid sample composition analysis must give reproducible results within the limits of the analytical procedure.

c) Disturbance of equilibrium due to sampling

The procedure of sampling the liquid or vapour phase may produce a change in the volume of the equilibrium cell. The disturbance of the equilibrium condition is directly proportional to the change in the volume associated with sampling. Since volume is linked to pressure, the change in the volume due to sampling can be quantified by the change in the cell pressure. Besserer and Robinson [1971], and Wagner and Wichterle [1987] reported changes of 0.1 and 0.01 bar respectively due to sampling. Mühlbauer [1990] also encountered this problem in his sampling technique.

There are two volume changes that are associated with sampling in the static method which result in the disturbance of the equilibrium condition. They are:-

- i) the volume change associated with the withdrawn sample, and
- ii) the volume change associated with the sampling method that is employed, e.g. Mühlbauer [1990] used a sliding rod sampler.

Thus to minimise the effects of volume change, the ideal method is to have the smallest possible volume change as compared to the method of sampling employed. Practically this has been achieved in the following fashion:-

- A large equilibrium cell volume in comparison to the withdrawn sample. This dampens the volumetric disturbances as the percentage cell volume change is decreased. The drawbacks of a large equilibrium cell however are increased use of chemicals. Sagara et al. [1972], Klink et al. [1975], Aschroft et al. [1983], Reiff et al. [1987], and Mühlbauer [1990] all report the use of large equilibrium cells to minimise the percentage volume change during sampling.
- A very rapid sampling method to minimise the disturbance in equilibrium. This method was employed by Figuiere et al. [1980] using rapid-acting pulse valves.
- A sampling method that eliminates the volume change due to the sampling method. Rogers and Prausnitz [1970], and Nakayama et al. [1987] used a sampling rod which traversed the entire equilibrium cell.
- Making use of a variable-volume equilibrium cell. The pressure change due to sampling can then be compensated by pressure adjustment [Nakayama et al., 1987].

- Not disturbing the cell contents, by making use of in-situ phase composition analyses. Konrad et al. [1983] made use of optical methods to determine composition, as did Besserer and Robinson [1971].

The equipment in this study made use of a novel impeller-induced flow, through a sampling valve, which is discussed later in Chapter 4.

d) Sample homogenisation

One of the major problems in liquid sampling is a tendency for the more volatile component to flash preferentially. This produces a concentration gradient in the resultant vapour. Therefore, if no method is employed to homogenise the withdrawn sample and also prevent partial condensation, quantitative analysis of the sample will be in error. The following are examples of procedures that have been adopted in an attempt to eliminate this problem:-

- Wagner and Wichterle [1987] made use of a stirred homogenisation vessel in the sample line.
- Kalra et al. [1978], Ng and Robinson [1979] and Nakayama et al. [1987] employed a forced circulation system to homogenise the vapourised liquid sample.
- Mühlbauer [1990] made use of a jet mixer. The liquid sample is expelled into the evacuated jet mixer in which swirling recirculation homogenises the vapour. This device has also been used in the present study.
- Kobayashi and Katz [1953], Rogers and Prausnitz [1970], Simnick et al. [1977], and Inomata et al. [1986] made use of the method of analysing the more and less volatile components separately. This method basically entailed the separation of the more and less volatile components in the sample by expanding the sample into an evacuated vessel. The amount of supercritical component could then be calculated from the total pressure. The condensed less volatile components are then flushed out of the vessel with an organic solvent. A calibration standard was then added and the resulting mixture then analysed by gas chromatography. This procedure appears unnecessarily complex and may introduce error.
- Chou et al. [1990] made use of microcells to homogenise the withdrawn samples. The equilibrium samples were trapped in the microcells and the microcells were then put into a microcell housing in which the sample analysis was undertaken.

e) Accurate analysis of the withdrawn sample

The most commonly used methods to analyse the withdrawn samples are by gas chromatography (GC) and spectroscopy. Refractive index measurement in conjunction with GC analysis has also been reported by Besserer and Robinson [1971], and Kalra et al. [1978].

Thermal conductivity detectors (TCD) and Flame ionisation detectors (FID) are the two most commonly used types of detectors in GC analysis. An advantage of the TCD, compared to the FID is that the TCD can be used to detect hydrocarbon and non-hydrocarbons, whereas the FID can only detect organics. However, the FID is more sensitive than the TCD. The main disadvantage of analysis by GC is that the high-pressure equilibrium state is different from the state at which the sample enters the GC. It is stated by Deiters and Schneider [1986] that the quantitative determination of the composition does not usually present a problem, but it is the handling and preparation of the sample that does.

Spectroscopic or photometric methods make use of in-situ composition analysis to overcome the sample preparation difficulties that are associated with GC analysis. Infrared spectroscopy has been reported by Price and Kobayashi [1959], Konrad et al. [1983], and Swaid et al. [1986] to determine phase compositions. However, there are also difficulties that are associated with spectroscopy or Raman scattering methods. They are as follows:-

- i) extensive calibration procedures,
- ii) application of visual or ultraviolet spectroscopy is largely restricted to aromatic or coloured compounds, and
- iii) there is the possibility that the absorption bands of different compounds may overlap.

Accurate GC detector calibration still remains a considerable problem for gas mixtures or gas-liquid mixtures as reliable commercial standards are usually not available and the full mole fraction range must be covered. However, this problem has been recently overcome with a precision volumetric calibration device (Raal, 1992 and Raal and Mühlbauer, 1998).

f) Temperature and pressure measurement

The most commonly used temperature sensors are platinum resistance thermometers (Pt-100 Ω), thermocouples, thermistors, and quartz thermometers. High stability thermistors and quartz thermometers have very high sensitivities to temperature and are generally used as primary measuring devices against which one can calibrate the commonly used sensors.

In recent years pressure transducers, differential manometers and Bourdon-type pressure gauges have primarily been used as the measuring devices for pressure. Some pressure transducers have temperature compensation over wide ranges, and are thus favoured. Dead weight piston gauges are generally used as a primary measuring device against which the transducers can be calibrated.

g) Degassing of the less volatile component

At low compositions of the more volatile component in the liquid phase, dissolved gases will compete with the more volatile component. Thus degassing is required of the less volatile (liquid) component to remove dissolved gases. Degassing is especially important in systems where the two components are partially mutually soluble. Figuiere et al. [1980] and Legret et al. [1981] stress the importance of degassing in order to obtain accurate VLE data. Liquid degassing is usually done in-situ or before sample introduction into the equilibrium cell. Equipment used for degassing are described by Van Ness and Abbott [1978], Battino et al. [1971], and Mühlbauer [1990].

2.4. DYNAMIC METHODS

Dynamic methods can be divided into one of three categories, depending on the phases that are circulated or passed through the equilibrium cell. The three types of flow methods are:-

- the single vapour pass method;
- the phase recirculation method; and
- the single vapour and liquid pass method.

2.4.1. Single Vapour Pass Method

2.4.1.1. Description of the single vapour pass method

The typical features of a single vapour pass method are shown in Figure 2-3.

The vapour feed (gaseous component) is passed through the stationary liquid phase in the equilibrium cell. It is fed at constant pressure. With time the gaseous component progressively

dissolves in the liquid phase until equilibrium is reached. This method has very short equilibration times (Young [1978] claims an equilibration time of 15 minutes), but in general the equilibration time will depend on the transport coefficients of mass and momentum transfer between both phases. It is also dependent on the equilibrium solubilities of the system. Once equilibrium has been achieved, a vapour phase sample is obtained by diverting a portion of the effluent stream, whilst a liquid phase sample is withdrawn from the equilibrium cell.

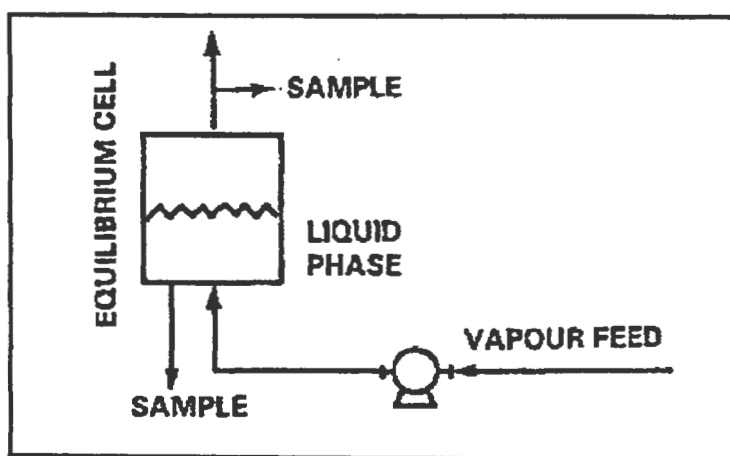


Figure 2-3: Schematic illustrating typical features of a single vapour pass method (extracted from Raal and Mühlbauer [1994])

The single vapour pass method was the original dynamic method. This method can be used to generate isobaric or isothermal VLE data, depending on whether one controls the pressure of the gaseous component or the temperature of the liquid phase respectively. It is also the simplest and easiest method to operate; however it has several disadvantages. Therefore this method has largely been replaced by recirculation methods.

2.4.1.2. Selected examples from literature for the single vapour pass method

Wan and Dodge [1940]

Figure 2-4 below illustrates the flowsheet of the apparatus used by Wan and Dodge. The more volatile component (delivered from its storage vessel) enters at point A, and flows through the presaturators (B and C), before entering the equilibrium cell (D). After the equilibrium cell, it is expanded into the sample line (I). Liquid samples are withdrawn from the apparatus through line E. A Bourdon pressure gauge (G) is used to control the pressure, and equilibrium pressures are

measured with a dead-weight piston gauge. Agitation of the equilibrium cell contents is achieved via a magnetic stirrer which is operated by a solenoid (line connections indicated by F).

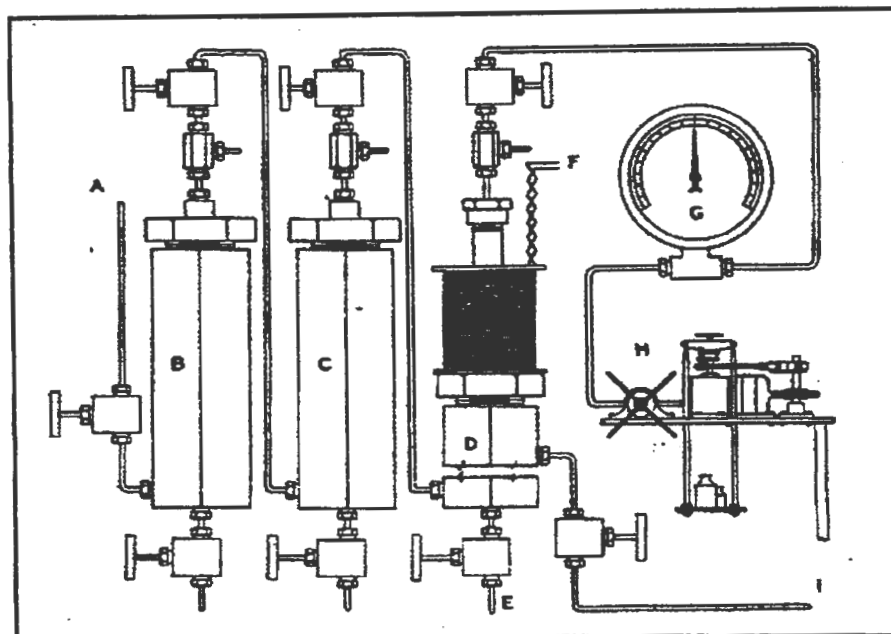


Figure 2-4: Flowsheet of the experimental apparatus used by Wan and Dodge [1940]
 A - inlet; B,C - presaturators; D - equilibrium cell; E - sampling point; F - solenoid line connections; G - Bourdon pressure gauge; H - screw press.

The apparatus makes use of two oil baths for the control of temperature. The first oil bath is used to control the temperature in the first presaturator (control to within 0.1°C), while the second oil bath is used to control the temperature of the second presaturator and the equilibrium cell (control to within 0.01°C). Heating is achieved with an electric immersion heater.

Because the gas phase makes a single pass through a given column of liquid and must become saturated with the less volatile component during this relatively short time, use is made of presaturators. The first presaturator temperature was maintained 10°C higher than the equilibrium temperature, so as to over-saturate the gas relative to the equilibrium temperature. The second presaturator and equilibrium cell then reduce the concentration of the less volatile component to the proper equilibrium value.

At least two hours were allowed to elapse before any samples were taken. Samples of both phases were taken at one hour intervals. Equilibrium composition was taken as the value when consecutive liquid samples agreed within the limit of experimental error. To ensure consistent

results, Wan and Dodge [1940] developed a technique for sampling the liquid. The main features were very slow sampling and flushing of the contents of the sampler.

2.4.1.3. Difficulties associated with the single vapour pass method

The following are the difficulties that are encountered with the single vapour pass method:-

- large quantities of gaseous component are used, which becomes an important factor in the choice of method when very rare, high purity, and expensive gases are used;
- establishing whether the vapour phase is saturated with liquid in the short contact time available;
- liquid component is constantly being removed, which places constraints on the amount of data obtained from one experimental run;
- liquid components that are used are restricted to ones which have low partial pressures (e.g. below 0.01 MPa (Young, 1978)) and thus this method is not suitable to critical region studies;
- ensuring that there is no droplet entrainment in the effluent vapour stream;
- maintaining accurate control of the gas flow rate. High gas flowrates produce rapid liquid saturation, at the expense of vapour saturation, as a result of the shorter contact time. The opposite effect occurs for a lower gas flowrate. This flowrate problem is heightened when either the gas is highly soluble in the liquid or vice versa;
- maintaining a constant liquid level ; and
- some form of liquid agitation is required if the components are slightly soluble in one another.

Table 2-1 lists the single vapour pass apparatus that were surveyed. Greater detail on apparatus design and systems investigated is available in Appendix A.2.

2.4.2. Phase re-circulation methods

2.4.2.1. Description of the phase recirculation method

Phase recirculation methods may be subdivided into one of two categories, depending on whether recirculation of one or both phases occurs (in the case of VLE). As a result they are termed single

phase and two-phase recirculation respectively. Figure 2-5 illustrates the features of the phase recirculation method.

The components of interest are charged into the equilibrium cell. Achieving the desired level in the equilibrium cell is difficult and considerable experience is required to determine the quantity added [Freitag and Robinson, 1986]. One or both phases are withdrawn from the cell and recirculated. The temperature and pressure of the equilibrium cell contents are maintained at the desired setting. For the case of two-phase recirculation the phases are circulated counter-currently through the equilibrium cell and either phase may be dispersed. The liquid phase enters the equilibrium cell at the top and pours down through the vapour phase, whilst the vapour phase enters at the bottom of the cell and bubbles up through the liquid phase. As a result equilibrium between the phases in a well-designed equilibrium cell should be rapidly achieved due to good contacting between the phases. This arrangement removes some of the problems associated with the single vapour pass method, e.g. ensuring that equilibrium is achieved; that the liquid component is not continuously removed from the system, and that large quantities of the gaseous component are not wasted. Also liquids possessing high partial pressures may be studied.

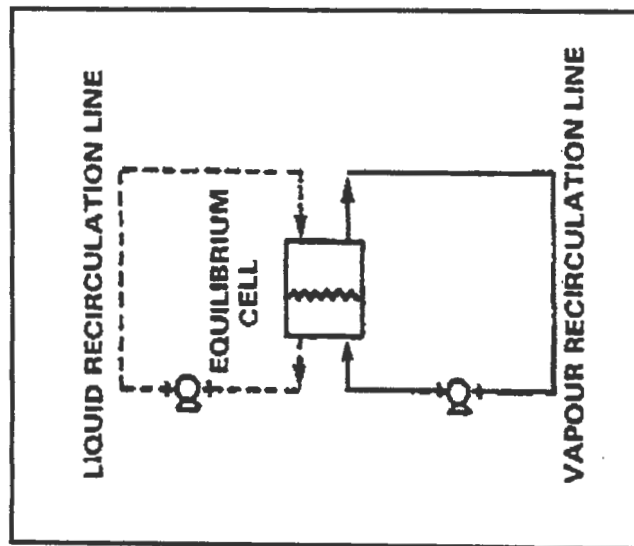


Figure 2-5: Schematic illustrating the features of the phase recirculation method (extracted from Raal and Mühlbauer [1994])

References	Cell volume (cm ³)	Operating Range		Equilibrium cell (1)	Measurement Device		Equilibration time (min)	Sample size (μl)	
		Temp (K)	Pressure (bar)		Temp (2)	Pressure (3)		Vapour	Liquid
Wan and Dodge [1940]	-	273-573	1013	cold-rolled steel	-	B/DWP	120	-	3000
Duncan and Hiza [1970]	-	10-150	203	electrolytic tough pitch copper	PR	B	-	-	-
Legret et al. [1983]	-	423	200	-	TC	BM/PT	-	-	N/A
Lee and Chao [1988]	300	-	345	-	TC	B	-	-	-
Di Giacomo et al. [1989]	100	473	1000	stainless steel	TC	PT	60-300	-	-

Table 2-1: Single vapour pass apparatus surveyed

Key:

(1) Materials of construction

(2) PR - platinum resistor; TC - thermocouple

(3) B - Bourdon type pressure gauge; DWP - Dead weight piston gauge; BM - Bourdon manometer; PT - Pressure transducer

2.4.2.2. Selected examples from literature for the single phase recirculation method

The single-phase recirculation method can be sub-divided into two groups, depending on whether one has recirculation of either the liquid or vapour phase. Selected examples of each of these groups will now be presented.

2.4.2.2.1. Liquid phase recirculation

Kim et al. [1986(a)]

The apparatus was designed for rapid determination of equilibrium compositions for temperatures and pressures up to 423K and 13.7 MPa respectively. The equilibrium cell had an internal volume of 100 cm³, and was constructed from 316 stainless steel. A schematic of the experimental apparatus is shown in Figure 2-6.

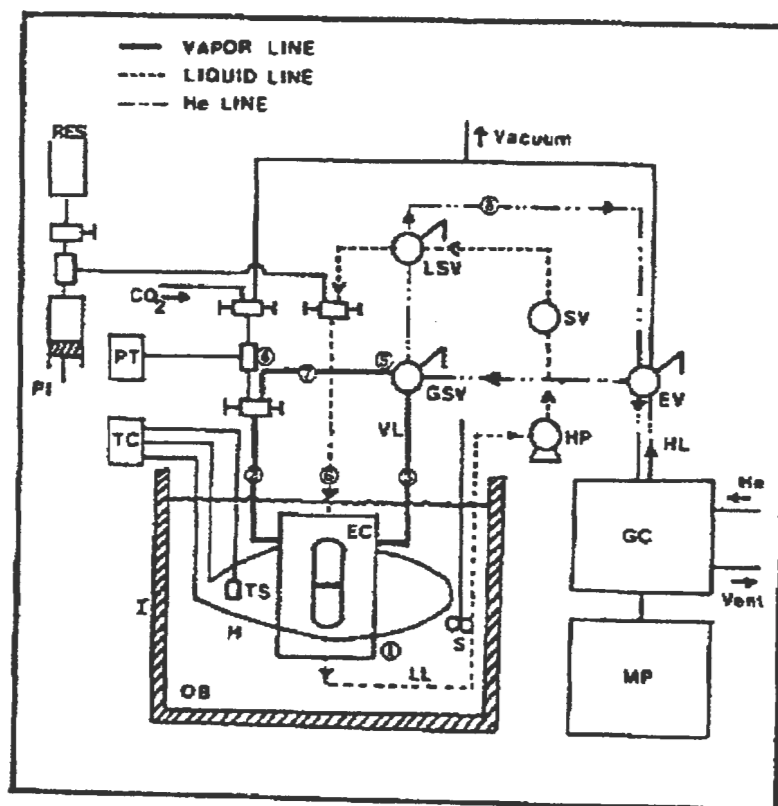


Figure 2-6: Schematic of the experimental apparatus of Kim et al. [1986(a)]

PI - piston injector; PT - pressure transducer; TC - temperature controller; I - insulation; OB - oil bath; H - heater; TS - temperature sensor; EC - equilibrium cell; S - stirrer; LL - liquid line; VL - vapour line; HL - carrier gas (helium) line; LSV - liquid sampling valve; GSV - gas sampling valve; SV - safety valve; EV - evacuation valve; MP - microprocessor; GC - gas chromatograph; HP - high pressure pump; numbers 1 to 8 give the position of thermocouples.

The equilibrium cell has two glass windows and is housed in a temperature controlled oil bath. The bath is heated by 1000 W and 200 W electrical heaters and the oil bath temperature is controlled to within 0.1 K. A pressure transducer is used to measure the equilibrium cell pressure, and temperatures are measured with iron-constantan thermocouples.

All connections between the equilibrium cell and valves are 1/8" o.d. stainless steel tubing. All the valves and tubing for the vapour line were wrapped with heating wire and insulated. Insulation of all other lines is achieved with heavy-duty heating tapes. The vapour and liquid sampling lines are also maintained at approximately the system temperature.

Kim et al. [1986(a)] state that circulation of the liquid phase results in rapid equilibration. The equilibrium vapour phase reaches the vapour-sampling valve by diffusion. Despite this, representative vapour compositions were usually obtained in less than 10 minutes. Rapid equilibration was achieved as a result of pulsation in liquid flow, a short vapour line, and repeated injections.

Sampling of the vapour phase was achieved with an external sampling loop of volume 25 μl and the liquid phase with an internal sampling loop of volume 0.5 μl . The vapour and liquid samples were transported from the sampling valves to the GC with helium as the carrier gas.

Table 2-2 lists the liquid phase recirculation apparatus that were surveyed. Greater detail on apparatus design and systems investigated is available in Appendix A.2.

2.4.2.2.2. Vapour phase recirculation

Fredenslund et al. [1973]

The apparatus was designed for an operating temperature range of -180°C to 25°C and pressure range from 3 to 350 atm. Fredenslund et al. [1973] state that the outstanding features of the apparatus are the liquid sampling device and the method of liquid nitrogen feed to the thermostat.

The equilibrium cell is placed in a cryostat to maintain constant temperature. The equilibrium cell is constructed from type 304 stainless steel, and has windows made of fused quartz. Equilibrium cell volume is approximately 15 cm^3 .

References	Cell volume (cm ³)	Operating Range		Equilibrium cell (1)	Measurement Device		Equilibration time (min)	Sample size (μl)	
		Temp (K)	Pressure (bar)		Temp (2)	Pressure (3)		Vapour	Liquid
Kim et al. [1986(a)]	100	423	137	316 stainless steel	TC	PT	10	25	0.5
Mohamed and Holder [1987]	100	-	-	Stainless steel	TC	PT	-	-	-

Table 2-2: Liquid phase recirculation apparatus surveyed

Key:

- (1) Material of construction
- (2) TC - thermocouple
- (3) PT - pressure transducer

With the method of nitrogen fed to the thermostat the temperature can be controlled to within 0.01°C and the nitrogen consumption is very low.

The liquid sampling device consists of a 5 mm diameter rod that protrudes into the liquid phase in the cell. The part of the rod that is immersed in the liquid has a $3.5\ \mu\text{l}$ hole drilled vertically through it. By activation of a piston, which is connected to the rod and is mounted outside the thermostat, the sample of liquid is drawn into the cell wall. From here the liquid sample is flushed with GC carrier gas into the GC. The packing gland that surrounds the rod is constructed of Invar, graphite, and graphite- and glass impregnated Teflon. The packing gland is also thermally compensated so that the volumetric decrease of the packing gland equals that of the stainless steel hole containing the gland in going from room temperature to -100°C . This method of sampling has the advantage of small sampling volume and therefore minimal disturbance of the equilibrium during sampling. Figure 2-7 shows the liquid sampling unit of Fredenslund et al. [1973].

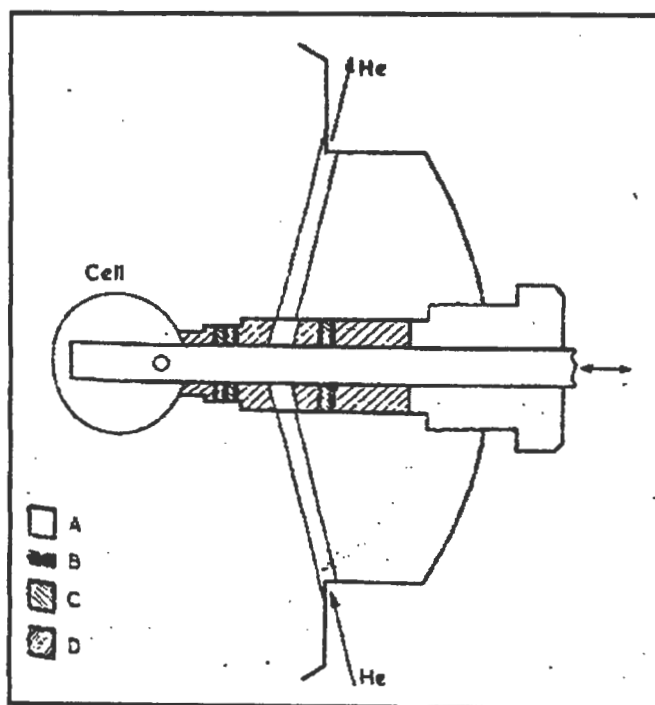


Figure 2-7: Illustration of the liquid sampling unit of Fredenslund et al. [1973]
 A - 304 stainless-steel; B - graphite; C - Teflon; D - Invar

Weber et al. [1984]

The equilibrium cell (Figure 2-8) was constructed of chromium-nickel steel, and had a volume of $230\ \text{cm}^3$. Visual observation of the equilibrium cell contents was possible as a result of high-

pressure glass windows being incorporated into the wall of the equilibrium cell. The windows also assisted in the control of the height of the liquid-level and of the distribution of the vapour injected in the liquid, as well as detection of the appearance of two liquid phases.

The vapour that is recycled is introduced back into the equilibrium cell at the bottom through a distribution nozzle, and leaves at the top through a mist separator made of wire mesh. A temperature sensor can be inserted into the mist separator.

Liquid samples are taken through a capillary, and vapour samples are isolated in a bypass of the recycling system after equilibrium has been established (Figure 2-9 and Figure 2-10). Samples are collected in sample bottles from which they are injected into a GC.

The vapour can be recycled either by a reciprocating double acting compressor (Method I, Figure 2-9) located in the bath, or by a membrane compressor (Method II, Figure 2-10) operated at ambient temperature. Method II is the preferred method for the investigation of ternary systems.

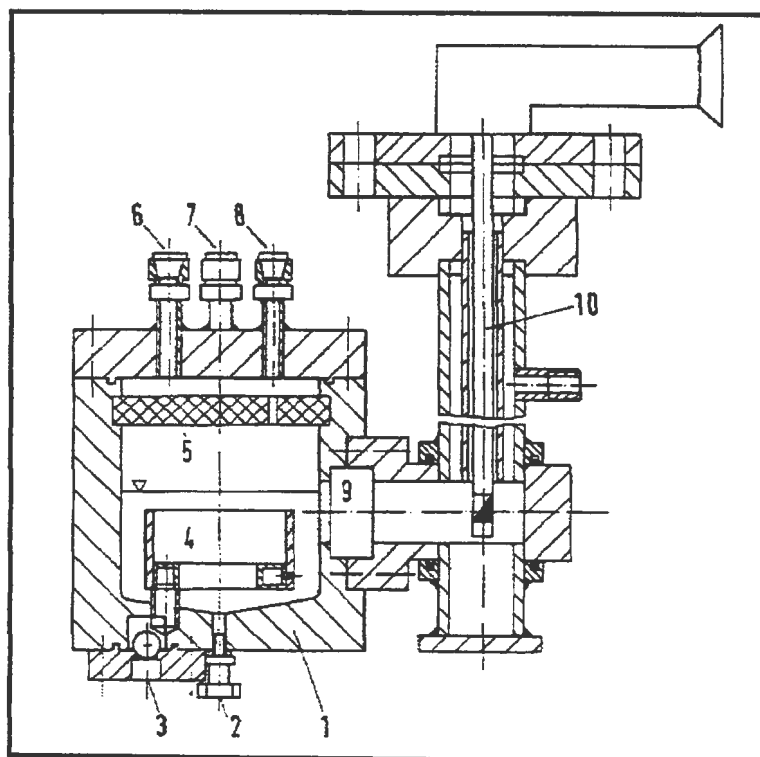


Figure 2-8. The high-pressure equilibrium cell of Weber et al. [1984]

1 - cell body; 2 - solvent inlet; 3 - gas inlet; 4 - distribution nozzle; 5 - mist separator; 6 - gas outlet; 7 - connection for temperature sensor; 8 - connection for capillary; 9 - high pressure glass window; 10 - inspection and illumination device.

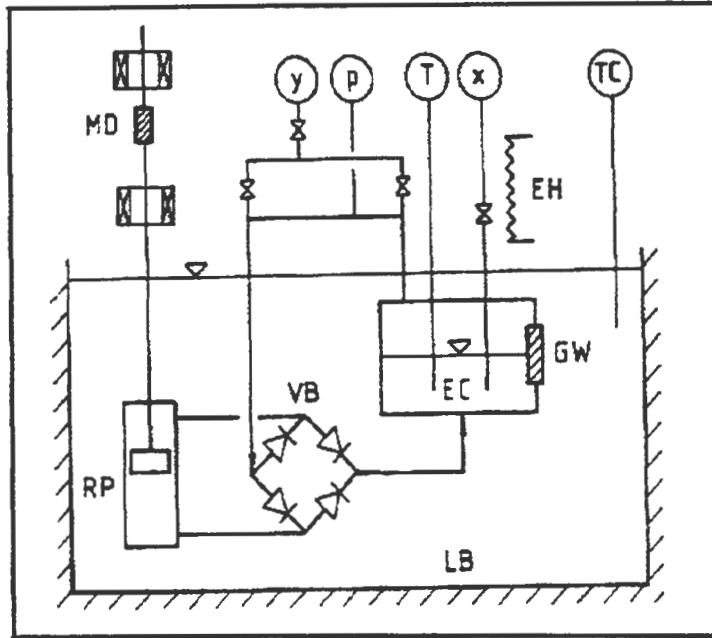


Figure 2-9: Schematic of the vapour-liquid equilibrium apparatus of Weber et al. [1984] with internal recycle

EC - equilibrium cell; TC - temperature control; RP - reciprocating pump; EH - electric heater; GW - glass window; LB - liquid bath; VB - valve box; MD - magnetic drive; P - pressure measurement; T - temperature measurement; Y - vapour sampling device; X - liquid sampling device.

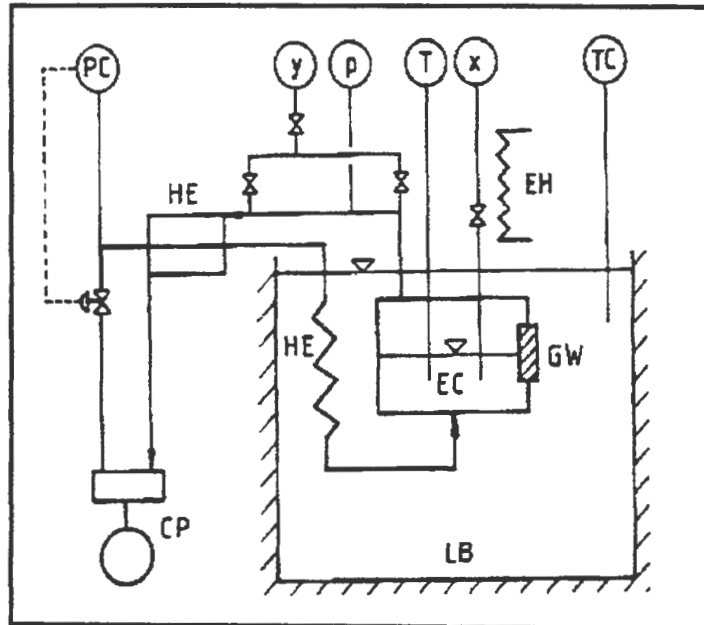


Figure 2-10: Schematic of the vapour-liquid equilibrium apparatus of Weber et al. [1984] with external recycle

HE - heat exchanger; PC - pressure control; CP - compressor (remaining symbols as in Figure 2-9 above)

Temperature was measured by Pt-100 Ω electrical resistance sensors and pressure by a precision Bourdon-tube pressure gauge.

Because the liquid sample will flash as soon as the temperature increases or the pressure decreases, it is difficult to transfer a representative sample into the GC. To overcome this problem, the liquid sample is withdrawn through a capillary tube (the tubing and the sample valve are heated electrically to ensure complete vapourization of the sample). The vapour sample was collected in a two-litre stainless steel vessel that was evacuated. The maximum pressure in the vessel was kept below the dew point at ambient temperature.

Chou et al. [1990]

The apparatus consists of two main sections:-

- i) one for achieving phase equilibria, and
- ii) another for analysing fluid samples.

The equilibrium cell which is approximately 100 cm³ in volume is connected to two sampling ports; one for the vapour phase and the other for the liquid phase. Each sampling port contains a specially designed sampling valve which Chou et al. [1990] refer to as a microcell.

Each microcell has a sample cavity of approximately 30 μ l. During sampling, it collects an equilibrium-phase sample at conditions of the equilibrium cell; thereafter it is taken from the apparatus to the sample analysis system for composition analysis. Figure 2-11 shows a cross-sectional view of the microcell.

The sample analysis system consists primarily of a temperature-controlled microcell oven and a GC. The microcell oven contains a microcell housing, a flash vessel, a recirculation system, and a GC sampling valve connected to a sample loop.

The microcell containing a fluid sample is inserted into the microcell housing from which the high-pressure sample is vapourized into the flash vessel. The flash vessel is a variable-volume bellows assembly that also acts as a pump to recirculate the flashed sample through the sampling valve so that the fluid inside the sample loop is homogeneous. The sample is injected into the GC by purging carrier gas (Helium) through the loop. In the present project homogenisation of the sample is achieved with the use of a jet-mixer.

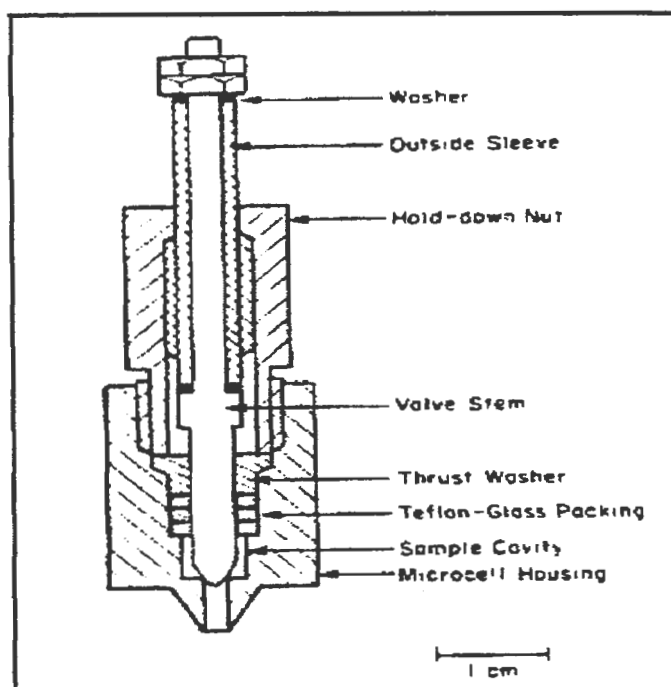


Figure 2-11: Cross-sectional view of microcell of Chou et al. [1990]

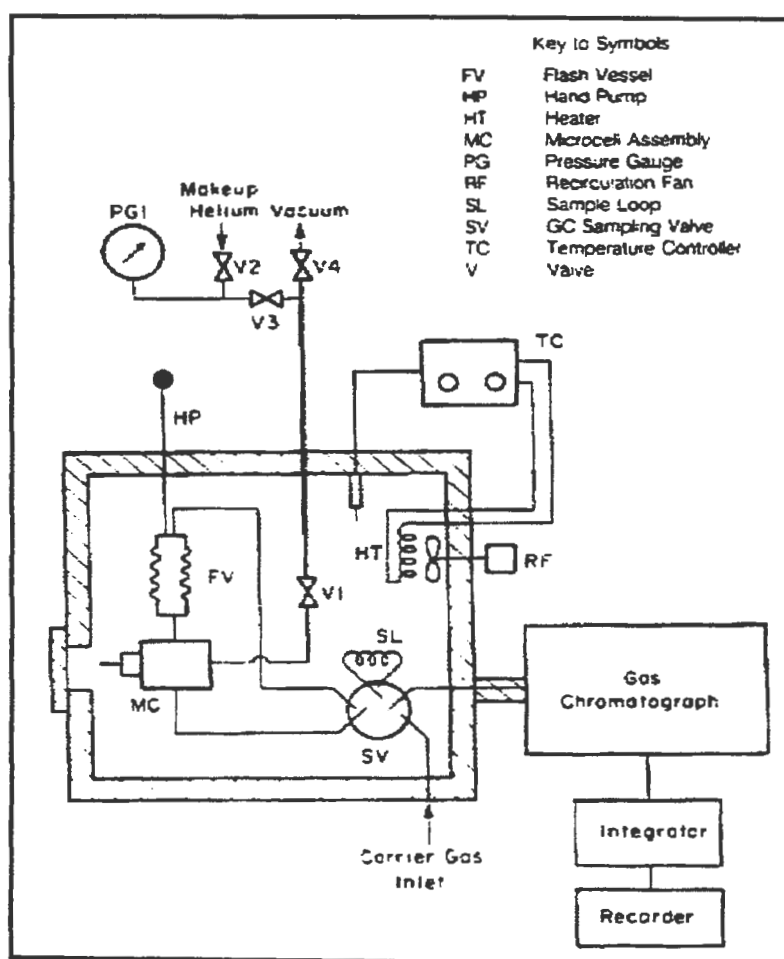


Figure 2-12: Schematic diagram of the sample-analysis system of Chou et al. [1990]

Figure 2-12 illustrates the sample analysis set-up of Chou et al. [1990]. Their set-up is analogous to the one in this project, except that this project makes use of a GC valve and a jet mixer to sample and homogenise respectively.

Table 2-3 lists the vapour phase experimental apparatus surveyed in this project. Greater detail on apparatus and systems measured is available in Appendix A.2.

2.4.2.3. Selected examples from literature for the two phase recirculation method

Muirbrook and Prausnitz [1965]

The equilibrium apparatus consists of basically a heavy-walled, stainless steel equilibrium cell with circulating lines and pumps, all of which are enclosed in a constant temperature bath. Figure 2-13 shows a simplified flow diagram of the equilibrium cell. Vapour is pumped out of the top of the equilibrium cell and bubbles through the liquid. The liquid is pumped out of the equilibrium cell by pump P-1 and returned to the top of the cell.

The bottom of the cell and the top of the pressure head are each fitted with two Aminco tubing fittings which serve as entrance and exit points for the pumped fluids. A piece of tubing attached to the inlet on the pressure head directs the liquid flow against the inner wall of the cell. A baffle was attached to the thermowell to prevent liquid entrainment in the vapour stream. A level indicator was also attached to the thermowell. Figure 2-14 below illustrates the equilibrium cell.

The problems of sampling and agitation of the phases were both overcome with the means of circulation of the phases. Each phase was circulated through tubing external to the equilibrium cell, providing adequate agitation. Samples were obtained by locking off sections of the circulation lines. Sampling was rather complex, and the high-pressure liquid and vapour samples from the equilibrium system were moved to glassware which were at pressures less than atmospheric where both samples are gases.

One of the major design problems was that of a pump to circulate the vapour and liquid streams. The pumps were required to withstand internal pressures of up to 15000 psi without substantial leaks and pump at a rate of 10 to 100 cc/min, and produce a head of 1 ft of fluid. Muirbrook and Prausnitz [1965] solved the problem by design a pump that was a variation of a vane pump with

References	Cell volume (cm ³)	Operating Range		Equilibrium cell (1)	Measurement Device		Equilibration time (min)	Sample size (μl)	
		Temp (K)	Pressure (bar)		Temp (2)	Pressure (3)		Vapour	Liquid
Price and Kobayashi [1959]	V.V.	115-293	138	stainless steel	TC	B	30-60	-	-
Toyama et al. [1962]	V.V.	88-298	69	stainless steel	TC	B	-	-	-
Fredenslund and Sather [1970]	-	-	-	stainless steel	QT	B	-	-	-
Fredenslund et al. [1973]	15	93-298	350	304 stainless steel	PR	DWP	120-180	-	3.5
Katayama et al. [1975]	-	-	-	stainless steel	T	B	-	-	-
Streett and Calado [1978]	4.2	-	10000	stainless steel A-286	PR	PT	5-10	5000-10000	5000-10000
Somait and Kidnay [1978]	-	-	138	stainless steel	PR	B	-	-	-
Stead and Williams [1980]	34	>300	90	copper	PR	B	60	-	-
Tsang and Streett [1981]	10	313-523	2000	stainless steel	PR	PT	5-10	-	-
Chang et al. [1982]	75	-	-	stainless steel	PR	PT	5-10	-	-
Dorau et al. [1983]	168	70-300	200	austenitic steel	PR	B	-	-	-
Pozo and Streett [1984]	-	523	290	stainless steel	PR	PT	10-15	-	-

Table 2-3: Vapour phase recirculation apparatus surveyed

References	Cell volume (cm ³)	Operating Range		Equilibrium cell (1)	Measurement Device		Equilibration time (min)	Sample size (μl)	
		Temp (K)	Pressure (bar)		Temp (2)	Pressure (3)		Vapour	Liquid
Pozo and Streett [1984]	-	233-343	80	pyrex tubing	PR	PT	10-15	-	-
Weber et al. [1984]	230	223-300	3-180	chromium-nickel steel	PR	B	-	-	-
Freitag and Robinson [1986]	100	256-405	280	Hastealloy C-276	TC	B	30	-	50-200
Jou et al. [1987]	150	-	-	316 stainless steel	TC	B	-	-	-
Chou et al. [1990]	100	-	-	-	TC	B	60	30	30
Shah et al. [1990]	-	325-530	-	stainless steel	PR	PT	5-10	-	-
Shah et al. [1990]	-	>325	-	sapphire tube	PR	PT	5-10	-	-
Suzuki et al. [1991]	300	373	350	316 stainless steel	QT	PT	-	-	-

Table 2-3: (continued) Vapour phase recirculation apparatus surveyed

Key:

(1) Materials of construction

(2) TC - thermocouple; QT - quartz thermometer; PR - platinum resistance thermometer; T - thermometer

(3) B - Bourdon type pressure gauge; DWP - dead weight piston gauge; PT - pressure transducer

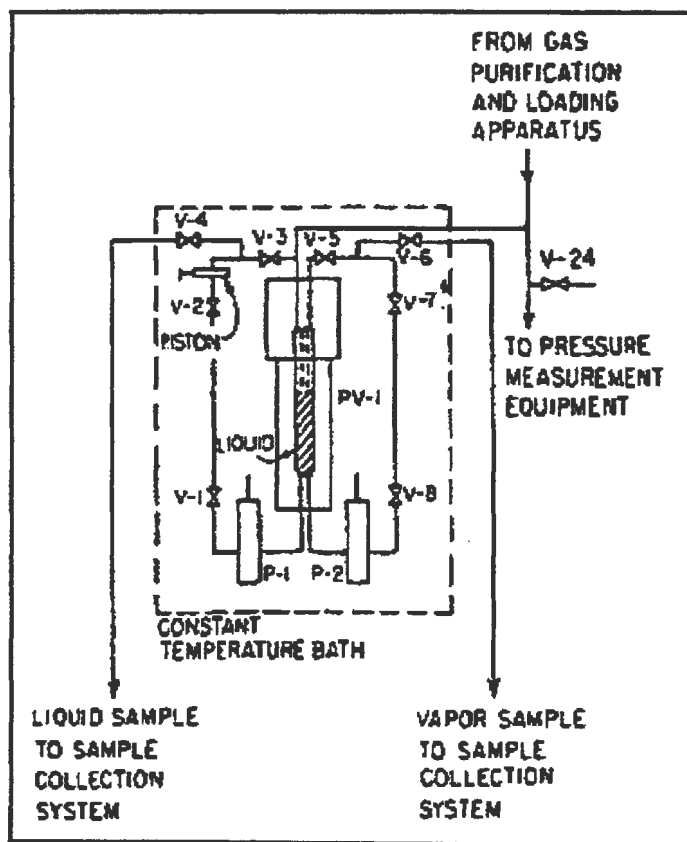


Figure 2-13: Flow diagram of equilibrium system of Muirbrook and Prausnitz [1965]

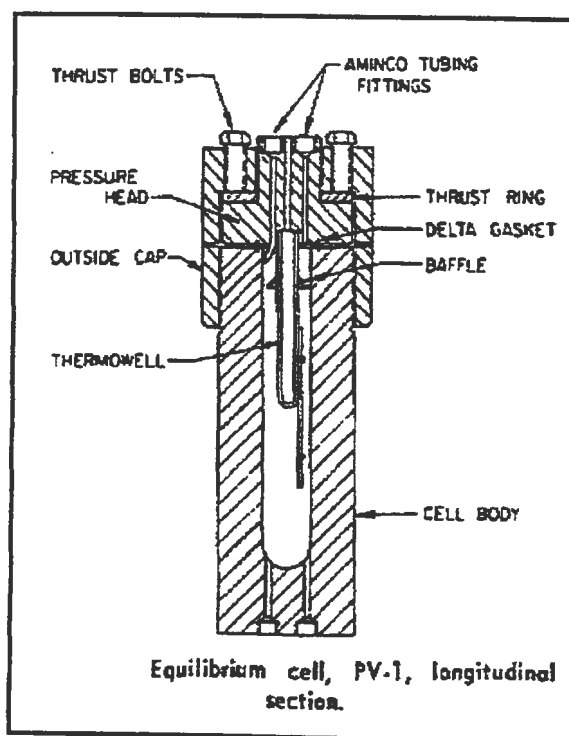


Figure 2-14: Longitudinal section through the equilibrium cell (extracted from Muirbrook and Prausnitz [1965])

cylindrical rollers acting as vanes moving the fluid from inlet to outlet. Figure 2-15 illustrates the sections through the high pressure pumps.

Temperature measurement in the equilibrium cell was via thermocouples, whilst pressure was measured with an Aminco pressure balance.

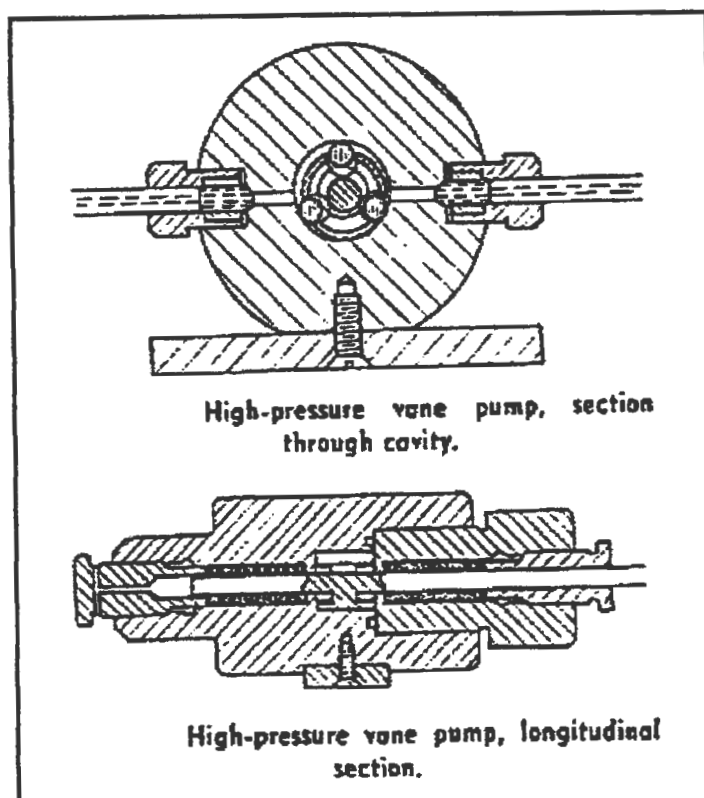


Figure 2-15: Sections through the vane pumps designed by Muirbrook and Prausnitz [1965]

Kubota et al. [1983]

The apparatus has an operating temperature range of 283 to 353 K and operates under pressures of up to 80 MPa. The authors name the following as the main features of the apparatus:-

- Minimal disturbance of the vapour of liquid phase during sampling because the apparatus is a circulating type for both phase.
- No dead volume in the sampling system because the samples are trapped in a 4-port ball valve.
- The change from the vapour-circulating path to the liquid-circulating path is facilitated by a 6-port ball valve.

The cell was constructed from 304 stainless steel and had an internal volume of approximately 106 cm^3 . In the middle of the cell, a pair of Pyrex glass windows, 21 mm in diameter and 20 mm thick, were placed to allow observation of mixing and circulation conditions of the cell contents and to observe the behaviour of the interface in the critical region. An agitator rotated by an external magnet was used to stir the contents of the cell. Figure 2-16 illustrates the equilibrium cell.

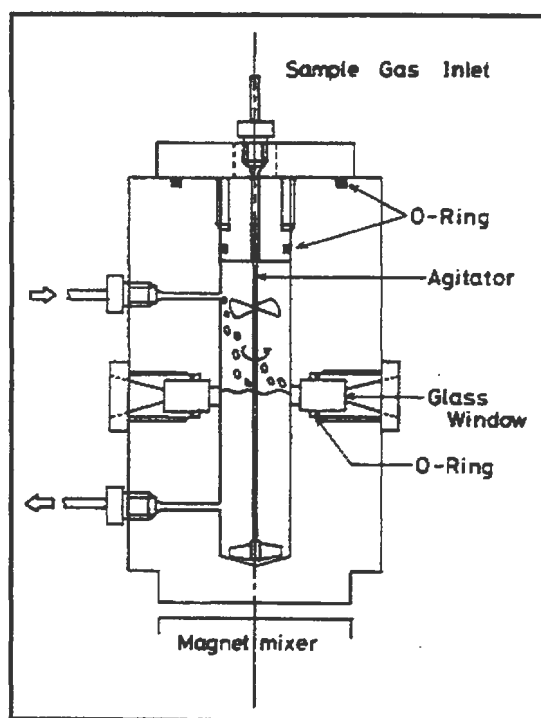


Figure 2-16: Equilibrium cell of Kubota et al. [1983]

Sampling of the phases was achieved using a four-port ball valve. The change from the vapour circulating path to the liquid circulating path was achieved using a six-port ball valve. Figure 2-17 shows the configuration of the valves on the experimental apparatus. The sample trapped in the four-port ball valve was introduced into the low-pressure analysis system.

The low-pressure analysis system consisted of a bellows type diaphragm pump. This pump circulated the equilibrium sample in the low-pressure analysis system to ensure uniform composition throughout the low-pressure line. Once homogenised the sample was injected into the GC.

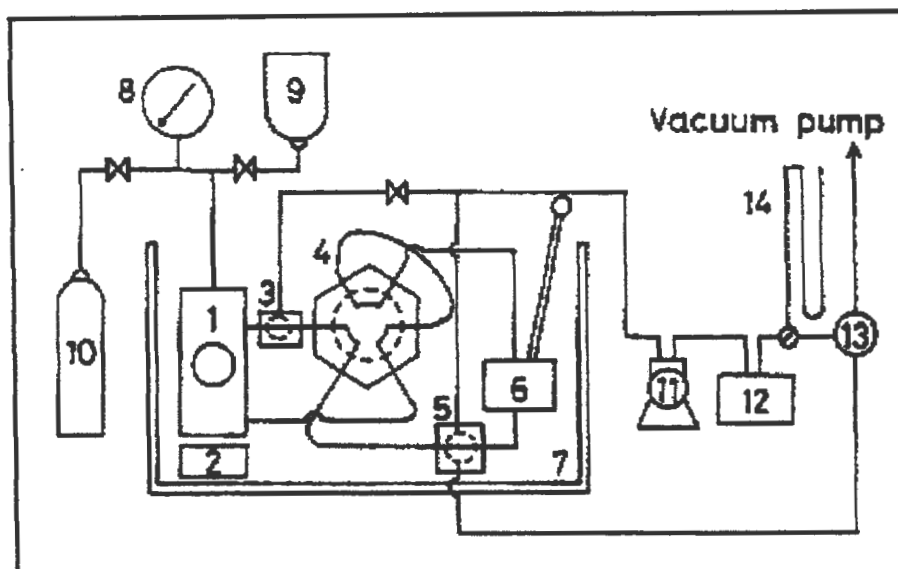


Figure 2-17: Illustration of the layout of the experimental apparatus of Kubota et al. [1983]
 1 - equilibrium cell; 2 - magnet mixer; 3 - 2-way (3-port) ball valve; 4 - 6-way (6-port) ball valve; 5 - 2-way (4-port) ball valve; 6 - high-pressure circulating pump; 7 - constant-temperature bath; 8 - Bourdon tube gauge; 9 - propylene cylinder; 10 - ethylene cylinder; 11 - low-pressure circulating pump; 12 - gas chromatograph; 13 - expansion vessel; 14 - mercury manometer.

Radosz [1984]

The experimental apparatus used by Radosz is capable of measuring two- (VLE, LLE) and three-phase (VLLE) equilibria. It also has variable-volume capability. The equilibrium cell (see Figure 2-18) has a window and has an operating temperature range of 280 to 530 K and an operating pressure up to 35 MPa. Mixing is achieved with the use of two circulation pumps. The variable-volume cylinder that forms part of the top phase recirculating loop is used to help maintain constant pressure during sampling. All parts of the apparatus which are in contact with any of the phases are housed in an air-bath.

Radosz [1984] states that the most serious difficulty with batch cells is the problem of avoiding pressure drop during sampling. To resolve the problem he added a variable-volume cylinder to the top-phase recirculating loop. Pressure was thus maintained constant with this cylinder by pressurising the piston with one of the feed components.

Evaporation and homogenisation of the withdrawn sample was accomplished in a 100 cm³ chamber. Radosz [1984] states that the key requirement to avoid condensation in the chamber, was to maintain a high temperature. This method is analogous to the sampling procedure in this project using jet-mixers.

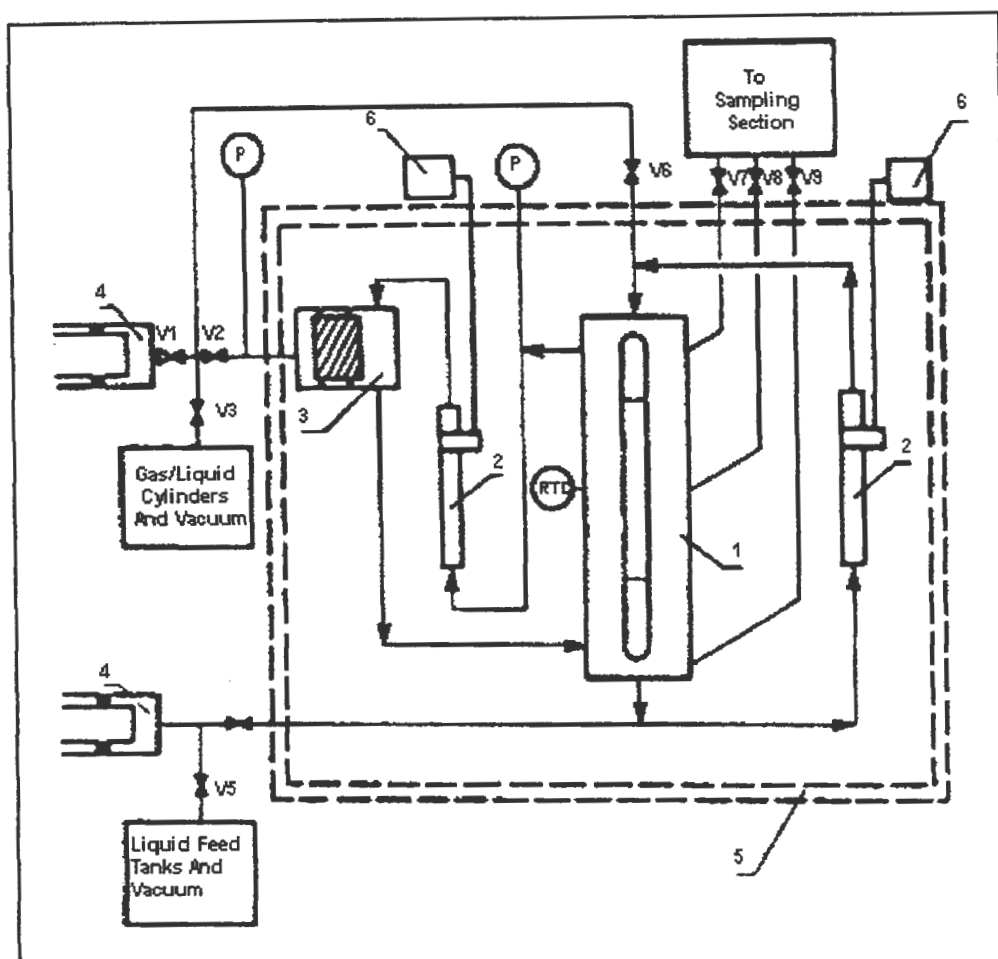


Figure 2-18: Mixing and separation section of apparatus of Radosz [1984]

1 – Windowed Mixing and Separation Vessel; 2 – Magnetic Recirculating Pumps; 3 – Variable-volume Cylinder; 4 – Positive Displacement Pump; 5 – Constant Temperature Air Bath; 6 – Motors for Magnetic Recirculating Pumps; P – Pressure Transducer; RTD – Platinum Resistance Thermometer; V – Valves.

Adams et al. [1988]

The apparatus was designed to perform P-V-T and X-Y phase equilibria studies in the temperature range from 200 to 400 K. Foreseeing the requirement that almost all supercritical fluid process design requires phase density information, Adams et al. [1988] incorporated volumetric measurement capabilities into their apparatus. For observation of phase behaviour over wide temperature and pressure ranges the equilibrium cell was constructed from sapphire.

The equilibrium cell (pressure vessel) consists of a 3.175 cm o.d., 1.27 cm i.d., by 10.16 cm long sapphire tube sealed against stainless steel end flanges by spring-loaded Teflon washers. Recirculation of the phases is achieved via magnetically actuated pumps. Adams et al. [1988] claim an equilibration time of 5 to 10 minutes.

Sampling of the phases is performed with a Rheodyne six-port sample injection valve. To obtain a sample the recirculated phase is pumped through the sample loop of the injection valve. From the injection valve the sample is flushed to the GC (See Figure 2-19 below).

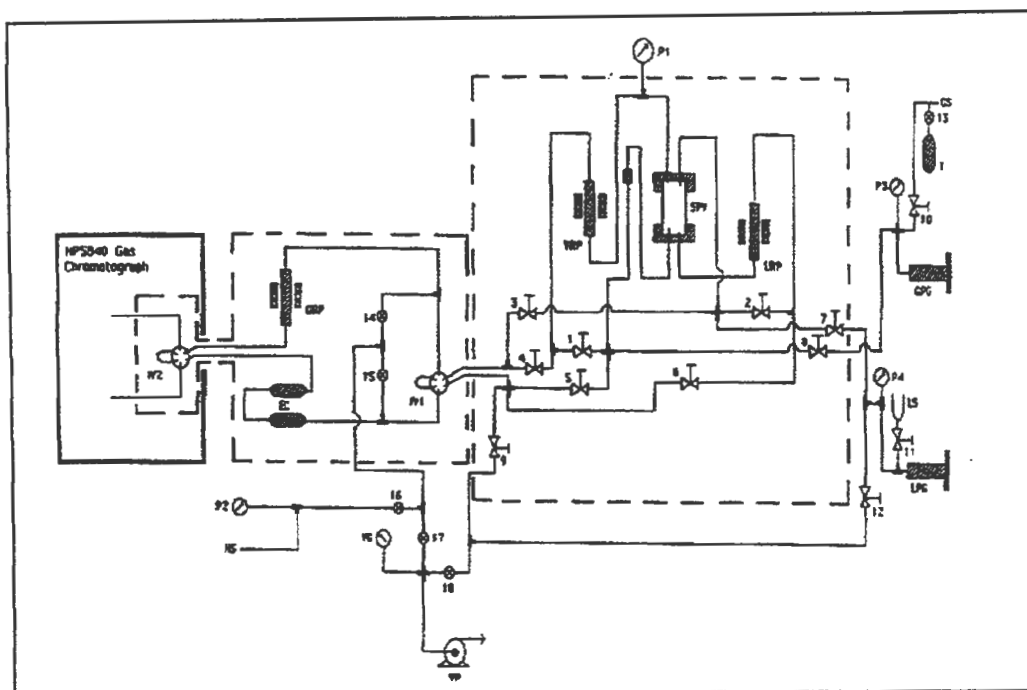


Figure 2-19: Apparatus of Adams et al. [1988]

EC – Expansion chambers; GPG – Gas pressure generators; GRP – Gas recirculation pump; GS – gas supply; HS – Helium supply; IV1 – Rheodyne 6-port injection valve; IV2 – Valco 6-port injection valve; LPG – Liquid pressure generator; LRP – Liquid recirculation pump; LS – Liquid supply; P(1-4) – Pressure gauges; SPV – Sapphire pressure vessel; T – Trap; VG – Vacuum gauge; VP – Vacuum pump; VRP – Vapour recirculation pump; 1-18 – Shut-off valves.

The temperature-controlled region in which the injection valve is housed also serves to dilute, vaporise, and homogenise all the sample material for subsequent injection into the GC. The carrier gas used was helium. Adams et al. [1988] state that to keep the dilution volume low and still vaporise all the mixture components, the temperature of the sampling section is increased to a level at which the ratio of the partial pressure to saturation pressure for all components is less than 0.1. They state that at this value the physical adsorption effects should be insignificant.

Sample homogenisation is promoted by gas recirculation using a pump. The pump continuously circulates the gas mixture of helium and sample components around the circulation loop. Two loops were used with the Rheodyne valve. A 0.018 cm^3 loop was used for liquid phase as well as

for near critical, highly dense vapour phase samples. For the vapour phase samples, which are less dense, a 0.455 cm^3 loop was used.

2.4.2.4. Difficulties associated with the phase recirculation methods

The following are some of the difficulties encountered in the phase recirculation methods:-

- maintaining an adequate level in the equilibrium cell. This is normally effected by the use of a liquid-level measuring device (cathetometer); by visual observation; or by optical observation e.g. Hsu et al. [1985].
- ensuring that there is no droplet entrainment in the effluent vapour stream. Muirbrook and Prausnitz [1965] made use of a demisting device.
- ensuring that the pumps used do not contaminate the equilibrium mixture or create stagnant spaces. The former problem has largely been overcome by the use of magnetically coupled pumps.
- avoiding the possibility of partial condensation and vapourisation of the recirculated vapour and liquid streams respectively.
- avoiding undesirable pressure gradients across the equilibrium cell, that can be brought about by circulating pumps. This is a weakness, in principle, of the circulation method since flow cannot be produced without a pressure gradient. However, in practice data from circulation methods compare well with those from the static type cells. In the present project, the liquid stirrer itself provides a small recirculating flow through a sampling valve mounted on the outside of the cell wall.

Table 2-4 lists the two-phase recirculation apparatus surveyed. Greater detail on apparatus design and systems investigated is available in Appendix A.2.

References	Cell volume (cm ³)	Operating Range		Equilibrium cell (1)	Measurement Device		Equilibration time (min)	Sample size (µl)	
		Temp (K)	Pressure (bar)		Temp (2)	Pressure (3)		Vapour	Liquid
Griswold et al. [1943]	600	273-553	207	steel	TC	B	300	30000	60000
Muirbrook and Prausnitz [1965]	200	233-303	1034	403 stainless steel	TC	B	-	-	-
Behrens and Sandler [1983]	1000	283-373	-	316 stainless steel	PR	PT	240-360	2000	2000
Kubota et al. [1983]	106	283-353	800	304 stainless steel	T	B	120	-	-
Radosz [1984]	60	283-533	350	-	PR	PT	15	100	100
Morris and Donohue [1985]	100	311 588	147 109	316 stainless steel	TC	PT	10-15	20/250	0.5
Hsu et al. [1985]	-	422	690	stainless steel	PR	PT	120-360	-	-
Takishima et. al. [1986]	700	-	-	-	QT	B	-	-	-
Adams et al. [1988]	-	513	346	sapphire	PR	PT	5-10	455	18
D'Souza et al. [1988]	100	-	-	stainless steel	PR	B	60	300/1000	300/1000
Kneisl et al. [1988]	-	310-425	60-345	stainless steel	PR	PT	90	1	1
Inomata et al. [1988]	750	-	-	316 stainless steel	TC	PT	-	-	-

Table 2-4: Two-phase recirculation apparatus surveyed

References	Cell volume (cm ³)	Operating Range		Equilibrium cell (1)	Measurement Device		Equilibration time (min)	Sample size (μl)	
		Temp (K)	Pressure (bar)		Temp (2)	Pressure (3)		Vapour	Liquid
Shibata and Sandler [1989(a)]	100	422	345	-	TC	PT	60	-	-
Kim et al. [1989]	150	293-430	250	316 stainless steel	TC	PT	10	100	1
Jennings and Teja [1989]	40	-	-	stainless steel	TS	B	-	1	0.2
Suzuki et al. [1990]	500	453	250	-	PR	B	480	1000- 10000	750
Wisniewska et al. [1993]	50	-	30	stainless steel	PR	B	-	300	300

Table 2-4: (continued) Two-phase recirculation apparatus surveyed

Key:

(1) Materials of construction

(2) TC - thermocouple; PR - platinum resistance thermometer; T - thermometer; QT - quartz thermometer; TS - thermistor

(3) B - Bourdon type pressure gauge; PT - pressure transducer;

2.4.3. The single vapour and liquid pass method

This is a relatively recent development in the dynamic method. This method was specifically developed for HPVLE measurements where thermal degradation of the components of interest could occur e.g. specific hydrocarbons.

2.4.3.1. Description of the single vapour and liquid pass method

Features of the single vapour and liquid pass method are illustrated in Figure 2-20.

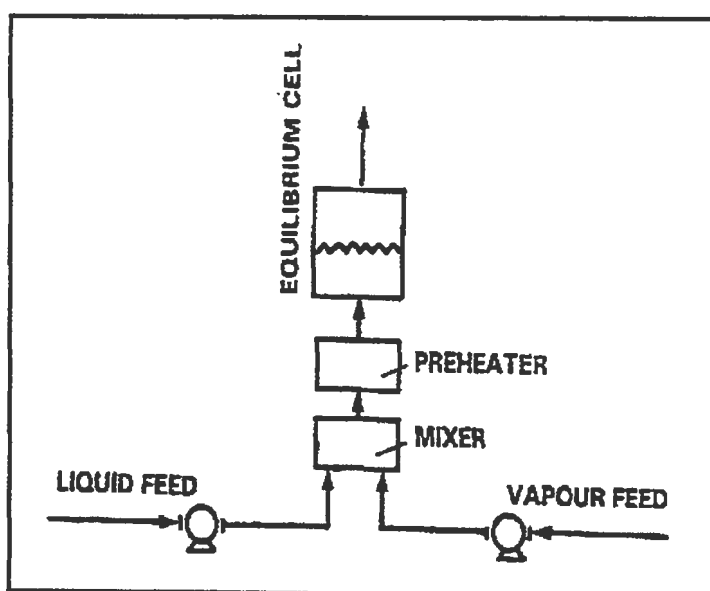


Figure 2-20: Schematic illustrating the single vapour and liquid pass method (extracted from Raal and Muhlbauer [1994])

The vapour and liquid components are contacted co-currently at a controlled temperature and pressure in a mixing unit. The combined streams are then passed into the equilibrium cell where the mixture separates into the vapour and liquid phases. The phases exit from the equilibrium cell separately and sampling is achieved by diversion of the effluent streams.

2.4.3.2. Selected examples from literature of the single vapour and liquid pass method

Lin et al. [1985]

The apparatus was developed to withstand pressures and temperatures up to 25 MPa and 710 K respectively. The main feature of the equilibrium cell is the transparent sapphire window sealed with gold “o”-rings for visual observation of the liquid level.

The equilibrium cell was approximately 10 cm³ in volume and was a horizontal cylindrical opening as illustrated in Figure 2-21. The transparent sapphire windows (2.54 cm in diameter and 1.27 cm thick) enclosed the open space at both ends to make visual observation of the liquid level possible. The sapphire windows were secured to the cell body with stainless steel flanges and bolts. Stacks of Belleville spring washers were installed between the bolt head and flange to compensate for thermal expansion effects.

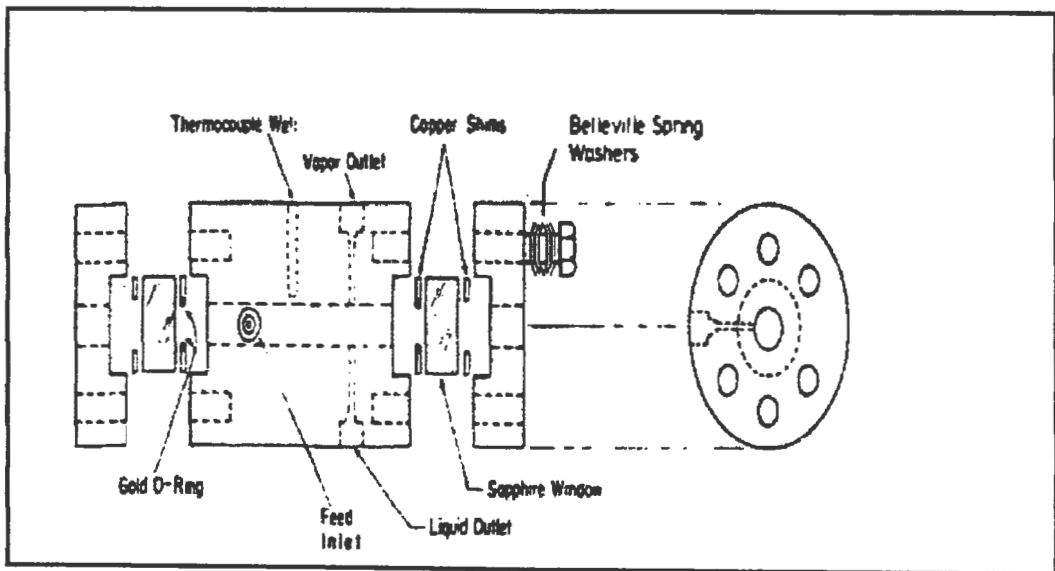


Figure 2-21: Equilibrium cell of Lin et al. [1985]

The major difficulty in the apparatus design, was the sealing of the transparent sapphire windows. Lin et al. [1985] state that no organic elastomer can be used for sealing at the high temperatures, therefore they used a gold “o”-ring backed by a copper shim. The gold “o”-ring was made from 20 B&S gauge gold wire, which was flattened and fused with pressure and temperature while in service.

Chen et al. [1994]

The apparatus of Chen et al. [1994], constructed of Nimonic, was designed for pressures up to 700 bar and temperatures up to 700 K. The cell contents could be viewed through a transparent sapphire window. Figure 2-22 illustrates the housing and ring that hold the sapphire windows in place. The housing is amazingly similar to the design in this project.

The sapphire windows (3" in diameter and 1" thick) are held in a housing that is clamped in a cavity at the end of the bar stock by a massive collar. The windows are pressed into the housing by a ring acting through a spring gasket. Sealing of the fluid pressure is achieved with a hollow gold plated "o"-ring that seals the contact between the housing and the body of the cell. The gasket seals the contact between the sapphire window and the housing. It is made of copper with two gold "o"-rings on the outer edge to resist any corrosive action of the cell fluid.

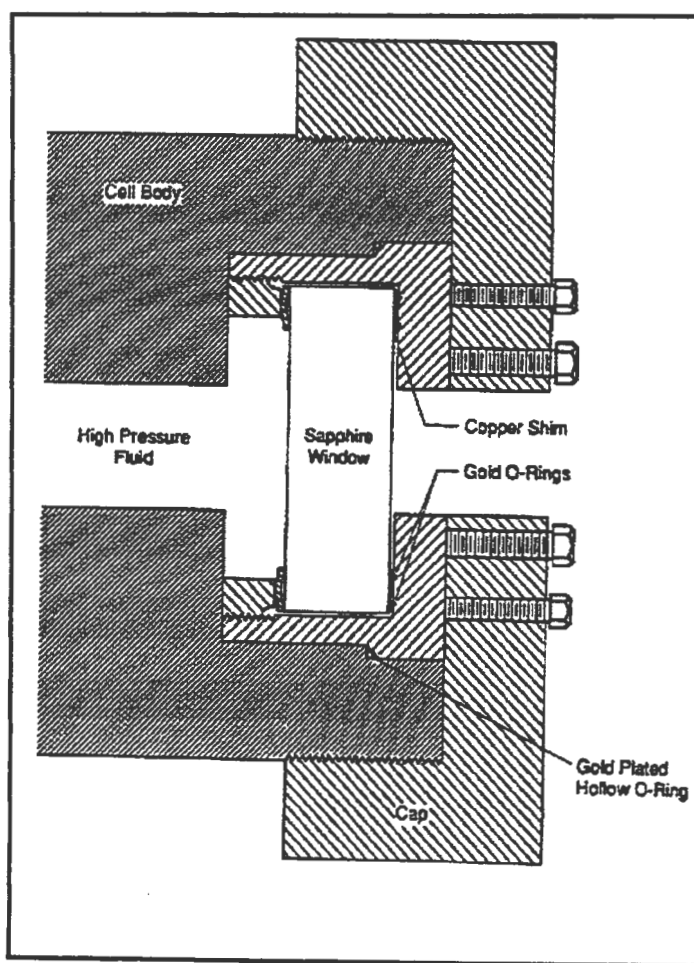


Figure 2-22: Sapphire window housing of Chen et al. [1994]

Sealing pressure at the contact of the sapphire and its housing is derived mainly from the cell pressure. Since sapphire is a brittle mineral, it is essential not to have it subjected to excessive pressure such as that due to turning bolts of flanges, thus the use of a housing. Figure 2-23 shows in greater detail the housing and ring to hold the sapphire window.

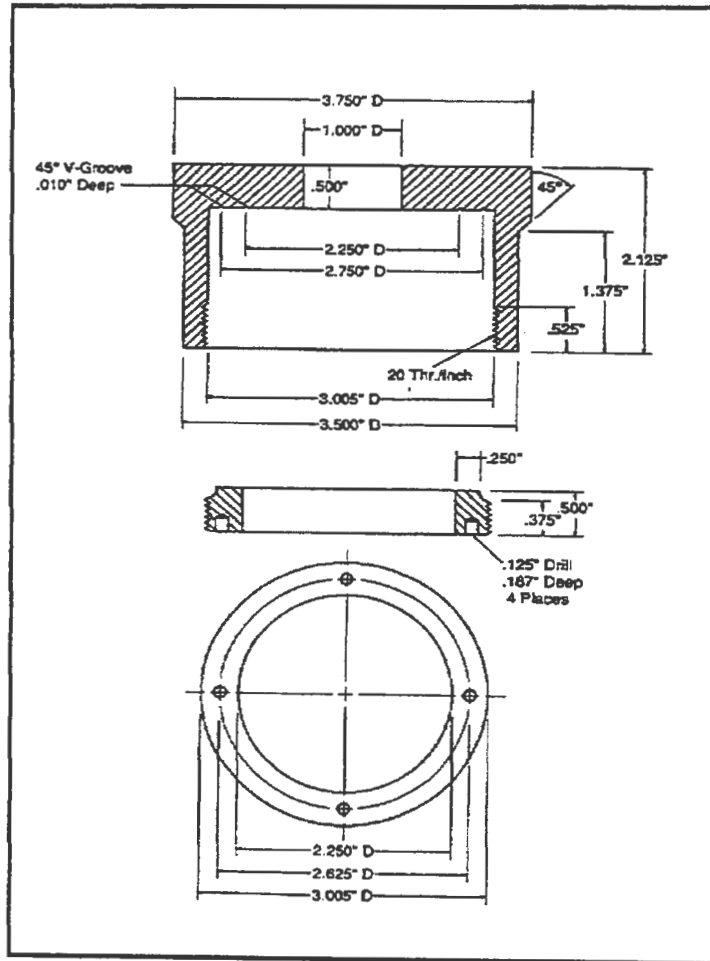


Figure 2-23: Machine drawing of the sapphire window housing (extracted from Chen et. al. [1994])

There are regions of stagnant volume in the equilibrium cell. Referring to Figure 2-22, one can immediately observe a stagnant region between the cell body and the sapphire window. This will certainly translate into the “equilibrium condition” samples analysed by Chen et al. [1994] not being a true equilibrium sample of the equilibrium cell contents.

2.4.3.3. Difficulties associated with the single vapour and liquid pass method

The following are some of the problems encountered in the single vapour and liquid pass method:-

- ensuring that equilibrium has been reached in one pass.
- ensuring complete separation in the equilibrium cell.
- achieving a steady level in the equilibrium cell.
- ensuring no droplet entrainment in the effluent stream.
- ensuring that the pumps do not contaminate the equilibrium mixture.
- minimising the effect of undesirable pressure gradients across the equilibrium cell.
- material selection problems, due to the high temperature and pressure requirements.
- large chemical usage.

Table 2-5 lists the single liquid and vapour pass apparatus surveyed. Greater detail on apparatus design and systems investigated is available in Appendix A.2.

References	Cell volume (cm ³)	Operating Range		Equilibrium cell (1)	Measurement Device		Equilibration time (min)	Sample size (μl)	
		Temp (K)	Pressure (bar)		Temp (2)	Pressure (3)		Vapour	Liquid
Simnick et al. [1977]	90	703	-	316 stainless steel	TC	B	-	-	-
Thies and Paulaitis [1984]	60	723	345	316 stainless steel	PR	B	-	-	-
Lin et al. [1985]	10	710	250	316 stainless steel	TC	B	-	-	-
Niesen et al. [1986]	-	625	100	316 stainless steel	PR	PT/B	-	-	-
Inomata et al. [1986]	30	710	250	316 stainless steel	TC	B	-	-	-
Jennings et al. [1991]	-	-	-	stainless steel	TS	B	20-30	-	-
Chen et al. [1994]	100	700	700	Nimonic	TC	B	-	-	-

Table 2-5: Single liquid and vapour pass apparatus surveyed

Key:

(1) Materials of construction

(2) TC - thermocouple; PR - platinum resistance thermometer; TS - thermistor

(3) B - Bourdon type pressure gauge; PT - pressure transducer

2.5. STATIC METHODS

The apparatus used in the present study is a modified static cell apparatus with dynamic flow sampling, and it is appropriate to review here similar equipment used by other researchers.

The static method can be divided into three sub-divisions, namely:-

- static analytical method,
- static non-analytical method, and
- static combined method.

2.5.1. The Static Analytical Method

2.5.1.1. Description of the static analytical method

Figure 2-24 below illustrates the features of a typical static analytical apparatus.

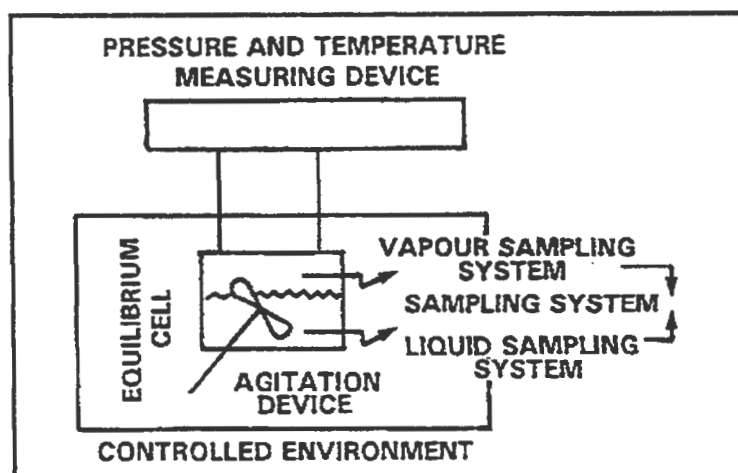


Figure 2-24: Schematic illustrating the typical feature of the static analytical method
(extracted from Raal and Muhlbauer [1994])

The components that are being studied are charged into the equilibrium cell. The liquid component is introduced into the equilibrium cell by flushing with the more volatile component or by a pump. The more volatile component is usually supplied directly from its storage cylinder,

whilst high boiling more volatile components such as propane and butane may have to be heated and pumped into the equilibrium cell by a compressor type device [Muhlbauer, 1990]. Agitation of the cell contents is then begun so as to facilitate contact between the phases and hence decreases the time take to reach equilibrium. Once equilibrium has been reached the temperature and pressure are recorded and liquid or vapour or both samples are withdrawn from the equilibrium cell and their compositions analysed. To generate the desired VLE equilibrium phase diagram, the temperature or pressure of the mixture is regulated.

2.5.1.2. Selected examples from literature of the static analytical method

Rogers and Prausnitz [1970]

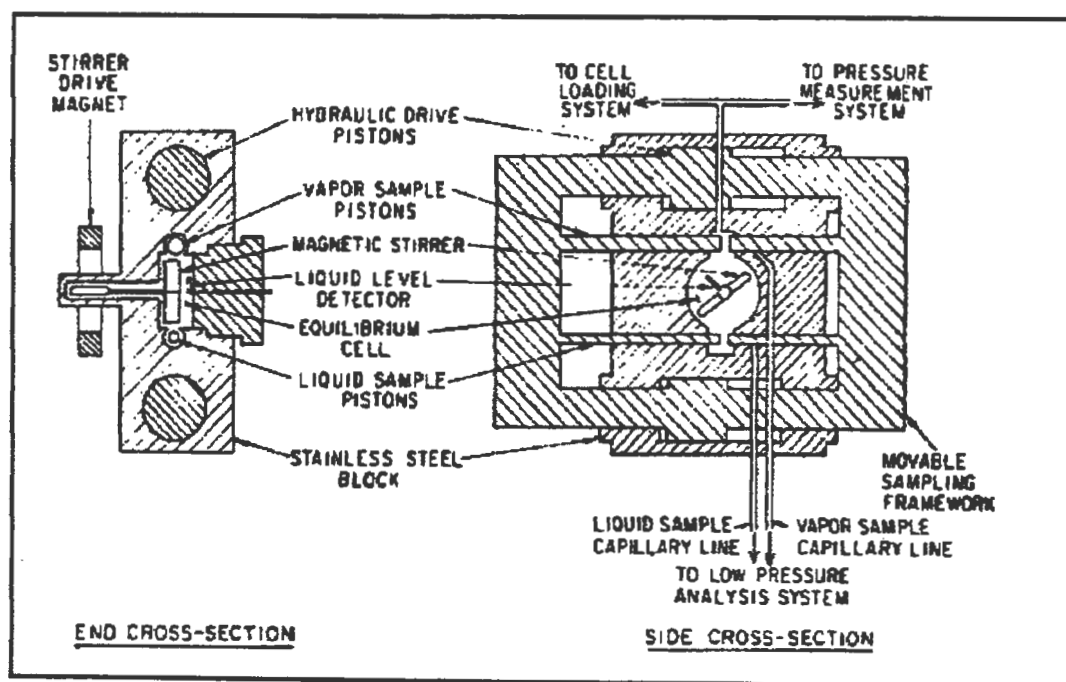


Figure 2-25: Schematic of the Equilibrium cell and sampling system of Rogers and Prausnitz [1970]

The sampling system of Rogers and Prausnitz [1970] transfers samples from the equilibrium cell to the low-pressure analysis system via two sets of moveable pistons. Movement of the sampling piston is achieved with a hydraulic drive. Each set of pistons (one for liquid sampling and the other for vapour sampling) contains two pistons, between which is a small variable-volume.

During sampling, this volume is extruded from the cell into a cylinder and moves down the cylinder until the sample ports are reached; the sample then expands through capillary tubing into the low-pressure zone. This technique has the primary advantage that the equilibrium cell pressure is not disturbed during withdrawal of the samples. A tight pressure seal around the moving piston is maintained by use of specially fabricated “o”-rings made of Rulon LD, a heavy-duty filled Teflon material. Figure 2-25 illustrates the equilibrium cell and the sampling system.

The contents of the cell are agitated with a magnetic stirrer. This method avoids the problem of pressure sealing a rotating shaft. The stirrer paddle was designed to stir both phases, to agitate the vapour-liquid interface without splashing liquid up into the region near the vapour-sampling pistons, and to dislodge any vapour bubbles near the vapour-sampling pistons.

Rogers and Prausnitz [1970] used a movable thermistor, whose response depends on whether it is in the vapour or the liquid phase to avoid withdrawal of a two-phase sample, and to aid in the loading of the equilibrium cell.

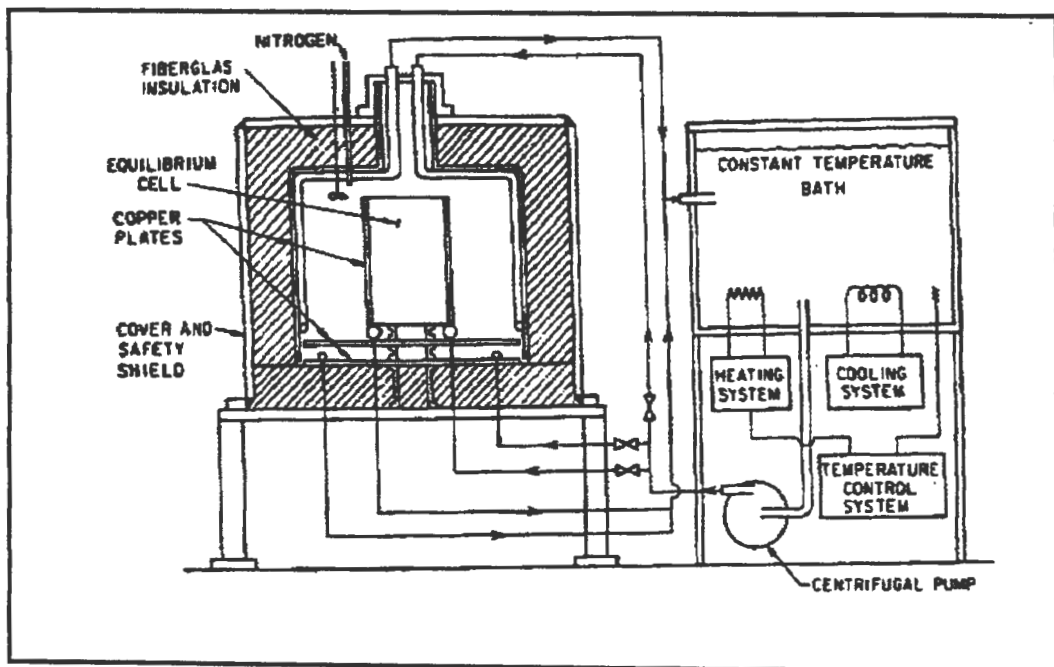


Figure 2-26: Thermostat system for the equilibrium cell of Rogers and Prausnitz [1970]

Temperature of the equilibrium cell is controlled by placing it in a thermostated enclosure, through which liquid from a temperature controlled bath is pumped. The enclosure also serves as

a thermal and safety shield. Temperature stability of the enclosure is promoted by having the inside constructed of copper plates. Fibreglass insulation was inserted between the steel exterior of the enclosure and the copper plates. Copper shielding and a layer of insulation was also used in the present project to ensure thermal stability in the air-bath.

Just as in the apparatus used in this project, nitrogen was continuously fed into the thermostated enclosure to avoid formation of an explosive mixture, should a leak develop in the equilibrium cell.

Besserer and Robinson [1971]

The apparatus is a rather complex double-piston equilibrium cell and was designed to permit the simultaneous measurement of the composition and the refractive index of the co-existing equilibrium phases.

Equilibrium between phases is achieved by mechanically spraying the entire liquid contents into the vapour phase and then allowing the phases to separate. Besserer and Robinson [1971] state that no more than 8 to 10 cycles are required to achieve equilibrium and the normal time was about 10 minutes.

The sampling system was such that samples could be removed from either phase and three or more analyses obtained from each sample. The sampling valves are internally mounted micro-metering valves with provision made for flushing out and evacuation of the low pressure sampling lines.

The equilibrium cell (Figure 2-27) was machined from a 316 stainless steel cylinder. It consists of three parts, two cylinder piston end sections and a central windowed section. The three sections are bolted together with the high-pressure seals between them, made by flattened Teflon "o"-rings. Each piston has a 10 cm travel and is confined to its respective cylinder. The piston seal is effected by four "o"-rings, one Teflon and three neoprene. The function of the pistons is to isolate the cell from the hydraulic fluid and to provide a means for varying the cell volume.

Besserer and Robinson [1971] do not explicitly state the purpose of the variable-volume capability of the equilibrium cell. The main purpose of the moveable pistons seems to be to facilitate the mixing of the equilibrium cell contents.

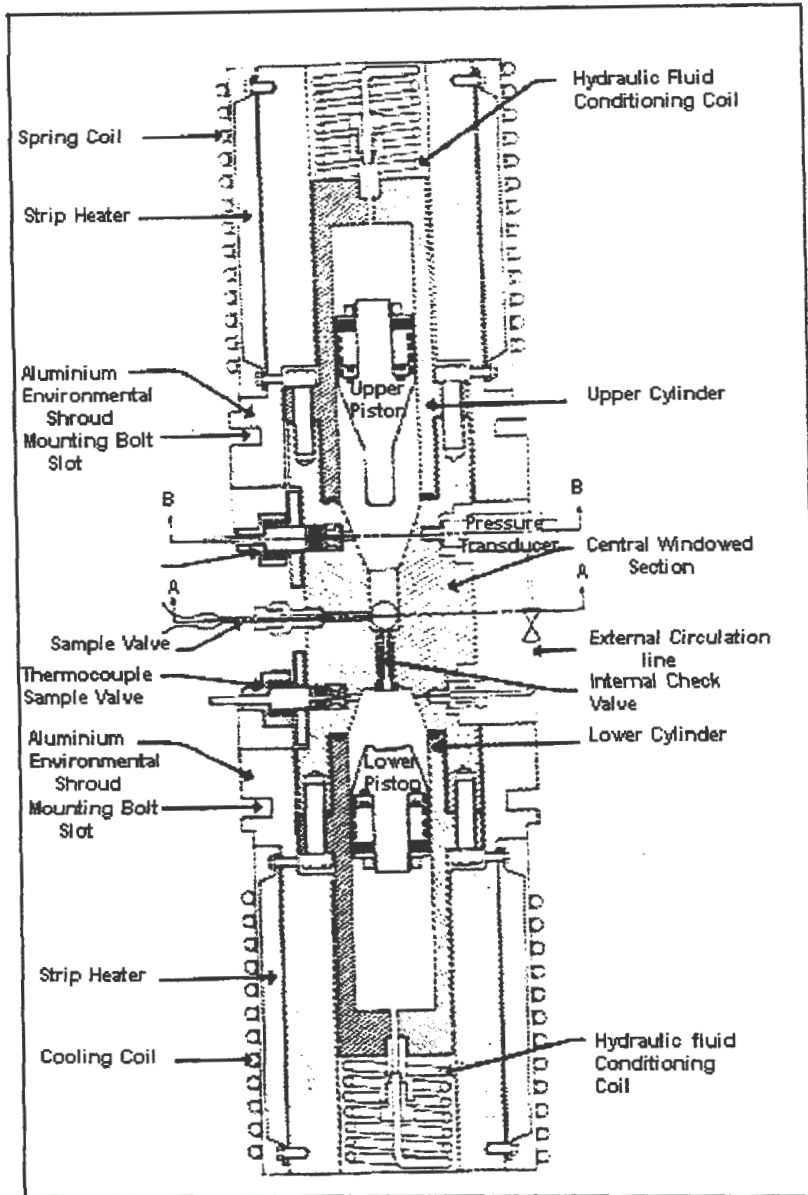


Figure 2-27: Equilibrium cell of Besserer and Robinson [1971]

Figuiere et al. [1980]

Figuiere et al. [1980] found existing sampling methods at their time to be not entirely satisfactory, and this led them to devise a new sampling method. The sampling procedure made use of micro-expansion which is obtained through rapid opening of small aperture valves. The amount of withdrawn sample is small enough (about $1 \mu\text{l}$) so as not to modify equilibrium conditions in a 50 cm^3 cell.

The sampling system is located at the bottom of the cell body. Two holes were drilled through the cell bottom. The lower one is used to sample the liquid phase, and the higher one samples the gas phase. These holes contain the stems of the two valves, the seats of which are machined in the

cell body material. The samples flow through slits machined along the valve stems and encounter the GC carrier gas. Sampling is achieved by rapid vertical percussions generated by a hammer activated by an electromagnet and transmitted to the valves by pushers.

In order to rapidly reach equilibrium inside the cell, efficient stirring is achieved by means of a magnetic stirrer rotating in an orientable magnetic field induced by four coils located outside the cell. The arrangement is analogous to the one used by us in this project to effect stirring in the second liquid phase (if it exists).

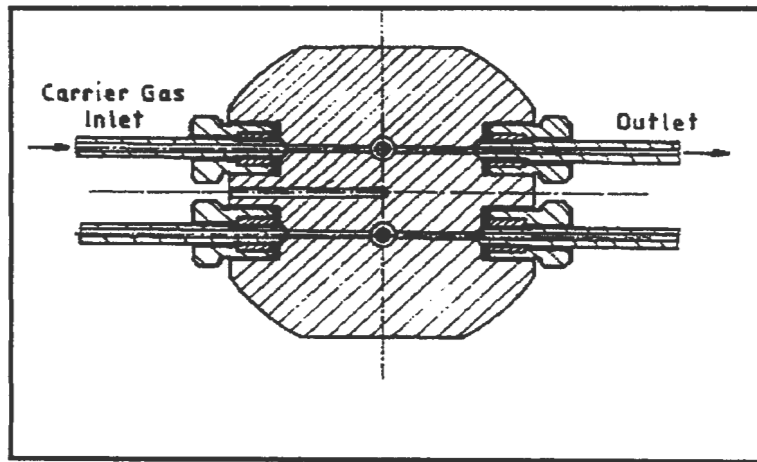


Figure 2-28: Schematic of the carrier gas circulation through the cell to carry off the samples [Figuiere et al., 1980]

The sampling method of Figuiere et al. [1980] is very reliant on the opening time of the valves. They state that the valve opening had to be calibrated by supplying different powers to the electromagnets that actuate the valve openings and closings. This sampling method seems to be cumbersome and not very reliable. The reproducibility of sample volumes, which will be dependent on physical properties and pressures, is not mentioned.

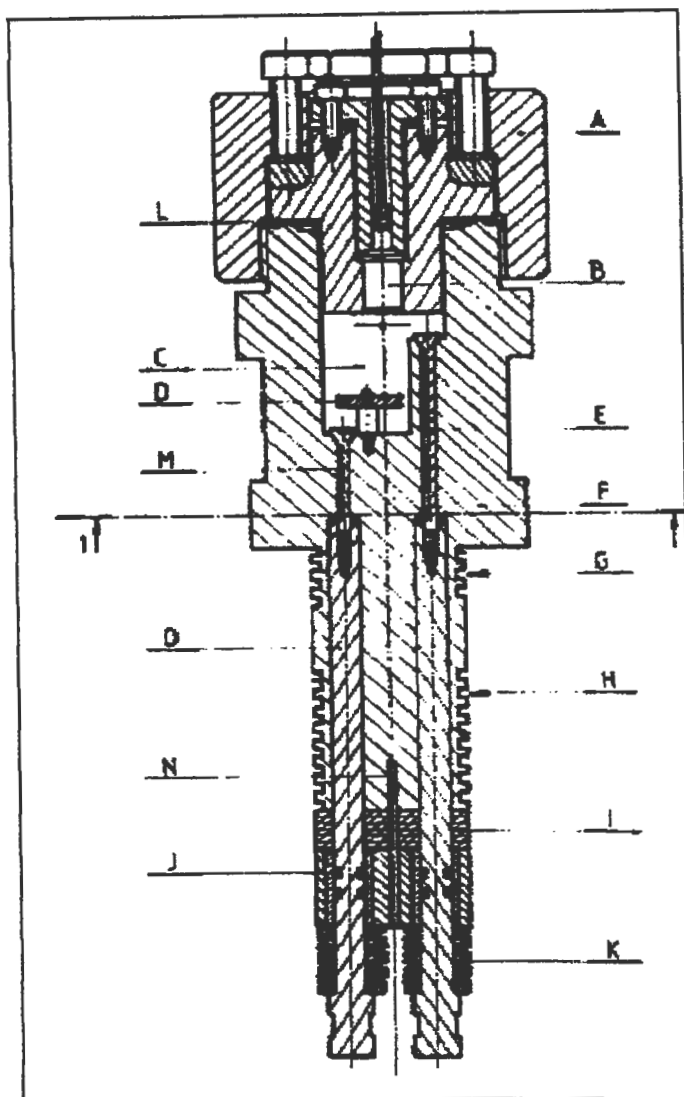


Figure 2-29: Equilibrium cell assembly of Figuiere et al. [1980]

A – cell cap; B – pressure transducer; C – equilibrium compartment; D – magnetic stirrer; E – valve; G – heating resistance place; H – cooling coil place; I – teflon thermal shield; J – viton O-ring; K – spring washers; L – copper gasket; M – channel; N – thermocouple well; O – valve pusher.

Legret et al. [1981]

Legret et al. [1981] made use of a sampling microcell for sampling of the equilibrium phases. These microcells could be detached from the equilibrium cell after filling and transferred to a specially designed chromatographic injection port. The sampling microcells were designed to trap a sample of volume 15 μl . Figure 2-30 illustrates the sampling microcell.

Legret et al. [1981] state that their sampling method is simple and fast, because no displacement fluid like mercury or circulation pumps is required. The expansion of the fluid into the valve is very small in amplitude; it represents 5×10^{-4} in relative value of the volume and it results in no

observable effect on the sample reproducibility, because the dead volume between the equilibrium cell and the sampling microcell is only approximately 4 μl .

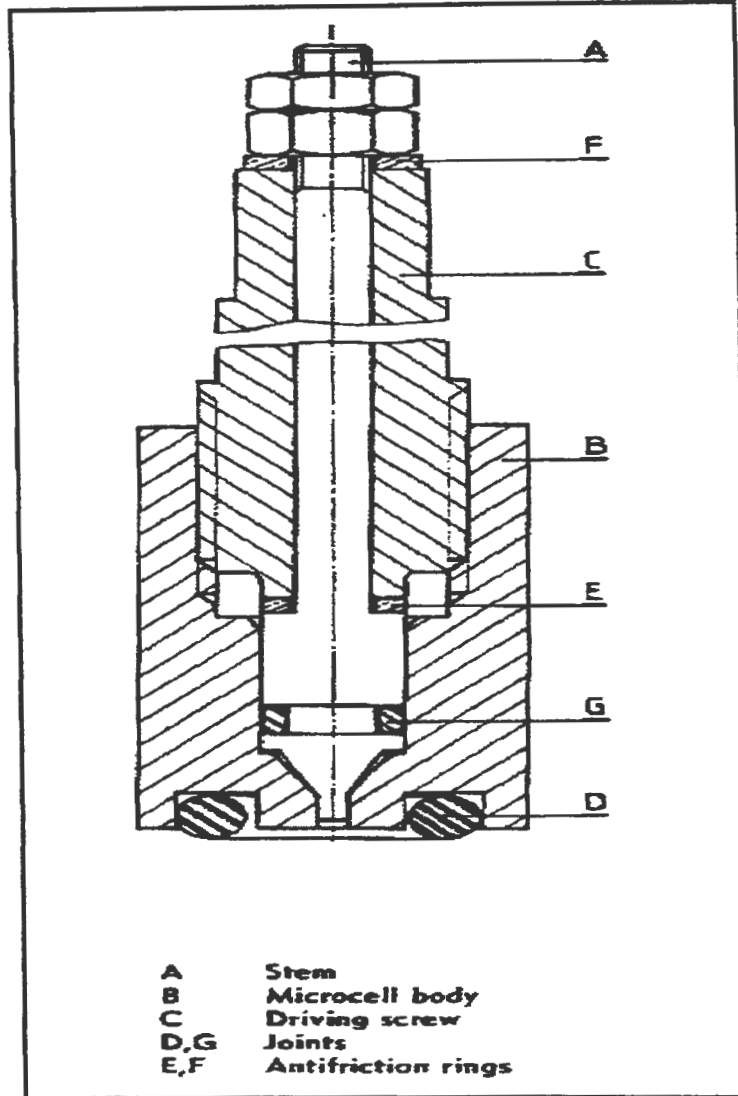


Figure 2-30: Sampling microcell of Legret et al. [1981]

Konrad et al. [1983]

The optical equilibrium cell was constructed from stainless steel Nimonic 90 and was designed for pressures up to 200 MPa and temperatures between 300 and 450 K. The equilibrium cell had two pairs of synthetic sapphire windows (12 mm diameter and 9 mm long). The windows were mounted at the bottom and the half heights of the cell on supporting steel cones with Poulter type seals. Sealing between the steel window plugs and the windows was accomplished with Teflon foil.

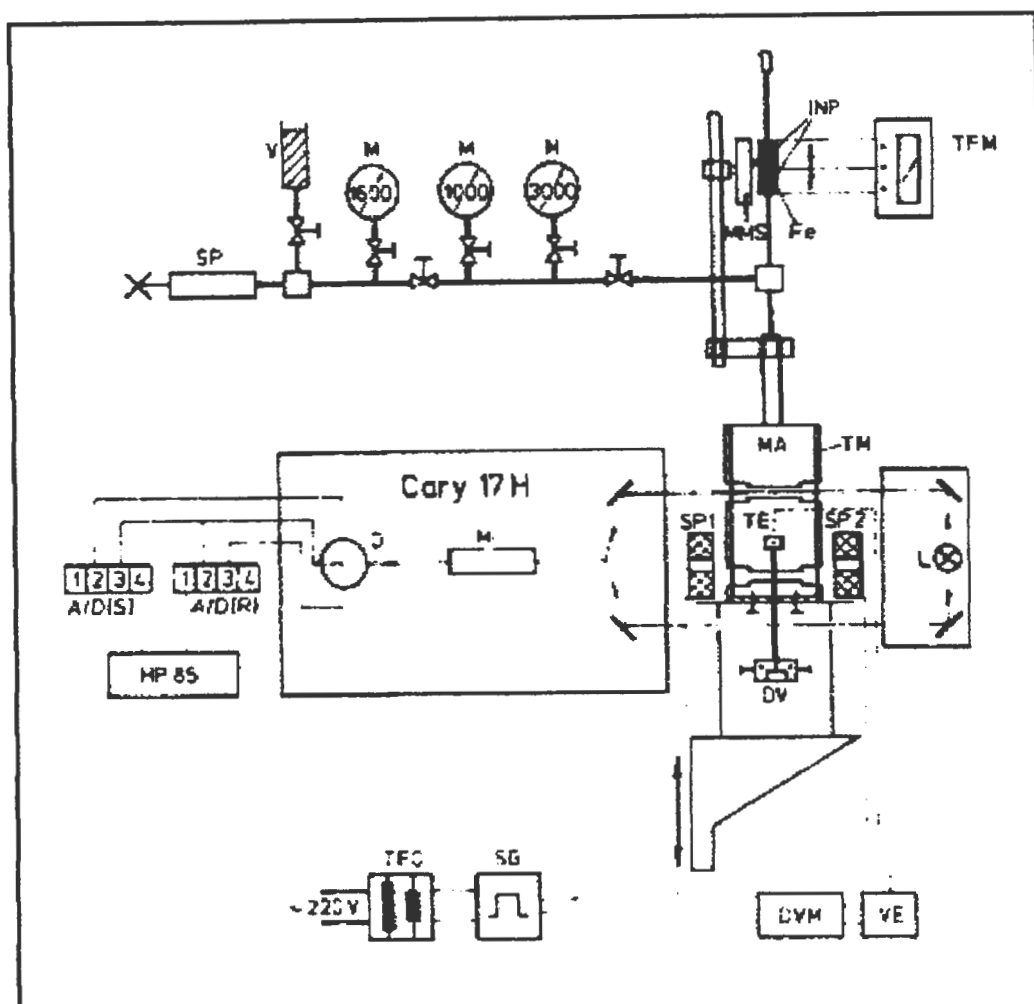


Figure 2-31: Schematic of the apparatus of Konrad et al. [1983]

A/D (S) - analogue-digital convertor for sample signal; A/D (R) - analogue-digital convertor for reference signal; Cary 17H - spectrophotometer; D - detector; DV - inlet valve; DVM - digital voltmeter; Fe - ferrite tip; HP85 - microcomputer; INP - thermostatically controlled solenoid for volume measurement; L - lamp; M - pressure gauges; MA - high pressure cell; MMS - micrometer screw; Mo - monochromator; SG - signal generator; SP - screw press; SP1, SP2 - solenoids; TE - thermocouple; TFM - carrier wave amplifier; TFO - transformer; TM - thermostating jacket; V - hydraulic oil reservoir; VE - reference junction.

Konrad et al. [1983] positioned the sapphire windows such that their optical axes were parallel to the cylindrical axes. This was done so as to prevent double refraction and accordingly interference between ordinary and extraordinary rays (Near infrared spectroscopy was used for determination of compositions). Window support plugs of varying kinds were used to obtain different optical path lengths.

Pressure in the equilibrium cell was created by a silicon oil in a screw press. It was transmitted to the fluid mixture by a separator system. A piston was used as a separator system and the position of the piston was detected by an inductive device. This allowed determination of cell volume. The

method of using a stepper motor and manipulating an EOS is much simpler, and has been used in this project to determine cell volume.

Ashcroft et al. [1983]

Pressure to the equilibrium cell was applied by mercury in the lower section and by a steel piston in the upper section (see Figure 2-32). Sealing was achieved with “U”-rings and the piston was actuated by hydraulic oil. Using this system the cell contents could be raised and lowered without pressure changes, merely by the dual action pumping of the oil and mercury.

Equilibrium of the cell contents was achieved by a rather cumbersome mechanical rocking system. The apparatus had swivel joints, and Ashcroft et al. [1983] state that rocking was maintained for three hours to attain thermodynamic equilibrium in the cell.

The thermostatted air-bath used by Ashcroft et al. [1983] is similar to the one designed in this project. The Ashcroft et al. [1983] air-bath was constructed of steel and had dimensions of 1.2m x 0.6m x 1.1m high. The temperature in the bath was regulated to ± 0.1 K by an air circulator and heater operated by a thermistor-fed proportional controller. The maximum temperature that could be maintained in the bath for long periods of time was 333 K.

The sampling mechanism of Ashcroft et al. [1983] consisted of a stainless steel sampling rod (10 mm diameter) bored with a hole of diameter 2 mm. Figure 2-34 illustrates the sampling mechanism. The mechanism and its operation are very similar to that of Fredenslund et al. [1973].

The equilibrium cell contents could be observed by means of a mirror and optical system. Observation was made through the window assembly and a glass capillary tube (refer to Figure 2-32). The cylindrical windows were of toughened soda glass and the glass capillary tube was pyrex. There was a rather cumbersome method to maintain a small pressure differential across the capillary tube.

A measuring rod that was equipped with a vernier accurately determined the position of the piston. This however required an additional sealing point for the equilibrium cell.

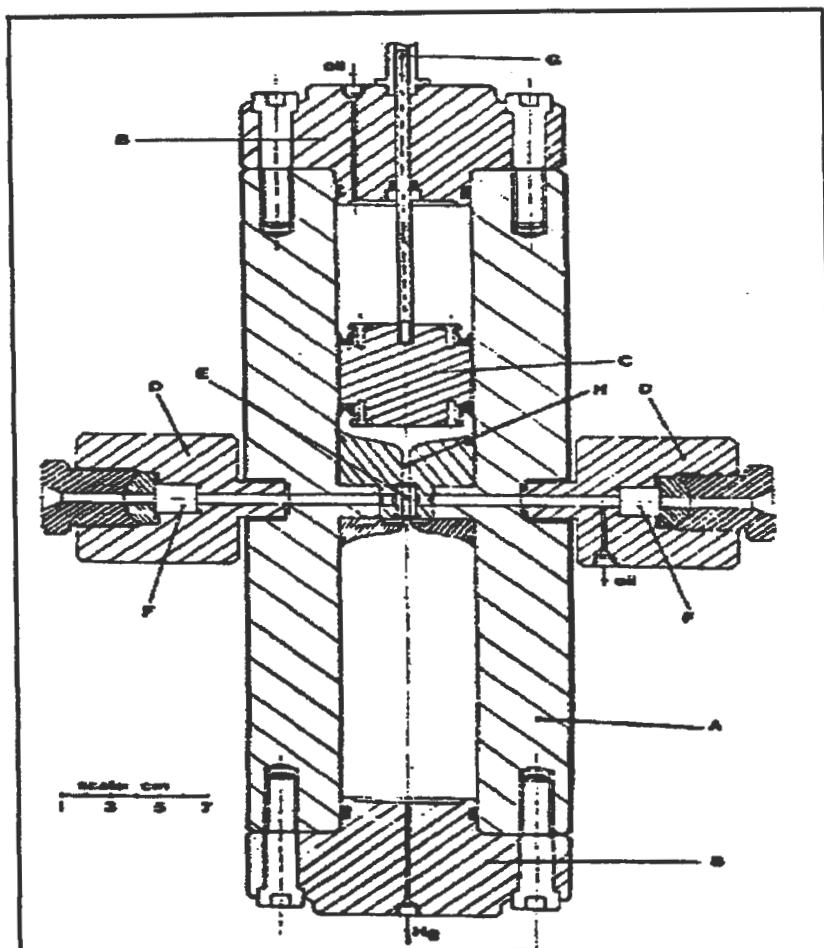


Figure 2-32: Equilibrium cell of Ashcroft et al. [1983]

A - cell body; B - end caps; C - piston; D - window assemblies; E - glass capillary; F - toughened glass windows; G - piston indicating rod; H - sampling valve.

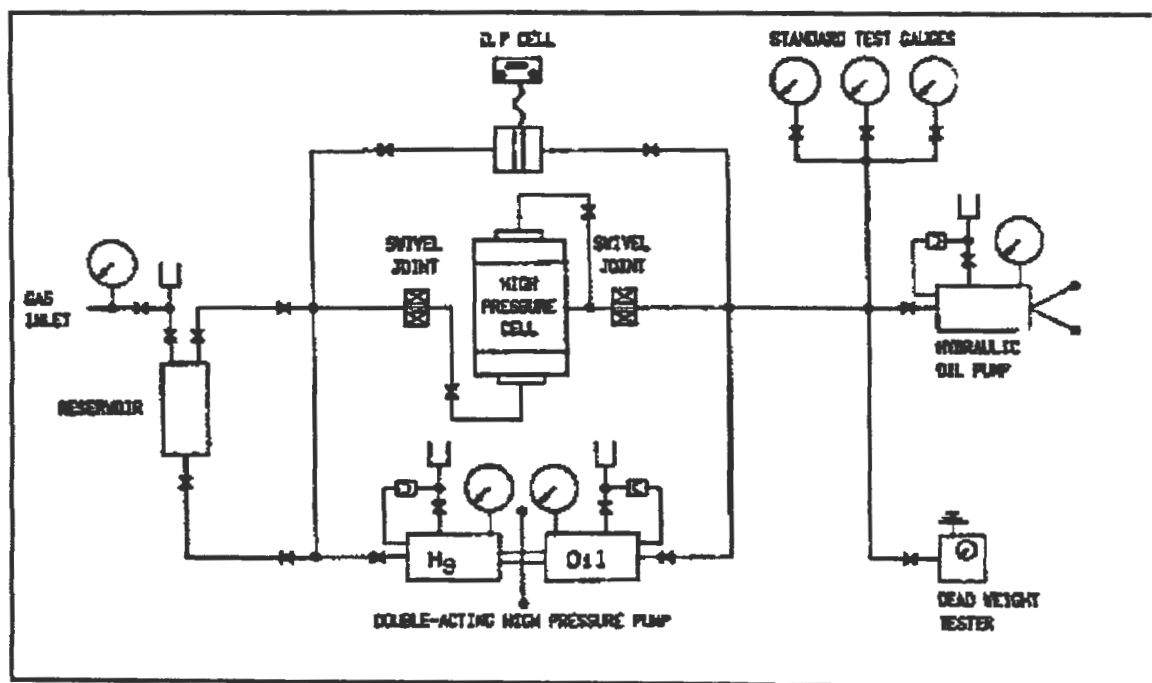


Figure 2-33: Schematic of the overall equipment layout of Ashcroft et al. [1983]

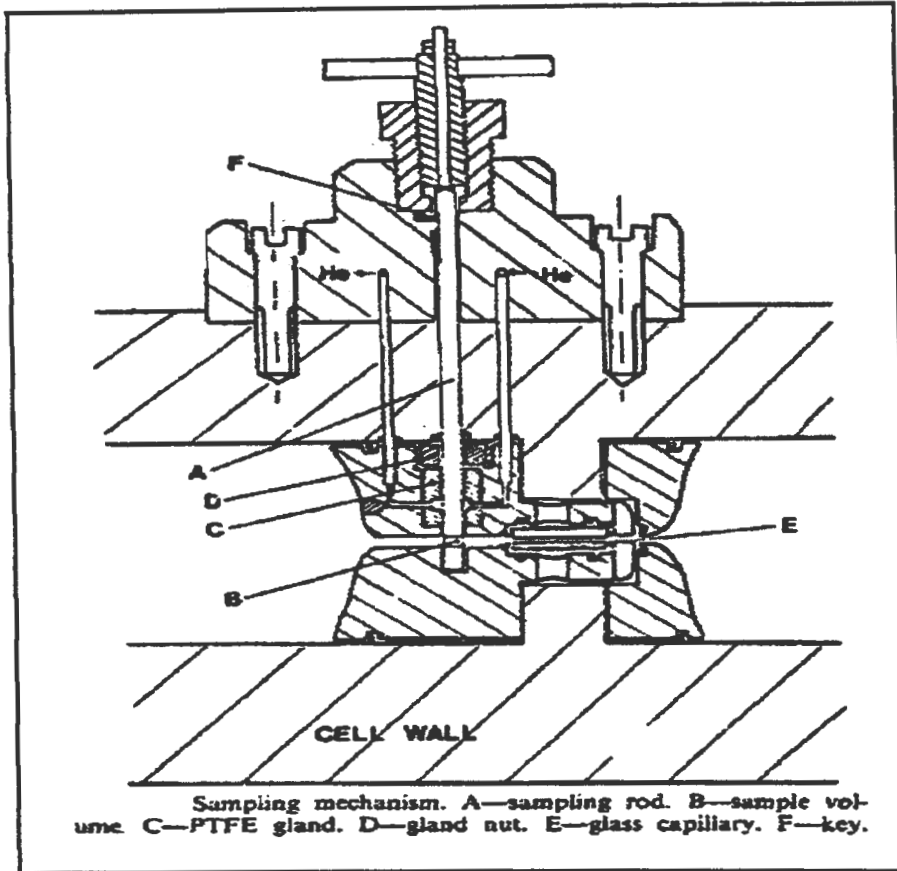


Figure 2-34: Sampling apparatus of Ashcroft et al. [1983]

Occhiogrosso et al. [1986]

The equilibrium cell which was variable in volume was designed to operate at up to pressures and temperatures of 700 bar and 535 K respectively. The cell had a maximum internal volume of 45 cm³ and was constructed from 316 stainless steel. The cell contents were illuminated by a fibre-light pipe and was viewed through a 3.81 cm diameter quartz window which was secured by a cell end cap which had a 0.64 cm by 1.91 cm view slit. A leak-proof seal of the end cap was ensured by using a Viton “o”-ring which was placed in an “o”-ring groove located between the quartz window and the cell body.

The contents of the cell could be compressed to the desired operating pressure by a movable piston fitted with two Viton “o”-rings and driven by a low-vapour-pressure silicone oil which was pressurised by a syringe-type pressure generator. The equilibrium cell contents were mixed by a magnetic stirring bar activated by a magnet situated below the cell. Pressure of the equilibrium mixture could be isothermally adjusted at a fixed overall composition by varying the interior cell volume.

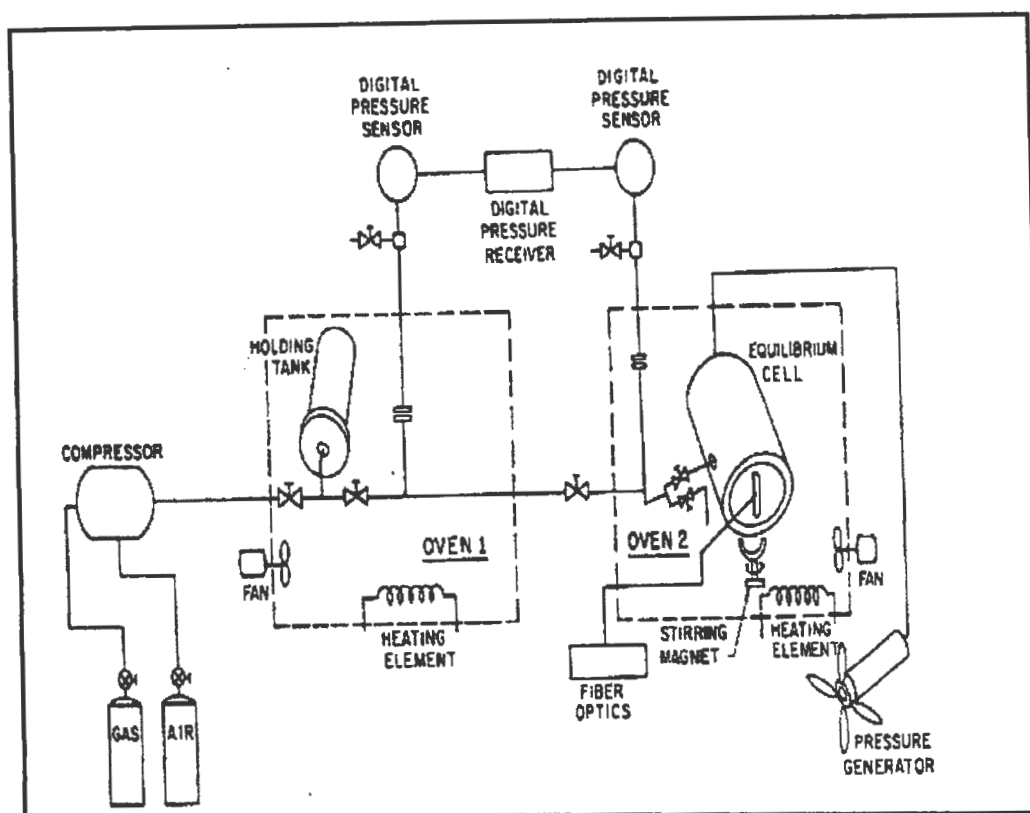


Figure 2-35: Experimental apparatus of Occhiogrosso et al. [1986]

The experimental method of Occhiogrosso et al. [1986] was that of the dew- and bubble point method. The data that they consequently obtained was an isopleth (constant composition at various temperatures and pressures). This meant that the equilibrium cell contents did not need to be sampled and analysed for each experimental point.

Laugier and Richon [1986]

The originality of the apparatus was the sampling system. Two capillaries of internal diameter, 0.1 mm, are fixed in the cylindrical wall of the cell at levels designed to withdraw the vapour and liquid samples. These capillaries also connect the equilibrium cell to a metallic chromatographic injector. Carrier gas flows through the expansion chambers of each of the injectors where a kalrez gasket inserted on the end of a movable axis can obstruct the extremity of the capillary. The kalrez gasket is held in place at the end of the capillary by a helicoidal spring. Thrust blocks are used to limit the linear movement of the axis and the path of the movable axis. This in turn controls the period of aperture time for the extraction of very small amounts of phase samples. The capillary is maintained short so as to ensure that the amount of mixture contained within it is

negligible compared to that of the withdrawn samples. The injectors are also heated to vapourise the samples. Figure 2-36 illustrates the flow diagram of the apparatus.

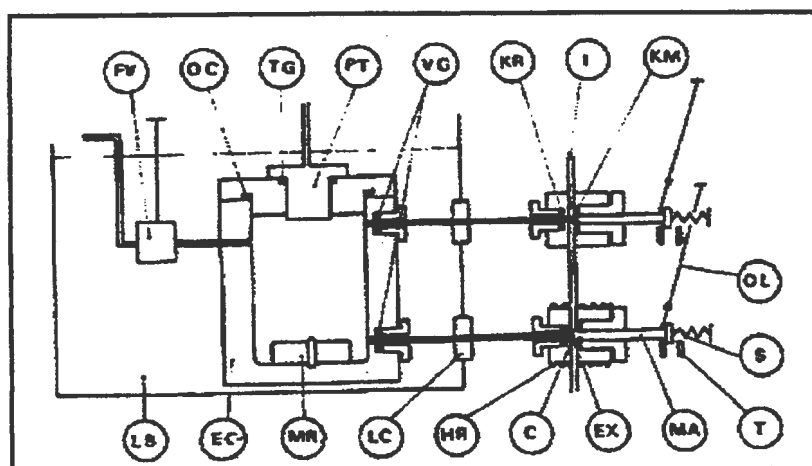


Figure 2-36: Flow diagram of the experimental apparatus of Laugier and Richon [1986]
 B - buffer; C - capillary; EC - equilibrium cell; EX - expansion chamber; FV - feeding valve; HR - heating resistance; I - carrier gas inlet; KG - kalrez gasket; KM - kalrez membrane; KR - kalrez "O"-ring; LB - liquid bath; LC - leakproof connection; MA - movable axis; MI - metallic injector; MR - magnetic rod; O - carrier gas outlet; OL - operating lever; OC - cell "O"-ring; PT - pressure transducer; S - helicoidal spring; T - thrust; TG - Teflon gasket; VG - Viton gasket.

Laugier and Richon [1986] claim that the apparatus is very simple and that measurement in the critical region does not involve significant experimental difficulty. They made comparisons with experimental data of Kay and Albert [1956] and stated that there was a strong similarity over the entire pressure range.

Mühlbauer [1990]

The apparatus of Mühlbauer [1990], developed in the same laboratory as the equipment in this project, was the predecessor of the current HPVLE static apparatus. A number of the features of the current equilibrium apparatus were used directly from the Mühlbauer [1990] apparatus. They include :-

- the design of the externally mounted heating unit;
- the design of the bottom stirrer in the equilibrium cell;
- the design of the jet-mixers for the homogenisation of the withdrawn equilibrium sample;
- and
- the design of the propane compression device.

The apparatus of Mühlbauer [1990] was capable of measurement of pressures and temperatures up to 200 bar and 200 °C respectively. The equilibrium cell volume was approximately 350 cm³ and the cavity was drilled eccentrically to accommodate the liquid sampling device and the sampling port.

The liquid phase sampling device was similar to that used by Fredenslund et al. [1973] (discussed earlier). The sampler was a polished stainless-steel sampling rod with a small hole (1.5 mm) drilled near the tip. The sampling rod was moved through the cell wall by an air-activated piston with Viton “o”-rings and guide rods to prevent rotation and misalignment of the sample hole with the carrier-gas channels drilled through the cell wall.

Sampling of the vapour phase was achieved through a capillary with entrapment of a small volume (approximately 0.75 cm³) of vapour in an evacuated space. The vapour sampling assembly was heavy and very cumbersome. The vapour sample, like the liquid sample was conveyed with helium gas, which was the carrier gas, to the jet-mixers before being sent to the GC for analysis.

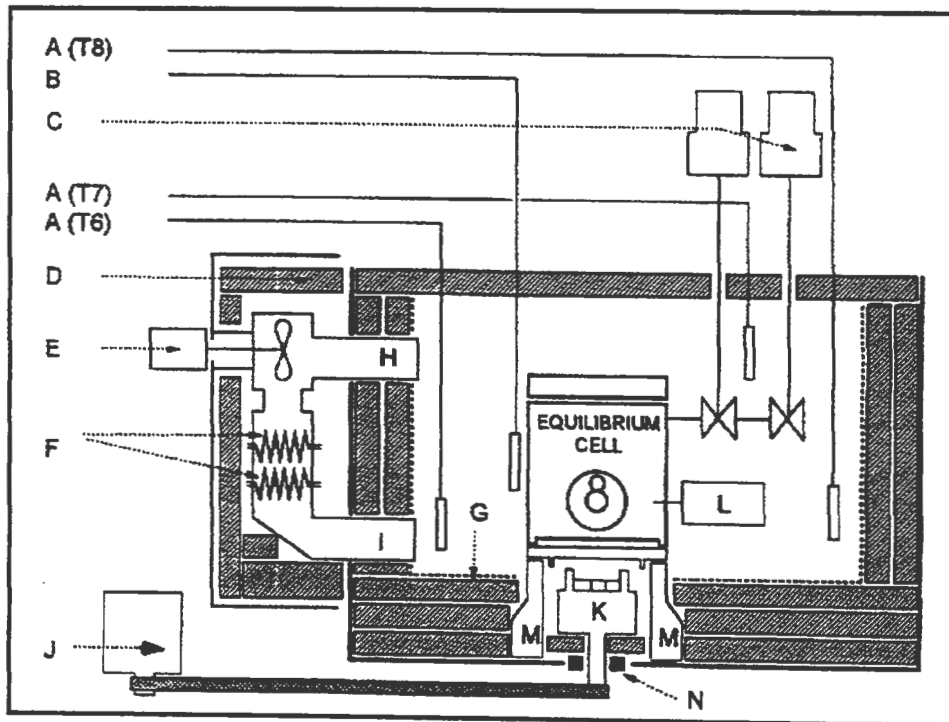


Figure 2-37: Equilibrium cell and air-bath arrangement of Mühlbauer [1990]

A - air bath temperature profile measuring thermocouples; B - Eurotherm 818 controller; C - vapour sampling valves; D - fiberglass insulation; E - Siflo air circulation fan; F - aluminium finned cartridge heaters; G - copper lining; H - air inlet; I - air outlet; J - variable speed motor; K - magnetic stirrer; L - jet mixer; M - rotating magnet well; N - graphite bush; O - liquid sampling device.

Figure 2-37 illustrates the equilibrium cell and air-bath arrangement of Mühlbauer [1990]. The air-bath arrangement used by Mühlbauer [1990] was directly used in this project. A number of the recommendations that were proposed by Mühlbauer [1990] were also incorporated into the design of the apparatus in this project, e.g. the variable-volume equilibrium cell, viewing windows and the use of GC sampling valves to sample the equilibrium phases.

Results obtained by Mühlbauer [1990] for the system carbon dioxide + toluene were in excellent agreement with literature. Other systems measured by Mühlbauer [1990] were propane + 1-propanol and propane + water.

2.5.2. The static non-analytical method

2.5.2.1. Description of the static non-analytical method

As described under synthetic methods earlier in the chapter, a mixture of known composition is made up and introduced into the equilibrium cell. Depending on whether isothermal (method of pressure variation) or isobaric (method of temperature variation) measurements are being undertaken, the temperature or pressure of the mixture is adjusted until phase separation of the homogeneous phase occurs. At the commencement of homogeneous phase separation, the pressure and temperature is recorded. Since the initial loading quantities of each of the components is exactly known, the composition of the mixture can be easily calculated. The temperature and pressure is readjusted after the appearance of the second phase to form the homogeneous region. This prevents de-mixing and layering of the phases. Adjustment of the temperature or pressure is again undertaken until the formation of a new phase is observed. The pressure, temperature and composition (mole fraction) at which these phase separations commence map out the phase envelope. Phase compositions are not analysed.

2.5.2.2. Selected examples from literature of the static non-analytical method

Meskel-Lesavre et al. [1981]

The apparatus was designed for the simultaneous determination of VLE and saturated liquid molar volumes. Bubble pressure and saturated molar volumes of the liquid phase are directly measured for a mixture of given composition. Determination of molar volumes as a function of composition makes it possible to obtain the partial molar volumes, which are very useful to test

the validity of the mixing rules in EOS of mixtures. This data is useful for determining the effect of pressure on the non-ideality in the liquid phase and to obtain the Poynting correction factor.

The equilibrium cell was designed to be very light and small, so that it could be weighed with an accurate balance and thermostated without any temperature gradient. Compositions of the binary or multi-component mixtures were determined by weighing each component in the equilibrium cell. A pressurising device was used to vary the equilibrium cell volume. The pressure was transmitted by a free moving piston. The equilibrium pressure in the cell was read by a pressure transducer and was known as a function of total volume of the cell. A discontinuity in the pressure versus total volume plot corresponded to the bubble point of the mixture. Accurate values of the bubble pressure and of the saturated liquid phase molar volume were simultaneously obtained from the pressure versus total volume plot. At the bubble point the liquid mole fraction is exactly the mole fraction obtained by weighing on a very accurate balance.

Experimental data obtained with the equipment of Meskel-Lesavre et al. [1981] for the system ethane + n-dodecane were in good agreement with literature. For greater detail on dew- and bubble point methods for VLE determination, refer to Appendix A.

Fontalba et al. [1984]

The piston assembly of Fontalba et al. [1984] is very similar to that utilized in this project. The total volume of the equilibrium chamber is obtained by precise determination of the position of the piston with respect to a reference. The reference position was defined by the stop screw at the bottom of the cell. The internal volume of the equilibrium chamber for any position of the piston was calculated from the position of the piston, the internal diameter of the equilibrium cell, and the maximum volume. A micrometer (see Figure 2-38) enabled the position of the piston to be measured to within 10^{-3} cm. Fontalba et al. [1984] state that measurement of the piston level to within 10^{-3} cm results in an accuracy of about 7×10^{-3} cm³ in the volume determination.

Fontalba et al. [1984] made use of a probe to measure the interface level. The bottom of the probe body ended in a very small thermistor (see Figure 2-39) powered by continuous current through wires passing in the probe body. Using a regulated current, a difference of thermal conductivity in the space around the thermistor resulted in an induced change of potential at the bounds of the thermistor.

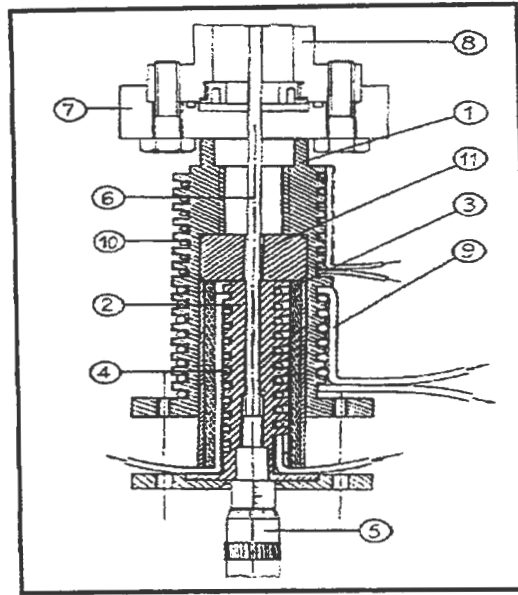


Figure 2-38: Total volume measuring device of Fontalba et al. [1984]

1 – Sleeve; 2 – cooled slide; 3 – Teflon insulating jacket; 4 – helicoidal groove to receive a cooling coil; 5 – micrometer; 6 – probe connected to the piston; 7 – pressurizing assembly; 8 – cell body; 9 – cooling coil; 10 – helicoidal groove to receive a heating electrical coil; 11 – spacer.

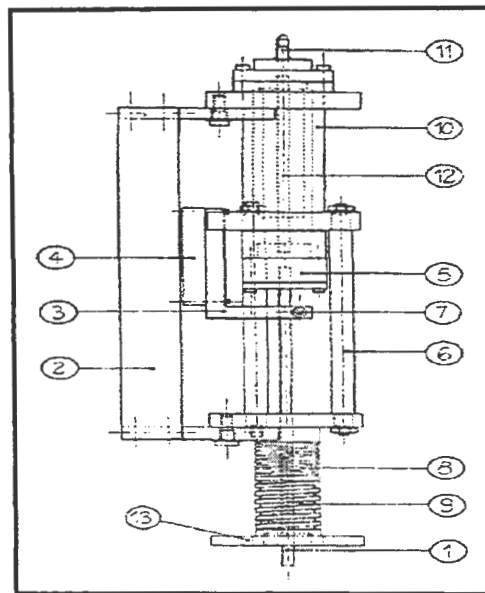


Figure 2-39: Interface level measuring device of Fontalba et al. [1984]

1 – Probe body; 2 – displacement transducer; 3 – corner plate to make a rigid connection between the probe body and the cursor (4); 4 – displacement transducer cursor; 5 – screw-nut device to move the probe; 6 – column assembly for axial adjustment of the probe; 7 – rigid connection between (1) and (3); 8 – helicoidal groove to receive a cooling coil; 9 – helicoidal groove to receive an electrical coil; 10 – pressurizing jacket; 11 – inlet-outlet of the pressurizing liquid; 12 – metallic rod; 13 – holes for the fixation on the cell.

2.5.2.3. Advantages of the static non-analytical method

The following are some of the advantages of the static non-analytical method as outlined by Raal and Muhlbauer [1994] :-

- As a result of no sampling of the equilibrium phases being required, there is no need for complicated and expensive analytical devices.
- Equilibrium data can be generated very rapidly and efficiently, as there is no need to wait for equilibration between phases.
- P-V-T relationships and even orthobaric densities can be measured.
- Critical property measurements can be undertaken on the apparatus.
- An entire isopleth can be obtained from a single charging of the equilibrium cell.

2.5.2.4. Disadvantages of the static non-analytical method

The following are some of the disadvantages of the static non-analytical method as outlined by Raal and Muhlbauer [1994] :-

- For multicomponent (in particular greater than two components) systems, limited information is obtained from experimentation.
- Observation of iso-optic systems, i.e. where the coexisting phases have approximately the same refractive index, is extremely difficult.
- The method is not suitable for measurements in the region away from the critical state.
- Dew points can easily be undetected if the liquid phase condenses as a thin film on the wall of the equilibrium cell instead of as a mist.

2.5.3. The static combined method

2.5.3.1. Description of the static combined method

This method combines the features of the analytical and non-analytical static methods into a single equilibrium cell. As a result provisions are made for the viewing of the cell contents, sampling of the vapour and liquid equilibrium phases, and determination of the equilibrium cell

volume. The analytical method does not lend itself to the study of phase equilibria near the critical state, since it entails the sampling of the equilibrium phases. In the critical region the gradients of the isobars or isotherms are generally very flat [Deiters and Schneider, 1986]. This means that a slight disturbance in the equilibrium conditions (e.g. during sampling), be it of temperature or pressure, can lead to large fluctuations in the equilibrium phase compositions. Thus if one designs a HPVLE apparatus for accurate measurement up to and including the critical point, the combined method will have to be adopted.

2.5.3.2. Selected examples from literature of the static combined method

Japas and Franck [1985]

The equilibrium cell was basically a cylinder constructed from a nickel-base, corrosion-resistant, high-strength alloy. On both ends, windows of synthetic sapphire were mounted, which, with a light source and mirror, permitted the observation of the interior.

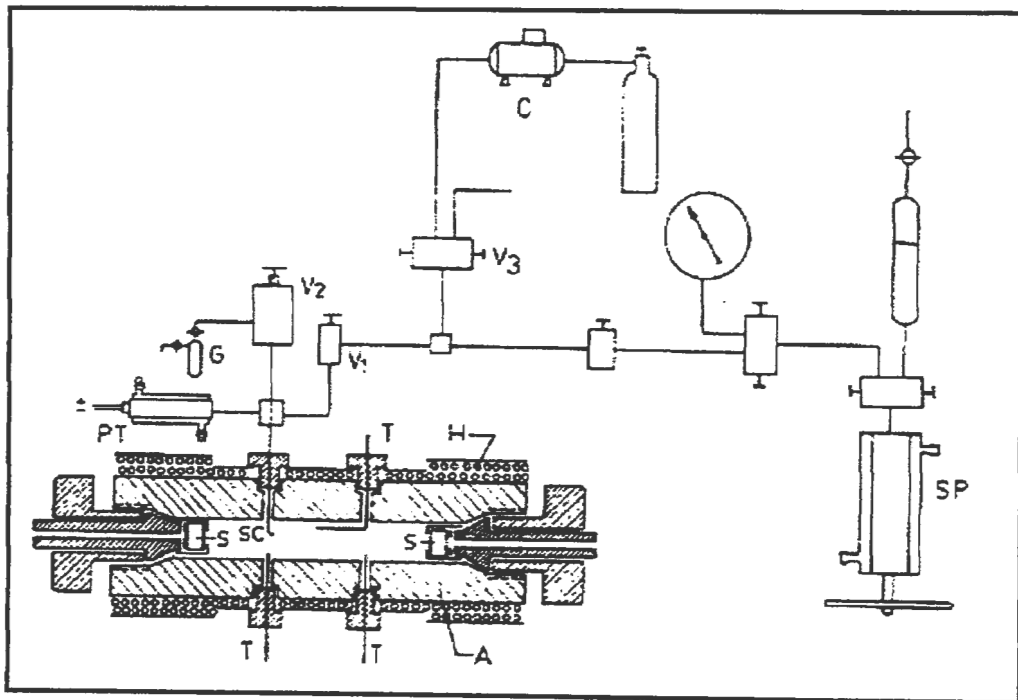


Figure 2-40: High pressure equipment of Japas and Franck [1985]

A - autoclave; C - air driven compressor; G - glass vessel; H - heating jackets; PT - pressure transducer; S - sapphire windows; SC - capillaries; SP - screw press; T - thermocouple; V - valves.

The apparatus could be operated in both the analytical and synthetic methods of investigation. In the analytical method a thin stainless steel capillary was applied to extract samples from the liquid phase through a micrometer valve. In the synthetic mode of operation, the precise amounts of gas and liquid introduced into the equilibrium cell were determined. After filling, the temperature was slowly increased and recorded simultaneously with the pressure. The P-T curves at constant volume, "isochors", showed a break point at the transition from a two-phase to a homogeneous one-phase system. Each break point of this kind was one point on the three dimensional P-T-x phase boundary surface and supplied also a value for the molar volume at this condition. Continuation of the heating permitted the determination of the P-V-T data of the system. The knick-points were also determined by cooling and in the majority of cases simultaneously by visual observation of the disappearance or appearance of a second phase and critical opalescence. This method of VLE determination is analogous to the dew point and bubble point method outlined in Appendix A.

The apparatus designed in the present project is also capable of operation in the synthetic mode, and thus could also be classified under a static combined method of operation.

Table 2-6 lists the static apparatus surveyed. Greater detail is available in Appendix A.

References	Cell volume (cm ³)	Operating Range		Equilibrium cell (1)	Measurement Device		Equilibration time (min)	Sample size (μl)	
		Temp (K)	Pressure (bar)		Temp (2)	Pressure (3)		Vapour	Liquid
Kobayashi and Katz [1953]	-	367	207	-	TC	B	120	-	-
Akers et al. [1954]	500	-	670	stainless steel	T	B	30	-	-
Din [1960]	-	-	-	copper	PR	DM	-	2500000	-
Kohn [1961]	5/12	-	69/104	pyrex glass	PR	B	-	N/A	N/A
Rogers and Prausnitz [1970]	150	223-423	1013	stainless steel	TC	PT	-	-	-
Besserer and Robinson [1971]	V.V. 10-175	255-395	207	316 stainless steel	TC	PT	10	10 ⁻³ g	10 ⁻³ g
Brunner et al. [1974]	1000	623	1000	316 stainless steel	TC	B	-	-	-
Ohgaki and Katayama [1975]	300	-	152	stainless steel	PR	DWP/PT	-	V.V.	150
Slocum [1975]	V.V.	223-523 223-598	69 35	pyrex glass	-	-	-	-	-
Antczana and Cheh [1975]	800	-	-	316 stainless steel	TC	DWP	300-1500	-	-
Nieto and Thodos [1978]	V.V.	325-425	56	stainless steel	TC	PT	640	50	50

Table 2-6: Static apparatus surveyed

References	Cell volume (cm ³)	Operating Range		Equilibrium cell (1)	Measurement Device		Equilibration time (min)	Sample size (μl)	
		Temp (K)	Pressure (bar)		Temp (2)	Pressure (3)		Vapour	Liquid
Ng and Robinson [1978]	150	310-589	173	316 stainless steel	TC	B	180	-	-
Kalra and Robinson [1979]	241.1	77-298	104	stainless steel	TC	PT	-	-	-
Figuiere et al. [1980]	50	673	400	stainless steel	TC	PT	-	1	1
Legret et al. [1981]	100	233-433	50-1000	stainless steel	TC	PT	10	15	15
Bae et al. [1981]	300	223-323	100	304 stainless steel	PR	PT	120	-	8
Meskel-Lesavre et al. [1981]	V.V.	373	50	titanium	TC	PT	60	N/A	N/A
Konrad et al. [1983]	100	293-473	2000	stainless steel Nimonic 90	TC	B	-	50 mg	50 mg
Konrad et al. [1983]	100	300-450	2000	stainless steel Nimonic 90	TC	B	-	N/A	N/A
Rousseaux et al. [1983]	V.V.	573	600	stainless steel	TC	PT	300	N/A	N/A
Guillevic et al. [1983]	V.V.	558	70	316 stainless steel	TC	PT	-	-	-
Ashcroft et al. [1983]	885	333	690	manganese steel	TS	PT	180	60	60

Table 2-6: (continued) Static apparatus surveyed

References	Cell volume (cm ³)	Operating Range		Equilibrium cell (1)	Measurement Device		Equilibration time (min)	Sample size (µl)	
		Temp (K)	Pressure (bar)		Temp (2)	Pressure (3)		Vapour	Liquid
de Loos et al. [1984]	-	-	-	stainless steel	PR	DWP	-	-	-
Fontalba et al. [1984]	V.V. (60 max)	433	450	titanium alloy	TC	PT	-	N/A	N/A
Fall and Luks [1984]	7-8	398	104	pyrex glass	PR	PT	-	N/A	N/A
Huang et al. [1985]	V.V. (45 max)	523	345	sapphire and stainless steel	TC	PT	-	-	-
Japas and Franck [1985]	-	673	2900	nickel-base corrosion-resistant high strength alloy	TC	PT	-	-	-
Laugier and Richon [1986]	50	423	100	316 stainless steel	TC	PT	-	-	-
Occhiogrosso et al. [1986]	V.V. (45 max)	535	700	316 stainless steel	PR	PT	-	N/A	N/A
Wagner and Wichterle [1987]	65	-	100	stainless steel	QT	B	-	-	-
Nakayama et al. [1987]	270	450	200	316 stainless steel	TC	PT	720	100 250	100 250
Kalra et al. [1987]	V.V.	-	200	316 stainless steel	TC	B	720-900	-	-

Table 2-6: (continued) Static apparatus surveyed

References	Cell volume (cm ³)	Operating Range		Equilibrium cell (1)	Measurement Device		Equilibration time (min)	Sample size (µl)	
		Temp (K)	Pressure (bar)		Temp (2)	Pressure (3)		Vapour	Liquid
Kalra et al. [1987]	V.V.	-	240	316 stainless steel	TC	PT	1440	-	-
Reiff et al. [1987]	2000	273-473	300	chromium+nickel+molybdenum steel	PR	B/PT	-	-	-
Laugier et al. [1990]	V.V. (10 max)	353	200	sapphire	TC	PT	-	N/A	N/A
Mühlbauer [1990]	350	453	200	stainless steel	PR	PT/B	-	900	8.8
Xu et al. [1991]	500	-	500	stainless steel	PR	PT	-	600	300
Brunner et al. [1994]	1000	773	350	-	TC	PT	-	-	-
Verneau et al. [1994]	500	273-423	1-20	-	PR	PT	-	-	-
Sako et al. [1995]	500	480	300	-	PR	B	240-300	-	3000
Pfohl et al. [1997]	1100	-	520	stainless steel	TC	PT	720	-	-

Table 2-6: (continued) Static apparatus surveyed

Key:
(1) Materials of construction
(2) TC - thermocouple; T - thermometer; PR - platinum resistance thermometer; QT - quartz thermometer
(3) B - Bourbon type pressure gauge; DM - differential manometer; PT - pressure transducer; DWP - dead weight piston gauge

CHAPTER THREE

REVIEW OF THE COMPUTATION AND THERMODYNAMIC INTERPRETATION OF HPVLE

The interpretation and modelling of HPVLE data thermodynamically is very much more difficult than for the low-pressure case. Measurement of this type of data is both expensive and complex and considerable experimental skill, experience and patience is required of the researcher. It is therefore very important that the data be correctly theoretically interpreted as this allows for interpolation and extrapolation of data to new conditions (Wong et al. [1992]) and proper correlation of phase behaviour from the minimum amount of experimental data.

Moser and Kistenmacher [1987] have estimated the financial and experimental time requirements for the measurement of VLE data. It is when one views these figures that one realizes the need for better extrapolation and predictive techniques in HPVLE. Moser and Kistenmacher [1987] estimate the cost of VLE measurement for a single set of data points at \$2000 (in terms of 1987 dollar value), and the time required to measure VLE for a single isotherm of a single binary system at approximately 30 days. These figures are quoted for low pressure VLE via the dew point and bubble point method. The large experimental set-up time is not included in these estimates. From our experience in HPVLE, we estimate HPVLE total cost and time values being two- or three-fold those quoted by Moser and Kistenmacher [1987].

Thermodynamics provides the framework for interpreting phase equilibrium data. At low pressure this thermodynamic analysis is common. However, when one progresses to mixtures at high pressures, the analysis is much more complicated and less common. Van Ness [1964], Van Ness et al. [1973], Van Ness and Abbott [1982] and Van Ness and Abbott [1983] discuss data reduction methods in detail. Baker et al. [1982] discuss the Gibbs energy analysis of phase equilibria in a publication.

Prausnitz et al. [1986] refer to high pressure as any pressure sufficiently large so as to have an appreciable effect on the thermodynamic properties of all the phases under consideration. At these conditions, to enable one to correlate or predict data, the non-idealities introduced by the high pressures need to be described. This is one of the aspects that are covered in this chapter.

A review of the theoretical aspects of high temperature and pressure VLE has been excellently covered by Sandler [1994], Mühlbauer and Raal [1995] and Raal and Mühlbauer [1998]. Some of the methods reviewed by them, coupled with the recently developed methods of Wong and Sandler [1992] were employed in this project and will be concentrated on. A brief summary of other methods is provided in Appendix B.

There are basically two categories of theoretical methods:-

- i) the direct method, and
- ii) the combined method [Wichterle, 1978 (a,b)].

In the direct method, computation of both the liquid and vapour phase fugacity coefficients is required. These are computed via a single appropriate EOS. The combined method on the other hand requires the computation of the liquid phase activity coefficient using an appropriate liquid phase model and the vapour phase fugacity coefficients using an EOS.

The history of the development of EOS models will be discussed with particular emphasis placed on the models used in this project. A similar discussion will be undertaken for liquid phase activity coefficient models. Consistency testing and critical property prediction will also be briefly discussed so as to ensure a complete review of HPVLE computation and thermodynamic interpretation. Chueh and Prausnitz [1967(a,b,c)] cover HPVLE computation well in their series of publications.

3.1. CRITERION FOR PHASE EQUILIBRIA

The thermodynamic treatment of phase equilibria is excellently covered in most undergraduate thermodynamic texts e.g. Walas [1985], Smith and van Ness [1987], Smith et al. [1996] and Winnick [1997]. The development of the criterion for phase equilibrium is covered in Appendix B.1.

The criterion for phase equilibria as stated by Smith and Van Ness [1987] is:

“Multiple phases at the same temperature and pressure are in equilibrium when the fugacity or chemical potential of each species is uniform throughout the system.”

$$\mu_i^\alpha = \mu_i^\beta = \dots = \mu_i^\pi \quad i = 1, \dots, N \quad (3-1)$$

$$\hat{f}_i^\alpha = \hat{f}_i^\beta = \dots = \hat{f}_i^\pi \quad i = 1, \dots, N \quad (3-2)$$

A description of the fugacity based on first principles from the total differential of the logarithm of fugacity is:

$$d \ln \hat{f}_i = \left(\frac{d \ln \hat{f}_i}{dT} \right)_{(P,x)} dT + \left(\frac{d \ln \hat{f}_i}{dP} \right)_{(T,x)} dP + \sum_{j=1}^{n-1} \left(\frac{d \ln \hat{f}_i}{dx_j} \right)_{(P,T,x)} dx_j \quad (3-3)$$

In Equation (3-3) the first, second, and third terms (RHS) may be related to the partial molar enthalpy, volume, and excess Gibbs free energy respectively. However, there is some difficulty in calculating the terms on the right hand side of Equation (3-3) which makes its use impractical.

For the case of equilibrium between a liquid and vapour phase at the same temperature and pressure, applying the general phase criteria yields:

$$\hat{f}_i^V = \hat{f}_i^L \quad (3-4)$$

However, knowing the relationship between component fugacities is of little practical value unless one can relate them to measurable properties e.g. temperature, pressure, and composition.

The problem of relating fugacities to measurable properties is overcome through the use of auxiliary functions such as activity coefficient, γ_i , and fugacity coefficient, ϕ_i .

3.2. THEORETICAL METHODS IN HPVLE

Wichterle [1978 (a,b)], Mühlbauer and Raal [1995], and Raal and Mühlbauer [1998] give excellent reviews on the two theoretical methods that have been developed for HPVLE. They are:

- i) the direct method, and
- ii) the combined method.

Since this project involved the design and construction of an isothermal HPVLE apparatus and the subsequent measurement of data isothermally, only the isothermal forms of these methods

will be discussed. Ramjugernath and Raal [1999] have undertaken a comparison of the direct and combined methods for isothermal HPVLE computation.

3.2.1. The Direct method

In the direct method, the vapour phase fugacity is described by:

$$\hat{f}_i^V = y_i \hat{\phi}_i^V P \quad (3-5)$$

and the liquid phase fugacity by:

$$\hat{f}_i^L = x_i \hat{\phi}_i^L P \quad (3-6)$$

This results in the equilibrium condition being described by:

$$x_i \hat{\phi}_i^L = y_i \hat{\phi}_i^V \quad (3-7)$$

The effects of temperature, pressure, and composition on the liquid and vapour phase fugacities are determined by the effect of these variables on the fugacity coefficients. This may be represented mathematically as:

$$\hat{\phi}_i^V = \phi(T, P, y_i, \dots, y_N) \quad (3-8)$$

$$\hat{\phi}_i^L = \phi(T, P, x_i, \dots, x_N) \quad (3-9)$$

The fugacity coefficients for both the vapour and liquid phases are calculated using a suitable EOS which describes the phase behaviour through exact thermodynamic relationships.

For the vapour phase,

$$\ln \hat{\phi}_i^V = \left(\frac{1}{RT} \right) \int_{V^V}^{\infty} \left[\left(\frac{dP}{dn_i} \right)_{(T, y, n_j)} - \frac{RT}{V^V} \right] dV - \ln \left[\frac{PV^V}{n_T RT} \right] \quad (3-10)$$

and for the liquid phase,

$$\ln \hat{\phi}_i^L = \left(\frac{1}{RT} \right) \int_{V^L}^{\infty} \left[\left(\frac{dP}{dn_i} \right)_{(T,V,n_j)} - \frac{RT}{V^L} \right] dV - \ln \left[\frac{PV^L}{n_T RT} \right] \quad (3-11)$$

The equilibrium ratio, K , is then defined as:

$$K_i = \frac{y_i}{x_i} = \frac{\hat{\phi}_i^L}{\hat{\phi}_i^V} \quad (3-12)$$

The description of phase equilibria via the direct method applies to both low- and high pressures. However at higher pressure the application of Equation (3-7) is not simple since:

- vapour phase non-idealities become pronounced i.e. $\hat{\phi}_i^V \neq 1$.
- the total pressure differential term in the isothermal Gibbs-Duhem equation becomes significant, especially near the critical region.

3.2.1.1. Difficulties associated with the application of the direct method

- a) Selecting the most appropriate EOS to describe both the liquid and vapour phase non-idealities can be a trial and error procedure, since there are literally hundreds of EOS's described in literature. In the selection of an EOS, the main criterion is that the EOS must be flexible enough to fully describe the system behaviour (P, V, T) for both phases in the temperature, pressure, and composition ranges under study.
- b) Selection of mixing rules further complicates the method. Mixing rules extend the pure component form of an EOS to mixtures. Generally most mixing rules are somewhat empirical in nature and tend to be system specific. Mühlbauer and Raal [1995] have elegantly classified the mixing rules.
- c) The problem of locating the appropriate liquid and vapour molar densities when higher than cubic order EOS's are used. This problem has been reviewed by Raal et al. [1980].
- d) The computational techniques for the calculation of dew-points and bubble-points are usually unreliable and do not converge to a solution at conditions close to the critical point, especially for multicomponent mixtures. Anderson and Prausnitz [1980 (a),(b)] describe a technique that

is robust and generally ensures convergence for dew-point, bubble-point and flash calculations.

For isothermal analysis, a bubble-pressure computation is generally undertaken. Figure 3-1 illustrates the computational procedure for the bubble-pressure calculation using the direct method.

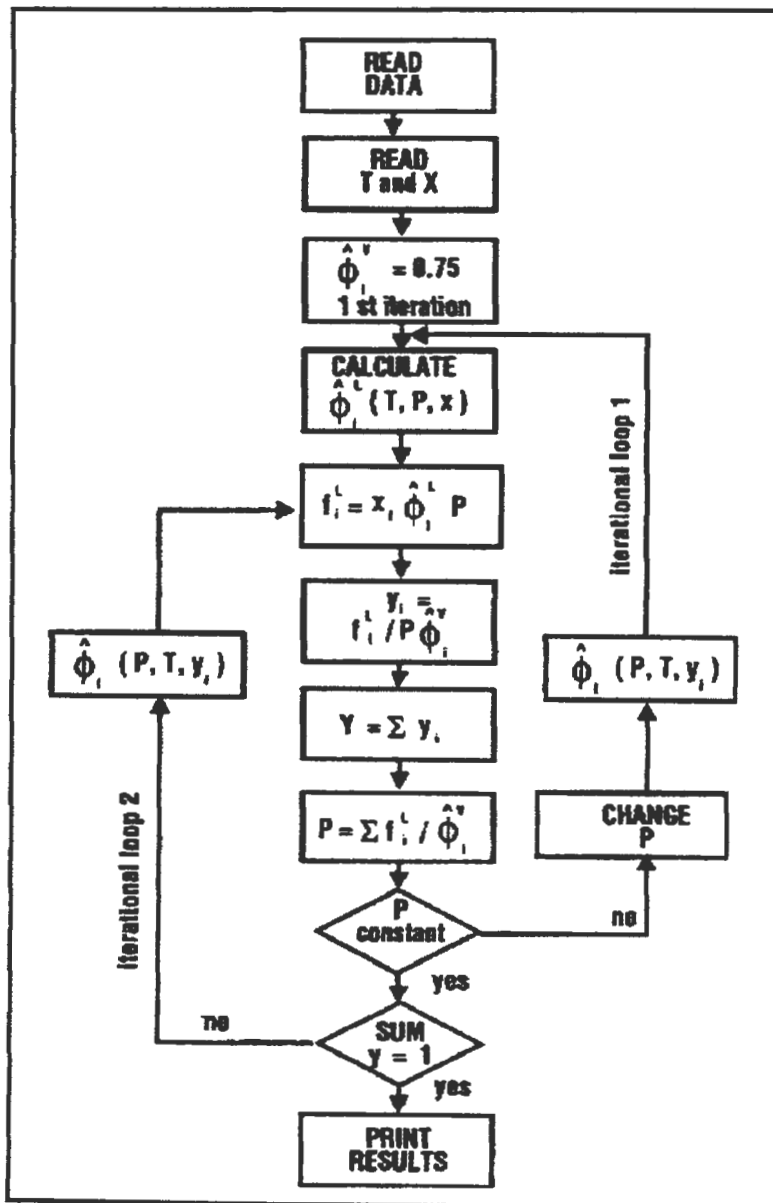


Figure 3-1: Computational procedure for the bubble pressure calculation using the direct method [Muhlbauer and Raal, 1995]

With the development of mixing rules that have built in Gibbs excess model dependency (Huron and Vidal [1978], Wong and Sandler [1992]), there has been the development of one may say, the “modern” direct method (Raal and Mühlbauer [1998]). The liquid and vapour fugacity coefficients are still calculated using an EOS, but the EOS have a built in Gibbs excess model in their mixing rules. More detail follows later in the chapter.

3.2.2. The Combined method

The main feature of this method of analysis is the use of separate auxiliary functions to describe the non-ideality of each phase.

For the vapour phase fugacity,

$$\hat{f}_i^V = y_i \hat{\phi}_i^V P \quad (3-13)$$

and for the liquid phase fugacity,

$$\hat{f}_i^L = x_i \gamma_i f_i^o \quad (3-14)$$

This results in the equilibrium condition becoming,

$$y_i \hat{\phi}_i^V P = x_i \gamma_i f_i^o \quad (3-15)$$

Here again, the effects of temperature, pressure and composition on the fugacity in the liquid and vapour phases are determined not only by the effect of these variables on the fugacity coefficient, but this time also on the activity coefficients. Therefore, the following relationships are required:

$$\gamma_i = \gamma(T, P, x_1, \dots, x_N) \quad (3-16)$$

$$\hat{\phi}_i^V = \phi(T, P, y_1, \dots, y_N) \quad (3-17)$$

$$f_i^o = f(T, P) \quad (3-18)$$

The equilibrium ratio, K , for the case of the combined method is now,

$$K_i = \frac{y_i}{x_i} = \frac{\gamma_i f_i^o}{\hat{\phi}_i^V P} \quad (3-19)$$

The fugacity coefficient is calculated using a suitable EOS that describes the vapour phase behaviour through the exact thermodynamic relationship,

$$\ln \hat{\phi}_i^V = \left(\frac{1}{RT} \right) \int_{V^V}^{\infty} \left[\left(\frac{dP}{dn_i} \right)_{(T,V,n_j)} - \frac{RT}{V^V} \right] dV - \ln \left[\frac{PV^V}{n_T RT} \right] \quad (3-10)$$

as in the direct method.

The activity coefficient can be determined from the Gibbs-Duhem equation by relating the activity coefficients to the molar Excess Gibbs free energy:

$$\sum x_i d \ln \gamma_i = \sum x_i d \left(\frac{\bar{G}_i^E}{RT} \right) = \left(-\frac{\Delta H}{RT^2} \right) dT + \left(\frac{\Delta V}{RT} \right) dP \quad (3-20)$$

The activity coefficient γ_i relates the liquid fugacity \hat{f}_i^L at conditions T , P , and x to some other condition where its value is accurately known. The “other condition” is referred to as the *standard state* and it represents the known and defined thermodynamic condition of a component at which its activity coefficient is unity.

3.2.2.1. Standard states

The conditions of pressure and composition of the standard state should always be chosen such that the numerical values of the activity coefficients are close to unity. This is to ensure that the real conditions are not drastically different from the standard ones. The standard state temperature, however, is always established at the system temperature.

At extreme pressures it may occur that the system temperature is greater than the critical temperature of one of the components in the system. As a result, this component cannot exist in

the liquid phase. This makes it difficult to define the component's standard liquid state, as it has to be a hypothetical quantity. Since any uncertainties in the hypothetical extrapolation from the sub-critical region affect the evaluated activity coefficients, and hence fugacity, the condensable and non-condensable components may require different standard states. Mühlbauer and Raal [1995] have listed the most commonly used standard states for condensable and non-condensable components as listed in Table 3-1.

For greater detail on condensable and non-condensable component standard states, refer to Appendix B.2.

Standard State	Temperature (<i>T</i>)	Pressure (<i>P</i>)	Composition (<i>x_i</i>)	Note
Condensable components				
1	<i>T_{system}</i>	<i>P_{system}</i>	1	Pure liquid component
2	<i>T_{system}</i>	<i>P_{reference}</i>	1	Pure liquid component
3	<i>T_{system}</i>	<i>P_o</i>	1	Pure liquid component
4	<i>T_{system}</i>	<i>P_{infinity}</i>	1	Pure liquid component
5	<i>T_{system}</i>	<i>P</i>	1	Pure liquid component
Non-condensable components				
7	<i>T_{system}</i>	<i>P_{system}</i>	0	component i infinitely diluted in component j
8	<i>T_{system}</i>	<i>P_{reference}</i>	0	component i infinitely diluted in component j
9	<i>T_{system}</i>	<i>P_o</i>	0	component i infinitely diluted in component j

Table 3-1: Standards states available as listed by Mühlbauer and Raal [1995]

3.2.2.2. Activity Coefficients

The use of a constant pressure activity coefficient is advantageous for isothermal conditions as it greatly simplifies equation (3-20) to :

$$\sum x_i d \ln \gamma_i = 0 \quad (\text{const. } T \text{ and } P) \quad (3-21)$$

Another reason is that the well-known semi-empirical mixture models e.g. van Laar, Margules, NRTL, UNIQUAC, etc. are particular mathematical solutions of Equation (3-21). Equation (3-21) applies equally well to both symmetric and unsymmetric conventions of normalisation of activity coefficients.

The pressure dependency of the liquid phase activity coefficient varies from a very weak function of pressure at low to moderate pressures, to one which needs to be taken account of at high pressures. Thus at low to moderate pressures one could consider the liquid phase activity coefficient to be a function of just temperature and composition.

At constant temperature and composition, the constant pressure activity coefficient can be determined by the following rigorous thermodynamic relation:

$$\gamma_i^{(P')} = \gamma_i^{(P)} \exp \int_P^{P'} \left(\frac{\bar{V}_i}{RT} \right) dP \quad (3-22)$$

where $\gamma_i^{(P')}$ is the activity coefficient at the arbitrary reference pressure (P').

For the condensable component, applying Equation (3-22), the liquid phase fugacity can be determined by:

$$\hat{f}_i^L = x_i f_i^{OL} \gamma_i^{P'} \exp \int_{P'}^P \frac{\bar{V}_i^L}{RT} dP \quad (3-23)$$

Similarly, for the non-condensable component:

$$\hat{f}_i^L = x_i f_i^{OL} \gamma_i^{*(P')} \exp \int_{P'}^P \frac{\bar{V}_i^L}{RT} dP \quad (3-24)$$

In systems where the total pressure varies widely with liquid composition, Equations (3-23) and (3-24) are very useful. Refer to Appendix B.3. for greater detail on condensable and non-condensable activity coefficients.

3.2.2.3. Difficulties associated with the application of the Combined Method

- a) In most cases one of the components is usually supercritical at the equilibrium temperature. This results in some difficulty in defining an appropriate standard-state fugacity, f_i^{OL} , for this supercritical component since it cannot exist as a pure liquid at the system temperature.

Prausnitz et al. [1980] suggest methods to overcome this problem as proposed by Lyckman et al. [1965] and Spencer and Danner [1972].

- b) At high pressures the vapour phase non-idealities have to be accounted for i.e. $\hat{\phi}_i^v \neq 1$. An appropriate EOS model has to be chosen to calculate the vapour phase non-ideality.
- c) The total pressure differential term in the isothermal Gibbs-Duhem equation becomes significant at high pressures. Prausnitz et al. [1980] suggests methods to calculate this.
- d) Finding an appropriate model for the excess Gibbs free energy. Gess et al. [1991] and Sandler [1989] comprehensively list the most widely used excess Gibbs free energy models.
- e) Evaluating the liquid molar volume as a function of temperature and pressure. Prausnitz et al. [1980] suggests methods to evaluate this property, as proposed by Lyckman et al. [1965] and Spencer and Danner [1972].
- f) Determining the large number of parameters needed in this method. Generally, the parameters are obtained by fitting. The two most common methods for fitting are the least squares method (described by Gess et al. [1991] and Marquardt [1963]) and the maximum likelihood principle (described by Gess et al. [1991], Prausnitz et al. [1980], Anderson et al. [1978] and Rubio et al. [1983]).

Seeing that there are more difficulties associated with the combined method, most researchers make use of the direct method. The computational procedure for the isothermal bubble-pressure calculation via the combined method of Prausnitz et al. [1967], Prausnitz and Chueh [1968], and Prausnitz et al. [1980] is illustrated in Figure 3-2.

Combined methods reviewed in literature are briefly discussed in Appendix B.4.

There will always be the debate on which is the better analytical method to use. However, there is no objective and general criterion that could be used for testing of a particular method. Wichterle [1978(b)] gives some estimation surveys dealing with evaluation of the direct and combined methods. They are as listed in Table B-4.

Wichterle [1978(b)] states that if a good EOS is available which is suitable in its description of phase behaviour, then the direct method should be used in preference. He also states that the final choice of the method is subject to the type and particularity of the system; the availability and quality of data; the accuracy requested etc. Wichterle [1978(b)] recommends that at least two independent methods should be used for each computation.

A similar table of comparison between the direct and combined methods has been drawn up by Raal and Muhlbauer [1998]. They also drew up a table rating the capabilities of various classes of equations of state. Refer to Appendix B.5. for these tables.

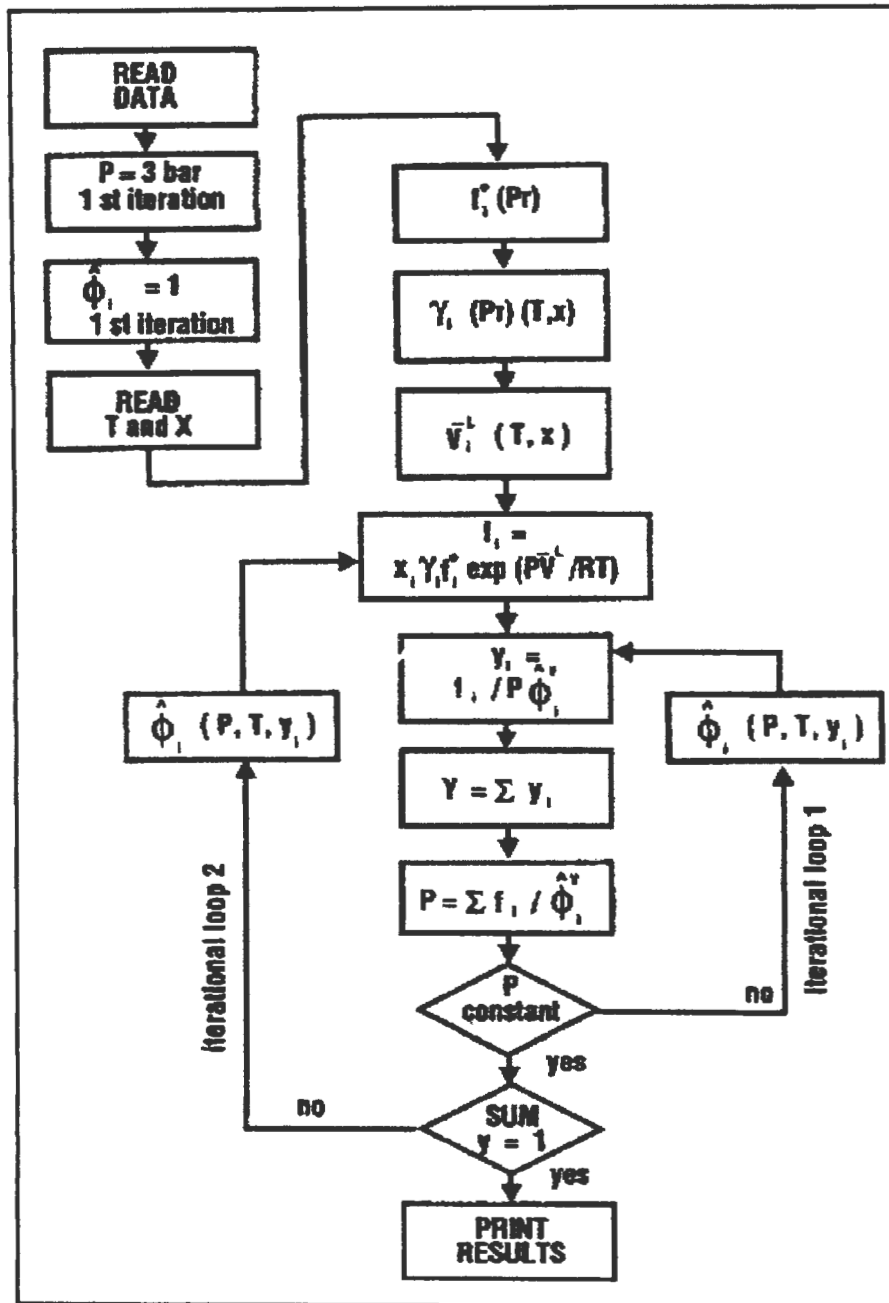


Figure 3-2: Computational procedure for the bubble pressure calculation using the combined method [Mühlbauer and Raal, 1995]

Table 3-2 below details a comparison drawn between the direct and combined method based on experience gained in this project (Ramjugemath and Raal [1999]).

Criterion	Direct method	Combined Method
Accuracy of the calculation	Good. Includes calculations in the critical region. Accuracy depends on the EOS model chosen and the number of adjustable parameters. The mixing rules chosen also have a significant effect on the accuracy.	Excellent, except in the critical region. Is also model dependent.
Range of conditions	Works well up to the critical region.	Works well at conditions well below the critical region. Begins to become unreliable as the critical region is approached.
Type of components	The method rates poor to fair in the ability to model highly polar and structurally complex systems. However, various models have been proposed in literature (e.g. Wong and Sandler [1992], Sandler et al. [1994], Raal and Muhlbauer [1998] and Malanowski and Anderko [1992]) that model these types of systems very well using this method.	The method is rated as fair to good depending on the liquid phase model chosen and the EOS chosen to describe the vapour phase non-ideality.
Calculation within the critical region	Good correlation and prediction is possible in the critical region, especially with the new Wong and Sandler mixing rules [1992].	Poor correlation of data in the critical region.
Computational times	This depends on the complexity of the EOS chosen. For high order EOS's, the computation may be slow depending on the number of roots. Also depends on the number of interaction parameters in the EOS state model chosen and the mixing rules. As an example, performing a calculation with the new Wong and Sandler mixing rules [1992] with the Peng-Robinson-Stryjek-Vera EOS takes approximately 2 to 3 minutes on a Pentium 150 PC (time taken to fit the parameters to experimental data).	It depends on the complexity of the liquid phase model chosen and the EOS used to describe the vapour-phase non-ideality. With the new combined method model described in this paper the parameters took approximately 4 minutes to determine on a Pentium 150 PC.
Input parameters	The number of parameters depends on the degree of generalization. If one has to take a simple cubic EOS of state as an example, the input parameter is generally the interaction parameter.	Usually generalized better, but more parameters are required. The choice of a standard-state is crucial (especially for HPVLE) and is discussed in Raal and Muhlbauer [1998].
Sensitivity to initial guess	With the methods for convergence adopted (as described in Anderson and Prausnitz [1980 a,b] and least squares techniques as described by Marquardt [1963]) the problem of an initial guess is not so significant.	Not as sensitive to the initial guess as the direct method.

Table 3-2: Comparison of the Direct and Combined Methods

Correlation abilities	Depending on the complexity of the EOS, mixing rules and the number of adjustable parameters, the correlating ability varies. For the simple EOS's, one has just the binary interaction parameters. With more complex EOS's and mixing rules such as Huron and Vidal [1979], modifications of Huron and Vidal (Orbey and Sandler [1997]) and Wong and Sandler [1992] the correlation ability increases, as now we have binary interaction parameters along with adjustable parameters that are related to excess Gibbs free energy models. It is not necessarily the case that the correlation ability increases with the number of adjustable parameters.	The number of adjustable parameters can be unlimited. Correlation ability depends on the excess Gibbs free energy model chosen for the liquid phase and the EOS and mixing rules that are used to describe the vapour phase. Generally the correlation is excellent at conditions well below critical.
Consistency of computation	Good for all conditions.	Reliable results cannot be expected at higher pressures, especially at pressures close to the critical condition.
Extrapolation Ability	The new Wong and Sandler (Wong et. al. [1992]) mixing rules permit for data to be extrapolated to conditions of pressure and temperature vastly different from the conditions at which measurements were undertaken.	No extrapolation ability.
Interpolation Ability	Even with very simple EOS's data can be interpolated in small ranges.	Not as flexible as the direct method.
Prediction Ability	With the newer EOS's with mixing rules that incorporate the description of an excess Gibbs free energy model, the models can be totally predictive if the UNIFAC group contribution model or modification thereof is used to determine the excess Gibbs free energy (Orbey et al. [1993], Fischer and Gmehling [1996], and Kurihara and Kojima [1995(a),(b)]). HPVLE can also be predicted from infinite dilution activity coefficients and other methods as described by Feriui and Geană [1996], and Yoo et al. [1996]. Huang and Sandler [1993] describe how their new mixing rules enable one to predict HPVLE data from existing low-pressure activity coefficient parameters.	Has no predictive abilities. Can become predictive, however, if we use the UNIFAC model or any group contribution model to describe the liquid phase and an EOS with mixing rules as described by Orbey et al. [1993] to describe the vapour phase. This is a suggestion by the authors, but has not been tested.

Table 3-2 (continued): Comparison of the Direct and Combined Methods

3.3. SURVEY OF EQUATIONS OF STATE

The mechanical state of a substance is known when the pressure, temperature, and volume are fixed. These three properties are related by a so-called equation of state represented mathematically as:

$$f(P, V, T) = 0 \quad (3-25)$$

Many important properties of pure substances and mixtures (e.g. vapour pressures, critical properties, densities, and VLE relations) can be evaluated from a suitable EOS. It is interesting to note that at present no one EOS exists that is equally suitable for all these properties of any large variety of substances.

3.3.1. Brief history of Equations of State

The history of EOS's began with Boyle's experiments with air in 1662. He deduced that at a given temperature the volume of a gas is inversely proportional to its pressure, written mathematically as:

$$PV = \text{constant} \quad (3-26)$$

In 1802, Charles and Gay-Lussac quantified the effect of temperature. Clapeyron combined these results in 1834 into the first statement of the ideal gas law as:

$$PV = R(T + 267) \quad (3-27)$$

The ideal gas relation that eventually followed is:

$$PV = RT \quad (3-28)$$

or

$$Z = \frac{PV}{RT} = 1 \quad (3-29)$$

where R is the gas constant and Z is the compressibility factor.

At the very onset it was realised that the ideal gas law often is only a rough approximation of true behaviour of real gases. To achieve a closer approximation one has to account for the fact that real gases have size, shape and structure and as a result their molecules occupy space and attract or repel each other physically and/or electrically. These deviations from the ideal gas structure determine the forces between molecules and their PVT behaviour. As a result of their structure, molecules exhibit electrical properties. They are either:-

1. Non-polar symmetrical molecules which are usually electrically neutral;
2. Molecules having residual valences that usually result in association and hydrogen bonding;
or
3. Polar unsymmetrical molecules usually possessing dipole moments.

While forces of repulsion and attraction are present in all molecules they are more pronounced in associating and polar molecules. Consequently the PVT correlations proposed to that point in time had not been successful in modelling polar substances.

In 1873 van der Waal took these factors into account quantitatively in an equation that is the basis for many currently accepted PVT relations, the van der Waals EOS. Many EOS's which are much more accurate have since been proposed. They are conveniently classified (Sandler [1994]) according to their origins as follows:-

1. van der Waal family of equations;
2. Family of extended virial equations;
3. Corresponding states equations;
4. Equations derived from statistical thermodynamics based on lattice models, perturbation, and integral equation theory; and
5. Fitting computer simulation data.

Excellent reviews on the various classes of EOS's are available in Walas [1985], Sandler [1994], and Raal and Mühlbauer [1998]. The literature is too extensive to summarise all of the EOS's. In this project, use was made of the virial and cubic EOS's and therefore they will be detailed. A brief summary of other EOS's surveyed will be presented in Appendix B.

3.3.2. Virial Equation of State

This is an infinite power series in inverse molar volume, and is given by:

$$Z = \frac{PV}{RT} = 1 + \frac{B}{V} + \frac{C}{V^2} + \frac{D}{V^3} + \dots \quad (3-30)$$

The coefficients B , C , D , etc. are called “virial coefficients”; B is the second virial coefficient, C is the third coefficient, and so on. From statistical mechanics, these coefficients are related to the forces between molecules, i.e. the second virial coefficient represents the interaction between two molecules, the third virial coefficient reflects the simultaneous interaction among three molecules, etc. For pure fluids these virial coefficients are functions of temperature only.

Despite its theoretical basis, the virial equation has not been widely used, mainly because values of the virial coefficients are often not known. The second virial coefficient has been studied extensively for simple fluids and some light hydrocarbons, but less is known about the third virial coefficient. Moreover, the infinite series converges very slowly at the higher densities, requiring a greater number of terms to get a correct value of compressibility factor, Z , while little information is available for the higher virial coefficients. It is suggested by Smith and Van Ness [1987] that the truncated two- and three-parameter virial EOS be used for pressures up to 15 and 50 bars respectively.

Prausnitz et al. [1980] regard the integrated form of the truncated three-parameter virial equation as one of the most useful equations developed for phase equilibrium thermodynamics. The equation can be applied to any component in a mixture regardless of whether that component can exist as a pure vapour at the temperature and pressure of the mixture. This implies that no hypothetical standard states are required. Also this equation is equally valid for both polar and non-polar substances.

Experimental data for the second and third virial coefficients are available in a compilation by Dymond and Smith [1980]. Correlations for the second virial coefficient have been proposed, and the most commonly used correlations are those of Tsonopoulos [1974] and Hayden and O’Connell [1975]. For greater detail on these correlations and variations of the virial EOS, refer to Appendix B.6.

Interactions between the molecules making up a mixture affects the behaviour of the mixture. The most popular and widely used methods of accounting for these interactions via an EOS is provided in the form of interaction parameters.

For an n -component mixture, there are n single, $\frac{n(n-1)}{2}$ binary, $\frac{n(n-1)(n-2)}{6}$ tertiary, etc. interaction parameters. The mixture virial coefficient is then a summation of the individual virial coefficients appropriately weighted with respect to the composition of the mixture. Interactions between dissimilar molecules is usually small (depending on whether the molecules are non-polar or not) at low to moderate pressures. The higher-order interactions (greater than two) are usually masked by the imperfections of the EOS. They are also difficult to determine and therefore usually not available for computational purposes.

In the virial equation, interactions between gases are incorporated in the two-parameter virial EOS as the mixture second virial coefficient, which is related to the pure component and cross second virial coefficient:

$$B_{mix} = \sum_{i=1}^m \sum_{j=1}^m y_i y_j B_{ij} \quad (3-31)$$

where $B_{ij} = B_{ji}$, y_i is the mole fraction, and m is the number of components.

For a binary system the exact expression is:

$$B_{mix} = \sum_{i=1}^2 \sum_{j=1}^2 y_i y_j B_{ij} = y_1^2 B_{11} + 2y_1 y_2 B_{12} + y_2^2 B_{22} \quad (3-32)$$

The fugacity coefficient $\hat{\phi}_i$ is determined by equation (3-10). For the truncated two-parameter virial EOS it yields:

$$\ln \hat{\phi}_i = \frac{P}{RT} \left[2 \sum_{j=1}^2 y_j B_{ij} - B_{mix} \right] \quad (3-33)$$

As mentioned before, Hayden and O'Connell [1975] provide expressions for predicting pure component and second virial cross coefficients for simple and complex systems requiring only the

component's critical temperature and pressure, mean radius of gyration, dipole moment and if appropriate a parameter to describe chemical associations. The correlation of Hayden and O'Connell [1975] is detailed in Appendix B.6.

3.3.3. van der Waals Family of Cubic Equations

The simplest equations capable of representing both the liquid and vapour states are equations cubic in volume. They have found considerable applications in VLE calculations. These equations represent a compromise between ease of use in computation and sufficient flexibility to describe wide-ranging phase behaviour. The formulation of the empirical cubic EOS is based essentially in the expression of pressure as the sum of two terms, a repulsion pressure (P_r) and an attraction pressure (P_a). The P_r term is usually expressed by the van der Waals hard-sphere equation:

$$P_r = \frac{RT}{V-b} \quad (3-34)$$

where b is a constant related to the size of the hard sphere.

The P_a term can be expressed as:

$$P_a = \frac{a}{g(V)} \quad (3-35)$$

where a is a constant and is regarded as a measure of the intermolecular attraction force, and $g(V)$ is a function of molar volume. The general form of the cubic EOS is therefore:

$$P = \frac{RT}{(V-b)} - \frac{a}{g(V)} \quad (3-36)$$

The determination of the parameters in the van der Waals and other EOS's is briefly discussed in Appendix B.7.

The famous cubic equation of van der Waals, proposed in 1873, was the first EOS to give a qualitative description of the vapour and liquid phases and phase transitions. Mathematically represented as:

$$P = \frac{RT}{(V-b)} - \frac{a}{V^2} \quad (3-37)$$

The van der Waals EOS though is not quantitatively accurate. For example, it predicts that the critical compressibility is 0.375 for all fluids. In reality the value varies from 0.24 to 0.29 for different hydrocarbons and the range is wider for non-hydrocarbons. Also, the predicted vapour pressures are inaccurate.

One of the first important modifications to the van der Waals equation was made by Redlich and Kwong [1949]. They recognised the temperature dependence of the attraction term and tried to account for it with the following EOS (Redlich-Kwong EOS):

$$P = \frac{RT}{(V-b)} - \frac{a}{T^{0.5}V(V+b)} \quad (3-38)$$

The Redlich-Kwong equation has limited accuracy, and is generally successful only for nearly ideal systems. It gives a somewhat better critical compressibility of 0.333, but is still not very accurate for the phase boundary (vapour pressure) and the liquid density. To overcome the deficiencies of the van der Waals and the Redlich-Kwong EOS's, many modifications have been proposed over the years. Two of these many modifications have achieved widespread acceptance. They are the Soave [1972] and Peng and Robinson [1976] EOS's.

In a recent publication (Soave et al. [1995]) the Redlich-Kwong parameters for a and b have been determined without the use of critical constants. The proposed method by Soave et al. [1995] makes it possible to treat substances whose critical constants are not known (heavy or thermally unstable compounds) by using one density value and the vapour pressure curve.

Soave, in 1972, proposed the following modification of the attractive term in the Redlich-Kwong EOS,

$$P_a = \frac{a(T)}{V(V+b)} \quad (3-39)$$

$$a(T) = a_c \alpha(T) \quad (3-40)$$

$$\sqrt{\alpha} = 1 + \kappa(1 - \sqrt{T_r}) \quad (3-41)$$

$$\kappa = 0.48 + 1.574\omega - 0.176\omega^2 \quad (3-42)$$

The temperature dependence of the attractive term had been incorporated into the value of a , and the term was also a function of the acentric factor, ω .

The resulting Soave EOS is as follows:

$$P = \frac{RT}{(V-b)} - \frac{a(T,\omega)}{V(V+b)} \quad (3-43)$$

For the calculation of the fugacity coefficients, it is convenient to write the equation in terms of the compressibility factor, Z . In this form the Soave EOS is:

$$Z^3 - Z^2 + Z(A - B - B^2) - AB = 0 \quad (3-44)$$

where

$$A = \frac{aP}{R^2 T^2} \quad (3-45)$$

$$B = \frac{bP}{RT} \quad (3-46)$$

$$Z = \frac{PV}{RT} \quad (3-47)$$

The fugacity coefficient is then given by:

$$\ln \phi = Z - 1 - \ln(Z - B) - \frac{A}{B} \ln\left(\frac{Z + B}{Z}\right) \quad (3-48)$$

This cubic equation results in more accurate vapour pressure predictions (especially above one bar) for light hydrocarbons. It was actually this equation which led to cubic EOS becoming an important tool for the prediction of VLE at moderate and high pressures for non-polar fluids. However, the Soave EOS failed to generate satisfactory liquid densities. The equation predicts specific liquid volumes greater than the literature values and the deviations increase from about 7% at $T_r = 0.65$ to 27% at the critical point [Peng and Robinson, 1976].

The Soave EOS was modified for handling of polar fluids by Soave [1979]. The modification involved the introduction of two empirical parameters into the expression for the α function given in equation (3-41). For more detail on the modification and develop thereon, refer to Valderrama et al. [1994].

The Peng and Robinson [1976] EOS was proposed to address the weakness of the Soave EOS in the area of the critical region instabilities and inaccurate liquid density predictions. As such, it is very closely related to the Soave EOS. The proposed equation by Peng and Robinson is:

$$P = \frac{RT}{(V - b)} - \frac{a(T, \omega)}{(V + b) + b(V - b)} \quad (3-49)$$

where

$$a = a_c \alpha \quad (3-50)$$

$$\sqrt{\alpha} = 1 + \kappa(1 - \sqrt{T_r}) \quad (3-51)$$

$$\kappa = 0.37464 + 1.5426\omega - 0.26992\omega^2 \quad (3-52)$$

For the determination of the fugacity coefficient,

$$Z^3 - (1 - B)Z^2 + Z(A - 3B^2 - 2B) - (AB - B^2 - B^3) = 0 \quad (3-53)$$

where

$$A = \frac{aP}{R^2 T^2} \quad (3-54)$$

$$B = \frac{bP}{RT} \quad (3-55)$$

$$Z = \frac{PV}{RT} \quad (3-47)$$

$$\ln \phi = Z - 1 - \ln(Z - B) - \frac{A}{2\sqrt{2}B} \ln \left[\frac{Z + (1 + \sqrt{2})B}{Z + (1 - \sqrt{2})B} \right] \quad (3-56)$$

The Peng-Robinson EOS gives slightly improved liquid volumes ($Z_c = 0.307$) and gives accurate vapour pressure predictions for hydrocarbons in the C6 to C10 range.

Modifications for the Peng-Robinson EOS have been numerous e.g. Lin [1984], Stryjek and Vera [1986 (a,b)], Valderrama and Molina [1986], Xu and Sandler [1987 (a,b)], Mohamed and Holder [1987], Melhem et al. [1989] and Twu et al. [1995] to name a few. The most widely used modification is that of Stryjek and Vera [1986 (a,b)]. The modification is to the temperature dependent α function is shown in Table 3-3.

For a detailed description of the general capabilities and shortcomings of the various cubic EOS's, refer to Martin [1979] and Abbott [1979]. Knapp [1986], Tsonopoulos and Heidman [1986] and Mathias and Klotz [1994] review the widely used EOS's from an industrial perspective. For a general review on EOS's refer to Wei and Sadus [2000].

Various α functions (temperature-dependency models of the attractive term for cubic EOS) have been proposed. Sandler [1992] lists a representative sample of them. Table 3-3 below lists α functions that have been surveyed in this project.

As mentioned before, the greatest utility of cubic EOS's is for phase equilibrium calculations involving mixtures. At present there are essentially two basic methods of applying a cubic EOS

Reference	Temperature-dependency model
Redlich and Kwong [1949]	$\alpha = (\sqrt{T_r})^{-1}$
Soave [1972]	$\alpha = [1 + \kappa(1 - \sqrt{T_r})]^2$ $\kappa = 0.485 + 1.551\omega + 0.156\omega^2$
Peng and Robinson [1976]	$\alpha = [1 + \kappa(1 - \sqrt{T_r})]^2$ $\kappa = 0.374 + 1.542\omega + 0.269\omega^2$
Mathias and Copeman [1983]	$\alpha = [1 + C_1(1 - \sqrt{T_r}) + C_2(1 - \sqrt{T_r})^2 + C_3(1 - \sqrt{T_r})^3]^2$
Mathias [1983]	$\alpha = [1 + \kappa(1 - \sqrt{T_r}) - p(1 - T_r)(0.7 - T_r)]^2$ $\kappa = 0.485 + 1.551\omega + 0.156\omega^2$
Soave [1984]	$\alpha = 1 + \kappa(1 - T_r) + n(T_r^{-1} - 1)$
Stryjek and Vera [1986 (a,b)]	$\alpha = [1 + \kappa(1 - \sqrt{T_r})]$ $\kappa = \kappa_0 + \kappa_1(1 + \sqrt{T_r})(0.7 - T_r)$ $\kappa_0 = 0.378 + 1.489\omega + 0.171\omega^2 + 0.019\omega^3$
Twu et al. [1995]	$\alpha = T_r^{N(M-1)} e^{L(1-T_r)^{NM}}$

Table 3-3: List of α functions surveyed

to a mixture. Both are discussed briefly in Appendix B.8., as outlined in Walas [1985] and Mühlbauer and Raal [1995]. The most commonly used method is that of mixing rules to determine mixture parameters derived from those of individual components. Pure component a_i and b_i parameters are calculated using pure component properties. Mixing rules are then employed to express the EOS mixture parameters a_m and b_m as some function of composition and pure component a_i and b_i parameters. The simplest mixing rules are just mole-fraction-weighted sums of the corresponding parameters for each of the components of the mixture. The most commonly used mixing rule is the van der Waals one-fluid mixing rules:

$$a_m = \sum \sum x_i x_j a_{ij} \quad (3-57)$$

$$b_m = \sum \sum x_i x_j b_{ij} \quad (3-58)$$

In addition, combining rules are needed for the parameters a_{ij} and b_{ij} . The usual combining rules are:

$$a_{ij} = \sqrt{a_i a_j} (1 - k_{ij}) \quad (3-59)$$

$$b_{ij} = \frac{1}{2} (b_i + b_j) (1 - l_{ij}) \quad (3-60)$$

where k_{ij} and l_{ij} are the binary interaction parameters obtained by fitting EOS predictions to experimental VLE data for k_{ij} or VLE and density data for k_{ij} and l_{ij} . Generally, l_{ij} is set equal to zero, in which case,

$$b_m = \sum x_i b_i \quad (3-61)$$

For the fugacity coefficient of component i in a mixture, we now have for the Soave EOS:

$$\ln \hat{\phi}_i = \frac{b_i}{b_m} (Z - 1) - \ln(Z - B) - \frac{A}{B} \left[\frac{2 \sum_{j=1}^m x_j a_{ij}}{a_m} - \frac{b_i}{b_m} \right] \ln \left(\frac{Z + B}{Z} \right) \quad (3-62)$$

For the Peng-Robinson EOS:

$$\ln \hat{\phi}_i = \frac{b_i}{b_m} (Z - 1) - \ln(Z - B) - \frac{A}{2\sqrt{2}B} \left[\frac{2 \sum_{j=1}^m x_j a_{ij}}{a_m} - \frac{b_i}{b_m} \right] \ln \left(\frac{Z + (1 + \sqrt{2})B}{Z + (1 - \sqrt{2})B} \right) \quad (3-63)$$

The justification of the van der Waals one-fluid mixing rule comes from the virial EOS. From statistical mechanics, the second virial coefficient B , for pure components can be shown to be a function of temperature only, and the only composition dependence of these virial coefficients in mixtures is given by equation (3-31),

$$B = \sum \sum x_i x_j B_{ij}(T) \quad (3-31)$$

Expanding the van der Waals equation in powers of $\left(\frac{b}{V}\right)$, one has:

$$\frac{PV}{RT} = 1 + \sum_{n=1}^{\infty} \left(\frac{b}{V}\right)^n - \frac{a}{VRT} \quad (3-64)$$

Therefore,

$$B(x_i, T) = \sum \sum x_i x_j B_{ij}(T) = b - \frac{a}{RT} \quad (3-65)$$

From this one can deduce that for the low-density composition dependence of a cubic EOS to be the same as the theoretically correct virial expansion, a sufficient, but not necessary condition is that the cubic EOS parameters satisfy the van der Waals one-fluid mixing rule.

A shortcoming of the van der Waals one-fluid mixing rule is that it is applicable only to mixtures of relatively moderate solution non-ideality. Since many mixtures of chemical industrial interest exhibit great degrees of non-ideality, a mixing rule had to be determined to model the systems. Traditionally systems of a high degree of non-ideality have been described by activity coefficient models. Vidal [1978] and Huron and Vidal [1979] developed a mixing rule to produce successful description of some highly non-ideal systems. They did this by assuming that the excess Gibbs free energy is independent of pressure (which is an incorrect assumption [Sandler, 1992]) and then equated the excess free energy and EOS results at infinite pressure. Since,

$$G^E = A^E + PV^E \quad (3-66)$$

for G^E to remain finite at infinite pressure, V^E must be zero which requires that the van der Waals mixing rule for the b parameter be used. The mixing rule for the a parameter, then is:

$$a_m = b_m \left[\sum x_i \left(\frac{a_i}{b_i}\right) - \sigma G^E \right] \quad (3-67)$$

where σ is a numerical constant which depends on the particular EOS used. This mixing rule was the first to combine an EOS with an excess Gibbs free-energy model to represent strongly non-ideal solutions.

The Huron-Vidal mixing rule, however, has a collection of theoretical and computational difficulties as listed by Sandler et al. [1994]:-

1. The mixing rule may not be successful in describing non-polar hydrocarbon systems.
2. It does not satisfy the quadratic composition dependence required of the second virial coefficient.
3. Even though the Huron-Vidal approach allows the use of G^E models with EOS's, the parameters are not the same as those obtained when correlating data directly with the activity coefficient model. As a result, one cannot use parameter tables developed for excess Gibbs free energy models at low pressure with this EOS model. Tables are available in the DECHEMA Data Series.

Mollerup [1986], Gupte et al. [1986(b)], Michelsen [1990 (a),(b)], and Heidemann and Kokal [1990] have tried to correct for the inconsistencies of using excess Gibbs free energy models at the infinite pressure limit, as used in the Huron-Vidal model. The most successful of the proposed models was the Huron-Vidal second-order model. The advantage this model has over the Huron-Vidal was that current activity coefficient parameter tables could be used and this model when combined with the modified UNIFAC group contribution method, could be totally predictive. Sandler [1994] excellently outlines the model and illustrates its use with some results. However, the Huron-Vidal second-order model being a variation of the Huron-Vidal formulation, still does not satisfy the second virial coefficient boundary condition.

Another method to correct for the deficiencies of the Huron-Vidal is along the empirical approach and that is simply to add an additional composition dependence and parameter to the combining rules of the a parameter in the van der Waals one-fluid mixing rules. Generally the b parameter rule is left unchanged. Examples of the combining rules are listed in Table 3-4.

The combining rules indicated in Table 3-4 have provided good correlations of complex binary mixtures. However, these combining rules still have theoretical and conceptual difficulties associated with them.

1. These mixing rules when used in the van der Waals one-fluid mixing rules, result in the second virial coefficient being non-quadratic in composition, as a result not satisfying a theoretical boundary condition.

2. The second problem is the so-called “Michelsen-Kistenmacher Syndrome” as pointed out by Michelsen and Kistenmacher [1990]. If one applies the combining rule to a ternary system, the value of a_m obtained if two of the three components are considered to be identical is not the same as the a_m value calculated for the equivalent binary mixture.
3. Another problem, also pointed out by Michelsen and Kistenmacher [1990], is that for some combining rule, as above, the added composition-dependent term depends explicitly on mole fractions rather than on mole ratios. As a result, the added terms become less important as the number of components in a mixture increases, decreasing the mole fraction of each component. Thus, for example, the value of parameter a_{12} will be different in binary and multicomponent mixtures with the same species mole ratio.

Author	Combining Rule
Panagiotopolos and Reid [1986 (a,b)]	$k_{ij} = K_{ij} - (K_{ij} - K_{ji})x_i$
Adachi and Sugie [1986]	$k_{ij} = K_{ij} + l_{ij}(x_i - x_j)$
Sandoval et al. [1989]	$k_{ij} = K_{ij}x_i + K_{ji}x_j + 0.5(K_{ij} + K_{ji})(1 - x_i - x_j)$
Schwartzentruber and Renon [1989 (a,b)]	$k_{ij} = K_{ij} + l_{ij} \frac{m_{ij}x_i - m_{ji}x_j}{m_{ij}x_i + m_{ji}x_j} (x_i + x_j)$ <p>where</p> $K_{ji} = K_{ij}, l_{ji} = -l_{ij}, m_{ji} = 1 - m_{ij}, \text{ and } K_{ii} = l_{ii} = 0$

Table 3-4: Some of the combining rules surveyed

The perfect mixing and combining rule would need to satisfy known boundary conditions, i.e. at low density, result in a second virial coefficient which is quadratic in composition; and at high liquid-like densities produce G^E behaviour similar to that of current activity coefficient models. Researchers have believed that for a mixing and/or combining rule to satisfy the boundary condition, it would have to be density-dependent [Michel et al., 1989; Copeman and Mathias, 1986; and Sandler et al., 1986]. However, there is a conceptual problem with density-dependent mixing rules and that is that the order of the EOS with respect to volume changes depending on the number of components. This unfortunately violates the one-fluid model.

Fortunately, there is hope as a mixing rule has been developed which satisfies the boundary conditions without being density-dependent. The Wong and Sandler mixing rule [Wong and Sandler, 1992] is claimed to be “the theoretically correct mixing rule for cubic EOS’s”. In addition:

1. It allows the use of existing G^E parameter tables [Wong and Sandler, 1992];
2. Allows extrapolation over wide ranges of temperature and pressure [Huang and Sandler, 1993]; and
3. Provides the simplest method of extending UNIFAC or other low pressure prediction methods to high temperatures and pressures [Orbey et al., 1993].

The new mixing rules of Wong and Sandler are based on the following important observation:-

1. Although the van der Waals one-fluid mixing rule is a sufficient condition to ensure the proper composition dependence of the second virial coefficient, it is not a necessary condition. The van der Waals one-fluid mixing rule places constraints on two functions, a and b , to satisfy the single relation:-

$$B(x_i, T) = \sum \sum x_i x_j B_{ij}(T) = \sum \sum x_i x_j \left(b_{ij} - \frac{a_{ij}}{RT} \right) = b - \frac{a}{RT} \quad (3-68)$$

The mixing rule of Wong and Sandler uses the last equality of equation (3-68) as one of the restrictions on the EOS a and b parameters together with the following combining rule:

$$b_{ij} - \frac{a_{ij}}{RT} = \frac{1}{2} \left[\left(\frac{b_i - a_i}{RT} \right) + \left(\frac{b_j - a_j}{RT} \right) \right] (1 - k_{ij}) \quad (3-69)$$

where k_{ij} is a second virial coefficient binary interaction parameter.

2. The excess Helmholtz free energy on mixing is much less pressure dependent than the excess Gibbs free energy (refer to Figure 3-3).

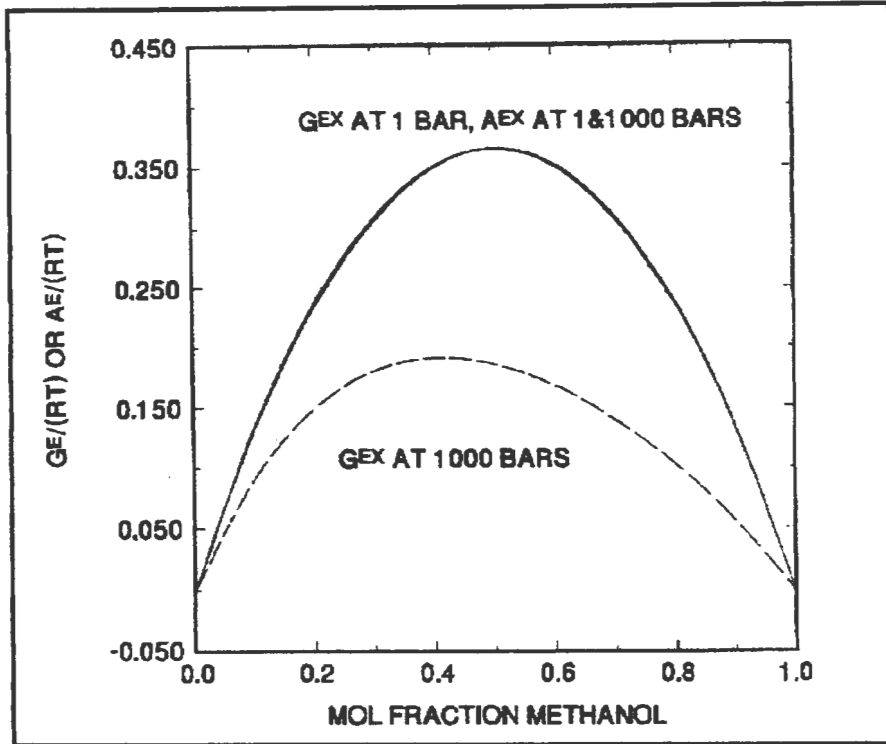


Figure 3-3: The excess Gibbs energy and Helmholtz energies of mixing for the methanol + benzene system at 1 bar and 1000 bar calculated from the Stryjek-Vera modification of the Peng-Robinson equation of state and the Wong and Sandler mixing rule (extracted from Sandler et al. [1994])

The second equation for the a and b parameters then comes from the condition that:

$$\begin{aligned}
 A_{EOS}^E(T, P = \infty, x_i) &= A^E(T, P = \infty, x_i) \\
 &= A^E(T, low P, x_i) \\
 &= G^E(T, low P, x_i)
 \end{aligned}
 \tag{3-70}$$

where the subscript EOS refers to the Helmholtz free energy derived from an EOS, while A^E and G^E without the subscripts indicate the free energy from activity coefficient models.

Combining the equations gives the following mixing rules:-

$$\frac{a_m}{RT} = Q \frac{D}{1-D'}
 \tag{3-71}$$

$$b_m = \frac{Q}{1-D} \quad (3-72)$$

where

$$Q = \sum \sum x_i x_j \left(b - \frac{a}{RT} \right)_{ij} \quad (3-73)$$

$$D = \sum x_i \frac{a_i}{b_i RT} + \frac{G^E(x_i)}{\sigma RT} \quad (3-74)$$

σ is a constant which depends on the EOS used (e.g. $\sigma = [\ln(\sqrt{2} - 1)]\sqrt{2}$ for the Peng-Robinson EOS. Any excess free energy (activity coefficient) model may be used for G^E .

Sandler et al. [1994] summarized the advantages of the mixing rule as follows:-

1. It extends the range and applicability of equations of state to mixtures that previously could only be correlated with activity coefficient models.
2. Activity coefficient parameters reported in databanks, such as the DECHEMA Data Series can be used directly and with good accuracy.
3. In many mixtures the free-energy model parameters in the EOS can be taken to be independent of temperature, thereby allowing extrapolation over large ranges of temperature and pressure.
4. The mixing rule can be used to make predictions at high pressure based on low-pressure prediction techniques, such as UNIFAC and other group contribution methods.

The full formulation of the Wong-Sandler mixing rules appears in Appendix B.

Mixing rule formulations for the Huron-Vidal (HV) (Huron and Vidal [1979]) and modifications thereof (Michelsen [1990(b)] (MHV1), Dahl and Michelsen [1990] (MHV2), Boukouvalas et al. [1994] (LCVM) and Orbey and Sandler [1995(b)] (HVO)) used in this project appear in Appendix B. A comprehensive classification of mixing rules was undertaken by Mühlbauer and Raal [1995] and is shown in Figure 3-4. Comprehensive comparisons of the abilities of the various mixing rules are available in Knudsen [1993], Wang et al. [1996], Orbey and Sandler

[1996], Pan and Guo [1996] and Orbey and Sandler [1997]. Michelsen [1996] even advises on the choice of matching mixing rules to excess models and Michelsen and Heideman [1996] list properties of EOS mixing rules derived from excess models.

There have been modifications and corrections to the Wong and Sandler mixing rule since its formulation in 1992. Orbey and Sandler [1995(a)] reformulated the mixing rule, in the process eliminating one of its parameters. Satyro and Trebble [1998] showed that at extremely high pressures (in the order of 15000 bar) the Wong and Sandler mixing rules produced negative heat capacities. They modified the Wong and Sandler mixing rule, however at the expense of maintaining the quadratic compositional relationship of the predicted second virial coefficient.

Twu and Coon [1996] recently developed a mixing rule (evolved from the work of Wong and Sandler [1992]) that they claim is more flexible than the Wong-Sandler mixing rules and avoids the problems associated with the Wong-Sandler mixing rules. The mixing rules depends only on composition and temperature. They have applied the mixing rule successfully to complex mixtures. The mixing rules for the a_m and b_m parameters are defined by Twu and Coon [1996] as follows:

$$b^* = \frac{b_{vdw}^* - a_{vdw}^*}{1 - \left(\frac{a_{vdw}^*}{b_{vdw}^*} + \frac{1}{c} \frac{A_{nr}^E}{RT} \right)} \quad (3-75)$$

$$a^* = b^* \left(\frac{a_{vdw}^*}{b_{vdw}^*} + \frac{1}{c} \frac{A_{nr}^E}{RT} \right) \quad (3-76)$$

Equations (3-75) and (3-76) reduce to the van der Waals one fluid mixing rules when A_{nr}^E is zero. Twu and Coon state that the major difference between their mixing rule and that of Wong-Sandler is that Wong-Sandler mixing rules do not reduce to the van der Waals mixing rules when A_{ws}^E is zero. The entire formulation for the Twu and Coon mixing rule is available in Twu and Coon [1996].

MIXING RULES

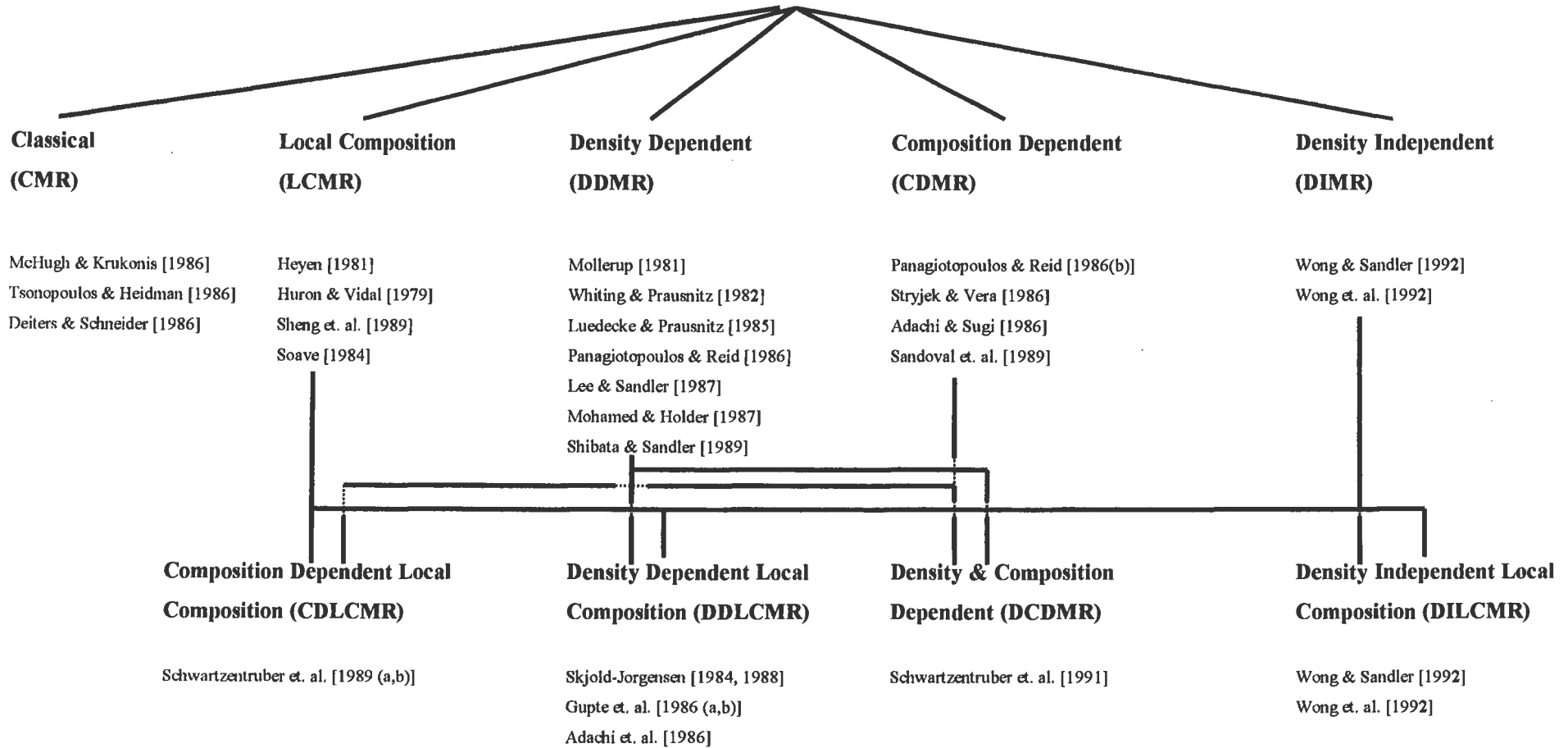


Figure 3-4: Classification of the various mixing rules according to Mühlbauer and Raal [1995]

3.4. ACTIVITY COEFFICIENTS

Excess properties provide global measures of deviations from ideal solution behaviour i.e. attention is focused on the mixture. However, it is useful to have in addition a local measure of deviation from ideal solution behaviour, which refers to a chemical component. The activity coefficient, γ_i , for component i in solution, provides such a measure.

Activity coefficients are derived from excess Gibbs energies and are related as follows:

$$\overline{G}_i^E = RT \ln \gamma_i \quad (3-77)$$

$$\ln \gamma_i = \frac{1}{RT} \left(\frac{\partial n G^E}{\partial n_i} \right)_{P,T,n_j} \quad (3-78)$$

where, \overline{G}_i^E is the partial molar excess Gibbs energy of component i and G^E is the excess Gibbs energy.

In practice, however, the process is reversed and excess Gibbs energies are evaluated from knowledge of activity coefficient as follows:

$$\frac{G^E}{RT} = \sum x_i \ln \gamma_i \quad (3-79)$$

For more detail on excess Gibbs energies and partial molar Gibbs free energy refer to Smith et al. [1996].

Many functional forms of the Gibbs energy have been proposed over the years. They have been expressed with respect to mole fraction, volume fraction and molecular surface fractions (volume fractions and molecular surface fractions are preferential when the molecules differ widely in size or chemical nature) with activity coefficients. Most of these correlations are purely empirical, based on intuition. There are eight well-known correlations for activity coefficient in use. They are as follows:

1. Margules
2. van Laar
3. Wilson
4. NRTL
5. UNIQUAC
6. Regular solution theory and its modification of Scatchard-Hildebrand
7. UNIFAC
8. ASOG

The latter three can be classified under Group contribution liquid-phase models.

A brief description of each of the above Gibbs excess models will now be presented. For more detail on these and other related models refer to Walas [1985], Gess et al. [1991], Milanowski and Anderko [1992] and Sandler [1994].

3.4.1. Margules Equation

This is the oldest of all correlations for activity coefficient. Margules originally proposed it in 1895. It is still in common use today and is capable of producing highly accurate results. The form of the equation is equivalent to a pure expansion in composition e.g. it can be derived from the Redlich-Kister expansion (for more detail on activity coefficient from series expansion refer to Gess et al. [1991]).

The simplest form of the Margules equation is known as the two-suffix equation (because Gibbs energy is a second order function of mole fractions (x_i):

$$\frac{G^E}{RT} = Ax_1x_2 \quad (3-80)$$

The activity coefficient are then given by the following expressions:

$$\ln\gamma_1 = Ax_2^2 \quad (3-81)$$

$$\ln\gamma_2 = Ax_1^2 \quad (3-82)$$

The applicability of the two-suffix Margules equation is limited because of its simplicity. The function is symmetric in relationship between x_1 and G^E . However, most real systems exhibit asymmetric behaviour, making the equation inadequate in the representation of non-ideal systems.

To account for more complicated behaviour, the three-suffix Margules equation was proposed. The equation is defined as follows:

$$\frac{G^E}{RT} = x_1 x_2 [A_{21} x_1 + A_{12} x_2] \quad (3-83)$$

The expressions for activity are now defined as follows:

$$\ln \gamma_1 = [A_{12} + 2(A_{21} - A_{12})x_1]x_2^2 \quad (3-84)$$

$$\ln \gamma_2 = [A_{21} + 2(A_{12} - A_{21})x_2]x_1^2 \quad (3-85)$$

The three-suffix Margules equation can be successfully applied to a wider range of systems than the two-suffix form. Gess et al. [1991] evaluates the performance of each of the variations of the Margules equations.

The four-suffix Margules equation, which is a fourth order function of mole fraction (x_i) is given by:

$$\frac{G^E}{RT} = x_1 x_2 [Ax_2 + Bx_1 - Dx_1 x_2] \quad (3-86)$$

The Margules equations can also be derived from Wohl's expansion for a binary system (Gess et al. [1991]).

The Margules equation, especially the high order forms, perform reasonably well for certain non-ideal systems. When these equations perform poorly, however, it can be attributed to the assumption of equal sized molecules.

3.4.2. van Laar Equation

The equation was developed to account for the size differences of the molecules. It can be developed from Wohl's expansion, with $q_1 \neq q_2$ (Gess et al. [1991]). The model was proposed by van Laar in 1910 and is based on the van der Waals equation. The excess Gibbs energy model is as follows:

$$\frac{G^E}{RT} = \frac{A_{12}A_{21}x_1x_2}{x_1A_{12} + x_2A_{21}} \quad (3-87)$$

The expressions for activity coefficients are given by:

$$\ln \gamma_1 = A_{12} \left[\frac{A_{21}x_2}{A_{12}x_1 + A_{21}x_2} \right]^2 \quad (3-88)$$

$$\ln \gamma_2 = A_{21} \left[\frac{A_{12}x_1}{A_{12}x_1 + A_{21}x_2} \right]^2 \quad (3-89)$$

Although the van Laar equation does take into account the size differences between molecules, it still does not model highly non-ideal systems well. This is as a result of the interactions between molecules not being properly characterized. Another problem with the activity coefficient correlations so far is that the effect of temperature on the excess Gibbs energy is not addressed. Since the constants are not dependent on temperature, the equations are limited to the treatment of isobaric systems.

3.4.3. Wilson Equation

The Wilson equation, developed by Wilson [1964] is an extension of the work done by Flory and Huggins. The model addresses the case where molecules of each component differ in size, and also incorporated an expression for the energy of interaction between two molecules. The Wilson equation is as follows:

$$\frac{G^E}{RT} = -x_1 \ln(x_1 + \Lambda_{12}x_2) - x_2(x_1\Lambda_{21} + x_2) \quad (3-90)$$

The expressions for the activity coefficients are given by:

$$\ln \gamma_1 = -\ln(x_1 + \Lambda_{12}x_2) + x_2 \left[\frac{\Lambda_{12}}{x_1 + \Lambda_{12}x_2} - \frac{\Lambda_{21}}{\Lambda_{21}x_1 + x_2} \right] \quad (3-91)$$

$$\ln \gamma_2 = -\ln(x_2 + \Lambda_{21}x_1) - x_1 \left[\frac{\Lambda_{12}}{x_1 + \Lambda_{12}x_2} - \frac{\Lambda_{21}}{\Lambda_{21}x_1 + x_2} \right] \quad (3-92)$$

where,

$$\Lambda_{ji} = \frac{\bar{V}_i}{\bar{V}_j} \exp\left(-\frac{\lambda_{ji} - \lambda_{jj}}{RT}\right) \quad (3-93)$$

and

\bar{V}_i is the molar volume of pure liquid component i ,

λ_{ji} is the interaction energy between components j and i , and

$(\lambda_{12} - \lambda_{11}), (\lambda_{21} - \lambda_{22})$ are the adjustable parameters.

The major disadvantage of the Wilson equation is the inability to predict limited miscibility regions for a system. This problem was noted and addressed by adding an additional C parameter to the Wilson equation (3-90) as follows:

$$\frac{G^E}{RT} = C[x_1 \ln(x_1 + \Lambda_{12}x_2) + x_2 \ln(x_1\Lambda_{21} + x_2)] \quad (3-94)$$

Equation (3-94) is known as the three-parameter Wilson model. The introduction of the C parameter, which has no physical significance, creates two serious problems:-

1. Extension of equation (3-94) to multicomponent mixtures becomes very complicated because the binary interaction parameter Λ_{ij} cannot be extended for use in the equation.

2. The Wilson parameters are inherently correlated and introduction of the C parameter further increases the interdependence of the parameters.

Another commonly used modification of the Wilson equation is that of Tsuboka and Katayama [1975].

3.4.4. NRTL Equation (Non-Random Two-Liquid Model):

Renon and Prausnitz [1968] proposed the three-parameter NRTL equation. It also used the concepts of local composition (like the Wilson equation), but had an additional term to account for the non-randomness in the solution. The NRTL equation is as follows:

$$\frac{G^E}{RT} = x_1 x_2 \left[\frac{\tau_{21} G_{21}}{x_1 + x_2 G_{21}} + \frac{\tau_{12} G_{12}}{x_2 + x_1 G_{12}} \right] \quad (3-95)$$

where,

$$\tau_{ji} = \frac{g_{ji} - g_{ii}}{RT} \quad (3-96)$$

$$G_{ji} = \exp(-\alpha_{ji} \tau_{ji}) \quad (3-97)$$

g_{ji} is a parameter for interaction between components j and i ,

$\alpha_{ji} = \alpha_{ij}$ is a non-randomness parameter, and

$(g_{12} - g_{22}), (g_{21} - g_{11}), \alpha_{12}$ are the adjustable parameters.

The expressions for the activity coefficients are given by:

$$\ln \gamma_1 = x_2^2 \left[\tau_{21} \left(\frac{G_{21}}{x_1 + x_2 G_{21}} \right)^2 + \frac{\tau_{12} G_{12}}{(x_2 + x_1 G_{12})^2} \right] \quad (3-98)$$

$$\ln \gamma_2 = x_1^2 \left[\tau_{12} \left(\frac{G_{12}}{x_2 + x_1 G_{12}} \right)^2 + \frac{\tau_{21} G_{21}}{(x_1 + x_2 G_{21})^2} \right] \quad (3-99)$$

The NRTL equation is more complicated in that there are three adjustable parameters. The equation can predict limited visibility ranges and has the added advantage that two of the parameters are temperature dependent. A disadvantage of the model though is the increased computer times in calculation encountered with the addition of the third parameter, and the correlation or interdependence of the parameters. Renon and Prausnitz [1968] vaguely related the third parameter to the inverse of the co-ordination number. The co-ordination number, a function of the number of molecules just touching a reference molecule, α was however found to be a strictly empirical factor not related to any mechanism in general.

Maria and Tassios [1973] found that $\alpha = -1$ gave an excellent representation of both miscible and partially immiscible binaries. Sandler [1997] suggests a value of $\alpha = 0.3$ for VLE and $\alpha = 0.2$ for liquid-liquid equilibria (LLE).

Raal and Brouckaert [1992] have reviewed the use of the NRTL equation in the prediction of LLE from experimental heats-of-mixing.

3.4.5. UNIQUAC Model (Universal Quasi-Chemical Theory)

The model was proposed by Abrams and Prausnitz [1975] and was an extension of the quasi-chemical lattice theory of Guggenheim. The major characteristics of the equation are:

1. Its applicability to multicomponent mixtures in terms of binary parameters only;
2. Applicability to LLE;
3. Built-in temperature dependence valid over at least a moderate range;
4. Superior representation for molecules of widely different molecular sizes; and
5. Its basis for predictive group contribution methods such as UNIFAC.

The only major disadvantage of the model is its algebraic complexity and the availability of r and q parameters.

In the model the excess Gibbs energy is represented by two parts:

$$G^E = G^E(c) + G^E(r) \quad (3-100)$$

where, $G^E(c)$ is the contribution owing to the difference in sizes and shapes of the molecules (configurational or combinatorial part); and

$G^E(r)$ is the contribution owing to energetic interactions (residual part).

The expressions for the excess Gibbs energies for the configurational and residual parts are given by equations (3-101) and (3-102) respectively.

$$\frac{G^E(c)}{RT} = x_1 \ln \frac{\Phi_1}{x_1} + x_2 \ln \frac{\Phi_2}{x_2} + \frac{z}{2} \left(q_1 x_1 \ln \frac{\theta_1}{\phi_1} + q_2 x_2 \ln \frac{\theta_2}{\phi_2} \right) \quad (3-101)$$

$$\frac{G^E(r)}{RT} = -q_1 x_1 \ln(\theta_1 + \theta_2 \tau_{21}) - q_2 x_2 \ln(\theta_2 + \theta_1 \tau_{12}) \quad (3-102)$$

The expression for activity coefficient is also comprised of two parts:

$$\ln \gamma_i = \ln \gamma_i^C + \ln \gamma_i^R \quad (3-103)$$

The configurational and residual components of activity coefficient are defined by equations (3-104) and (3-105) respectively.

$$\ln \gamma_i^C = \ln \frac{\Phi_i}{x_i} + \frac{z}{2} q_i \ln \frac{\theta_i}{\Phi_i} + \Phi_j \left(l_i - \frac{r_i}{r_j} l_j \right) \quad (3-104)$$

$$\ln \gamma_i^R = -q_i \ln(\theta_i + \theta_j \tau_{ji}) + \theta_j q_i \left(\frac{\tau_{ji}}{\theta_i + \theta_j \tau_{ji}} - \frac{\tau_{ij}}{\theta_j + \theta_i \tau_{ij}} \right) \quad (3-105)$$

where, γ_i^C is the combinatorial contribution of activity coefficient;

γ_i^R is the residual contribution of activity coefficient;

$$\tau_{ji} = \exp \left(\frac{-(u_{ji} - u_{ii})}{RT} \right) \quad (3-106)$$

u_{ji} is the parameter of interaction between components j and i ;

q_i is the area parameter of component i ;

r_i is the size parameter of component i ;

z is the coordination number (set equal to 10);

$$l_i = \frac{z}{2}(r_i - q_i) - (r_i - 1) \quad (3-107)$$

$$\Phi_i = \frac{x_i r_i}{x_1 r_1 + x_2 r_2} \quad (3-108)$$

$$\theta_i = \frac{x_i q_i}{x_1 q_1 + x_2 q_2} \quad (3-109)$$

$(u_{12} - u_{22}), (u_{21} - u_{11})$ are the adjustable parameters.

The modified UNIQUAC equation as proposed by Anderson and Prausnitz [1978] is also widely used to model complex systems. The activity coefficient for this modification is given by:

$$\ln \gamma_i = \ln \frac{\Phi_i}{x_i} + \frac{z}{2} q_i \ln \frac{\theta_i}{\Phi_i} + \Phi_j \left(l_j - \frac{r_i}{r_j} l_j \right) + C q'_i \left[- \ln \left(\theta'_i + \theta'_i \tau_{ji} + \frac{\theta'_j \tau_{ji}}{\theta'_i + \theta'_j \tau_{ji}} - \frac{\theta'_j \tau_{ij}}{\theta'_j + \theta'_j \tau_{ij}} \right) \right] \quad (3-110)$$

where the parameters are as defined before, but the primed parameters are now modified parameters of Anderson and Prausnitz [1978]. The modified structural area parameter (q') was introduced by Anderson and Prausnitz [1978] to obtain better agreement between mixture containing polar components such as water or alcohol. In the modified UNIQUAC equation, C is an adjustable parameter that is usually set equal to unity. If C is set equal to unity and q' is set equal to q for both components, the modified UNIQUAC reduces to the original UNIQUAC of Abrams and Prausnitz [1975].

To improve the temperature dependence of the UNIQUAC equation Skjold-Jorgensen et al. [1980] proposed an equation for the co-ordination number (z) described as a function of temperature:

$$z = 35.2 - 0.1272T + 0.00014T^2 \quad (3-111)$$

Raal and Naidoo [1990] proposed an exponential temperature dependence for z as follows:

$$z = A + \frac{B}{\exp\left(\frac{T - T_o}{T_o}\right)} \quad (3-112)$$

where $T_o = 273.15$ K and the constants A and B are evaluated from H^E data.

3.4.6. Group contribution liquid-phase models

Up to this point, all activity coefficient models mentioned required experimental data so that the binary interaction parameters could be determined. However, as the variety of organic compounds of interest in chemical processes is large, it leads to an uncountable number of possible interaction parameters. A situation may arise where an engineer needs to make activity coefficient prediction for a system, or at conditions, for which experimental data are not available. Thus if one could find a liquid model that is based on well-defined thermodynamics or statistical mechanical assumption, so that the parameters that appear can be related to the molecular properties of the species in the mixture, the resulting model would have a predictive ability. This is where group contribution liquid-phase model come in so handy. The most notable of these are as follows:

1. The regular solution theory which is determined from the theory of van Laar, and its modification as developed by Scatchard and Hildebrand (Hildebrand and Scott [1962]). The relationship developed for the excess Gibbs energy and activity coefficients are based on solubility parameters. The regular solution theory is derived and illustrated in detail in Sandler [1989].
2. The analytical solution of groups model (ASOG). It was developed by Derr and Deal [1969] and is based on the principle of independent action as proposed by Langmuir. The principle is that the properties of complex molecules can be evaluated on the basis that smaller groups of atoms within the molecule contribute in a fixed way to the molecule's property, independent of the group within the molecule. Group interaction parameter tables and greater detail is available in Kojima and Tochigi [1979].
3. The UNIFAC (UNIQUAC Functional-Group Activity Coefficient) method. It is a functional group method and was developed by Fredenslund et al. [1977]. The model is based on the UNIQUAC model. In the UNIFAC model, both the combinatorial and residual terms are obtained from group contribution methods. The activity coefficient for each species is

assumed to be made up of the two contributions (just as in the UNIQUAC method) by equation (3-103). However the combinatorial and residual terms are now expressed by equations (3-113) and (3-118) respectively.

$$\ln \gamma_i^C = \left(\frac{\ln \Phi_i}{x_i} + 1 - \frac{\Phi_i}{x_i} \right) - \frac{1}{2} z q_i \left(\frac{\ln \Phi_i}{\theta_i} + 1 - \frac{\Phi_i}{\theta_i} \right) \quad (3-113)$$

where,

$$\Phi_i = \frac{x_i r_i}{\sum_j x_j r_j} \quad (3-114)$$

$$\theta_i = \frac{x_i q_i}{\sum_j x_j q_j} \quad (3-115)$$

For equations (3-114) and (3-115) summation is over all components.

$$r_i = \sum_k v_{ki} R_k \quad (3-116)$$

$$q_i = \sum_k v_{ki} Q_k \quad (3-117)$$

For equations (3-116) and (3-117) summation is over all groups.

where, R_k is the volume parameters for group k ;

Q_k is the surface area parameter for group k ;

v_{ki} is the number of groups of type k in molecule i ;

x_i is the liquid mole fraction of component i ; and

z is the coordination number = 10.

The residual term is given by:

$$\ln \gamma_i^R = \sum_k v_{ki}^{(i)} (\ln \Gamma_k - \ln \Gamma_k^{(i)}) \quad (3-118)$$

where,

$$\ln \Gamma_k = Q_k \left[1 - \ln \left(\sum_m \theta_m \psi_{mk} \right) - \sum_m \left(\frac{\theta_m \psi_{km}}{\sum_n \psi_{nm}} \right) \right] \quad (3-119)$$

$$\psi_{nm} = \exp \left(-\frac{a_{nm}}{T} \right) \quad (3-120)$$

$$\theta_m = \frac{Q_m X_m}{\sum_n Q_n X_n} \quad (3-121)$$

$$X_m = \frac{\sum_j v_{mj} x_j}{\sum_j \sum_n v_{nj} x_j} \quad (3-122)$$

a_{mn} is the group interaction parameter for the interaction between groups m and n .

$\Gamma_k^{(i)}$ is the residual activity coefficient of group k in a reference solution containing only molecules of type i .

There have been modifications and further developments to the UNIFAC equation e.g. Fredenslund and Rasmussen [1985], Gmehling and Weidlich [1986] and Larsen et al. [1987].

Tables of the groups and values for the group parameters are available in Fredenslund et al. [1977].

3.5. CRITICAL PROPERTIES

The accurate knowledge of critical properties of pure fluids and mixtures is important from both a theoretical and practical viewpoint. Since the phenomena are closely linked with intermolecular interactions, they provide valuable insight into general fluid phase behaviour. In high-pressure distillation, supercritical extraction and the recovery of oil and gas from high-pressure reservoirs, accurate knowledge of the mixture critical properties and behaviour is necessary for efficient process design. The proximity of plant operating conditions to the critical region, for example, must be known precisely and inability to generate this information accurately may increase plant investment.

For a pure fluid the critical point is reached when the physical properties of the coexisting phases become identical. Considerable information is available on pure fluid critical properties, viz.

critical temperature, pressure and volume. For binary and other multicomponent systems the vapour-liquid critical point is in addition characterised by an equivalence of composition in both phases.

The prediction of multicomponent critical properties as a function of composition is mathematically very complex, and systems exhibit a considerable variety of behaviour in the critical region. Scott and van Konynenburg [1970], and Sadus [1994] give excellent reviews on critical region prediction, calculation, and classification. Reference should be made to Sadus [1994] for the classification of phase behaviour of binary mixtures with respect to different critical phenomena.

Earlier predictive techniques contain much approximation and are no longer satisfactory or advisable, since much more rigorous methods have been satisfactorily demonstrated. Modern techniques vary in complexity, but in essence, are all based on the fundamental condition required for the existence of a critical point, i.e. the critical state of an n -component mixture as given by Gibbs [1928], involving two simple mathematical expressions. They are in the form of the following determinants:

$$U = \begin{vmatrix} \frac{\partial^2 G}{\partial x_1^2} & \frac{\partial^2 G}{\partial x_1 \partial x_2} & \cdots & \frac{\partial^2 G}{\partial x_1 \partial x_{n-1}} \\ \frac{\partial^2 G}{\partial x_2 \partial x_1} & \frac{\partial^2 G}{\partial x_2^2} & \cdots & \frac{\partial^2 G}{\partial x_2 \partial x_{n-1}} \\ \vdots & \vdots & \ddots & \vdots \\ \frac{\partial^2 G}{\partial x_{n-1} \partial x_1} & \frac{\partial^2 G}{\partial x_{n-1} \partial x_2} & \cdots & \frac{\partial^2 G}{\partial x_{n-1}^2} \end{vmatrix} \quad (3-123)$$

$$M = \begin{vmatrix} \frac{\partial U}{\partial x_1} & \frac{\partial U}{\partial x_2} & \cdots & \frac{\partial U}{\partial x_{n-1}} \\ \frac{\partial^2 G}{\partial x_2 \partial x_1} & \frac{\partial^2 G}{\partial x_2^2} & \cdots & \frac{\partial^2 G}{\partial x_2 \partial x_{n-1}} \\ \vdots & \vdots & \ddots & \vdots \\ \frac{\partial^2 G}{\partial x_{n-1} \partial x_1} & \frac{\partial^2 G}{\partial x_{n-1} \partial x_2} & \cdots & \frac{\partial^2 G}{\partial x_{n-1}^2} \end{vmatrix} \quad (3-124)$$

where the partial derivatives with respect to x_i are obtained at constant values of P , T , and $x_{k, k \neq i, n}$. Both of these, equations (3-123) and (3-124), must equal zero at the critical point.

For the case of a binary system, equations (3-123) and (3-124) are drastically simplified to equations (3-125) and (3-126) respectively.

$$\left(\frac{\partial^2 G}{\partial x_1^2} \right)_{P,T} = 0 \quad (3-125)$$

$$\left(\frac{\partial^3 G}{\partial x_1^3} \right)_{P,T} = 0 \quad (3-126)$$

The Gibbs free energy is a function of temperature, pressure and composition:

$$G = G(T, P, x_1, x_2, \dots, x_{n-1}) \quad (3-127)$$

To ensure that equations (3-123) and (3-124) are suitable for use with pressure explicit EOS's, it is necessary to express the partial derivatives of the Gibbs free energy in terms of partial derivatives of the molar Helmholtz free energy and partial derivatives of pressure through transformation of the independent variables. This is done using the following equation, which is a fundamental thermodynamic relation.

$$G = A + PV \quad (3-128)$$

Thus, by the use of an appropriate equation of state and the conditions imposed by equations (3-123) and (3-124), one can predict the critical temperature and pressure of a fluid mixture.

However, in reality the mathematical techniques for solving the problem are not trivial, as in instances it leads to the solution of two highly non-linear algebraic equations. Hence the use of various prediction techniques which are well documented (Chueh and Prausnitz [1967(b)], Spear et al. [1969, 1971], Pak and Kay [1972], Hicks and Young [1975, 1976], Peng and Robinson [1977], Heidemann and Khalil [1980], Michelsen [1984], Billingsley and Lam [1986], Sadus and Young [1987], and Christou et. al. [1989, 1991(a,b)]).

The solution of simultaneous non-linear algebraic equations is not needed in all techniques. Some techniques are more correlative than predictive. Chueh and Prausnitz [1967(b)] used correlations to determine the variation of critical temperature and volume with mole fraction. Having obtained

the critical temperature and volume, they then used an altered form of the Redlich-Kwong equation of state to predict the critical pressure. Other techniques are rigorous and have large computational times (Joffe and Zudkevitch [1967]). This is as a result of the solution of non-linear differential equations. Here again techniques vary on how the sets of equations are solved. Numerical methods (Spear et al. [1969, 1971]), graphical search procedures (Heidemann and Khalil [1980]), etc. are used as tools for the various methods. Various review papers are available which go into great detail on the predictive techniques and the problems associated with these techniques (Sadus [1994], and Hicks and Young [1975]). Recently greatly enhanced speed and reliability have been achieved in search methods developed by Nagarajan et al. [1991(a,b)]. These methods are mathematically very complex and have not been tackled in this project.

The method adopted in this project is based on the publication by Deiters and Schneider [1976]. Instead of solving equations (3-125) and (3-126), the critical condition equations were replaced by an equivalent equation written in terms of the derivatives of Helmholtz free energy.

$$\frac{1}{A_{vv}} (A_{vv}A_{xx} - A_{vx}^2) = 0 \quad (3-129)$$

$$\frac{1}{A_{vv}^2} (A_{xxx}A_{vv}^2 - 3A_{vxx}A_{vx}A_{vv} + 3A_{vxx}A_{vx}^2 - A_{vvv}A_{xx}A_{vx}) = 0 \quad (3-130)$$

Here each subscript “v” and “x” denotes a partial differentiation of the molar Helmholtz energy (A) with respect to volume (V) and mole fraction (x). Solving this set of equations for an appropriate EOS generates a series of solutions for critical pressure and critical temperature for varying mole fraction. From these solutions the critical volume and critical compressibility factor can also be calculated. From a cross-plot of critical pressure against mole fraction and critical temperature against mole fraction, a plot of critical pressure against critical temperature (T - P locus) can be obtained. This is the typical diagram for illustrating the phase behaviour of a binary mixture.

A sufficiently accurate computation of the T - P critical locus should permit placement of the critical point in a P - x - y HPVLE data set, particularly for systems or conditions where the critical region is difficult to determine experimentally. Critical locus information can thus define the practical operating range for high-pressure separation equipment more precisely.

The method adopted from Deiters and Schneider [1976] is demonstrated in their paper for the Redlich-Kwong EOS. In this project the method was modified for the Peng-Robinson EOS. The derivation for the Peng-Robinson EOS modification is available in Appendix B.19. The predictive abilities of the Redlich-Kwong, Soave, Peng-Robinson and Peng-Robinson-Stryjek-Vera have been compared by Ramjugernath et al. [1997].

3.6. CONSISTENCY TESTS FOR HPVLE

The measurement of temperature, pressure and both liquid and vapour compositions represents an “overdetermination” of VLE for a binary system since any one of these variables can be determined from the Gibbs-Duhem equation. It is therefore possible to calculate any one of these variables and to compare its value over the entire composition range with the measured data. This constitutes a test of thermodynamic consistency of the data.

However, the computation of the vapour phase compositions in HPVLE is much more difficult and less certain than for LPVLE since in HPVLE there is a strong pressure dependence of the mixture molar volume at saturation. Also, to account for vapour phase non-idealities an equation of state is used to model the vapour phase. In addition, the more volatile component is frequently supercritical and special attention must be paid to the standard state definitions (as discussed earlier).

Raal and Mühlbauer [1998] and Ramjugernath et al. [1997] have reviewed HPVLE consistency tests. They have described the essential elements of four thermodynamic consistency testing procedures. The consistency tests are as follows:-

- 1) Chueh et al. [1965];
- 2) Won and Prausnitz [1973];
- 3) Christiansen and Fredenslund [1975]; and
- 4) Mühlbauer and Raal [1991].

The first two tests are extensions of the area test for LPVLE (LPVLE consistency testing is reviewed by Raal and Mühlbauer [1998]), and as a result suffer, although to a lesser extent, from the deficiencies of the area tests. The Mühlbauer and Raal [1991] test is a modification of the Chueh et al. [1965] test, but is based only on the vapour phase compositions. Adler et al. [1960], Chang and Lu [1969], Kollar-Hunek et al. [1986], and Jackson and Wilsak [1995] have also reviewed generalised consistency tests. In a recent publication by Bertuccio et al. [1997] a method for the testing of binary and isothermal vapour-liquid equilibrium data at moderate and high pressures has been proposed that makes use of a direct method approach.

Of the four consistency test procedures reviewed by Raal and Mühlbauer [1998] and Ramjugernath et al. [1997], the Won and Prausnitz [1973] and Christiansen and Fredenslund

[1975] tests are the most rigorous. The Won and Prausnitz [1973] also requires a model equation for the excess free energy. The latter test contains fewer assumptions, but is also more complex. Both tests yield vapour phase compositions from high pressure P - x data and fulfil the role of a high-pressure reduction procedure. They also produce Henry's constant.

Greater details on the four consistency tests are available in Appendix B.19.

3.7. DETERMINATION OF SECOND VIRIAL COEFFICIENTS

The second virial coefficients are generally obtained from P - V - T measurement using equipment described in Appendix A.4. Jones and Kay [1967], Barber et al. [1982] and Wilson et al. [1984] detail the computational methods for the determination of the second virial coefficient from P - V isotherms, which are summarized here.

Jones and Kay [1967] and Barber et al. [1982] represented low-pressure data by a truncated virial equation as follows:

$$\frac{PV}{nRT} = 1 + \frac{Bn}{V} + \frac{Cn^2}{V^2} \quad (3-131)$$

Equation (3-131) was rearranged to give for each data point (along an isotherm):

$$y_k = \left(\frac{P_k V_k}{nRT} - 1 \right) \frac{V_k}{n} = B + \frac{Cn}{V_k} \quad (3-132)$$

Values of the virial coefficients (B and C) and the number of moles (n) were obtained from a set of isothermal compressibility measurements by minimizing the sum of the squares of the deviations of all the experimental points from the regression line given by equation (3-132).

The computation method of Wilson et al. [1984] made use of the truncated virial equation:

$$Z = 1.0 + \frac{B}{V} \quad (3-133)$$

The computational procedure involved adjusting the intercept in equation (3-133) to unity in order to determine the number of moles. The second virial coefficient (B) was then determined by least squares from equation (3-133) using only those points that are linear (determined by standard statistical tests).

A slightly modified approach for computation of virial coefficients, developed in this project, is described in Section 8.8.

CHAPTER FOUR

EXPERIMENTAL APPARATUS: DESIGN, CONSTRUCTION AND DEVELOPMENT

4.1. HISTORY OF HPVLE STUDIES IN THE DEPARTMENT

The experimental apparatus developed and its associated equipment used in this project are as a result of nearly two decades of research and development undertaken in the School of Chemical Engineering at the University of Natal under the supervision of Prof. J.D. Raal.

The study and subsequent development of HPVLE equipment began in the early 1980's when SASOL commissioned the School to measure VLE data for certain components of interest to them in their coal liquefaction process, at the extreme conditions of 500 °C and 200 bars. Harel initiated the study in 1982. Preliminary design and construction of equipment was undertaken during this period. Bradshaw furthered the studies between 1983 to 1985 and proceeded to select and construct liquid and vapour sampling devices. During Bradshaw's study, the extreme conditions of temperature and pressure requested by SASOL were changed to slightly less demanding operating conditions of 250 °C and 200 bars. The development and research undertaken by Bradshaw are detailed in his MSc thesis (Bradshaw [1985]). The major difficulty encountered by Bradshaw, one that seems to be encountered by all researchers, is that of sampling the equilibrium liquid phase.

At the end of Bradshaw's study, the measurement of HPVLE (in particular the sampling of the equilibrium phases) had not been perfected. Bradshaw had problems with uniformity of the air-bath and equilibrium cell temperatures and the liquid phase compositions measured showed an incorrect bias towards the more volatile component in the systems measured. Due to time constraints these problems were not rectified and it was left to Mühlbauer to deal with them when he began his research into HPVLE in 1987.

Mühlbauer [1990] extensively modified the equipment of Bradshaw [1985]. He perfected the liquid and vapour sampling devices, re-designed the air-bath and constructed certain auxiliary equipment. Details of the work undertaken by him are available in his thesis (Mühlbauer [1990]).

However, Mühlbauer's research still left some unanswered questions and prompted us to determine how far one could push technology to produce a more advanced HPVLE apparatus.

Some questions asked at the beginning of the project to determine objectives are:-

1. Could the experimental apparatus be made more compact and versatile?
2. Could a better sampling method be developed for analysis of the equilibrium phases?
3. Could one detect the formation of a second liquid phase (if it did exist)?
4. Could multiple phases be sampled with the sampling method chosen?
5. Was the experimental data obtained for the propane + 1-propanol system measured by Mühlbauer [1990] correct? The data had to be verified and it had to be determined if the system could be better modelled.

All of these questions led to the design and construction of a HPVLE apparatus that will be described in this section. The responses to the questions posed produced the following equipment design in summary:-

1. The equipment was of the static type. It was extremely compact, with the isothermal environment being an air-bath with dimensions of 1 m x 0.75 m x 0.5 m. The equilibrium cell was variable in volume, which made it capable of undertaking P - V - T measurements and VLE measurements via the dew and bubble point methods.
2. The sampling method chosen was based on a recommendation of Raal and Mühlbauer [1994]. Use was made of six-port two-position GC sampling valves as the sampling device. The equilibrium phase samples were circulated through the sample loop of the GC sampling valves by centrifugal action of the stirrers on the equilibrium cell contents.
3. The formation of multiple phases and the phase interfaces could be detected visually. This was possible as the equilibrium cell had two pairs of illuminated sapphire viewing windows. The windows were 33 mm in diameter and were 14 mm thick. Each set of windows, once installed, offered a viewing diameter of 22 mm.
4. The apparatus was designed to enable the sampling of two liquid phases and a vapour phase. Each of the sampling devices was a six-port two-position GC sampling valve. A composite stirrer had to be designed to enable stirring of all the phases and to enable flow of each of the phases through the sampling loops of their respective sampling valves.

The apparatus designed was of the static type for the following reasons:-

1. The research group had extensive experience in the use of static equipment.
2. The experimental work involved with the static method was capable of being undertaken by a single researcher.
3. Static type equipment is generally much cheaper and less time consuming to construct than dynamic types. Long delays for delivery of equipment and spare parts for specialised dynamic methods were expected in South Africa where these items are usually not available.

Aspects of the experimental apparatus that will be covered in this sections are as follows:-

1. The equilibrium cell and piston assembly.
2. Method of agitation of the equilibrium cell contents.
3. Method of sampling the liquid and vapour phases.
4. Method of homogenising the equilibrium samples (Jet-mixers).
5. Isothermal environment for the equilibrium cell (Air-bath).
6. Safety features.
7. Temperature and pressure measurement.

Ancillary equipment that was used in this project is described in Appendix C.

4.2. EXPERIMENTAL APPARATUS: DESCRIPTION AND CONSTRUCTION

4.2.1. The equilibrium cell and piston assembly

The main body of the experimental apparatus consisted of an equilibrium cell and a piston assembly. The piston, which was driven by a stepper motor, enabled the equilibrium cell volume to be varied by displacement of the piston in the equilibrium cell. Figure 4-1 illustrates the body of the experimental apparatus. See also Photograph 4-1.

The equilibrium cell was machined from a solid billet (stainless steel type 316) of diameter 120 mm and height 200 mm. The billet was bored to a diameter of 40 mm and length of 190mm (this gave a compression ratio of 2:1 with the piston). The effective resulting internal volume (including composite stirrer) of the equilibrium cell was approximately 200 ml. Two pairs of synthetic sapphire windows (33 mm in diameter and 14 mm thick, supplied by LABOTEC) were

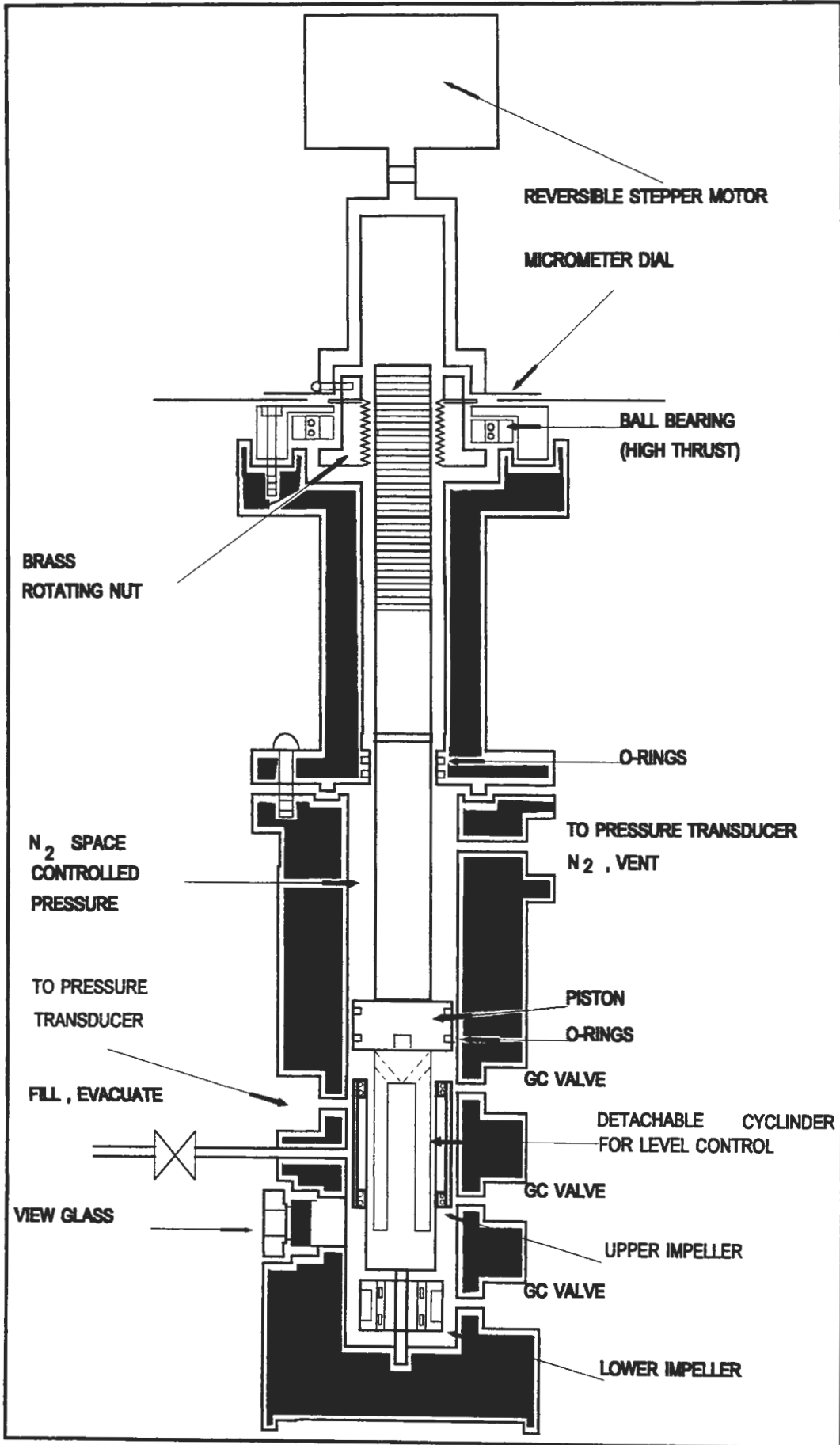
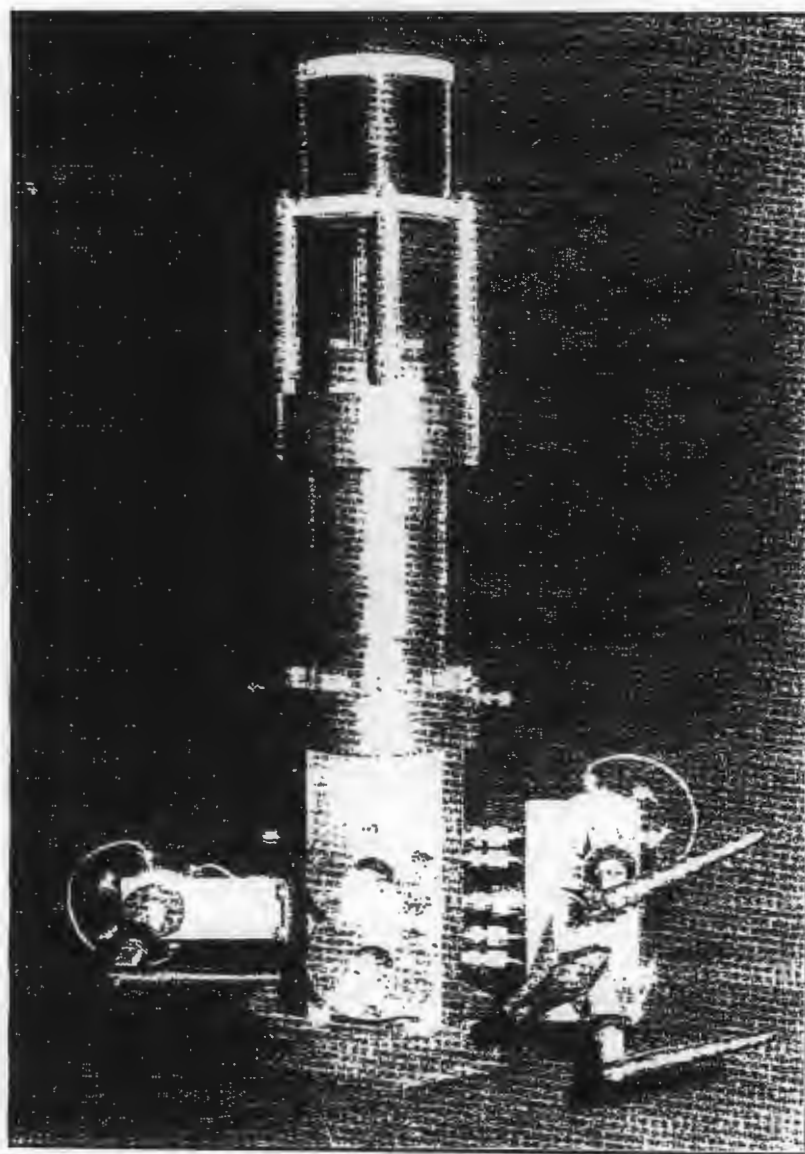


Figure 4-1: Schematic of the equilibrium cell assembly

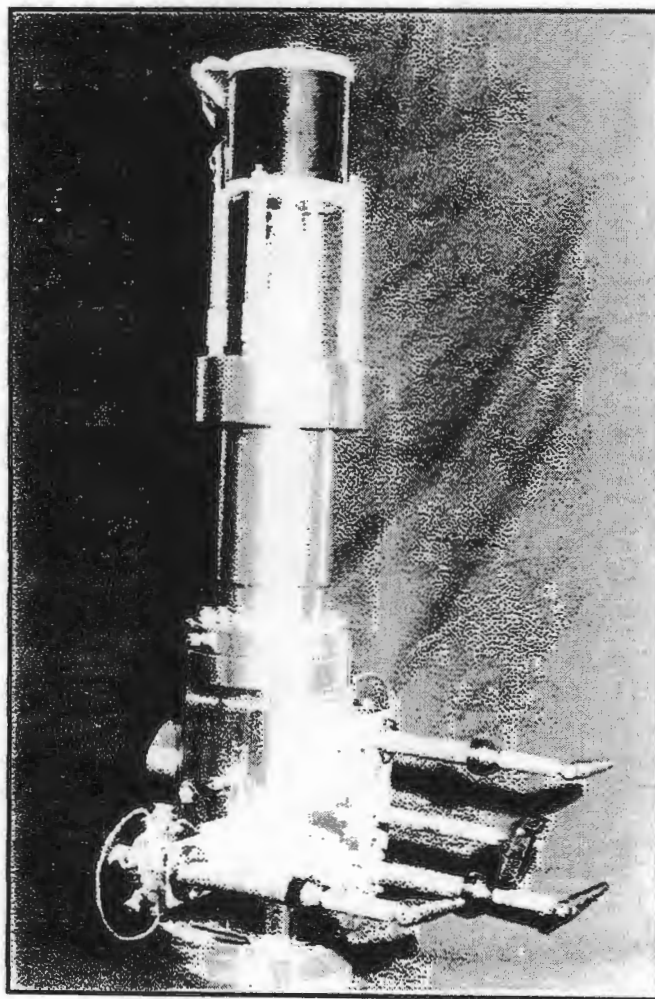
placed in special housings that bolted onto the equilibrium cell body (see Photograph 4-1). Five 8 mm mild steel bolts positioned and held each housing onto the equilibrium cell body. Figures 4-2 and 4-3 illustrate the details of the sapphire window housings.

Sealing between the sapphire window housings and the equilibrium cell body was achieved with Viton "o"-rings. The sapphire window housings were constructed of 316 stainless steel (see Figure 4-2 and Photograph 4-1) and the sapphire windows were encased in a gasket type material (see Figure 4-3) which then fitted snugly into the stainless steel housing. Sealing of the sapphire windows against the gasket type material housing was also accomplished with Viton "o"-rings.



Photograph 4-1: Front view of the main assembly of the apparatus

Various problems were encountered in the sealing of the sapphire windows. The first gasket type material used was Rulon. However, Rulon suffered from creep at high temperatures and pressures and was also attacked by some of the chemicals used in this study. Bronze impregnated Teflon was then tried, but it also suffered from creep and extruded under high temperatures and pressures. Finally, we resorted to a sapphire window encasing made from a combination of two materials, Axiol and bronze impregnated Teflon. This worked very satisfactorily and no sealing problems have been experienced on the sapphire window housings since its use, even at the operating limits of the equilibrium cell that are 175 °C and 175 bar. The material that many researchers claim to be the ultimate for sealing purposes and for use as housing is Kalrez. Unfortunately, Kalrez is not available in South Africa and a supplier for the material could not be located.



Photograph 4-2: Side-view of the main assembly of the apparatus

The viewing paths for the sapphire windows were illuminated with small 5 watt light bulbs. The small light bulbs were housed in a pyrex tube. They were therefore not in direct contact with the isothermal air-bath environment, which when in operation is at high temperature.

The piston was housed in a piston assembly (see Figure 4-1 and Photograph 4-1). The piston housing was machined from a solid stainless steel billet of 120 mm diameter. The piston was held in place by a high strength brass nut and a high-trust ball bearing. Figure 4-4 illustrates the piston. Sealing of the piston in the equilibrium cell was via two Viton "o"-rings fitted into grooves cut onto the head of the piston (see Figure 4-4). Sealing of the nitrogen compartment was also via Viton "o"-rings fitted into a groove on the shaft of the piston. The piston shaft (M16) was partially threaded. The pitch was 2 mm threads. A slot was cut into the shaft and together with a guide pin, which fitted into the slot, acted as a guide mechanism for the piston. The pin and slot also acted as a limiter for displacement of the piston. The piston was driven by a stepper motor (details of the stepper motor and its circuitry are available in the Appendix C).

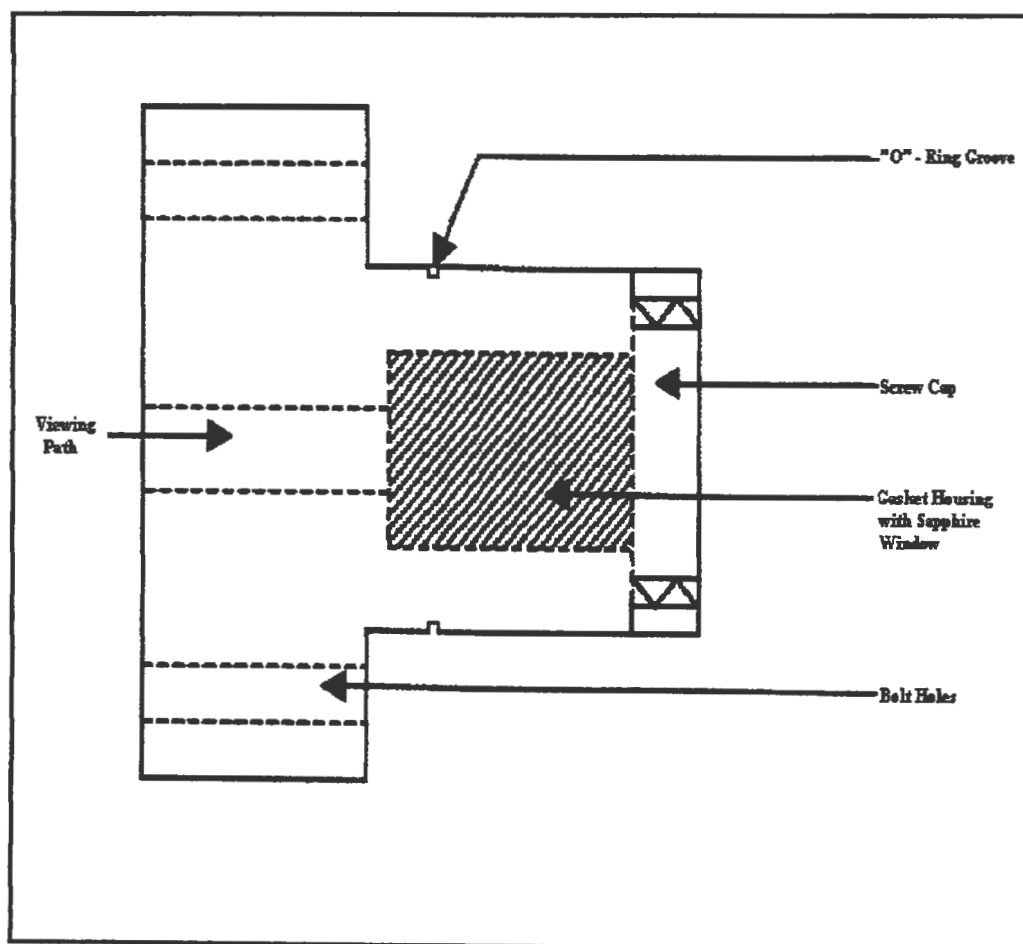


Figure 4-2: Stainless-steel housing for the sapphire window

A liquid manipulation attachment was also designed. It could be screwed into the piston head. Figures 4-1 and 4-4 illustrate the attachment. The attachment has two channels drilled into it, as indicated in Figure 4-1, to allow for vapour flow, which facilitated the entrainment of vapour into the liquid during stirring (this sped up the rate of attainment of equilibrium). The attachment was used to manipulate the liquid-level in the cell. This was achieved by moving the piston, which results in displacement of fluid in the equilibrium cell, changing the liquid-level.

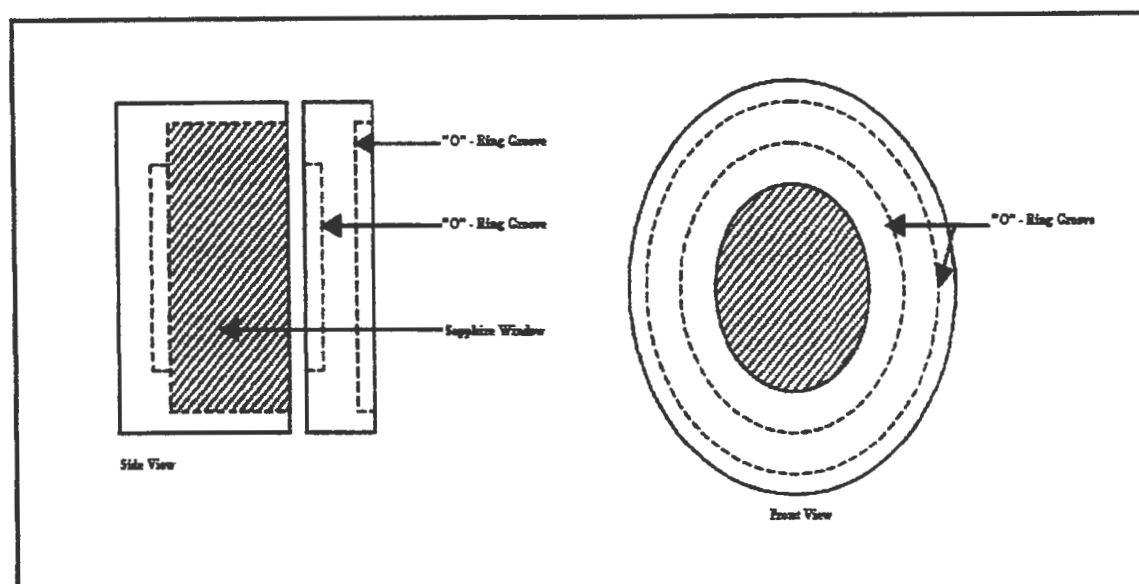


Figure 4-3: Housing for the sapphire windows that was made from gasket-type material

A micrometer dial was incorporated into the design, so that the exact number of revolutions that the stepper motor had made could be measured. By counting the number of revolutions made by the motor and knowing the pitch of the threads on the threaded portion of the piston, the length that the piston had moved in the equilibrium cell could be calculated.

A problem encountered by a number of researchers is the determination of the liquid-level and control thereof. The sapphire windows and the variable-volume piston with liquid-level manipulation device solved this problem relatively easily. Refer to Appendix C for other methods for liquid-level detection. An added advantage of the variable-volume piston is that in the high-density region of measurement, movement of the piston could alter the phase compositions of the equilibrium cell contents significantly, i.e., without addition or removal of system components.

Sealing of the piston assembly onto the equilibrium cell body was attained with the use of a flange type fitting between the two assemblies. A raised edge on the piston assembly fitted into a groove in the equilibrium cell body and a Viton “o”-ring in the groove attached as a gasket. The two assemblies were bolted together with six stainless steel bolts that were 8 mm in diameter.

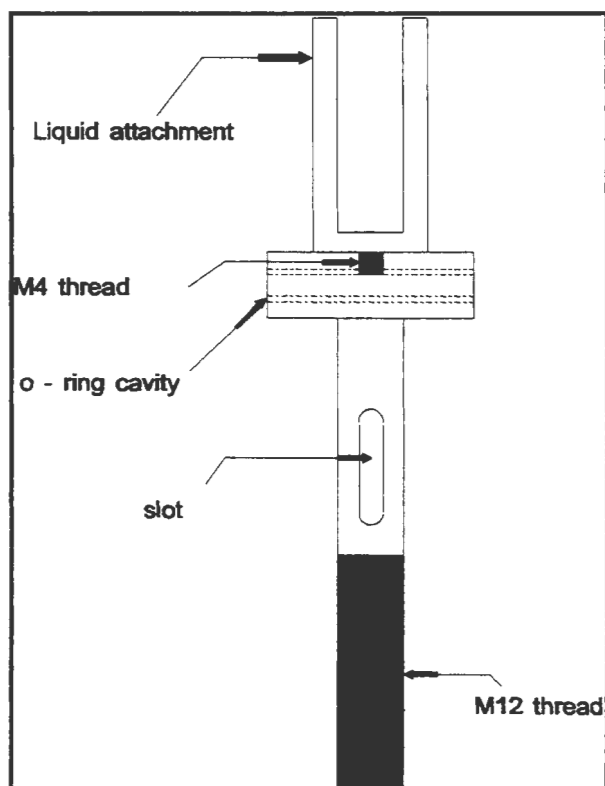
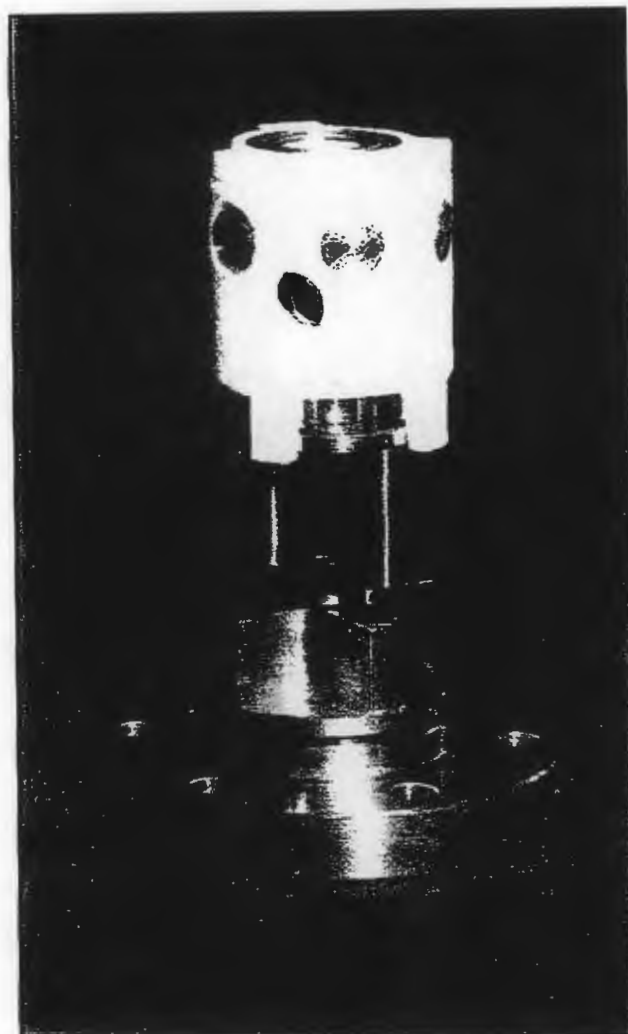


Figure 4-4: Illustration of the piston with the liquid manipulation attachment

The equilibrium cell has a removable base. The removable base was incorporated into the design for basically two reasons:-

1. It made construction and attachment of the composite impeller much simpler. The composite impeller attaches to the removable base and is supported by a screw that screws into the base.
2. It makes cleaning of the entire equilibrium cell possible. Mechanical cleaning of the equilibrium cell would be required if the components in the cell were to form residues during experimentation.

The base is basically a flange with a raised edge that bolts into the equilibrium cell body. Sealing between the base and the equilibrium cell body is achieved with Viton "o"-rings. Photograph 4-3 shows the removable base supporting the composite impeller.



Photograph 4-3: The removable base supporting the composite impeller

All fittings and valves on the equilibrium cell and piston assembly, besides the fill/evacuate valve, were Swagelok. All valves and fittings were purchased from Johannesburg Valve and Fitting.

The reasons why we decided to have the nitrogen compartment were:-

1. **Safety.** By pulsing nitrogen into the upper compartment, in the piston assembly, we maintain the same pressure on both sides of the piston. Thus, the threads on the piston shaft experience less force.

2. Assisting the stepper motor. The stepper motor can only drive against a pressure of approximately 10 bar. By maintaining the pressure differential across the piston to a value less than the above mentioned, the stepper motor could move the piston. An electronic circuit which was referred to as the pressure equalization circuit was designed to maintain a pressure differential across the piston of approximately one bar. Details of the pressure equalization circuit are available in Appendix C.

Holes were drilled through equilibrium cell body into the cell for the GC valve sampling lines, pressure transducer lines, and fill/evacuate line. The holes were 3 mm in diameter. This was undertaken so as to ensure as small a dead-volume as possible in the equilibrium cell.

The fill/evacuate valve on the equilibrium cell was a Whitey valve. It was bi-directional and could withstand a combined temperature and pressure effect of 175 °C and 10000 psi respectively.

4.2.2. Method of agitation of the equilibrium cell contents

Two sets of stirrers were designed for the equilibrium cell. Both were mounted onto one assembly (see Figure 4-5 and Photograph 4-4). Each stirrer had a different mode of operation. The lower stirrer was to intensively mix the equilibrium cell content to enable the rapid attainment of equilibrium. The second stirrer (or top stirrer) was to stir the second liquid phase (if it existed) and also to circulate the vapour (although this was not its main purpose) and second liquid phases through the sample loop of the upper GC sampling valve.

Rotation of the bottom stirrer is achieved by magnetic coupling. The impeller design was basically the same as that used by Bradshaw [1985] and Muhlbauer [1990]. It has four vanes, two of which were wider. The two wide veins housed two cylindrical rare earth magnets (obtained from LABOTEC). The impeller was constructed from 316 stainless steel (Figure 4-6). The impeller rotated on a stainless steel pin. A horse-shoe magnet mounted on a Maxon motor provided the magnetic coupling for the rotation of the bottom impeller. The impeller served two purposes:-

1. It mixed the equilibrium cell contents and promoted equilibrium. This was achieved by rapid rotation, thus creating a vortex into which vapour is entrained. This produced rapid mass transfer and equilibration of the phases.
2. The stirrer (impeller) created a centrifugal force that forced liquid through the sampling loop on the GC valve. This ensured that a representative sample of the equilibrium liquid phase was always flowing through the GC sampling loop.

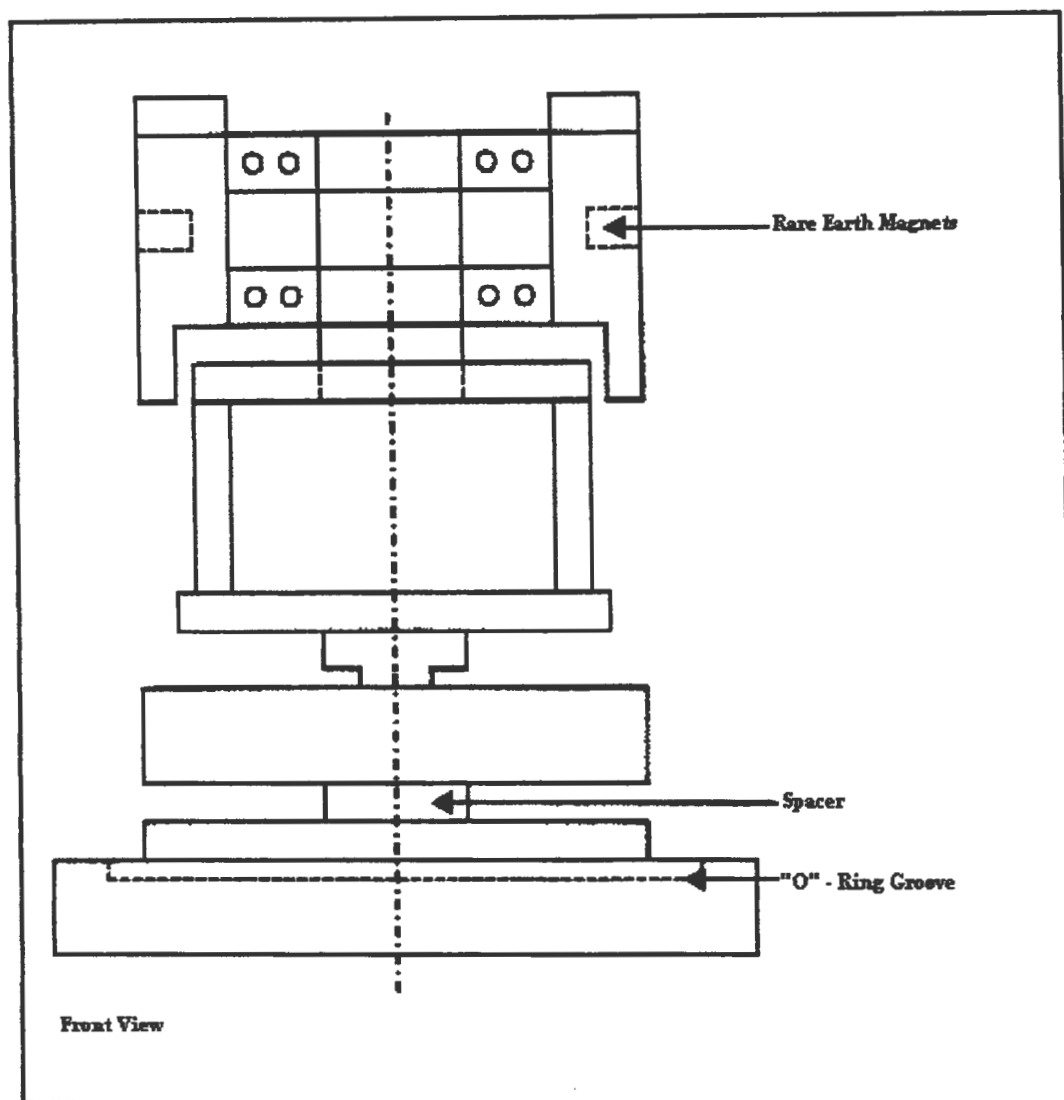


Figure 4-5: Schematic of the composite stirrer

The Maxon motor that turned the horse-shoe magnet was housed in a well situated below the equilibrium cell. The well protruded into the air-bath and the cover-plate on the well supported the equilibrium cell body. This construction allowed the air in the well to become heated and so reduce the temperature gradient across the well support plate. Good thermal insulation between

the cell body and the plate was achieved by machining a shallow recess on the bottom of the equilibrium cell body, to entrap a stagnant pocket of air.

The upper stirrer was constructed from 316 stainless steel and Teflon. It operated according to the principles of magnetic induction. The impeller had four rare earth magnets imbedded in it and it was positioned in an orientable magnetic field that was induced by the four coils. The decision was made to insert the upper stirrers some time after the equilibrium cell had been machined. This left very limited space in which to insert the impeller and the coils that induced the magnetic field. With the limited surface on the equilibrium cell body, the coil configuration in the equilibrium cell body was such that the coils were at angles of 120 and 60 degrees to each other instead of the symmetric 90 degrees. This left some rather complex electronic circuitry to be designed so as to drive the stirrers efficiently. Details of the coils and the circuitry are discussed in Appendix C.

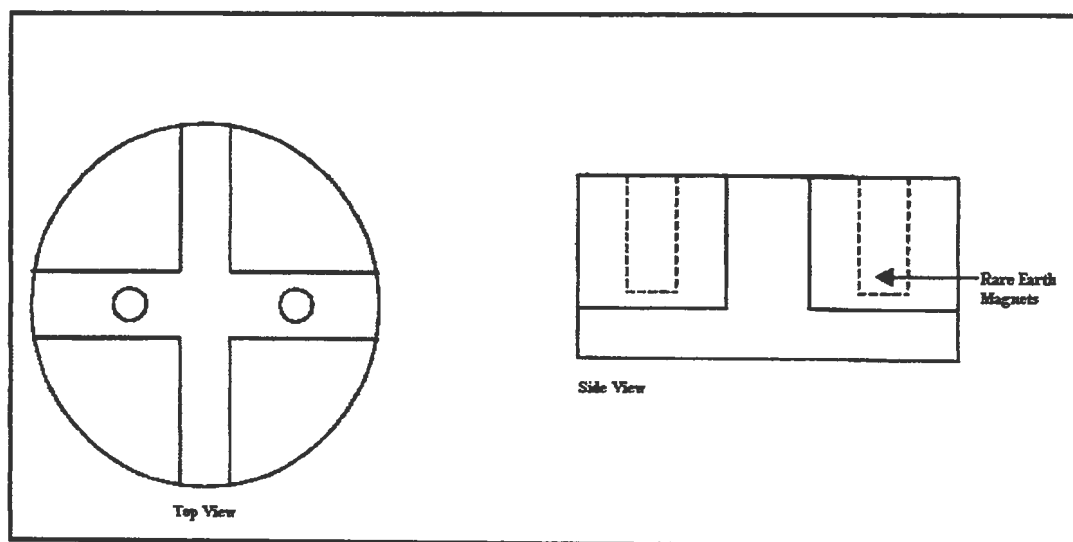


Figure 4-6: Schematic of the bottom stirrer

The upper stirrer served the following purpose:-

1. It ensured that if a second liquid phase were present, it would be stirred independently of the bottom liquid phase. This would avoid mixing of the two liquid phases.
2. Its centrifugal action forced liquid through the sample loop on the GC sampling valve, ensuring a representative sample of the second liquid equilibrium phase for GC analysis.

3. It mixed the vapour phase and also created a pressure gradient for the flow of equilibrium vapour through the sample loop of the vapour GC sampling valve.

4.2.3. Method of sampling vapour and liquid phases

Probably the most difficult aspect of HPVLE equipment design is that of designing a sampling device that allows for a small representative sample to be removed from the high-pressure equilibrium cell without disturbing the equilibrium conditions.

A number of sampling devices have been proposed and used by various researchers. A few of these have been discussed in Chapter 2. The sampling method opted for in this project was one that permitted no change in the cell volume and no disturbance to the system during sampling. The sampling device was a commercial six-port two position GC sampling valve. The only difference between a standard GC sampling valve and the one used in this project is that the GC valve in this project could withstand very high temperatures and pressures (175 bar and 175 °C). The six-port two position GC sampling valves were manufactured by VALCO and supplied by Anatech Instruments.

The two modes of operation of the GC sampling valve are as indicated in Figure 4-7. In the sampling position, the stirrers force fluid through the sampling loop and back into the equilibrium cell. Thus there is always a flow of a representative sample of the equilibrium phase through the sample loop. The volume of the withdrawn sample from the equilibrium cell is determined by the size of the sample loop. Very fine bore, thick walled stainless-steel tubing was used for the sample loop (1/8" tubing with internal diameter of 1 mm). A problem encountered during construction was that the ports for the sample loops were spaced a significant distance apart. This meant that a very long sampling loop had to be inserted (approximately 21 cm). This resulted in a sample volume of approximately 165 μl (much larger than the volume the jet-mixers had been designed for). There was nothing that could be done to reduce the sample loop size and therefore the operating parameters for the jet-mixers had to be altered to cope with the large sample volume.

In the flushing mode, the equilibrium cell is shut off from the sampling loop and the sampling loop is opened to the carrier-gas (in this project helium was used). The carrier-gas flushes the representative sample out of the sample loop and into a jet-mixer. As can be seen, this sampling

procedure causes no disturbances to the equilibrium condition and the cell volume is not affected for a particular set of conditions.

There were three GC sampling valves on the apparatus (see Figure 4-1 and Photograph 4-3). They were positioned at appropriate heights along the wall of the equilibrium cell body so that the appropriate phases could be sampled. The first sampling valve was positioned at the bottom of the equilibrium cell body adjacent to the bottom stirrer. It sampled the bottom liquid phase. The second sampling valve was positioned adjacent to the upper stirrer, about a third of the way up the equilibrium cell body. It sampled the second or upper liquid-phase (if it existed). Finally, the third GC sampling valve was for the vapour phase. It was positioned about half way up the equilibrium cell body.

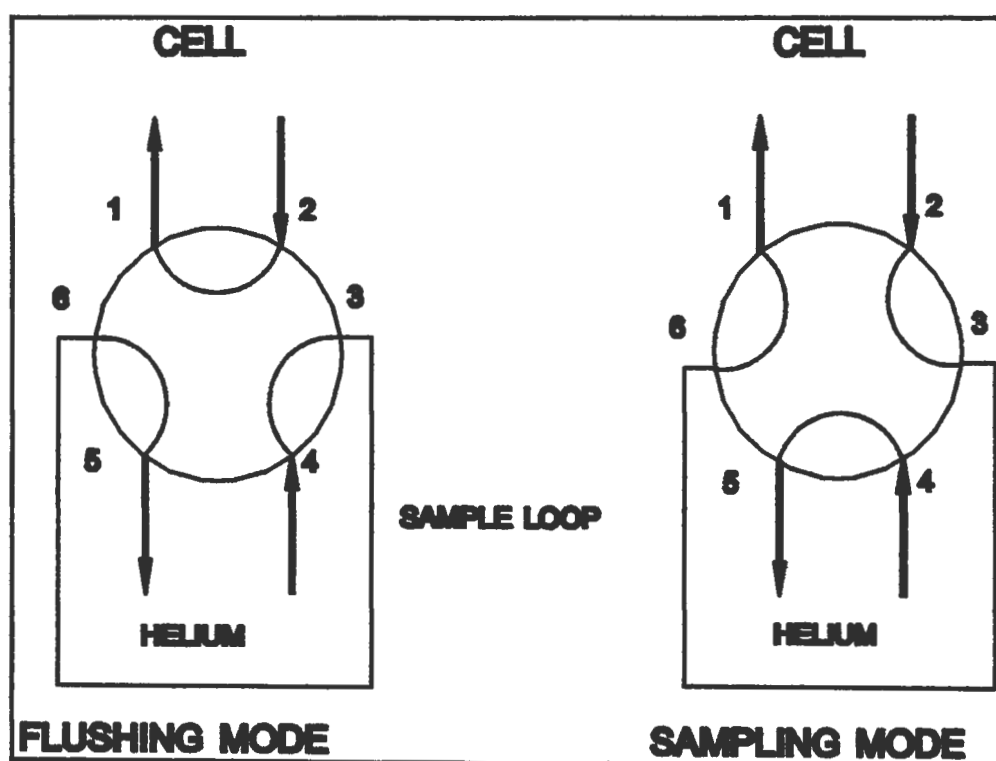


Figure 4-7: Schematic showing the two modes of operation of the six-port GC valves

4.2.4. Jet-mixers

During the flushing of a volatile/non-volatile mixture into an evacuated space, there is a tendency for the more volatile component to flash preferentially. This creates a non-homogenous gas-liquid mixture. If no method is used to homogenise the withdrawn equilibrium phase sample, the

analysis of the withdrawn sample will be in error. Various methods have been proposed and tried by various researchers. Some of them have been briefly discussed in Chapter 2 and Appendix A.

The method/device used in this project is the same as was used by Muhlbauer [1990]. The device is known as a jet-mixer. It vapourises and homogenises the withdrawn sample in preparation for GC analysis. The sample from the sample loop on the GC sampling valve is flushed into an initially evacuated jet-mixer. The jet-mixer has a nozzle through which the flushed sample passes at a reasonably high velocity to produce a swirling, recirculating flow in the jet-mixer until the pressure becomes uniform. By flushing carrier-gas through the sampling loop into the jet-mixer at a controlled flow, further mixing of the sample is ensured. Figure 4-8 illustrates a cross-section through a jet-mixer. Photograph 4-3 shows the jet-mixers attached to the equilibrium cell.

The jet-mixer has no moving parts and external devices. It was machined from 316 stainless steel. The mixing chamber has an internally mounted cylindrically shaped baffle. The baffle has a restriction nozzle that accelerates and vapourizes the withdrawn sample (in the case of a liquid sample). It creates a swirling circulating flow until the pressure equalizes. The internal space has rounded corners, as shown, to eliminate stagnant areas.

The inlet to the jet-mixer was via a 1/8" stainless steel tube that was welded into the jet-mixer body. The inlet line protruded into the jet-mixer mixing chamber and ensured that flow occurred through the restricted nozzle in the chamber. The inlet line comes from the GC sampling valve. Flow out of the jet-mixer is through a Whitey valve that screwed into the jet-mixer body. It regulated the venting of the jet-mixer.

Three 100 Watt heater cartridges were embedded in the body of the jet-mixer, as can be seen in Figure 4-8. They are evenly spaced along the circumference of the jet-mixer body. The large body of the jet-mixer ensures good temperature uniformity. The heater cartridges maintained the jet-mixers at a temperature higher than the equilibrium mixture and the surrounding air-bath. An Eurotherm 808 temperature controller regulated the temperature of the jet-mixer. The temperature sensor used was a Pt-100 that was also embedded in the jet-mixer body. The controller maintained the temperature of the jet-mixers to within 0.1 °C of the set-point. The jet-mixers were insulated with Fibrefrax. This was done as they were at a higher temperature than the air-bath and thus radiated heat to the surrounding air-bath. This could lead to thermal gradients and thus instabilities and non-uniformity's in the bath and equilibrium cell

Two sizes of jet-mixers were designed in this project. The larger jet-mixers had a volume of approximately 65 cm^3 and the smaller ones a volume of approximately 40 cm^3 . The larger jet-mixers were used to homogenise the liquid phase, while the smaller ones were used to homogenise the vapour sample and for further homogenisation of the liquid samples. There was one large jet-mixer for each of the liquid phases (if two liquid phases existed). There were two smaller jet-mixers, one to homogenise the vapour sample and the other for further homogenisation of the liquid sample.

The pressure in the jet-mixer was measured with a Sensotec TJE pressure transducer. The transducer was not directly attached to the jet-mixer, but by appropriate opening of valves, could be linked to the jet-mixer (see Figure 5-3). The operating range of the transducer was from 0 to 5 bar absolute and it had temperature compensation. Its accuracy was $\pm 0.25\%$ of full-scale pressure. The pressure transducer gives very useful information on the operation of the jet-mixer and the reproducibility of the phase sampling. The determination of the operating pressure and temperature ranges for the jet-mixers is discussed in Appendix D. The design and sizing of the jet-mixers is discussed in Appendix C.

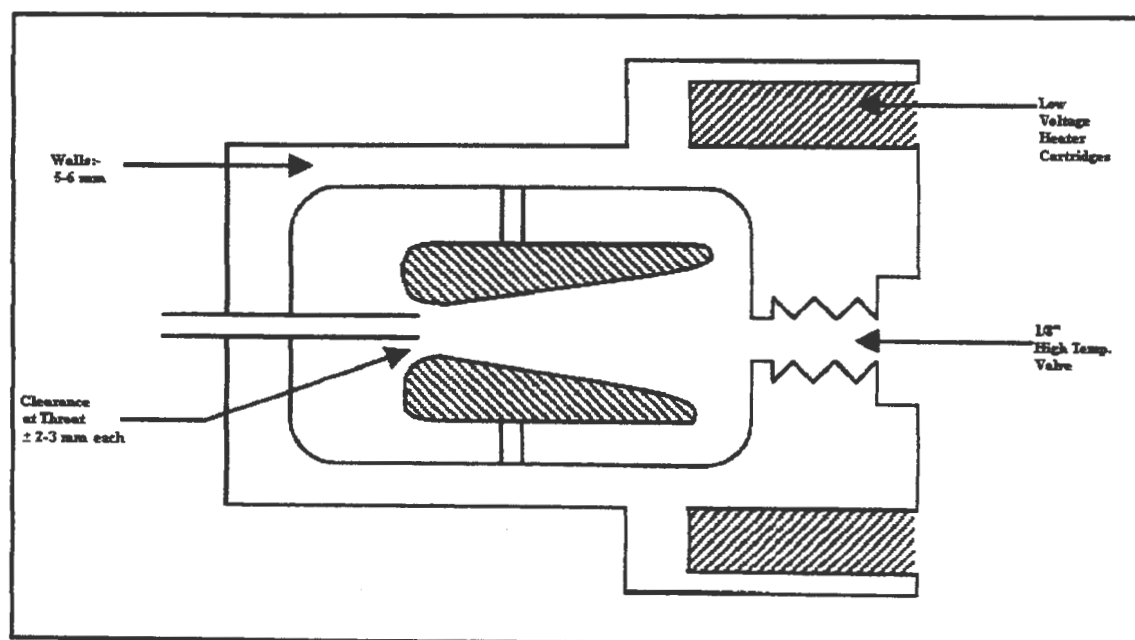


Figure 4-8: Cross-section through the jet-mixer

4.2.5. Air-bath

True vapour-liquid equilibrium can only be established in an equilibrium cell that is free of thermal gradients. This means designing an air-bath that maintains a stable and uniform temperature. The air-bath was designed to be very compact and functional. Some of the design concepts used by Muhlbauer [1990] were used directly in this project (Meacham et al. [1994] details isothermal thermostated air-baths). The actual bath was constructed from mild steel (4 mm thick) and it had dimensions of 1 m x 0.75 m x 0.5 m. Photographs 4-4 and 4-5 show the outside and inside of the air-bath.

The bath had a blow-off lid. This was to ensure that if there was a sudden rise in pressure in the bath the lid will easily lift off to release the pressure and thus prevent an explosion. The bath also had holes cut in it for the valve stems and handles, the viewing ports for the equilibrium cell, the holders for the light source, and for cabling to the jet-mixers, Pt-100 sensors and solenoid coils.

The main design features of the air-bath were as follows:-

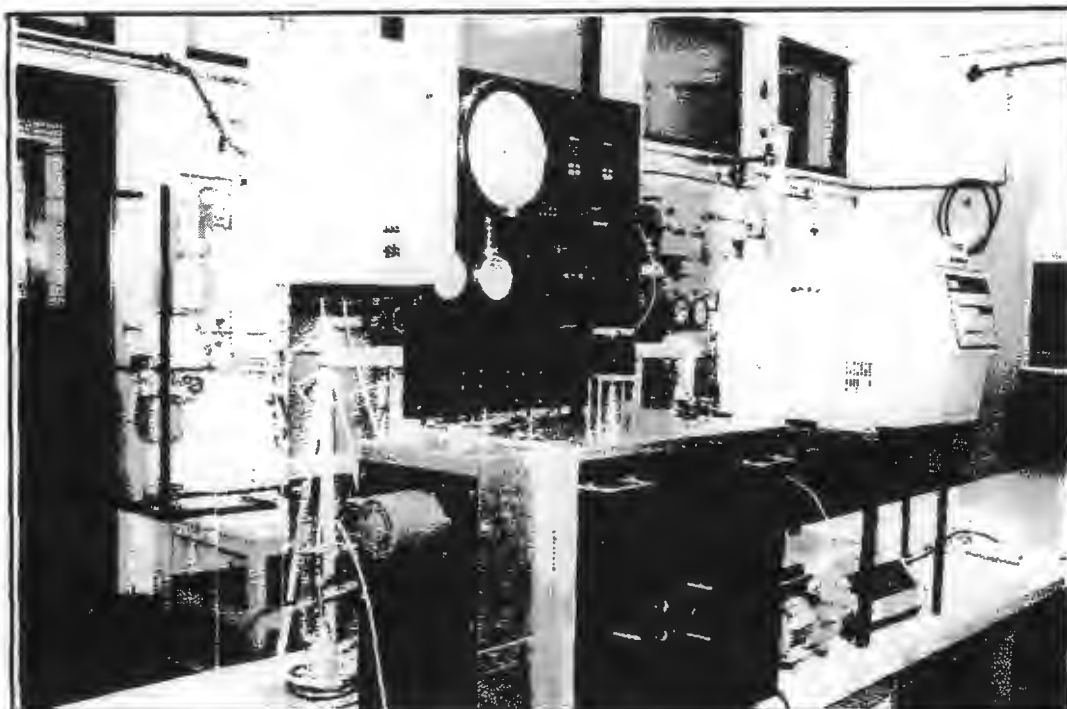
1. Insulation
2. Interior copper lining
3. Air-agitation
4. Temperature control
5. Minimising all possible thermal leaks, conductive paths and thermal disturbances.

4.2.5.1. Insulation

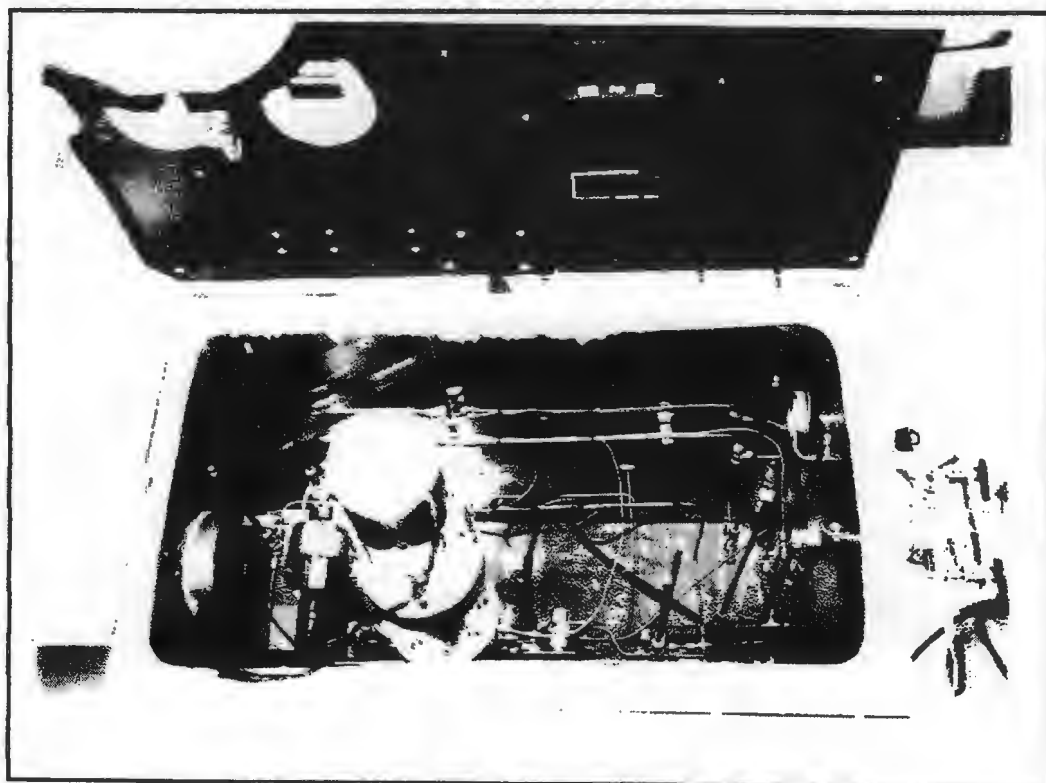
A layer of insulation was inserted between the walls of the air-bath and the interior copper lining. The thermal insulation material used was Fibrefrax. The specifications of Fibrefrax are available in Appendix C. The thickness of the insulation was approximately 50 mm. The lid of the air-bath was also padded on the inside with Fibrefrax (thickness approximately 40 mm).

4.2.5.2. Interior copper lining

To promote high thermal stability and avoid any local temperature disturbances, a copper lining



Photograph 4-4: The HPVLE apparatus designed in this project together with its ancillary equipment



Photograph 4-5: The interior of the air-bath showing the copper jacket, insulation, equilibrium cell and plumbing.

(approximately 2 mm thick) was placed against the insulation in the air-bath. The lining also served to hold the insulation in place in the bath. Copper has a high thermal conductivity (approximately $401 \text{ Wm}^{-1}\text{K}^{-1}$ at 300 K, Incropera and DeWitt [1996]) and quickly disperses and transmits any local temperature disturbances.

4.2.5.3. Air agitation

The heating elements had to be shielded from direct view of the equilibrium cell to avoid radiative heat transfer and consequently local heating effects between the equilibrium cell and the heating elements. As a result, the heating elements were placed in an insulated box external to the air-bath (Photograph 4-4 shows the box that housed the heating elements and the Siflo Universal Fan). A Siflo Universal Fan was used to circulate air through the box (over the heating elements) and into the air-bath. In order to avoid burnout of the heating elements an air flowrate of approximately 2.51 ms^{-1} was required. To also prevent burnout of the heating elements, a circuit was designed that ensured power to the heaters was applied only once the fan had been switched on. The air was drawn in from the top of the bath by the fan, blown over the heaters, and out at the bottom of the bath (Photograph 4-5 shows the interior of the air-bath and the inlet and outlet to the heater box). The fan was able to displace approximately 72 l/s of air under no load conditions. To avoid the air from the heater box being blown directly on the equilibrium cell, a deflector plate was fitted on the outlet. The deflector plate also aided circulation in the air-bath, as it created an upward spiral motion of air.

To decrease the likelihood of an explosion in the air-bath should there be any leaks on the equilibrium cell, nitrogen from the pressure equalization circuit was bled into the air-bath. This produced an air-bath environment that was less conducive to ignition.

4.2.5.4. Temperature control

The temperature in the air-bath was controlled with a Eurotherm 818 PID controller which was supplied by PREI Instruments. The temperature sensor was a Pt-100 Ω resistor. The output from the temperature controller was a 4 to 20 mA signal that drove a fast cycle firing Eurotherm thyristor. The thyristor supplied the energy to three aluminium finned stainless steel cartridge heaters. The total power output of the heater cartridges was approximately 1700 W.

Calibration of the temperature sensors and tuning of the temperature controller is discussed in Appendix C.

4.2.5.5. Minimizing all possible thermal leaks, conductive paths and thermal disturbances

Possible thermal leaks and conductive paths identified were:

- The cover-plate for the well that housed the horse-shoe magnet and MAXON motor.
- The valve stems for all the valves in the air-bath, including the GC sampling valves.
- Sampling lines from the air-bath.
- Holes in the air-bath for valve stem extensions, sample lines and electrical cabling.
- Piston assembly external to the air-bath

Great precautions were taken to ensure effective thermal insulation between the cell bottom and the rotating magnet. Rotation of the horse-shoe magnet produced a high convective heat transfer coefficient between the cold air (room temperature) in the well and the heated support plate. The well was thus sealed and an air gap was left between the equilibrium cell bottom and the cover-plate for the well. This ensured good thermal insulation between the bottom of the equilibrium cell body and the support plate.

Thermal breaks were inserted in all the valve stem extensions out of the air-bath. The material used for the thermal breaks was Teflon. The thermal breaks reduced conduction of heat to a minimum.

All sample lines outside of the air-bath were wrapped in heating tape. This prevented or at worst reduced thermal gradients.

All holes in the air-bath walls drilled for valve stem extensions, sampling lines and electrical cables were fitted with Teflon plugs. This reduced radiative heat transfer from the air-bath tremendously.

The jet-mixers situated in the air-bath were the source of two thermal disturbances. They are as follows:-

- Due to the higher operating temperatures of the jet-mixer, the equilibrium cell could be thermally disturbed if there were any conductive paths leading from the jet-mixer to it. To prevent conductive paths to the equilibrium cell, the jet-mixers were supported on brackets that attached to the air-bath bottom. This ensured that there were no conductive paths back to the equilibrium cell except for a small piece of piping that connected the jet-mixer to the GC sampling valve and in turn it to the equilibrium cell.
- The surface of the jet-mixer was at a higher temperature than the surrounding air-bath. To prevent or reduce radiative disturbances to the air-bath and equilibrium cell, the surface was insulated with Fibrefrax.

Part of the piston assembly was situated outside of the air-bath. This was as a result of the stepper motor having to be situated external to the air-bath. To prevent thermal gradients due to thermal conduction, thermal breaks were inserted in the support arms, of the piston assembly, for the stepper motor. The thermal breaks were made from Teflon.

4.2.5.6. Temperature Profiles

Pt-100 Ω resistance temperature sensors were strategically placed in wells in the walls of the equilibrium cell and in the air-bath to monitor the temperature profiles. Four sensors were placed in wells in the equilibrium cell body and four in the air-bath at different positions. Figure 4-9 indicates the locations of the sensors on the equilibrium cell and in the air-bath. All the temperature sensors were connected to a Eurotherm multichannel selector that enabled the temperatures for all the sensors to be scrolled through very rapidly. Temperature profiles for a few set-point temperatures are given in Chapter Seven.

For almost all of the operating temperatures for the air-bath, the maximum deviations in the temperature profiles were approximately 2 K for the air-bath and 0.4 K for the equilibrium cell body.

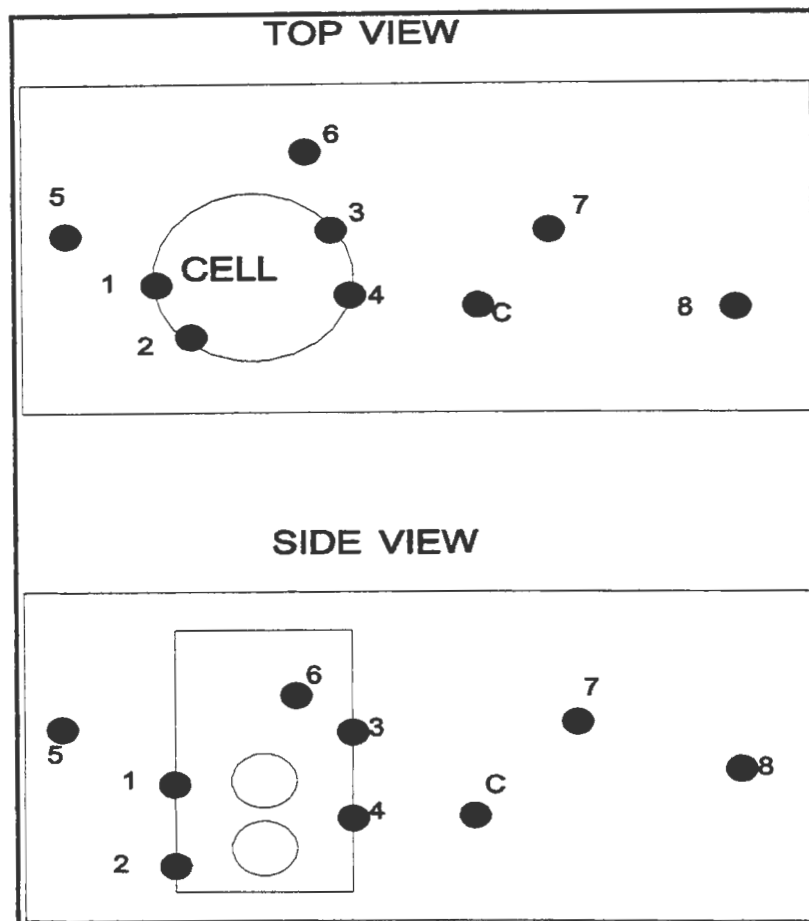


Figure 4-9: Location of the temperature sensors in the air-bath and on the equilibrium cell body (1 – 8 denote the number on the Eurotherm selector and C denotes the air-bath temperature controller sensor)

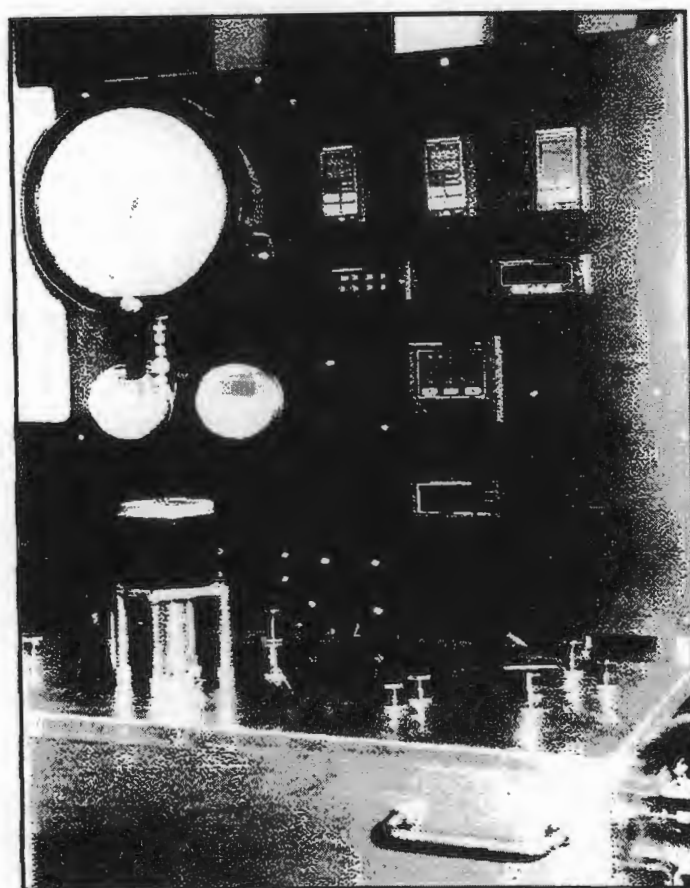
4.2.6. Temperature and Pressure Measurement

The measurement of temperature and pressure, along with phase composition are critical to the measurement of accurate VLE data. Excellent reviews on temperature and pressure measurement are available in literature (Benedict [1977], Kardos [1977], Nicholas and White [1982] and Kennedy [1983]).

4.2.6.1. Temperature measurement

Temperatures were measured with Pt-100 Ω resistor (class A) sensors and the values were displayed on Eurotherm temperature displays. The Pt-100's were certified as being accurate to within 0.05%. The sensors were calibrated against a Hewlett Packard Quartz Thermometer. For

a wide range of temperature measurements the quartz thermometer and Pt-100 Ω resistors were within 0.3% of each other. Photograph 4-6 shows the display panel of the apparatus with the temperature displays mounted on it.



Photograph 4-6: The control/display panel for the apparatus with displays units for temperature and pressure measurement

4.2.6.2. Pressure measurement

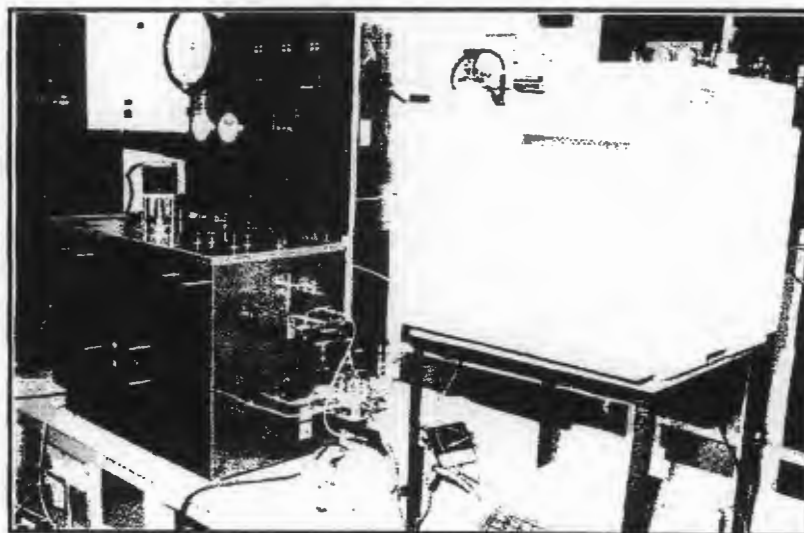
Pressure measurements were undertaken with Sensotec TJE pressure transducers. The transducers are certified accurate to within 0.25% of their readings. Two Bourdon type Heisse gauges were also used to measure pressure and to calibrate the pressure transducers. There were three pressure transducer used in this project. One each for measuring the equilibrium cell and nitrogen compartment pressures (0 – 175 bar absolute) and another for measuring the pressures of the jet-mixers (0-5 bar absolute) (the pressure transducer displays can be seen on the control/display panel in Photograph 4-6). One of the Heisse gauges (0 – 5000 psi) was connected

in parallel to the pressure transducer that measured the equilibrium cell pressure. The other Heisse gauge (0-500 psi) was used to calibrate the other pressure transducers. The Heisse gauges had certified calibrations traceable to the National Bureau of Standards. They were claimed to be accurate to 0.1% of their full scale reading by the manufacturer.

The procedure for the calibration of the pressure transducers to the Heisse gauges is discussed in Appendix C.

4.2.7. Composition measurement

A few of the various methods used to determine the composition of the equilibrium phases in phase equilibrium studies have been discussed in Chapter 2. In this project, use was made of a GC with a TCD detector for phase composition analysis. The calibration of the TCD detector is discussed in Appendix D and the calibration charts (response factors) for the various components studied are presented in Chapter 7.



Photograph 4-7: Arrangement of the high-pressure apparatus and the GC facilitating online analysis of the equilibrium phase compositions.

The GC used in this project was the Chrompack CP 9000 which was equipped with both a TCD and FID detector. However, all analyse undertaken in this project were performed on the TCD detector, as it enabled one to detect the presence of water. For all the systems studied, separation

of the components was possible on a 3 m length stainless steel column (1/8" diameter). The column packing was Poropak N with an 80/100 mesh. The output signal from the GC was analysed and converted into peak area signals by a Varian 4270 Integrator.

The GC operating conditions for the various systems studied are presented in Chapter 7.

4.2.8. Safety features

High-pressure and temperature phase equilibrium experimentation can be extremely hazardous (as a result of the high temperature and pressures involved) and it is thus imperative that the utmost safety precautions be undertaken to protect the researcher and the equipment. These are some of the safety precautions undertaken to safe-guard the researcher and equipment:-

1. Safety relief valves were installed on all high-pressure line. They were positioned just before the pressure transducers.
2. The pressure transducers used had a 150% over-pressure safety feature.
3. A shut-off valve was inserted before the 0–5000 psi Heisse gauge to prevent a negative strain on the gauge during evacuation.
4. Nitrogen was bled into the air-bath. This produced an environment that was not conducive to ignition. Ignition could occur if there was a leak on the equilibrium cell and some flammable material with a very low flash or fire point was released into the air-bath.
5. The air-bath had a blow-off lid that ensured rapid decompression of the air-bath contents.
6. Simple circuitry ensured that the heater cartridges for the air-bath were only energized once the fan had been turned on. This prevented burnout of the cartridges, which could possibly result in a fire.
7. A number of the chemicals used were fairly toxic. At all times the exhaust fans in the laboratory were switched on and all relief valves and exhaust lines (e.g. from the vacuum pump) were connected to the fume cupboard.
8. The viewing windows in the walls of the air-bath were tempered and were also shatterproof.
9. Proper insulation and the installation of thermal breaks on all valve stems exiting the air-bath also served to prevent burns to the researcher.
10. All design calculations were undertaken such that there was at least a 100% over-design, as a safety precaution.

CHAPTER FIVE

EXPERIMENTAL PROCEDURE

In this chapter the preparation, start-up, and sampling procedures for the experimental apparatus and its associated equipment will be discussed. These experimental procedures are the result of numerous trial runs so as to obtain a reproducible experimental method that produces the most accurate experimental results.

The method of calibration of the gas chromatograph is also discussed in this chapter.

Operating procedures for the auxiliary equipment are given in Appendix D.

Sections 5.1 to 5.4 describe the experimental procedure for vapour-liquid equilibria measurement. The procedure for the P - V - T measurements is described in section 5.5.

5.1. THE PREPARATION STAGE

5.1.1. Preparation of the Equilibrium Cell

Since pressure is one of the primary measurements in our experimentation, one has to ensure that there are no leaks in the equilibrium cell or any of the lines that convey the equilibrium sample to the gas chromatograph. Thus, before every experimental run the equilibrium cell was pressurised to a value in excess of the expected maximum operating pressure and was thoroughly scrutinised for leaks. Snoop leak detector was used as the primary tool in detecting leaks. The same procedure was undertaken for the lines conveying the equilibrium sample to the gas chromatograph. Generally the cell and the lines were left pressurised overnight. The pressure drop was noted the next morning. If the pressure drop was within a specified tolerance (temperature effects, as well as the leak rates of fittings were taken into account), then the equilibrium cell was deemed ready for use in experimentation.

At the beginning of a study of a new system or isotherm all seals on the equilibrium cell were replaced. This was to ensure that there would be little risk of failure during experimental runs. Seals that were replaced were as follows:-

1. Viton “o”-rings on the sapphire window housings;
2. Viton “o”-ring on the bottom of the equilibrium cell (impellor mounting);
3. Viton “o”-rings on the piston; and
4. Viton “o”-ring between upper nitrogen compartment and equilibrium cell.

The equilibrium cell was “cleaned” by applying a vacuum in the equilibrium cell and raising the temperature of the equilibrium cell. Thus any solvents that were present in the equilibrium cell were removed by evaporation. Successive flushing of the equilibrium cell, with the gaseous component under investigation, removed any trace amounts of impurities.

The sampling lines, which convey the equilibrium sample to the GC, were also flushed with the carrier gas between runs to clean the sample lines. A GC trace of the flush could be undertaken at this time to determine if the flushed sample had any significant amount of impurity.

5.1.2. Preparation of the liquid component for experimentation

The liquid component was thoroughly degassed before being introduced into the equilibrium cell. This was done so as to remove any impurities, such as dissolved gases, from the liquid. Degassing was carried out in a specially designed apparatus. The description of the degassing apparatus and its operating procedure appear in Appendices C and D respectively.

5.1.3. Verification of gas chromatograph detector calibration factor

The calibration factor for the gas chromatograph detector was checked before each experimental run by injecting a few standards through the gas chromatograph. This was undertaken, as in some instances there was slight drift in the calibration factor for the detector. This phenomenon was also noted by Mühlbauer [1990].

5.1.4. Calibration of the pressure transducers

The Sensotec pressure transducer once calibrated still tended to have slight drift. The drift tended to be on the atmospheric pressure reading or the zero. The span did not seem to be affected over

a short period. Thus, before every experimental run the Sensotec pressure transducers were zeroed to atmospheric pressure for the day. The atmospheric pressure was read on a barometer (to within 0.1 mbar) and the pressure transducer display was then adjusted to the correct barometric pressure. Every month, the pressure transducers were fully calibrated i.e. zero and span. Calibration of the pressure transducer is explained in Appendix C. The accuracy of the pressure transducers is detailed in Chapter 4 and 7.

5.2. THE START-UP PROCEDURE

The start-up procedure was dependent on the system that was being measured. Figures 5-1 and 5-2 show the equipment arrangements used for the carbon dioxide + toluene or carbon dioxide + methanol, and the propane + 1-propanol systems respectively. Essentially the difference in the two arrangements is the method in which the liquid and gas are fed into the equilibrium cell. In the procedure for the propane + 1-propanol system the gas first goes through a compressor before it is introduced into the equilibrium cell. The reasons for this arrangement follows in the discussion preceding each of the arrangements.

5.2.1. The Carbon dioxide + Toluene and Carbon dioxide + Methanol systems

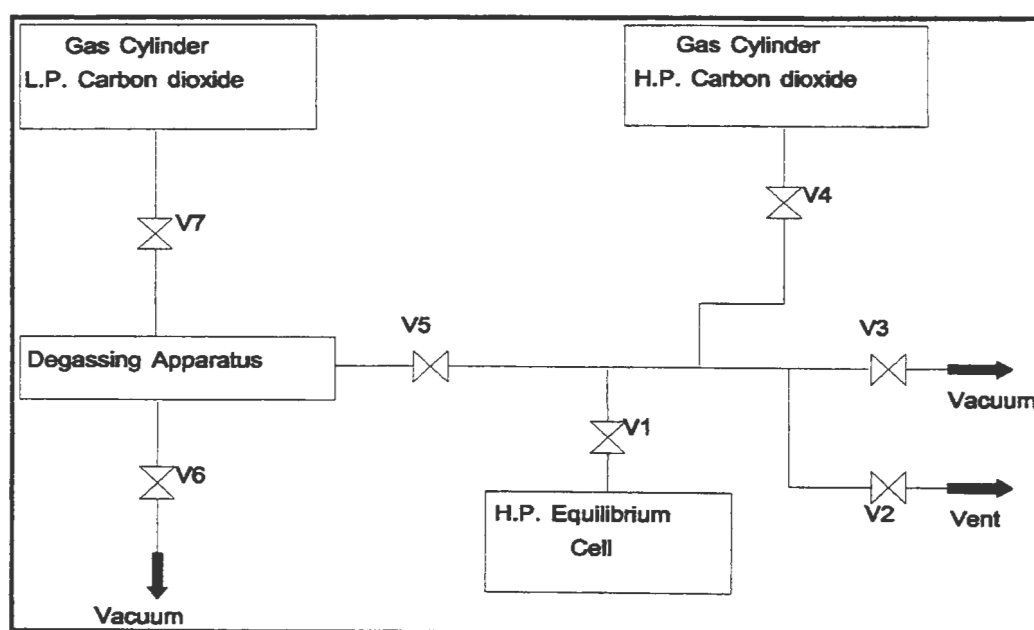


Figure 5-1: Equipment arrangement for the carbon dioxide + toluene and carbon dioxide + methanol systems.

Before introduction of any of the components into the equilibrium cell, the cell was evacuated. It was then subsequently filled with carbon dioxide and vented to the atmosphere. This filling and venting procedure was carried out on average about five times. This ensured that only trace amounts of residual air or any other impurities remained in the equilibrium cell. The equilibrium cell was once again evacuated (typical vacuum achieved in the equilibrium cell was about 1 mbar). The toluene/methanol was then sucked into the equilibrium cell from the degassing apparatus (after the liquid had been degassed). To assist, some carbon dioxide was used to flush the remaining toluene/methanol into the cell. The toluene/methanol was degassed again in situ under vigorous stirring and vacuum. This degassing in situ was carried out for about 15 minutes. It also served to position the liquid-level in the equilibrium cell by expelling the excess toluene/methanol.

Carbon dioxide was then introduced into the equilibrium cell from its gas cylinder. The cell was pressurised to a value close to the desired experimental pressure and the temperature controller was set to the desired isothermal temperature. The stirrer was switched on and its speed adjusted so that there was vigorous stirring. Once the cell had heated up to the desired temperature (this normally took about 6 hours), the contents were ready for sampling. During the initial heat-up procedure the cell had to be vented so as to keep the pressure close to the desired experimental value. The cell was then left for a further few hours to reach complete thermal and thermodynamic equilibrium.

5.2.2. The Propane + 1-Propanol System

The introduction procedure for the components, i.e. propane and 1-propanol, varied from that used in the carbon dioxide + toluene and carbon dioxide + methanol systems because propane at room temperature is sub-critical. As a result the quantity (moles) of gas that can be introduced into the equilibrium cell is extremely small when compared to the amount of 1-propanol introduced. The vapour pressure of propane at room temperature is approximately 8 bar. An increase in the equilibrium cell temperature does not drastically increase the cell pressure. Therefore, a method had to be sought to introduce a greater number of moles of propane into the equilibrium cell. Two methods were investigated:-

- 1) Introducing the propane into the equilibrium cell as a liquid; or
- 2) Compressing the propane before introduction into the equilibrium cell.

Alternative two was decided on as :-

- 1) We could not obtain a cylinder with a port for liquid withdrawal;
- 2) Commercial equipment to liquefy propane was both expensive and complex; and
- 3) Mühlbauer [1990] had already used a compression device and obtained reasonable pressures in the equilibrium cell.

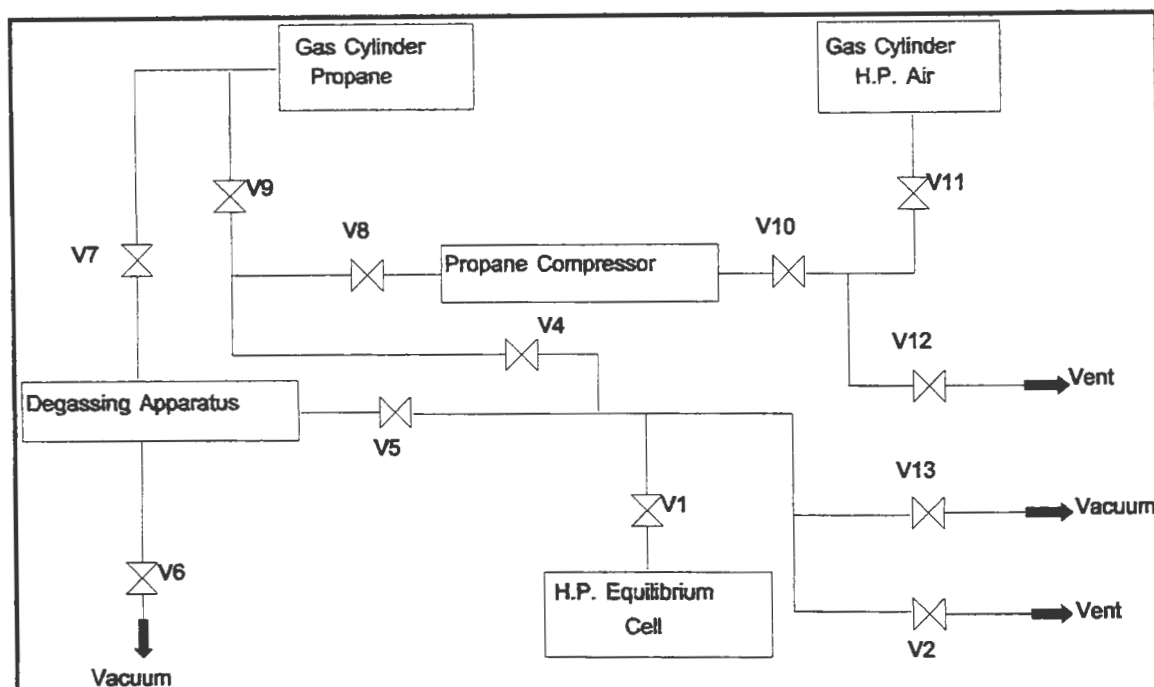


Figure 5-2: Equipment arrangement for the propane + 1-propanol system.

The equilibrium cell was evacuated and flushed with propane in a similar procedure as explained in Section 5.2.1. The degassed 1-propanol was introduced from the degassing apparatus to the equilibrium cell by suction due to a vacuum applied in the equilibrium cell. Propane flushed through the degassing apparatus was used to assist the flow into the equilibrium cell. In the equilibrium cell, the 1-propanol was again degassed, this time in-situ. The procedure was similar to that of Section 5.2.1. from then onwards.

The difference in the introductory procedure for the propane + 1-propanol system is the method of introduction of propane into the equilibrium cell. For investigation at low system pressures, propane is introduced into the equilibrium cell straight from the storage cylinder. When one requires experimental pressures in excess of the vapour pressure of propane at room temperature,

the propane is fed into the equilibrium cell via a compression device. Description of the compression device and its operating procedure is available in Appendices C and D respectively.

5.2.3. Positioning of the liquid-level

During the pressurising procedure the liquid-level can rise drastically as the more volatile component absorbs into the liquid phase. Mühlbauer [1990] states that the liquid-level can under some conditions increase approximately three-fold. It is thus crucial that one positions the liquid-level so that the appropriate phases are situated at the appropriate heights in the equilibrium cell for sampling of the equilibrium phases.

If the liquid-level is too high, the following could occur :-

- 1) During venting, some of the liquid phase will also be vented; or
- 2) if the liquid-level is alongside the vapour sampling port, the liquid phase will be sampled instead of the vapour phase; or
- 3) if the liquid-level is too close to the vapour sampling port, splashing could result in droplets of the liquid phase being entrained into the vapour sampling port.

During the filling process, one can view the liquid-level through the sapphire viewing windows. Generally the equilibrium cell was filled with the liquid component to a height half way up the bottom window. This constituted a volume of approximately 45 to 50 cm³.

5.4. THE SAMPLING PROCEDURE

The sampling procedure for the equilibrium liquid and vapour samples was developed by performing various runs on the carbon dioxide + toluene system. The sampling procedure was essentially the same for all systems measured. Differences in the sampling procedures for systems were:-

1. The final pressure to which the jet-mixers were pressurised; and
2. The temperature of the jet-mixers.

Reference must be made to Figure 5-3, which illustrates the plumbing in the sampling section, when going through the sampling procedure. Assume at the beginning that all valves are closed.

5.4.1. Sampling of the liquid phase

Once the cell contents had reached equilibrium (the cell contents were deemed to be at equilibrium when the equilibrium pressure remained constant over a period of 30 minutes) the following procedure was followed:-

1. The bottom stirrer speed was reduced to a setting of approximately half of its original value. This was to ensure that there would be no splashing of liquid in the equilibrium cell, and that no vapour bubbles would lodge themselves in the liquid sampling loop.
2. The internal jet-mixer (inside the air-bath) temperature was set on the Eurotherm 818 temperature controllers. The temperature of the jet-mixer was set to a value that was typically between 240 and 300 °C, depending on the system being investigated. The external jet-mixer (outside the air-bath) temperature was also set, typically 5 to 10 °C higher than the internal jet-mixers.
3. The sampling lines external to the air-bath were heated to a temperature comparable to the jet-mixer temperature.
4. The 8-port GC sampling valve was heated to a temperature comparable to the jet-mixer temperatures. Steps 1 to 4 were generally undertaken about an hour before the sample was actually taken for analysis.
5. All the lines from the sampling valve to the GC were evacuated, along with all the lines from the helium inlet to the sampling valve. This was achieved by opening the three-way valves T1 and T2 to vacuum. Valves V14, V13, V1, V9, V11, and V8 were also opened. The lines were evacuated to the approximately 0.8 mbar (this was the rating of the vacuum pump used). Once the desired vacuum was achieved all the above mentioned valves were closed.
6. Valve T2 was then opened to helium. Metering valve V13 was then slightly opened to allow a slow flow of helium into the line. The pressure in the line was built-up to 0.75 bar and then valve V13 was closed. The helium was then allowed to heat up in the line to the temperature of the air-bath (this took approximately 10 minutes). The helium is heated to the equilibrium temperature so as to ensure that no condensation of the equilibrium sample takes place in the line during sampling.

7. The bottom GC sampling valve was then turned from the *sampling* to the *flushing* position and valve V1 was opened. This flashed the equilibrium sample into the internal jet-mixer. To facilitate the homogenisation of the equilibrium sample valve V13 was again opened slightly. A slow flowrate of helium was set so as to create a swirling action in the jet-mixer and thus facilitate mixing. Flowrate was judged by the rate of increase in the line/jet-mixer pressure. A rate of approximately 0.005 bar per second was generally set. The pressure in the jet-mixer was built-up to 1.8-bar. A slow flowrate of helium ensured that:-
 - a) As the helium gas flowed slowly through the heating loops it was heated to the air-bath temperature. Thus any less-volatile component that may have deposited in the sampling line after flashing would be displaced into the jet-mixer;
 - b) The constant flow of helium ensured that the equilibrium sample was trapped in the jet-mixer; and
 - c) The additional mixing of the carrier gas with the equilibrium sample, due to circulation created by the continuous flow of helium, resulted in a totally vapourised and homogenised sample ready for GC analysis.
8. Valve V13 was then closed. The line/jet-mixer pressure reading was then checked to see if there was any decrease in pressure. A decrease in pressure was a sure sign that there was condensation in the line or in the jet-mixer.
9. Valve V9 was opened. The diluted equilibrium sampled was thus flushed from the internal jet-mixers to the external jet-mixers. This produced further homogenisation of the equilibrium sample.
10. Valve V13 was opened and a slow flowrate of helium (approximately 0.005 bar/sec) was allowed. The pressure was built up to approximately 1.8 bar, at which point valve V13 was closed.
11. Valve V11 was opened. The micrometer needle valve V12 was then opened so as to allow a slow flow (approximately 0.01 bar/sec) of diluted homogenised equilibrium sample through the 8-port GC valve. The 8-port GC valve was then switched and the sample was conveyed to the GC for analysis. Valve V12 was then closed and the analysis results awaited. This step was repeated about five times. Generally sample was sent to the GC for analysis at every 0.1 bar decrease in pressure.

It should be noted that with this design the liquid sampling method does not affect the cell interior volume or pressure and so there is no disturbance of the equilibrium condition.

5.4.2. Sampling of the vapour phase

Sampling of the vapour phase was simpler than for the liquid as the sample was only homogenised once and this occurred in a jet-mixer external to the air-bath. The procedure was very similar to that for the liquid sample and we assume for this procedure that the liquid sample has been taken first. Thus steps 1 to 4 in the liquid phase sampling procedure have already been carried out. The procedure from then on is as follows:-

1. The sampling lines and the jet-mixers had to be evacuated. This was accomplished by opening the three-way valves T1 and T2 to vacuum. Valves V2, V7, and V10 were also opened. The lines/jet-mixer were evacuated to approximately 0.8 mbar. Once the desired vacuum was achieved all the above mentioned valves were closed.
2. Valve T2 was then opened to helium. Metering valve V13 was slightly opened to allow a slow flow of helium into the line. The pressure in the line was built-up to 0.75 bar and then valve V13 was closed. As in step 6 for the liquid sampling the helium was allowed to heat up to the bath temperature.
3. Valve V7 was opened and the vapour GC sampling valve turned from the *sampling* to the *flushing* position, followed by the opening of valve V2. This flashed the sample into the jet-mixer and promoted homogenisation via swirling action. Valve V13 was opened and slow flowrate of helium (approximately 0.005 bar/sec) was set. The pressure was built up to 2 bar.
4. Valve 13 was then closed and the pressure reading monitored for any decrease. Any decrease as mentioned before was a sign of condensation in the line/jet-mixer.
5. Valve V10 was opened and the step procedure was as discussed in step 11 for liquid sampling.

5.4.3. Some important notes on experimental procedure

Discussed below are some important points and observations on the experimental procedure. They are as follows:-

a) Overpressurization

This is to be avoided in the flushing and homogenising procedure. Overpressurisation may result in the less volatile component separating out in the jet-mixer. The jet-mixer then in

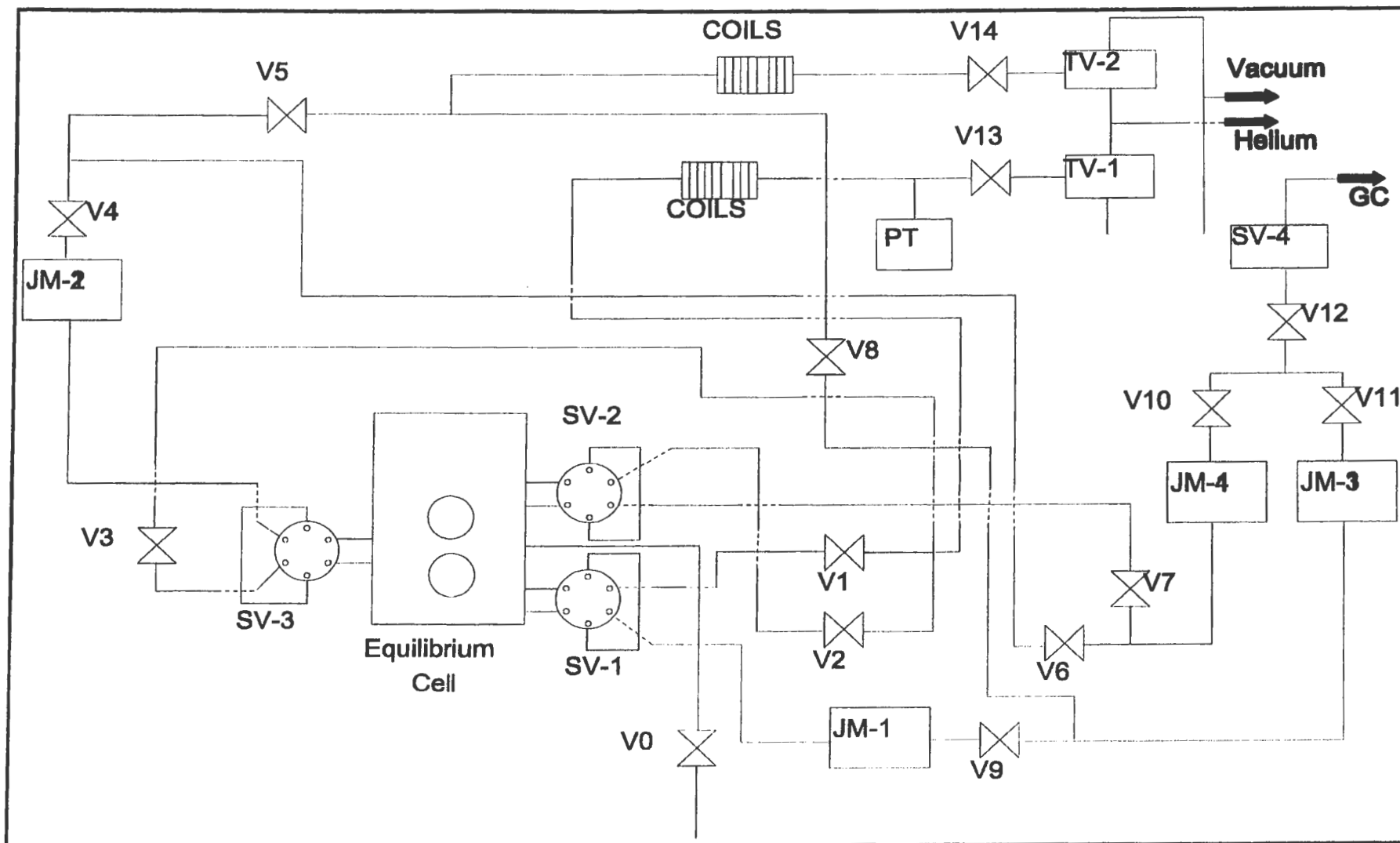


Figure 5-3: Layout of sampling lines for the apparatus

effect acts as an equilibrium cell. As a result the sample conveyed to the GC for analysis is not a representative equilibrium sample.

b) Purging of sample lines

The lines conveying the equilibrium samples from the equilibrium cell to the GC have to be evacuated and purged between successive liquid and vapour samples. This is to ensure that no residual traces of components from previous samples are present in the sampling lines. The purging procedure is explained under the liquid and vapour sampling procedure.

c) Sample line length

When the equilibrium samples are flushed from the sampling device to the GC, there is a tendency for the volatile and non-volatile components to separate due to the volatile component travelling faster than the non-volatile component. A concentration profile is evident during successive flushings to the GC. The concentration of the non-volatile component increases with successive flushings. Mühlbauer [1990] noted this observation, and thanks to this observation, we kept the length of sampling lines to the shortest possible length. We also inserted the second jet-mixer as recommended by Mühlbauer [1990]. Despite these precautions, there was still a very slight non-random spread in the successive vapour mole fractions. As observed by Mühlbauer [1990], the first flushing produced a slightly rich volatile component sample, and the final flushing a slightly lean volatile component sample.

5.5. PROCEDURE FOR P-V-T MEASUREMENTS

The experimental procedure for the measurement of P-V-T behaviour of gases and gas mixtures is relatively simple. It basically involves varying the volume of the equilibrium cell and noting the equilibrium cell pressure under varying isothermal conditions.

The procedure maybe outlined as follows:-

1. The air-bath temperature is set on the Eurotherm 808 controller to the temperature of interest. In this study the temperatures under investigation were 50 °C, 75 °C, and 100 °C. It generally took about 6 hours for the air-bath and the equilibrium cell to reach thermal equilibrium at the set-point temperature.
2. The piston is moved to its zero position. This gives the equilibrium cell its maximum possible volume.

3. The equilibrium cell is filled with the gas to be investigated. When a binary gas mixture is to be studied the gases are charged into the equilibrium cell consecutively. The pressure increments on filling were also noted and could be used as a means of calculating the composition of the binary mixture in the equilibrium cell. In the case of binary gas systems the upper stirrers are switched on and the cell contents stirred to ensure homogenisation of the cell contents.
4. At thermal equilibrium and once the pressure had stabilised, the pressure of the equilibrium cell was noted.
5. The piston is then moved downwards in the equilibrium cell. The distance that the piston moves is calculated from the micrometer dial on the piston assembly. The stepper motor drive can be moved in steps and therefore the distance moved by the piston can be calculated in increments or steps of the stepper motor. When the piston was to be moved the pressure equalisation circuit was switched on. This maintained a pressure differential across the piston of 1 bar. This assisted the stepper motor in driving the piston.
6. At the new position of the piston which constituted a new equilibrium cell volume (once the pressure had stabilised) the equilibrium pressure was noted.
7. Steps 5 and 6 were then repeated for as many measurements as were required.
8. Once a particular isotherm had been completed, the air-bath temperature was set to the new temperature under investigation and steps 4 to 7 were carried out.
9. For the binary gas system the composition of the system could be measured by following the procedure as outlined for the vapour phase sampling (Chapter 5.4.2).

5.6. GC CALIBRATION PROCEDURE

The detector used in this study was the Thermal conductivity detector (TCD) and therefore calibration of the GC in fact meant calibration of the TCD. There are basically two methods of calibrating a detector to achieve accurate results. The method of internal standardisation is the more accurate, while the other is the method of direct injection. Unfortunately the method of internal standardisation could not be used in this project, for the following reasons:-

1. The systems being studied consisted of components that were a liquid and a gas at room temperature. This meant that internal standardisation could not be used.
2. The equilibrium samples to be analysed were routed directly from GC sampling valves. This precluded the addition of a standard of known quantity to the sample before analysis.

As a result the method of direct injection had to be adopted. A major concern when using this method of calibration though is the reliance on the accuracy of the injected volume and the syringe. A new precision volumetric GC calibration apparatus, developed in the Department for gas mixtures could not be used since the micro-liquid injection feature had not been completed yet. The precautions taken and the methods of calibration are described in Appendix D.2.

The operating conditions for the GC and the method are summarised in Chapter 7.

CHAPTER SIX

SYSTEMS CHOSEN FOR EXPERIMENTATION

Before any systems were thoroughly investigated, the experimental apparatus and procedure was put to the test with the carbon dioxide + toluene system. Once the apparatus had been shown capable of accurately measuring HPVLE data, the carbon dioxide + methanol system was tackled. As one of the objectives was to verify the experimental results of Mühlbauer [1990] for the propane + 1-propanol system, this system was investigated last.

P-V-T investigations were also undertaken to demonstrate the versatility of the apparatus. The second virial coefficients were determined for pure components and for a binary mixture. Pure components investigated were nitrogen and propane. The binary mixture studied was nitrogen + propane.

Published data for the systems of interest to this project are available in table format in Appendix E.

6.1. THE CARBON DIOXIDE + TOLUENE SYSTEM

Carbon dioxide + toluene was used as a test system as it is a very severe test of the experimental equipment and procedure. In addition the system has been used in the past by various authors (Ng and Robinson [1978], Sebastian et al. [1980], Morris and Donohue [1985], Kim et al. [1986], Fink and Hershey [1990], and Mühlbauer [1990]) as a test system for their equipment and procedures.

The reasons why the carbon dioxide + toluene system is generally used as a test system are as follows :-

1. Carbon dioxide and toluene are easily available in high purity. In addition they are relatively cheap and non-toxic, also, carbon dioxide is non-combustable. These are important factors to take into consideration during initial experimentation when leaks have to be eliminated and experimental procedures finalised. During the test phase large quantities of material are used.

2. There is a large difference in the volatility between the two component which makes it difficult to obtain a liquid sample which is representative. Thus it serves as a very severe test for the sampling method used.
3. The system is very difficult to handle once a sample has been withdrawn. The liquid sample has to be vaporised before analysis by a gas chromatograph and partial condensation of the non-volatile in the sample lines is always a major problem, and must be avoided.
4. True equilibrium conditions are not very easily obtained.
5. Carbon dioxide is supercritical at room temperature, and thus the desired experimental pressure can be achieved by merely heating the cell.

Table 6-1 below lists the authors who have studied the carbon dioxide + toluene system as reviewed in this project.

Author/s	System Temperature (K)	Pressure Range (Bar)	Number of experimental data sets
Ng and Robinson [1978]	311.26	3.34 - 77.43	8
	352.59	3.76 - 123.07	10
	393.71	4.03 - 152.93	8
	477.04	11.79 - 152.24	8
Sebastian et al. [1980]	393.25	9.76 - 51.98	4
	422.45	19.79 - 51.88	5
	476.95	12.37 - 50.97	5
	502.75	20.62 - 50.36	4
	542.85	31.66 - 51.57	3
Lin et al. [1985]	477	11 - 49	5
Morris and Donohue [1985]	353.15	2.59 - 119.30	12
	383.15	5.93 - 128.00	10
	413.15	7.10 - 131.70	9
Kim et al. [1986]	353.4	6.72 - 61.77	8
	373.2	5.15 - 54.89	7
	393.2	13.13 - 64.50	7
Fink and Hershey [1990]	308.16	8.04 - 69.21	15
	323.17	6.40 - 87.73	16
	353.18	5.18 - 123.50	19
Mühlbauer [1990]	352.15	8.76 - 109.97	9
Mühlbauer and Raal [1991]			

Table 6-1: Survey of measured data for the Carbon Dioxide + Toluene System

Volumetric properties for the system have been undertaken at high pressure and are available in Pohler and Kiran [1996].

6.2. THE CARBON DIOXIDE + METHANOL SYSTEM

The reasons for studying the carbon dioxide + methanol system were as follows :-

1. The system is generally used as a test system and has been well studied. It thus serves as a further test for the experimental apparatus and experimental procedure.
2. SASOL approached us to determine HPVLE data for a multicomponent system of interest to them. One of the constituent binaries in the multicomponent system was the carbon dioxide + methanol system. They however required HPVLE data at low temperatures (approximately 200 K). The equipment used in this study is not at this stage capable of measuring HPVLE at such low temperatures. We thus decided to perform HPVLE measurements at higher temperatures, test the extrapolation ability of the Wong and Sandler mixing rule (Wong et. al. [1992]), and then extrapolate the measured data that we obtained to the temperatures required by SASOL.

Table 6-2 lists the authors who have studied the carbon dioxide + methanol system as reviewed in this project.

Reighard et al. [1996] have also determined HPVLE for the carbon dioxide + methanol system, however, their data was measured at constant composition i.e. P - T data.

6.3. THE PROPANE + 1-PROPANOL SYSTEM

Only two researchers had studied the HPVLE behaviour for the system. Nagahama et al. [1971] performed HPVLE measurements for the system at low temperature, but did not measure the vapour phase compositions. Mühlbauer [1990] measured both the liquid and vapour phases; however he could not achieve proper modelling of the system. Mühlbauer [1990] could also not attain a relatively high pressure in his equilibrium apparatus. He suspected that there was liquid phase splitting occurring at this higher pressure, although he did not have a visual cell and therefore could not confirm this. We thus decided to verify the experimental data of Mühlbauer [1990] to determine if the measured data were accurate and to determine if there was liquid phase splitting at the higher pressures.

Table 6-3 lists the authors who have studied the propane + 1-propanol system as reviewed in this project.

Excess molar properties for the propane + 1-propanol system are available in Brown et al. [1996].

Author/s	System Temperature (K)	Pressure Range (Bar)	Number of experimental data sets
Katayama et al. [1975]	298.15	2.19 - 61.28	13
Ohgaki and Katayama [1976]	298.15	7.90 - 59.53	8
	313.13	5.77 - 80.58	9
Weber et al. [1984]*	233.15	3.00 - 8.90	6
	248.15	3.30 - 16.85	7
	253.15	5.55 - 15.20	6
	273.15	4.48 - 33.00	9
	273.15	6.59 - 34.86	20
	298.15	7.80 - 50.83	11
Chang and Rousseau [1985]**	243.15	2.05 - 13.46	6
	258.15	2.21 - 21.57	6
	273.15	1.93 - 32.35	6
	298.15	2.60 - 54.54	8
Brunner [1985] Brunner et al. [1987]***	298.15	17.3 - 62.3	17
	323.15	9.9 - 95.5	14
	373.15	20.1 - 154.2	12
	423.15	36.7 - 161.3	11
	473.15	75.2 - 129.3	4
Hong and Kobayashi [1988]	230	6.89 - 8.83	6
	250	11.55 - 17.51	3
	250	6.89 - 15.86	4
	273.15	6.89 - 34.47	10
	290	6.89 - 51.64	9
	310	6.89 - 77.43	19
	330	6.89 - 106.46	13
Suzuki et al. [1990(b)]	313.4	6.83 - 77.13	8
Chang et al. [1997]	291.15	5.6 - 49.3	12
	298.16	9.2 - 57.1	17
	303.18	8.9 - 63.2	16
	308.15	13.2 - 70.1	16
	313.14	13.2 - 80.3	17

* Weber [1984] did not measure vapour phase compositions.

** Chang and Rousseau [1985] did not measure vapour phase compositions.

*** The liquid and vapour compositions are not at the same pressure.

Table 6-2: Survey of measured data for the Carbon Dioxide + Methanol System

Author/s	System Temperature (K)	Pressure Range (Bar)	Number of experimental data sets
Nagahama et. al. [1971]*	293.05	1.43 – 7.99	10
Mühlbauer [1990]**	354.75	4.53 – 22.39	14
Mühlbauer and Raal [1993]**	378.15	4.58 – 35.49	16
	393.15	4.46 - 40.45	18

*Nagahama et. al. [1971] did not measure vapour phase compositions

** The liquid and vapour phase compositions are not at the same pressure

Table 6-3: Survey of measured data for the Propane + 1-Propanol System

6.4. *P-V-T* MEASUREMENTS

P-V-T measurements were undertaken for nitrogen and propane so as to obtain the second virial coefficients for the gases. This was undertaken to examine the variable volume capabilities of the apparatus and thus its versatility. Nitrogen and propane were decided on because: -

1. We had worked with them during the VLE studies, and thus these gases were available to us; and
2. These gases had been extensively studied before, and values for the second virial coefficient are available in Dymond and Smith [1980].

The determination of the second virial coefficient for the nitrogen + propane system was also undertaken. Dymond and Smith [1980] contains extensive data on the second virial coefficient for pure gases, however, cross-term second virial coefficients for the system nitrogen + propane are sparse. Data for the system are available in Wormald et al. [1996].

CHAPTER SEVEN

EXPERIMENTAL RESULTS

The factors that affect the accuracy of the equilibrium measurements will be discussed in this chapter. The measured experimental data will also be presented. The properties that are measured in VLE experimentation are temperature, pressure and phase compositions. It is thus crucial that proper calibration be undertaken for these properties. Therefore GC calibrations for composition measurements, as well as pressure and temperature sensor calibrations will also be presented in this section.

7.1. PURITY OF CHEMICALS

The chemicals used in this project can be grouped into one of two categories, viz. gaseous and liquid components at standard conditions.

7.1.1. Gaseous materials

The gaseous chemicals used in this project were carbon dioxide, nitrogen, propane and helium. Fedgas supplied carbon dioxide, nitrogen and helium, whereas Afrox supplied propane.

7.1.1.1. Carbon Dioxide

Carbon dioxide with a certified minimum purity of 99.995 % was supplied in a 75l cylinder. The cylinder was pressurised to between 70 and 75 bar. GC analysis of the carbon dioxide verified a purity of greater than 99.99 %. The major impurities in carbon dioxide were oxygen, nitrogen, water, sulphur dioxide and some hydrocarbons. All of these were in less than 10 ppm quantities.

7.1.1.2. Nitrogen

Nitrogen was used for PVT measurements, as well as for pressurisation of the upper nitrogen compartment (equalisation of the pressures across the piston head). The nitrogen, which came pressurised at 200 bar in a 75l cylinder, was certified as having a minimum purity of 99.998 %.

GC analysis confirmed purity in excess of 99.99 %. The major impurities in nitrogen were oxygen, water, ethane, propylene, isobutane, and n-butane.

7.1.1.3. Helium

Helium was used as a carrier gas and as a reference gas in gas chromatography. It was supplied in a 75l cylinder, pressurised at 200 bar, with a certified minimum purity of 99.998 %. The major impurities in helium were oxygen, nitrogen, water, and hydrocarbons. All major impurities were in ppm quantities.

7.1.1.4. Propane

Instrument grade propane with a certified minimum purity of 99.5 % was supplied in an A1 cylinder as a liquefied gas under its vapour pressure. GC analysis of the propane indicated a purity of approximately 99 %. The major impurities in propane were ethane, propylene, isobutane and n-butane.

7.1.2. Liquid materials

Liquid materials used in this project were toluene, methanol and 1-propanol. For all of the liquids, purity was verified by GC analysis and refractive indices measurement (refer to Table 7-1).

7.1.2.1. Toluene

Toluene was supplied by SAARCHEM. The minimum purity was claimed to be 99.8 %. Major impurities were benzoic acid (0.002 %), ammonia (0.0002 %), benzene (0.05 %) and water (0.02 %).

7.1.2.2. Methanol

Riedel-de Haën supplied methanol. The minimum purity was claimed to be 99.8 %. The major impurity was water (0.03 %).

7.1.2.3. 1-Propanol

1-Propanol was obtained from MERCK. The minimum purity was claimed to be 99.7 %. Major impurities in 1-propanol were acetone (0.01 %), ethanol (0.05 %), methanol (0.05 %), 2-propanol (0.05 %) and water (0.05 %).

Chemical	Refractive Index		GC Analysis % purity
	Measured	Literature [Weast et al., 1986]	
Toluene	1.4962	1.4961	99.7
Methanol	1.3292	1.3290	99.8
1-Propanol	1.3848	1.3850	99.5

Table 7-1: Purity of the liquid materials verified by refractive index measurement (20 °C) and GC analysis.

Refractive indices were measured with a high precision refractometer and GC analysis was undertaken with the instrument (detailed in Chapter 4) at the conditions mentioned later in this chapter.

7.2. ACCURACY OF MEASURED PROPERTIES

The primary properties that were measured were temperature, pressure and composition.

7.2.1. Temperature

Temperature was measured with a Pt-100 Ω resistor (class A). It was certified as being accurate to within 0.05 %. This corresponds to a temperature uncertainty of approximately 0.2 K at 100 °C. The Pt-100 Ω resistor was calibrated against a quartz thermometer. For a wide range of temperatures (30 to 250 °C) the quartz thermometer and Pt-100 Ω resistor readings were within 0.3 % of each other.

7.2.2. Pressure

Sensotec pressure transducers were used to measure pressure. The transducers were certified accurate to within 0.25 %. This corresponds to a pressure uncertainty of approximately 0.25 bar at a pressure of 100 bar. The pressure transducers were calibrated against a Heisse gauge. Two Heisse gauges were used to calibrate the pressure transducers. For the 0 to 5 bar range transducer, the 0 to 500 psi range Heisse gauge was used. For the 0 to 175 bar range transducers, the 0 to 5000 psi range Heisse gauge was used. For calibration of all the transducers, the transducer and Heisse gauge readings corresponded to within a tenth of a bar over the entire pressure range. The Heisse gauges were certified as having an uncertainty of approximately 0.034 bar.

7.2.3. Composition

Phase compositions were determined by GC analysis. GC calibration is discussed in Chapter 5 and Appendix D. Performing a literature survey and taking into account all known possible factors that affect accuracy of composition measurement via GC (for GC calibration, a plot was made of GC area versus number of moles injected), the maximum errors for composition measurement were determined. They correspond to approximately 1.0 % for the non-volatile component and 1.5 % for the volatile component. Since mole fraction measurements relate the ratio of volatile or non-volatile number of moles to total number of moles, the uncertainty in mole fractions is approximately 2.5 %.

7.3. GC CALIBRATION CURVES

The method of calibration for the GC and the conditions of operation are discussed in Appendix D and later in this chapter. Presented in Figures 7-1 to 7-5 are the GC calibration curves for the various chemicals used in this study. For all of the GC calibrations, the calibration factor appears to be extremely linear in the range of calibration. The calibration factor obtained by linear regression through the data points is also given in Figures 7-1 to 7-5.

Figure 7-1: GC calibration for Toluene

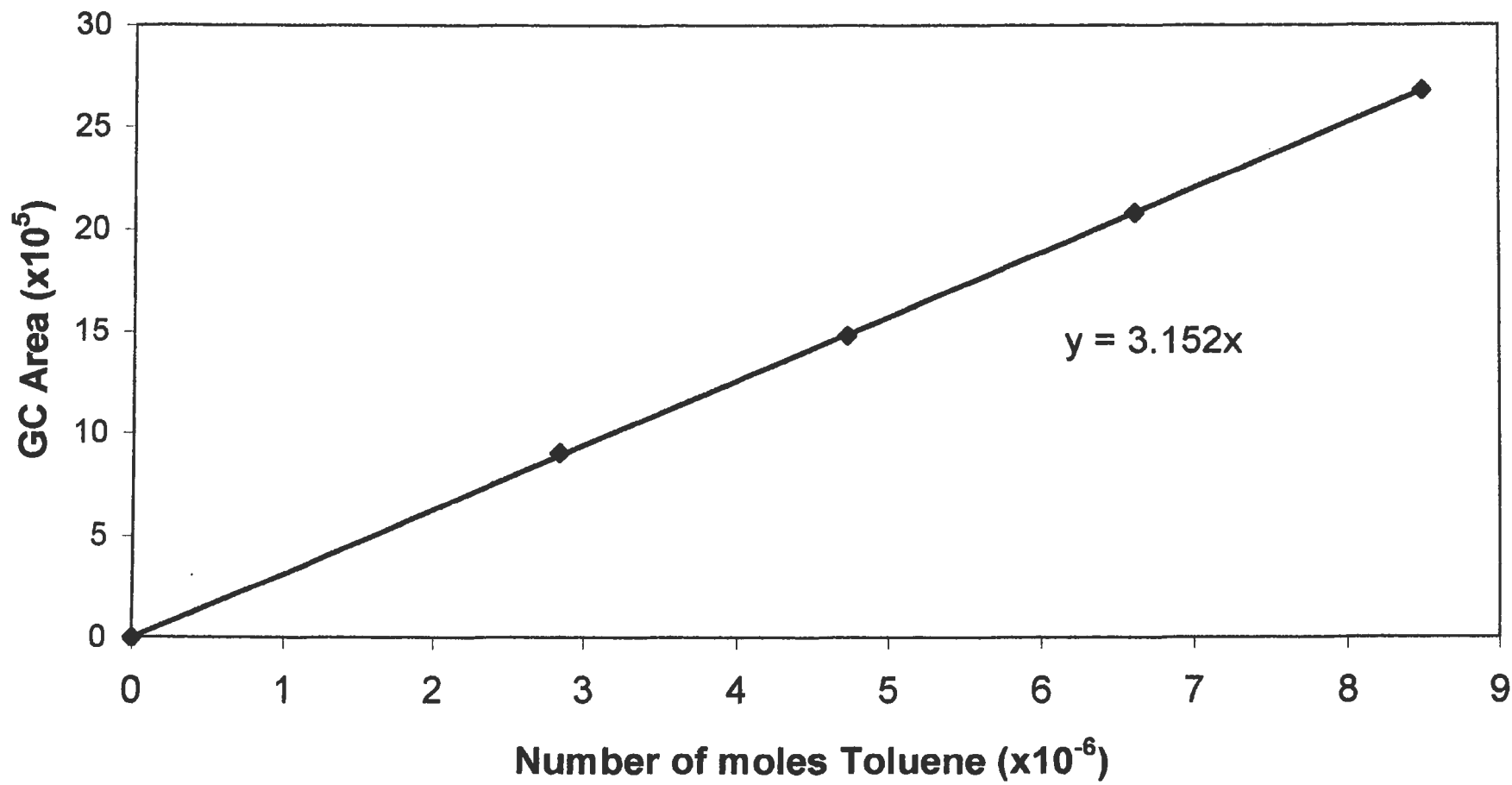


Figure 7-2: GC calibration for Methanol

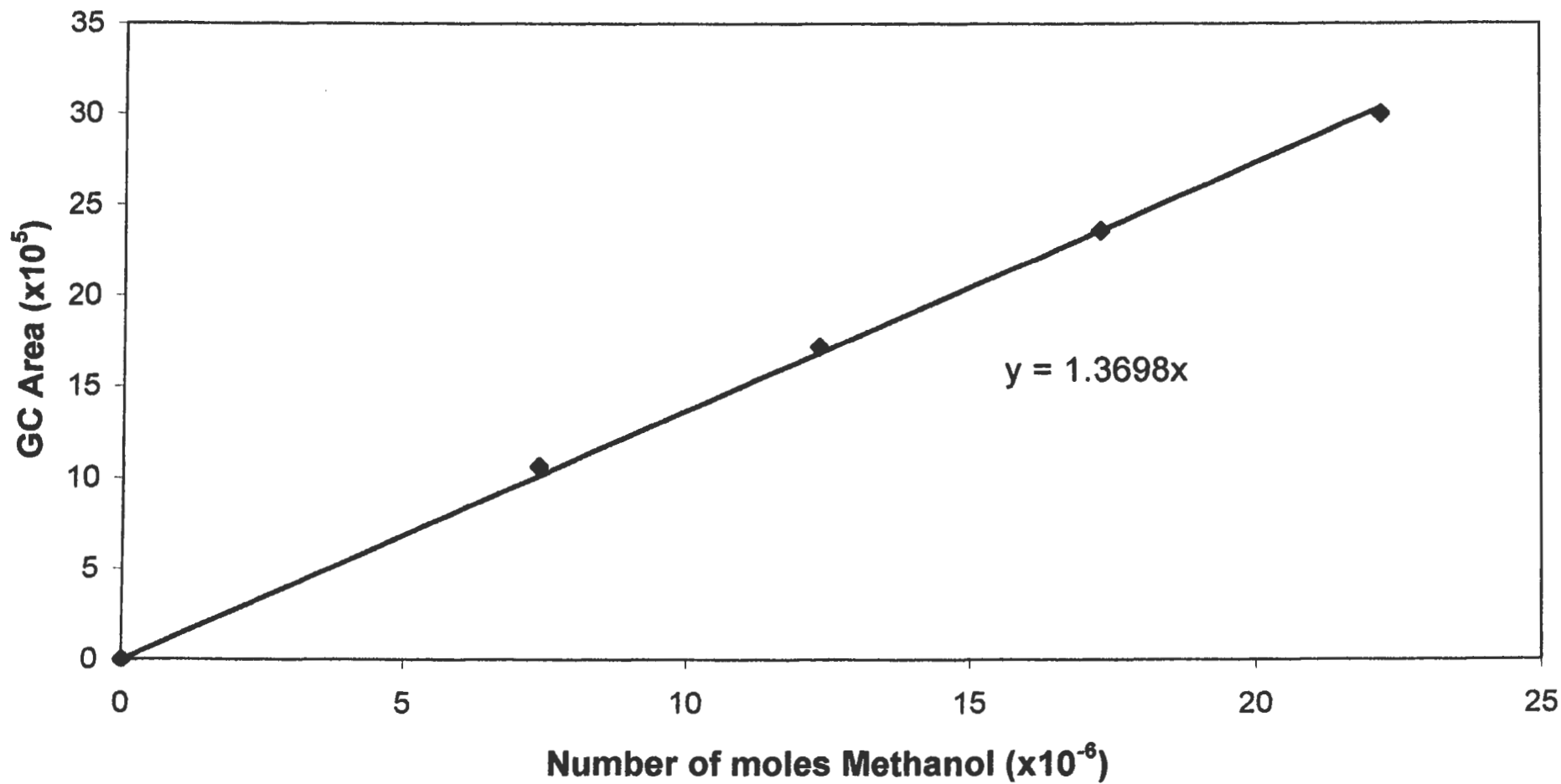


Figure 7-3: GC calibration for 1-Propanol

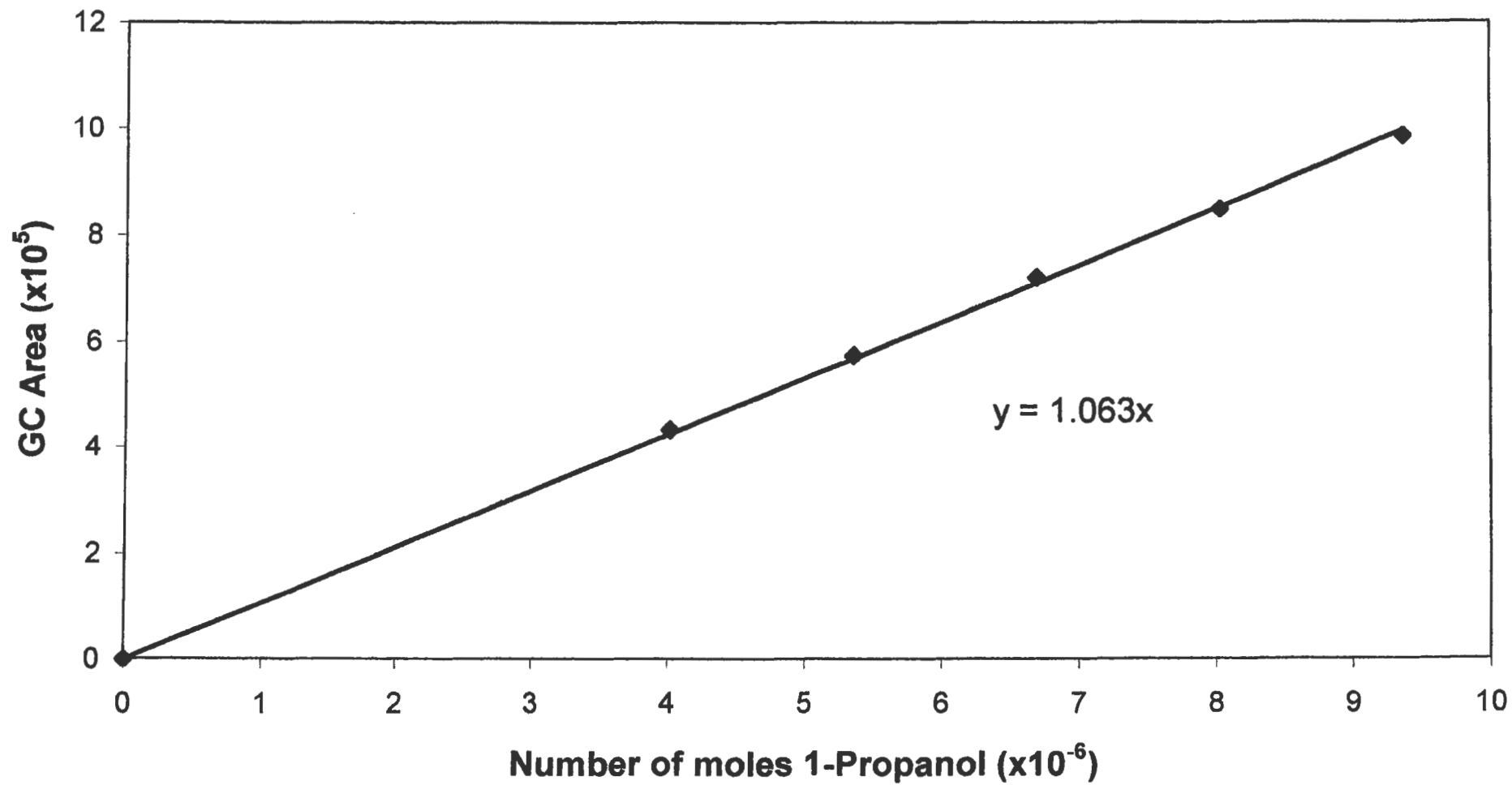


Figure 7-4: GC calibration for Carbon Dioxide

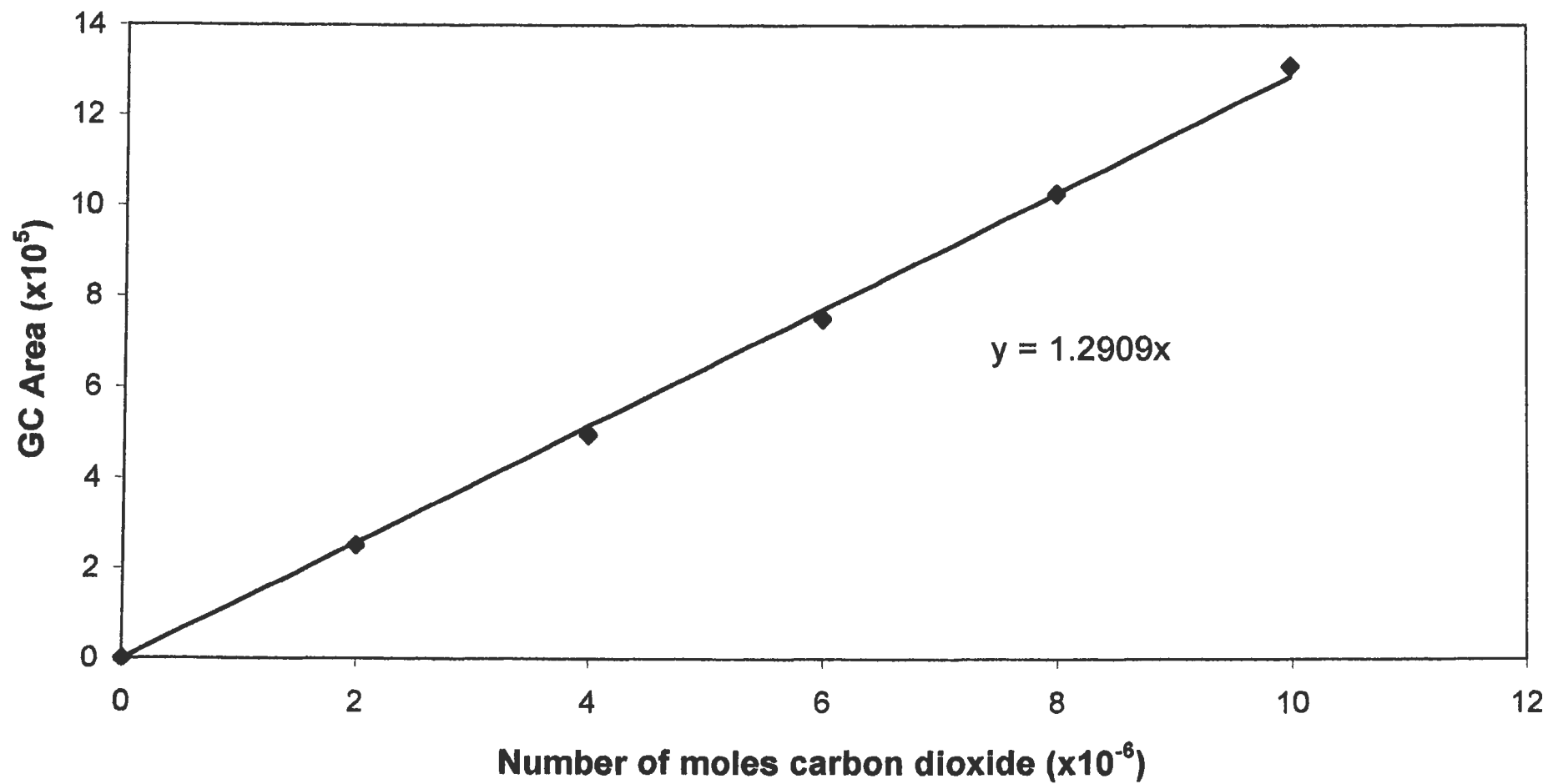
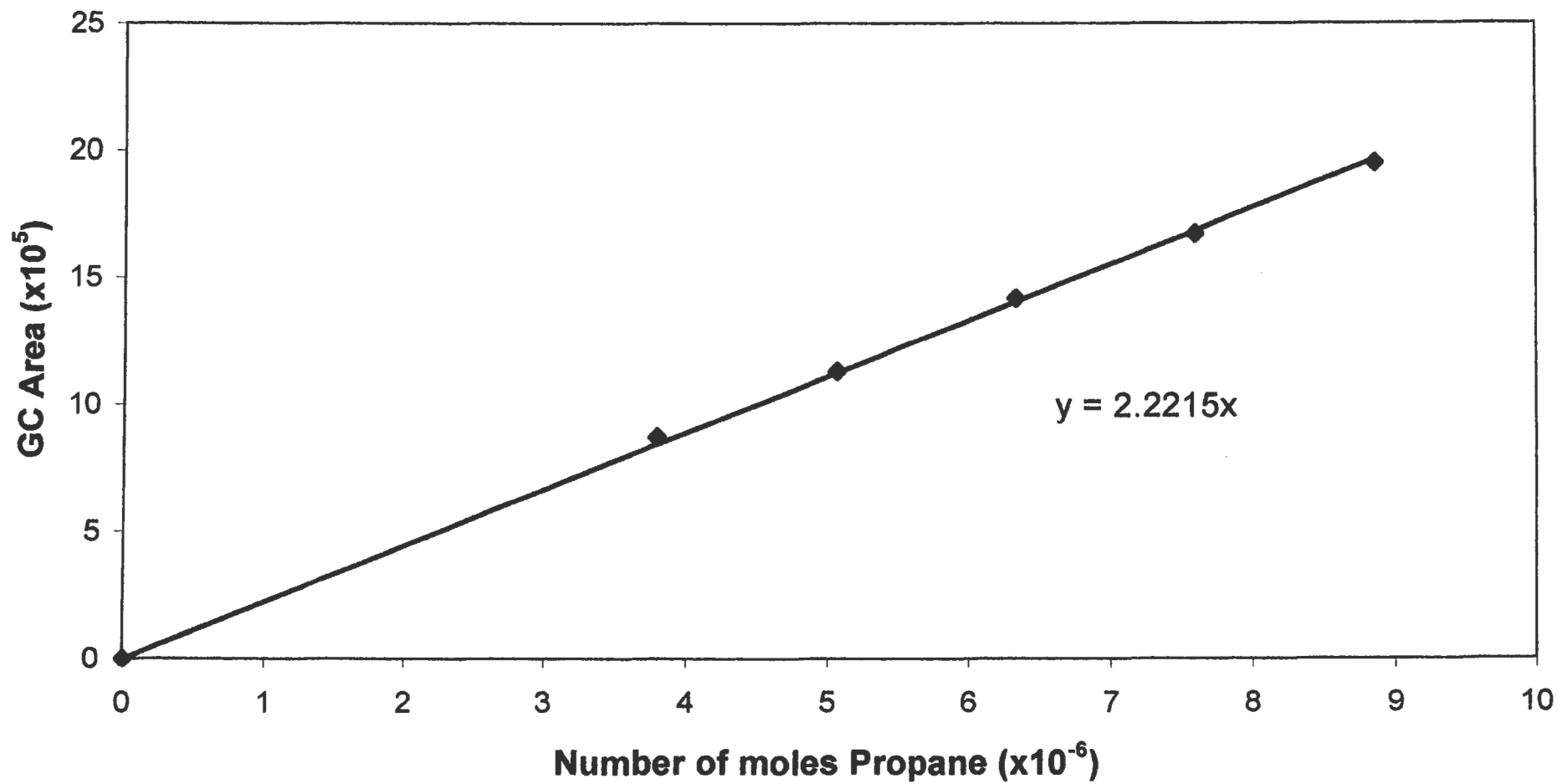


Figure 7-5: GC calibration for Propane



7.4. VAPOUR-LIQUID EQUILIBRIUM MEASUREMENTS

HPVLE measurements were performed for three systems, viz. carbon dioxide + toluene, carbon dioxide + methanol and propane + 1-propanol. For each of the systems a few isotherms were measured.

7.4.1. Carbon Dioxide + Toluene System

The carbon dioxide + toluene system was measured at three isotherms, viz. 38 °C, 80 °C and 118.3 °C.

7.4.1.1. Carbon Dioxide + Toluene - 38 °C isotherm

Table 7-2 lists the experimental data points (liquid and vapour phase mole fractions and pressure) for the carbon dioxide + toluene system at the given isotherm. Figure 7-6 gives the graphical illustration of the data points. Figure 7-7 compares the data measured in this project to literature. Unfortunately a direct comparison at 38 °C could not be made, as literature data was only available at 38.11 °C (Ng and Robinson [1978]) and 35.01 °C (Fink and Hershey [1990]).

Pressure (bar)	Liquid Composition (X_{CO_2})	Vapour Composition (Y_{CO_2})
4.58	0.0382	0.9921
11.23	0.1181	0.9932
20.39	0.1997	0.9935
31.33	0.2867	0.9955
50.14	0.5335	0.9941
60.64	0.6986	0.9945
64.29	0.7613	0.9936

Table 7-2: Experimental data for the Carbon Dioxide + Toluene System at 38 °C

7.4.1.2. Carbon Dioxide + Toluene - 80 °C isotherm

Table 7-3 lists the experimental data points (liquid and vapour phase mole fractions and pressure) for the carbon dioxide + toluene system at the given isotherm. Figure 7-8 gives the graphical illustration of the data points. Figures 7-9 and 7-10 compare the data measured in this

project to literature. Literature data compared to were, Ng and Robinson [1978] (79.44 °C), Morris and Donohue [1985] (80.0 °C), Kim et al. [1986] (80.25 °C), Fink and Hershey [1990] (80.03 °C) and Mühlbauer and Raal [1991] (79 °C).

Pressure (bar)	Liquid Composition (X_{CO_2})	Vapour Composition (Y_{CO_2})
5.89	0.0357	0.9048
12.52	0.0715	0.9562
21.38	0.1215	0.9749
35.63	0.2045	0.9755
51.58	0.2935	0.9841
65.69	0.3816	0.9845
78.15	0.4484	0.9836
84.35	0.4972	0.9828

Table 7-3: Experimental data for the Carbon Dioxide + Toluene System at 80 °C

7.4.1.3. Carbon Dioxide + Toluene – 118.3 °C isotherm

Table 7-4 lists the experimental data points (liquid and vapour phase mole fractions and pressure) for the carbon dioxide + toluene system at the given isotherm. Figure 7-11 gives the graphical illustration of the data points. Figure 7-12 compares the data measured in this project to literature. Literature data compared to were, Ng and Robinson [1978] (120.56 °C), Sebastian et al. [1980] (120.1 °C), and Kim et al. [1986] (120.05 °C).

Pressure (bar)	Liquid Composition (X_{CO_2})	Vapour Composition (Y_{CO_2})
20.64	0.0986	0.9285
33.9	0.1381	0.9462
52.4	0.2382	0.9541
74.29	0.3213	0.9536
94.39	0.3997	0.9485
100.14	0.4335	0.9484
121.33	0.5467	0.9325

Table 7-4: Experimental data for the Carbon Dioxide + Toluene System at 118.3 °C

Figure 7-6: Experimental HPVLE data for the Carbon Dioxide + Toluene System at 38 °C

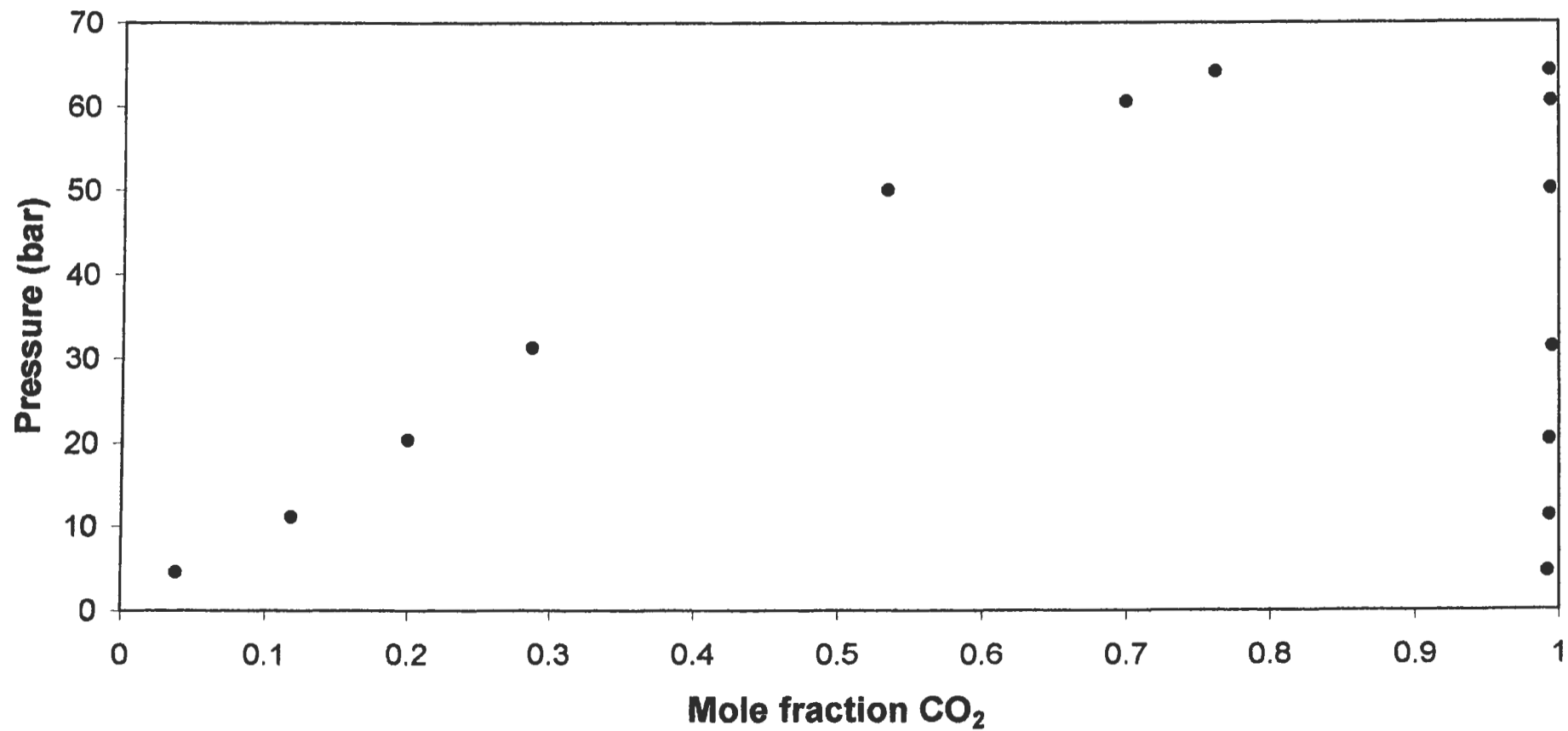


Figure 7-7: HPVLE data for Carbon Dioxide + Toluene System at 38 °C (Comparison with literature)

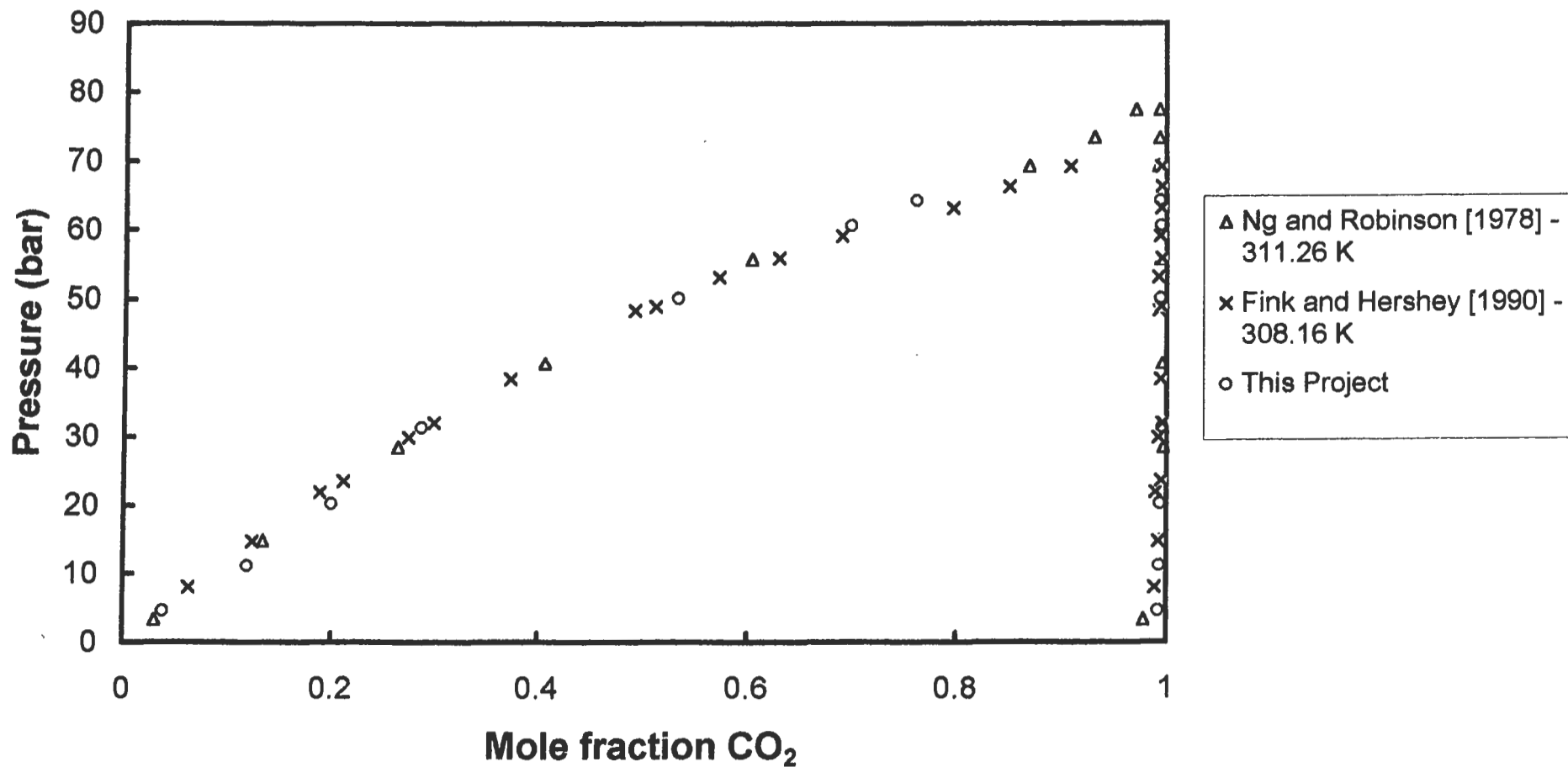


Figure 7-8: Experimental HPVLE data for the Carbon Dioxide + Toluene System at 80 °C

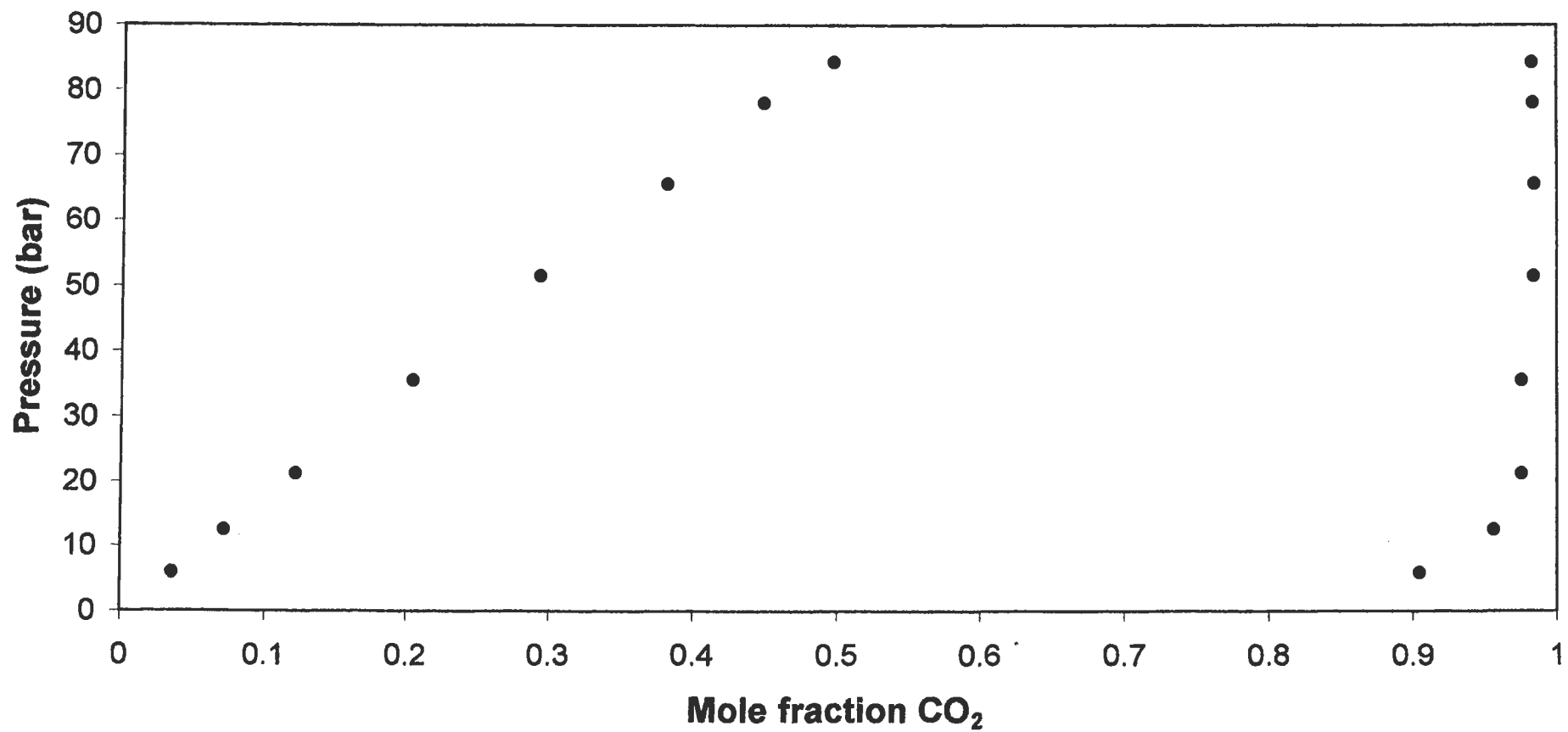


Figure 7-9: HPVLE data for Carbon Dioxide + Toluene System at 80 °C (Comparison with literature)

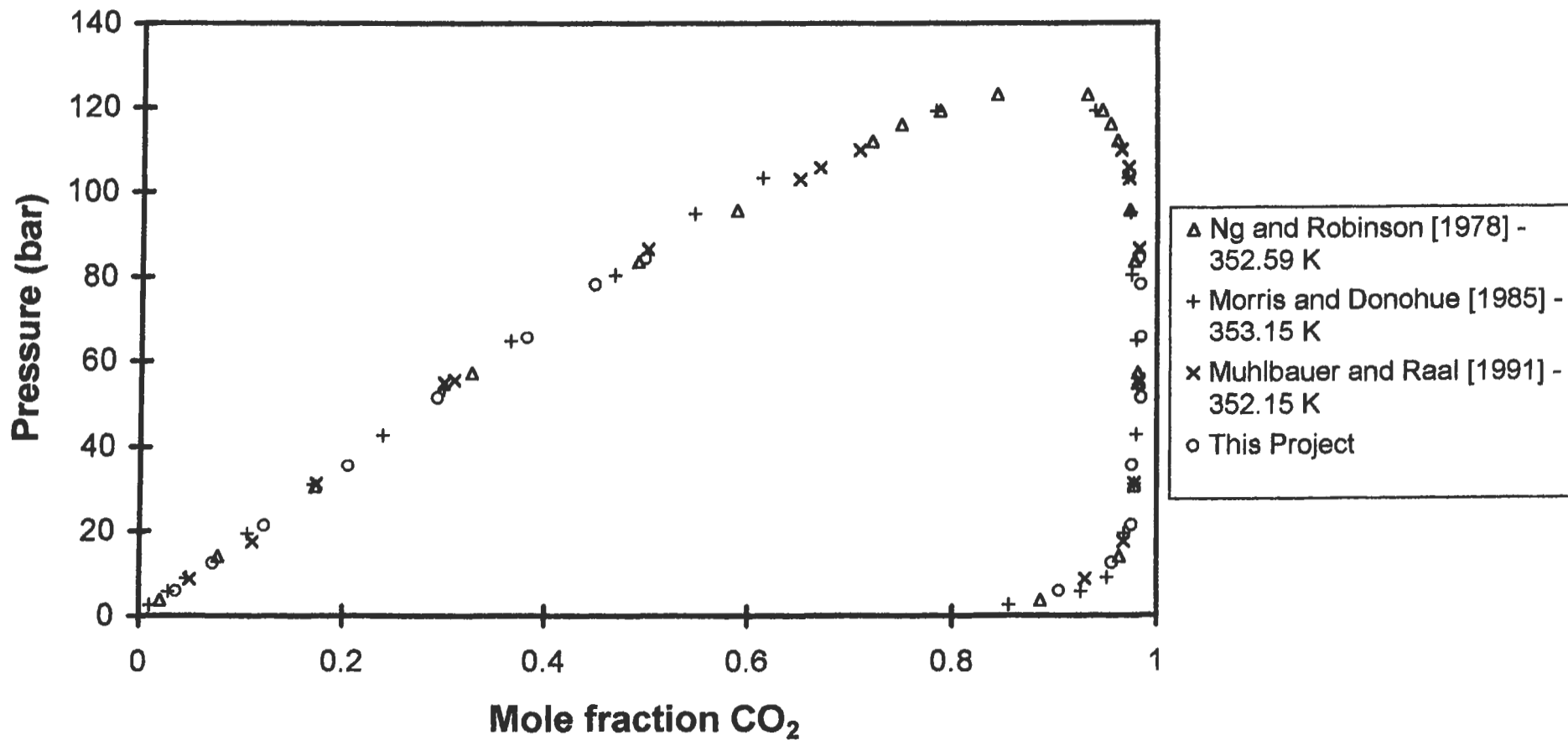


Figure 7-10: HPVLE data for Carbon Dioxide + Toluene System at 80 °C (Comparison with literature)

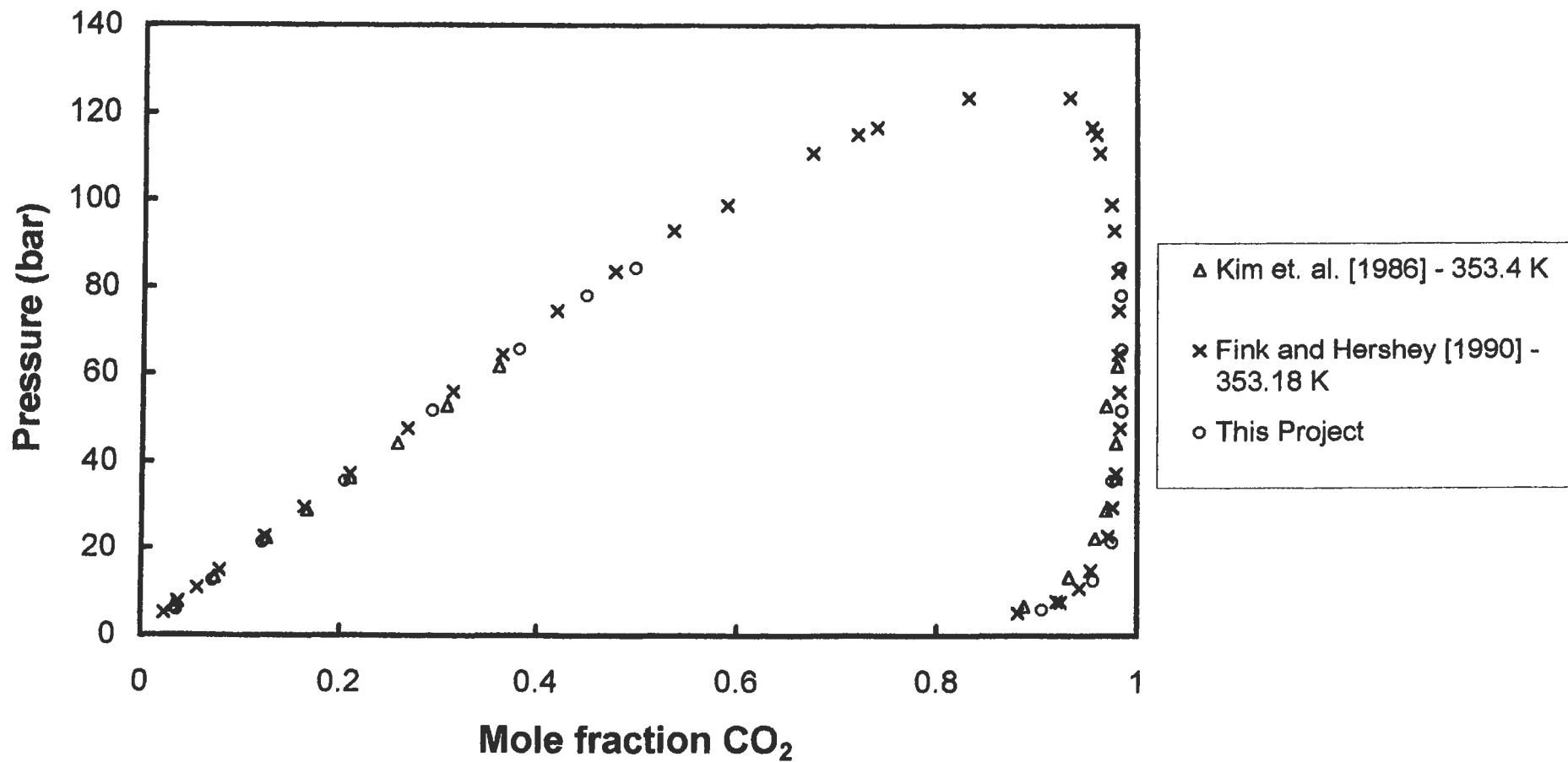


Figure 7-11: Experimental HPVLE data for the Carbon Dioxide + Toluene System at 118.3 °C

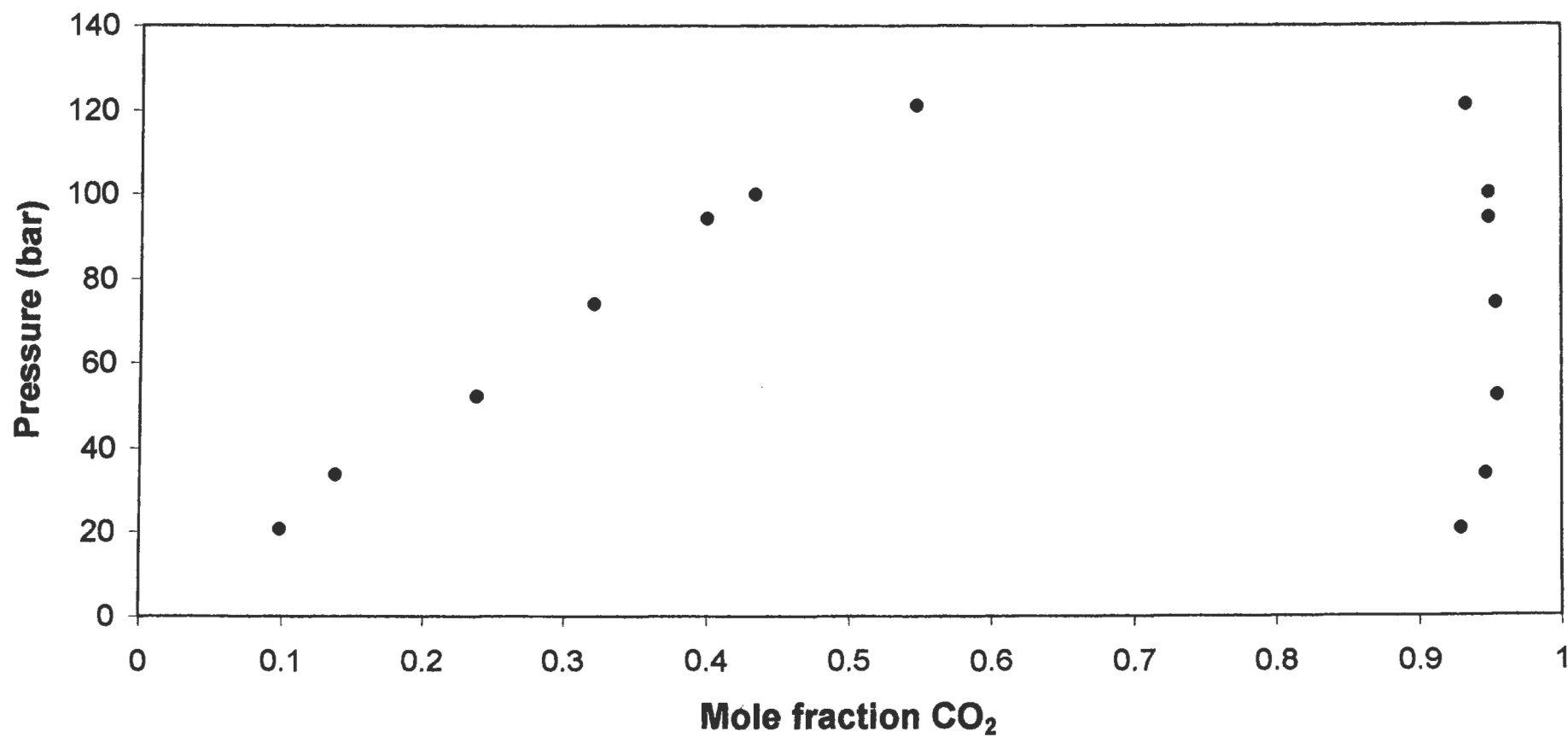
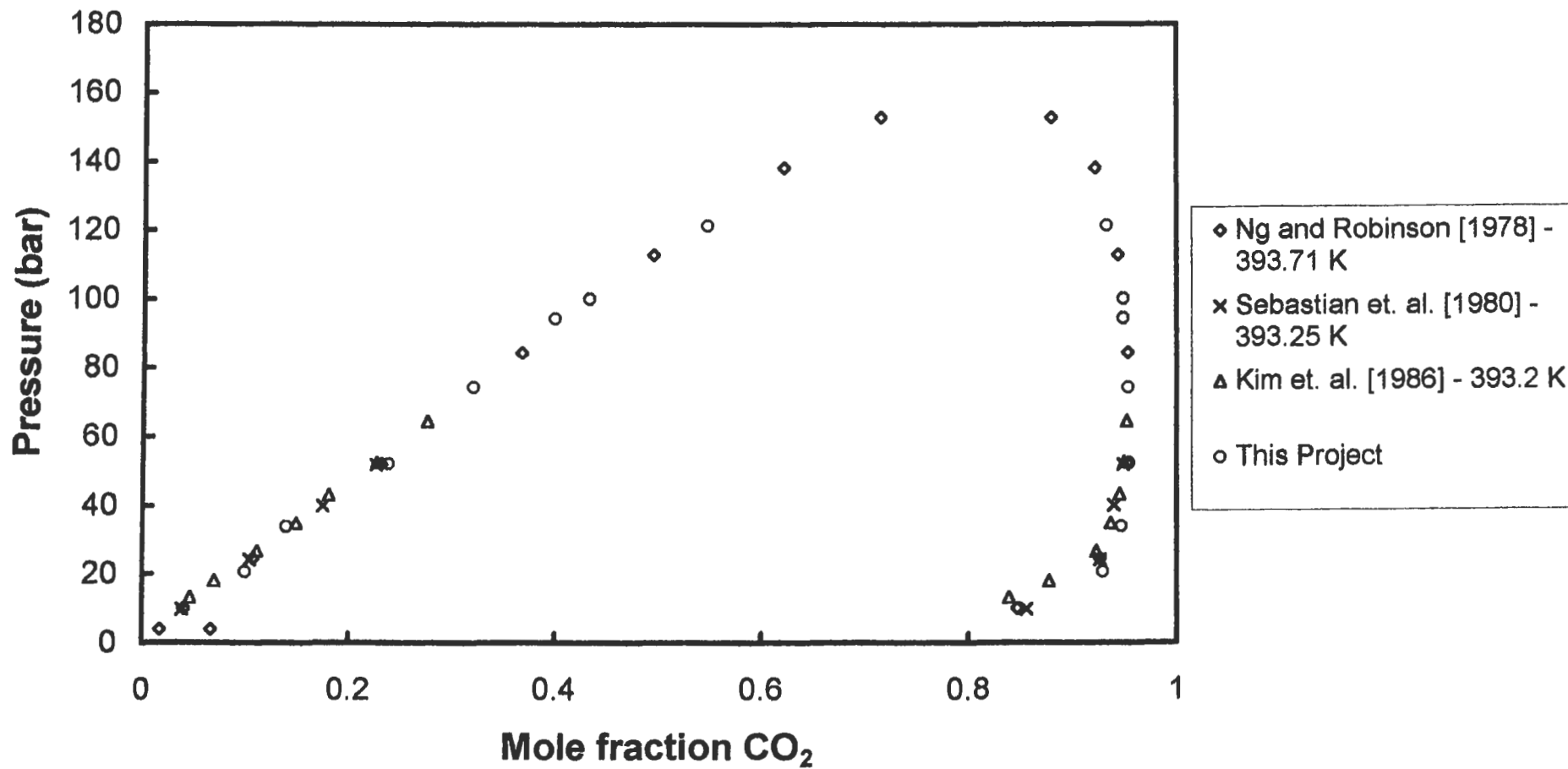


Figure 7-12: HPVLE data for Carbon Dioxide + Toluene System at 118.3 °C (Comparison with literature)



7.4.2. Carbon Dioxide + Methanol System

The carbon dioxide + methanol system was measured at three isotherms, viz. 40 °C, 90 °C and 100 °C.

7.4.2.1. Carbon Dioxide + Methanol - 40 °C isotherm

Table 7-5 lists the experimental data points (liquid and vapour phase mole fractions and pressure) for the carbon dioxide + methanol system at the given isotherm. Figure 7-13 gives the graphical illustration of the data points. Figure 7-14 compares the data measured in this project to literature. Literature data compared to were Ohgaki and Katayama [1976] (40.0 °C), Suzuki et al. [1990] (40.25 °C) and Chang et al. [1997] (39.99 °C).

Pressure (bar)	Liquid Composition (X_{CO_2})	Vapour Composition (Y_{CO_2})
12.91	0.0653	0.9732
23.13	0.1233	0.9825
31.45	0.1856	0.9856
43.39	0.2516	0.9826
51.92	0.3227	0.9845
55.46	0.347	0.986
61.31	0.3968	0.9849
67.58	0.4736	0.9866

Table 7-5: Experimental data for the Carbon Dioxide + Methanol System at 40 °C

7.4.2.2. Carbon Dioxide + Methanol - 90 °C isotherm

Table 7-6 lists the experimental data points (liquid and vapour phase mole fractions and pressure) for the carbon dioxide + methanol system at the given isotherm. Figure 7-15 gives the graphical illustration of the data points. No literature data were available for the system at 90 °C and therefore no comparisons could be made for the measured data.

Pressure (bar)	Liquid Composition (X_{CO_2})	Vapour Composition (Y_{CO_2})
9.67	0.0273	0.7254
15.69	0.0469	0.7991
24.6	0.0701	0.8715
26.54	0.0734	0.8874
40.21	0.1138	0.9132
55.45	0.1646	0.9253
76.89	0.2389	0.9362
85.64	0.2713	0.9419

Table 7-6: Experimental data for the Carbon Dioxide + Methanol System at 90 °C

7.4.2.3. Carbon Dioxide + Methanol – 100 °C isotherm

Table 7-7 lists the experimental data points (liquid and vapour phase mole fractions and pressure) for the carbon dioxide + methanol system at the given isotherm. Figure 7-16 gives the graphical illustration of the data points. Figure 7-17 compares the data measured in this project to literature. Literature data compared against were that of Brunner et al. [1987] (100 °C).

Pressure (bar)	Liquid Composition (X_{CO_2})	Vapour Composition (Y_{CO_2})
21.57	0.0451	0.8042
30.89	0.0697	0.8629
38.73	0.0887	0.8837
50.94	0.1258	0.9053
68.22	0.1783	0.9138
75.28	0.2033	0.9127
90.67	0.2531	0.9118
105.94	0.3103	0.91
120.68	0.3611	0.8927

Table 7-7: Experimental data for the Carbon Dioxide + Methanol System at 100 °C

Figure 7-13: Experimental HPVLE data for the Carbon Dioxide + methanol System at 40 °C

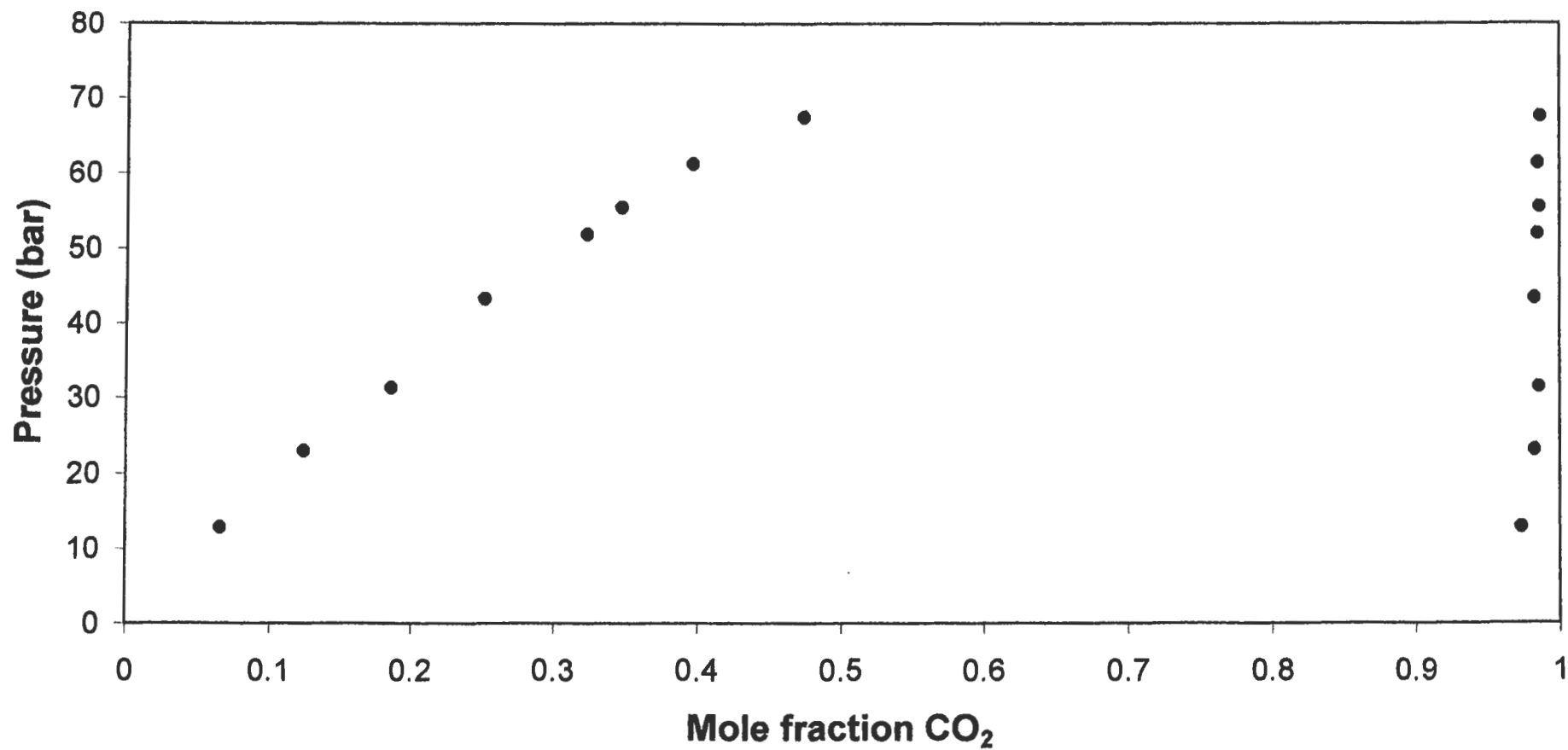


Figure 7-14: HPVLE data for the Carbon Dioxide + Methanol System at 40 °C (Comparison with literature)

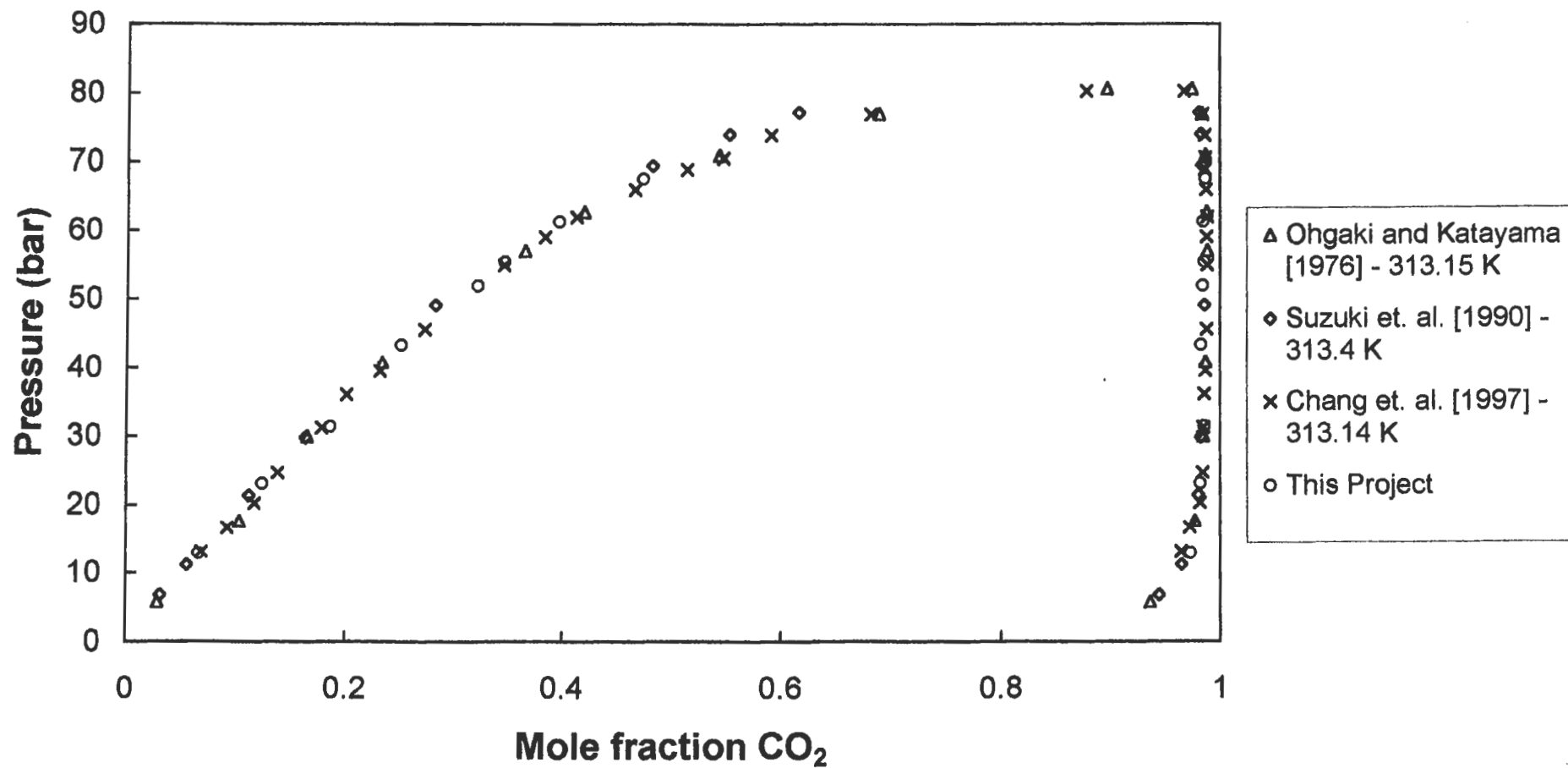


Figure 7-15: Experimental HPVLE data for the Carbon dioxide + Methanol System at 90 °C

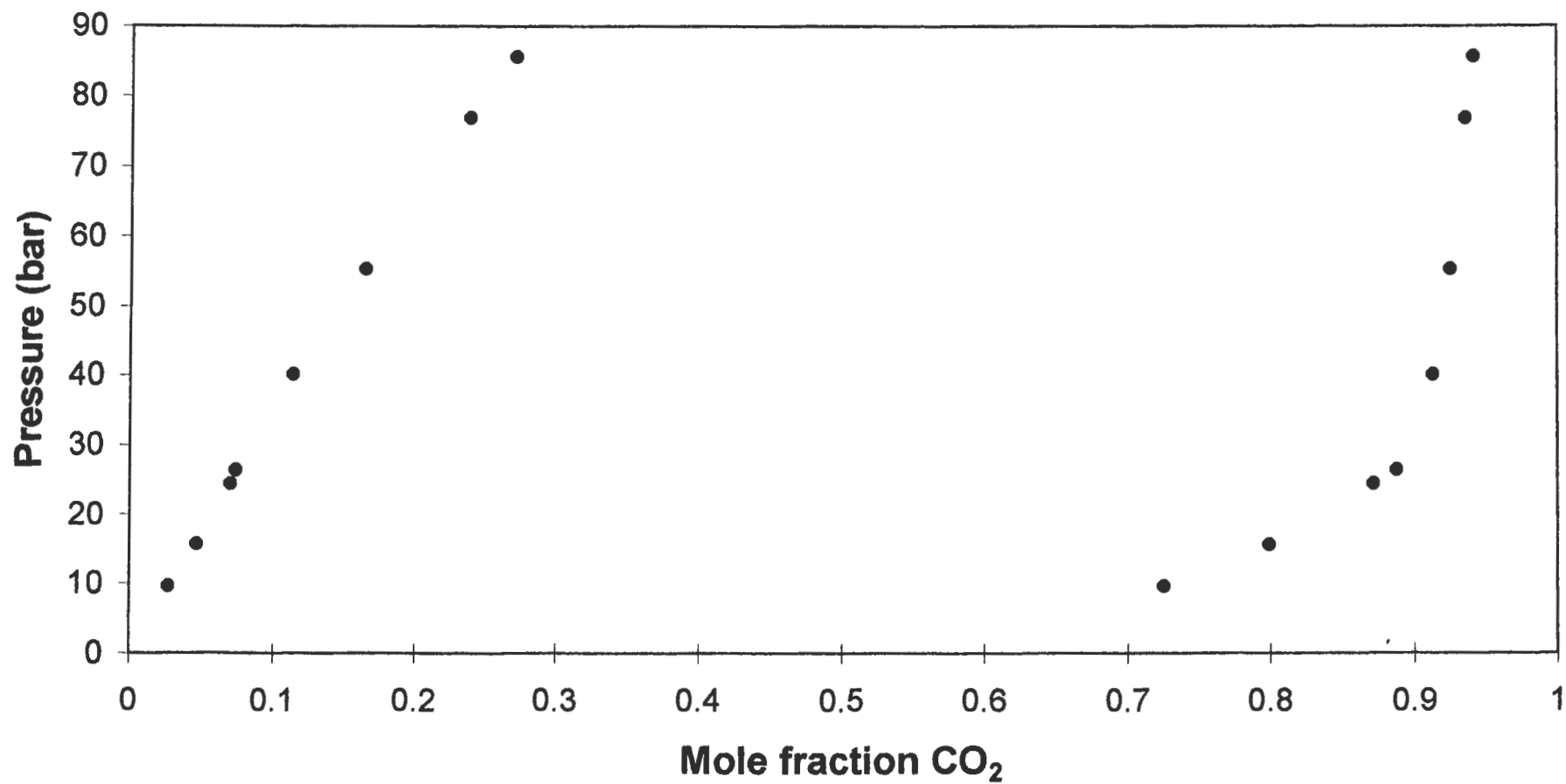


Figure 7-16: Experimental HPVLE data for Carbon Dioxide + Methanol at 100 °C

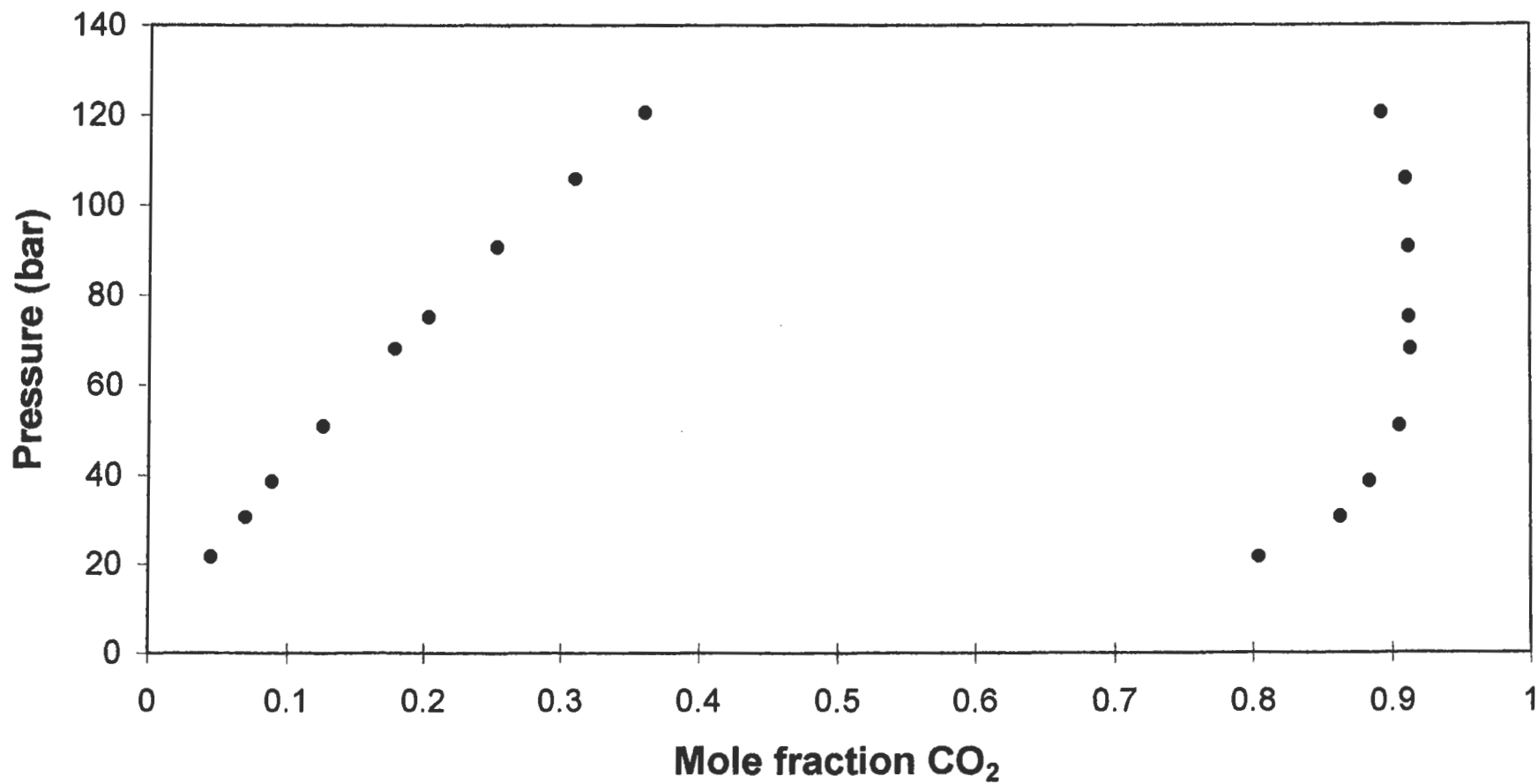
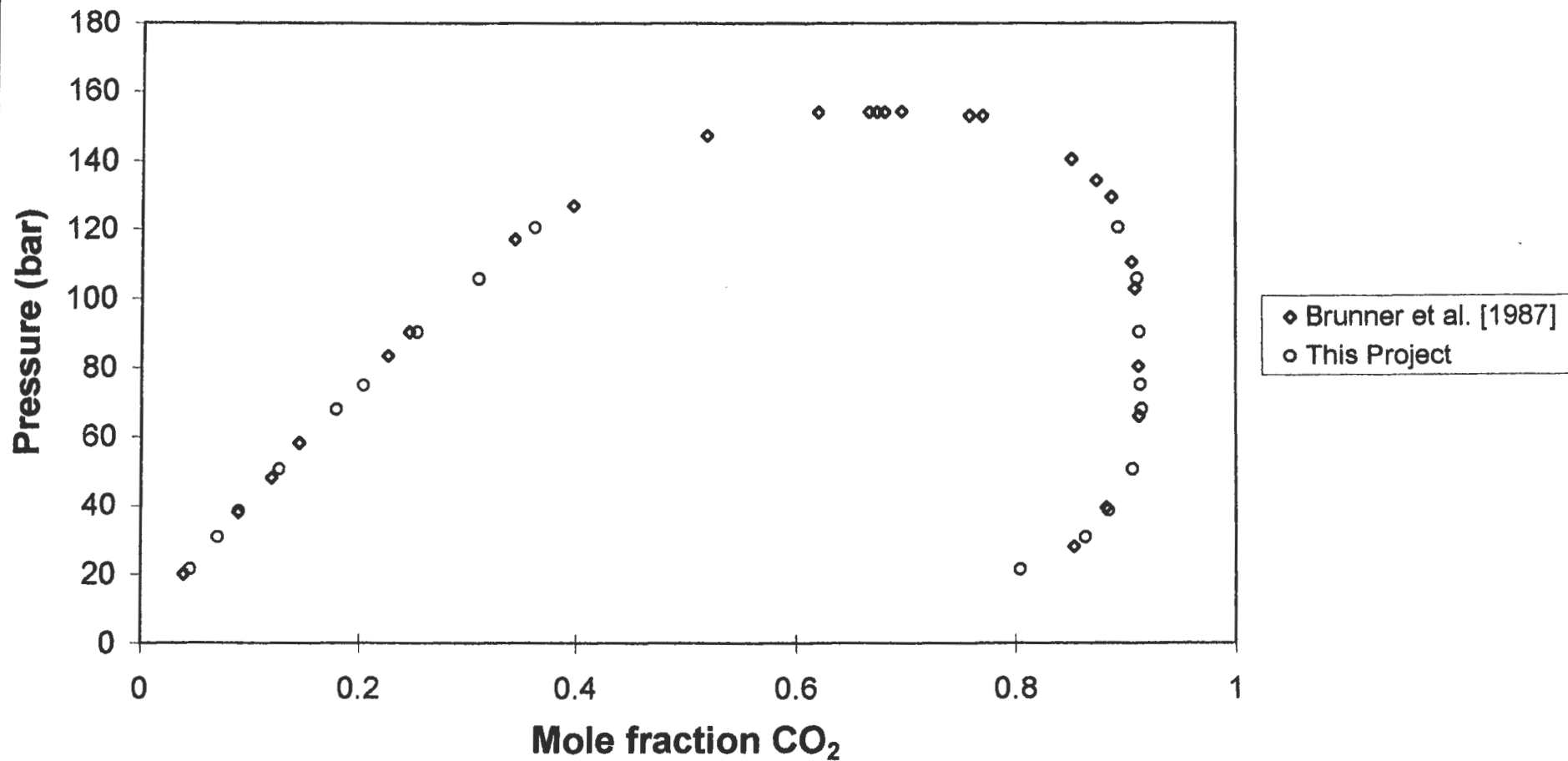


Figure 7-17: HPVLE data for Carbon Dioxide + Methanol at 100 °C (Comparison with literature)



7.4.3. Propane + 1-Propanol

The propane + 1-propanol system was measured at two isotherms, viz. 105.1 °C and 120 °C.

7.4.3.1. Propane + 1-Propanol – 105.1 °C isotherm

Table 7-8 lists the experimental data points for (liquid and vapour phase mole fractions and pressure) for the propane + 1-propanol system at the given isotherm. Figure 7-18 gives the graphical illustration of the data points. Figure 7-19 compares the data measured in this project to literature. Literature data compared to were that of Mühlbauer and Raal [1993] (105.1 °C).

Pressure (bar)	Liquid Composition ($X_{propane}$)	Vapour Composition ($Y_{propane}$)
5.89	0.07092	0.7168
8.91	0.1053	0.8437
13.54	0.1559	0.8837
19.67	0.2512	0.8998
23.31	0.3193	0.9089
26.47	0.3719	0.9128
28.54	0.4268	0.9179
29.62	0.4417	0.9187
31.81	0.4897	0.9258

Table 7-8: Experimental data for the Propane + 1-Propanol System at 105.1 °C

7.4.3.2. Propane + 1-Propanol – 120 °C isotherm

Table 7-9 lists the experimental data points for (liquid and vapour phase mole fractions and pressure) for the propane + 1-propanol system at the given isotherm. Figure 7-20 gives the graphical illustration of the data points. Figure 7-21 compares the data measured in this project to literature. Literature data compared to were that of Mühlbauer and Raal [1993] (120 °C).

The only other set of literature data available for the propane + 1-propanol system was that of Nagahama et al. [1971]. The experimental data however was at a much lower temperature (293.05 K) and Nagahama et al. [1971] did not make measurements of the vapour phase composition.

Figure 7-18: Experimental HPVLE data for the Propane + 1-Propanol System at 105.1 °C

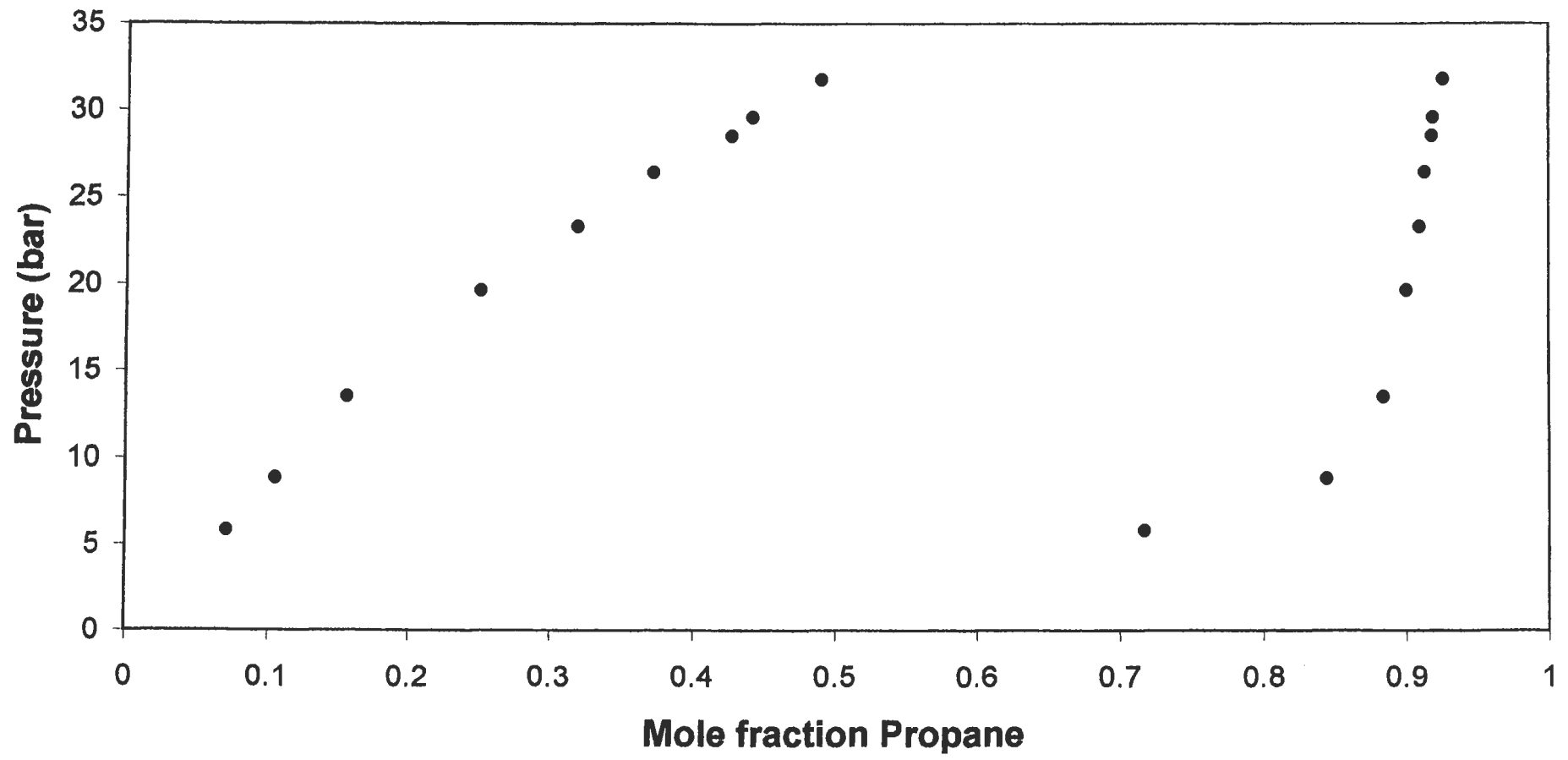


Figure 7-19: HPVLE data for the Propane + 1-Propanol System at 105.1 °C (Comparison with literature)

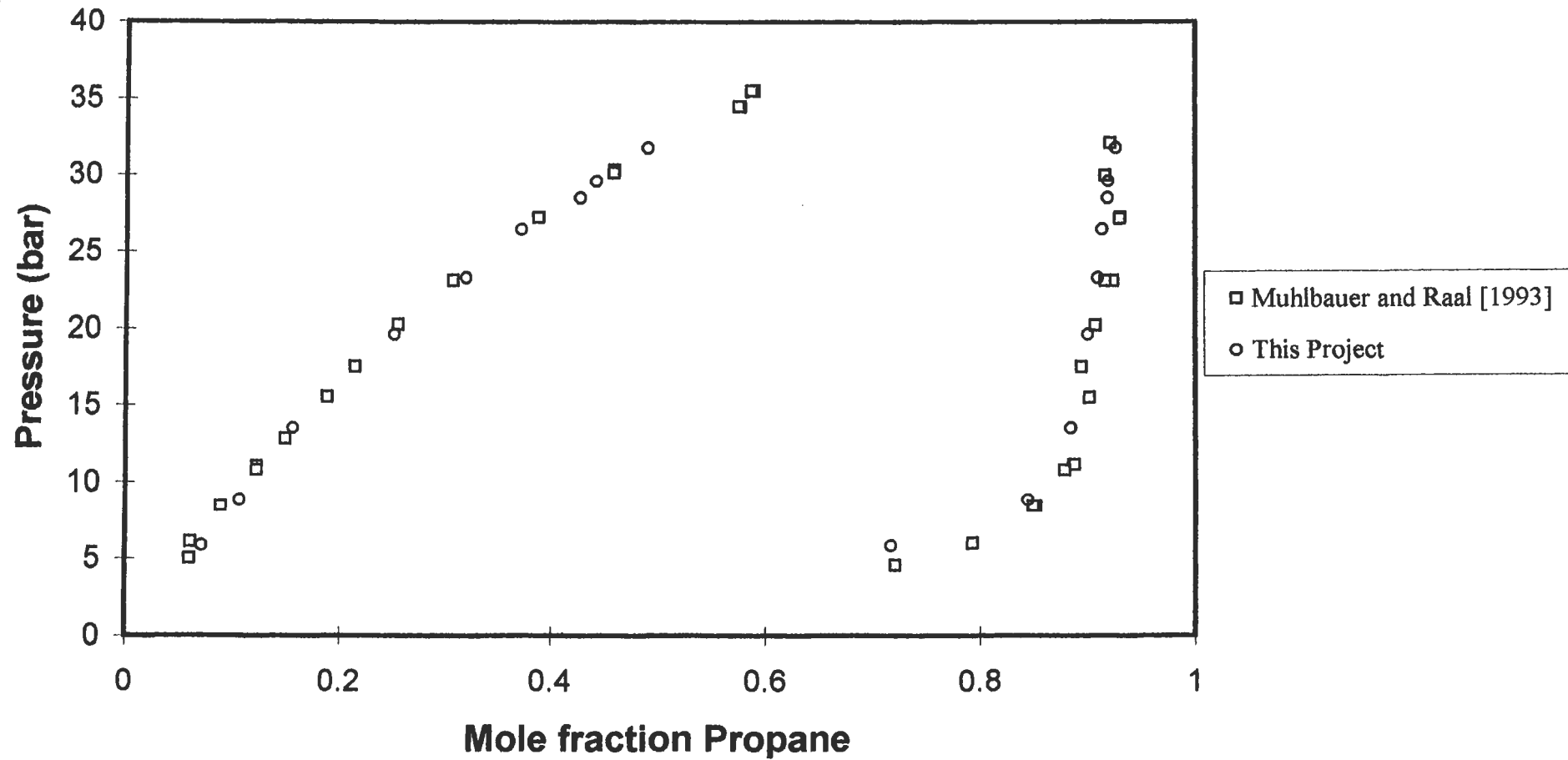


Figure 7-20: Experimental HPVLE data for the Propane + 1-Propanol System at 120 °C

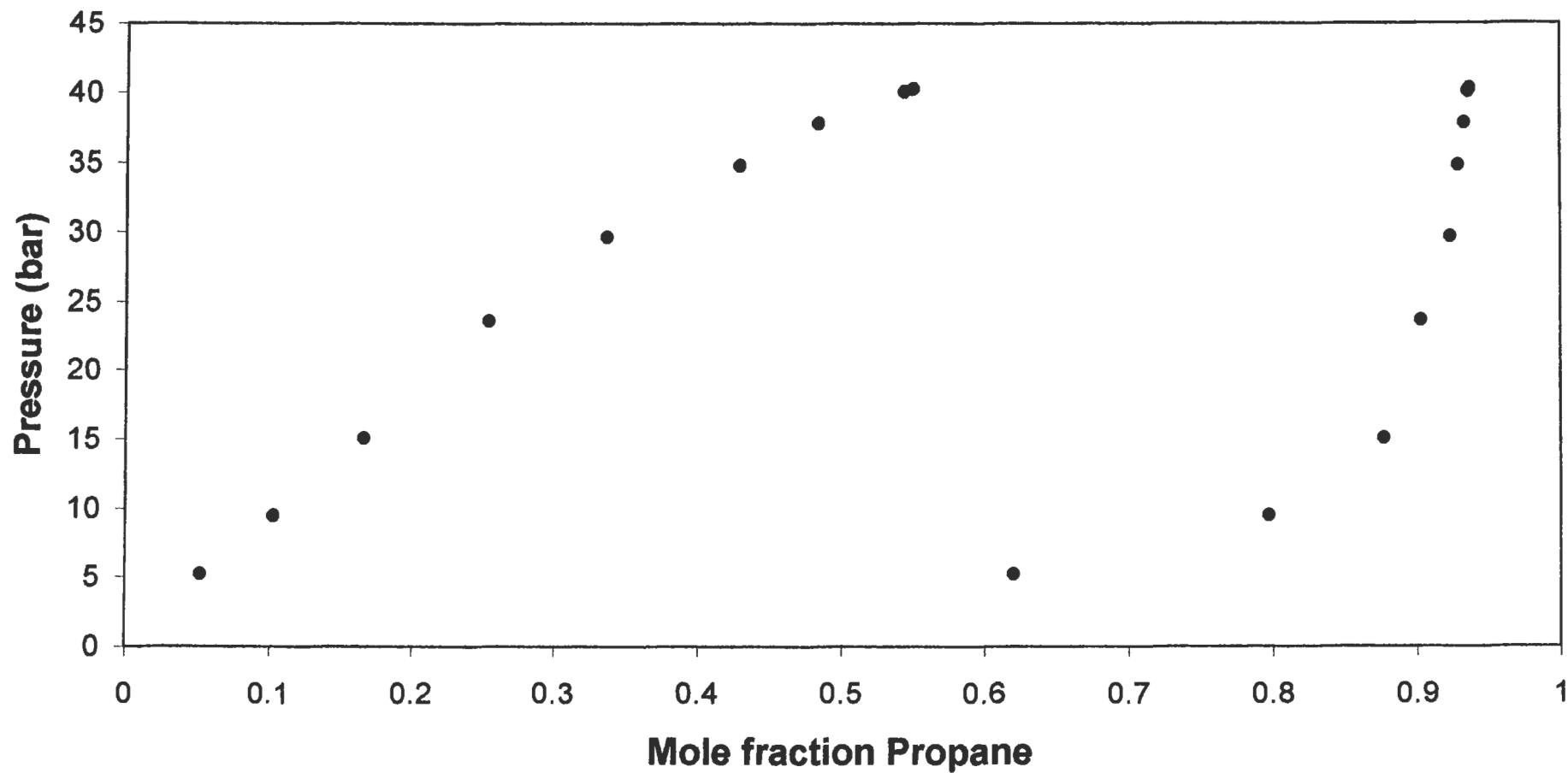
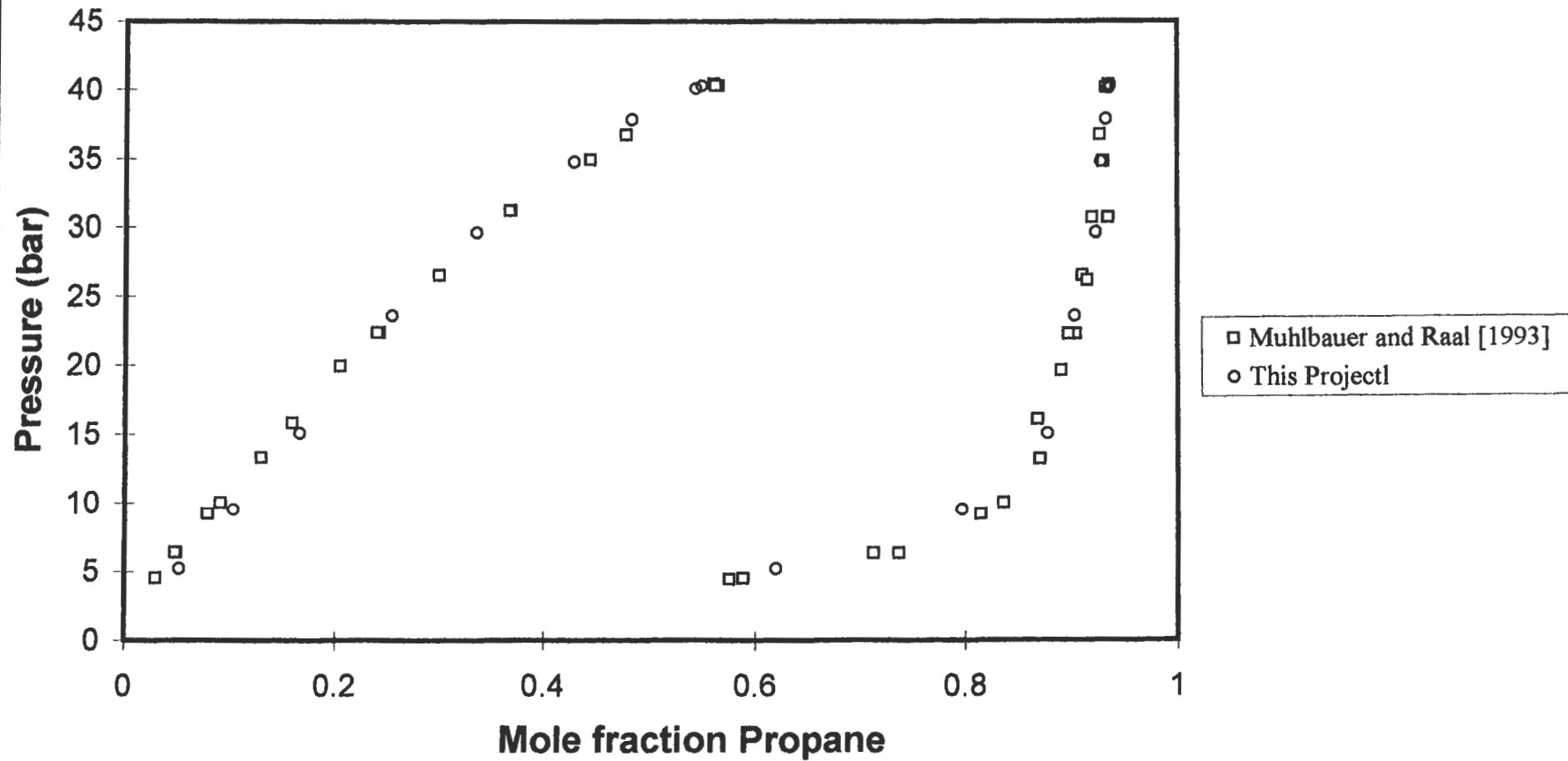


Figure 7-21: HPVLE data for the Propane + 1-Propanol System at 120 °C (Comparison with literature)



Pressure (bar)	Liquid Composition (X_{propane})	Vapour Composition (Y_{propane})
5.23	0.0521	0.6198
9.56	0.1023	0.7967
15.12	0.1659	0.8767
23.65	0.2542	0.9028
29.66	0.3363	0.9229
34.84	0.4289	0.9284
37.89	0.4838	0.9329
40.12	0.5437	0.9357
40.31	0.5497	0.9368

Table 7-9: Experimental data for the Propane + 1-Propanol System at 120 °C

7.5. P-V-T MEASUREMENTS

P-V-T measurements were undertaken to demonstrate the equipment's variable-volume capability and versatility. Measurements were undertaken for nitrogen, propane and for a nitrogen + propane binary. The second virial coefficients were then derived from the P-V-T measurements, as discussed in Section 8.8.

7.5.1. Nitrogen

Measurements were undertaken for nitrogen at three isotherms viz. 50 °C, 75 °C and 100 °C. Tables 7-10 to 7-12 list the experimental data for the three isotherms respectively.

Pressure (bar)	Volume (m^3/kmol)
2.67	10.0642
2.81	9.5959
2.95	9.1275
3.11	8.6591
3.28	8.1908
3.48	7.7224
3.7	7.2540
3.96	6.7857

Table 7-10: P-V data for nitrogen at the 50 °C isotherm

Pressure (bar)	Volume (m ³ /kmol)
2.95	9.8164
3.09	9.3652
3.25	8.9141
3.42	8.4629
3.62	8.0117
3.83	7.5606
4.07	7.1094
4.35	6.6582

Table 7-11: P-V data for nitrogen at the 75 °C isotherm

Pressure (bar)	Volume (m ³ /kmol)
3.33	9.3229
3.48	8.8959
3.66	8.4689
3.85	8.0419
4.07	7.6149
4.32	7.1879

Table 7-12: P-V data for nitrogen at the 100 °C isotherm

Second virial coefficients calculated from the P-V-T measurements for nitrogen are listed in Table 7-13.

Temperature (°C)	Experimental B (cm ³ /gmol)	*Literature B (cm ³ /gmol)
50	1.20	-0.50 to -0.25
75	3.88	3.20 to 3.38
100	6.57	6.14 to 6.56

Table 7-13: Second virial coefficients for nitrogen

*Dymond and Smith [1980]

7.5.2. Propane

Measurements were undertaken for propane at three isotherms viz. 50 °C, 75 °C and 100 °C. Tables 7-14 to 7-16 lists the experimental data for the three isotherms respectively.

Second virial coefficients calculated from the P-V-T measurements for nitrogen are listed in Table 7-17.

Pressure (bar)	Volume (m ³ /kmol)
2.45	11.0960
2.52	10.5797
2.64	10.0633
2.78	9.5469
2.88	9.0305
3.04	8.5141
3.22	7.9977
3.44	7.4813

Table 7-14: P-V data for propane at the 50 °C isotherm

Pressure (bar)	Volume (m ³ /kmol)
2.41	11.8052
2.51	11.2626
2.63	10.7200
2.77	10.1775
2.91	9.6349
3.07	9.0923
3.26	8.5498
3.46	8.0072

Table 7-15: P-V data for propane at the 75 °C isotherm

Pressure (bar)	Volume (m ³ /kmol)
2.49	12.2866
2.59	11.7238
2.71	11.1611
2.85	10.5984
2.99	10.0356
3.15	9.4729
3.33	8.9101
3.53	8.3474

Table 7-16: P-V data for propane at the 100 °C isotherm

Temperature (°C)	Experimental B (cm ³ /gmol)	*Literature B (cm ³ /gmol)
50	-319.49	-338.2 to -315
75	-268.79	-293
100	-279.54	-256 to -242.1

Table 7-17: Second virial coefficients for propane

*Dymond and Smith [1980]

7.5.3. Propane + Nitrogen Binary

The propane + nitrogen binary system's P-V properties were measured at 75 °C. The experimental data are listed in Table 7-18.

Pressure (bar)	Volume (m ³ /kmol)
2.33	12.3492
2.43	11.7816
2.55	11.2140
2.68	10.6465
2.83	10.0789
2.99	9.5113
3.17	8.9437
3.38	8.3762

Table 7-18: P-V data for propane (1) + nitrogen (2) binary at the 75 °C isotherm for $y_1 = 0.78$ mole fraction.

The cross second virial coefficient for the system was calculated to be -57.57 cm³/gmol. This compares reasonably well with the interpolated literature value of -46.03 cm³/gmol (Wormald et al. [1996]).

7.6. GC OPERATING CONDITIONS

The GC operating conditions are summarized in Table 7-19.

Operating Condition	Binary Systems being separated in GC		
	CO ₂ + Toluene	CO ₂ + Methanol	Propane + 1-Propanol
Column Temperature (°C)	200	140	150
TCD Detector Temperature (°C)	240	240	240
Elution Times (mins)	CO ₂ : 0.49 Toluene: 9.2	CO ₂ : 1.15 Methanol: 4.07	Propane: 2.11 1-Propanol: 7.15
Injector Temperature (°C)	200	200	200
Carrier gas flowrate (cc/min)	30	30	30
Reference gas flowrate (cc/min)	30	30	30

Table 7-19: Operating conditions for the Chrompack CP 9000 with Poropak N column

7.7. TEMPERATURE PROFILES

Temperature profiles for three different operating temperatures (40 °C, 80 °C and 120 °C) for the equilibrium apparatus are listed in Table 7-20. Reference must be made to Figure 4-9 when identifying the location of the Pt-100 sensors.

Sensor Number	Set-point Temperature (°C)		
	40	80	120
1	40.1	79.8	120.1
2	40.0	80.0	120.0
3	40.2	79.8	119.8
4	40.3	79.7	119.8
5	40.2	79.9	119.9
6	40.2	79.9	119.9
7	40.0	79.9	119.8
8	39.9	80.0	120.1

Table 7-20: Temperature profiles for three operating temperatures for the experimental apparatus

Temperature profiles for all other operating temperatures were very much the same. For all of the operating temperatures, the maximum difference between the highest and lowest temperatures in the profile was approximately 0.4 °C.

CHAPTER EIGHT

DISCUSSION OF EXPERIMENTAL RESULTS

Due to the costly and demanding nature of HPVLE measurement, it is essential that experimental data be properly interpreted and modeled. The methods adopted in this project for the interpretation and modeling of the systems measured are discussed in Chapter 3. In this section the details for the calculation methods will be comprehensively discussed.

Modeling of the measured HPVLE for the systems carbon dioxide + toluene, carbon dioxide + methanol and propane + 1-propanol was based on both the direct and combined methods. In the direct method, use was made of the Soave (SRK), Peng-Robinson (PR) and Peng-Robinson-Stryjek-Vera (PRSV) EOS's with various mixing rules (including Wong-Sandler mixing rules). For the combined method, various activity coefficient models (Van Laar, Wilson, NRTL and UNIQUAC) were used in conjunction with the Virial, Soave, PR and PRSV EOS's (with classical van der Waals mixing rules and Wong-Sandler mixing rules). A newly proposed combined method (Ramjugernath and Raal [1999]) was also used.

The extrapolative ability of the Wong-Sandler mixing rules were investigated for the carbon dioxide + methanol and propane + 1-propanol systems. In additions for the propane + 1-propanol system HPVLE data were predicted using the UNIFAC group contribution method in conjunction with Wong-Sandler and Huron-Vidal mixing rules.

Since measurements were not undertaken in the critical region for the systems investigated, the critical region for the systems measured were computed using the computational method of Deiters and Schneider [1976].

The experimental data for the various systems were tested for thermodynamics consistency using the consistency area test of Chueh et al. [1965]. Plots of the residuals were also undertaken as an indication of the consistency of experimental data.

The second virial coefficients were calculated from measured P-V-T data for nitrogen, propane and the nitrogen + propane binary at temperatures of 50, 75 and 100 °C. A slightly modified approach to that used by Wilson et al. [1984] and Barber et al. [1982] was used and is discussed later.

8.1. COMPARISON OF EXPERIMENTAL HPVLE DATA

8.1.1. Carbon Dioxide + Toluene

For the 38 °C isotherm comparisons were made to the experimental data of Ng and Robinson [1978] and Fink and Hershey [1990]. It must be borne in mind that the data of Fink and Hershey is at 35.01 °C. Figure 7-7 shows the graphical comparison. There is very good agreement between data measured and that reported in literature. There is only a slight discrepancy for the liquid phase around the 0.2 mole fraction region.

A comparison with literature data of Ng and Robinson [1978], Morris and Donohue [1985], Kim et al. [1986], Fink and Hershey [1990] and Mühlbauer and Raal [1991] was made for the 80 °C isotherm. There was excellent agreement with literature. The experimental data of Morris and Donohue [1985] showed a slight discrepancy for the liquid composition around the 0.6 mole fraction region.

For the 120 °C isotherm comparisons were made to the experimental data of Ng and Robinson [1978], Sebastian et al. [1980] and Kim et al. [1986]. Once again there was very good agreement with literature data, with only a slight discrepancy for the vapour phase around the 20 bar measurement.

8.1.2. Carbon Dioxide + Methanol

Data measured at the 40 °C isotherm were compared to the literature data of Ohgaki and Katayama [1976], Suzuki et al. [1990] and Chang et al. [1997]. There was excellent agreement with the measurements of the various researchers, especially for the P-y data.

No literature data could be found to compare the data measured for the 90 °C isotherm.

For the 100 °C isotherm the experimental data were compared to that of Brunner et al. [1987]. There was excellent agreement between the two sets of data.

8.1.3. Propane + 1-Propanol

Only two researchers viz. Nagahama et al. [1971] and Mühlbauer and Raal [1993] had previously measured the system. The experimental data of Nagahama et al. was at 19.9 °C, and

so a comparison could not be made to experimental data of this project (measured at 105.1 and 120.0 °C). A comparison with the data of Mühlbauer and Raal at the 105.1 and 120.0 °C isotherms indicated some differences between the data sets, especially for the vapour phase. For the 105.1 °C isotherm there is an appreciable difference between the vapour phase measurements of this project compared to those of Mühlbauer and Raal [1993]. The experimental data of this project is however much smoother than those of the latter authors.

8.2. THE DIRECT METHOD

The direct method of data reduction is the method preferred by a vast majority. The direct method uses a single EOS to describe both the liquid and vapour phases. The preferred fugacity coefficient model is a cubic EOS. The reason for choosing a cubic EOS is as a result of its simplicity, accuracy and ease of use. The roots of a cubic EOS of state can very easily be determined, which is not the case with high order EOS's.

8.2.1. EOS models and mixing rules used

In this project use was made of the following EOS's and mixing rules in the direct method:-

1. Soave EOS with van der Waals mixing rules (Soave [1972]) – SRK.
2. Peng-Robinson EOS with van der Waals mixing rules (Peng and Robinson [1976]) – PR.
3. Peng-Robinson-Stryjek-Vera EOS with van der Waals mixing rules (Stryjek and Vera [1986(a,b)]) – PRSV-1vdw.
4. Peng-Robinson-Stryjek-Vera (PRSV) EOS with two-parameter van der Waals mixing rules (Panagiotopolos and Reid [1986(a,b)]) – PRSV-2vdw.
5. PRSV EOS with Huron-Vidal mixing rules (Huron and Vidal [1979]) – HVO.
6. PRSV EOS with modified Huron-Vidal first order mixing rules (Michelsen [1990(b)]) – MHV1.
7. PRSV EOS with modified Huron-Vidal second order mixing rules (Dahl and Michelsen [1990]) – MHV2.
8. PRSV EOS with a linear combination of Huron-Vidal and Michelsen model mixing rule (Boukouvalas et al. [1994]) – LCVM.
9. PRSV EOS with Orbey-Sandler modification of Huron-Vidal mixing rule (Orbey and Sandler [1995(b)]) – HVOS.
10. PRSV EOS with Wong-Sandler mixing rules (Wong and Sandler [1992])– PRSV-WS.

For the Huron-Vidal mixing rules and modifications thereof, use was made of the NRTL liquid phase model. For the Wong-Sandler mixing rules computations were undertaken for a range of liquid phase models (Van Laar, Wilson, NRTL and UNIQUAC liquid phase models).

Details of each of the EOS's and mixing rules are given in Chapter 3 and Appendix B.

8.2.2. Data fitting/correlation

The reduction of the measured data involved determining the fitting parameters for each of the models. The parameters were determined by least squares regression of the experimental data. The objective function for the least squares regression was:

$$S = \sum_{i=1}^n \left[\left(\frac{P_i^{cal} - P_i^{exp}}{P_i^{exp}} \right)^2 + \left(\frac{y_i^{cal} - y_i^{exp}}{y_i^{exp}} \right)^2 \right] \quad (8-1)$$

Thus the sum of the errors between the *calculated* or *predicted* properties and the experimental properties must be minimized. The *calculated* system pressure and vapour compositions are computed via a bubble pressure computation. A flow diagram of the bubble pressure algorithm used in this project is shown in Figure 8-1. Algorithms for the computation of high-pressure phase equilibrium are discussed in depth in Heidemann [1983].

Inputs into the bubble pressure algorithm are the temperature and liquid composition, critical properties (temperature and pressure), accentric factors, K_i (fitted vapour pressure parameter for the PRSV EOS) and Gibbs excess free energy model parameters (for mixing rules which incorporate a Gibbs excess free energy model, e.g. Wong-Sandler and Huron-Vidal).

The PRSV EOS K_i parameter was determined by least squares regression of experimental vapour pressure data. The objective function in the least square regression was:

$$S = \sum_{i=1}^n \left(\frac{P_i^{cal} - P_i^{exp}}{P_i^{exp}} \right)^2 \quad (8-2)$$

Depending on the method used to calculate a new pressure in the algorithm, one or two initial guesses must be made for the pressure. In this project use was made of the secant method

(Anderson and Prausnitz [1980(a,b)] for the determination of the new pressure. The new pressure is determined by the following expression for the secant method:

$$P_{k+1} = P_k - \frac{f(P_k)(P_k - P_{k-1})}{f(P_k) - f(P_{k-1})} \quad (8-3)$$

where

$$f(P) = \ln \sum K_i x_i \quad (8-4)$$

There are a number of different methods to determine a new pressure, some of which are described in Anderson and Prausnitz [1980(a,b)]. Another commonly used method is that of interval halving described in Gerald and Wheatley [1989]. It is interesting to note that the secant method fails for cases where the denominator in Equation (8-3) equals zero.

The fugacity coefficients in solution are calculated from expressions given in Chapter 3 and Appendix B, for the appropriate EOS and mixing rule combinations. The equilibrium ratio's (K_i) are calculated from Equation (3-12), knowing the liquid and vapour fugacity coefficients in solution.

There are two convergence checks in the algorithm. For both convergence checks the tolerances (ϵ_1 and ϵ_2) were set to $1E-5$.

The least square regression routine used was based on the work of Marquardt [1963]. Other methods for the determination of the fitting parameters can also be used e.g. the least square method described by Gess et al. [1991] and the maximum likelihood principle described by Anderson et al. [1978], Prausnitz et al. [1980] and Gess et al. [1991].

Calculation of the fugacity coefficient using a cubic EOS involved solving of an equation cubic in compressibility factor. There were three roots for this cubic equation, two of which were real, and one that was imaginary. It should be noted that the largest real root is the vapour compressibility factor and that the smallest real root is the liquid compressibility factor. Anderson and Prausnitz [1980(a,b)] explain the determination of roots for cubic EOS's in terms of density.

Depending on the EOS and mixing rules used, one to three parameters were fitted. For the SRK, PR and PRSV-1vdw EOS's, one parameter was fitted i.e. k_{12} . For the PRSV-2vdw EOS two

parameters were determined i.e. k_{12} and k_{21} . When fitting was undertaken with the PRSV EOS and Huron-Vidal (or modifications thereof) mixing rules two parameters were fitted viz. the Gibbs excess free energy model parameters. In the NRTL Gibbs excess free energy model, the third parameter (α_{12}) was set equal to 0.3 for all computations. For the PRSV-WS EOS's three parameters were fitted viz. k_{12} and the Gibbs excess free energy model parameters. The NRTL third parameter was set equal to 0.3 for these computations as well.

In this project all computations were undertaken using MATLAB software. Depending on the EOS and mixing rules chosen, the MATLAB fitting program for the direct method took approximately between 30 seconds to 10 minutes. This may seem like a large amount of computational time, but bear in mind that the MATLAB processor and programming language is approximately a quarter, or less, of the speed of other processor and programming languages e.g. FORTRAN or BASIC. The reason that MATLAB was still used is because of its ease of use and extensive library especially for matrix manipulation and numerical methods.

Once the fitted parameters were obtained, a bubble pressure computation could be undertaken to determine the entire P-x-y diagram. Figures 8-2 to 8-25 compare the experimental data measured in this project to the predicted/correlated data using the direct method with the appropriate EOS and mixing rules.

8.2.3. Fitted parameters

8.2.3.1. Carbon Dioxide + Toluene System

Table 8-1 summarizes the interaction parameters, k_{12} , obtained for the SRK, PR and PRSV-1vdw EOS's. Table 8-2 summarizes the interaction parameters, k_{12} and k_{21} , for the PRSV-2vdw EOS.

EOS	Interaction parameter (k_{12})		
	Temperature ($^{\circ}$ C)		
	38	80	118.3
SRK	0.0837	0.1007	0.0954
PR	0.0831	0.0964	0.0888
PRSV-1vdw	0.0837	0.1072	0.1128

Table 8-1: Interaction parameter obtained for various EOS's, from fitting of experimental data measured in this project, using the direct method for the Carbon Dioxide +Toluene System

Figure 8-1: Flowchart for the bubble P computation via the direct method

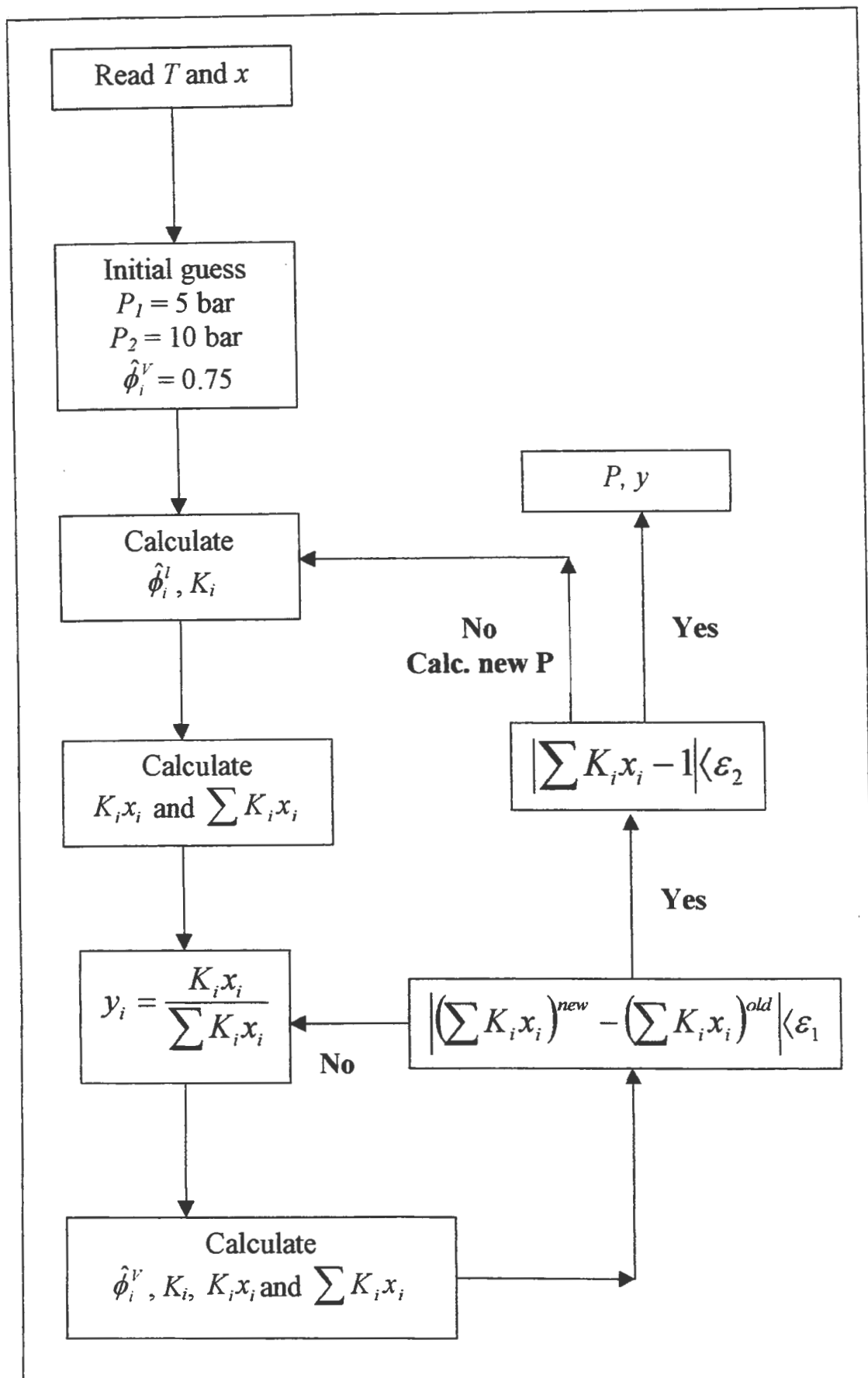


Table 8-3 compares the binary interaction parameter obtained in this project with those published in literature. The trend seen in Table 8-1 indicates that the binary interaction parameter generally increases with increasing temperature, except for the SRK and PR EOS's at the 118.3 °C isotherm.

EOS	Interaction parameters (k_{12} and k_{21})					
	Temperature (°C)					
	38		80		118.3	
PRSV-2vdw	0.0783	0.1174	0.0964	0.1276	0.0943	0.1506

Table 8-2: Interaction parameters obtained for PRSV EOS with 2-parameter van der Waals mixing rules, from fitting of experimental data measured in this project, using the direct method for the Carbon Dioxide + Toluene System

Reference	EOS	k_{ij}
Ng and Robinson [1978]	PR	0.09 (no specific temperature given)
Kim et al. [1986]	PR	0.108 (no specific temperature given)
Mohamed and Holder [1987]	PR	0.1056 (38.11 °C) 0.09424 (79.44 °C) 0.09331 (120.51 °C)

Table 8-3: Literature values for the binary interaction parameters for the Carbon Dioxide + Toluene System

The binary interaction parameters obtained in this project are comparable to those mentioned in literature. For the 38 °C isotherm there is substantial difference in the interaction parameters. This can be attributed to the experimental data being slightly varied and therefore the interaction parameter (which is just a fit of the experimental data) is different.

Table 8-4 summarizes the interaction parameters obtained by the fitting of the Huron-Vidal and modifications thereof mixing rules with the PRSV EOS. In all of the mixing rule/EOS combinations summarized in Table 8-4, use was made of the NRTL activity coefficient model to describe the activity coefficient incorporated into the mixing rules. In all cases the α_{ij} term in parameter in the NRTL model was set equal to 0.3.

Table 8-5 summarizes the interaction parameters obtained by the fitting of the Wong-Sandler mixing rules with the PRSV EOS. α_{ij} was set equal to 0.3 in the NRTL model.

EOS	Interaction parameters (a_{12} and a_{21} (cal.mol ⁻¹))					
	Temperature (° C)					
	38		80		118.3	
HVO	1390.08	-301.26	1408.53	-317.60	1480.97	-388.95
MHV1	391.21	-248.07	-117.08	169.70	-201.78	192.72
MHV2	119.80	286.23	97.04	186.15	-46.67	185.39
LCVM	1023.23	-484.08	132.05	133.34	513.97	-231.49
HVOS	959.57	-520.01	35.25	134.63	-49.32	155.09

Table 8-4: Interaction parameters obtained for PRSV EOS with Huron-Vidal (and modifications thereof) mixing rules, from fitting of experimental data measured in this project, using the direct method for the Carbon Dioxide + Toluene System

G ^E model	Interaction parameters (k_{ij} , p_{12} and p_{21} (reduced parameters))								
	Temperature (° C)								
	38			80			118.3		
NRTL	0.5291	1.5736	-0.1344	0.6213	0.4384	0.2578	0.6000	0.8408	0.0000
Wilson	0.5073	1.0660	0.1179	0.6001	0.9163	0.4471	0.5200	1.1709	0.0865
Van Laar	0.5029	0.7206	1.9195	0.5076	0.7224	2.1252	0.5046	0.7249	2.1372
UNIQUAC	0.5218	0.8368	0.5107	0.5588	0.8728	0.5532	0.5444	0.8136	0.5691

Table 8-5: Interaction parameters obtained for PRSV EOS with Wong-Sandler mixing rules, from fitting of experimental data measured in this project, using the direct method for the Carbon Dioxide + Toluene System

For NRTL: $p_{ij} = a_{ij}/RT$ (a_{ij} in cal.mol⁻¹)

For Wilson: $p_{ij} = (V_{Lj}/V_{Li})\exp(-a_{ij}/RT)$ (a_{ij} in cal.mol⁻¹)

For Van Laar: $p_{ij} = a_{ij}$

For UNIQUAC: $p_{ij} = \exp(-a_{ij}/RT)$ (a_{ij} in cal.mol⁻¹)

8.2.3.2. Carbon Dioxide + Methanol System

Table 8-6 summarizes the interaction parameters, k_{12} , obtained for the SRK, PR and PRSV-1vdw EOS's. Table 8-7 summarizes the interaction parameters, k_{12} and k_{21} , for the PRSV-2vdw EOS.

EOS	Interaction parameter (k_{12})		
	Temperature (° C)		
	40	90	100
SRK	0.0587	0.0808	0.0950
PR	0.0654	0.0837	0.0953
PRSV-1vdw	0.0668	0.0953	0.1075

Table 8-6: Interaction parameter obtained for various EOS's, from fitting of experimental data measured in this project, using the direct method for the Carbon Dioxide + Methanol System

Figure 8-2: Comparison between the predicted and experimental VLE data for the Carbon Dioxide + Toluene System at 38 °C

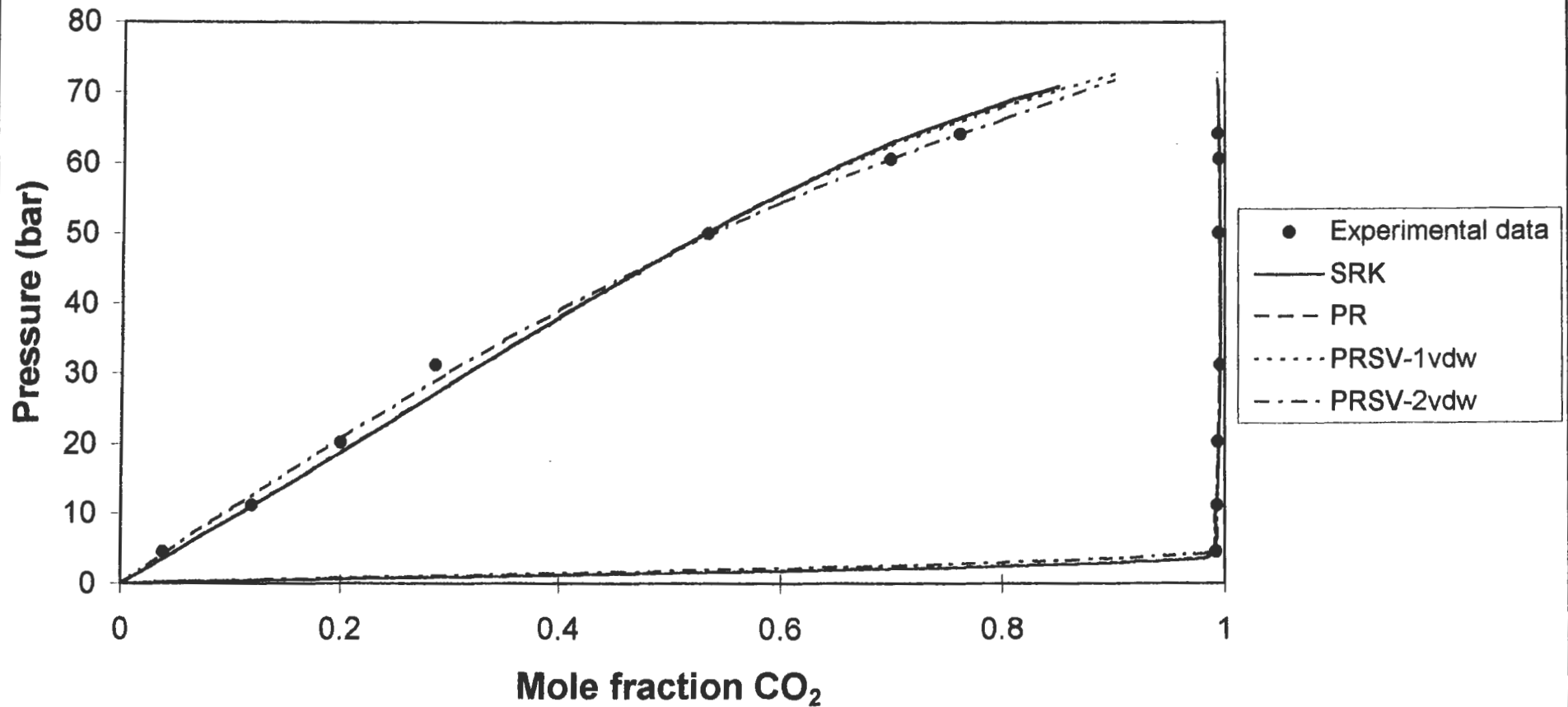


Figure 8-3: Comparison between the predicted and experimental VLE data for the Carbon Dioxide + Toluene System at 38 °C

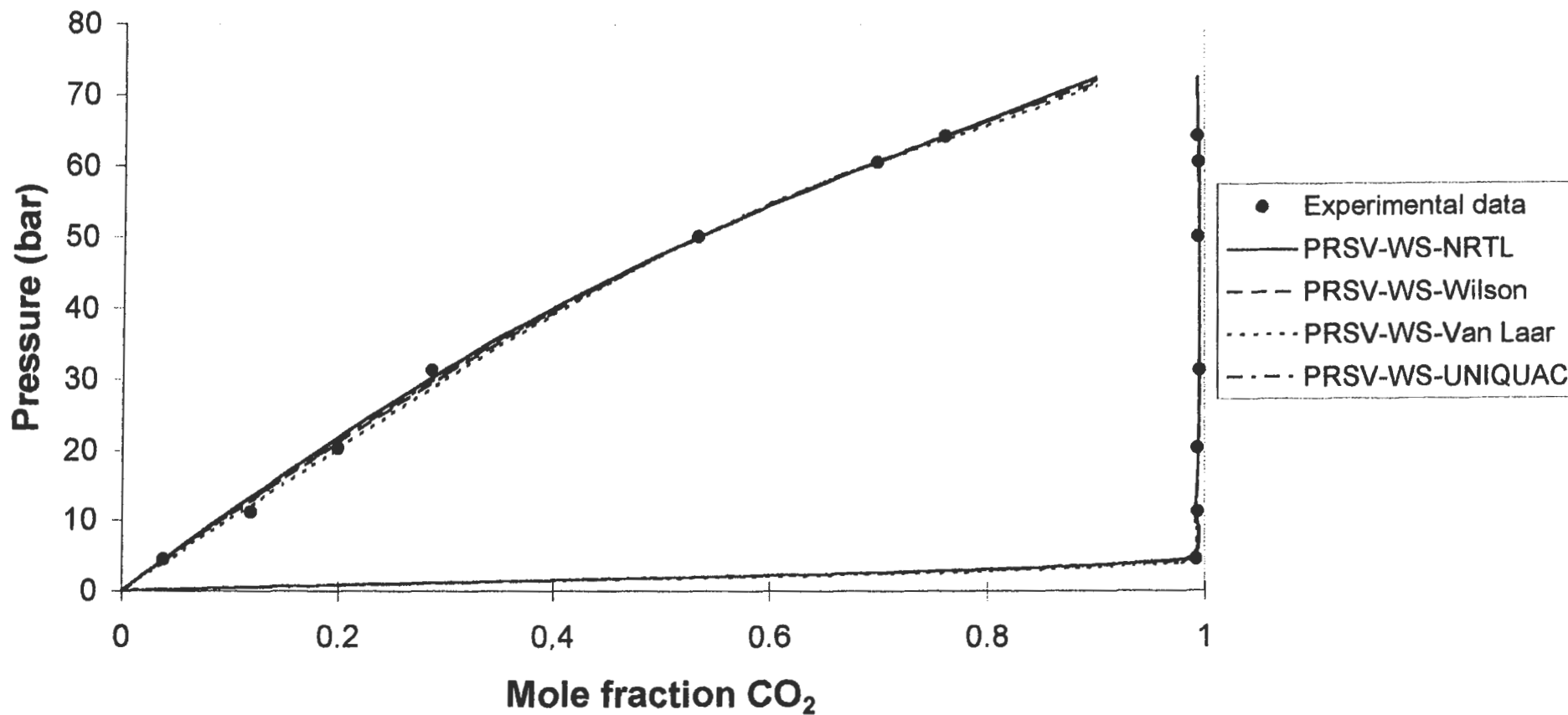


Figure 8-4: Comparison between the predicted and experimental VLE data for the Carbon Dioxide + Toluene System at 38 °C

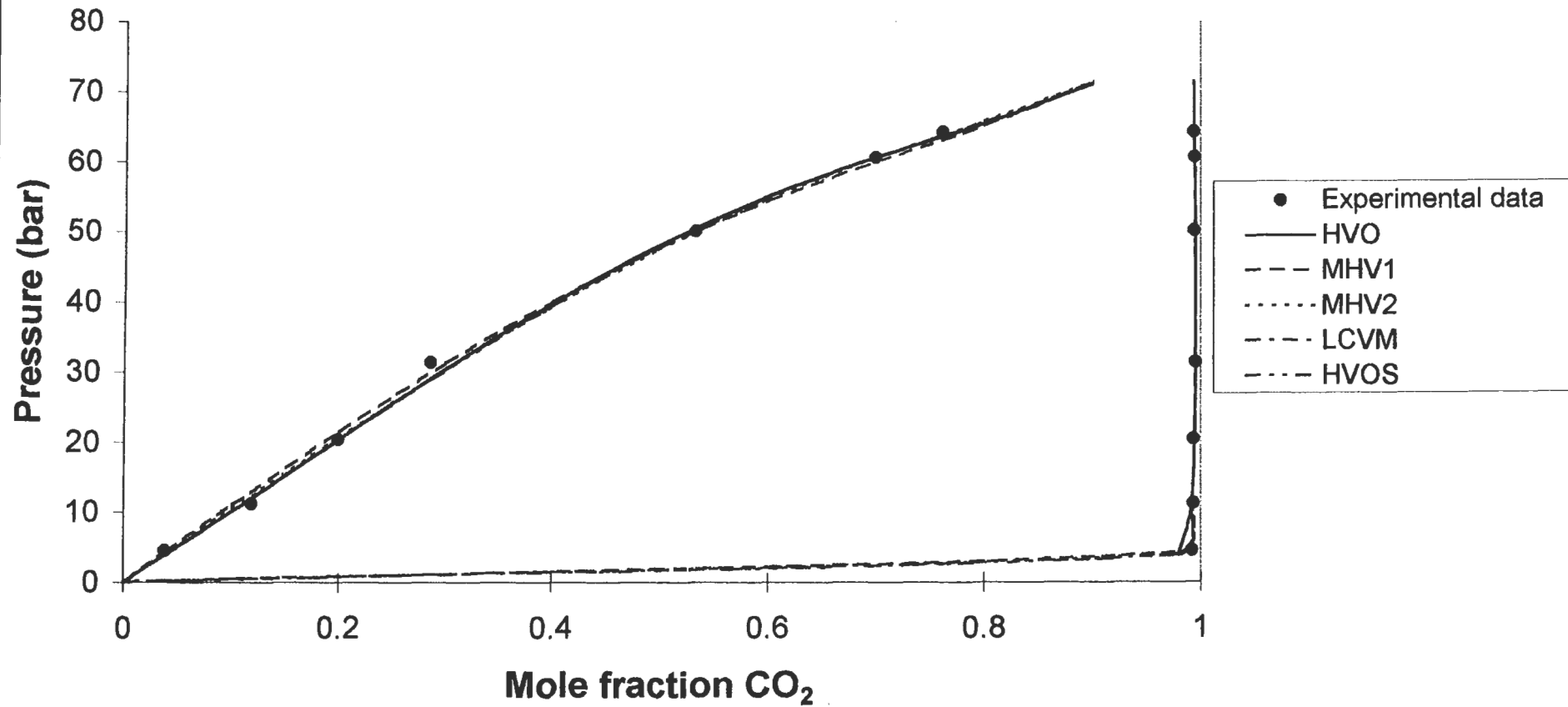


Figure 8-5: Comparison between the predicted and experimental VLE data for the Carbon Dioxide + Toluene System at 80°C

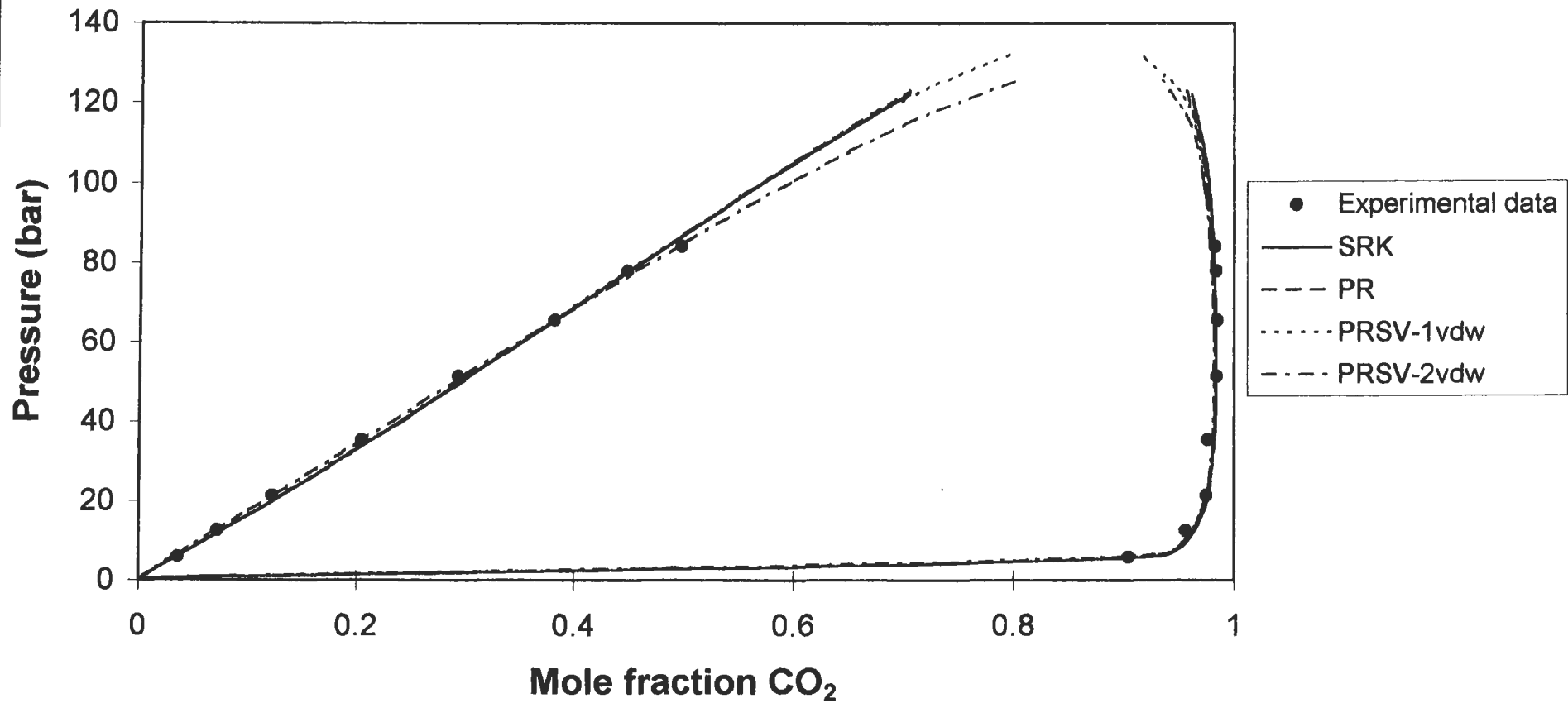


Figure 8-6: Comparison between the predicted and experimental VLE data for the Carbon Dioxide + Toluene System at 80°C

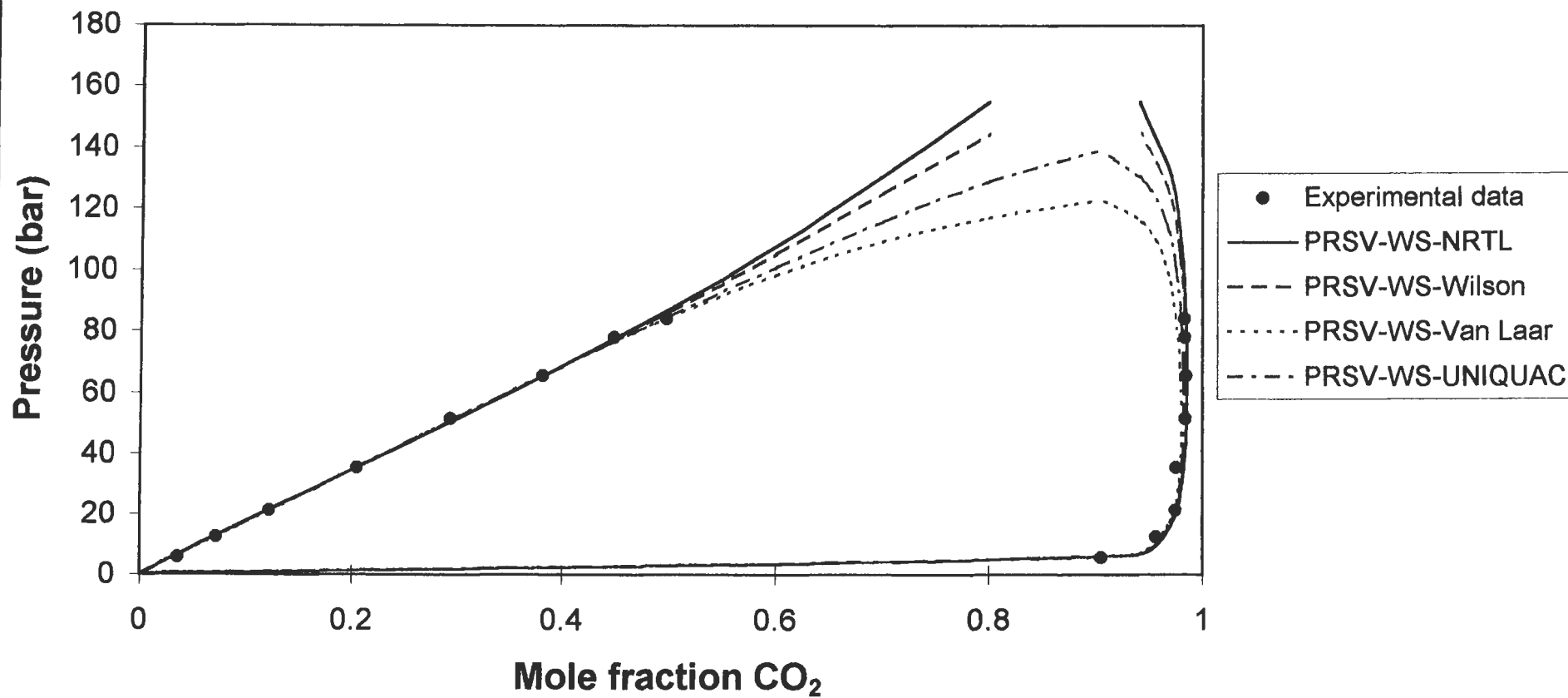


Figure 8-7: Comparison between the predicted and experimental VLE data for the Carbon Dioxide + Toluene System at 80°C

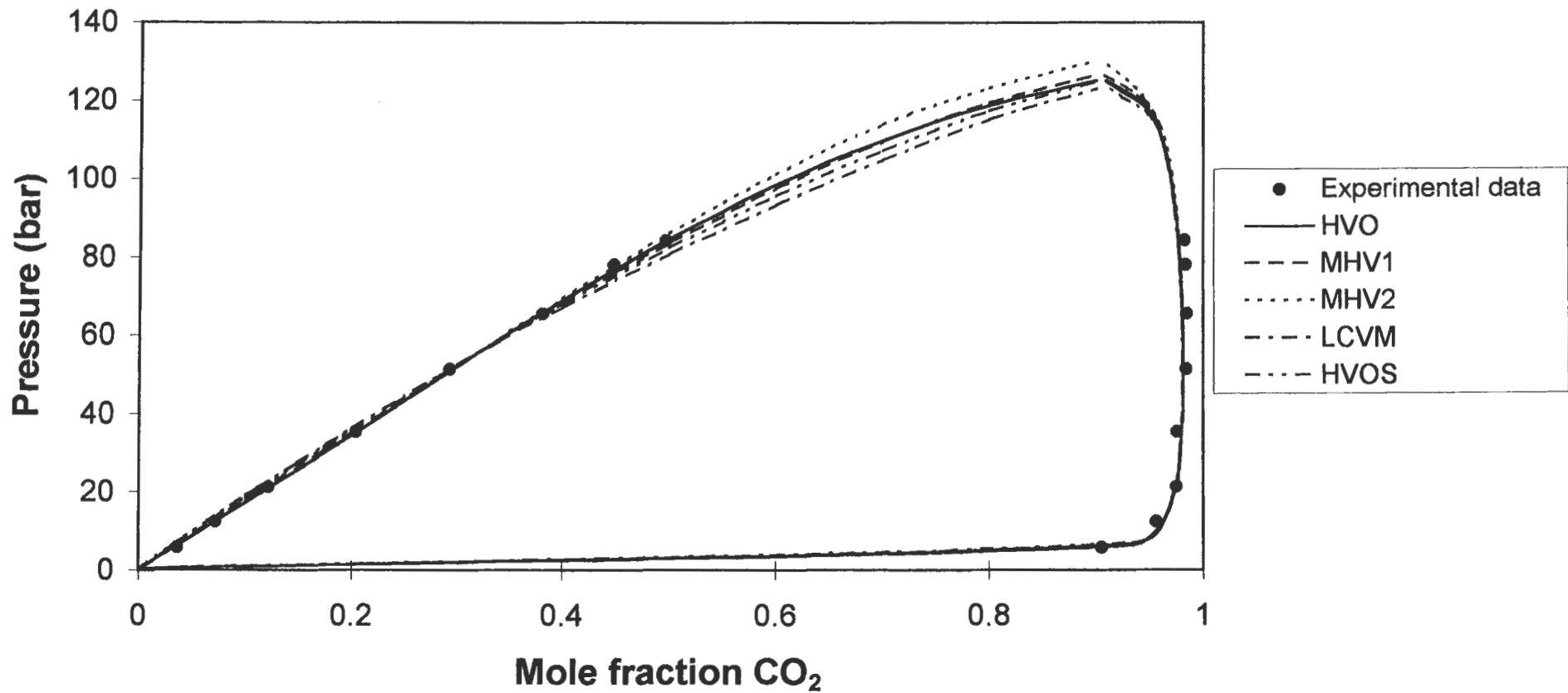


Figure 8-8: Comparison between the predicted and experimental data for the Carbon Dioxide + Toluene System at 118.3°C

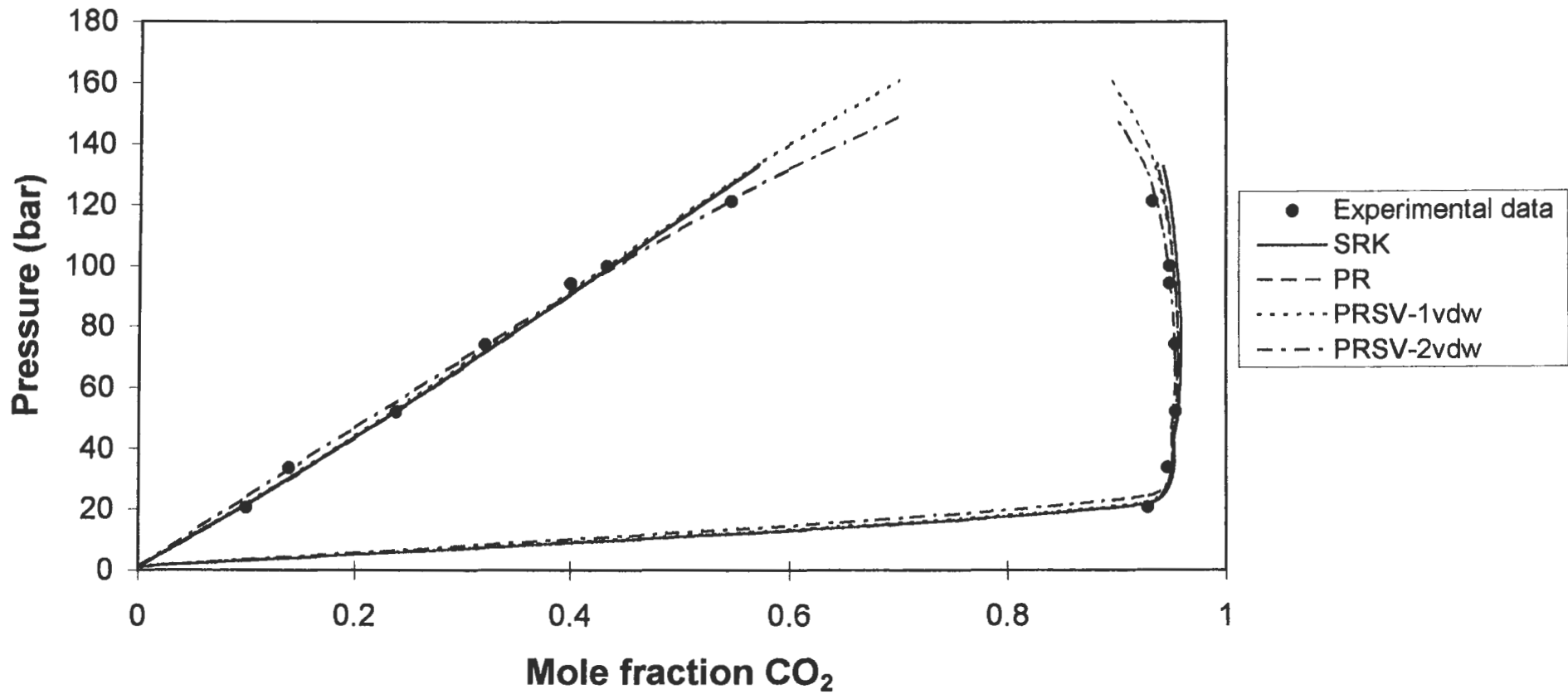


Figure 8-9: Comparison between the predicted and experimental data for the Carbon Dioxide + Toluene System at 118.3°C

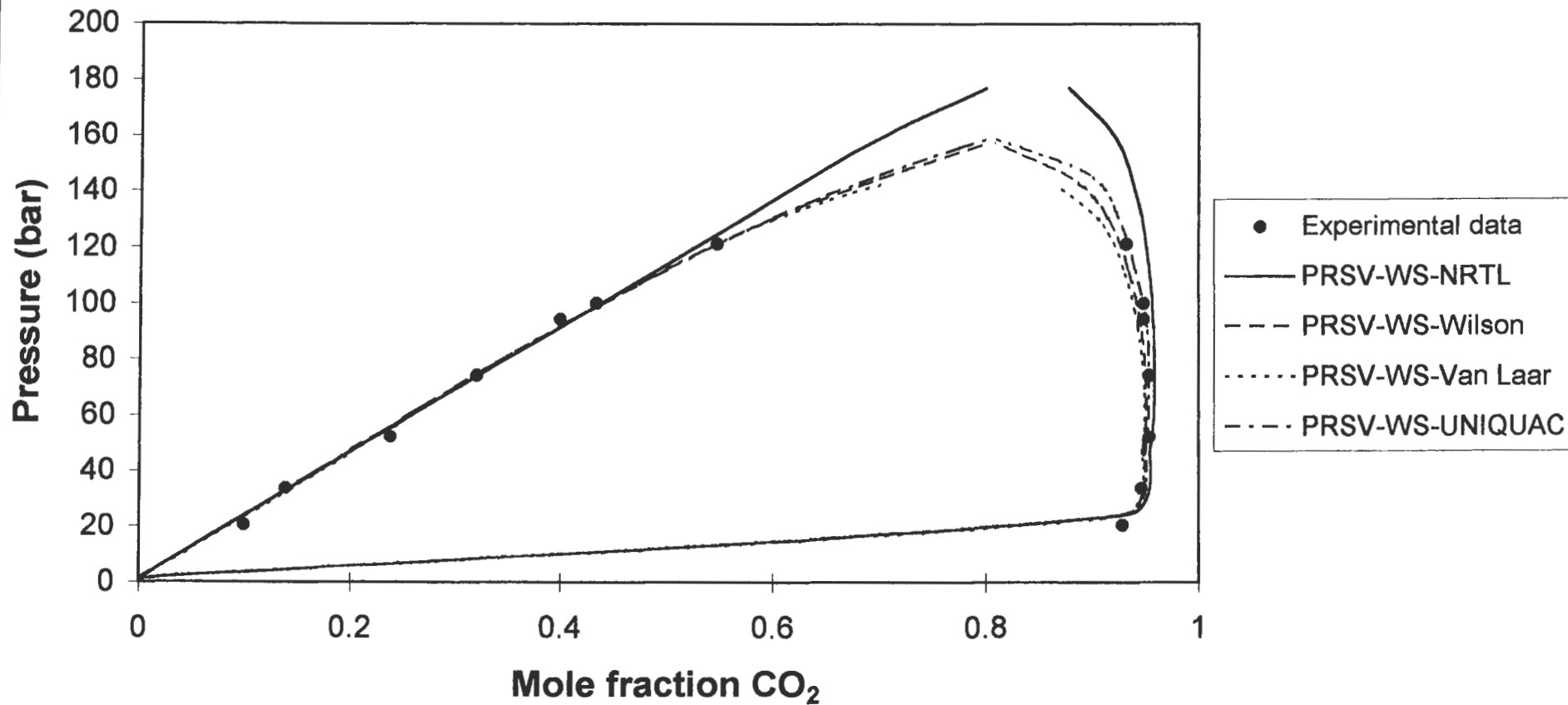


Figure 8-10: Comparison between the predicted and experimental data for the Carbon Dioxide + Toluene System at 118.3°C

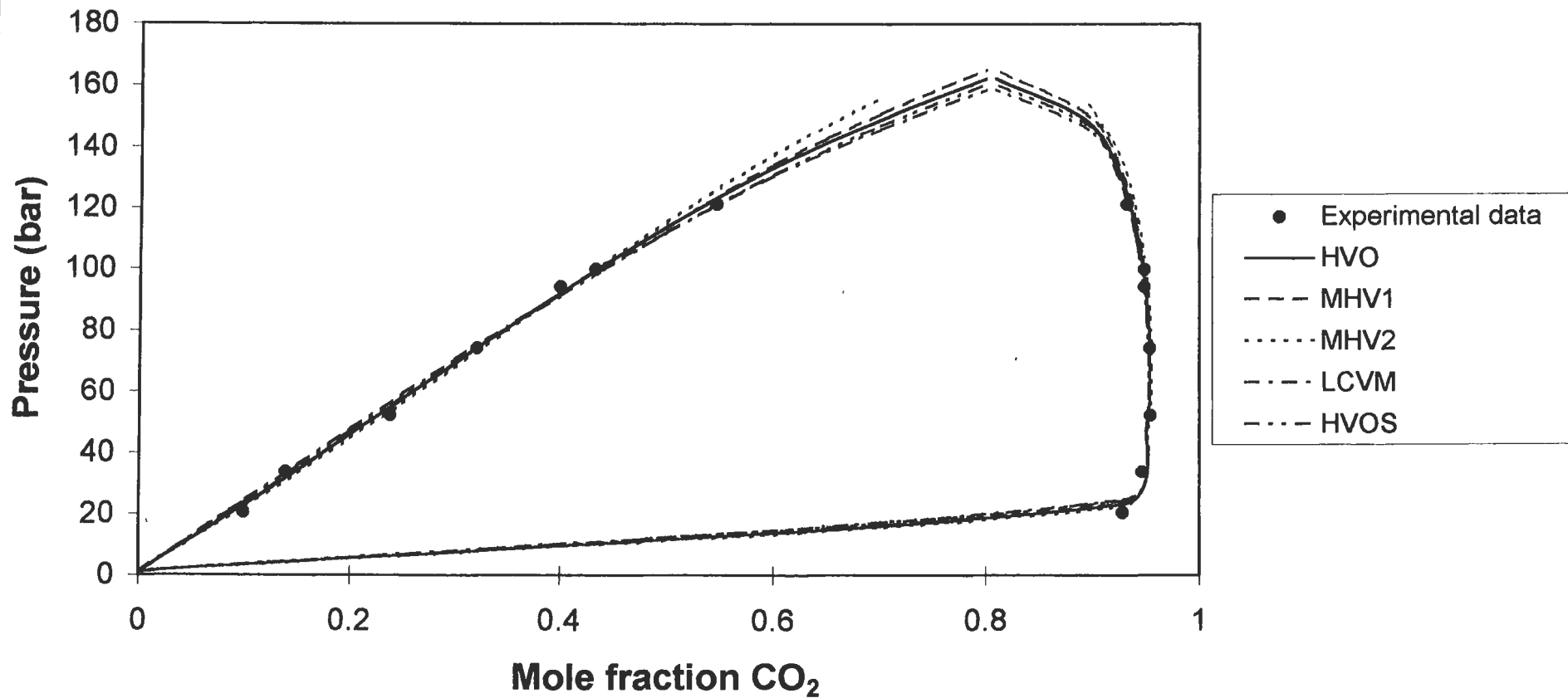


Table 8-8 compares the binary interaction parameter obtained in this project to that published in literature. The trend seen in Table 8-6 indicates that the binary interaction parameter generally increases with increasing temperature.

EOS	Interaction parameters (k_{12} and k_{21})					
	Temperature ($^{\circ}$ C)					
	40		90		100	
PRSV-2vdw	0.0744	0.0579	0.0924	0.0973	0.0918	0.1221

Table 8-7: Interaction parameters obtained for PRSV EOS with 2-parameter van der Waals mixing rules, from fitting of experimental data measured in this project, using the direct method for the Carbon Dioxide + Methanol System

Reference	EOS	k_{ij}
Weber et al. [1984]	PR	0.025 (-40 $^{\circ}$ C) 0.027 (-20 $^{\circ}$ C) 0.044 (0 $^{\circ}$ C) 0.041 (25 $^{\circ}$ C)

Table 8-8: Literature values for the binary interaction parameters for the Carbon Dioxide + Methanol System

The binary interaction parameters obtained in this project can not be directly compared to those mentioned in literature, as the isotherms measured in this project are higher than those mentioned in literature.

Table 8-9 summarizes the interaction parameters obtained by the fitting of the Huron-Vidal and modifications thereof mixing rules with the PRSV EOS. In all of the mixing rule/EOS combinations summarized in Table 8-9, use was made of the NRTL activity coefficient model to describe the activity coefficient incorporated into the mixing rules. In all cases the α_{ij} term in the NRTL model was set equal to 0.3.

Table 8-10 summarizes the interaction parameters obtained by the fitting of the Wong-Sandler mixing rules with the PRSV EOS. α_{ij} was set equal to 0.3 in the NRTL model.

Figures 8-11 to 8-19 illustrate graphically the fit of the various EOS/mixing rule combinations for the carbon dioxide + methanol system for the measured VLE data.

EOS	Interaction parameters (a_{12} and a_{21} (cal.mol ⁻¹))					
	Temperature (° C)					
	40		90		100	
HVO	1070.34	-62.38	937.81	74.13	778.16	239.57
MHV1	979.04	-186.69	874.39	-87.70	617.40	132.21
MHV2	759.61	185.77	723.43	149.37	486.88	370.77
LCVM	962.36	-125.14	994.27	-96.11	645.13	183.51
HVOS	1073.21	-118.47	985.42	-20.08	727.49	203.17

Table 8-9: Interaction parameters obtained for PRSV EOS with Huron-Vidal (and modifications thereof) mixing rules, from fitting of experimental data measured in this project, using the direct method for the Carbon Dioxide + Methanol System

G ^E model	Interaction parameters (k_{ij} , p_{12} and p_{21} (reduced parameters))								
	Temperature (° C)								
	40			90			100		
NRTL	0.4001	0.3519	0.4877	0.5000	0.0724	0.4884	0.3932	0.4445	0.6361
Wilson	0.4085	0.6367	0.6623	0.4997	1.0200	0.5216	0.4725	0.3443	1.0754
Van Laar	0.3992	0.7923	0.8062	0.4999	0.5546	0.4971	0.4942	1.0025	0.4720
UNIQUAC	0.4713	1.0442	0.5168	0.5326	1.1161	0.5519	0.4798	0.9547	0.4795

Table 8-10: Interaction parameters obtained for PRSV EOS with Wong-Sandler mixing rules, from fitting of experimental data measured in this project, using the direct method for the Carbon Dioxide + Methanol System

For NRTL: $p_{ij} = a_{ij}/RT$ (a_{ij} in cal.mol⁻¹)

For Wilson: $p_{ij} = (V_{Lj}/V_{Li})\exp(-a_{ij}/RT)$ (a_{ij} in cal.mol⁻¹)

For Van Laar: $p_{ij} = a_{ij}$

For UNIQUAC: $p_{ij} = \exp(-a_{ij}/RT)$ (a_{ij} in cal.mol⁻¹)

8.2.3.3. Propane + 1-Propanol

Table 8-11 summarizes the interaction parameters, k_{12} , obtained for the SRK, PR and PRSV-1vdw EOS's. Table 8-12 summarizes the interaction parameters, k_{12} and k_{21} , for the PRSV-2vdw EOS.

EOS	Interaction parameter (k_{12})	
	Temperature (° C)	
	105.1	120
SRK	0.0483	0.0606
PR	0.0548	0.0654
PRSV-1vdw	0.0631	0.0769

Table 8-11: Interaction parameter obtained for various EOS's, from fitting of experimental data measured in this project, using the direct method for the Propane + 1-Propanol System

Figure 8-11: Comparison between the predicted and experimental data for the Carbon Dioxide + Methanol System at 40°C

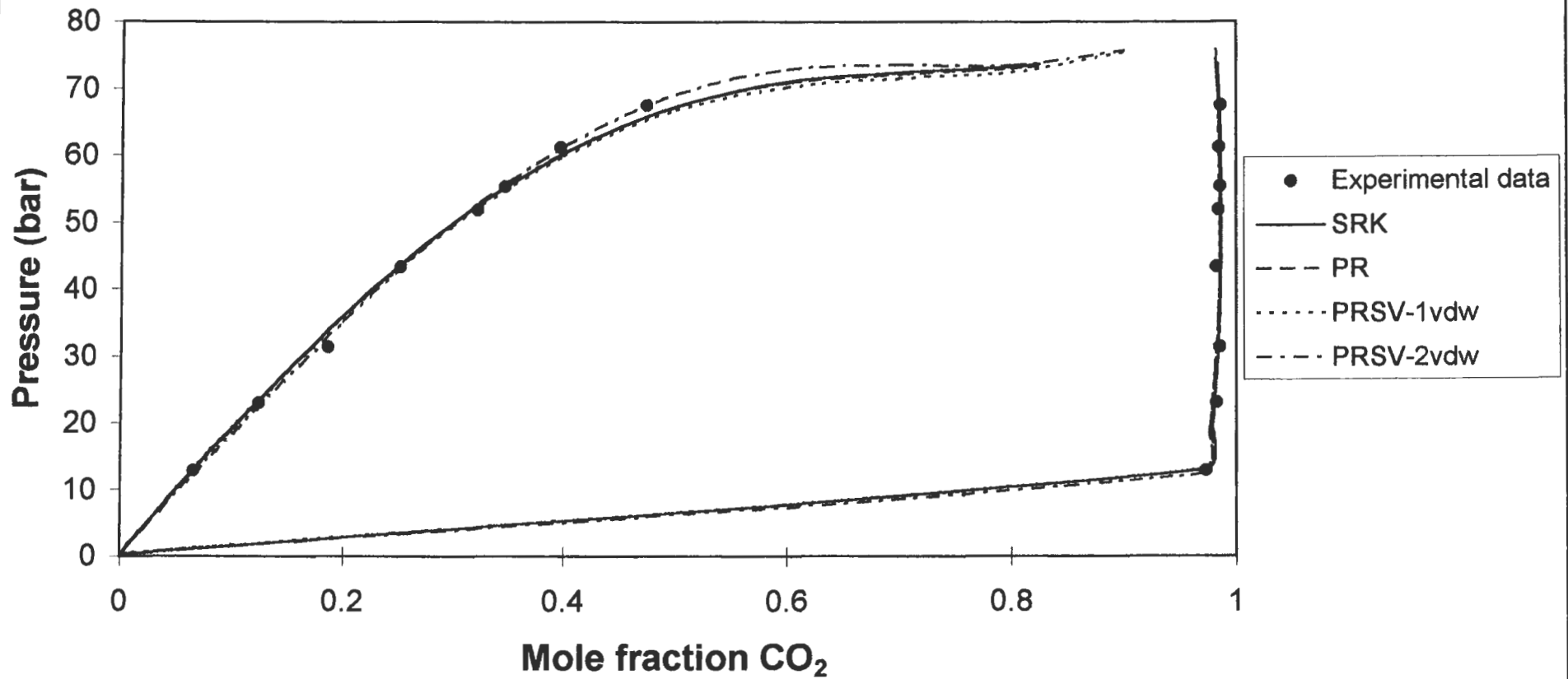


Figure 8-12: Comparison between the predicted and experimental data for the Carbon Dioxide + Methanol System at 40°C

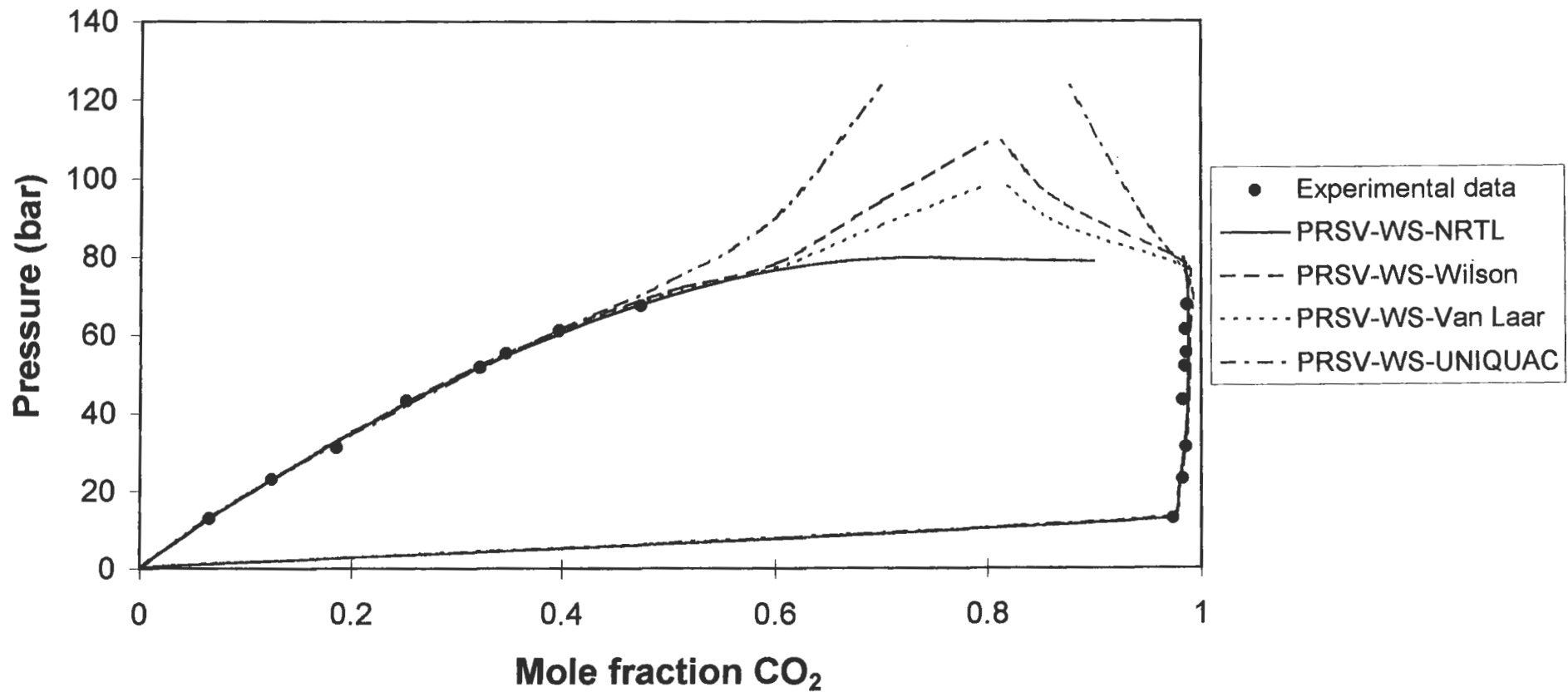


Figure 8-13: Comparison between the predicted and experimental data for the Carbon Dioxide + Methanol System at 40°C

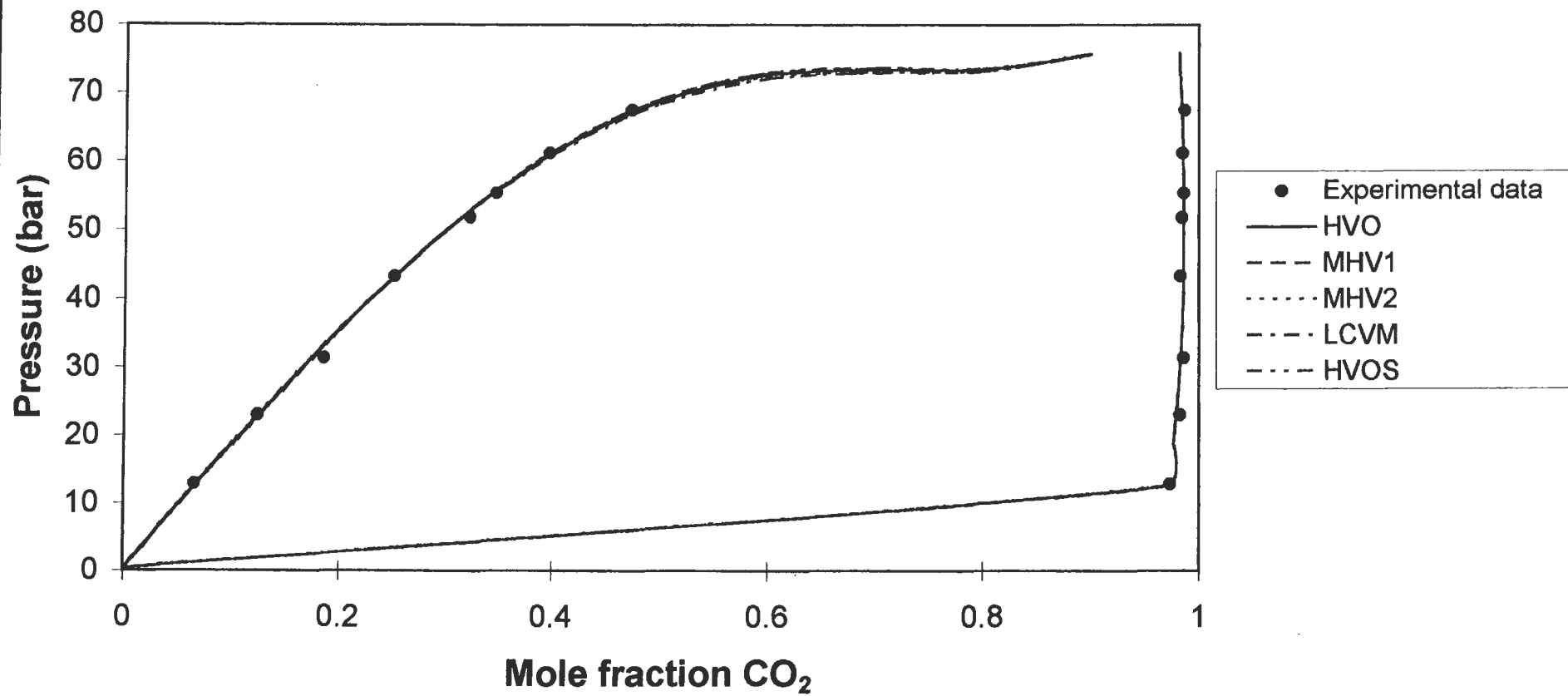


Figure 8-14: Comparison between the predicted and experimental data for the Carbon Dioxide + Methanol System at 90°C

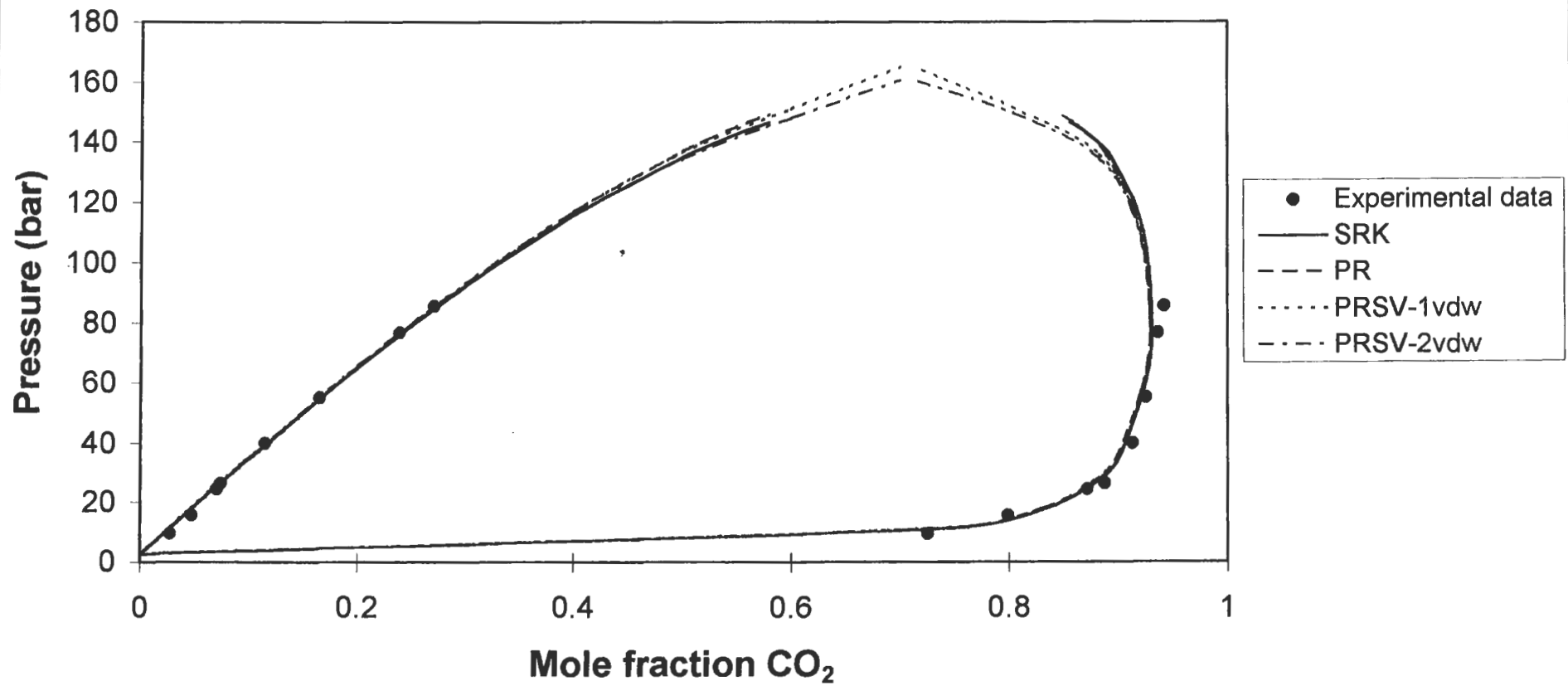


Figure 8-15: Comparison between the predicted and experimental data for the Carbon Dioxide + Methanol System at 90°C

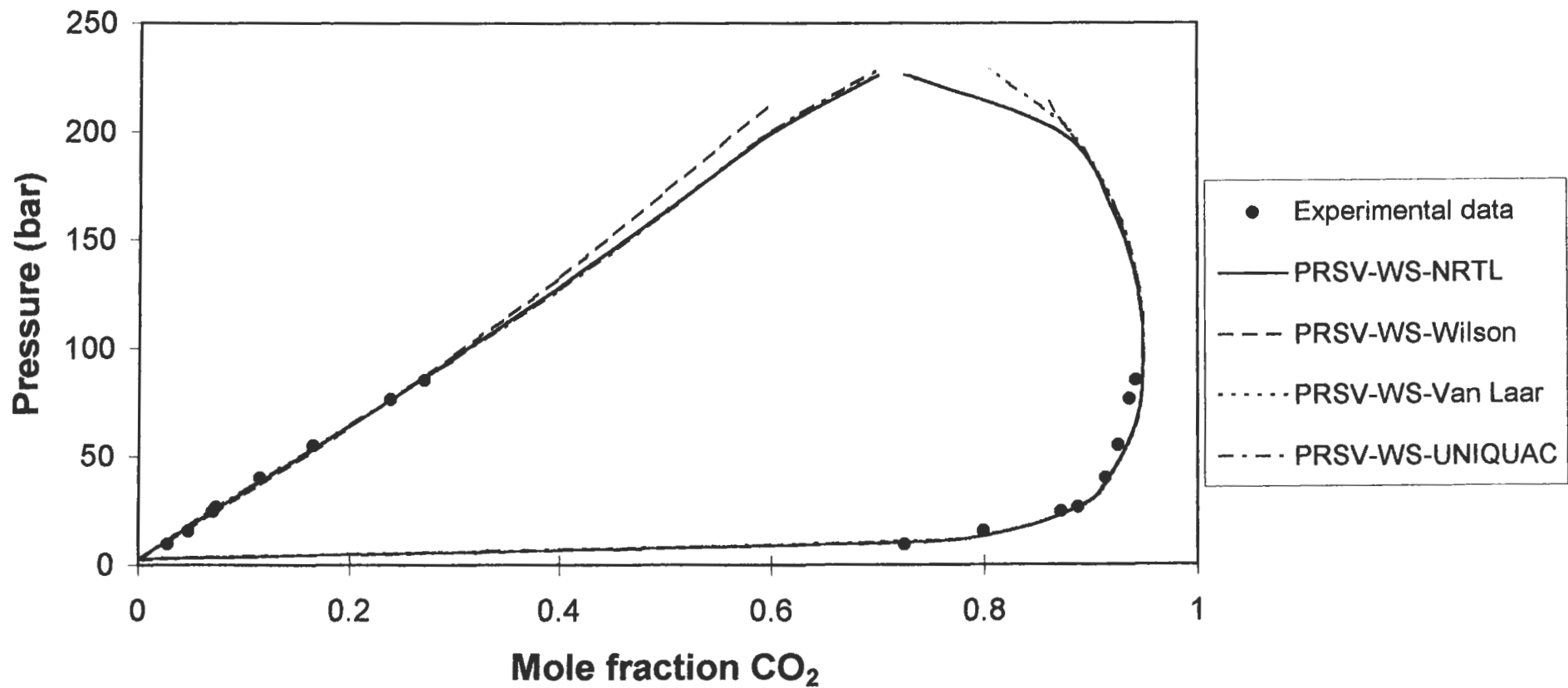


Figure 8-16: Comparison between the predicted and experimental data for the Carbon Dioxide + Methanol System at 90°C

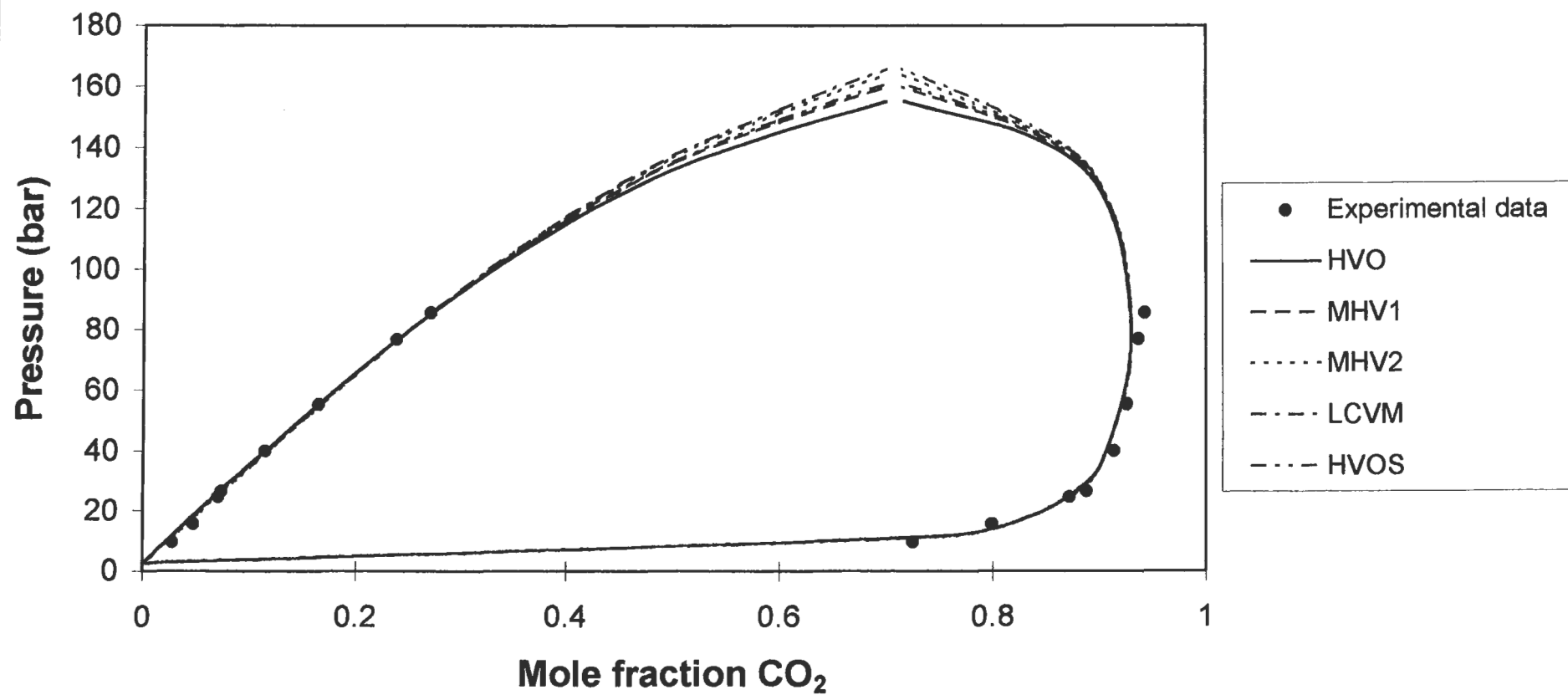


Figure 8-17: Comparison between the predicted and experimental data for the Carbon Dioxide + Methanol System at 100°C

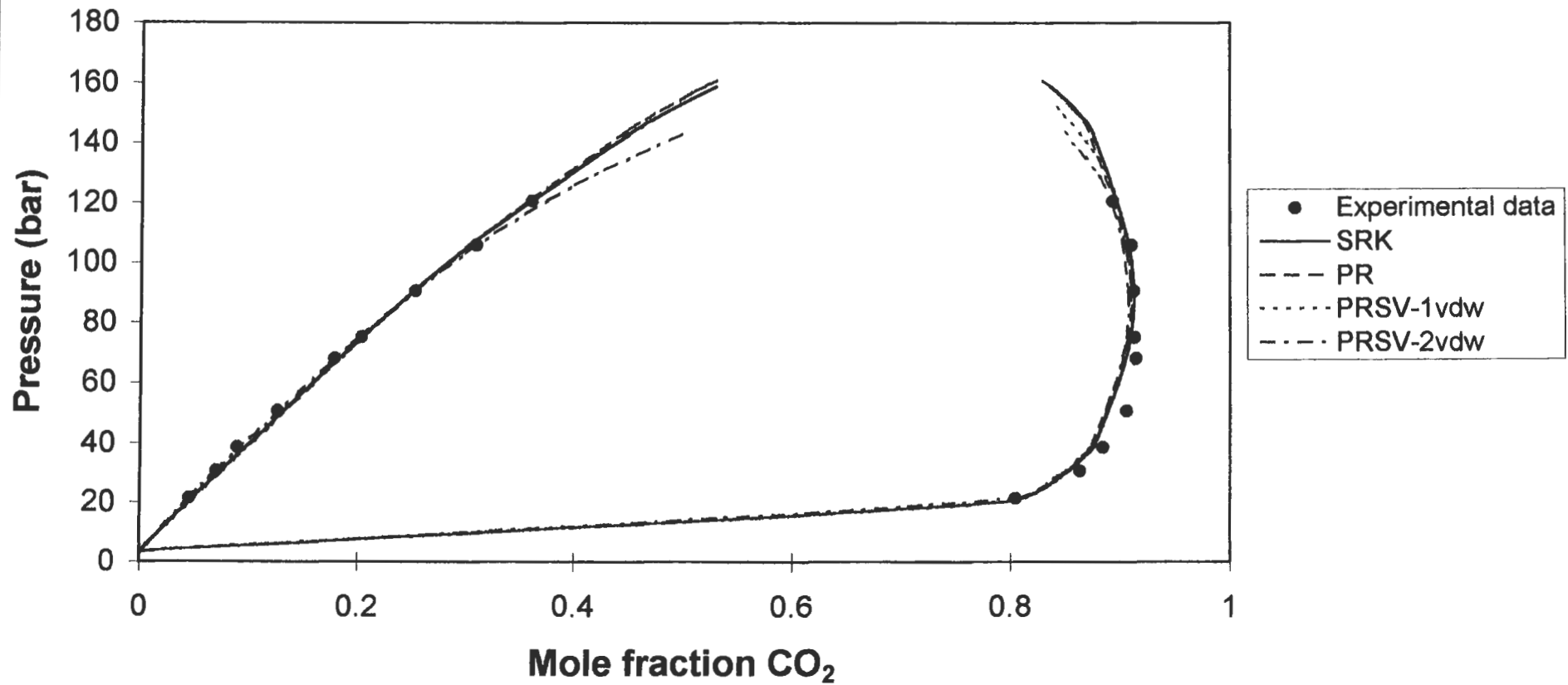


Figure 8-18: Comparison between the predicted and experimental data for the Carbon Dioxide + Methanol System at 100°C

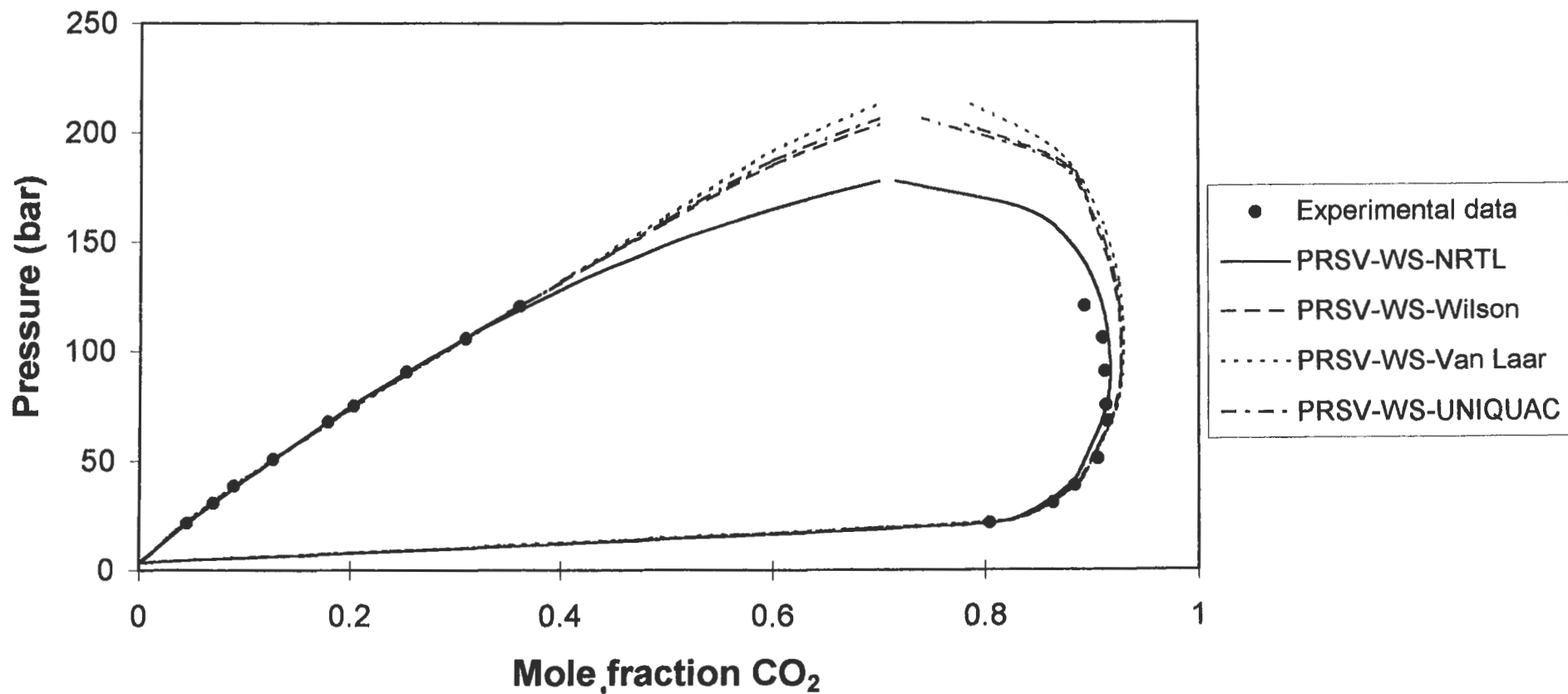
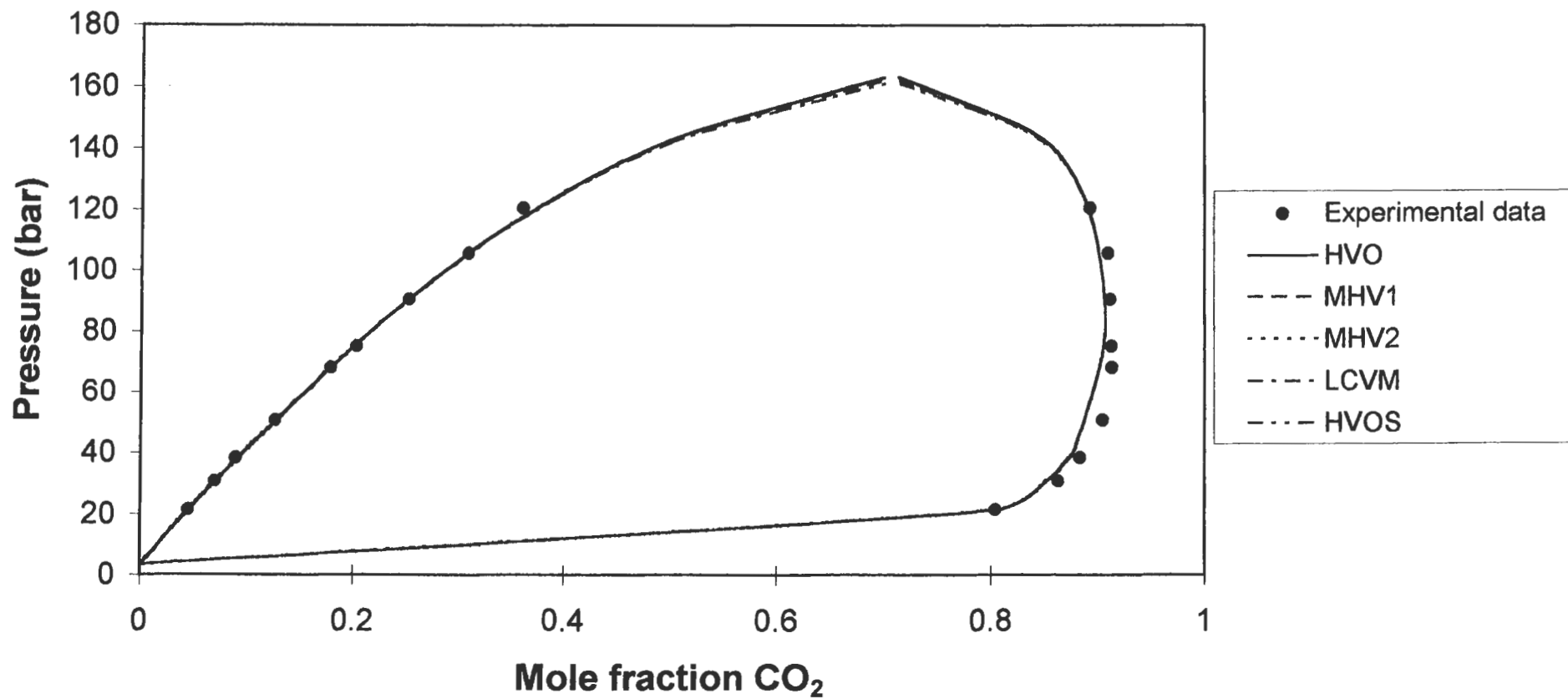


Figure 8-19: Comparison between the predicted and experimental data for the Carbon Dioxide + Methanol System at 100°C



A trend very easily seen in Tables 8-11 is that the value of the interaction parameter increases with increasing temperature. This trend is not evident in the fitting of Mühlbauer and Raal [1993] shown in Table 8-13. The values for the interaction parameter, k_{ij} , obtained by Mühlbauer and Raal [1993] for the propane + 1-propanol system using the Peng-Robinson EOS with van der Waals mixing rules are also significantly different from those obtained in this work for the appropriate temperatures. This can be attributed to the fact that there was a difference in the measured vapour compositions between the two sets of measurements.

EOS	Interaction parameters (k_{12} and k_{21})			
	Temperature ($^{\circ}$ C)			
	105.1		120	
PRSV-2vdw	0.0890	0.0241	0.0972	0.0236

Table 8-12: Interaction parameters obtained for PRSV EOS with 2-parameter van der Waals mixing rules, from fitting of experimental data measured in this project, using the direct method for the Propane + 1-Propanol System

Reference	EOS	k_{ij}
Mühlbauer and Raal [1993]	PR	0.0587 (81.62 $^{\circ}$ C)
		0.06859 (105.11 $^{\circ}$ C)
		0.06831 (120.05 $^{\circ}$ C)

Table 8-13: Literature values for the binary interaction parameters for the Propane + 1-Propanol System

EOS	Interaction parameters (a_{12} and a_{21} (cal.mol $^{-1}$))			
	Temperature ($^{\circ}$ C)			
	105.1		120	
HVO	1488.64	-258.09	1539.51	-286.55
MHV1	1417.81	-364.19	1422.98	-368.60
MHV2	1262.70	-210.94	1212.55	-199.20
LCVM	1523.15	-375.03	1451.52	-338.28
HVOS	1570.67	-312.33	1545.83	-302.13

Table 8-14: Interaction parameters obtained for PRSV EOS with Huron-Vidal (and modifications thereof) mixing rules, from fitting of experimental data measured in this project, using the direct method for the Propane + 1-Propanol System

Table 8-14 summarizes the interaction parameters obtained by the fitting of the Huron-Vidal and modifications thereof mixing rules with the PRSV EOS. In all of the mixing rule/EOS combinations, use was made of the NRTL activity coefficient model to describe the activity coefficient incorporated into the mixing rule. The α_{ij} parameter was set to 0.3 for all cases.

The interaction parameters obtained by the fitting of the Wong-Sandler mixing rules with the PRSV EOS are summarized in Table 8-15. Once again the α_{ij} parameter for the NRTL activity coefficient was set to 0.3.

G^E model	Interaction parameters (k_{ij} , p_{12} and p_{21} (reduced parameters))					
	Temperature ($^{\circ}$ C)					
	105.1			120		
NRTL	0.3534	-0.2618	0.6770	0.3082	0.4985	0.0553
Wilson	0.3209	1.1046	0.5236	0.3000	1.2651	0.3878
Van Laar	0.2982	0.4200	0.7200	0.2340	0.3001	7.3113
UNIQUAC	0.3824	1.3231	0.4972	0.3798	1.7758	0.4014

Table 8-15: Interaction parameters obtained for PRSV EOS with Wong-Sandler mixing rules, from fitting of experimental data measured in this project, using the direct method for the Propane + 1-Propanol System

For NRTL: $p_{ij} = a_{ij}/RT$ (a_{ij} in cal.mol^{-1})

For Wilson: $p_{ij} = (V_{Lj}/V_{Li})\exp(-a_{ij}/RT)$ (a_{ij} in cal.mol^{-1})

For Van Laar: $p_{ij} = a_{ij}$

For UNIQUAC: $p_{ij} = \exp(-a_{ij}/RT)$ (a_{ij} in cal.mol^{-1})

Figure 8-20 to 8-25 summarize graphically the fitting of the various EOS/mixing rule combinations for the direct method for the Propane + 1-Propanol system.

8.3. THE COMBINED METHOD

The combined method, which is otherwise known as the gamma-phi method, is used very infrequently in the modeling of HPVLE. The method as, its name suggests, makes use of an EOS to describe the vapour phases and an activity coefficient model to describe the liquid phase. The combined method is much more difficult to apply, as it requires the definition of standard states or reference conditions. It also has many drawbacks, which are discussed in Chapter 3, but when applied correctly can give considerably improved modeling over the direct method.

There is no means to determine whether the direct or combined method produces better fits for a specific system. Therefore one has to apply both methods to the system.

Figure 8-20: Comparison between the predicted and experimental data for the Propane + 1-Propanol System at 105.1 °C

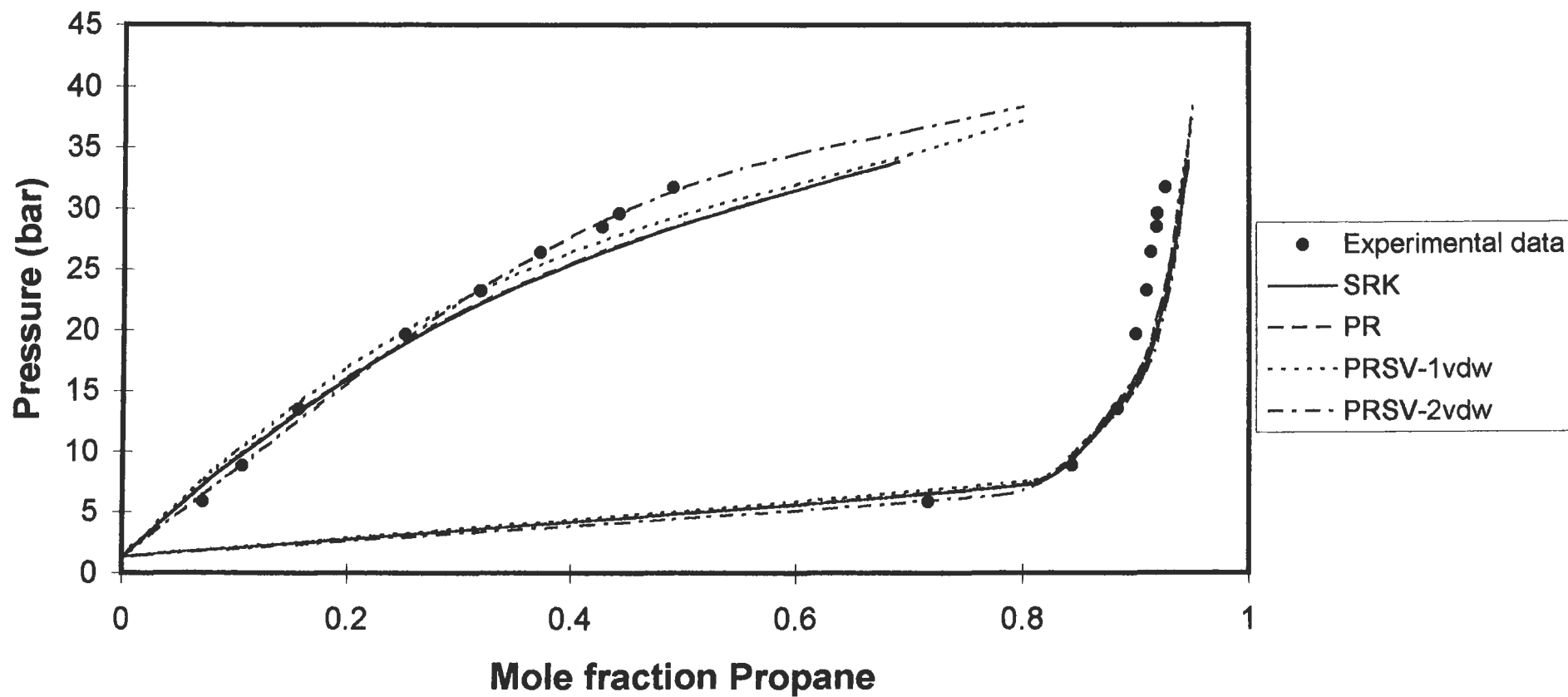


Figure 8-21: Comparison between the predicted and experimental data for the Propane + 1-Propanol System at 105.1 °C

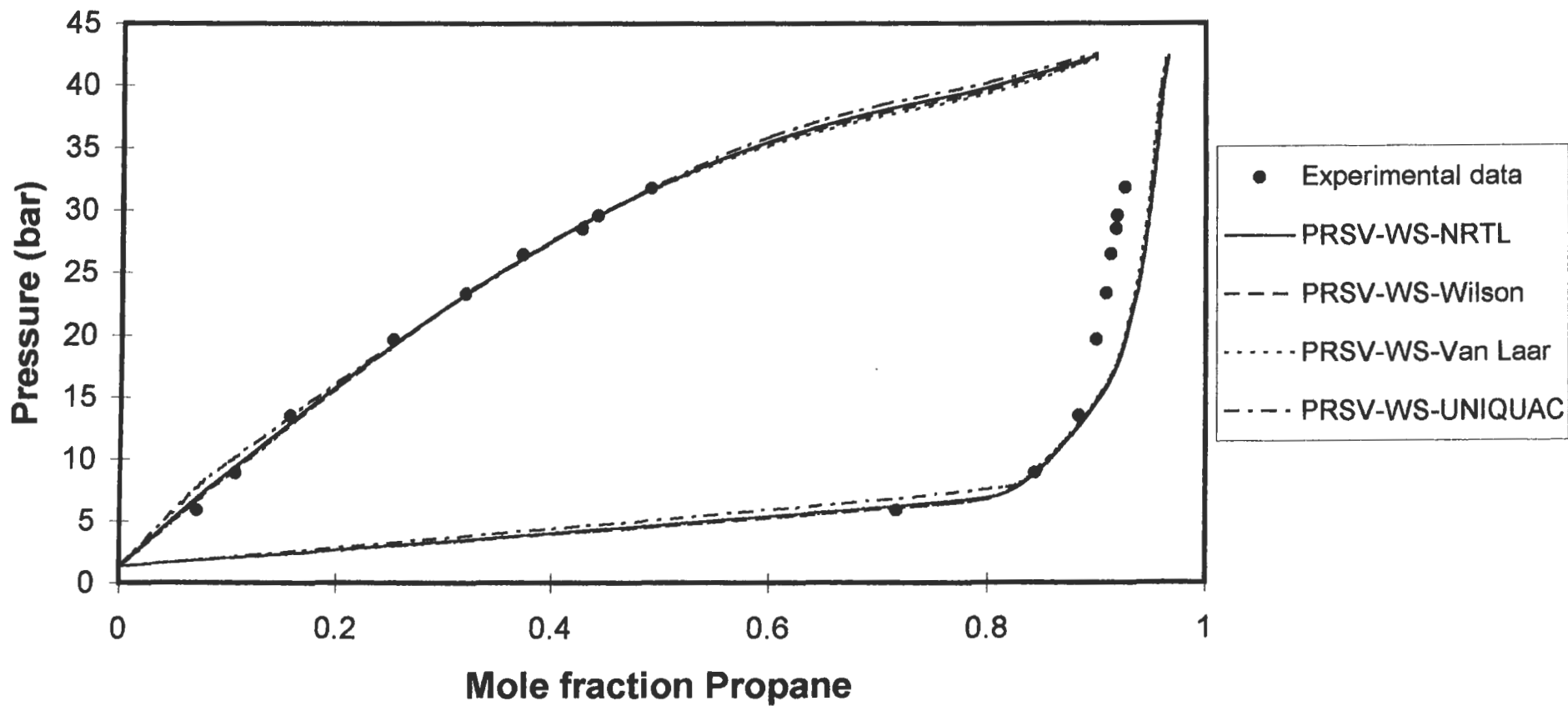


Figure 8-22: Comparison between the predicted and experimental data for the Propane + 1-Propanol System at 105.1 °C

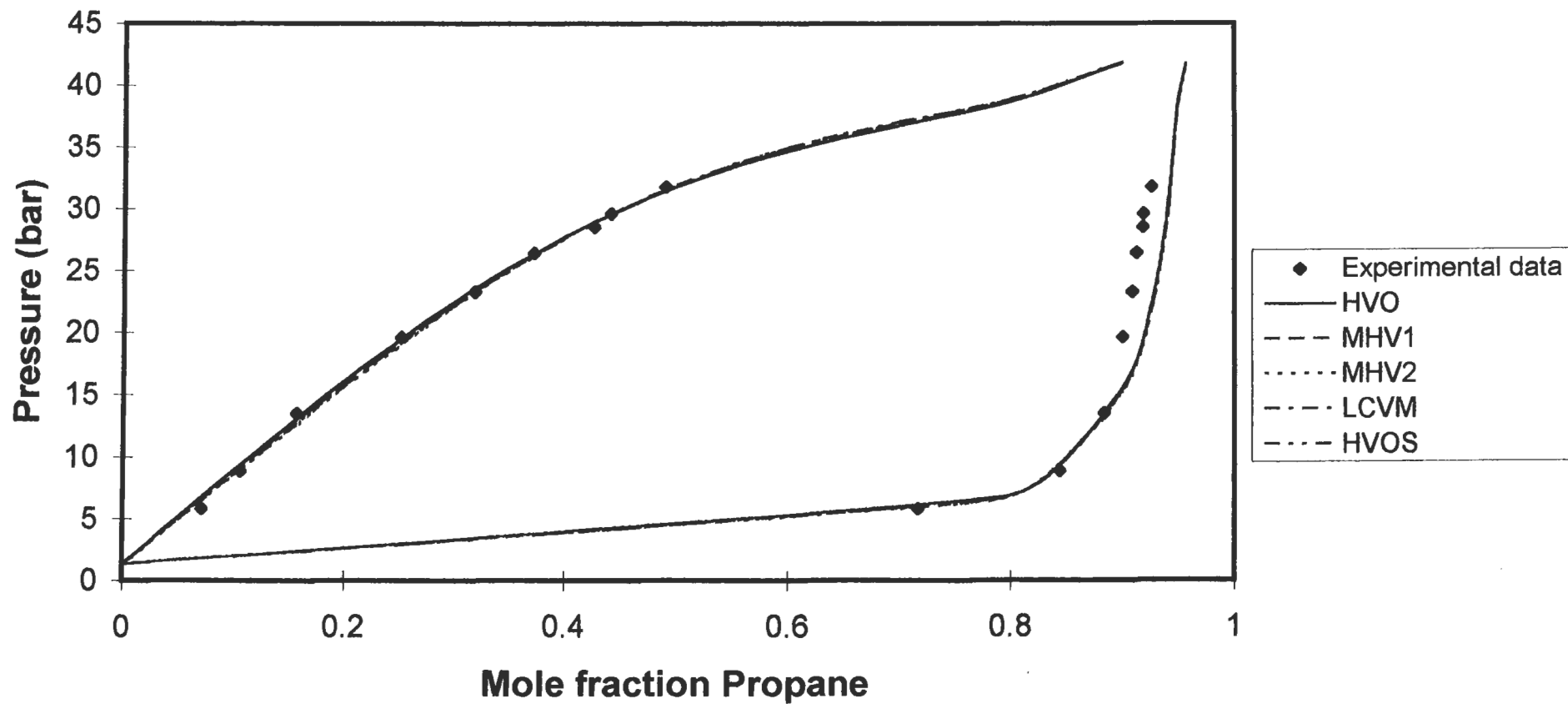


Figure 8-23: Comparison between the predicted and experimental data for the Propane + 1-Propanol System at 120 °C

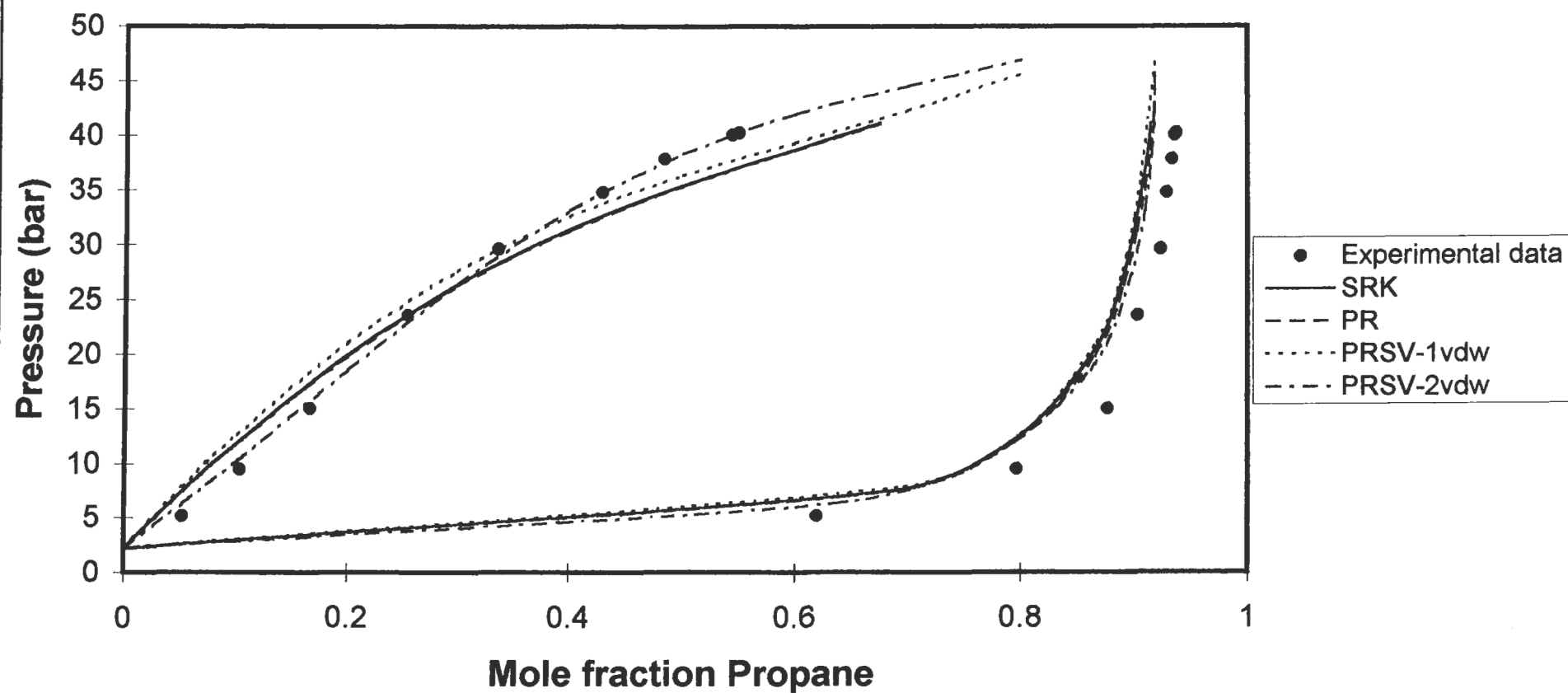


Figure 8-24: Comparison between the predicted and experimental data for the Propane + 1-Propanol System at 120 °C

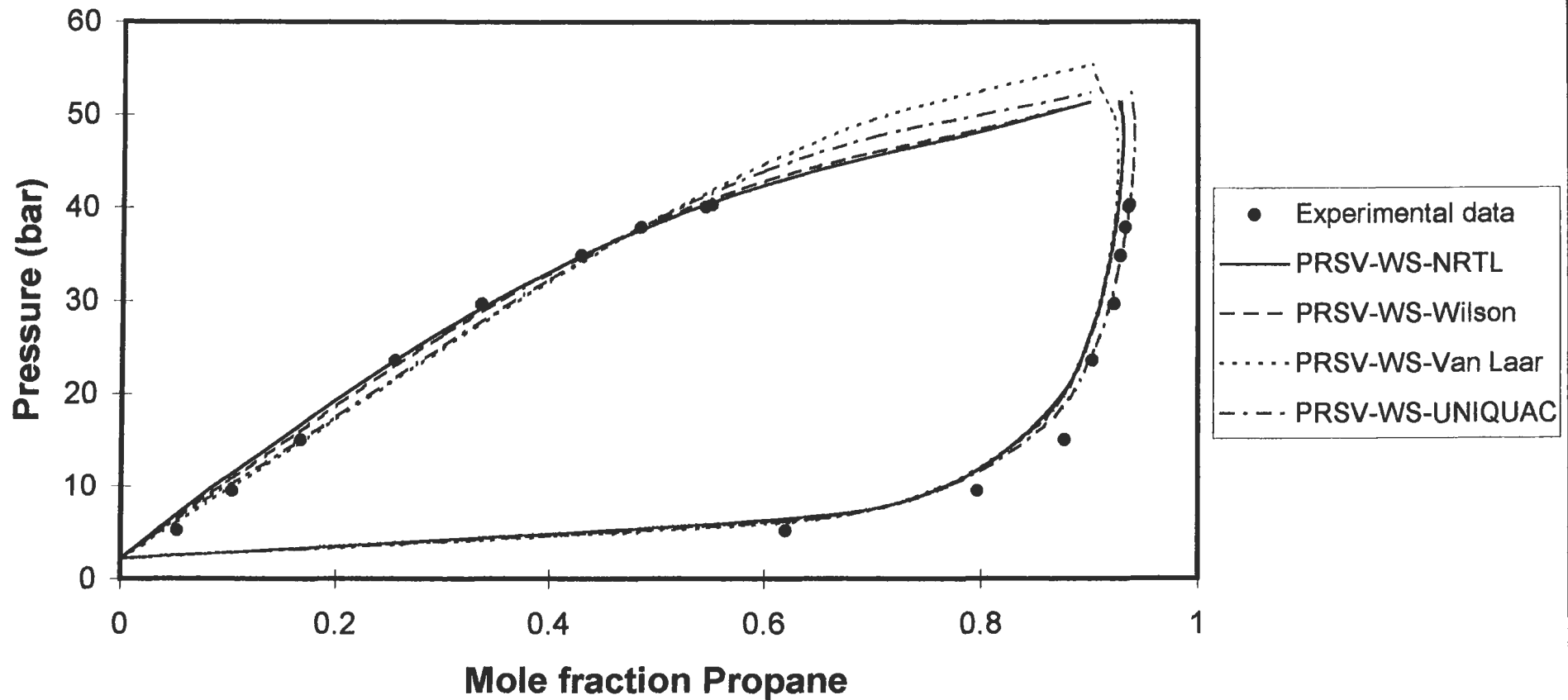
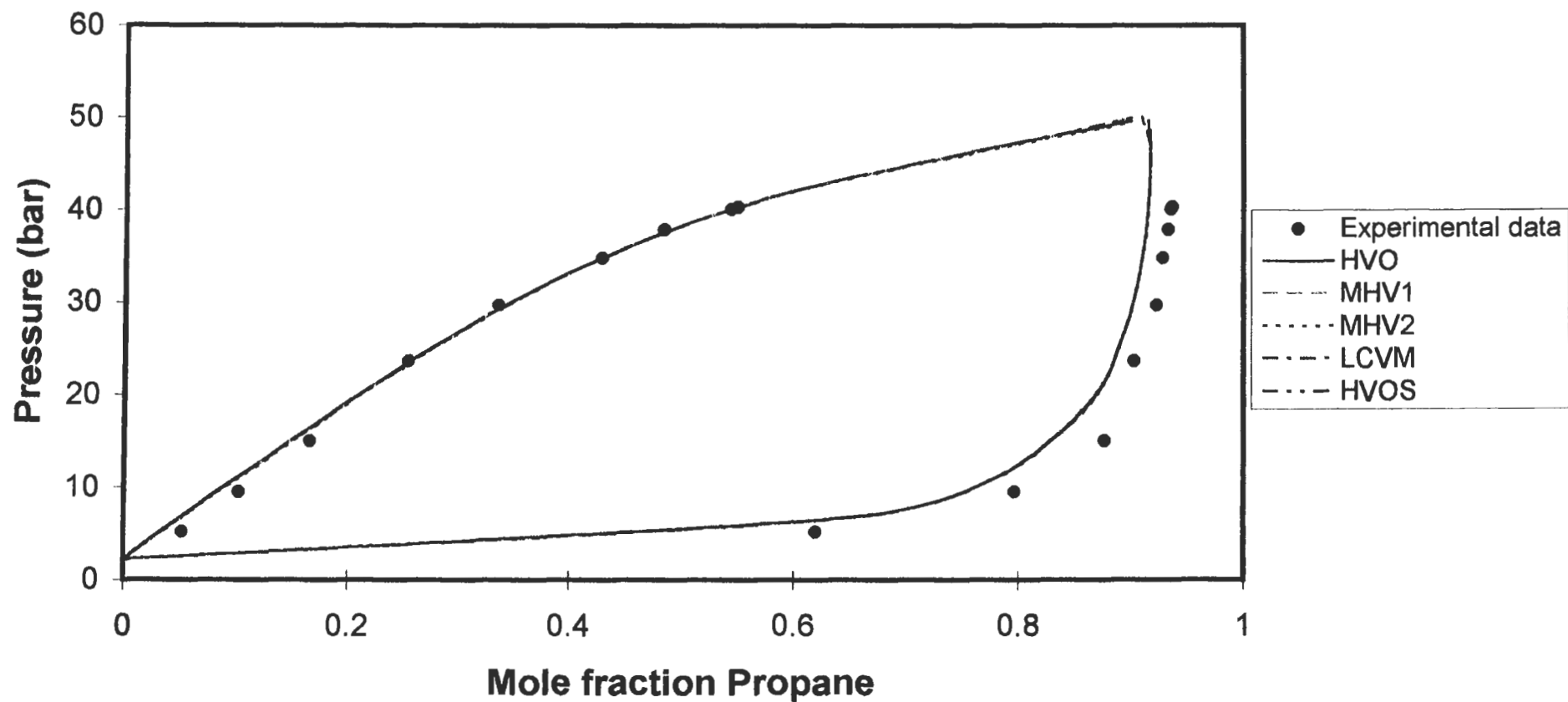


Figure 8-25: Comparison between the predicted and experimental data for the Propane + 1-Propanol System at 120 °C



8.3.1. Model combinations for the Combined Method

The following combinations of EOS/mixing rule and activity coefficient models were applied in this project:-

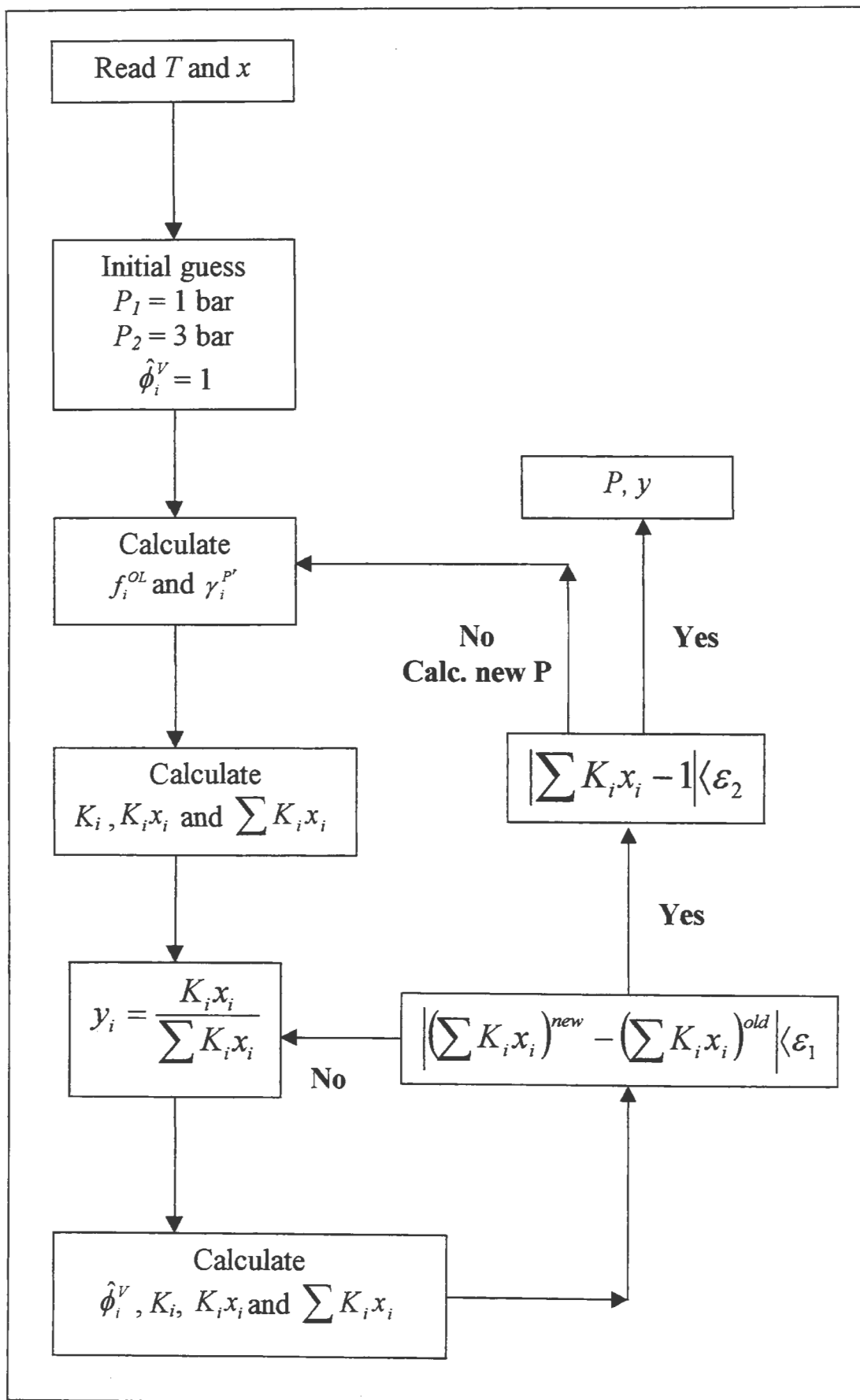
1. Peng-Robinson-Stryjek-Vera EOS with van der Waals mixing rules and the UNIQUAC activity coefficient model – PRSV + Uniquac.
2. Peng-Robinson-Stryjek-Vera EOS with van der Waals mixing rules and the NRTL activity coefficient model – PRSV + NRTL.
3. Peng-Robinson-Stryjek-Vera EOS with van der Waals mixing rules and the Van Laar activity coefficient model – PRSV + Van Laar.
4. Peng-Robinson-Stryjek-Vera EOS with van der Waals mixing rules and the Wilson activity coefficient model – PRSV + Wilson.
5. Peng-Robinson-Stryjek-Vera EOS with Wong and Sandler mixing rules (NRTL activity coefficient model in mixing rule) and the NRTL activity coefficient model – PRSVWS-NRTL + NRTL (new combined method).
6. Virial EOS and the UNIQUAC activity coefficient model – Virial + Uniquac.
7. Virial EOS and the NRTL activity coefficient model – Virial + NRTL.
8. Virial EOS and the Van Laar activity coefficient model – Virial + Van Laar.
9. Virial EOS and the Wilson activity coefficient model – Virial + Wilson.

8.3.2. Data fitting/Correlation

Determination of the fitting parameters for the combined method was undertaken with the method analogous to that used for the direct method (Marquardt non-linear regression) except that the bubble pressure algorithm was modified so as to accommodate the use of an activity coefficient model to account for liquid phase non-idealities. Figure 8-26 illustrates the flow chart for the bubble pressure computation via the combined method. The objective function for the least square regression was the same as for the direct method, viz. Equation (8-1).

Inputs for the bubble pressure algorithm were the temperature and liquid compositions, critical properties (temperature and pressure), acentric factors, K_i (fitted vapour pressure parameter for the PRSV EOS), Gibbs excess free energy model parameters (for activity coefficient models and for mixing rules which incorporate a Gibbs excess free energy model, e.g. Wong-Sandler) and correlation parameters for the standard-state fugacity coefficient (Prausnitz et al. [1980]). In

Figure 8-26: Flowchart for the bubble P computation via the combined method



addition, modified Rackett parameters were required for the computation of liquid molar volumes. When the Virial EOS was used to compute the vapour phase fugacity coefficient the dipole moments, radii of gyration and association and solvation parameters were required as well.

The Secant method was used for the determination of the new computed pressure in the bubble pressure algorithm and therefore two initial guesses were made for the pressure. Depending on the system and the experimental measurements, initial guesses on $P_1 = 1$ and $P_2 = 3$ bar would ensure the computation procedure started smoothly and converged to a solution. The equations for the computation of the new pressure via the Secant method were given by Equations (8-3) and (8-4).

The algorithm shown in Figure 8-26 is a combination of algorithms given by Mühlbauer [1990] and Smith and Van Ness [1987]. Each of the algorithms on their own did not perform well for HPVLE computation, but the combination of the two produced an algorithm that performed very well, except in the region approaching the critical state.

The standard-state fugacity was computed using the following expression:

$$f_i^{OL} = P_i^S \phi_i^S \exp \int_{P_i^S}^{P'} \frac{V_i^L}{RT} dP \quad (8-5)$$

The reference pressure was set equal to zero for all components. Prausnitz et al. [1980] also had a correlation for the zero-pressure reference fugacity given by the following expression:

$$\ln f_i^{OL} = C_1 + \frac{C_2}{T + C_6} + C_3 T + C_4 \ln T + C_5 T^2 \quad (8-6)$$

The constants for Equation (8-6) as well as all inputs for both the direct and combined method bubble pressure computations are given in Appendix F.

The liquid molar volumes were computed via the O'Connell modification (Prausnitz et al. [1980]) of the modified Rackett equation of Spencer and Danner [1972]. The saturated-liquid molar volume was given by the following equation:

$$V_i^L = \frac{RT_{C_i} Z_{f_i}^\tau}{P_{C_i}} \quad (8-7)$$

where, $\tau = 1 + (1-T_r)^{0.286}$ for $T_r \leq 0.75$

$\tau = 1.6 + 0.00693/(T_r - 0.655)$ for $T_r > 0.75$

In all computations in the bubble pressure calculation it was assumed that the liquid partial molar volume (\bar{V}_i^L) for each of the components was equal to the liquid molar volume (V_i^L). This was undertaken as liquid partial molar volumes are not available and the assumption that $V_i^L = \bar{V}_i^L$ is a reasonable one.

The activity coefficient at some reference pressure, P^r , was computed using Equation (3-22). This correction is undertaken because the isothermal activity coefficients are not evaluated at the same pressure and therefore must be corrected from the experimental pressure P to the same arbitrary reference pressure designated P^r . The activity coefficient was computed using one of the following activity coefficient models, viz. NRTL, Van Laar, Wilson or UNIQUAC.

The fugacity coefficients in solution for the vapour phase were calculated from expressions given in Chapter 3 and Appendix B, for the appropriate EOS and mixing rule combinations. The equilibrium ratio (K_i) was calculated from Equation (3-19). For the virial EOS, the Hayden and O'Connell [1975] method was used to compute the pure component and cross virial coefficients. The Hayden and O'Connell method is detailed in Appendix B.

There were two convergence checks in the algorithm. For both convergence checks the tolerances (ϵ_1 and ϵ_2) were set equal to $1E-5$.

Depending on the EOS used for the description of the vapour phase and the activity coefficient model for the liquid phase, two or three parameters were fitted. When the virial EOS was used to describe the vapour phase, two parameters were fitted, viz. the liquid phase activity coefficient model parameters. For the NRTL model, the third parameter (α_{ij}) was set equal to 0.3 for all computations. For description of the vapour phase via the PRSV EOS, with van der Waals one-fluid mixing rules, three parameters were fitted, viz. the interaction parameter for the van der Waals one-fluid mixing rule and the two parameters for the liquid phase activity coefficient model. Once again the α_{ij} parameter for the NRTL model was set equal to 0.3.

A modified combined method (Ramjugernath and Raal [1999]) was also used to correlate the experimental data. The modified method basically adopts the same method as the *normal* combined methods, viz. that the vapour phase is described by an EOS and the liquid phase by an activity coefficient model. However, the vapour phase is now described by an EOS, which has mixing rules that incorporate an activity coefficient model, e.g. Wong-Sandler, and Huron-Vidal mixing rules. Correlation or fitting involves the fitting of just three parameters, the k_{ij} interaction parameter for the mixing rule and the activity coefficient model parameters, which occur in the mixing rule and in the activity coefficient for the description of the liquid phase. The same activity coefficient model is used to describe the liquid phase and the Gibbs excess energy in the mixing rule for the vapour phase. The activity coefficient parameters were simultaneously fitted to the liquid phase model and the activity coefficient model in the mixing rule. For the NRTL excess free energy model, the α_{ij} was set equal to 0.3. The decision to simultaneously fit the activity coefficient model parameters to the liquid phase activity coefficient and the mixing rule was intuitive. The method is further discussed in Section 8.4.

Computational times for the combined method were on average longer than those for the direct method. Depending on the combinatorial choice of EOS and activity coefficient model the combined method took approximately 1 to 10 minutes to converge to a solution.

Once the fitted parameters were obtained, a bubble pressure computation could be undertaken to determine the entire P-x-y diagram. Figures 8-27 to 8-42 compares the experimental data measured in this project to the predicted/correlated data using the combined method with the appropriate combinations of EOS's and activity coefficient models.

It seems that the fit for the combined method using the Marquardt method is very tight and when the bubble pressure computations are undertaken for liquid compositions significantly higher than those fitted, the bubble pressure computation had problems converging and may in fact give erroneous results. This is true for combined methods in general and is especially evident near the critical region.

Both the direct and combined methods and the modeling/correlating combinations are discussed in Section 8.4. The absolute averages errors for both the vapour composition and pressure are summarized and the models rated for the three systems modeled, viz. the carbon dioxide + toluene, carbon dioxide + methanol and propane + 1-propanol systems.

8.3.3. Fitted parameters

8.3.3.1. Carbon Dioxide +Toluene System

Table's 8-16 and 8-17 summarizes the fitted parameters for the Virial and PRSV EOS's respectively with the appropriate liquid phase activity coefficient models. For the PRSV EOS, the van der Waals one-fluid mixing rule was used for all computations via the combined method.

Interaction parameters (p_{12} and p_{21} (reduced parameters))						
Temperature ($^{\circ}$ C)						
G^E model	38		80		118.3	
NRTL	0.6076	0.4619	1.5955	-0.1841	1.6261	-0.1956
Wilson	0.5812	0.5506	0.9431	0.2266	0.9308	0.2299
Van Laar	0.9618	1.0072	0.8131	1.4174	0.8158	1.4310
UNIQUAC	-0.2360	1.2267	0.1056	0.7325	0.1079	0.7340

Table 8-16: Interaction parameters obtained for various activity coefficient models with the Virial EOS, from fitting of experimental data measured in this project, using the combined method for the Carbon Dioxide + Toluene System

For NRTL: $p_{ij} = (a_{ij}/RT)$ (a_{ij} in cal.mol $^{-1}$)

For Wilson: $p_{ij} = (V_{Lj}/V_{Li})\exp(-a_{ij}/RT)$ (a_{ij} in cal.mol $^{-1}$)

For Van Laar: $p_{ij} = a_{ij}$

For UNIQUAC: $p_{ij} = (a_{ij}/RT)$ (a_{ij} in cal.mol $^{-1}$)

Interaction parameters (k_{ij} , p_{12} and p_{21} (reduced parameters))									
Temperature ($^{\circ}$ C)									
G^E model	38			80			118.3		
NRTL	-0.1657	2.9855	-0.5291	0.0103	10.2769	0.3900	-0.0689	3.542	-0.5318
Wilson	-0.0381	1.1784	0.0188	-0.1192	1.0952	0.0000	-0.0874	1.0819	0.0000
Van Laar	-0.1004	0.7522	2.5642	-0.0102	0.7819	3.2257	-0.0639	0.7642	3.6086
UNIQUAC	-0.1083	0.7910	0.2314	-0.0101	1.0957	0.1314	-0.0643	1.2980	0.0522

Table 8-17: Interaction parameters obtained for various activity coefficient models with the PRSV EOS, from fitting of experimental data measured in this project, using the combined method for the Carbon Dioxide + Toluene System

For NRTL: $p_{ij} = (a_{ij}/RT)$ (a_{ij} in cal.mol $^{-1}$)

For Wilson: $p_{ij} = (V_{Lj}/V_{Li})\exp(-a_{ij}/RT)$ (a_{ij} in cal.mol $^{-1}$)

For Van Laar: $p_{ij} = a_{ij}$

For UNIQUAC: $p_{ij} = (a_{ij}/RT)$ (a_{ij} in cal.mol $^{-1}$)

The modified combined method (Ramjugernath and Raal [1999]) yielded fitted parameters summarized in Table 8-18.

There are very few references in literature for the comparison of fitted parameters for the Carbon Dioxide + Toluene System using the combined method. Only literature source found was Mühlbauer and Raal [1991]. They used the Virial, Peng-Robinson and Group Contribution

EOS's with the UNIQUAC liquid phase activity coefficient model. Table 8-19 and 8-20 summarizes their fitted parameters.

Interaction parameters (k_{ij} , p_{12} and p_{21} (reduced parameters))									
Temperature ($^{\circ}$ C)									
Model	38			80			118.3		
PRSVWS-NRTL+NRTL	0.2551	2.9972	-0.5252	0.4125	3.4366	-0.5026	0.3353	3.9687	-0.5417

Table 8-18: Interaction parameters obtained for the NRTL activity coefficient model with the PRSV EOS with Wong-Sandler mixing rules (NRTL activity coefficient model), from fitting of experimental data measured in this project, using the modified combined method for the Carbon Dioxide + Toluene System

$$p_{ij} = (a_{ij}/RT) \text{ (} a_{ij} \text{ in cal.mol}^{-1}\text{)}$$

Interaction parameters (p_{12} and p_{21}) (K)						
Temperature ($^{\circ}$ C)						
G^E model	38.11		79		120	
UNIQUAC	170.13	112.10	232.48	99.09	237.27	122.25

Table 8-19: Interaction parameters obtained the Virial EOS with the UNIQUAC model using the combined method for the Carbon Dioxide + Toluene System by Mühlbauer and Raal [1991]

$$P_{ij} = (a_{ij}/R) \text{ (} R = 83.147\text{)}$$

Interaction parameters (k_{ij} , p_{12} and p_{21} (K))									
Temperature ($^{\circ}$ C)									
G^E model	38.11			79			120		
UNIQUAC	0.1056	99.34	182.23	0.09424	256.66	84.07	0.09331	384.70	37.16

Table 8-20: Interaction parameters obtained for PR EOS with the UNIQUAC model using the combined method for the Carbon Dioxide + Toluene System by Mühlbauer and Raal [1991]

$$P_{ij} = (a_{ij}/R) \text{ (} R = 83.147\text{)}$$

No comparisons could be made between the fitted parameters of Mühlbauer and Raal [1991] and those obtained in this project for either the Virial or Peng-Robinson EOS using the combined method. The fitted parameters are different. The fit or correlation to the experimental data though for both this work and Mühlbauer and Raal [1991] seems to good for both cases. It is possible for different values for the parameters to be obtained and can be attributed to the fact that a local minimum could have been obtained for the objective function instead of the absolute minimum. Mühlbauer and Raal [1991] make no mention at all of the units for the UNIFAC fitted parameters. From their definition of R as having a value of 83.147 (again with no units), one presumes that R being the Universal gas constant, the units of the fitted parameter will be Kelvin (K).

Figure 8-27: Comparison between the predicted and experimental VLE data for the Carbon Dioxide + Toluene System at 38 °C

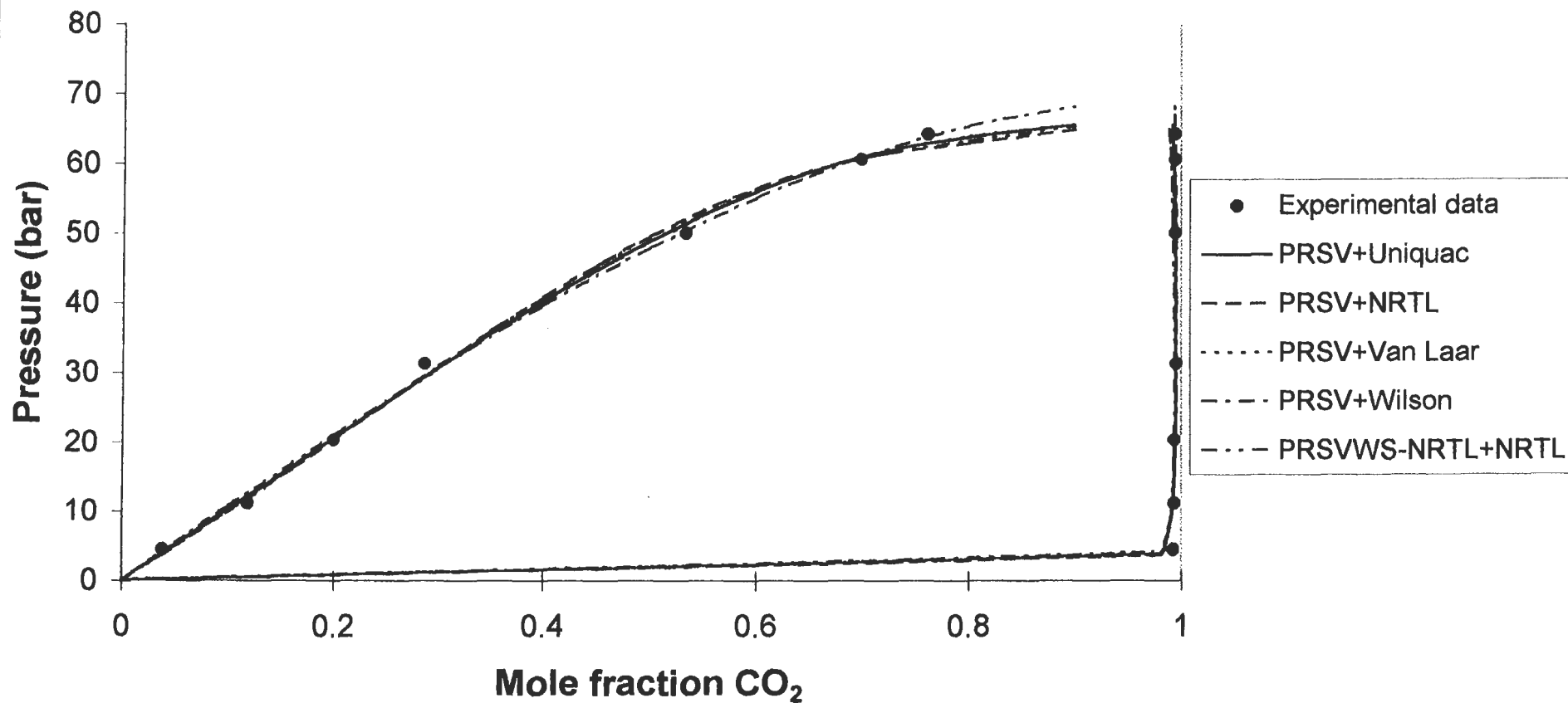


Figure 8-28: Comparison between the predicted and experimental VLE data for the Carbon Dioxide + Toluene System at 38 °C

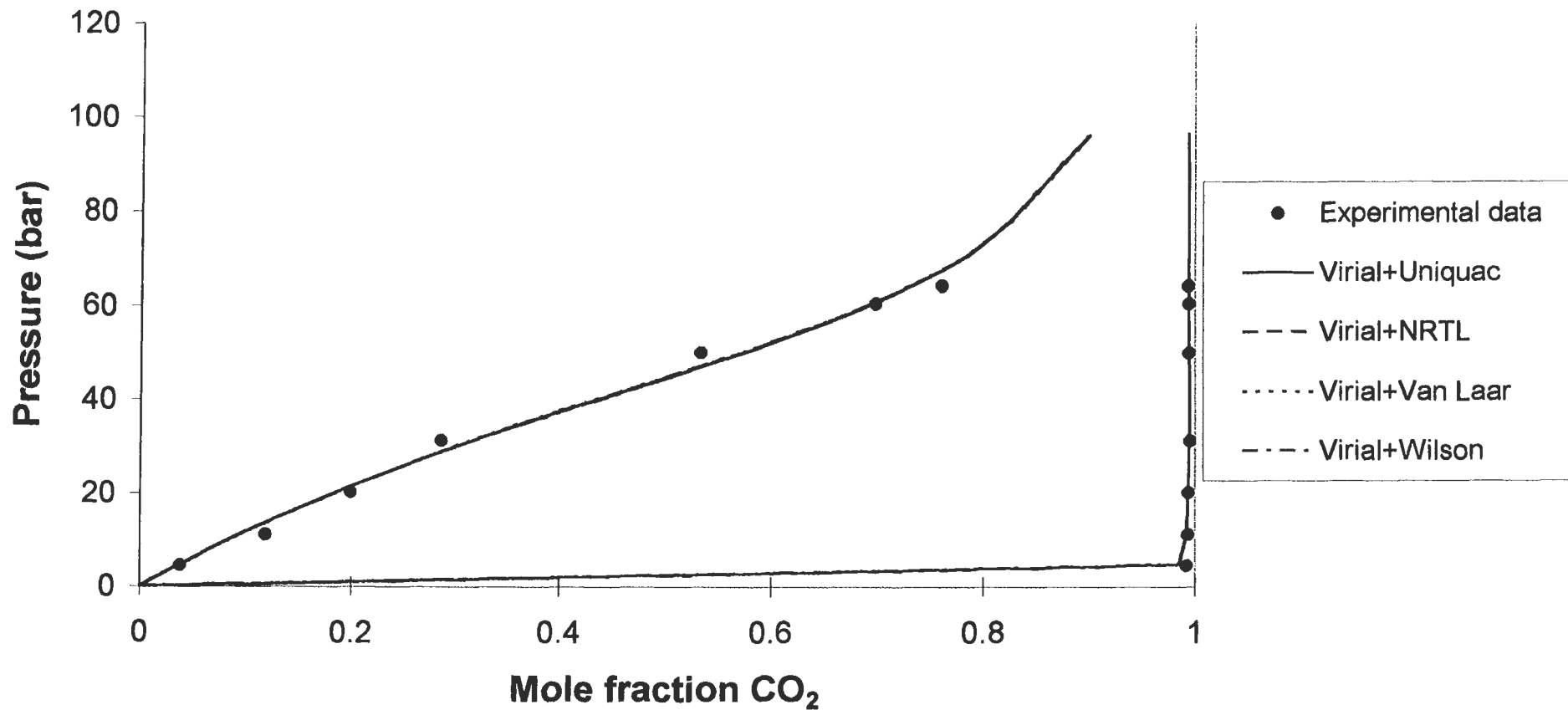


Figure 8-29: Comparison between the predicted and experimental VLE data for the Carbon Dioxide + Toluene System at 80°C

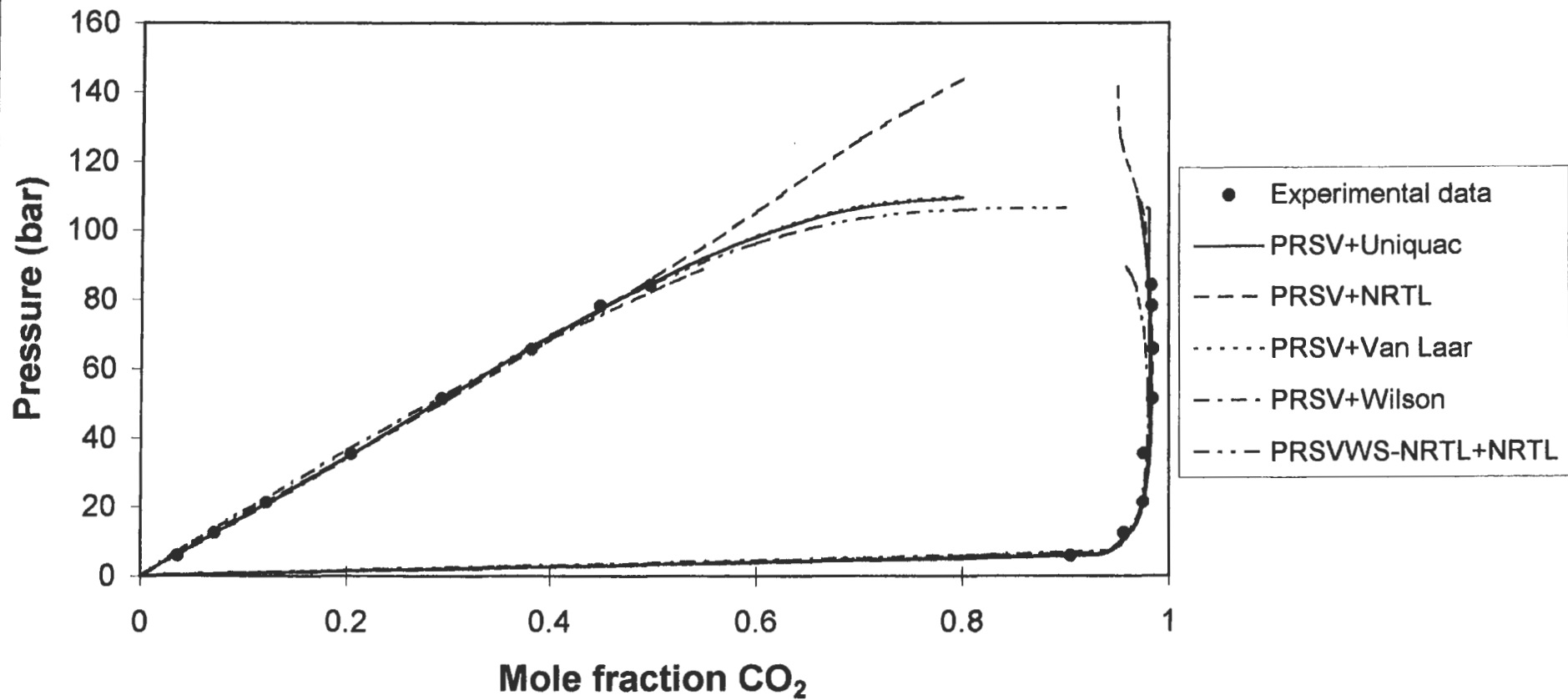


Figure 8-31: Comparison between the predicted and experimental data for the Carbon Dioxide + Toluene System at 118.3°C

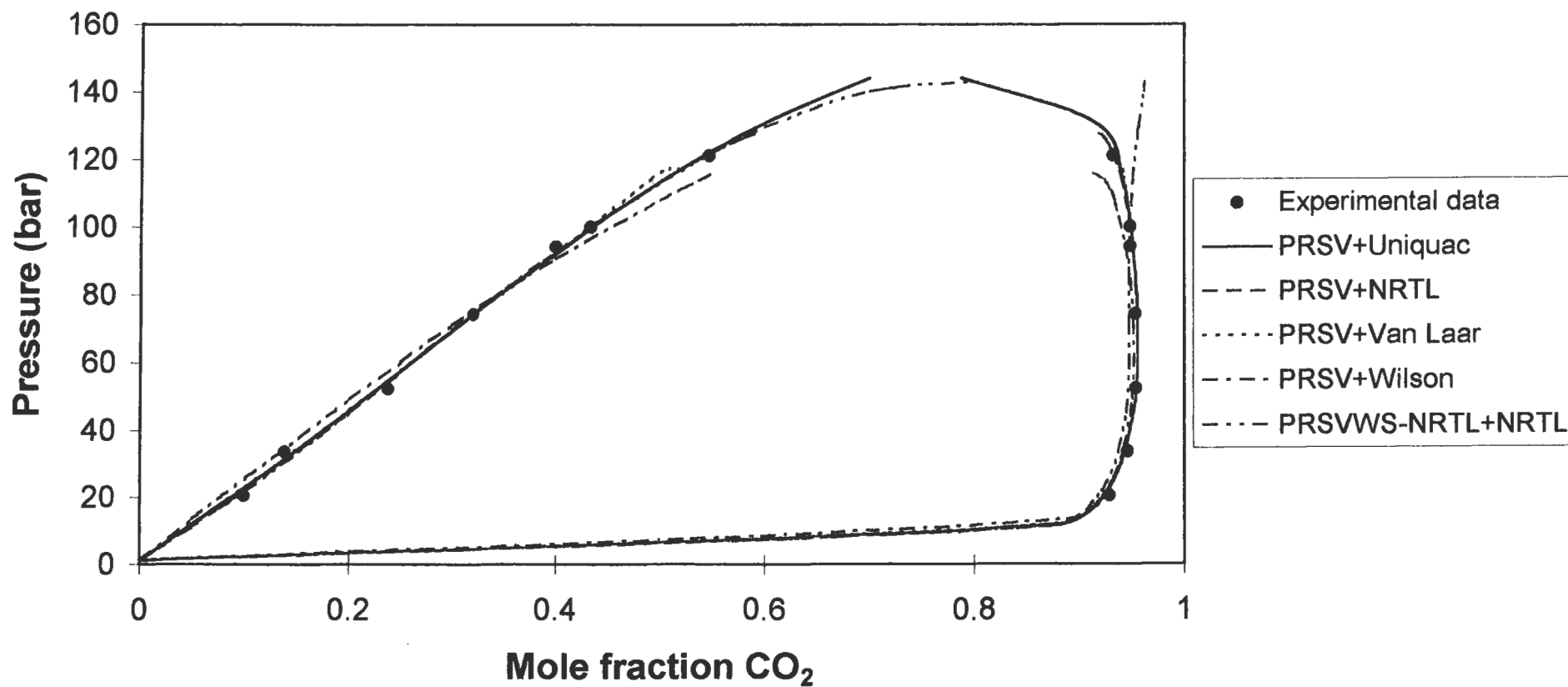
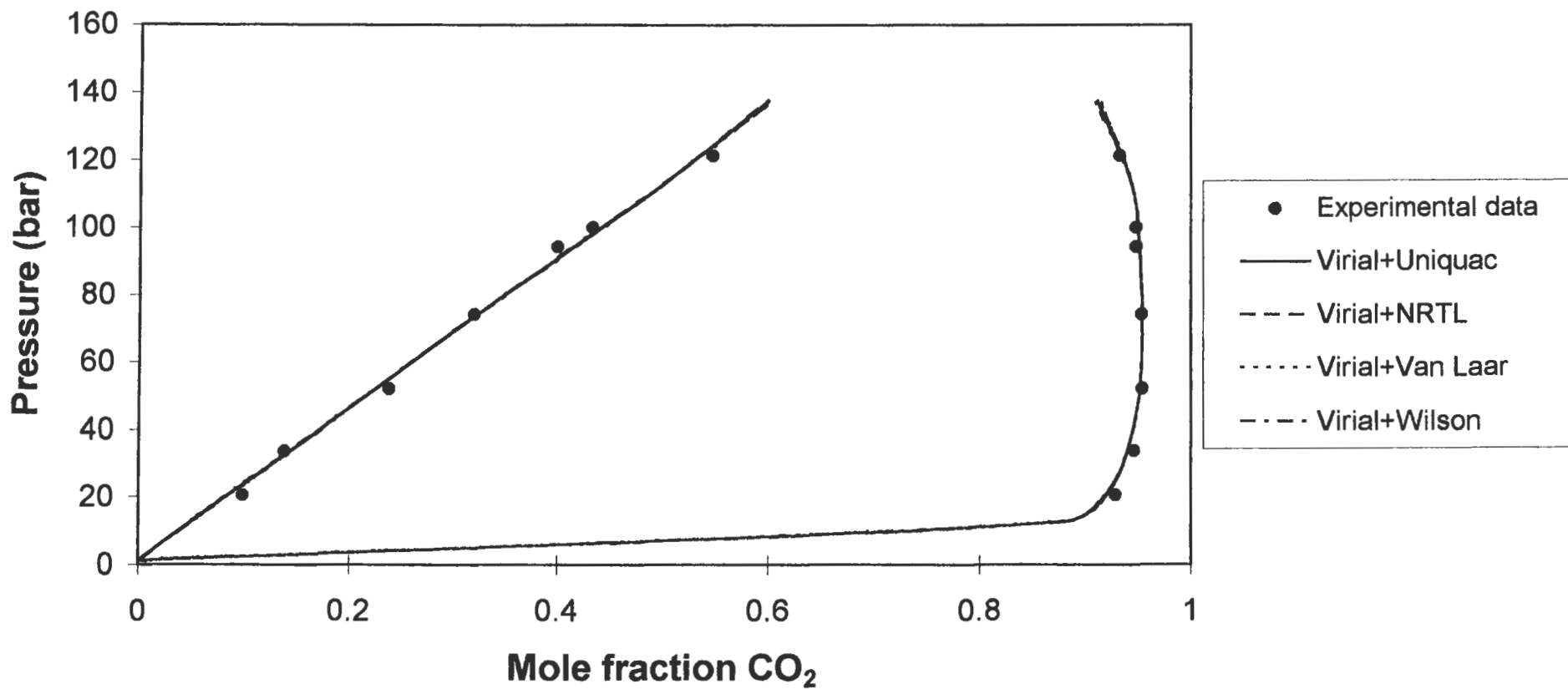


Figure 8-32: Comparison between the predicted and experimental data for the Carbon Dioxide + Toluene System at 118.3°C



The fitting of parameters by Mühlbauer and Raal [1991] for the combined method combination of the PR EOS with the UNIQUAC liquid model, was undertaken whereby a value for k_{ij} was set (typically a value obtained from literature or by regression via the direct method). The liquid model parameters were then fitted. This is an incorrect fitting procedure as it does not fit all three parameters simultaneously and therefore the values obtained by Mühlbauer and Raal [1991] are significantly different from those obtained in this project. In addition this project made use of the PRSV EOS and this would produce a difference in the fitted parameters.

8.3.3.2. Carbon Dioxide + Methanol System

G^E model	Interaction parameters (p_{12} and p_{21} (reduced parameters))					
	Temperature ($^{\circ}$ C)					
	40		90		100	
NRTL	1.6272	0.3495	1.7248	0.2964	1.1254	0.7044
Wilson	0.5651	0.1602	0.6493	0.0947	0.4454	0.2572
Van Laar	1.3315	1.9008	1.3214	1.9233	1.4917	1.6427
UNIQUAC	2.1874	0.2138	2.8180	0.1052	1.6459	0.3991

Table 8-21: Interaction parameters obtained for various activity coefficient models with the Virial EOS, from fitting of experimental data measured in this project, using the combined method for the Carbon Dioxide + Methanol System

For NRTL: $p_{ij} = (a_{ij}/RT)$ (a_{ij} in cal.mol^{-1})

For Wilson: $p_{ij} = (V_{L,j}/V_{L,i})\exp(-a_{ij}/RT)$ (a_{ij} in cal.mol^{-1})

For Van Laar: $p_{ij} = a_{ij}$

For UNIQUAC: $p_{ij} = (a_{ij}/RT)$ (a_{ij} in cal.mol^{-1})

G^E model	Interaction parameters (k_{ij} , p_{12} and p_{21} (reduced parameters))								
	Temperature ($^{\circ}$ C)								
	40			90			100		
NRTL	0.0089	3.1007	0.0948	-0.0573	3.9985	0.1004	-0.0288	3.0120	0.2438
Wilson	-0.2418	0.5675	0.0000	-0.1897	0.6070	0.0000	-0.0681	0.5267	0.0000
Van Laar	0.0070	1.3082	3.1326	-0.0552	1.3011	3.8565	-0.0296	1.4500	3.0513
UNIQUAC	-0.2699	15.0000	0.2384	-0.1999	15.0000	0.1803	-0.0672	15.0000	0.3057

Table 8-22: Interaction parameters obtained for various activity coefficient models with the PRSV EOS, from fitting of experimental data measured in this project, using the combined method for the Carbon Dioxide + Methanol System

For NRTL: $p_{ij} = (a_{ij}/RT)$ (a_{ij} in cal.mol^{-1})

For Wilson: $p_{ij} = (V_{L,j}/V_{L,i})\exp(-a_{ij}/RT)$ (a_{ij} in cal.mol^{-1})

For Van Laar: $p_{ij} = a_{ij}$

For UNIQUAC: $p_{ij} = (a_{ij}/RT)$ (a_{ij} in cal.mol^{-1})

Table's 8-21 and 8-22 summarizes the fitted parameters for the Virial and PRSV EOS's respectively with the appropriate liquid phase activity coefficient models for the carbon dioxide + toluene system. For the PRSV EOS, the van der Waals one-fluid mixing rule was used for all

computations via the combined method. The modified combined method yielded fitted parameters summarized in Table 8-23.

Interaction parameters (k_{ij} , p_{12} and p_{21} (reduced parameters))									
Temperature ($^{\circ}$ C)									
Model	40			90			100		
PRSVWS-NRTL+NRTL	0.2129	3.3558	0.0813	0.0855	5.0694	0.2165	0.1237	6.3411	0.5205

Table 8-23: Interaction parameters obtained for the NRTL activity coefficient model with the PRSV EOS with Wong-Sandler mixing rules (NRTL activity coefficient model), from fitting of experimental data measured in this project, using the modified combined method for the Carbon Dioxide + Methanol System

$$p_{ij} = (a_{ij}/RT) \text{ (} a_{ij} \text{ in cal.mol}^{-1}\text{)}$$

Searching the literature, no references could be found for the correlation of experimental data for the carbon dioxide + methanol system via the combined method. Thus no comparisons could be made for the system for the fitted parameters.

Figure's 8-33 to 8-38 summarize the modeling for the carbon dioxide + methanol system via the combined method.

8.3.3.3. Propane + 1-Propanol System

Interaction parameters (p_{12} and p_{21} (cal.mol $^{-1}$))				
Temperature ($^{\circ}$ C)				
G^E model	105.1		120	
NRTL	2.3987	-0.3530	2.3164	-0.2450
Wilson	1.1228	0.0341	0.9920	0.0944
Van Laar	0.8363	2.1337	0.8944	1.9202
UNIQUAC	4.5385	-0.6249	3.4901	-0.5712

Table 8-24: Interaction parameters obtained for various activity coefficient models with the Virial EOS, from fitting of experimental data measured in this project, using the combined method for the Propane + 1-Propanol System

For NRTL: $p_{ij} = (a_{ij}/RT)$ (a_{ij} in cal.mol $^{-1}$)

For Wilson: $p_{ij} = (V_{Lj}/V_{Li})\exp(-a_{ij}/RT)$ (a_{ij} in cal.mol $^{-1}$)

For Van Laar: $p_{ij} = a_{ij}$

For UNIQUAC: $p_{ij} = (a_{ij}/RT)$ (a_{ij} in cal.mol $^{-1}$)

Figure 8-33: Comparison between the predicted and experimental data for the Carbon Dioxide + Methanol System at 40°C

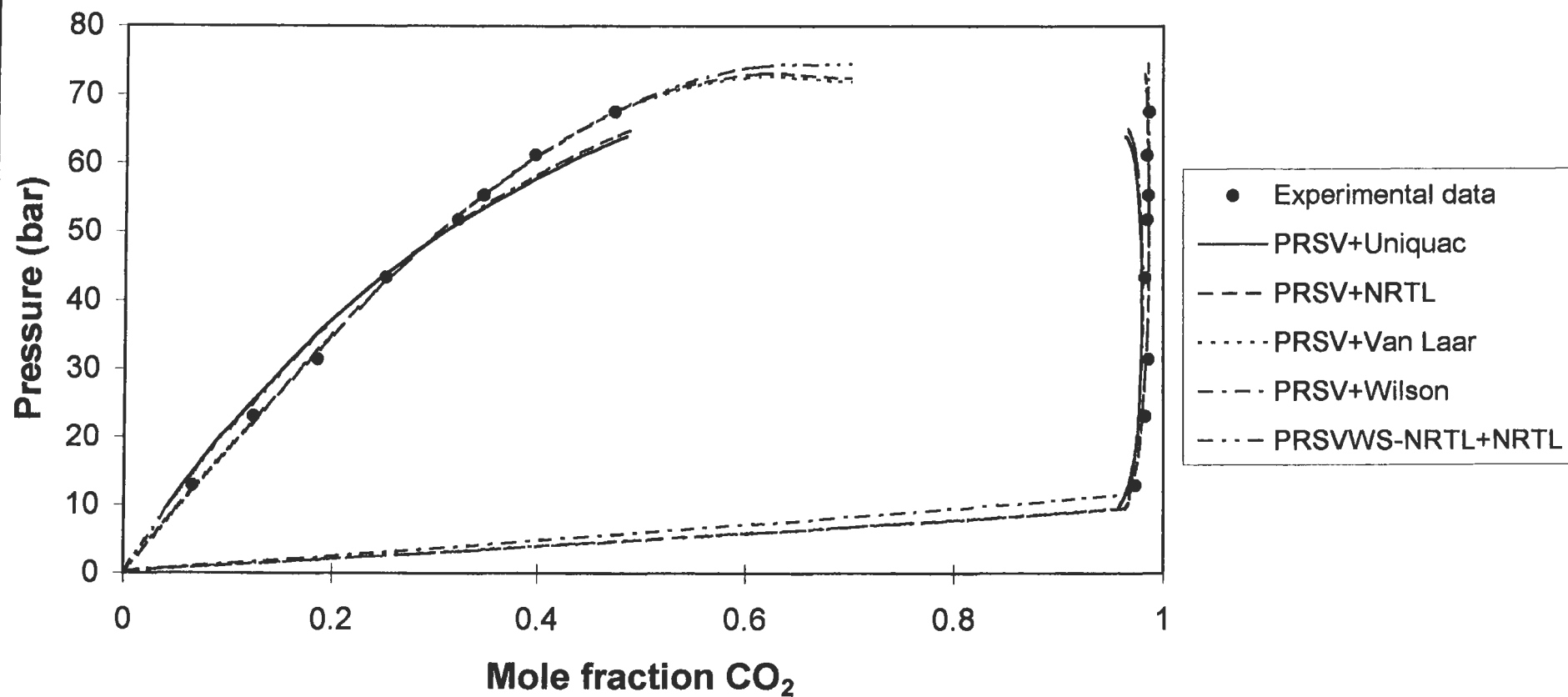


Figure 8-34: Comparison between the predicted and experimental data for the Carbon Dioxide + Methanol System at 40°C

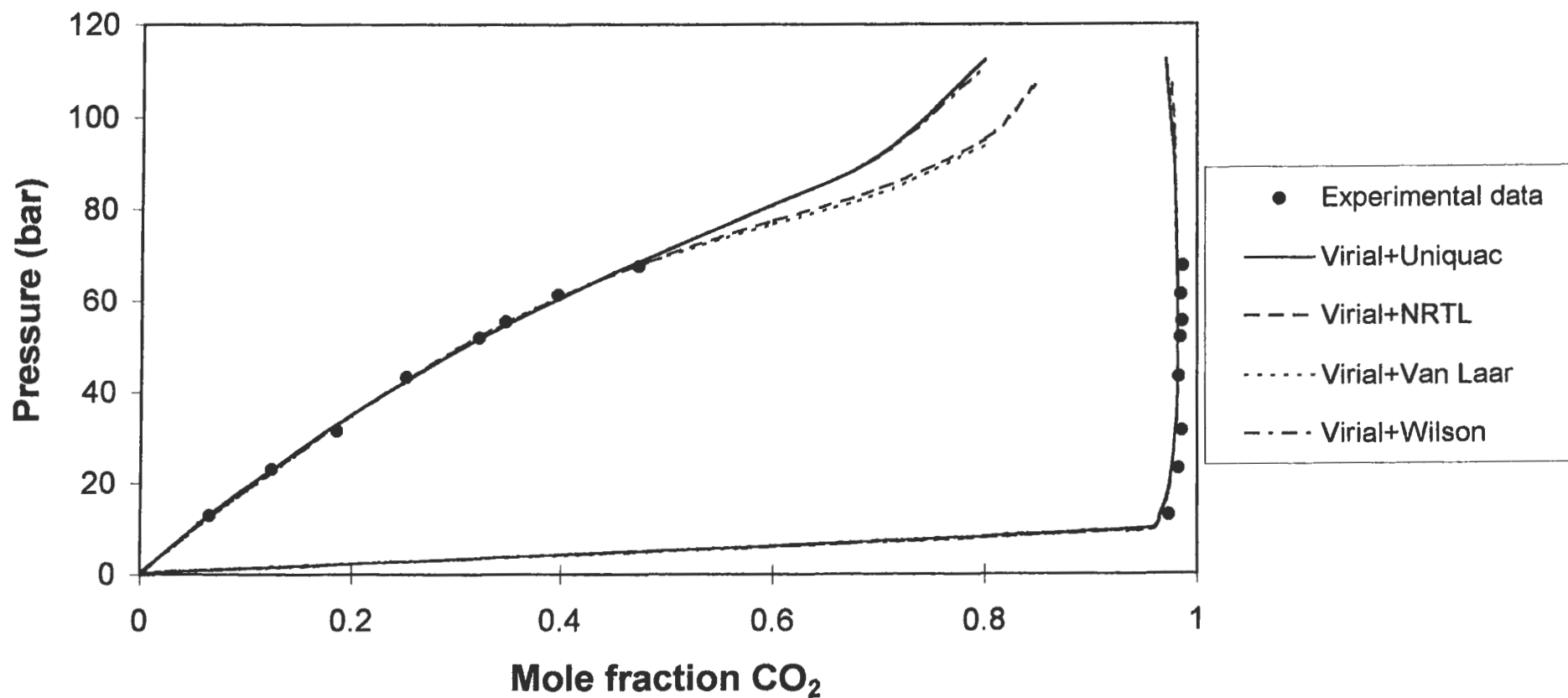


Figure 8-35: Comparison between the predicted and experimental data for the Carbon Dioxide + Methanol System at 90°C

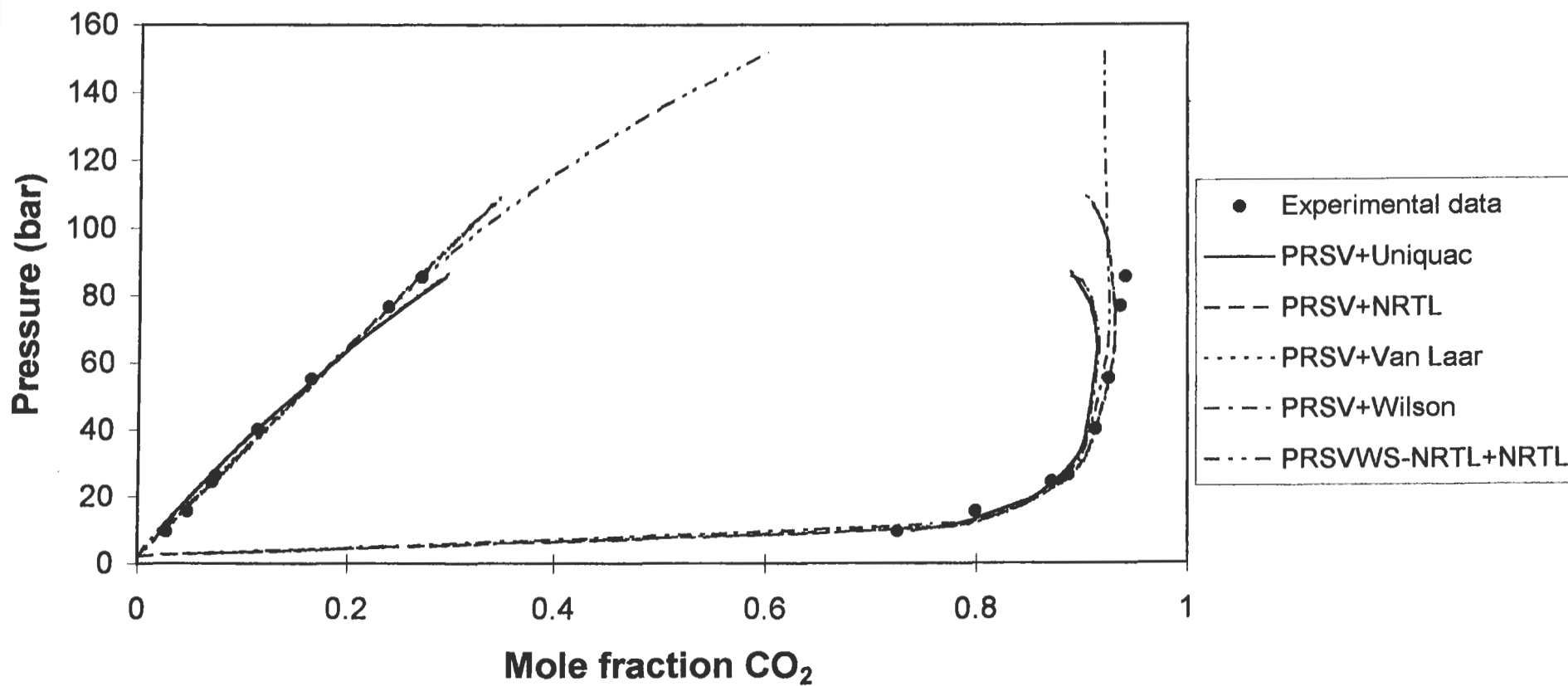


Figure 8-36: Comparison between the predicted and experimental data for the Carbon Dioxide + Methanol System at 90°C

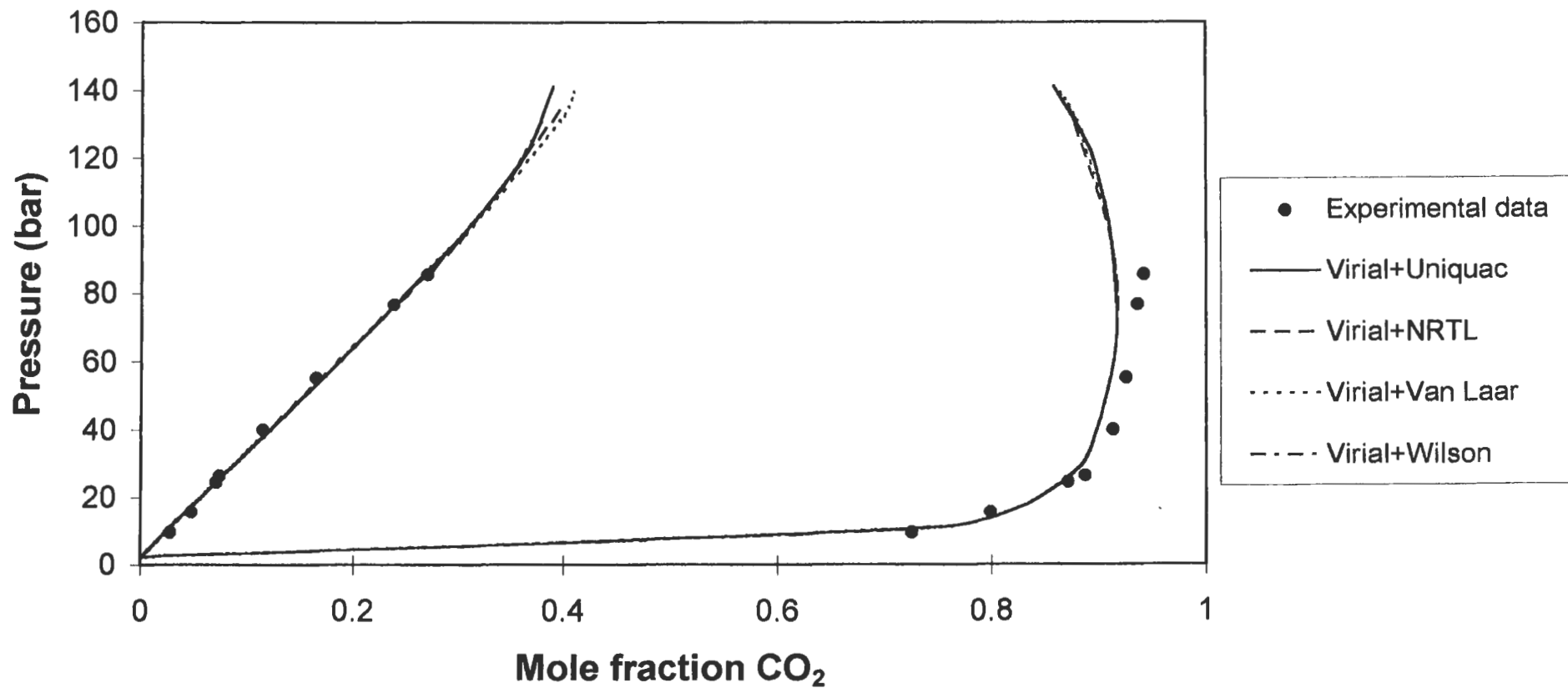


Figure 8-37: Comparison between the predicted and experimental data for the Carbon Dioxide + Methanol System at 100°C

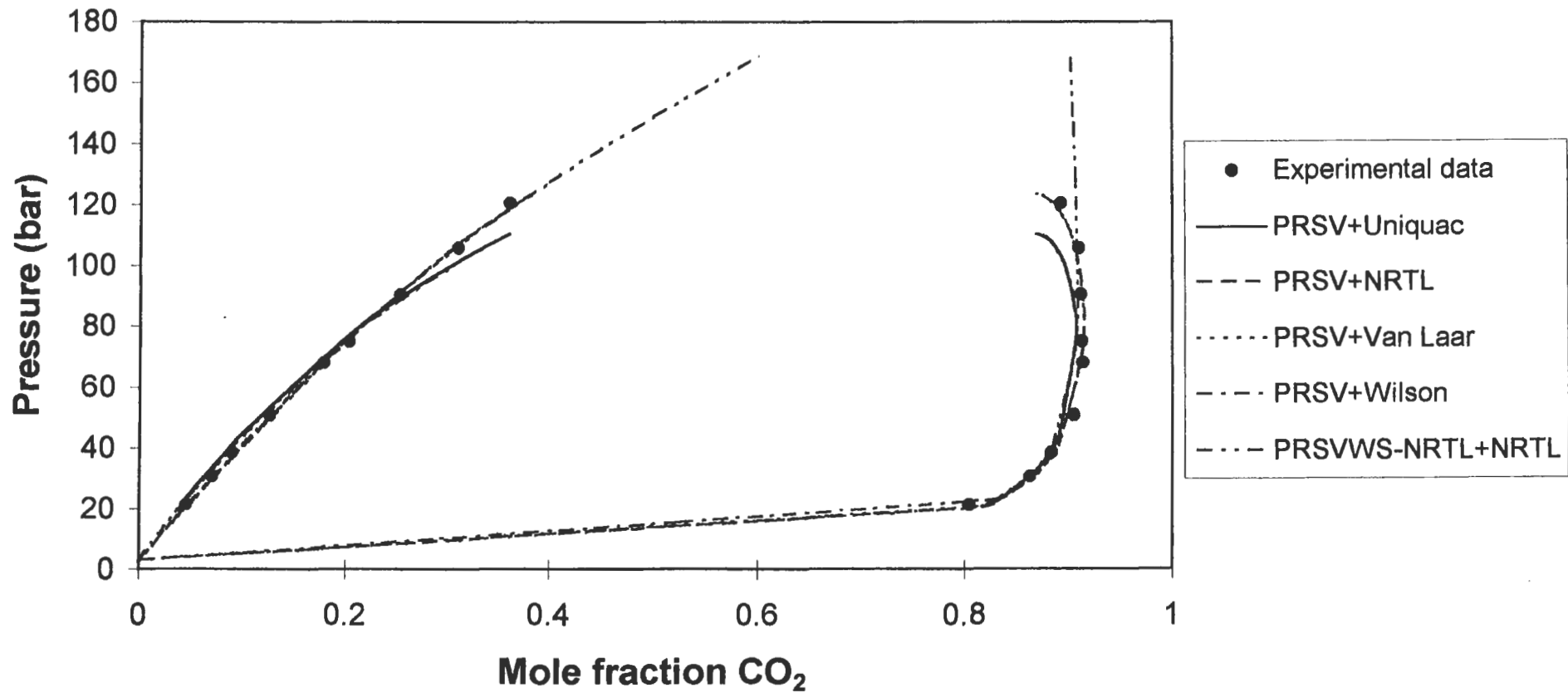
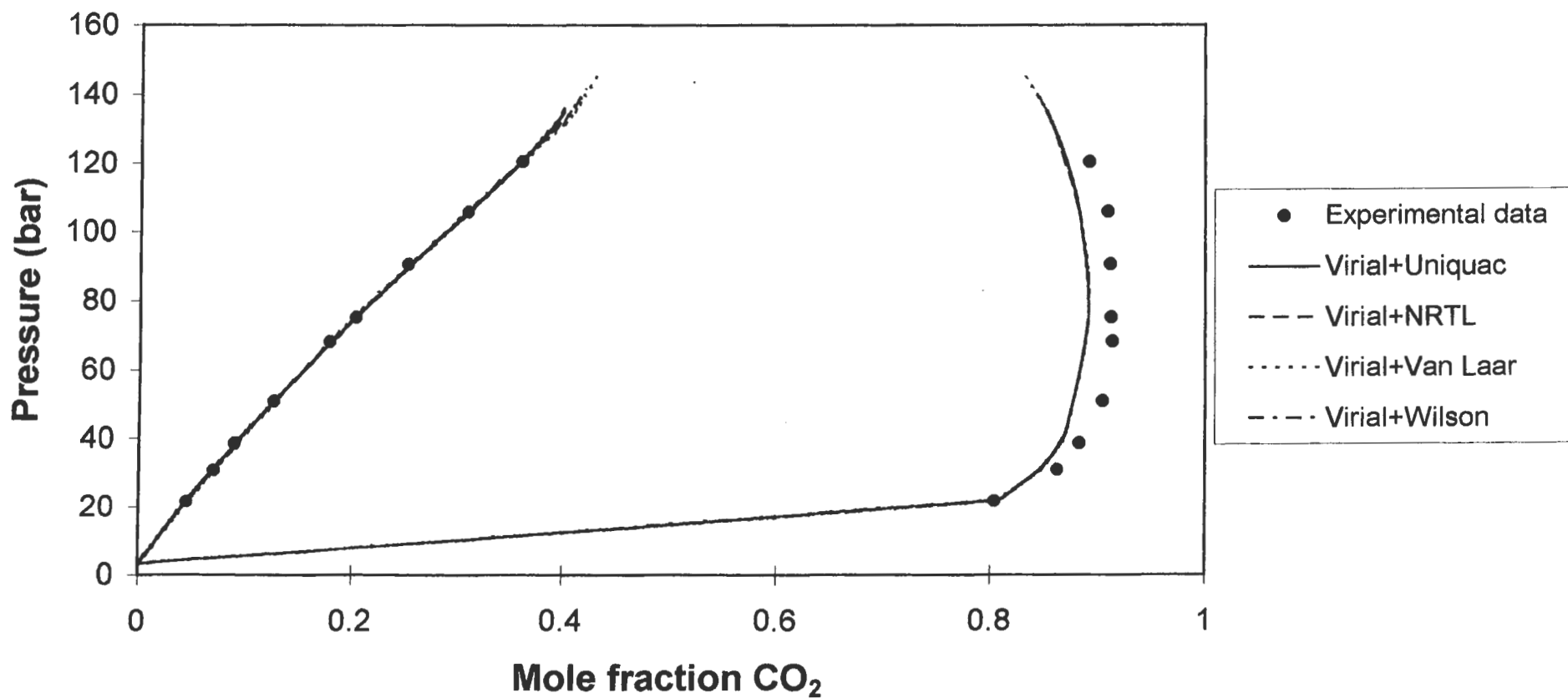


Figure 8-38: Comparison between the predicted and experimental data for the Carbon Dioxide + Methanol System at 100°C



Fitted parameters obtained by reduction of experimental data for the propane + 1-propanol system via the combined method are summarized in Table's 8-24, 8-25 for the virial and PRSV EOS with various activity coefficient models and in Table 8-26 for the new modified combined method.

Interaction parameters (k_{ij} , p_{12} and p_{21} (reduced parameters))						
Temperature ($^{\circ}$ C)						
G^E model	105.1			120		
NRTL	-0.1917	2.4978	-0.3736	0.2279	2.4507	-0.3210
Wilson	-0.1902	1.1425	0.0194	0.2244	1.0691	0.0383
Van Laar	-0.1915	0.8329	2.2249	0.2259	0.8754	2.1947
UNIQUAC	-0.1910	5.4400	-0.6349	0.2260	4.6987	-0.6044

Table 8-25: Interaction parameters obtained for various activity coefficient models with the PRSV EOS, from fitting of experimental data measured in this project, using the combined method for the Propane + 1-Propanol System

For NRTL: $p_{ij} = (a_{ij}/RT)$ (a_{ij} in cal.mol^{-1})

For Wilson: $p_{ij} = (V_{Lj}/V_{Li})\exp(-a_{ij}/RT)$ (a_{ij} in cal.mol^{-1})

For Van Laar: $p_{ij} = a_{ij}$

For UNIQUAC: $p_{ij} = (a_{ij}/RT)$ (a_{ij} in cal.mol^{-1})

Interaction parameters (k_{ij} , p_{12} and p_{21} (reduced parameters))						
Temperature ($^{\circ}$ C)						
Model	105.1			120		
PRSVWS-NRTL+NRTL	-0.1517	2.5611	-0.3802	0.3954	2.5665	-0.3433

Table 8-26: Interaction parameters obtained for the NRTL activity coefficient model with the PRSV EOS with Wong-Sandler mixing rules (NRTL activity coefficient model), from fitting of experimental data measured in this project, using the modified combined method for the Propane + 1-Propanol System

$p_{ij} = (a_{ij}/RT)$ (a_{ij} in cal.mol^{-1})

The propane + 1-propanol system had been previously modeled via the combined method by Mühlbauer and Raal [1993]. They made use of the UNIQUAC activity coefficient model to describe the liquid phase and utilized the Peng-Robinson, virial and Group Contribution EOS's to model the vapour phase. Table's 8-27 and 8-28 summarize the fitted parameters obtained by them for the propane + 1-propanol system using the virial and PR EOS's respectively.

Once again no comparisons could be made between the fitted parameters of Mühlbauer and Raal [1993] and this work. In addition, for this system the experimental data measured for both isotherms varied from those obtained by of Mühlbauer and Raal [1993], especially for the vapour phase compositions. This as well could contribute to the fitted parameters being

considerably different. The correlation of the experimental data for this work is however slightly better than that achieved by Mühlbauer and Raal [1993] for the vapour phase.

Interaction parameters (p_{12} and p_{21} (K))				
Temperature ($^{\circ}$ C)				
G^E model	105.11		120.05	
UNIQUAC	1153	-184.7	1055	-195.1

Table 8-27: Interaction parameters obtained the Virial EOS with the UNIQUAC model using the combined method for the Propane + 1-Propanol System by Mühlbauer and Raal [1993]

$$P_{ij} = (a_{ij}/R) \quad (R = 83.147)$$

Interaction parameters (k_{ij} , p_{12} and p_{21} (K))						
Temperature ($^{\circ}$ C)						
G^E model	105.11			120.05		
UNIQUAC	0.06859	846	-150.3	0.06831	747	-153.1

Table 8-28: Interaction parameters obtained the PR EOS with the UNIQUAC model using the combined method for the Propane + 1-Propanol System by Mühlbauer and Raal [1993]

$$P_{ij} = (a_{ij}/R) \quad (R = 83.147)$$

Figure's 8-39 to 8-42 summarize the modeling for the propane + 1-propanol system via the combined method graphically for the experimental data measured in this project.

8.4. ANALYSIS OF THE MODELLING

Under this section the modeling/correlation of the experimentally measured systems will be discussed. This will be undertaken globally for both the combined and direct methods.

To quantify the fit of a model to the experimental pressure and equilibrium vapour composition, the absolute average error in terms of pressure and vapour composition was computed. Equations (8-8) and (8-9) define the percentage absolute average error for pressure and vapour composition (mole fraction) respectively:

$$AAE - P\% = \frac{\sum_{i=1}^{NP} \left(\left| \frac{P_i^{calc} - P_i^{exp t}}{P_i^{exp t}} \right| * 100 \right)}{NP} \quad (8-8)$$

Figure 8-39: Comparison between the predicted and experimental data for the Propane + 1-Propanol System at 105.1 °C

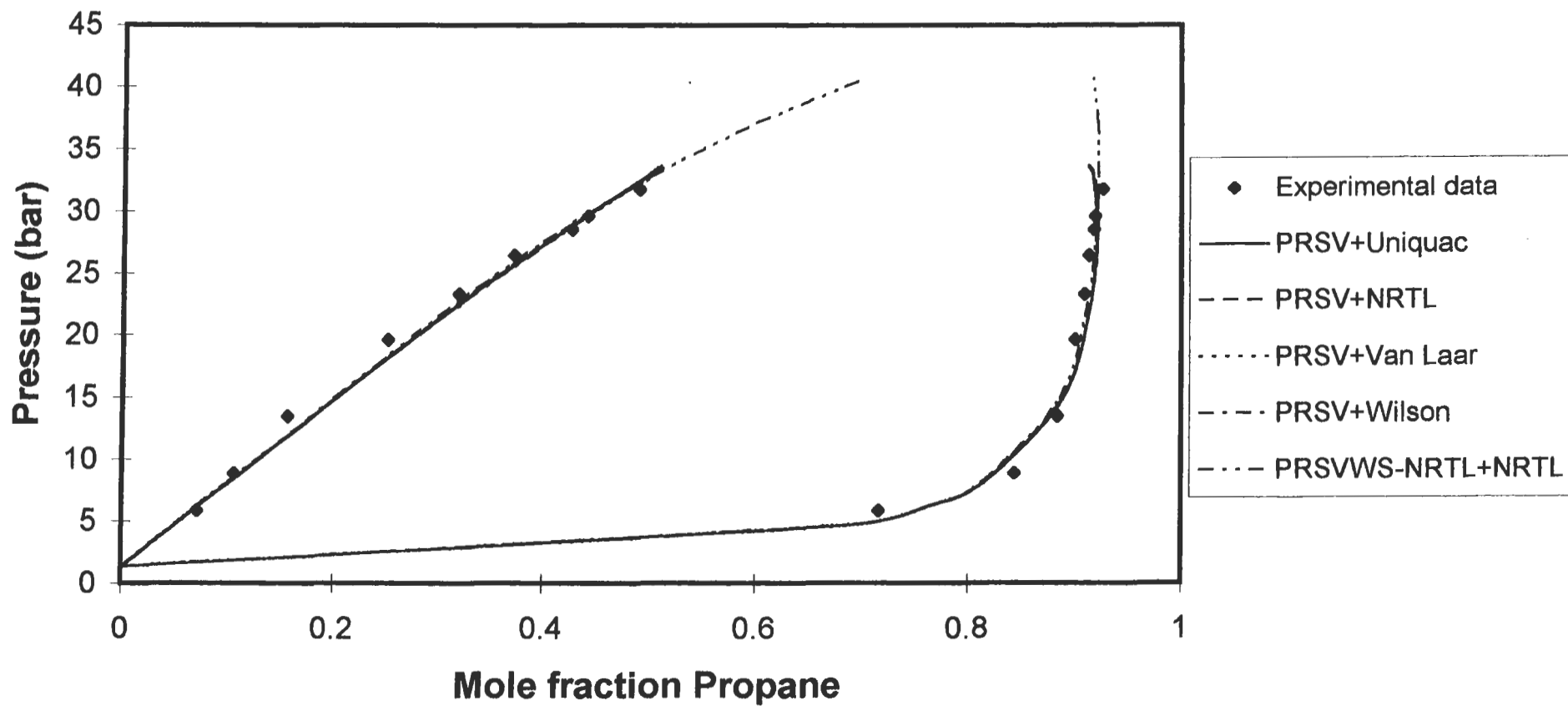


Figure 8-40: Comparison between the predicted and experimental data for the Propane + 1-Propanol System at 105.1 °C

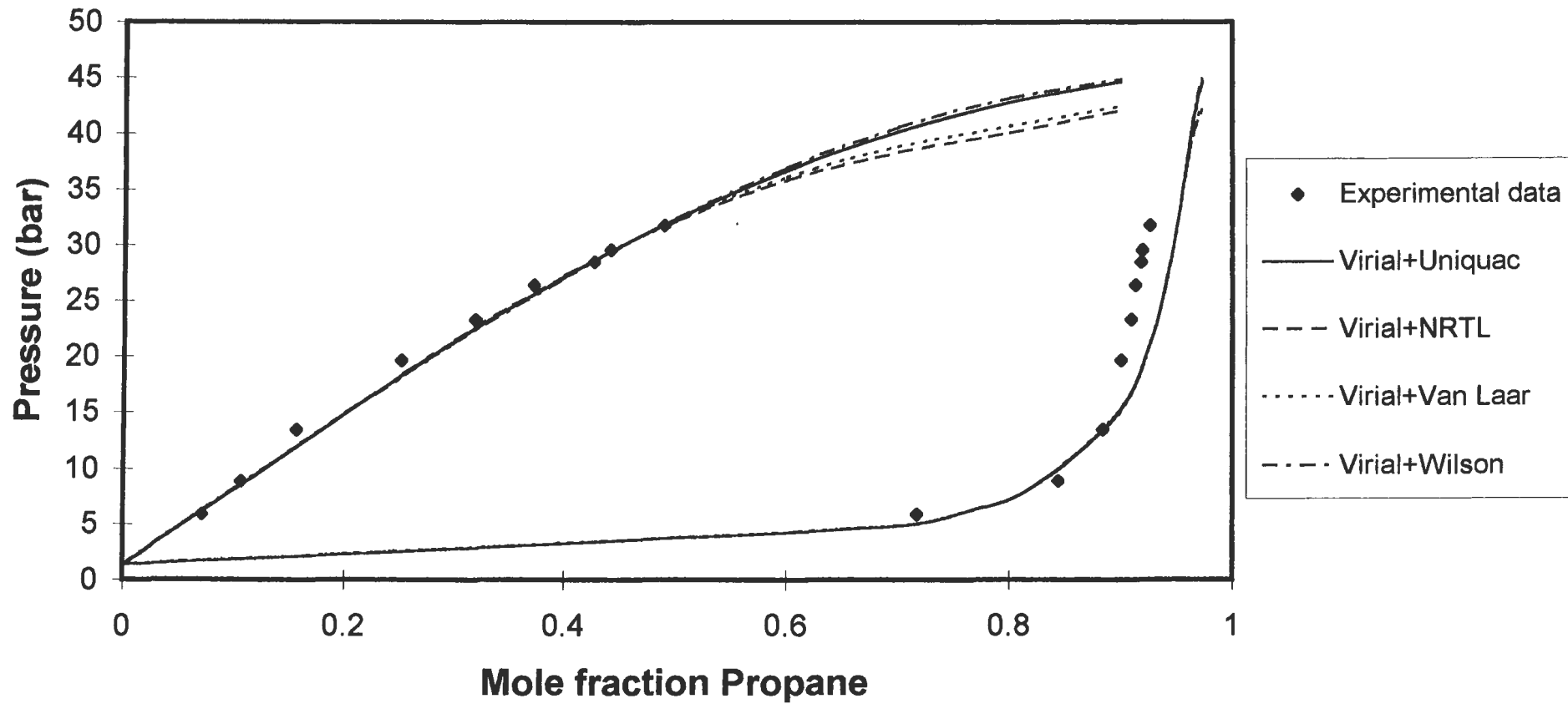


Figure 8-41: Comparison between the predicted and experimental data for the Propane + 1-Propanol System at 120 °C

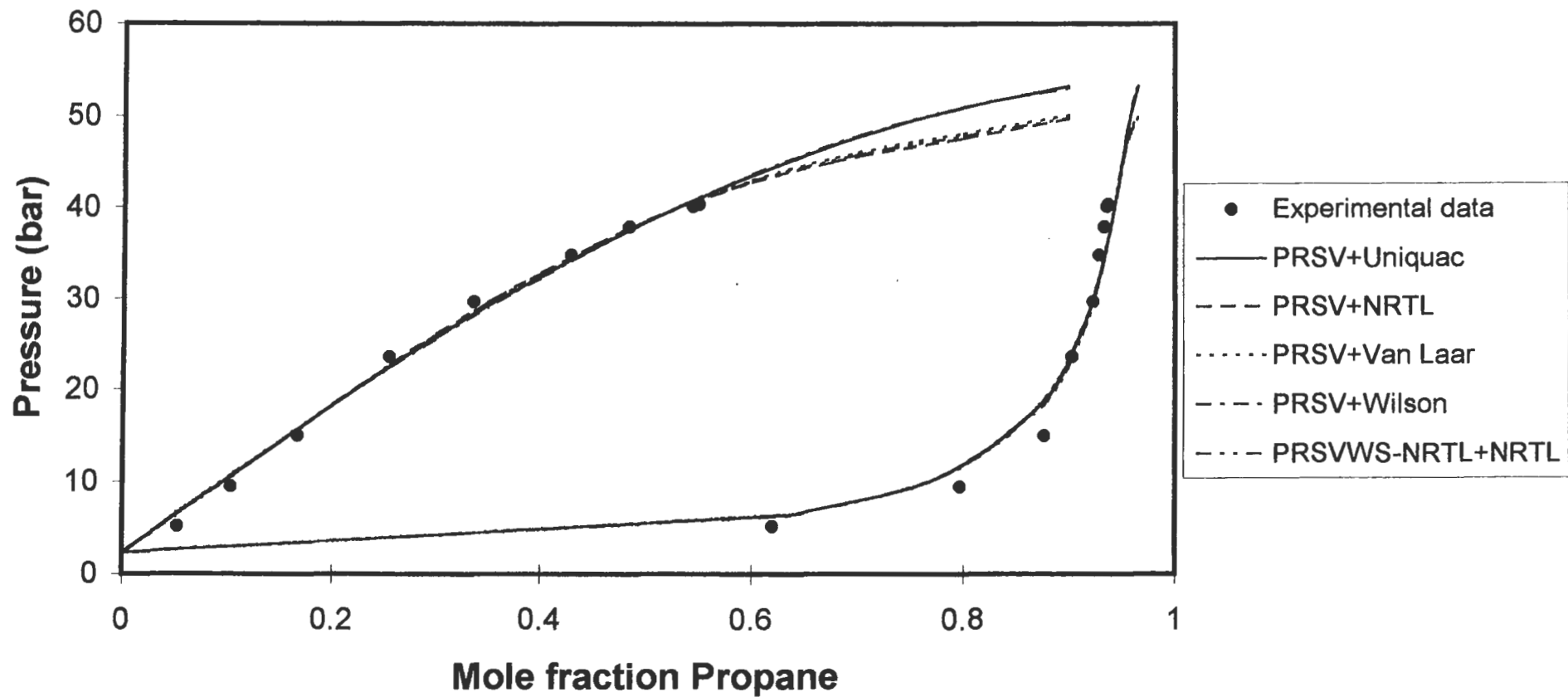
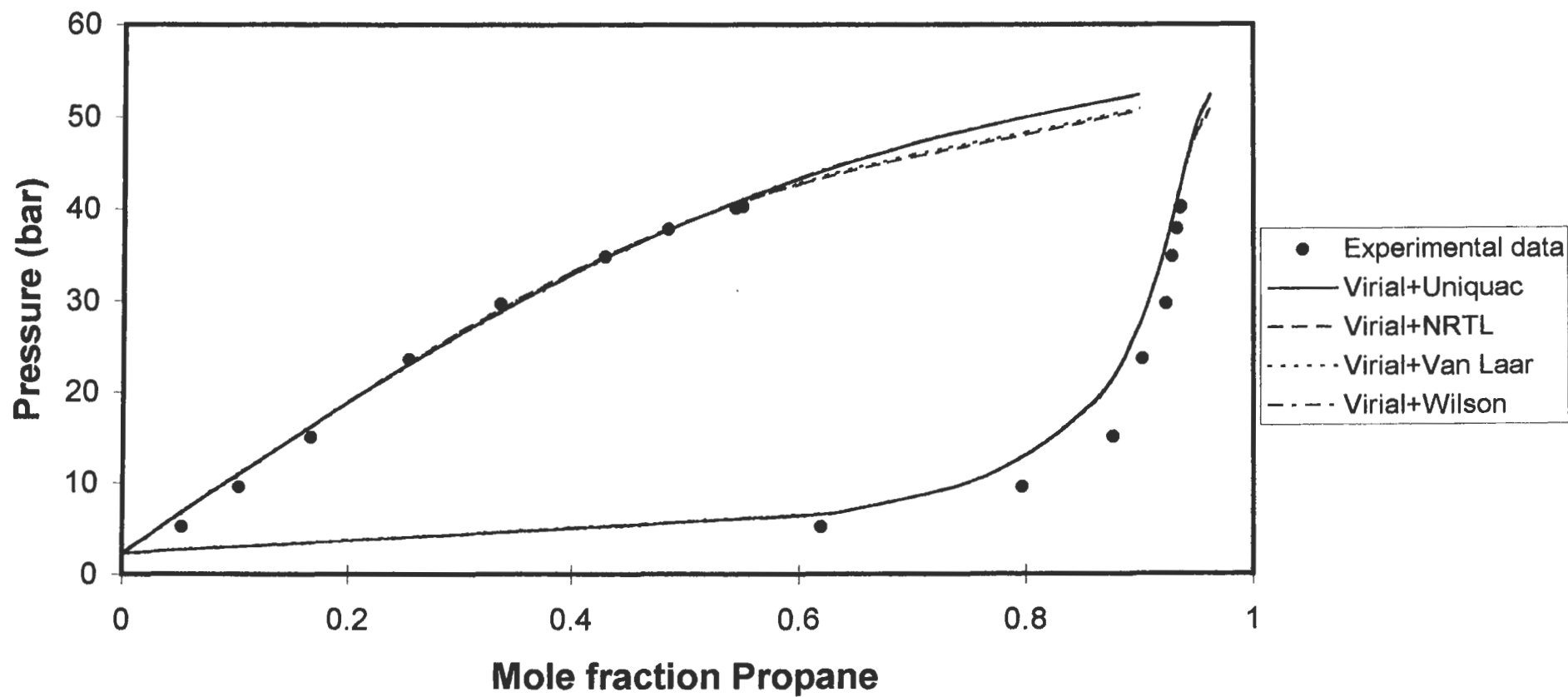


Figure 8-42: Comparison between the predicted and experimental data for the Propane + 1-Propanol System at 120 °C



$$AAE - Y\% = \frac{\sum_{i=1}^{NP} \left(\left| \frac{y_i^{calc} - y_i^{exp t}}{y_i^{exp t}} \right| * 100 \right)}{NP} \quad (8-9)$$

Table's 8-29, 8-30 and 8-31 summarize the percentage absolute average errors for pressure (AAE-P%) and vapour composition (AAE-y%) for the carbon dioxide + toluene, carbon dioxide + methanol and propane + 1-propanol systems respectively for the various direct and combined method models for the different isotherms.

8.4.1. Carbon Dioxide + Toluene System

Model	Isotherm (°C)					
	38		80		118.3	
	AAE-P%	AAE-y%	AAE-P%	AAE-y%	AAE-P%	AAE-y%
DIRECT						
SRK	7.091	0.276	3.220	0.581	4.127	0.653
PR	7.009	0.276	3.387	0.600	4.204	0.484
PRSV-1vdw	6.945	0.284	3.032	0.613	3.980	0.403
PRSV-2vdw	4.346	0.224	2.169	0.724	4.449	0.190
HVO	4.419	0.248	1.627	0.735	3.805	0.195
MHV1	4.825	0.217	3.521	0.784	4.007	0.189
MHV2	4.262	0.234	1.811	0.722	3.833	0.301
LCVM	4.357	0.247	7.405	0.874	4.581	0.228
HVOS	4.325	0.246	5.488	0.834	4.388	0.181
PRSVWS-NRTL	4.556	0.220	3.194	0.708	4.595	0.701
PRSVWS-Van Laar	4.210	0.242	1.778	0.790	3.991	0.685
PRSVWS-Wilson	4.382	0.220	2.606	0.611	4.382	0.438
PRSVWS-Uniquac	4.423	0.224	2.112	0.659	4.365	0.180
COMBINED						
PRSV+NRTL	5.183	0.338	3.266	0.692	3.204	0.186
PRSV+Van Laar	4.906	0.243	1.789	0.661	3.727	0.173
PRSV+Wilson	4.566	0.203	6.218	1.089	7.478	0.523
PRSV+Uniquac	4.931	0.248	1.814	0.655	3.628	0.181
PRSVWS-NRTL+NRTL	5.145	0.401	1.871	0.624	3.159	0.816
Virial+NRTL	7.438	0.191	2.049	0.740	4.492	0.312
Virial+Van Laar	7.319	0.191	2.159	0.748	4.580	0.302
Virial+Wilson	7.890	0.186	2.645	0.764	4.864	0.282
Virial+Uniquac	7.779	0.189	2.315	0.755	4.699	0.295

Table 8-29: Absolute average errors for the Carbon Dioxide + Toluene System

One of the very few things evident from Table 8-29 is that one can safely say that there is no model that performs the best for all three isotherms. For the 38 °C isotherm, the Huron-Vidal mixing rules (and modification thereof) models, along with the Wong-Sandler mixing rules perform the best, with the PRSVWS-Van Laar model probably describing the system the best. The combined method models produce on average a smaller AAE-y% than the direct method models (especially when the virial EOS is used to describe the vapour phase), but this is at the expense of the error in pressure.

For the 80 °C isotherm, the PRSVWS-Van Laar still rates very highly, but the best models are the combined method models, PRSV + Van Laar, and the modified combined method model, PRSVWS-NRTL + NRTL.

At the 118.3 °C isotherm, the best modeling was attained once again with the combined method, with the following models proving the best, viz. PRSV + NRTL, PRSV + Van Laar and PRSV + UNIQUAC.

It is evident that the Van Laar liquid phase model best describes the carbon dioxide + toluene system, be it as the excess free energy model in the mixing rule (Wong-Sandler mixing rules) or the liquid phase activity coefficient model in the combined method. For the NRTL liquid phase model the third parameter, α_{ij} , was set equal to 0.3 for all computations. Performing an investigation of varying the α_{ij} parameter, it was evident that other values did not produce an improvement in the modeling and therefore the recommendation of Sandler [1994] that α_{ij} be fixed at 0.3 was a very reasonable assumption. For the UNIQUAC liquid phase model, the co-ordination number (z) was set to 10. There are a number of correlations for the co-ordination number (discussed briefly in Chapter Two), but these correlations for co-ordination number produced little or no improvement in the modeling and it was decided to fix the co-ordination number at 10 for all computations.

The number of possible modeling combinations mushrooms as one chooses mixing rules and then possible excess free energy models for the mixing rules (in the case of the Huron-Vidal and modifications thereof, and the Wong-Sandler mixing rules). Therefore in this project, for the Huron-Vidal and modifications thereof mixing rules, the excess free energy model was restricted to the NRTL model.

There may be some concern that the temperatures at which modeling was undertaken for the carbon dioxide + toluene system was considerably higher than the critical temperature of carbon

dioxide and therefore the combined method might fail in the modeling of the system. This would probably be because carbon dioxide will have to be considered as a non-condensable component and the choice of a standard-state for the system would then be rather complex. The standard-state reference fugacity at zero pressure expression given by Prausnitz et al. [1980] is however valid up to reduced temperatures of 1.8 and, as can be seen from the modeling results, performs exceptionally well. The description and choice of standard-states for non-condensable components is briefly discussed in Appendix B.

A plot of experimental excess Gibbs free energy for the carbon dioxide + toluene system for the three isotherms in the present study is shown in Figure 8-43. Activity coefficient plots for the various isotherms are available in Appendix F.2.

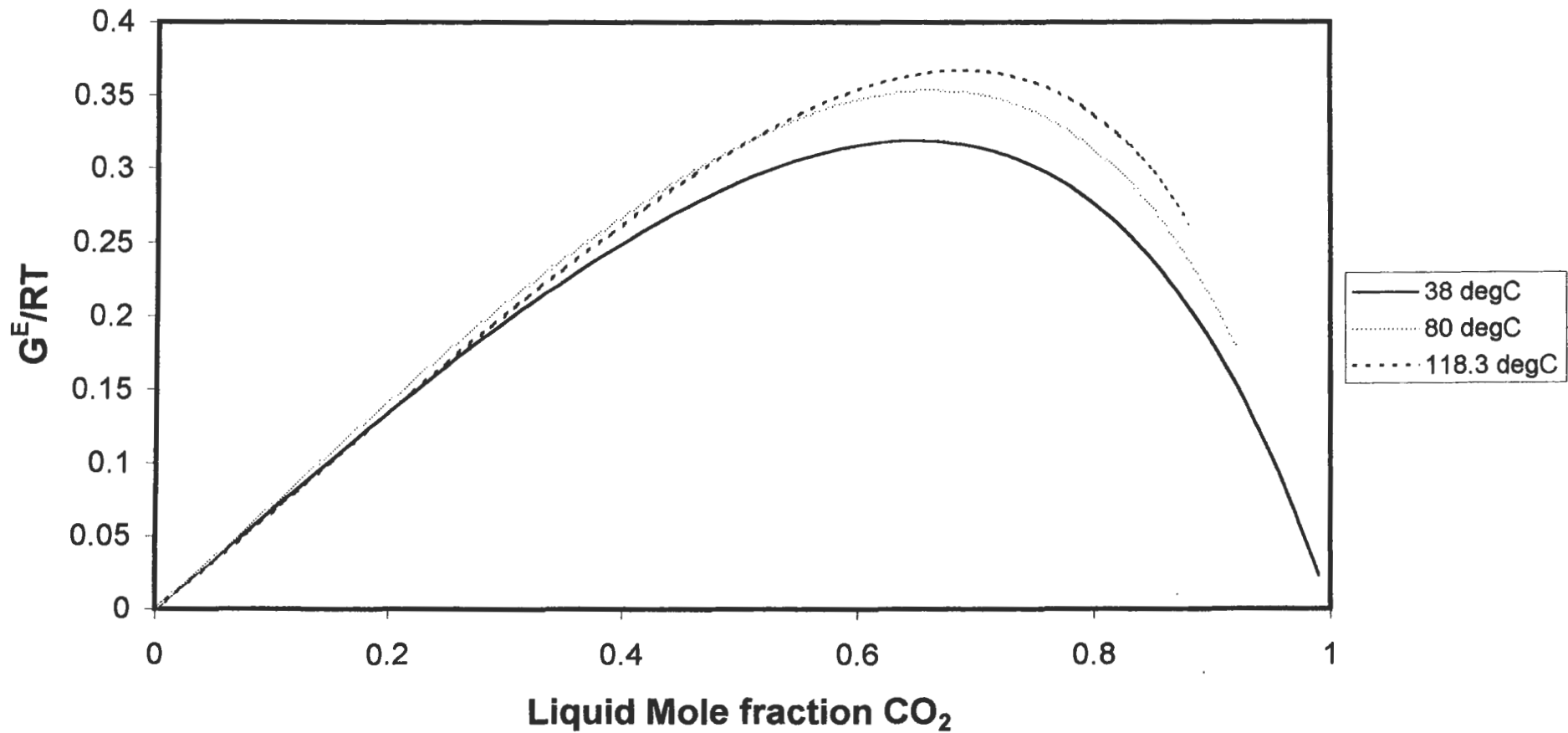
8.4.2. Carbon Dioxide + Methanol System

For the 40 °C isotherm, all the models performed reasonably well, except for the PRSV + Wilson and PRSV + UNIQUAC models. Even the *simple* SRK and PR EOS produced very good modeling of the system. In fact there was not much to choose from between the various models.

For the 90 °C isotherm (Figure 8-35), there were large errors in both the computed pressures and vapour compositions for all the models, again with the PRSV + Wilson and PRSV + UNIQUAC models fairing the worst. The only reasonable conclusions that could be drawn from this was that, there was either an error in the measurement of the experimental data at this particular isotherm or, that there was association in the system (indicative of the large errors in the vapour composition) and that the models could not account for this. There are no available literature data available for this isotherm and therefore one can not determine whether the measured data may have inaccuracies (there is high confidence in the measured data though). One does know, however that methanol undergoes association, which increases with temperature (Peschel and Wenzel [1984]) and it is therefore possible that the models utilized in this project could not account for the association of methanol. Peschel and Wenzel [1984] propose an EOS model to account for association of methanol, but this was not investigated in this project.

The Huron-Vidal and modifications thereof mixing rule models perform the best for the carbon dioxide + methanol system at the 90 °C isotherm. Reasonable modeling is also achieved with the PRSV + Van Laar and PRSVWS-Van Laar models.

Figure 8-43: Plot of G^E/RT versus liquid mole fraction CO_2 for the Carbon Dioxide + Toluene System



The theory of the utilized models not being able to describe the carbon dioxide + methanol system as a result of methanol associating, seems to be contradicted by the results of the modeling for the 100 °C isotherm. Very good modeling is obtained for this isotherm, again with the Huron-Vidal and modifications thereof mixing rule models performing very well. The best model though was the PRSVWS-NRTL model.

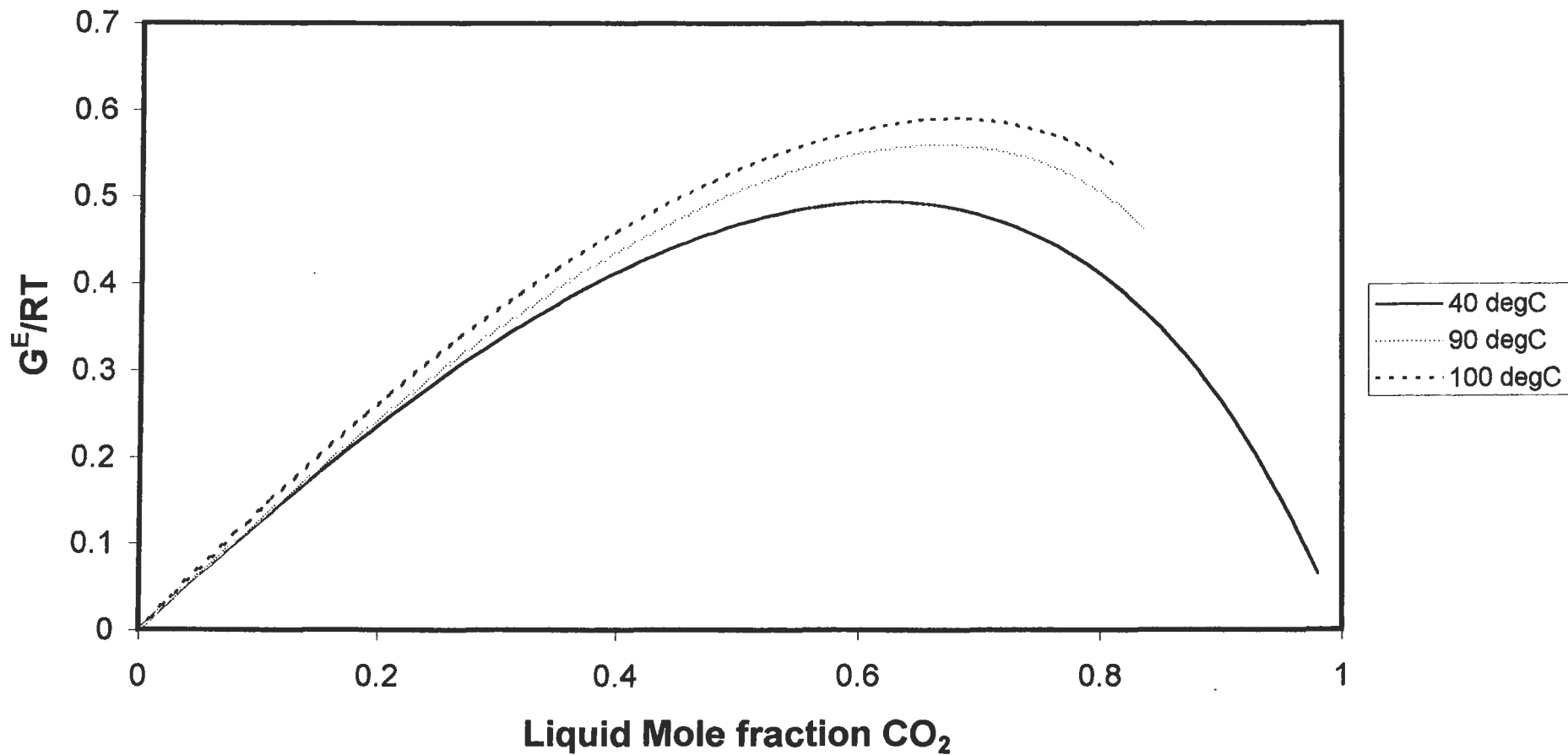
It seems that for this system, there is little to choose between the NRTL and Van Laar activity coefficient models as being the ones that best describe the system. The Wilson and UNIQUAC models fare poorly for this particular system, especially in the combined method.

Model	Isotherm (°C)					
	40		90		100	
	AAE-P%	AAE-y%	AAE-P%	AAE-y%	AAE-P%	AAE-y%
DIRECT						
SRK	2.246	0.173	5.753	1.579	2.744	1.011
PR	2.169	0.195	5.457	1.575	3.320	1.279
PRSV-1vdw	2.105	0.214	5.666	1.673	3.069	1.024
PRSV-2vdw	1.831	0.240	6.008	1.727	0.835	0.892
HVO	1.531	0.228	6.461	1.791	0.832	0.883
MHV1	1.622	0.232	5.791	1.708	0.861	0.890
MHV2	1.644	0.231	5.119	1.558	0.956	0.903
LCVM	1.541	0.226	5.180	1.585	0.822	0.877
HVOS	1.571	0.231	5.768	1.700	0.885	0.891
PRSVWS-NRTL	1.262	0.265	5.028	1.633	0.551	0.712
PRSVWS-Van Laar	1.223	0.264	4.995	1.620	1.264	1.298
PRSVWS-Wilson	1.374	0.270	5.321	1.345	0.910	1.139
PRSVWS-Uniquac	1.983	0.323	5.772	1.944	1.030	1.194
COMBINED						
PRSV+NRTL	1.875	0.227	4.669	1.779	1.853	0.410
PRSV+Van Laar	1.997	0.229	4.618	1.762	2.139	0.396
PRSV+Wilson	6.266	0.716	9.980	3.071	4.707	1.257
PRSV+Uniquac	6.970	0.688	10.528	3.169	5.884	1.341
PRSVWS-NRTL+NRTL	1.970	0.218	4.380	2.011	1.561	0.776
Virial+NRTL	1.658	0.461	4.860	2.183	0.489	2.165
Virial+Van Laar	1.773	0.461	4.784	2.174	0.565	2.181
Virial+Wilson	1.616	0.457	5.137	2.215	0.891	2.186
Virial+Uniquac	1.624	0.457	5.150	2.217	0.814	2.175

Table 8-30: Absolute average errors for the Carbon Dioxide + Methanol System

Figure 8-44 illustrate the excess Gibbs free energy plots for the carbon dioxide + methanol system for the three isotherms. Plots for the activity coefficient for the system are available in Appendix F.2.

Figure 8-44: Plot of G^E/RT versus liquid mole fraction CO_2 for the Carbon Dioxide + Methanol System



8.4.3. Propane + 1-Propanol System

The propane + 1-propanol system is probably one of the most difficult systems to model, and this is evident from the errors summarized in Table 8-31 for the various models. The system has been measured only twice before. Nagahama et al. [1971] undertook VLE measurements for the system at 19.9 °C. They however, did not measure the vapour phase composition and merely computed it using Barker's method. Mühlbauer and Raal [1993] undertook VLE measurement at much higher temperatures viz. 81.6, 105.1 and 120.1 °C, and they did measure the vapour phase composition. They could however not obtain proper modeling for the propane + 1-propanol system. There were always considerable discrepancies between the computed and the experimental pressure and vapour compositions. These discrepancies were most evident in the low-pressure region of the pressure versus vapour composition curve. Their reasoning for not being able to model the system accurately was that either, their experimental data were incorrect or, the models that they utilized (UNIQUAC with either the Peng-Robinson or virial EOS) were incapable of describing the system.

To determine which of the proposed reasons for inadequate modeling was correct, the decision was made in this project to measure the HPVLE for the propane + 1-propanol system at 105.1 and 120 °C. As can be seen in the experimental data of Figures 7-19 and 7-21, there is a slight difference in the vapour composition measurements between the experimental data of Mühlbauer and Raal [1993] and that produced in this project. The differences were the greatest in the low-pressure region. The vapour phase data measured in this project were also much smoother than those obtained by Mühlbauer and Raal [1993]. It is difficult though to determine which set of experimental data is *more correct*.

A range of models (more extensive than those used by Mühlbauer and Raal [1993]) were tried on the propane + 1-propanol system, but adequate modeling could not be obtained for either of the two isotherms. The Wong-Sandler mixing rules did however model the system the best of the entire range of models utilized. There were still however, discrepancies between the saturated vapour curve computed and the experimental curve for the low-pressure region. It was at that stage that an intuitive modified combined method was envisaged whereby the vapour phase would be described by an EOS with a mixing rule that incorporated an excess free energy model, and the liquid phase described by the same excess free energy model as that used for the mixing rule. A simultaneous fit of the excess free energy model parameters to the liquid phase excess free energy model and the mixing rule was thus achieved. This procedure was intuitively more attractive and consistent.

To test the new combined method (Ramjugernath and Raal [1999]), the PRSVWS-NRTL EOS was used to describe the vapour phase with the liquid phase description via the NRTL excess free energy model. As is evident from the graphical modeling results (Figures 8-39 and 8-41) and errors in pressure and vapour composition (Table 8-31), the new combined method performed extremely well when compared to the other models. There were still discrepancies though between the computed saturated vapour curve and the experimental vapour curve, especially for the 120 °C isotherm.

The following possibilities were initially thought to be the cause for the discrepancy in the modeling:-

1. The experimentally measured HPVLE data were incorrect.
2. There was hydrogen bonding and the models utilized were not adequate to describe the VLE behaviour.

Since the experiments were conducted with exceptional care there is considerable confidence in the measured data. The more likely candidate therefore, was that there was strong hydrogen bonding of some nature and the models utilized could not describe the behaviour of the system.

To account for the hydrogen bonding theory, an extensive literature survey was undertaken to determine if measurements for the system propane + 1-propanol had been undertaken before for other properties beside HPVLE. In a publication by Brown et al. [1996] measurements were made for excess molar enthalpy and excess molar volume for the system at a temperature of 348.14 K and at pressures of 5, 10 and 15 MPa. They had some very interesting results for the system and their explanation was that hydrogen bonds were broken when 1-propanol was diluted with propane. The propane then fitted into cavities in the hydrogen-bonded structure of the 1-propanol. The number of cavities decreased with increasing pressure.

This was exactly what was being observed for the system and the problem region was the low-pressure dilute region. Therefore, it was more probable that the system could not be described adequately because the models utilized could not describe the behaviour adequately.

To describe the complex behaviour of the system, a more complex EOS would be required. Because of the appearance of *holes* in the fluid, which were dependent on the pressure of the system, one would need to probably go to a Hole Theory model to obtain more adequate modeling of the system. Due to a lack of time, a literature survey was undertaken for the Hole Theory approach, but modeling of the system with the Hole Theory approach was not undertaken. Publications by Lacombe and Sanchez [1976], Sanchez and Lacombe [1976],

Panayiotou and Vera [1981], Nies et al. [1983] and Smirnova and Victorov [1987] describe the application of Hole Theory.

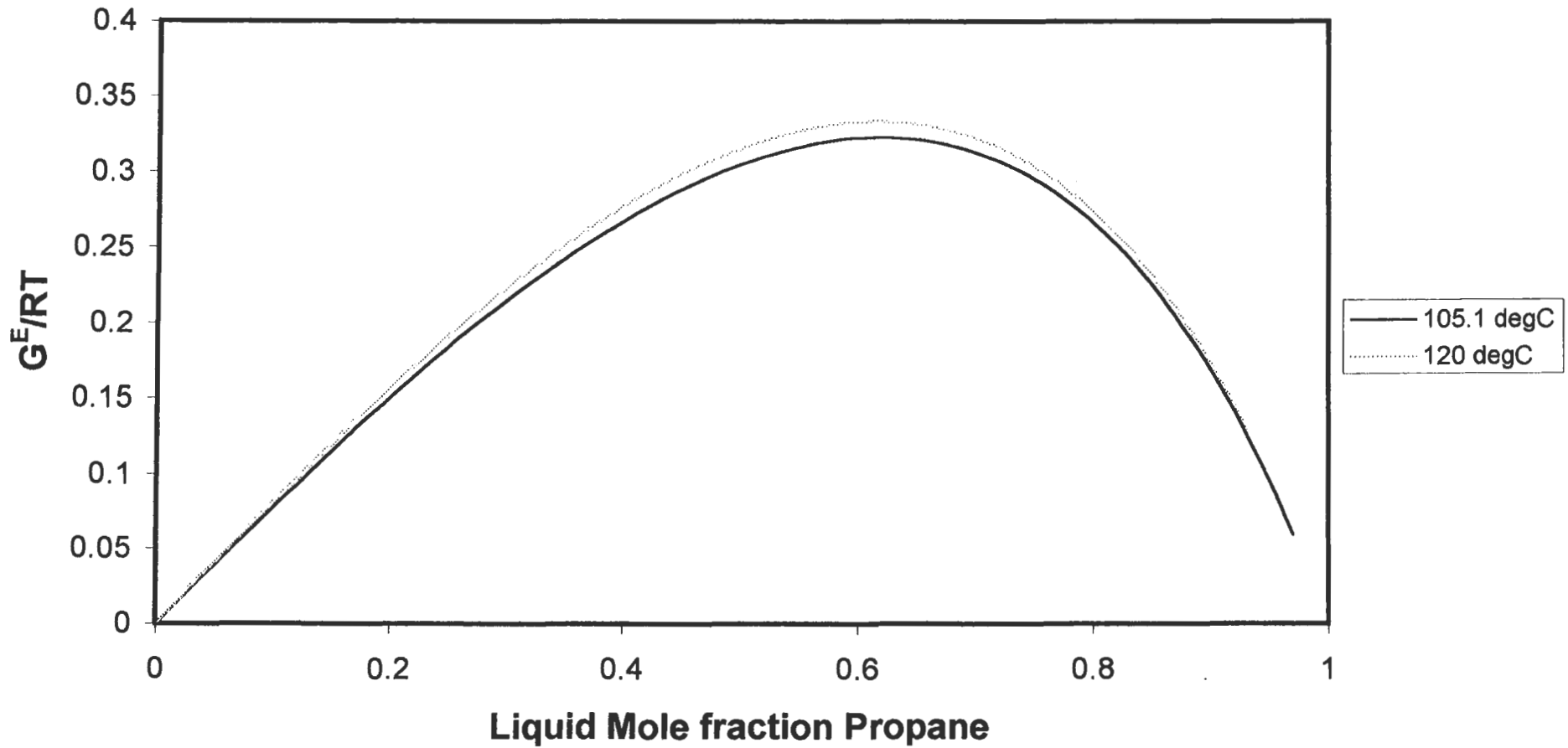
Model	Isotherm (°C)			
	105.1		120	
	AAE-P%	AAE-y%	AAE-P%	AAE-y%
DIRECT				
SRK	8.666	2.503	13.398	3.270
PR	8.578	2.260	14.728	3.456
PRSV-1vdw	8.521	2.761	14.980	3.716
PRSV-2vdw	2.539	2.531	4.757	2.474
HVO	3.354	2.647	6.851	2.742
MHV1	3.041	2.574	6.548	2.698
MHV2	2.904	2.572	6.746	2.739
LCVM	2.960	2.584	6.820	2.741
HVOS	3.113	2.583	6.815	2.737
PRSVWS-NRTL	3.472	3.502	7.630	2.025
PRSVWS-Van Laar	3.071	3.118	5.557	2.064
PRSVWS-Wilson	3.072	3.238	6.415	1.896
PRSVWS-Uniquac	5.692	3.955	6.135	1.487
COMBINED				
PRSV+NRTL	4.152	1.559	5.798	1.397
PRSV+Van Laar	4.178	1.563	6.226	1.440
PRSV+Wilson	4.419	1.577	6.829	1.510
PRSV+Uniquac	4.331	1.562	6.357	1.441
PRSVWS-NRTL+NRTL	3.971	1.437	5.651	1.310
Virial+NRTL	3.834	2.792	6.614	1.851
Virial+Van Laar	3.895	2.793	6.807	1.889
Virial+Wilson	4.135	2.798	7.305	1.938
Virial+Uniquac	3.985	2.788	6.946	1.875

Table 8-31: Absolute average errors for the Propane + 1-Propanol System

Figure 8-45 illustrates plots of excess Gibbs free energy for the two isotherms for the propane + 1-propanol system. Plots of activity coefficient for the system are available in Appendix F.2.

Mühlbauer [1990] suspected that liquid phase splitting occurred for the propane + 1-propanol system at the higher pressure, as he was not able to obtain convergence in his correlation program for the high-pressure region. Mühlbauer [1990] could also not obtain VLE measurements at much higher pressure in his apparatus. When the propane + 1-propanol system was measured in this project, it was possible to view the equilibrium cell contents, and at the higher pressure, no liquid phase splitting was observed. The problem of obtaining VLE measurements at much higher pressures was however encountered. The reason for this was

Figure 8-45: Plot of G^E/RT versus liquid mole fraction Propane for the Propane + 1-Propanol System



is simply because the single stage propane compressor utilized was not adequate to enable pressurization to the higher pressures.

Analysis of the excess Gibbs free energy versus liquid composition plot shows that there are no discontinuities in the curve, confirming the observation that there is no liquid phase splitting in the system at the measured isotherms. Criteria for the determination of liquid phase splitting are available in Walas [1985], Reid et al. [1988] and Schwartzeneruber et al. [1987].

8.4.4. Direct versus Combined Methods

Many researchers opt for the direct method approach for the reduction of HPVLE. There are many advantages to the approach as outlined in Chapter 3 and Table 3-1. However, what is evident from the three systems modeled in this project, is that for the various combinations of mixing rules and activity coefficient models available, one cannot simply decide that the direct method approach would be superior to the combined method approach. This is exactly what Wichterle [1978(b)] emphasized; one cannot easily make a decision on which is the better approach and both approaches should be undertaken to decide on which one produces the better modeling for the system.

8.5. EXTRAPOLATION AND PREDICTION OF HPVLE DATA

The cost of measurement of HPVLE data is extremely high as has been indicated by Moser and Kistenmacher [1987]. Methods are therefore continually being sought that would enable the extrapolation of existing data to some other conditions and preferably the prediction of HPVLE data entirely. The extrapolation and prediction of HPVLE data will be dealt with separately, with illustrations for the carbon dioxide + methanol and propane + 1-propanol systems.

8.5.1. Extrapolation methods

Extrapolation of HPVLE data can be undertaken very simply, if one utilizes the direct method with a cubic EOS. By assuming that the binary interaction parameter, k_{ij} , is temperature independent over a small temperature range (which is a reasonable assumption), VLE data can be computed at other temperatures over the small temperature range. Since the interaction parameter is temperature dependent, extrapolations over large a temperature range is not possible/accurate via this method.

The Wong and Sandler [1992] mixing rules utilized in this project and discussed in Chapter Three allow for the extrapolation of HPVLE over wide temperature and pressure ranges in one of two ways. They are as follows:-

1. Once reduced excess free energy parameters have been obtained for an EOS with Wong-Sandler mixing rules at one temperature, the reduced parameters can be used to compute HPVLE at any other temperature as the reduced parameters and the interaction parameter, k_{ij} , are temperature independent, according to Huang and Sandler [1993].
2. Excess free energy parameters are available for a number of systems at low pressure in the compilations of DECHEMA. Using the parameters given in DECHEMA, HPVLE data can be computed at other conditions of temperature and pressure (Wong and Sandler [1992]).

HPVLE data for the carbon dioxide + methanol system were correlated with the PRSVWS-NRTL model at 40 °C and the reduced parameters and k_{ij} values (at 40 °C) were used to determine HPVLE data for the system at 200 °C and -30 °C. This was to determine the extrapolation ability of the Wong-Sandler mixing rule for extrapolations above and below the temperature at which the correlated parameters were known. Figure 8-46 and Figure 8-47 shows the computed HPVLE curves for the carbon dioxide + methanol system at 200 °C and -30 °C respectively against literature data (experimental).

In Figure 8-46 the extrapolated data are compared to the literature data of Brunner et al. [1987] for the 200 °C isotherm. There is reasonable agreement in the liquid phase, but for the vapour phase there is a large difference between the extrapolated data and literature. Brunner et al. [1987] determined the critical composition to be 0.27 mole fraction carbon dioxide and the critical pressure to be 129.3 bar by graphical extrapolation. Using the Wong-Sandler extrapolation method, the critical point is considerably higher in composition and pressure, as can be seen in Figure 8-46.

For the -30 °C isotherm, there is very good agreement between the extrapolated data and the literature data of Chang and Rousseau [1985]. Chang and Rousseau did not measure the vapour phase as the values were all very close to unity. The vapour phase compositions computed by extrapolation were also extremely close to unity (approximately in the order of 0.999 mole fraction).

There is reasonable to very good agreement between the extrapolated and literature data for the carbon dioxide + methanol system for the 200 °C and -30 °C isotherms. The extrapolation for the -30 °C isotherm is probably better because the temperature range is smaller. On the other hand, one has no idea how accurate the experimental data of Brunner et al. [1987] or Chang and

Figure 8-46: Comparison between extrapolated and literature data for the carbon dioxide + methanol system at 200 °C

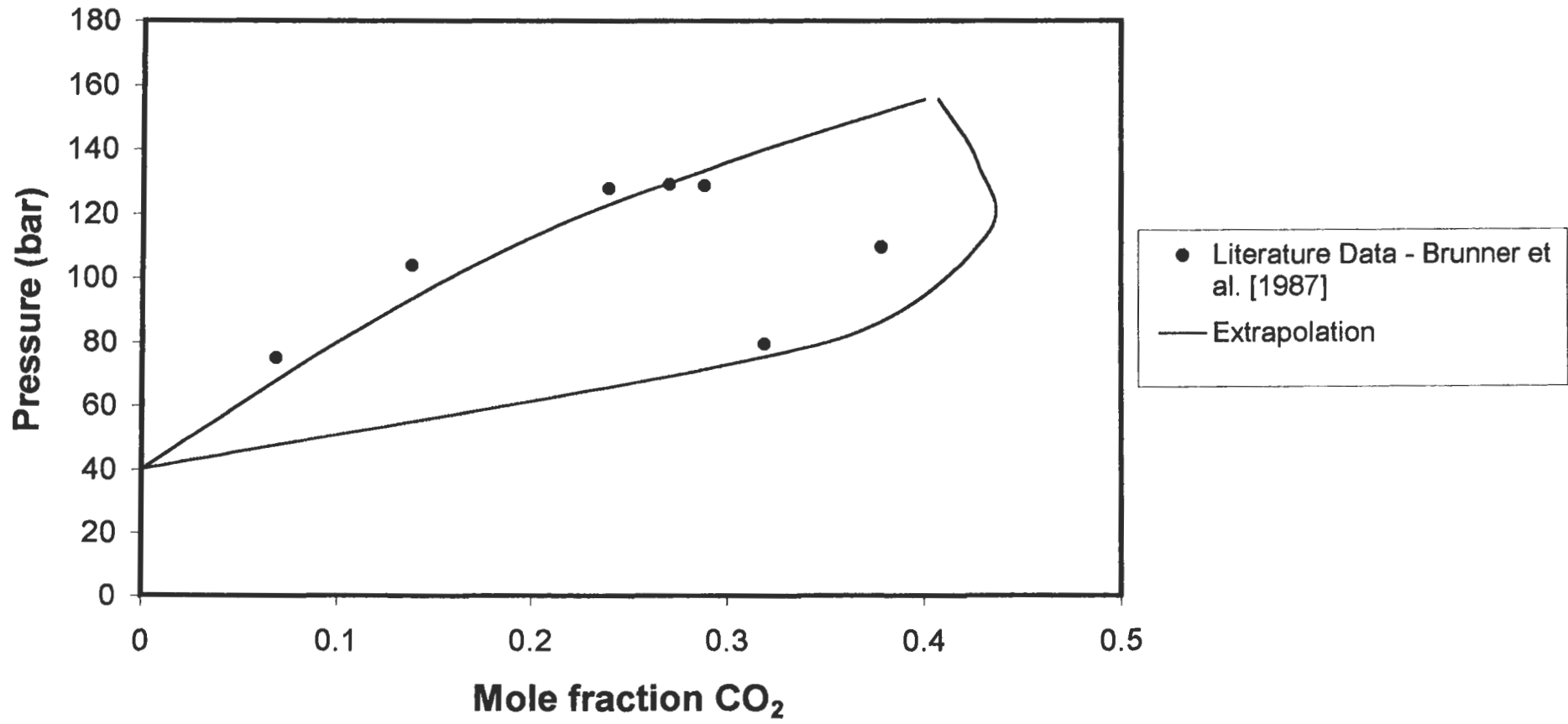
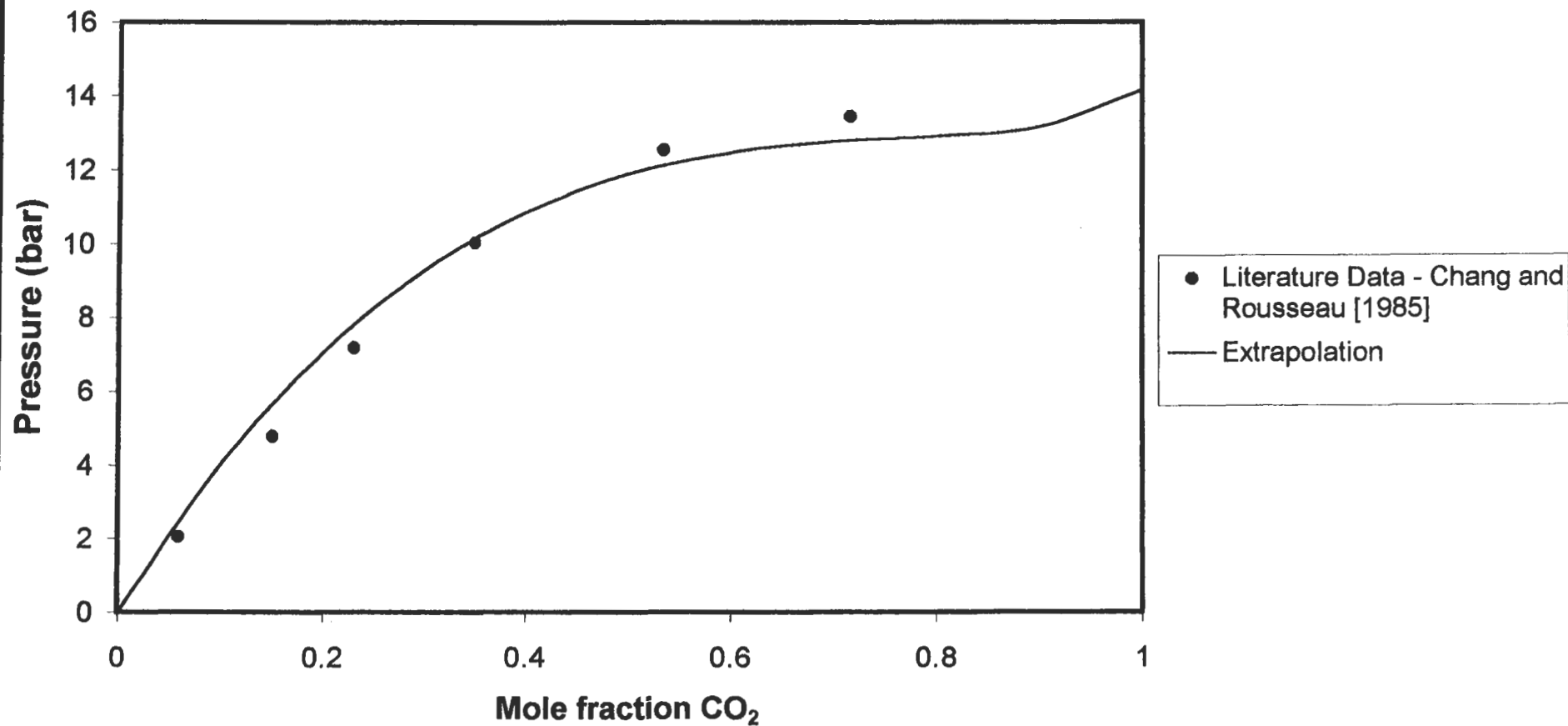


Figure 8-47: Comparison between extrapolated and literature data for the carbon dioxide + methanol system at -30 °C



Rousseau [1985] are and cannot dismiss that the extrapolation for either isotherm is better or worse. In general one could say that the method allows for very good approximation of HPVLE by extrapolation.

8.5.2. Predictive methods

The ultimate achievement in HPVLE computation would be the development of a totally predictive method. This would eliminate the need for costly and time-consuming HPVLE measurement. Therefore it is not surprising that a number of researcher have attempted or are attempting this task. There are numerous references in literature, e.g. Orbey et al. [1993], Kurihara and Kojima [1995(a),(b)], Fischer and Gmehling [1996], Feroiu and Geană [1996], Yoo et al. [1996] and Dünnebeil et al. [1996], some of which will be briefly discussed in this section.

The simplest predictive method would be to simply assume that the interaction parameter, k_{ij} , is zero in the mixing rule for the EOS via the direct method. This would enable prediction of HPVLE data for any isotherm. However, since k_{ij} for most system is not zero, and significantly away from zero, the predictions via this method would be significantly in error.

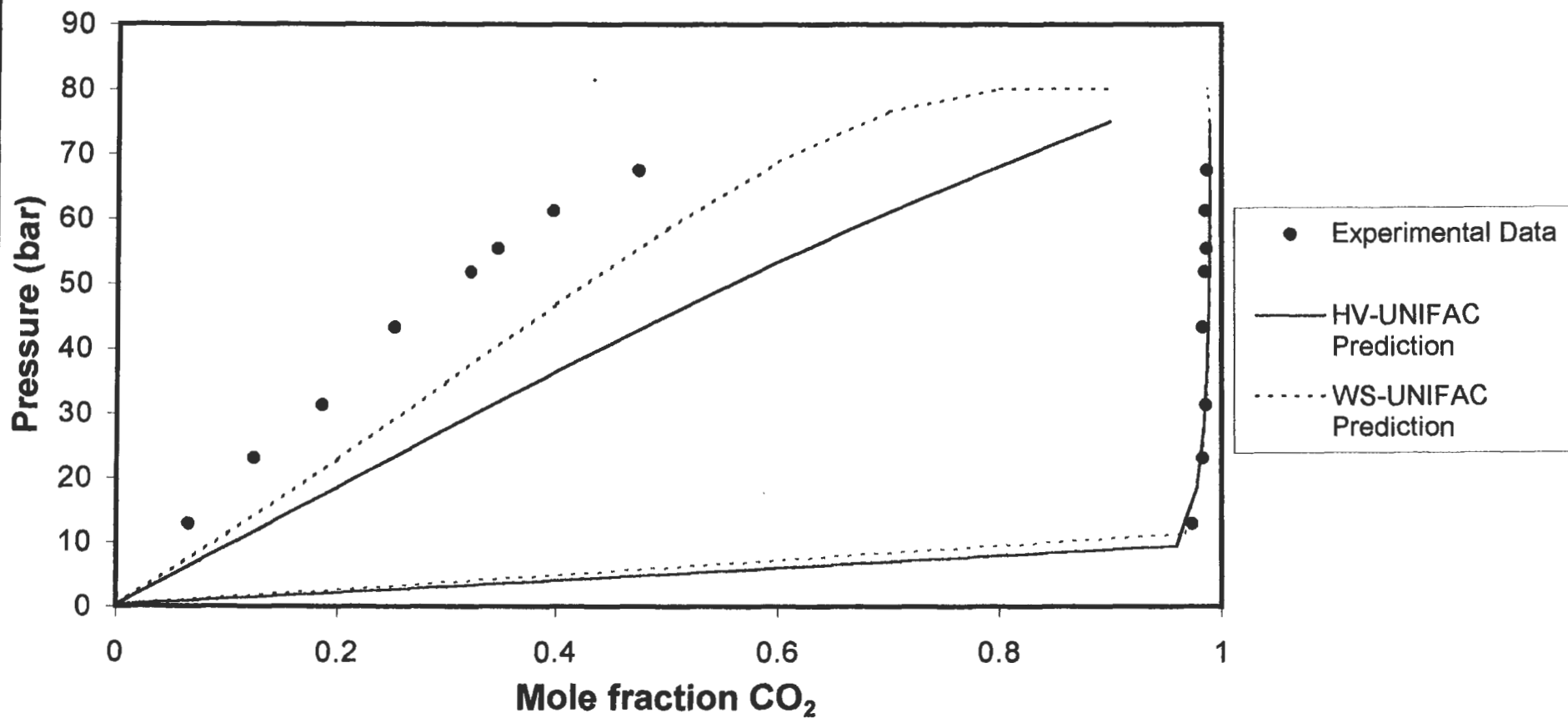
The method of Feroiu and Geană [1996] allows for the prediction of HPVLE from infinite dilution activity coefficient. The infinite dilution activity coefficients used are those at low-pressure which are generally readily available.

The method adopted in this project is that of Orbey et al. [1993]. The UNIFAC model is used to compute the activity coefficients at infinite dilution at 25 °C. These infinite dilution activity coefficients are then used to obtain the parameters for the excess Gibbs free energy model. The k_{ij} value is then obtained by matching the excess Gibbs free energy of the mixture calculated from the excess Gibbs free energy model and from the EOS at the single mid-concentration point, $x_i = 0.5$. The values for the parameters are then used for all other temperatures.

The method of Orbey et al. [1993] was used with the Wong-Sandler mixing rules with the NRTL excess Gibbs free energy model (WS-UNIFAC). It was also undertaken for the HVOS mixing rules (HV-UNIFAC). Predictions were undertaken for the carbon dioxide + methanol system at 40 °C and the propane + 1-propanol system at 120 °C.

Figure 8-48 illustrates the comparison of the predicted versus the experimentally measured data for the carbon dioxide + methanol system at 40 °C.

Figure 8-48: Comparison between experimental and predicted HPVLE data for the carbon dioxide + methanol system at 40 °C



As can be seen from Figure 8-48 the WS-UNIFAC model produced a more reasonable prediction for the carbon dioxide + methanol system than the HV-UNIFAC model. For both models the prediction of the vapour phase was excellent. The liquid phase was badly under-predicted by both models with the WS-UNIFAC faring better in the description of the liquid phase.

For the UNIFAC group selections, the following groups were selected:-

1. One CO₂ group to describe carbon dioxide; and
2. One CH₃OH group to describe methanol.

For this system the choice of UNIFAC groups was very simple as carbon dioxide and methanol have their own groups.

UNIFAC group contribution tables are available in Sandler [1989] and the group contributions for CO₂ were obtained from Apostolou et al. [1995].

Predictions were also undertaken for the propane + 1-propanol system at the 120 °C isotherm. Once again the WS-UNIFAC and HV-UNIFAC models were used. Figures 8-49 and 8-50 illustrate the comparison between predicted and experimentally measured data for the system for the different choice of UNIFAC groups to describe 1-propanol.

The UNIFAC group contributions for the propane + 1-propanol system were selected as follows:-

1. One CH₂ group and two CH₃ groups to describe propane;
2. One CH₃ group, two CH₂ groups and one OH group to describe 1-propanol (selection 1).
3. The 1-propanol group was also described by the choice of one CH₃OH group, one CH group and one CH₃ group (selection 2).

The choices of the UNIFAC contribution groups selected via the two methods were to determine the effect of the choice of contribution groups to the accuracy of the prediction.

Figure's 8-49 and 8-50 show the comparisons for representation of 1-propanol via selection 1 and 2 respectively. For both group selections for 1-propanol the HV-UNIFAC model was superior in predicting the behaviour of the system. Overall the best prediction was obtained with the HV-UNIFAC mode with selection 1 for the 1-propanol UNIFAC groups. However, even the best predictive model could not represent the vapour phase adequately. This is not a

Figure 8-49: Comparison between experimental and predicted HPVLE data for the propane + 1-propanol system at 120 °C

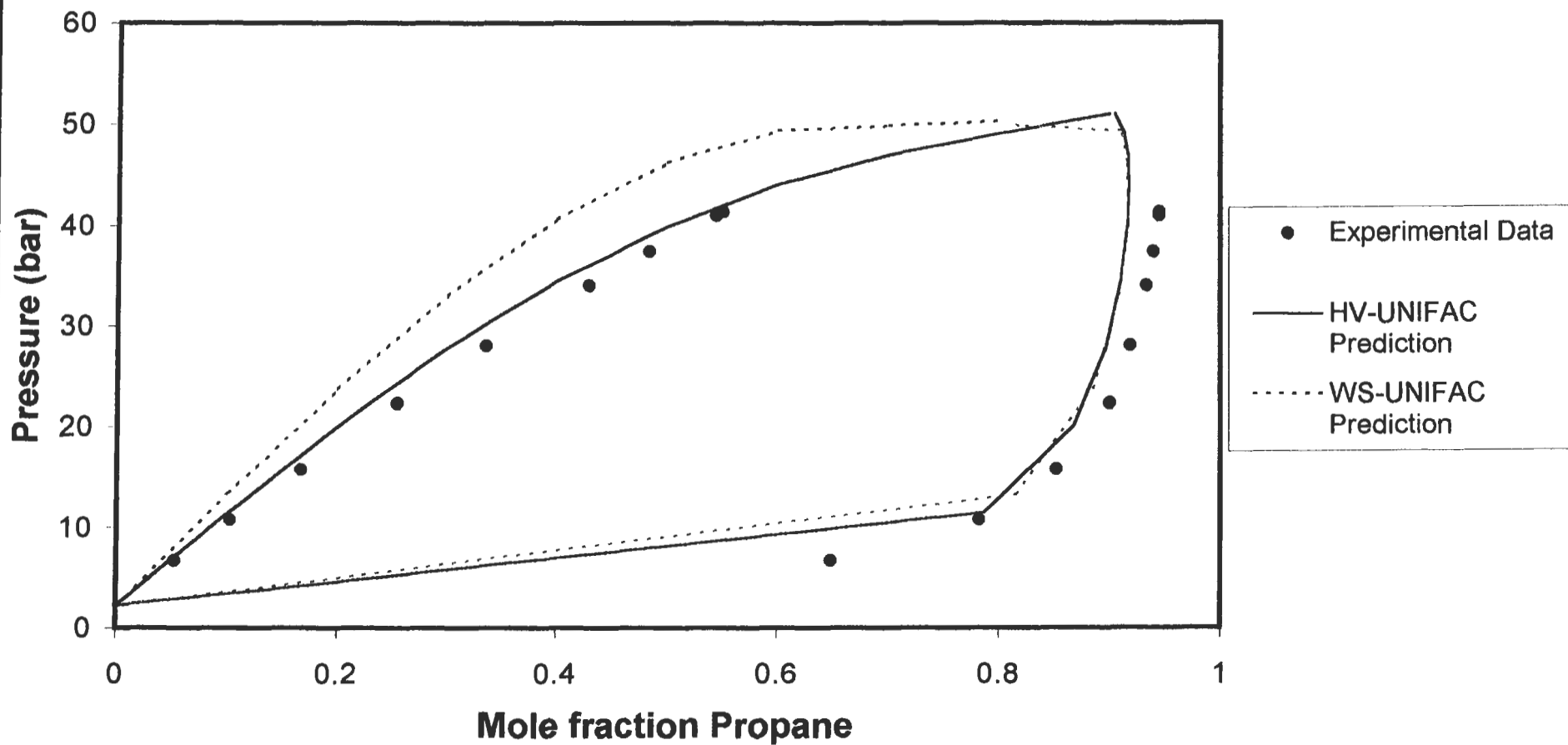
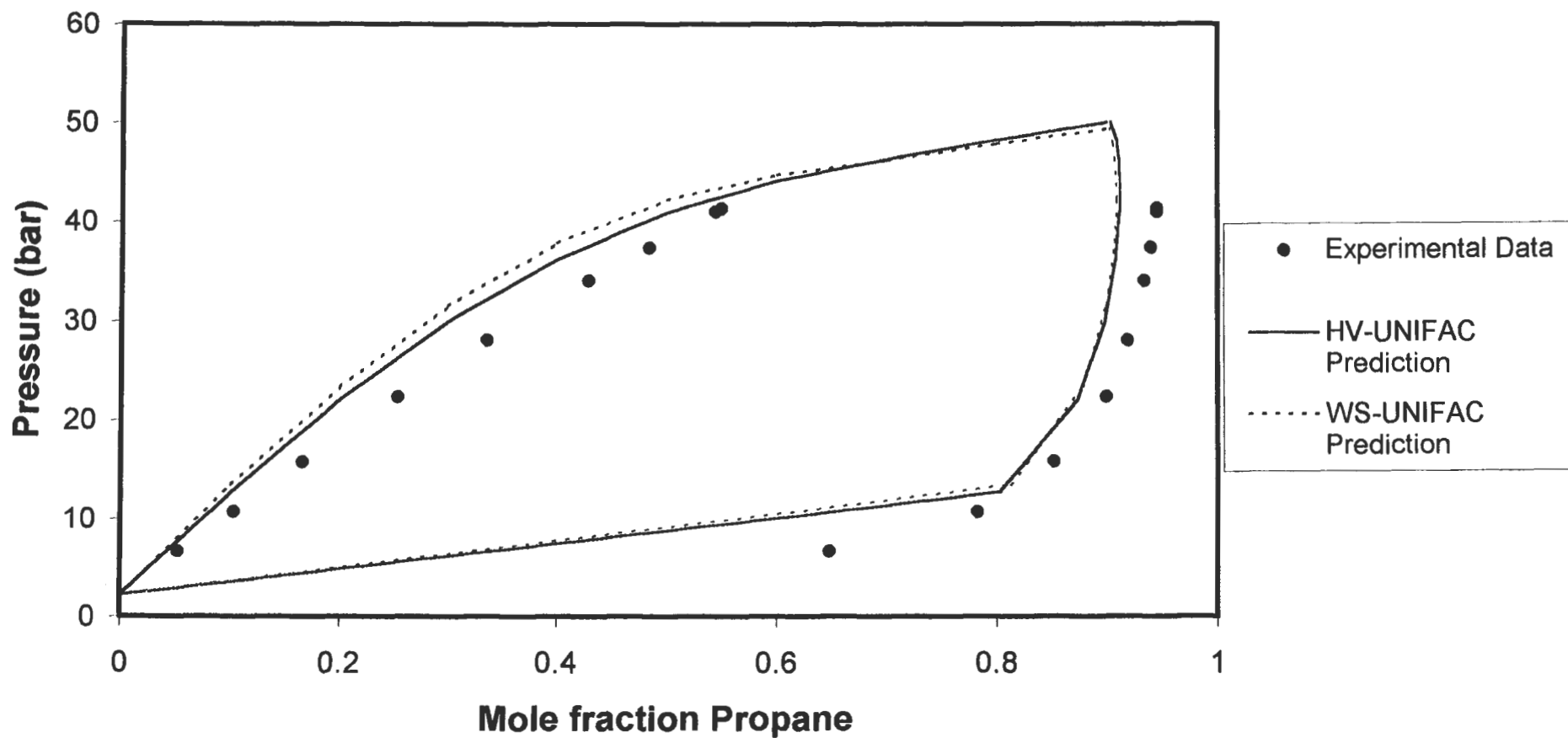


Figure 8-50: Comparison between experimental and predicted HPVLE data for the propane + 1-propanol system at 120 °C



downfall of the predictive method, but merely that the propane + 1-propanol system is highly non-ideal as discussed previously and difficult to model.

Overall, one can say that the predictive methods illustrated perform fairly, and would be an excellent tool for design engineers in the preliminary computations, as they provide a reasonably accurate (less than 10 %) representation of the system behaviour. They also indicate the correct trend exhibited by the systems.

8.6. CRITICAL PROPERTIES

In this project the critical properties (temperature and pressure) for the systems were not measured, mainly due to the fact that the conditions were beyond the maximum operating conditions for the apparatus designed. The critical properties were thus computed for the system studied using the method of Deiters and Schneider [1976]. Computations were undertaken using the SRK, PR and PRSV EOS's. The computational method is described in Chapter 3.5. and Appendix B. For each of the EOS's, the differential expressions given by Equations (3-129) and (3-130) were rigorously determined and solved using the Marquardt-Levenberg implementation of the Newton-Raphson technique. The following plots were then undertaken:-

1. Critical temperature versus composition;
2. Critical pressure versus composition;
3. Critical volume versus composition;
4. Critical compressibility factor versus composition; and
5. Pressure versus temperature plots.

The critical pressures versus critical temperature plots were obtained by cross plotting of the critical pressure versus composition and critical temperature versus composition plots.

Sadus [1994], in his excellent review of critical properties describes the classification of phase behaviour of binary mixture with respect to different critical phenomena. The classification is based on six type of critical phenomena illustrated on pressure versus temperature plots. For all of the system studied in this project, type one behaviour is predicted as shown in Figures 8-51 to 8-53.

Plots of critical temperature, pressure, volume and compressibility factor against composition are illustrated in Appendix F.3.

Figure 8-51: Plot of $\ln P$ versus temperature for the carbon dioxide + toluene binary system

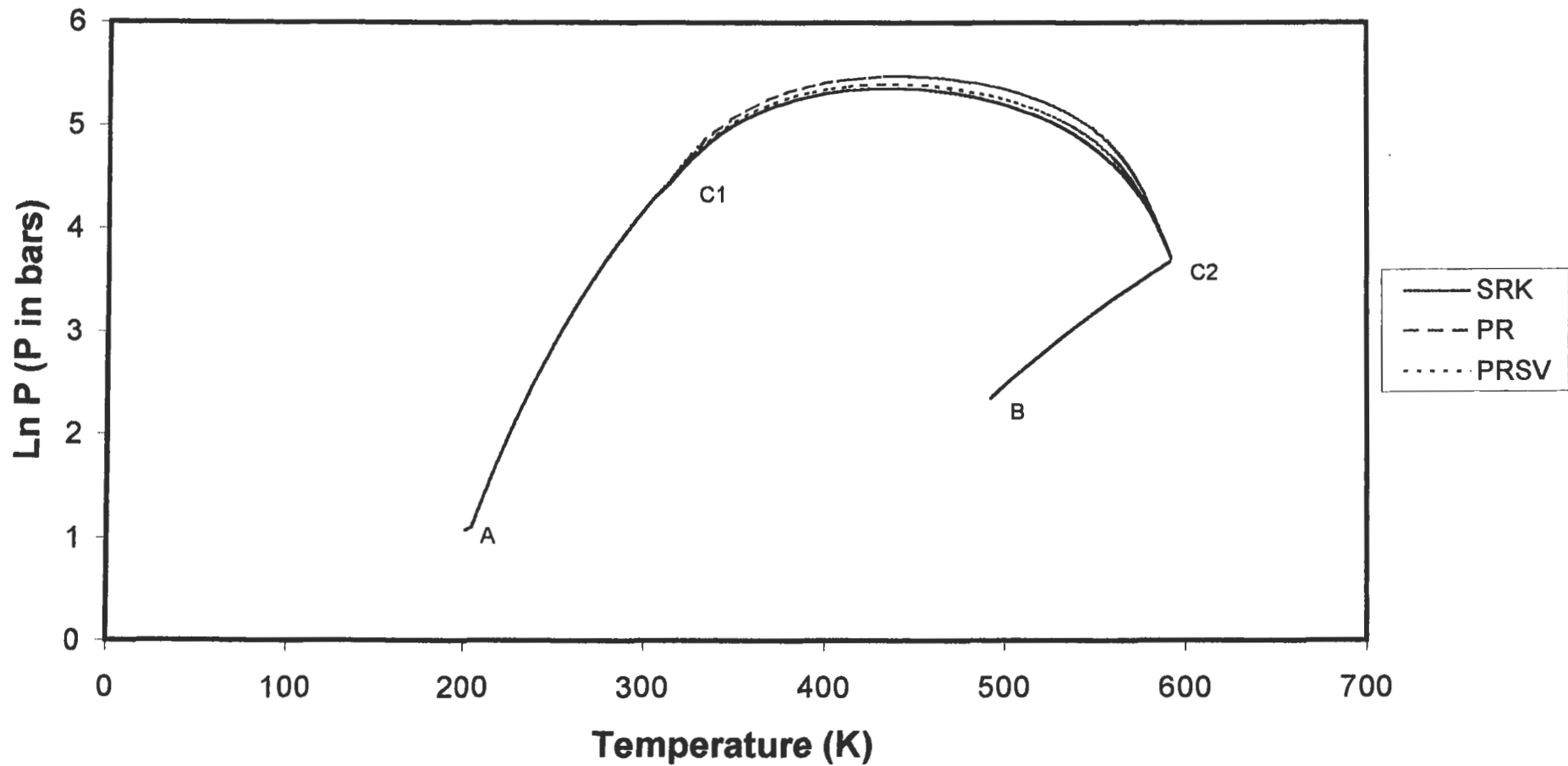


Figure 8-52: Plot of $\ln P$ versus temperature for the carbon dioxide + methanol binary system

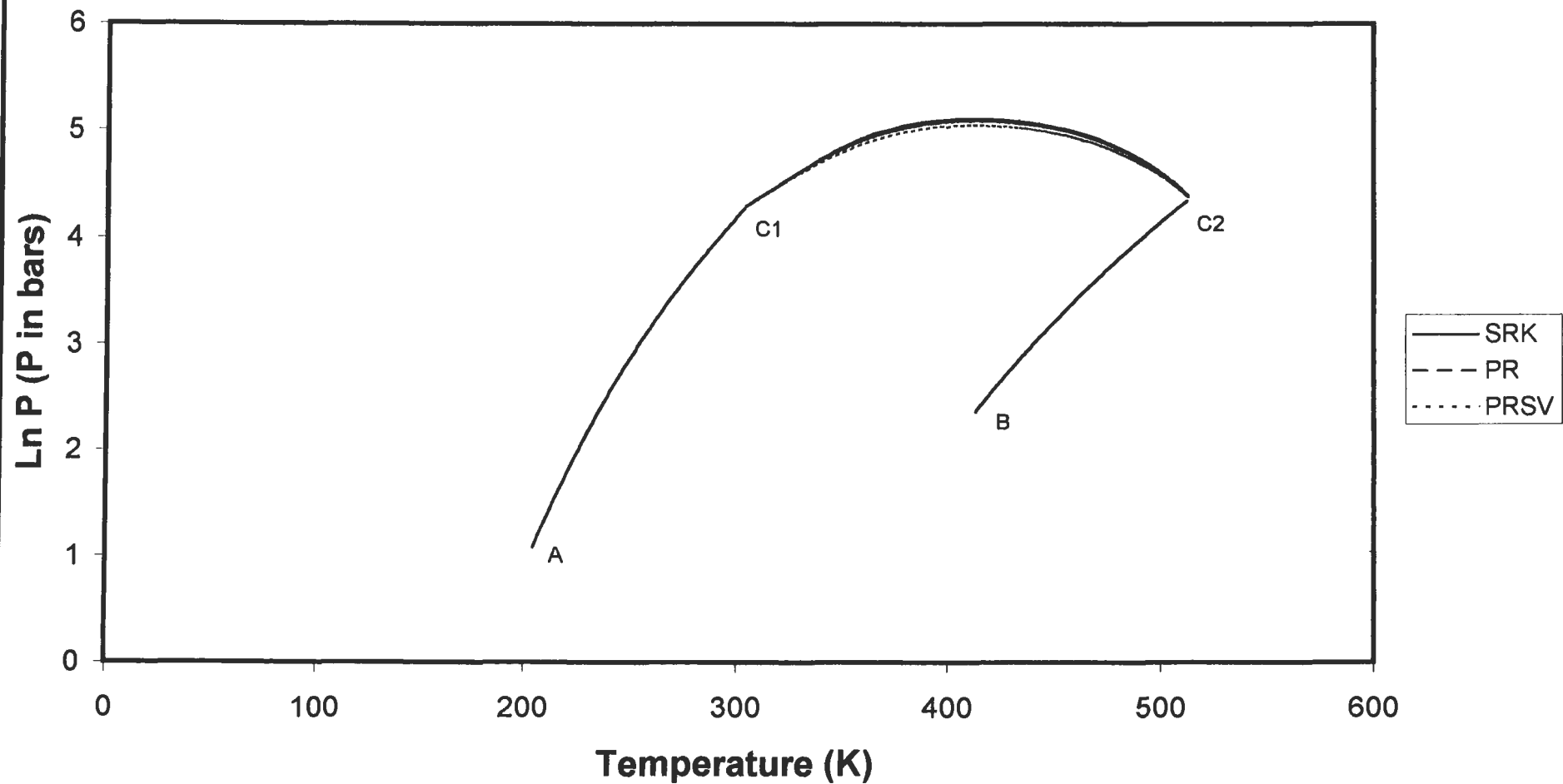
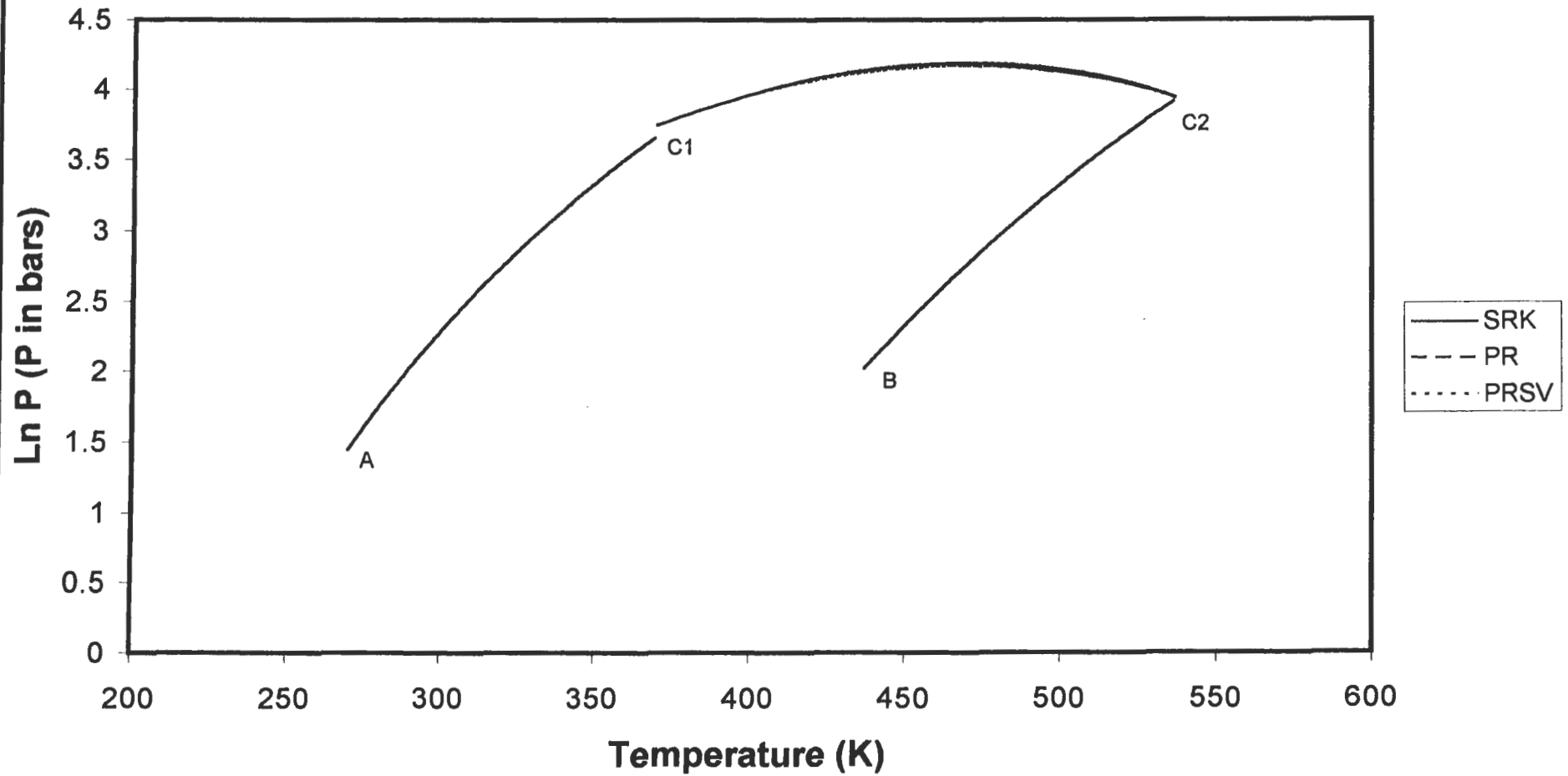


Figure 8-53: Plot of $\ln P$ versus temperature for the propane + 1-propanol binary system



In Figure's 8-51 to 8-53 curves A-C1 and B-C2 represent the vapour pressure curves for the two components, which were computed from either Antoine's equation or a vapour pressure correlation. Curve C1-C2 represents the critical pressure-temperature curve computed via the method of Deiters and Schnieder [1976].

The critical properties were computed for each of the isotherms for the carbon dioxide + toluene, carbon dioxide + methanol and propane + 1-propanol systems using the PRSV EOS. Tables 8-32 to 8-34 summarize the critical property data.

Temperature (°C)	Composition (x_{CO_2})	Critical Volume, cm ³ /gmol (V_c)	Critical Pressure, bar (P_c)	Critical Compressibility (Z_c)
38	0.9924	0.0891	82.7115	0.2831
80	0.9230	0.0663	161.4262	0.3646
118.3	0.8884	0.0744	205.3844	0.4694

Table 8-32: Computed Critical properties for the Carbon Dioxide + Toluene binary System using the PRSV EOS.

Temperature (°C)	Composition (x_{CO_2})	Critical Volume, cm ³ /gmol (V_c)	Critical Pressure, bar (P_c)	Critical Compressibility (Z_c)
40	0.9833	0.0954	82.4244	0.3018
90	0.8461	0.0744	135.2754	0.3335
100	0.8188	0.0755	142.9088	0.3477

Table 8-33: Computed Critical properties for the Carbon Dioxide + Methanol binary System using the PRSV EOS.

Temperature (°C)	Composition ($x_{propane}$)	Critical Volume, cm ³ /gmol (V_c)	Critical Pressure, bar (P_c)	Critical Compressibility (Z_c)
105.1	0.9773	0.2129	45.3468	0.3071
120	0.9302	0.2003	50.4070	0.3088

Table 8-34: Computed Critical properties for the Propane + 1-Propanol binary System using the PRSV EOS.

8.7. THERMODYNAMIC CONSISTENCY TESTING

A number of methods are available to determine the thermodynamic consistency of experimental HPVLE data. A few of these have been discussed in Section 3.6. and Appendix B.19. The Chueh et al. [1965] consistency test was utilized in this project in conjunction with residual plots to determine the thermodynamic consistency of the data measured for the carbon dioxide + toluene, carbon dioxide + methanol and propane + 1-propanol at the various isotherms.

The Chueh et al. test is a computational comparison between the value generated by Equations (B-140) and (B-141). Equation (B-140) has three integrals and in the tables summarizing the consistency test, each of the integrals will be refer to as Area 1, Area 2, and Area 3. Equation (B-140) will be referred to as the LHS and Equation (B-141) as the RHS. Equation (B-141) is comprised of three terms and in the tables they will be referred to as term 1, term 2 and term 3 respectively as they appear in the equation.

$$\int_{x_2=0}^{x_2} \ln\left(\frac{K_2}{K_1}\right) dx_2 + \int_{x_2=0}^{x_2} \ln\left(\frac{\hat{\phi}_2}{\hat{\phi}_1}\right) dx_2 + \frac{1}{RT} \int_{x_2=0}^{x_2} V^L dP = \text{LHS} \quad (\text{B-140})$$

$$\text{RHS} = \left[\ln K_1 + \ln\left(\frac{\hat{\phi}_2 P}{\hat{\phi}_1^{\text{sat}} P_1^{\text{sat}}}\right) + x_2 \left(\ln \frac{\hat{\phi}_2}{\hat{\phi}_1} + \ln \frac{K_2}{K_1} \right) \right]_{x_2=0}^{x_2} \quad (\text{B-141})$$

In Tables 8-35 to 8-42, Difference is defined as the absolute value difference between LHS and RHS and % inconsistency is defined as follows:

$$\% \text{inconsistency} = \frac{\text{Difference}}{\left| \frac{\text{LHS} + \text{RHS}}{2} \right|} * 100 \quad (8-10)$$

Chueh et al. [1965] performed their proposed consistency test for the carbon dioxide + nitrogen and carbon dioxide + oxygen system. For both cases they obtained % inconsistencies ranging from 4.5 % down to 0.9 %. According to them values of below 5 % are well within the uncertainties in the computations and they judged their data to be in terms of thermodynamic consistency, very good. This figure of 5 % inconsistency is being used as a benchmark to judge the quality of the measured data in terms of the Chueh et al. [1965] consistency test.

8.7.1. Carbon Dioxide + Toluene System

The carbon dioxide + toluene system was measured at three isotherms, viz. 38, 80 and 118.3 °C. Tables 8-35 to 8-37 summarize the Chueh et al. [1965] consistency test for the 38, 80 and 118.3 °C isotherms respectively. For the 38 and 80 °C isotherms the percentage inconsistency is less than 3.2 % across the composition range and in view of the uncertainties in the computations, it is probably fair to judge the thermodynamic consistency of this data as very good.

x_1	Area 1	Area 2	Area 3	LHS	RHS	term1	term2	term3	Diff.	% inconsistency
0.11810	0.82433	0.02560	0.03972	0.88963	0.90261	-4.62537	4.67886	0.84913	0.01298	1.44870
0.53350	3.21263	0.57029	0.14482	3.92920	4.03402	-4.02856	4.43531	3.62727	0.10482	2.63262
0.76130	4.13245	1.13087	0.15472	5.42852	5.58323	-3.13041	4.08227	4.63137	0.15471	2.80985
0.90000	4.52545	1.52132	0.14960	6.21554	6.38808	-2.09720	3.80644	4.67883	0.17254	2.73788

Table 8-35: Summary of Chueh et al. [1965] consistency test for the carbon dioxide + toluene system at 38 °C

x_1	Area 1	Area 2	Area 3	LHS	RHS	term1	term2	term3	Diff.	% inconsistency
0.12150	0.70732	0.02643	0.07070	0.80439	0.77979	-3.50323	3.55327	0.72975	0.02460	3.10523
0.29350	1.60647	0.15537	0.16597	1.92733	1.90603	-3.64200	3.80592	1.74210	0.02131	1.11165
0.49720	2.50030	0.45279	0.24906	3.20309	3.19758	-3.24934	3.60875	2.83817	0.00551	0.17216
0.90000	3.70572	1.27042	0.25373	5.26919	5.32163	-1.53016	3.41524	3.43656	0.05244	0.99029

Table 8-36: Summary of Chueh et al. [1965] consistency test for the carbon dioxide + toluene system at 80 °C

x_1	Area 1	Area 2	Area 3	LHS	RHS	term1	term2	term3	Diff.	% inconsistency
0.13810	0.65974	0.04315	0.10815	0.81088	0.73259	-2.59027	2.61887	0.70399	0.07828	10.14381
0.32130	1.41029	0.22808	0.24787	1.88505	1.74722	-2.55877	2.68153	1.62446	0.13783	7.58892
0.54670	2.12450	0.62458	0.36495	3.11605	2.95992	-2.27303	2.60272	2.63023	0.15613	5.13919
0.80000	2.74037	1.13237	0.37626	4.28204	4.16898	-1.67078	2.78168	3.05808	0.11306	2.67560

Table 8-37: Summary of Chueh et al. [1965] consistency test for the carbon dioxide + toluene system at 118.3 °C

For the 118.3 °C isotherm, the % inconsistency varied from approximately 10.2 % down to approximately 2.7 %. In light of the slightly larger inconsistency, one will have to rate the data as satisfactory to good in terms of thermodynamic consistency.

Another check for the thermodynamic consistency of the measured data is to view the residual plots for the system, especially the residual plot of vapour composition. If there is even scatter of the data about the zero x-axis, and the scatter is within 1% either side of the zero axis, then one can presume that the data are thermodynamically consistent (Prausnitz [1980]).

Making reference to Figures 8-54 to 8-56, there is even scatter for the carbon dioxide + toluene system for all isotherms. The scatter for almost all points is within the 1% region as well.

Figure 8-54: Residual plot of vapour composition for the Carbon Dioxide + Toluene System at 38 °C isotherm

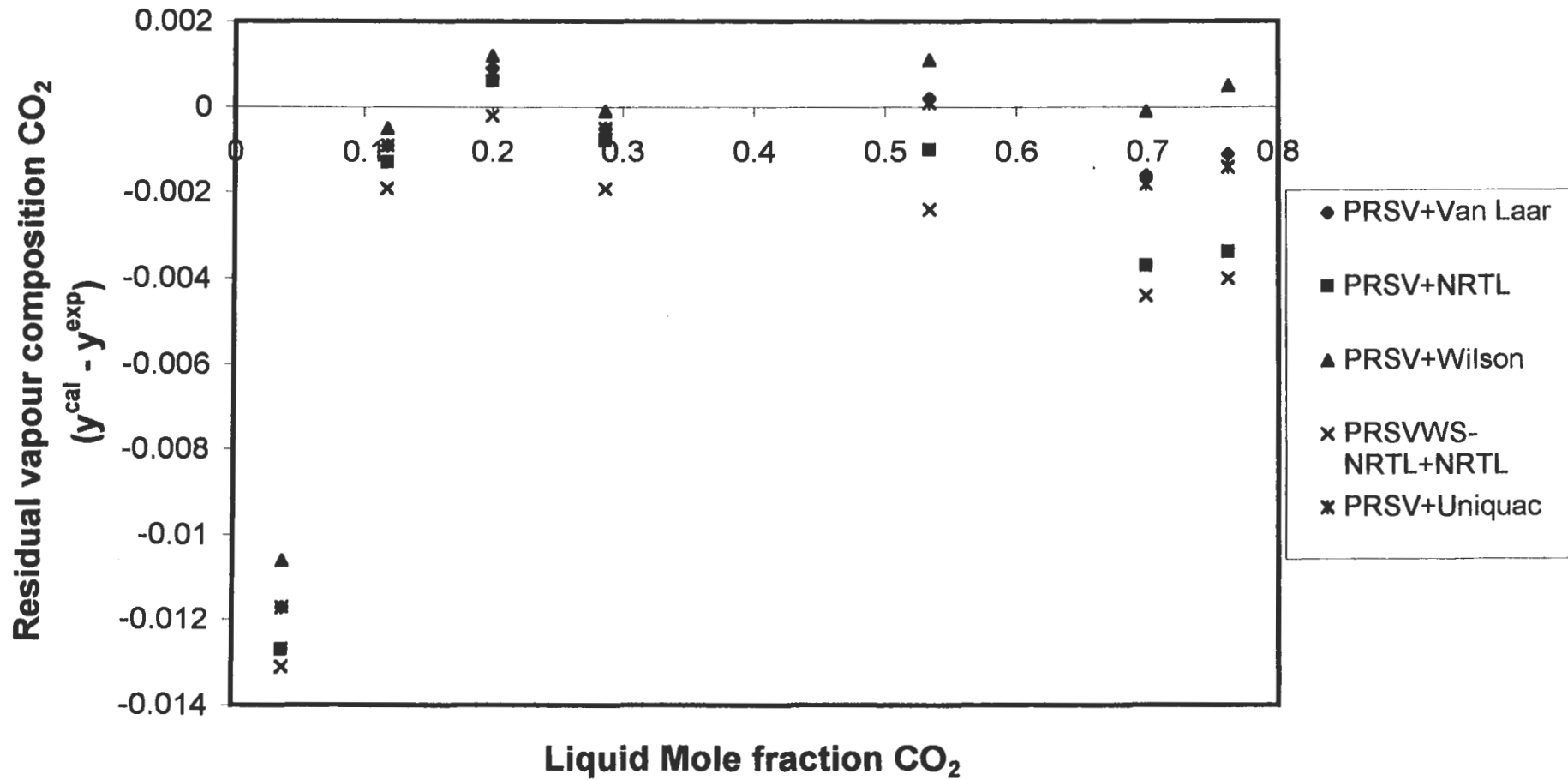


Figure 8-55: Residual plot of vapour composition for the Carbon Dioxide + Toluene System at 80 °C

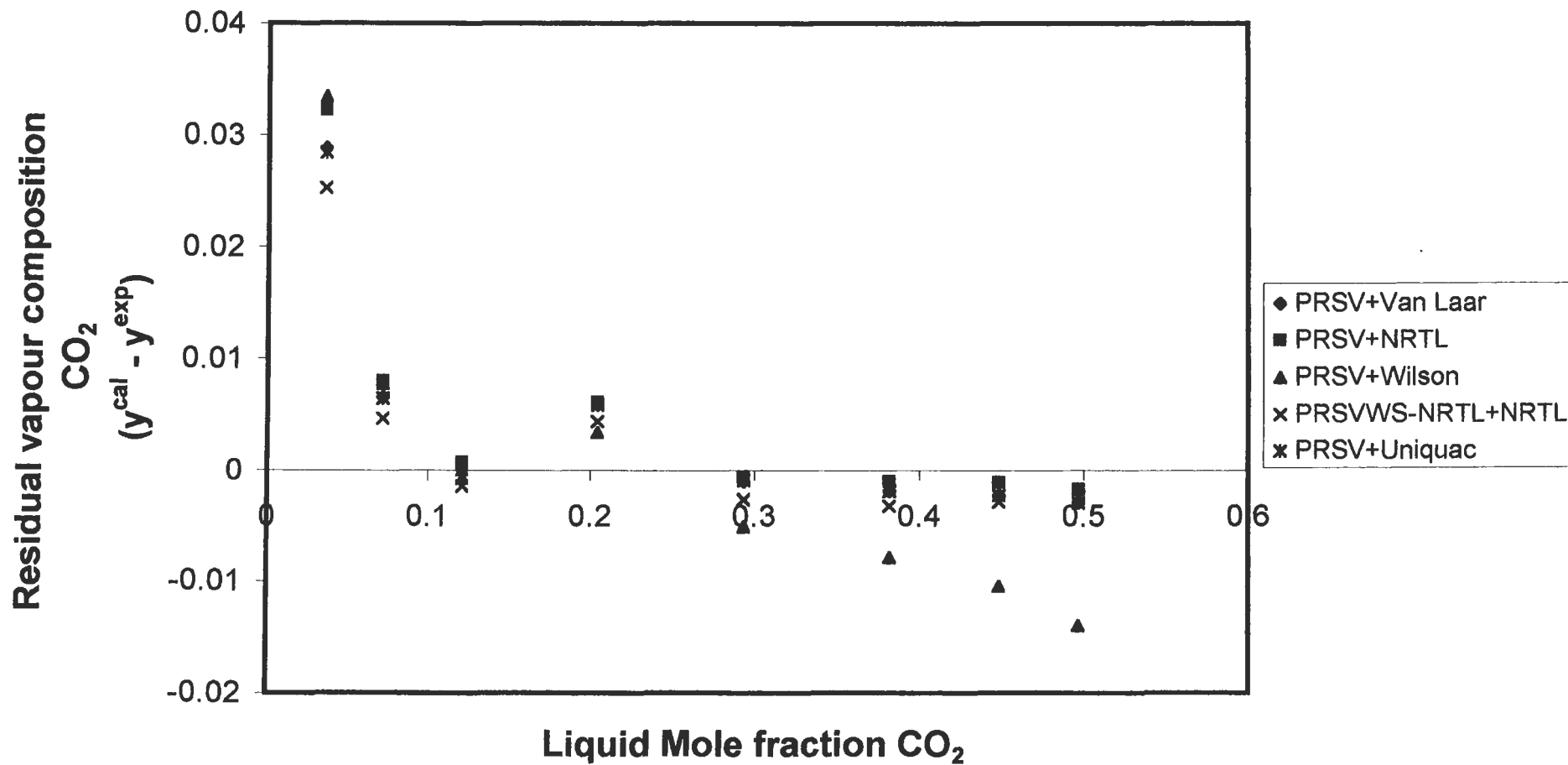
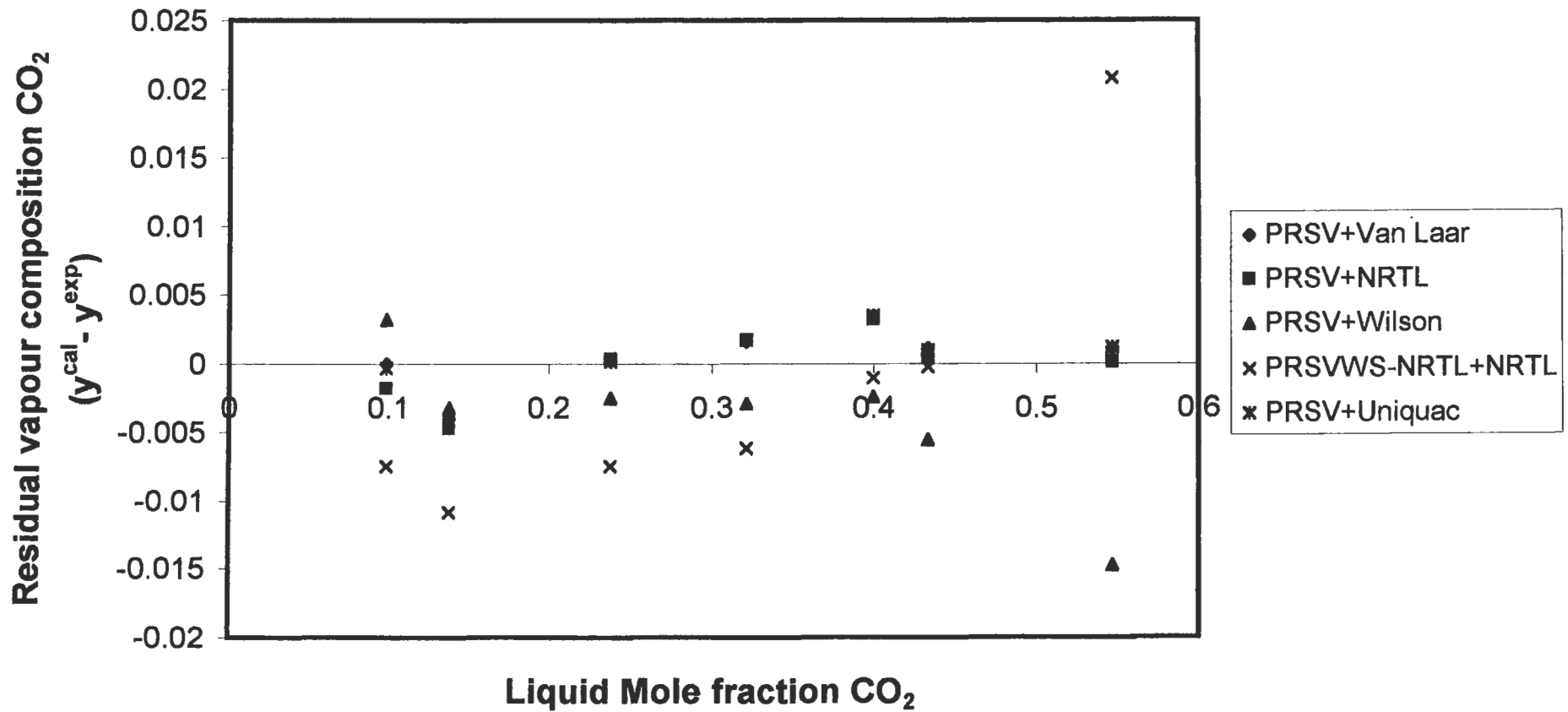


Figure 8-56: Residual plot of vapour composition for the Carbon Dioxide + Toluene System at 118.3 °C



Residual plots of pressure for the carbon dioxide + toluene system are available in Appendix F.4. All of the residual computations undertaken were performed for a number of models as indicated in the residual plots.

Plots for the computation of the areas for the Chueh et al. [1965] test are available in Appendix F.4. Simpson's one-third integration rule as outlined in Gerald and Wheatley [1989] was used to compute the areas under the curves.

8.7.2. Carbon Dioxide + Methanol System

Tables 8-38 to 8-40 summarize Chueh et al. consistency test computations for the carbon dioxide + methanol system for the 40, 90 and 100 °C isotherms respectively.

The % inconsistency for the 40 °C isotherm varies between approximately 8.5 % to 7%. This would rate the data as fair to good in terms of the Chueh et al. test. Viewing the vapour composition residual plot, one finds that there is even scatter and scatter is 1 % either side of the zero axis. This confirms the data as being consistent even though it does not rate that well according to the Chueh et al. test.

x_i	Area 1	Area 2	Area 3	LHS	RHS	Term1	term2	term3	% Diff.	% inconsistency
0.12330	0.75201	0.01835	0.02779	0.79815	0.86237	-3.77226	3.87790	0.75673	0.06422	7.73456
0.32270	1.82842	0.12748	0.06326	2.01940	2.01940	-3.89713	4.21729	1.87782	0.17858	8.46889
0.47360	2.54100	0.27471	0.07921	2.89592	3.13124	-3.62309	4.16464	2.58969	0.23532	7.80878
0.68000	3.34911	0.52078	0.08386	3.95737	4.24522	-3.11227	4.16598	3.19151	0.28786	7.01866

Table 8-38: Summary of Chueh et al. [1965] consistency test for the carbon dioxide + methanol system at 40 °C

x_i	Area 1	Area 2	Area 3	LHS	RHS	term1	term2	term3	% Diff.	% inconsistency
0.07010	0.33075	0.01064	0.03107	0.37245	0.37737	-2.03638	2.07434	0.33942	0.00492	1.31244
0.16460	0.73766	0.05408	0.07091	0.86266	0.90553	-2.36127	2.48693	0.77988	0.04287	4.84932
0.27130	1.14788	0.14850	0.11021	1.40676	1.46345	-2.27400	2.48949	1.24795	0.05668	3.94978
0.60000	2.04704	0.65552	0.18419	2.89028	3.04953	-1.62760	2.36041	2.31672	0.15924	5.36191

Table 8-39: Summary of Chueh et al. [1965] consistency test for the carbon dioxide + methanol system at 90 °C

x_i	Area 1	Area 2	Area 3	LHS	RHS	term1	term2	term3	% Diff.	% inconsistency
0.08870	0.39995	0.01838	0.04815	0.46649	0.47121	-2.01216	2.06765	0.41572	0.00472	1.00656
0.20330	0.86214	0.08976	0.10090	1.05299	1.07128	-2.15503	2.30971	0.91660	0.01830	1.72254
0.36110	1.37308	0.27033	0.15347	1.79807	1.82026	-1.93033	2.22011	1.53049	0.02219	1.79807
0.60000	1.92651	0.66732	0.20763	2.80145	2.90080	-1.40936	2.11326	2.19690	0.09935	3.48442

Table 8-40: Summary of Chueh et al. [1965] consistency test for the carbon dioxide + methanol system at 100 °C

Figure 8-57: Residual plot of vapour composition for the Carbon Dioxide + Methanol System at 40 °C

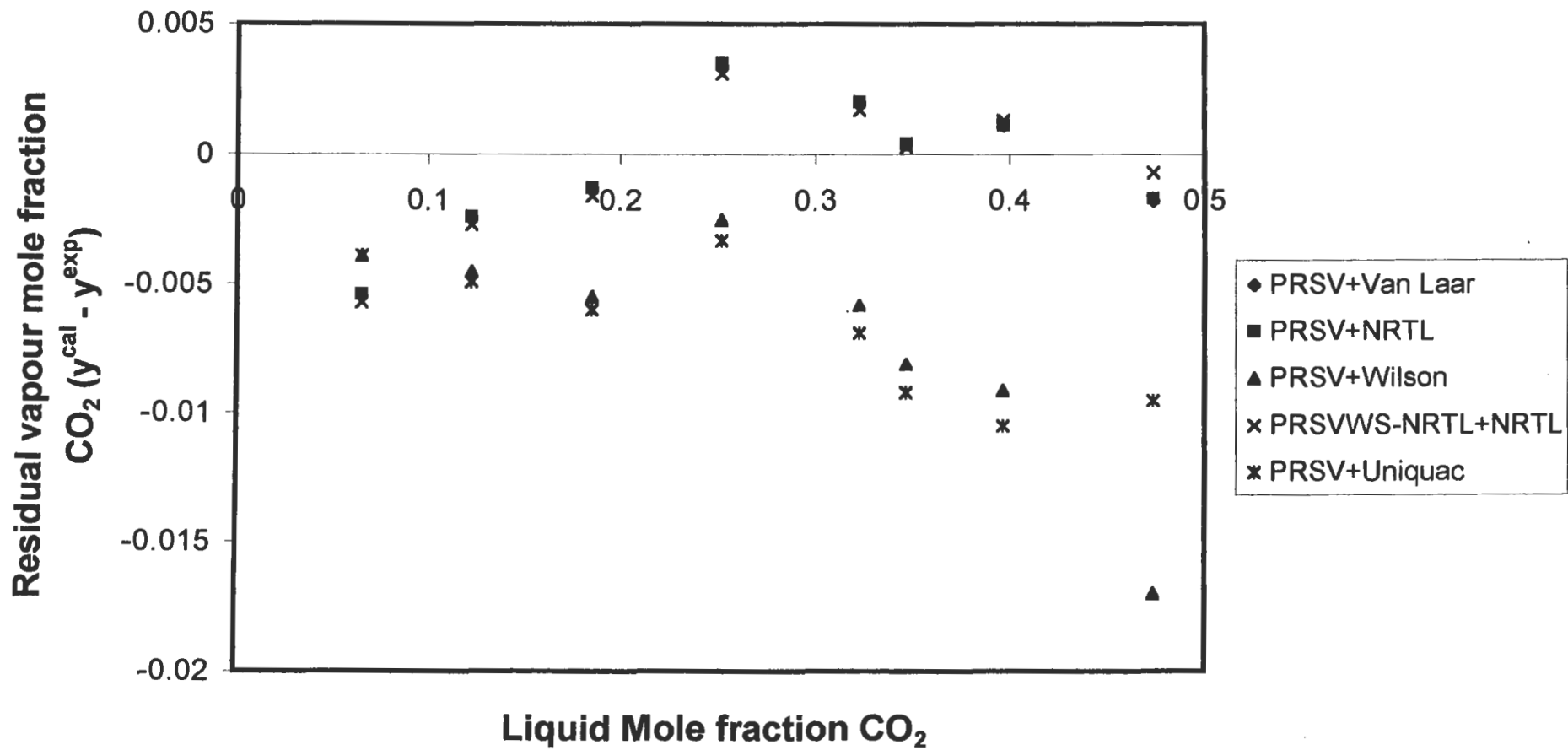


Figure 8-58: Residual plot of vapour composition for the Carbon Dioxide + Methanol System at 90 °C

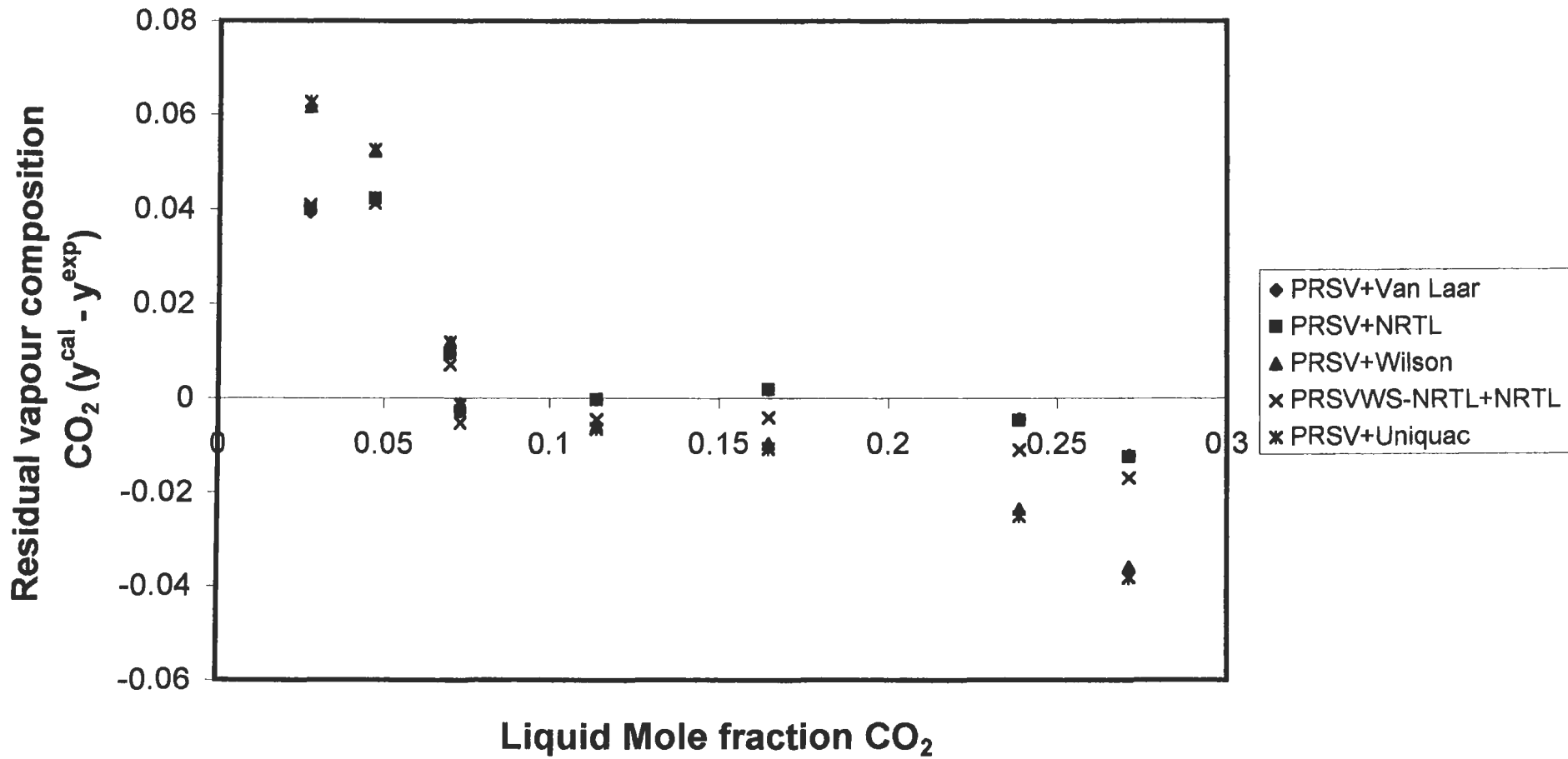
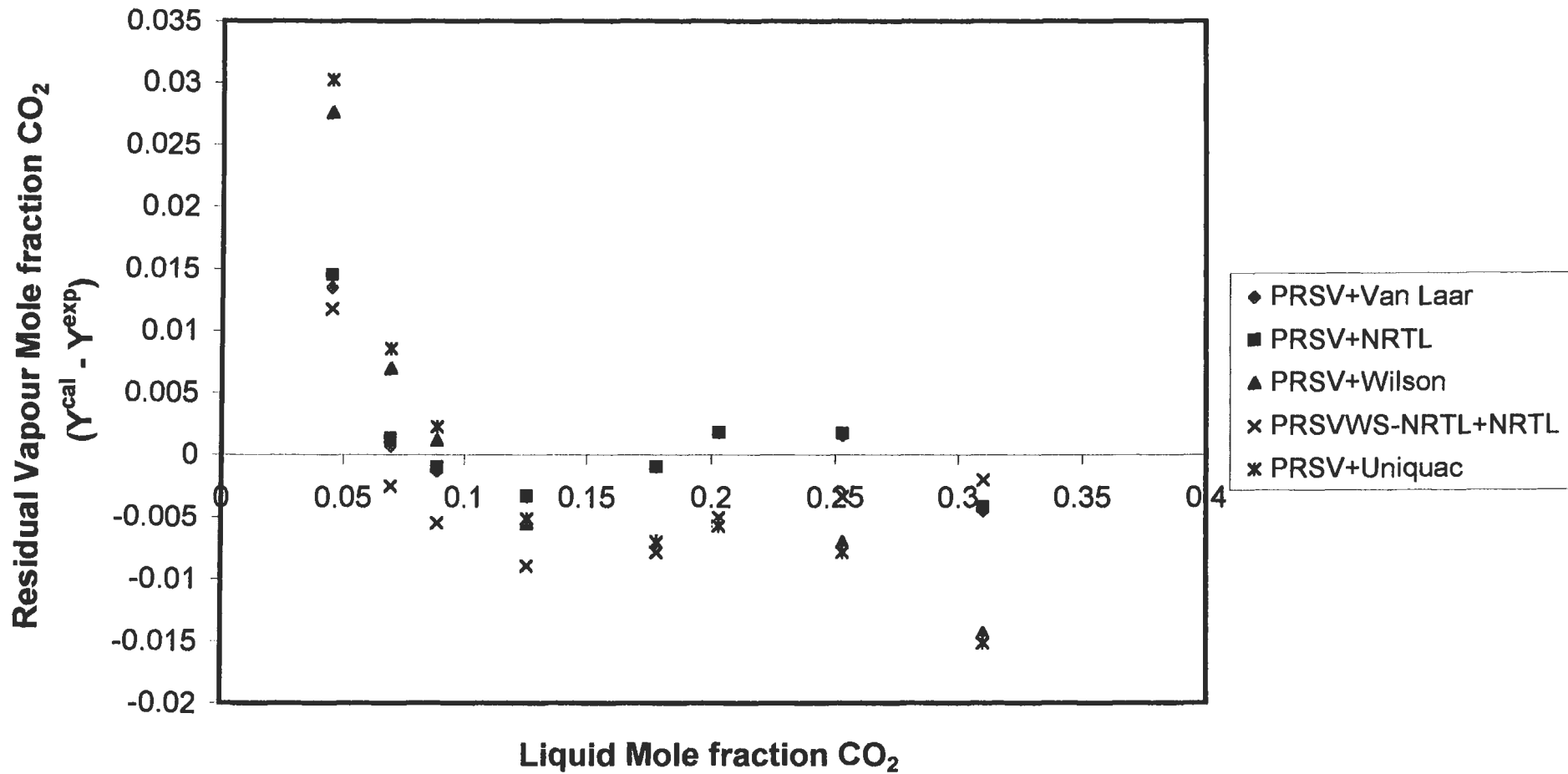


Figure 8-59: Residual plot of vapour composition for the Carbon Dioxide + Methanol System at 100 °C



The 90 and 100 °C isotherms have % inconsistencies below 5 % across the composition range. This implies the data are very good according to the Chueh et al. test, which is confirmed by the residual plot indicated in Figures 8-58 and 8-59.

8.7.3. Propane + 1-Propanol System

The Chueh et al. [1965] consistency test undertaken for the propane + 1-propanol system is summarized in Tables 8-41 and 8-42 for the 105.1 and 120 °C isotherms respectively. For both isotherms the % inconsistencies are fairly high, between approximately 8.7 % and 4.2 % for the 105.1 °C and 0.8 % and 8 % for the 120 °C isotherm.

x_1	Area 1	Area 2	Area 3	LHS	RHS	term1	term2	term3	% Diff.	% inconsistency
0.10530	0.39894	0.00965	0.01865	0.42724	0.44580	-1.60296	1.64588	0.40288	0.01856	4.25087
0.37190	1.28208	0.11599	0.06505	1.46208	1.58548	-2.02647	2.28323	1.32872	0.12341	8.09867
0.48970	1.60257	0.20531	0.08251	1.89028	2.05526	-1.87601	2.27677	2.27677	1.65450	8.36301
0.70000	2.03572	0.42793	0.10599	2.56912	2.80316	-1.28554	2.12240	1.96630	0.23404	8.71293

Table 8-41: Summary of Chueh et al. [1965] consistency test for the propane + 1-propanol system at 105.1 °C

x_1	Area 1	Area 2	Area 3	LHS	RHS	term1	term2	term3	% Diff.	% inconsistency
0.10230	0.35556	0.00718	0.02213	0.38487	0.38803	-1.41059	1.43796	0.36036	0.00316	0.81781
0.42890	1.40731	0.05465	0.08782	1.54970	1.67797	-2.15589	2.47764	1.35623	0.12827	7.94814
0.54970	1.74759	0.08641	0.10536	1.93912	2.09958	-2.08265	2.57941	1.60282	0.16046	7.94612
0.90000	2.43995	0.19798	0.13193	2.76849	2.99778	-1.03846	2.76589	1.27035	0.22929	7.95294

Table 8-42: Summary of Chueh et al. [1965] consistency test for the propane + 1-propanol system at 120 °C

According to the Chueh et al. test, one would have to rate the thermodynamic consistency of the data to be fair to good. Viewing the residual plots for the system, there is even scatter about the zero x-axis, but the deviation in the scatter is more than 1 %. For some points the scatter is as high as 3 to 5 % above and below the zero x-axis. Taking both tests into account, one would be doubtful about the thermodynamic consistency of the data, but would still rate it as satisfactory.

The models to compute the vapour phase fugacity coefficients and the residual vapour compositions were not able to properly correlate the experimental data for the propane + 1-propanol system, as has been discussed before, and this is the reason for the high % inconsistencies and large residuals computed. The true consistency/inconsistency of the data is therefore difficult to infer with conviction.

Figure 8-60: Residual plot of vapour composition for the Propane + 1-Propanol System at 105.1 °C isotherm

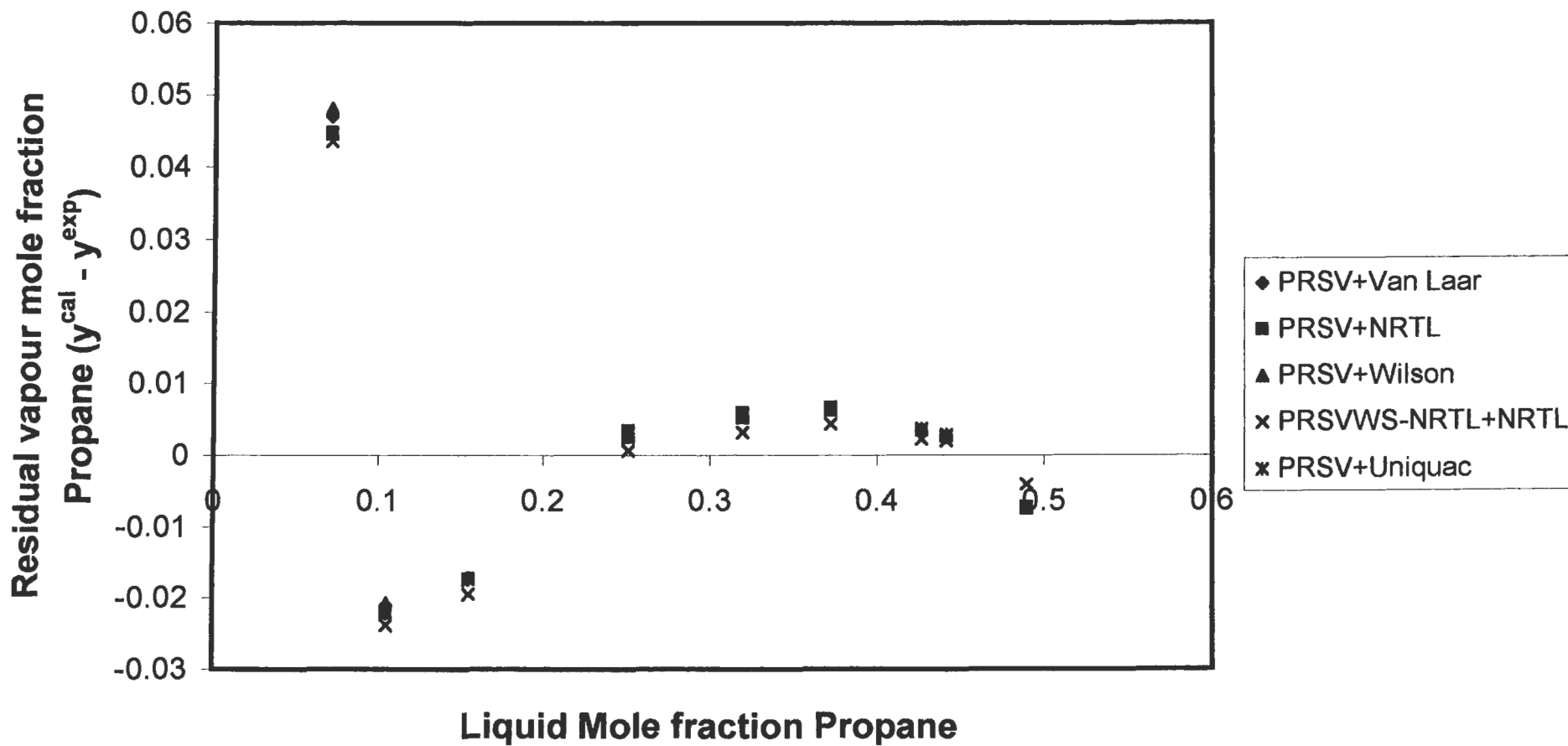
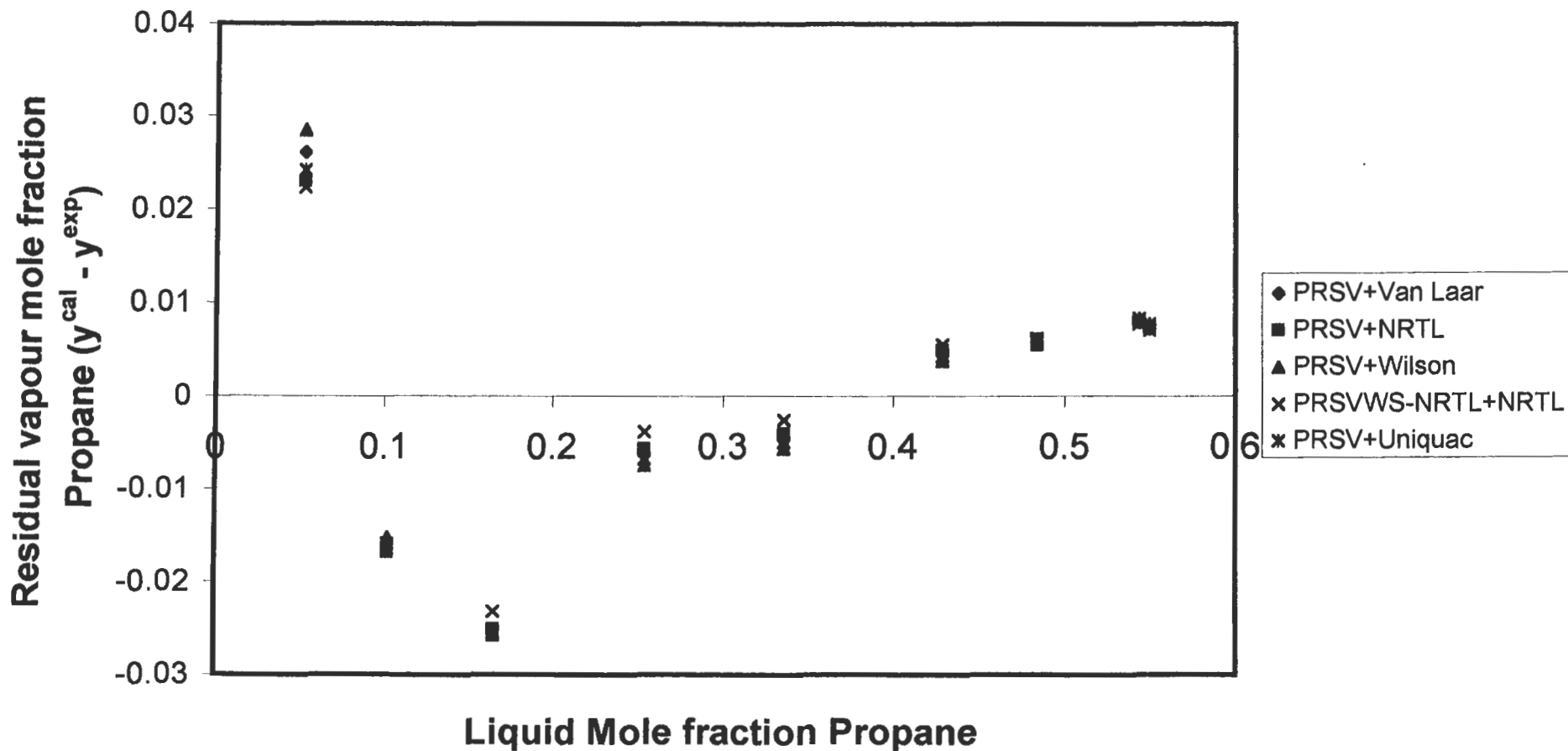


Figure 8-61: Residual plot of vapour composition for the Propane + 1-Propanol System at 120 °C isotherm



8.8. DETERMINATION OF SECOND VIRIAL COEFFICIENTS

The method of Jones and Kay [1967 (a,b)] and Wilson et al. [1984] was slightly modified to compute the second virial coefficients for the propane, nitrogen and propane + nitrogen binary system. The virial EOS was written in terms of volume, number of moles and the virial coefficient as follows:-

$$P = \frac{nRT}{V} + BRT + \frac{CRTn^3}{V^3} \quad (8-11)$$

The Marquardt [1963] least squares method was then used to minimize the error between the computed pressure via Equation (8-11) and the experimental pressure by varying the virial coefficients and the number of moles. The objective function was defined by Equation (8-12).

$$S = \sum_{i=1}^n \left(\frac{P_i^{calc} - P_i^{exp}}{P_i^{exp}} \right)^2 \quad (8-12)$$

The objective function was defined in terms of pressure because of all the measured variables, i.e. pressure, temperature and volume, the variable known with the greatest certainty was pressure. The volume (total volume) was computed by calibrating the cell with a gas of known virial coefficient. The initial volume was thus known with the least certainty. In fact, sensitivity analysis shows that the initial volume has the greatest affect on the computed second virial coefficients. A one percent uncertainty in the initial volume can produce as large as a 5 to 10 % uncertainty in the computed second virial coefficients.

For all P-V-T measurements undertaken, problems were encountered in zeroing the piston to the same initial total volume, and this is probably the reason why there are discrepancies between the computed second virial coefficients and literature data.

The computation method to determine the initial total volume and the change in volume is detailed in Appendix F.5.

CHAPTER NINE

CONCLUSIONS

A static type isothermal equilibrium apparatus for HPVLE measurements was designed that was very compact and user friendly. It has a maximum combined pressure- and temperature-operating limit of 175 bar and 175 °C respectively. The equilibrium cell has two pairs of sapphire viewing windows that permits direct viewing of the equilibrium cell contents. A novel sampling mechanism, utilizing a two-position six-port VALCO GC sampling valve was developed for sampling of the equilibrium liquid and vapour phases. With the sampling mechanism employed, no disturbances to the equilibrium phases occurred during the sampling procedure and the continuous flow of liquid through the valve sample loop ensured that the sampled liquid was always representative. This novel sampling method was very successful and gave highly reproducible results. The apparatus has a moveable piston that allows for the equilibrium cell volume to be varied. In the variable volume mode of operation, P-V-T measurements, as well as HPVLE measurements via the dew and bubble point method are possible. The P-V-T measurement capabilities have been demonstrated for the apparatus and HPVLE measurements for the carbon dioxide + toluene, carbon dioxide + methanol and propane + 1-propanol systems were undertaken. The apparatus produced experimental HPVLE data that compared excellently with published literature data and the P-V-T capability was shown to be satisfactory. With slight modification to the equipment and procedure, the accuracy of P-V-T data could be further improved. The design also incorporated a feature for analyzing two liquid phases in systems where they may occur. This feature awaits further testing and development and is discussed further under recommendations.

The equilibrium cell was positioned in an air-bath, which had an internal jacket of copper cladding and Fibrefrax insulation. The copper cladding and Fibrefrax insulation together with the externally mounted heating loop ensured that the equilibrium cell was shielded from radiative interchange and that highly isothermal control was achieved.

HPVLE measurements for the carbon dioxide + toluene system at 38, 80 and 118.3 °C were undertaken as a test of the equipment and experimental procedures. There was excellent agreement between literature data and data measured in this project. Further HPVLE measurements were undertaken for the carbon dioxide + methanol system at 40, 90 and 100 °C and the propane + 1-propanol system at 105.1 and 120 °C. There was very good agreement with

literature for the 40 and 100 °C isotherms of carbon dioxide + methanol. The 90 °C isotherm had not previously been measured. The measurements for the propane + 1-propanol system at the 105.1 and 120 °C indicated a slight discrepancy between the experimental data of this project and that of Mühlbauer and Raal [1993] for the vapour phase. It is believed though that the measured data are superior to the literature data as the equipment and sampling procedure utilized in this project were superior to those used in Mühlbauer and Raal [1993].

P-V-T measurements were undertaken for propane and nitrogen at 50, 75 and 100 °C. Measurements were also undertaken for the propane + nitrogen binary system at 75 °C. Second virial coefficients were computed from the measured P-V-T data and there were reasonable comparisons with literature data. The second virial coefficients and P-V-T data were found to be very sensitive to the initial cell volume, and recommendations have been made to rectify the problem by construction changes to the upper portion of the HPVLE cell or by PC control of the stepper motor.

Modeling of the HPVLE data measured was undertaken using both the direct and combined methods. Interaction parameters obtained by fitting of the experimental data to various models are available, but are too numerous to mention in this section. Modeling for the carbon dioxide + toluene and carbon dioxide + methanol was successfully achieved using a number of direct and combined method models. For the propane + 1-propanol system however, satisfactory modeling could not be achieved for the vapour curve and suggestions are made for the use of a Hole Theory EOS. The combined and direct method model used performed equally well for most systems, and for the systems studied there is no clear indication of which is the better method of data reduction.

Data extrapolation and prediction was illustrated using the Wong-Sandler and Huron-Vidal type mixing rules for the carbon dioxide + methanol and propane + 1-propanol systems. For these systems the extrapolation and prediction methods performed reasonably well.

Critical properties were successfully computed for the system investigated using the method of Deiters and Schneider [1976]. Predictions of critical temperature, pressure, volume and compressibility factor were undertaken using the SRK, PR and PRSV EOS.

Consistency testing was undertaken for all the systems measured with the criterion being whether the system passed the Chueh et al. [1965] test and the residual plots test as indicated in Prausnitz et al. [1980]. All the system passed the consistency tests and the HPVLE data measured were thus deemed to be thermodynamically consistent.

CHAPTER TEN

RECOMMENDATIONS

The apparatus discussed in this project was designed to be compact and versatile. It is capable of measuring P-V-T and HPVLE data, as well as HPVLE data via the dew- and bubble point methods. The following recommendations should enhance its ability in all of the modes of operation and increase its versatility:-

1. Larger jet-mixers.
2. Modification for larger operating temperature range.
3. Modification of the equipment for logging of data and control via a personal computer.
4. Greater compression ratio in the equilibrium cell and the "propane" compressor.
5. Insertion of a catalyst basket.

10.1. LARGER JET-MIXERS

The jet-mixers designed in this project were undersized. This was as a result of the sample loops on the GC sampling valves being larger than originally envisaged. This meant that the jet-mixer operating temperatures had to be set extremely high in order to ensure that no condensation occurred in the unit. The jet-mixers were at a far higher temperature than the surrounding air in the bath and this created hot spots in the air-bath despite appreciable thermal insulation. By increasing the size of the jet-mixer to approximately 500 cm³, the operating temperatures for the jet-mixers will be significantly reduced. This would also increase the feasibility of operation of the HPVLE apparatus at sub-ambient temperatures.

10.2. MODIFICATION FOR LARGER OPERATING TEMPERATURE RANGE

Currently the operating limits for the apparatus in terms of temperature are from room temperature to approximately 175 °C. By removal of the variable-volume piston and its assembly and replacement with a simple flange, the upper limit for temperature can be extended to approximately 230 °C. This is however at the expense of the upper limit of operation for pressure, which would decrease drastically (as a result of the limits of operation for the GC sampling valves). If all the Viton "o"-rings had to be replaced with some derivative that could

withstand higher temperature (e.g. Kalrez), then the upper limit for temperature could be extended to approximately 350 °C.

The lower limit of operation for temperature can be lowered by the addition of a refrigeration unit. This can simply and elegantly be undertaken by inserting refrigeration coils (cross-flow exchanger) into the box that currently houses the blower and the heating elements. Calculations indicate that an exchanger designed for this limited space would produce enough duty to reduce the temperature in the air-bath to approximately -25 °C. This would however mean that the air-bath would have to be more effectively insulated and sealed. It would probably require that the air-bath be filled with dry nitrogen so that condensation of water vapour does not occur in the bath. Condensation of water vapour leads to ice formation on the exchanger surfaces and this would effectively reduce the duty.

10.3. MODIFICATION OF EQUIPMENT FOR DATA-LOGGING AND CONTROL

All temperature and pressure measurements that are currently displayed on the instrumentation panel of the apparatus could be channeled to a personal computer and logged or controlled with the latter. The stepper motor could also be remotely operated from the personal computer. This would make operation in the dew- and bubble point mode of operation much more feasible, as there would be continuous logging of pressure and volume measurements. This would make identification of the breaks in the P-V curve much easier and consequently the vapour-liquid equilibria measurements more accurate.

P-V-T measurements could also be simplified and made more accurate. With computer operation, there would be exact control over the stepper motor, making it possible to exactly zero the piston position and change the volume of the equilibrium chamber. One of the drawbacks with the current setup for P-V-T measurements is that the zero position is not exactly known and this leads to inaccuracies in the P-V-T measurements.

10.4. GREATER COMPRESSION RATIO

The equilibrium cell currently has a compression ratio of approximately 2:1. Redesigning the cell such that the length to internal diameter ratio is larger can drastically increase the

compression ratio for the variable-volume cell. This would mean more travel for the piston and consequently a larger compression ratio. Currently the travel of the piston is limited by the placement of the sapphire windows, the upper stirrer and the sampling ports for the GC valves. This is as a result of the sealing mechanism for the piston head, which seals on a double “o”-ring.

The “propane” compressor was designed to compress propane to pressures higher than its bottle pressure so as to enable VLE measurements in the higher pressure region for the propane + 1-propanol system. With the current compressor problems were encountered in obtaining pressures higher than 40 bar for propane. A redesign of the compressor such that the propane chamber was much larger than the compressed air chamber, would produce larger compression pressures for propane.

10.5. INSERTION OF A CATALYST BASKET

The design of the upper stirrer lends itself ideally to the insertion of a basket. By inserting a basket filled with a catalyst of interest, one could undertake high-pressure VLE measurements with chemical reaction. With there being greater interest in phase equilibrium with chemical reaction, the equipment could very easily be adapted to permit measurement of VLE with chemical reaction at high pressure. According to a paper published by Verevkin and Heintz [1999, 2000], experiments of this nature would enable one to obtain heats of reaction for the specified reactions.

10.6. FUTURE WORK

The P-V-T measurement capabilities of the apparatus and the subsequent computation of second virial coefficients have been shown to be reasonable. With a bit more refinement as outlined above, publishable P-V-T and second virial coefficient data should be no problem.

The HPVLE capabilities of the apparatus have not been demonstrated by measurement of any test systems. The equipment is fully set up to undertake the measurements and all that is required is a suitable test system that produces sizeable quantities of the two liquid phases. The sampling mechanism for the second liquid phase has been tested and it works very well.

CHAPTER ELEVEN

REFERENCES

- Abbott, M. M. (1979). "Cubic equations of State: An Interpretative Review." Adv. Chem. Ser. **182**: 47-70.
- Abbott, M. M. and J. M. Prausnitz (1987). "Generalized Van der Waals Theory: A Classical Perspective." Fluid Phase Equilibria **37**(1): 29-62.
- Abbott, M.M. and J.M. Prausnitz (1994). Modeling the Excess Gibbs Energy. S. I. Sandler (ed.). New York, Marcel Dekker, Inc: 1-86.
- Abrams, D. S. and J. M. Prausnitz (1975). "Statistical Thermodynamics of Liquid Mixtures: A New Expression for the Excess Gibbs Energy of Partly or Completely Miscible Systems." AIChE Journal **21**(1): 116-127.
- Adachi, Y., B.C.-Y. Lu and H. Sugie (1983). "Three parameter equations of state." Fluid Phase Equilibria **13**: 133-143.
- Adachi, Y. and H. Sugie (1986). "A New Mixing Rule - A modified conventional mixing rule." Fluid Phase Equilibria **23**: 103-118.
- Adachi, Y., H. Sugie, K. Nakanishi and B.C.-Y. Lu (1989). "Density-dependent local-composition mixing rules for cubic equations of state." Fluid Phase Equilibria **52**: 83-90.
- Adachi, Y., H. Sugie and B.C.-Y. Lu (1990). "Taking Advantage of Available Cubic Equations of State." The Canadian Journal of Chemical Engineering **68**(August): 639-644.
- Adams, W. R., J. A. Zollweg, W. Streett and S.S.H. Rizvi (1988). "New Apparatus for Measurement of Supercritical Fluid-Liquid Equilibria." AIChE J. **34**(8): 1387-1391.
- Adler, S. B, L. Friend, R.L. Pigford and G.M. Roselli (1960). "Thermodynamic Consistency of Binary Liquid-Vapor Equilibrium Data When One Component Is Above Its Critical

Temperature.” AICHE Journal 6(1): 104-108.

Akers, W. W., J. F. Burns, and W.R. Fairchild (1954,a). “Low-Temperature Phase Equilibria: Methane-Propane System.” I&EC 46(12): 2531-2534.

Akers, W. W., R. E. Kelley, T.G. Lipscomb (1954,b). “Low-Temperature Phase Equilibria: Carbon Dioxide-Propane System.” I&EC 46(12): 2535-2536.

Akers, W. W., D. M. Kehn, and C. Kilgore (1954,c). “Volumetric and Phase Behavior of Nitrogen-Hydrocarbon Systems: Nitrogen + n-Heptane System.” Industrial and Engineering Chemistry 46(12): 2536-2539.

Akers, W. W., L. L. Attwel, and J.A. Robinson (1954,d). “Volumetric and Phase Behavior of Nitrogen-Hydrocarbon Systems : Nitrogen + Butane System.” Industrial and Engineering Chemistry 46(12): 2539-2540.

Anderko, A. (1990). “Equation of state methods for the modeling of phase equilibria.” Fluid Phase Equilibria 61: 145-225.

Anderson, T. F., D. S. Abrams and E.A. Grens II (1978). “Evaluation of Parameters for Nonlinear Thermodynamic Models.” AICHE Journal 24(1): 20-29.

Anderson, T.F. and J.M. Prausnitz (1978). “ Application of the UNIQUAC Equation to Calculation of Multicomponent Phase Equilibria. 1. Vapor-Liquid Equilibria.” Ind. Eng. Chem. Process Des. Dev. 17: 552-561.

Anderson, T.F. and J.M. Prausnitz (1980,a). “Computational Methods for high-pressure Phase Equilibria and Other Fluid-Phase Properties Using a Partition Function. 1. Pure Fluid.” Industrial and Engineering Chemistry Process Design and Development 19: 1-8.

Anderson, T.F. and J.M. Prausnitz (1980,b). “Computational Methods for high-pressure Phase Equilibria and Other Fluid-Phase Properties Using a Partition Function. 2. Mixtures.” Industrial and Engineering Chemistry Process Design and Development 19: 9-14.

Antezana, F. J. and H. Y. Cheh (1975). “Component Fugacities in Hydrogen-Ammonia-Propane Mixtures. I. The Fugacity of Hydrogen.” Ind. Eng. Chem. Fund. 14(3): 224-232.

- Anthanasios, Z., Panagiotopoulos, A. Z. and R. C. Reid (1986,a). "Multiphase high pressure Equilibria in Ternary aqueous systems." Fluid Phase Equilibria 29: 525-534.
- Apostolou, D.A., N.S. Kalospiros and D.P. Tassios (1995). "Prediction of gas solubilities using the LCVM equation of state/excess Gibbs free energy model." Ind. Eng. Chem. Res. 34: 948-957.
- Arai, K., H. Inomata and S. Saito (1982). "Vapor – Liquid Equilibrium Calculations using new Mixing rules combining functionally different Equations of State." J. Chem. Eng. Japan 15: 1-5.
- Ashcroft, S. J., R. B. Shearn, and G.J.J. Williams (1983). "A Visual Equilibrium Cell for Multiphase Systems at Pressure up to 690 bar." Chem. Eng. Res. Des. 61(1): 51-55.
- Aucejo, A., J. B. Monton, R. Munoz and J. Wisniak (1996). "Double Azeotropy in the Benzene + Hexafluorobenzene System." Journal of Chemical and Engineering Data 41(1): 21-24.
- Bae, H. K., K. Nagahama, and M. Hirata (1981). "Measurement and Correlation of High Pressure Vapour-Liquid Equilibria for the Systems Ethylene-1-Butene and Ethylene-Propylene." Journal of Chemical Engineering of Japan 14(1): 1-6.
- Bahlke, W. H. and W. B. Kay (1932). "Physical and Thermal Properties of Petroleum Distillates." Ind. Eng. Chem 24(3): 291-301.
- Baker, L. E., A. C. Pierce and K.D. Luks (1982). "Gibbs energy Analysis of Phase Equilibria." Society of Petroleum Engineers Journal 22(5): 731-742.
- Barber, J. R., W. B. Kay, and A.S. Teja (1982,a). "A Study of the Volumetric and Phase behavior of binary systems: Part I: Critical properties of propane - perfluorocyclobutane mixtures." AIChE Journal 28(1): 134-138.
- Barber, J. R., W. B. Kay, and A.S. Teja (1982,b). "A Study of the Volumetric and Phase behavior of binary systems: Part II: Vapor-Liquid Equilibria and Azeotropic states of Propane-Perfluorocyclobutane mixtures." AIChE Journal 28(1): 138-142.
- Barber, J. R., W. B. Kay, and A.S. Teja (1982,c). "A Study of the Volumetric and Phase

- Behavior of binary systems: Part 3: P-V-T-x Data and Second Virial Coefficients of Propane-Perfluorocyclobutane mixtures." *AIChE Journal* **28**(1): 142-147.
- Battino, R., M. Banzhof, M. Bogan, and E. Wilhelm (1971). "Apparatus for Rapid Degassing of Liquids: Part III." *Analytical Chemistry* **43**(6): 806-807.
- Behrens, P. K. and S. I. Sandler (1983). "Vapor-Liquid Equilibria for the Carbon Dioxide-1-Butene System at 37.7 and 45.0 °C." *J. Chem. Eng. Data* **28**(1): 52-56.
- Bennett, A., S. Lamm, H. Orbey and S.I. Sandler (1993). "Vapor-Liquid Equilibria of Hydrocarbons and Fuel Oxygenates. 2." *J. Chem. Eng. Data* **38**(2): 263-269.
- Bertucco, A., M. Barolo and N. Elvassore (1997). "Thermodynamic Consistency of Vapour-Liquid Equilibrium Data at High Pressure." *AIChE J.* **43**(2): 547-554.
- Besserer, G. J. and D. B. Robinson (1971). "A High Pressure Autocollimating Refractometer for Determining Coexisting Liquid and Vapor Phase Densities." *The Canadian Journal of Chemical Engineering* **49**(October): 651-656.
- Bian, B., Y. Wang, J. Shi, E. Zhao, and B. C.-Y. Lu (1993). "Simultaneous determination of vapor-liquid equilibrium and molar volumes for coexisting phases up to the critical temperature with a static method." *Fluid Phase Equilibria* **90**: 177-187.
- Billingsley, D. S. and S. Lam (1986). "Critical Point Calculation with Nonzero Interaction Parameters." *AIChE Journal* **32**(8): 1393-1396.
- Bolz, A., U.K. Deiters, C.J. Peters and T.W. de Loos (1998). "Nomenclature for Phase Diagrams with Particular Reference to Vapour-Liquid and Liquid-Liquid Equilibria (Technical Report)." *Pure and Appl. Chem.* **70**(11): 2233-2257.
- Boulouvalas, C., N. Spiliotis P. Coutisikos, N. Tzouvaras and D. Tassios (1994). "Prediction of vapor-liquid equilibrium with the LCVm model: a linear combination of the Vidal and Michelsen mixing rules coupled with the original UNIFAC and the *t*-mPR equation of state." *Fluid Phase Equilibria* **92**: 75-106.
- Bradshaw, S.M. (1985). *A Static Equilibrium Cell for High Pressure and Temperature Vapour-Liquid Equilibrium Measurements*. MSc.Eng.Dissertation, University of Natal, Durban.

- Braun, G. and H. Schmidt (1984). "High Pressure Extraction of Crude Montan Wax." Ber. Bunsenges. Phys. Chem. **88**(1): 891-894.
- Brignole, E. A., P. M. Andersen and Aa. Fredenslund (1987). "Supercritical Fluid Extraction of Alcohols from Water." Ind. Eng. Chem. Res. **26**(2): 254-261.
- Brown, P. R., J. D. Moore, A.C. Lewellan and J.B. Otto (1996). "Excess molar enthalpies and excess molar volumes for (propane + propan-1-ol) at a temperature of 348.15 K and at pressures of (5, 10, and 15) MPa." Journal of Chemical Thermodynamics **28**(4): 363-370.
- Brunner, G., S. Peter, and H. Wenzel (1974). "Phase equilibrium in the Systems n-Heptane-Nitrogen, Methylcyclohexane-Nitrogen and n-Heptane-Methylcyclohexane-Nitrogen at high Pressures." The Chem. Eng. Journal **7**(1): 99-104.
- Brunner, E. (1985). "Fluid mixtures at High Pressure I. Phase separation and critical phenomena of 10 binary mixture of (a gas + methanol)." J. Chem. Thermodynamics **17**: 671-679.
- Brunner, E., W. Hultenschmidt and G. Schlichtharle (1987). "Fluid mixtures at High Pressure IV. Isothermal phase equilibria in binary mixtures consisting of (methanol + hydrogen or nitrogen or methane or carbon monoxide or carbon dioxide)." J. Chem. Thermodynamics **19**: 273-291.
- Brunner, G., J. Teich, and R. Dohrn (1994). "Phase Equilibria in Systems Containing Hydrogen, Carbon Dioxide, Water and Hydrocarbons." Fluid Phase Equilibria **100**: 253-268.
- Burguet, M. C., J. B. Monton, R. Munoz, J. Wisniak and H. Segura (1996). "Polyazeotropy in Associating Systems: The 2-Methylpropyl Ethanoate + Ethanoic Acid System." Journal of Chemical and Engineering Data **41**(5): 1191-1195.
- Campanella, E. A., P. M. Mathias and J.P. O'Connell (1987). "Equilibrium Properties of Liquid Containing Supercritical Substances." AIChE J **33**(12): 2057-2066.

- Cha, S. B., A. Fenghour, G. Saville and W.A. Wakeham (1996). "Two fluid corresponding states model: a new mixing rule approximation." Fluid Phase Equilibria 125(1-2): 33-43.
- Chang, S. D. and B. C. Y. Lu (1969). "General Consistency Test." I. Chem. E. Symposium Series (32): 3:25-3:34.
- Chang, E., J. C. G. Calado, and W.B. Streett (1982). "Vapor-Liquid Equilibrium in the System Dimethyl Ether/Methanol from 0 to 180 °C and at Pressure to 6.7 MPa." J. Chem. Eng. Data 27(3): 293-298.
- Chang, T. and R. W. Rousseau (1985). "Solubilities of Carbon Dioxide in Methanol and Methanol-Water at High Pressures: Experimental Data and Modelling." Fluid Phase Equilibria 23: 243-258.
- Chang, C. J., C.-Y. Day, C.-H Ko and K.-L. Chiu (1997). "Densities and P-x-y diagrams for Carbon Dioxide dissolution in Methanol, Ethanol, and Acetone Mixtures." Fluid Phase Equilibria 131: 243-258.
- Carborundum Company Catalogue (1995). Properties of Fibrefrax Duraback.
- Chen, W.-L., K. D. Luks, and J.P. Kohn (1989). "Three-Phase Liquid-Liquid-Vapor Equilibria in the Nitrogen + Methane + n-Heptane System." J. Chem. Eng. Data 34: 312-314.
- Chen, Y. C. and Y. C. Chen (1993). "Vapor-liquid equilibria from an improved hard convex body expansion method. Part II. Non-polar mixtures." Fluid Phase Equilibria 86: 87-109.
- Chen, A. Q., G. J. Urbanus, and K.C. Chao (1994). "A new vapor-liquid equilibrium cell and VLE data for mixtures of 1-propanol + p-xylene." Fluid Phase Equilibria 94: 281-288.
- Chen, C.-C. (1996). "Molecular Thermodynamic Model for Gibbs Energy of Mixing of Nonionic Surfactant Solutions." AIChE Journal 42: 3231-3240.
- Chen, J. T. and M. J. Lee (1996). "Vapor-Liquid Equilibria of Cyclohexanol with Carbon Dioxide, Ethane, or Nitrogen at Elevated Pressures." Journal of Chemical and Engineering Data 41(2): 339-343.

- Cheng, H., M. E. Pozo de Fernandez, J.A. Zollweg, and W.B. Streett (1989). "Vapor-Liquid Equilibrium in the Carbon Dioxide + n-Pentane from 252 to 458K at Pressures to 10MPa." J. Chem. Eng. Data 34(3): 319-323.
- Chialvo, A. A., Y. V. Kalyuzhnyi and P.T. Cummings (1996). "Solvation Thermodynamics of Gas Solubility at Sub- and Near-Critical Conditions." AIChE Journal 42: 571-584.
- Chou, G. F., R. R. Forbert, and J.M. Prausnitz (1990). "High-Pressure Vapor-Liquid Equilibria for CO₂/n-Decane, CO₂/Tetralin, and CO₂/n-Decane/Tetralin at 71.1 and 104.4 °C." J. Chem. Eng. Data 35(1): 26-29.
- Chrisochoou, A. and K. Schaber (1996). "Design of supercritical fluid extraction process for separating mixtures incurred in enzyme-catalysed reactions." Chemical Engineering and Processing 35: 271-282.
- Christiansen, L. J. and A. Fredeslund (1975). "Thermodynamic Consistency Using Orthogonal Collocation or Computation of Equilibrium Vapor Compositions at High Pressures." AIChE Journal 21(1): 49-57.
- Christou, G., R. J. Sadus and C.L. Young (1989). "Gas-Liquid Critical Properties of Binary Mixtures of n-Alkanes and 2,2,4-Trimethylpentane with the Weakly Polar Halocarbons 1,2-Dichloroethane, cis-1,2-Dichloroethene, trans-1,2-Dichloroethene, and Tetrachloromethane." Ind. Eng. Chem. Res. 28(1): 481-484.
- Christou, G., R. J. Sadus and C.L. Young (1991,a). "Phase behaviour of 1-alkanol + alkane mixtures: gas-liquid critical temperatures." Fluid Phase Equilibria 67(1): 259-271.
- Christou, G., C. Tran and C. L. Young (1991,b). "Gas-Liquid Critical Temperatures of Binary Mixtures Containing a Low Molecular Weight Polydimethylsiloxane or Hexaethylidisiloxane." Fluid Phase Equilibria 62(1): 153-162.
- Chueh, P. L., N. K. Muirbrook and J.M. Prausnitz (1965). "Part II. Thermodynamic Analysis." AIChE J. 11(6): 1097-1102.
- Chueh, P. L. and J. M. Prausnitz (1967,a). "Vapor-Liquid Equilibria at High Pressures. Vapor-Phase Fugacity Coefficients in Nonpolar and Quantum-Gas Mixtures." I&EC Fund.

6(4): 492-498.

Chueh, P. L. and J. M. Prausnitz (1967,b). "Vapor-Liquid Equilibria at High Pressures: Calculation of Critical Temperatures, Volumes, and Pressure of Nonpolar Mixtures." AICHE Journal 13(6): 1107-1113.

Chueh, P. L. and J. M. Prausnitz (1967,c). "Vapor-Liquid Equilibria at High Pressure: Calculation of Partial Molar Volumes in Nonpolar Liquid Mixtures." AICHE J 13(6): 1099-1107.

Chun, K. W., T. C. Clinkscales R.R. Davison (1971). "Vapor-Liquid Equilibrium of Triethylamine-Water and Methyldiethylamine-Water." Journal of Chemical and Engineering Data 16(4): 443-446.

Chun, S. W., W. B. Kay, and A.S. Teja (1981). "Second virial coefficients of Propane-Isomeric Mixtures." J. Chem. Eng. Data 26(3): 300-303.

Cisternas, L. A. (1987). "A Simple and Accurate Technique to Obtain Component Parameters for the Three-Parameter Equation of State." Fluid Phase Equilibria 39(1): 75-87.

Copeman, T. W. and P. M. Mathias (1986). "Recent mixing rules for equations of state." ACS Symp. Ser. 300: 352-369.

Cotterman, R. L., D. Dimitrelis and J.M. Prausnitz (1984). "Supercritical-Fluid Extraction Calculations for High-Boiling Petroleum Fractions Using Propane. Application of Continuous Thermodynamics." Ber. Bunsenges. Phys. Chem. 88(1): 796-801.

Cuadros, F. and W. Okrasinski (1996). "Vapour pressure curves obtained from different equations of state-a quantitative analysis." Chemical Engineering Science 51(17): 4189-4198.

D'Souza, R., J. R. Patrick, and A.S. Teja (1988). "High Pressure Phase Equilibria in the Carbon Dioxide - n-Hexadecane and Carbon Dioxide - Water Systems." The Canadian Journal of Chemical Engineering 66(1): 319-323.

D'Souza, R. and A. S. Teja (1988). "High-Pressure Phase Equilibria in the System Glucose + Fructose + Water + Ethanol + Carbon Dioxide." Fluid Phase Equilibria 39(1): 211-224.

- Dahl, S. and M.L. Michelsen (1990). "High-pressure vapour-liquid equilibrium with a UNIFAC based equation of state." AIChE J. **36**: 1829-1836.
- Danner, R. P. and P. A. Gupte (1986). "Density Dependent Local Composition Models: An Interpretive Review." Fluid Phase Equilibria **29**(1): 415-430.
- David, R. and J. M. Bossoutrot (1996). "Thermodynamic properties of ternary fluid mixtures from the improved perturbation theory and van der Waals one-fluid theory-II. Real mixtures." Chemical Engineering Science **51**(21): 4933-4938.
- Day, C. H., C. J. Chang and C.Y. Chen (1996). "Phase Equilibrium of Ethanol + CO₂ and Acetone + CO₂ at elevated Pressures." Journal of Chemical and Engineering Data **41**(4): 839-843.
- de Loos, T. W., W. Poot, and R.N. Lichtenthaler (1984). "Fluid Phase Equilibria in Binary Ethylene + n-Alkane Systems." Ber. Bunsenges. Phys. Chem. **88**(1): 855-859.
- de Pablo, J. J. and J. M. Prausnitz (1988). "Thermodynamics of Liquid-Liquid Equilibria Including the Critical Region." AIChE Journal **34**(10): 1595-1606.
- de Pablo, J. J. and J. M. Prausnitz (1990). "Thermodynamics of liquid-liquid equilibria including the critical region. Transformation to non-classical coordinates using revised scaling." Fluid Phase Equilibria **59**(1): 1-14.
- de Swaan Arons, J. and T.W. de Loos (1994). "Phase Behaviour: Phenomena, Significance, and Models". S.I. Sandler (ed). Models For Thermodynamic and Phase Equilibria Calculations. Marcel Dekker, Inc. 363-506.
- Debbrecht, F. J. (1985). "Qualitative and Quantitative Analysis by Gas Chromatography". Modern Practise of Gas Chromatography. R. L. Grob (editor). New York, John Wiley and Sons: 261-420.
- Deiters, U. and G. M. Schneider (1976). "Fluid Mixtures at High Pressures. Computer Calculations of the Phase Equilibria and the Critical Phenomena in Fluid Binary Mixtures from the Redlich-Kwong Equation of State." Ber. Bunsenges. Phys. Chem. **80**(12): 1316-1321.

- Deiters, U. K. and G. M. Schneider (1986,a). "High Pressure Phase Equilibria: Experimental Methods." Fluid Phase Equilibria 29(1): 145-160.
- Derr, E.L. and C.H. Deal (1969). "Analytical solutions of groups: Correlation of activity coefficients through structural group parameters." Inst. Chem. Eng. Symp. Ser. (3): 40-51.
- Di Giacomo, G., V. Brandani, G. Del Re and V. Mucciante (1989). "Solubility of Essential Oil Components in Compressed Supercritical Carbon Dioxide." Fluid Phase Equilibria 52: 405-411.
- Di Giacomo, G., S. Brandani, and G. Del Re (1994). "High Pressure Phase Equilibria of the System Phenol-m-Cresol-Carbon Dioxide." Fluid Phase Equilibria 94: 313-327.
- Din, F. (1960). "The liquid-vapour equilibrium of the system nitrogen + oxygen at pressures up to 10 atm." Trans. Far. Soc. 56(1): 663-681.
- Donohue, M. D. and P. Vimalchand (1988). "The Perturbed-Hard-Chain Theory. Extensions and Applications." Fluid Phase Equilibria 40(1): 185-211.
- Dorau, W., H. W. Kremer, and H. Knapp (1983). "An Apparatus for the Investigation of Low-Temperature, High-Pressure, Vapor-Liquid and Vapor-Liquid-Liquid Equilibria." Fluid Phase Equilibria 11(1): 83-89.
- Duncan, A. G. and M. J. Hiza (1970). "A Multipurpose Phase Equilibrium Apparatus to Study Mixtures of Cryogenic Fluids: Application to Argon-Methane." Adv. in Cryogenic Engineering 15(1): 42-45.
- Dünnebeil, S., G. Sadowski and W. Arlt (1996). "Comparison of two predictive g^E models for vapor-liquid equilibrium calculations." The Chemical Engineering Journal 61(1): 21-26.
- Dymond, J. H. and E. B. Smith (1980). The Virial Coefficients of Pure Gases and Mixtures. New York, Oxford University Press.
- Eckert, C. J. and S. I. Sandler (1986). "Vapor-Liquid Equilibria for the Carbon Dioxide-

- Cyclopentane System at 37.7, 45.0, and 60.0 °C." J. Chem. Eng. Data **31**(1): 26-28.
- Elliot, D. G., R. J. J. Chen, P.S. Chappellear and R. Kobayashi (1974). "Vapor-Liquid Equilibrium of Methane-n-Butane System at Low Temperatures and High Pressures." J. Chem. Eng. Data **19**(1): 71-77.
- Eng, R. and S. I. Sandler (1984). "Vapor-Liquid Equilibria for Three Aldehyde/Hydrocarbon Mixtures." J. Chem. Eng. Data **29**(2): 156-161.
- Englezos, P., N. Kalogerakis and P.R. Bishnoi (1990). "Simultaneous Regression of Binary VLE and VLLE Data." Fluid Phase Equilibria **61**(1): 1-15.
- Eubank, P. T., K. R. Hall, and J.C. Holster (1980). A Review of Experimental techniques for Vapour-Liquid Equilibria. In: H. Knapp and S.I. Sandler (Editors). 2nd Int. Conf. on Phase Equilibria and Fluid Properties in the Chemical Industry, Frankfurt, DECHEMA, part II. 675-687.
- Eurotherm [1995]. Installation and Operating Instructions for 808 and 818 temperature controllers.
- Fall, D. J. and K. D. Luks (1984). "Phase Equilibria Behavior of the Systems Carbon Dioxide + n-Dotriacontane and Carbon Dioxide + n-Docosane." J. Chem. Eng. Data **29**(4): 413-417.
- Fall, D. J. and K. D. Luks (1985). "Liquid-Liquid-Vapor Phase Equilibria of the Binary System Carbon Dioxide + n-Tridecane." J. Chem. Eng. Data **30**(3): 276-279.
- Feroiu, V. and D. Geană (1996). "Prediction of vapor-liquid equilibria at high pressures using activity coefficients at infinite dilution." Fluid Phase Equilibria **120**(1-2): 1-10.
- Figuiere, P., J. F. Hom, S. Laugier, H. Renon, D. Richon, and H. Szwarc (1980). "Vapor-Liquid Equilibria Up to 40 000 kPa and 400 degrees C: A New Static Method." AIChE Journal **26**(5): 872-875.
- Fink, S. D. and H. C. Hershey (1990). "Modeling the Vapor-Liquid Equilibria of 1,1,1-Trichloroethane + Carbon Dioxide and Toluene + Carbon Dioxide at 308, 233 and 353 K." Ind. Eng. Chem. Res. **29**: 295-306.

- Fischer, K. and J. Gmehling (1996). "Further development, status and results of the PSRK method for the prediction of vapor-liquid equilibria and gas solubilities." Fluid Phase Equilibria 121(1-2): 185-206.
- Fontalba, F., D. Richon, and H. Renon (1984). "Simultaneous determination of vapor-liquid equilibria and saturated densities up to 45 MPa and 433 K." Rev. Sc. Instrum. 55(6): 944-951.
- Fotouh, K. and K. Shukla (1996). "Thermodynamic properties of ternary fluid mixtures from the improved perturbation theory and van der Waals one-fluid theory-I. Model mixtures." Chemical Engineering Science 51(21): 4923-4932.
- Fotouh, K. and K. Shukla (1996). "A comparative study of numerical methods for calculating phase equilibria in fluid mixtures from an equation of state." Chemical Engineering Science 51(15): 3763-3772.
- Fowles, I. A. (1995). Gas Chromatography. 2nd edition. Chichester, Wiley.
- Fredenslund, Aa. and G. A. Sather (1970). "Gas-Liquid Equilibrium of the Oxygen-Carbon Dioxide System." J. Chem. Eng. Data 15(1): 17-22.
- Fredenslund, Aa., J. Mollerup, and L.J. Christiansen (1973). "An apparatus for accurate determination of vapor-liquid equilibrium properties and gas P-v-t properties." Cryogenics 13(1): 414-419.
- Fredenslund, Aa., J. Gmehling and P. Rasmussen (1977). Vapor-Liquid Equilibria using UNIFAC. A Group Contribution Method. Elsevier, Amsterdam.
- Fredenslund, Aa. and P. Rasmussen (1985). "From UNIFAC to SUPERFAC - and back?" Fluid Phase Equilibria 24(1): 115-150.
- Freitag, N. P. and D. B. Robinson (1986). "Equilibrium Phase Properties of the Hydrogen-Methane-Carbon Dioxide, Hydrogen-Carbon Dioxide-n-Pentane and Hydrogen-n-Pentane Systems." Fluid Phase Equilibria 31(1): 183-201.
- Fu, Y. H., H. Orbey and S.I. Sandler (1996). "Prediction of Vapor-Liquid Equilibria of

- Associating Mixtures with UNIFAC models that include Association.” Industrial and Engineering Chemistry Research 35(12): 4656-4666.
- Fuller, G. G. (1976). “A modified Redlich-Kwong-Soave equation of state capable of representing the liquid phase.” Ind. Eng. Chem. Fund. 15: 254-257.
- Galivel-Solastiouk, F., S. Laugier, and D. Richon (1986). “Vapor-Liquid Equilibrium Data for the Propane-Methanol and Propane-Methanol-Carbon Dioxide System.” Fluid Phase Equilibria 28(1): 73-85.
- Gani, R., N. Tzouvaras, R. Rasmussen and Aa. Fredenslund (1989). “Prediction of Gas Solubility and Vapor-liquid Equilibria by Group Contribution.” Fluid Phase Equilibria 47(1): 133-152.
- Garcia-Sanchez, F., B. E. Otilio Hernandez-Garduza and G. Eliosa-Jimenez (1996). “Prediction of the Azeotropic Behaviour of Binary Mixtures from Gas-Liquid P-T-x Critical Data with Cubic Equations of State.” The Canadian Journal of Chemical Engineering 74: 967-976.
- Georgeton G.K., R.L. Smith Jr. and A.S. Teja (1986). “Application of cubic equations of state to polar fluids and fluid mixtures.” ACS Symp. Ser. 300: 434-451.
- Gerald, C.F. and P.O. Wheatley (1989). Applied Numerical Analysis. 4th ed. Addison-Wesley Publishing Company, Reading, Massachusetts, USA.
- Gess, M.A., R.P. Danner and M. Nagvekar (1991). Thermodynamic Analysis of Vapor-Liquid Equilibria: Recommended Models and a Standard Data Base. Design Institute for Physical Property Data, American Institute of Chemical Engineers.
- Gibbs, W. J. (1928). The Collected Works of J. Willard Gibbs: 1. Thermodynamics. New York, Longmans.
- Gomez-Nieto, M. and G. Thodos (1978). “Vapor-Liquid Equilibrium Measurements for the Propane-Ethanol System at Elevated Pressures.” AIChE J. 24(4): 672-678.
- Gregorowicz, J., J. P. O'Connell and C.J. Peters (1996). “Some characteristics of pure fluid properties that challenge equation-of-state models.” Fluid Phase Equilibria 116: 94-101.

- Griswold, J., D. Andres, and V.A. Klein (1943). "Determination of High-Pressure Vapor-Liquid Equilibrium." Petroleum Refiner 22(6): 99-106.
- Grob, R. L. (1995). Modern Practise of Gas Chromatography. 3rd edition. New York, John Wiley & Sons.
- Gros, H. P., M. S. Zabaloy and E.A. Brignole (1996). "High-Pressure Vapor-Liquid Equilibria for Propane + 2-Butanol, Propylene + 2-Butanol, and Propane + 2-Butanol + 2-Propanol." Journal of Chemical and Engineering Data 41(2): 335-338.
- Gullevic, J.-L., D. Richon, and H. Renon (1983). "Vapor-Liquid Equilibrium Measurements up to 558 K and 7 MPa: A New Apparatus." Ind. Eng. Chem. Fund. 22: 495-499.
- Gupte, P. A., P. Rasmussen and A. Fredenslund (1986,a). "A New Group-Contribution Equation of State for Vapor-Liquid Equilibria." Ind. Eng. Chem. Fund. 25(4): 636-645.
- Gupte, P. A., P. Rasmussen, and A. Fredenslund (1986,b). "Equation of state mixing rules from G^E models." Fluid Phase Equilibria 29(1): 485-494.
- Hampson, J. W. (1996). "A Recirculating Equilibrium Procedure for Determining Organic Compound Solubility in Supercritical Fluids. Anthracene in Carbon Dioxide." Journal of Chemical and Engineering Data 41(1): 97-100.
- Hanif, N. S. M., G. S. Shyu, K.R. Hall and P.T. Eubank (1996). "Areas of J.C. Maxwell for Pure-Component Fluid-Phase Equilibria from Equations of State." Industrial and Engineering Chemistry Research 35(7): 2431-2437.
- Harmens, A. and H. Knapp (1980). "Three-parameter cubic equation of state for normal substances." Ind. Eng. Chem. Fund. 19: 291-294.
- Hayden, J. G. and J. P. O'Connell (1975). "A Generalised method for predicting Second virial coefficients." Ind. Eng. Chem. Proc. Des. Dev. 14: 209-216.
- Heidemann, R.A. (1983). "Computation of High Pressure Phase Equilibria." Fluid Phase Equilibria 14: 55-78.

- Heideman, R. A. (1996). "Excess free energy mixing rules for cubic equations of state." Fluid Phase Equilibria **116**: 454-464.
- Heidemann, R. A. and A. M. Khalil (1980). "The Evaluation of Critical Points." AIChE Journal **26**(5): 769-779.
- Heidemann, R. A. and S. L. Kokal (1990). "Combined excess free energy models and equations of state." Fluid Phase Equilibria **56**: 17-37.
- Heyen, G. (1980). "Liquid and Vapour Properties from a cubic equation of state." Proceedings of 2nd International Conference on Phase Equilibrium Fluid Properties in the Chemical Industry (H. Knapp and S.I. Sandler eds.), DECHEMA, Frankfurt/Main, 9-13.
- Heyen, G. (1981). "A Cubic Equation of State with Extended Range of Application." S. Neuman (editor) Second World Congress on Chemical Engineering, Canada, Montreal: 41-46.
- Hiaki, T., K. Takahashi, T. Tsuji, M. Hongo and K. Kojima (1994,a). "Vapour-Liquid Equilibria of Ethanol + 2,2,4-Trimethylpentane at 333.15 K and 1-Propanol + 2,2,4-Trimethylpentane at 343.15 K." J. Chem. Eng. Data **39**: 605-607.
- Hiaki, T., K. Yamato, H. Miyazawa and K. Kojima (1994,b). "Computer-aided Measurement of Vapor-Liquid Equilibrium in a Still." The Canadian Journal of Chemical Engineering **72**: 142-147.
- Hiaki, T., K. Takahashi, T. Suji, M. Hongo and K. Kojima (1995). "Vapor-Liquid Equilibria of Ethanol + Octane at 343.15 K and 1-Propanol + Octane at 358.15 K." J. Chem. Eng. Data **40**: 271-273.
- Hicks, C. P. and C. L. Young (1975). "The Gas-Liquid Critical Properties of Binary Mixtures." Chemical Reviews **75**(2): 119-175.
- Hicks, C. P. and C. L. Young (1976). "Critical Properties of Binary Mixtures." J. Chem. Soc. Faraday I **72**: 122-133.
- Hildebrand, J.H. and R.L. Scott (1962). Regular Solutions. Prentice Hall, Englewood Cliffs, NJ.

- Hong, J. H. and R. Kobayashi (1988). "Vapor-Liquid Equilibrium Studies for the Carbon Dioxide-Methanol System." Fluid Phase Equilibria **41**: 269-276.
- Hottovy, J. D., J. P. Kohn, and K.D. Luks (1981). "Partial Miscibility Behavior of the Methane-Ethane-n-Octane System." J. Chem. Eng. Data **26**: 135-137.
- Hottovy, J. D., J. P. Kohn, and K.D. Luks (1982). "Partial Miscibility Behavior of the Ternary Systems Methane-Propane-n-Octane, Methane-n-Butane-n-Octane, and Methane-Carbon Dioxide-n-Octane." J. Chem. Eng. Data **27**: 298-302.
- Hsu, J. J.-C., N. Nagarajan, and J.R.L. Robinson (1985). "Equilibrium Phase Compositions, Phase Densities, and Interfacial Tensions for CO₂ + Hydrocarbon Systems. 1. CO₂ + n-Butane." J. Chem. Eng. Data **30**: 485-491.
- Huang, S. S. S. and D. B. Robinson (1984). "Vapor-Liquid Equilibrium in the selected aromatic binary systems: m-xylene-hydrogen sulfide and mesitylene-hydrogen sulfide." Fluid Phase Equilibria **17**(1): 373-382.
- Huang, S. S. S. and D. B. Robinson (1985). "The Equilibrium Phase Properties of Selected Mesitylene Binary Systems: Mesitylene-Methane and Mesitylene-Carbon Dioxide." The Canadian Journal of Chemical Engineering **63**(1): 126-130.
- Huang, S. S. S., A. D. Leu, H.-J. Ng, and D.B. Robinson (1985). "The Phase Behavior of two Mixtures of Methane, Carbon Dioxide, Hydrogen Sulfide, and Water." Fluid Phase Equilibria **19**(1): 21-32.
- Huang, H. and S. I. Sandler (1993). "Prediction of Vapor-Liquid Equilibria at High Pressures Using Activity Coefficient Parameters Obtained from low-pressure Data: A Comparison of Two Parameter Equation of State Mixing Rules." Ind. Eng. Chem. Res. **32**(7): 1498-1503.
- Huang, J. F. and L. S. Lee (1996). "Simultaneous estimation of excess enthalpy, excess Gibbs energy and vapor-liquid equilibrium using the modified Wilson model." Fluid Phase Equilibria **121**(1-2): 27-43.
- Huron, M. J. and J. Vidal (1979). "New Mixing Rules In Simple Equations of State for Representing Vapour-Liquid Equilibria of Strongly Non-Ideal Mixtures." Fluid Phase

Equilibria 3(1): 255-271.

- Incropera, F.P. and D.P. DeWitt (1996). Introduction to Heat Transfer. 3rd ed., John Wiley and Sons, New York.
- Inomata, H., K. Arai, and S. Saito (1986). "Measurement of Vapor-Liquid Equilibria at Elevated Temperatures and Pressures using a Flow Type Apparatus." Fluid Phase Equilibria 29: 225-232.
- Inomata, H., K. Arai, and S. Saito (1987). "Vapor-liquid Equilibria for CO₂/Hydrocarbons Mixtures at Elevated Temperatures and Pressure." Fluid Phase Equilibria 36(1): 107-119.
- Inomata, H., N. Ikawa, K. Arai, and S. Saito (1988). "Vapor-Liquid Equilibria for the Ammonia-Methanol-Water System." J. Chem. Eng. Data 33(1): 26-29.
- Inomata, H., N. Nakabayashi and S. Saito (1996). "Phase equilibrium calculation with a local composition model based on Lennard-Jones potential." Fluid Phase Equilibria 125(1-2): 13-20.
- Ishihara, K., A. Tsukajima, H. Tanaka, M. Kato, T. Sako, M. Sato and T. Hakuta (1996). "Vapor-Liquid Equilibrium for Carbon Dioxide + 1-Butanol at High Pressure." Journal of Chemical and Engineering Data 41(2): 324-325.
- Iwai, Y., M. R. Margerum and B.C.-Y Lu (1988). "A New Three-Parameter Cubic Equation Of State For Polar Fluids And Fluid Mixtures." Fluid Phase Equilibria 42: 21-41.
- Iwai, Y., T. Morotomi, K. Sakamoto, Y. Koga and Y. Arai (1996). "High-Pressure Vapor-Liquid Equilibria for Carbon Dioxide + Limonene." Journal of Chemical and Engineering Data 41(5): 951-952.
- Jackson, P. L. and R. A. Wilsak (1995). "Thermodynamic consistency tests based on the Gibbs-Duhem equation applied to isothermal, binary vapor-liquid equilibrium data: data evaluation and model testing." Fluid Phase Equilibria 103: 155-197.
- Japas, M. L. and E. U. Franck (1985). "High Pressure Phase Equilibria and PVT-Data of the Water-Nitrogen System to 673 K and 250 MPa." Ber. Bunsenges. Phys. Chem. 89(1):

793-800.

- Jenning, D. W. and A. S. Teja (1989). "Vapor-Liquid Equilibria in the Carbon Dioxide-1-Hexene and Carbon Dioxide-1-Hexyne Systems." J. Chem. Eng. Data **34**(3): 305-309.
- Jennings, D. W., R. J. Lee, and A.S. Teja (1991). "Vapor-Liquid Equilibria in the Carbon Dioxide + Ethanol and Carbon Dioxide + 1-Butanol Systems." J. Chem. Eng. Data **36**: 303-307.
- Jennings, D. W. and R. C. Schucker (1996). "Comparison of High-Pressure Vapor-Liquid Equilibria of Mixtures of CO₂ or Propane with Nonane and C₉ Alkylbenzenes." Journal of Chemical and Engineering Data **41**(4): 831-838.
- Joffe, J. and D. Zudkevitch (1967). "Prediction of Critical Properties of Mixtures: Rigorous Procedure for Binary Mixtures." Chemical Eng. Progress Symposium Series **63**(81): 43-51.
- Jones, A.E. and W.B. Kay (1967,a). "The Phase and Volumetric Relations in the Helium-n-Butane System: Part I. Phase and Volumetric Behavior of Mixtures of Low Concentration." AIChE Journal **13**(4): 717-720.
- Jones, A.E. and W.B. Kay (1967,b). "The Phase and Volumetric Relations in the Helium-n-Butane System: Part II. Second Virial Coefficients for Helium-n-Butane Mixtures." AIChE Journal **13**(4): 717-725.
- Jou, F.-Y., R. D. Deshmukh, F.D. Otto and A.E. Mather (1987). "Vapor-liquid equilibria for acid gases and lower alkanes in triethylene glycol." Fluid Phase Equilibria **36**: 121-140.
- Jou, F. -Y., A. E. Mather, F.D. Otto, and J.J. Carroll (1995). "Experimental Investigation of the Phase Equilibria in the Carbon Dioxide-Propane-3 M MDEA System." Ind. Eng. Chem. Res. **34**: 2526-2529.
- Jou, F. -Y., F. D. Otto and A.E. Mather (1996). "Solubility of Mixtures of Hydrogen Sulfide and Carbon Dioxide in Aqueous Solutions of Triethanolamine." Journal of Chemical and Engineering Data **41**(5): 1181-1183.
- Kakhu, A. I. and J. Homer (1996). "Evaluation of a model for the prediction of phase equilibria

- from general molecular parameters I: vapour-liquid equilibria and enthalpy at low pressures." Chemical Engineering Science 51(1): 127- 140.
- Kalra, H., H. Kubota, D.B. Robinson, and H.-J. Ng (1978). "Equilibrium Phase Properties of the Carbon Dioxide-n-Heptane System." J. Chem. Eng. Data 23(4): 317-321.
- Kalra, H. and D. B. Robinson (1979). "Vapor-Liquid Equilibrium in a Six-Component Simulated Sour Natural Gas System at Sub-Ambient Temperatures." Fluid Phase Equilibria 3(1): 133-144.
- Kalra, H., S. Y. K. Chung, (1987). "Phase Equilibria Data for Supercritical Extraction of Lemon Flavors and Palm Oils with Carbon Dioxide." Fluid Phase Equilibria 36(1): 263-278.
- Katayama, T., K. Ohgaki, G. Maekawa, M. Goto and T. Nagano (1975). "Isothermal Vapor-Liquid Equilibria of Acetone-Carbon Dioxide and Methanol-Carbon Dioxide Systems at High Pressure." J. Chem. Eng. Japan 8(2): 89-92.
- Kato, M., H. Konishi and Hirata (1970). "New Apparatus for Isobaric Dew and Bubble Point Method: Methanol-Water, Ethyl Acetate-Ethanol, Water-1-Butanol, and Ethyl Acetate-Water Systems." Journal of Chemical and Engineering Data 15(3): 435-439.
- Kay, W. B. (1936). "Density of Hydrocarbon gases and Vapors at High Temperature and Pressure." Ind. Eng. Chem. 28(9): 1014-1019.
- Kay, W. B. (1938). "Liquid-Vapor Phase Equilibrium relations in the Ethane-n-Heptane System." Ind. Eng. Chem. 30(4): 459-465.
- Kay, W. B. and G. M. Rambosek (1953). "Liquid-Vapor Equilibrium relations in Binary Systems." Ind. Eng. Chem. 45(1): 221-226.
- Kay, W.B. and Albert (1956). "Liquid-Vapor Equilibrium Relations in the Ethane-Cyclohexane System." Ind. Eng. Chem. 48: 422-426-+-.
- Kim, C. H., P. Vimalchand, and M.D. Donohue (1986,a). "Vapor-Liquid Equilibria for Binary Mixtures of Carbon Dioxide with Benzene, Toluene and p-Xylene." Fluid Phase Equilibria 31(1): 299-311.

- Kim, H., H. M. Lin, and K.C. Chao (1986,b). "Cubic Chain-of-Rotators Equation of State." Ind. Eng. Chem. Fund. 25(1): 75-84.
- Kim, C. H., A. B. Clark, P. Vimalchand, and M.D. Donohue (1989). "High - Pressure Binary Phase Equilibria of Aromatic Hydrocarbons with CO₂ and C₂H₆," J. Chem. Eng. Data 34(4): 391-395.
- Kiran, E, H. Pohler and Y. Xiong (1996). "Volumetric Properties of Pentane + Carbon Dioxide at High Pressures." Journal of Chemical and Engineering Data 41(2): 158-165.
- Klink, A. E., H. Y. Cheh, and E.H. Amick Jr. (1975). "The Vapor-Liquid Equilibrium of the Hydrogen-n-Butane System at Elevated Pressures." AIChE Journal 21(6): 1142-1148.
- Knapp, H. (1986). "Physical properties in process design - past, present and future." Fluid Phase Equilibria 29(1): 1-21.
- Kneisl, P., J. W. Zondlo, and W.B. Whiting (1988). "An Apparatus for Measurement of Multiple-Phase Equilibria at Elevated Pressures." Ind. Eng. Chem. Res. 27(8): 1541-1543.
- Knudsen, K., E. H. Stenby and Aa. Fredenslund (1993). "A Comprehensive Comparison Of Mixing Rules for Calculation Of Phase Equilibria In Complex Systems." Fluid Phase Equilibria 82: 361-368.
- Kobayashi, R. and D. L. Katz (1953). "Vapor-Liquid Equilibria for Binary Hydrocarbon-Water Systems." I&EC 45(2): 440-451.
- Kohn, J. P. (1961). "Heterogeneous Phase and Volumetric Behavior of the Methane n-Heptane System at Low Temperatures." AIChE Journal 7(3): 514-518.
- Kojima, K. and T. Tochigi (1979). Prediction of Vapor-Liquid Equilibrium by the ASOG Method. Elsevier, Amsterdam.
- Kollar-Hunek, K., S. Kemeny, Herberger, K., P. Angyal and E. Thury (1986). "Thermodynamic consistency test for binary VLE data." Fluid Phase Equilibria 27(1): 405-425.

- Konrad, R., I. Swaid, and G.M. Schneider (1983). "High-Pressure Phase Studies on Fluid Mixtures of Low-Volatile Organic Substances with Supercritical Carbon Dioxide." Fluid Phase Equilibria **10**: 307-314.
- Kontogeorgis, G. M., E. C. Voutsas, I.V. Yakoumis and D.P. Tassios (1996). "An Equation of State for Associating Fluids." Industrial and Engineering Chemistry Research **35**(11): 4310-4318.
- Kordikowski, A. and G. M. Schneider (1995). "Fluid phase equilibrium studies on ternary and quaternary mixtures of carbon dioxide with 1-dodecanol acid, quinoxaline and 1,8-octanediol at 393.2 K at pressures up to 40 MPa." Fluid Phase Equilibria **105**: 129-139.
- Kragas, T. K., J. Pollin, R.J. Martin and R. Kobayashi (1984). "A High-Pressure-High-Temperature Chromatographic Apparatus for the measurement of Vapor-Liquid Equilibria." Fluid Phase Equilibria **16**(1): 205-213.
- Kraska, T. and K. E. Gubbins (1996,a). "Phase Equilibria Calculations with a Modified SAFT Equation of State. 1. Pure Alkanes, Alkanols and Water." Industrial and Engineering Chemistry Research **35**(12): 4727-4737.
- Kraska, T. and K. E. Gubbins (1996,b). "Phase Equilibria Calculations with a Modified SAFT Equation of State. 2. Binary Mixtures of n-Alkanes, 1-Alkanols, and Water." Industrial and Engineering Chemistry Research **35**(12): 4738-4746.
- Kubota, H., H. Inatome, Y. Tanaka and T. Makita (1983). "Vapor-Liquid Equilibria of the Ethylene-Propylene System Under High Pressure." Journal of Chemical Engineering of Japan **16**(2): 99-103.
- Kuranov, G., B. Rumpf, N.A. Smimova and G. Maurer (1996). "Solubility of Single Gases Carbon Dioxide and Hydrogen Sulfide in Aqueous Solutions of N-Methyldiethanolamine in the Temperature Range 313-413 K at Pressures up to 5 MPa." Industrial and Engineering Chemistry Research **35**(6): 1959-1966.
- Kurihara, K. and K. Kojima (1995,a). "An implicit type EOS-GE(VP) model employing vapor pressure standard state. I. Prediction of high-pressure vapor-liquid equilibria based on low temperature data." Fluid Phase Equilibria **113**(1-2): 27-43.

- Kurihara, K. and K. Kojima (1995,b). "An implicit type EOS- G^E (VP) model employing vapor pressure standard state. II. Prediction of excess enthalpy using the EOS- G^E model." Fluid Phase Equilibria 113(1-2): 45-60.
- Lacombe, R.H. and I.C. Sanchez (1976). "Statistical Thermodynamics of Fluid Mixtures." J. Phys. Chem 80(23): 2568-2580.
- Landwehr, J. C., S. Yerazunis and H.H. Steinhauser (1958). "Vapor-Liquid Equilibria of Toluene-Ethyl Alcohol and Benzene-Ethyl Alcohol." Chemical and Engineering Data Series 3(2): 231-234.
- Larsen, B.L., P. Rasmussen and Aa. Fredenslund (1987). "A modified UNIFAC Group-Contribution Model for Prediction of Phase Equilibria and Heats of Mixing." Ind. Eng. Chem. Res. 26: 2274-2286.
- Laugier, S., D. Richon, and H. Renon (1980). "Vapor-Liquid Equilibria of Hydrogen-2,2,4-Trimethylpentane and Hydrogen-Toluene Systems at High Pressures and Temperatures." J. Chem. Eng. Data 25(3): 274-276.
- Laugier, S. and D. Richon (1986). "New apparatus to perform fast determination of mixture vapor-liquid equilibria up to 10 MPa and 423 K." Rev. Sc. Instrum. 57(3): 469-472.
- Laugier, S., D. Richon, and H. Renon (1990). "Simultaneous Determination of Vapor-Liquid Equilibria and Volumetric Properties of Ternary Systems with a New Experimental Apparatus." Fluid Phase Equilibria 54: 19-34.
- Laugier, S. and D. Richon (1996). "High-Pressure Vapor-Liquid Equilibria for Ethylene + 4-Methyl-1-pentene and 1-Butene + 1-Hexane." Journal of Chemical and Engineering Data 41(2): 282-284.
- Lee, R. J. and K. C. Chao (1986). "Cubic Chain-of-Rotators Equation of State with Density-Dependent Local Composition Mixing Rules." Fluid Phase Equilibria 29(1): 475-484.
- Lee, K. H. and S. I. Sandler (1987). "The generalized Van der Waals Function-IV. Local Composition Models for Mixtures of Unequal-Size Molecules." Fluid Phase Equilibria 34(1): 113-147.

- Lee, R. J. and K. C. Chao (1988). "Extraction of 1-Methylnaphthalene and m-Cresol with Supercritical Carbon Dioxide and Ethane." Fluid Phase Equilibria 43: 329-340.
- Lee, M. J. and J. T. Chen (1994). "Vapor-liquid equilibrium for carbon dioxide/alcohol systems." Fluid Phase Equilibria 92: 215-231.
- Leet, W. A., H. M. Lin and K.C. Chao (1986). "Cubic Chain-of-Rotators Equation of State II for Strongly Polar Substances and Their Mixtures." Ind. Eng. Chem. Fund. 25(4): 695-701.
- Legret, D., D. Richon and H. Renon (1981). "Vapor Liquid Equilibria up to 100 MPa: A New Apparatus." AIChE J. 27(2): 203-207.
- Legret, D., J. Desteve, D. Richon and H. Renon (1983). "Vapor-Liquid Equilibrium Constants at Infinite Dilution Determined by a Gas Stripping Method: Ethane, Propane, n-Butane, n-Pentane in the Methane-n-Decane System." AIChE Journal 29(1): 137-144.
- Leu, A. D. and D. B. Robinson (1988). "Equilibrium-Phase Properties of the Neopentane-Carbon Dioxide Binary System." J. Chem. Eng. Data 33(3): 313-316.
- Li, Y. and A. E. Mather (1996). "Correlation and Prediction of the Solubility of CO₂ and H₂S in Aqueous Solutions of Triethanolamine." Industrial and Engineering Chemistry Research 35(12): 4804-4809.
- Lin, H.M., H. Kim, T.M. Guo and K.C. Chao (1983). "Cubic chain of rotators equation of state and vapour-liquid equilibrium calculations." Fluid Phase Equilibria 13: 143-152.
- Lin, H.M. (1984). "Peng and Robinson Equation of State for Vapour-Liquid Equilibrium Calculations for Carbon Dioxide + Hydrocarbon Mixtures." Fluid Phase Equilibria 16: 151-169.
- Lin, M. M., H. Kim, W.A. Leet, and K.C. Chao (1985). "New Vapor-Liquid Equilibrium Apparatus for Elevated Temperatures and Pressures." Ind. Eng. Chem. Fund. 24(2): 260-262.
- Lin, Y.-L., P. R. Bienkowski, V.M. Shah and H.D. Cochran (1996). "Extension of a Generalized Quartic Equation of State to Pure Polar Fluids." AIChE Journal 42: 562-

570.

- Littlewood, A. B. (1970). Gas Chromatography: principles, techniques and applications. 2nd edition. New York, Academic Press.
- Luedecke, D. and J. M. Prausnitz (1985). "Phase Equilibria for strongly non-ideal mixtures from an equation of state with density-dependent mixing rules." Fluid Phase Equilibria 22(1): 1-19.
- Luyben, W.L. (1990). Process Modeling, Simulation and Control For Chemical Engineers (2nd ed.) McGraw-Hill Publishing Company, New York.
- Lyckman, E.W., C.A. Eckert and J.M. Prausnitz (1965). "Generalized reference fugacities for phase equilibrium thermodynamics." Chemical Engineering Science 20: 685-691.
- Malanowski, S. (1982,a). "Experimental Methods for Vapour-Liquid Equilibria. II. Dew and Bubble-Point Method." Fluid Phase Equilibria 9(1): 311-317.
- Malanowski, S. (1982,b). "Experimental Methods for Vapor-Liquid Equilibria. Part 1. Circulation Methods." Fluid Phase Equilibria 8: 197-219.
- Malanowski, S. and A. Anderko (1992). "Modelling Phase Equilibria: Thermodynamic Background and Practical Tools", John Wiley and Sons, Inc. New York, USA.
- Marathe, P. and S. I. Sandler (1991). "High-Pressure Vapor-Liquid Equilibrium of Some Binary Mixtures of Cyclopentane, Argon, Nitrogen, n-Butane, and Neopentane." J. Chem. Eng. Data 36(2): 192-197.
- Marina, J.M. and D.P. Tassios (1973). "Effective local compositions in Phase Equilibrium Correlations." Ind. Eng. Chem. Proc. Des. Dev. 12: 67-71.
- Marquardt, D.W. (1963). "An Algorithm for least-squares estimation of non-linear parameters." J. Soc. Indus. App. Math 11(2): 431-441.
- Marsh, K. N. (1989). "New Methods for Vapor-Liquid-Equilibria Measurements." Fluid Phase Equilibria 52(1): 169-184.

- Martins, J. J. (1979). "Cubic equations of state: Which?" Ind. Eng. Chem. Fund. **18**: 81-97.
- Mathias, P.M. (1983). "A versatile phase equilibrium equation of state." Ind. Eng. Chem. Process Design Dev. **22**: 385-391.
- Mathias, P. M. and T. W. Copeman (1983). "Extension of the Peng-Robinson equation of state to polar fluids and fluid mixtures." Fluid Phase Equilibria **13**: 91-108.
- Mathias, P. M. and H. C. Klotz (1994). "Take a Closer Look at thermodynamic Property Models." Chem. Eng. Process (June): 67-75.
- McHugh, M. and V. J. Krukonis (1986). Supercritical Fluid Extraction Principles and Practice. Stoneham, Butterworths.
- Meacham, R. I., B. A. Buffham, G. Mason and D.W. Drott (1992). "An Isothermal-Enclosure Air-Bath Thermostat for Experimental Apparatus." Chem. Eng. Res. and Design **72**(Part A): 263-271.
- Melhem, G. A., R. Saini and B.M. Goodwin (1989). "A Modified Peng-Robinson Equation of State." Fluid Phase Equilibria **47**(1): 189-237.
- Meskel-Lesavre, M., D. Richon, and H. Renon (1981). "New Variable Volume Cell for Determining Vapor-Liquid Equilibria and Saturated Liquid Molar Volumes by the Static Method." Ind. Eng. Chem. Fund. **20**(3): 284-289.
- Michel, S., H. H. Hooper and J.M. Prausnitz (1989). "Mutual solubilities of water and hydrocarbons from an equation of state. Need for an unconventional mixing rule." Fluid Phase Equilibria **45**: 173-189.
- Michelsen, M. L. (1984). "Calculation of critical points and phase boundaries in the critical region." Fluid Phase Equilibria **16**: 57-76.
- Michelsen, M. L. (1990, a). "A Method for incorporating excess Gibbs free energy models in equations of state." Fluid Phase Equilibria **60**: 47-58.
- Michelsen, M. L. (1990, b). "A Modified Huron-Vidal mixing rule for cubic equations of state." Fluid Phase Equilibria **60**: 213-219.

- Michelsen, M. L. (1996). "Matching equation of state mixing rules to activity coefficient model expressions." Fluid Phase Equilibria **121**(1-2): 15-26.
- Michelsen, M. L. and R. A. Heideman (1996). "Some Properties of Equation of State Mixing Rules Derived from Excess Gibbs Energy Expressions." Industrial and Engineering Chemistry Research **35**(1): 278-287.
- Michelsen, M.L. and H. Kistenmacher (1990). "On composition dependent interaction coefficients." Fluid Phase Equilibria **58**: 229-230.
- Mohamed, R. S. and G. D. Holder (1987). "High Pressure Phase Behavior in Systems Containing CO₂ and Heavier Compounds with similar Vapor Pressures." Fluid Phase Equilibria **32**(1): 295-317.
- Mollerup, J.M. (1980). "Thermodynamic Properties from Corresponding States Theory." Fluid Phase Equilibria **4**: 11-34.
- Mollerup, J. M. (1981). "A note on Excess Gibbs Energy Models, Equations of State and the local Composition Concept." Fluid Phase Equilibria **7**: 121-138.
- Mollerup, J. (1986). "A note on the derivation of mixing rules from excess Gibbs free energy models." Fluid Phase Equilibria **25**: 323-327.
- Morris, W. O. and M. D. Donohue (1985). "Vapor-Liquid Equilibria in Mixtures Containing Carbon Dioxide, Toluene, and 1-Methylnaphthalene." J. Chem. Eng. Data **30**(3): 259-263.
- Moser, B. and H. Kistenmacher (1987). "An Analysis of the industrial use of a phase equilibria prediction model based on Thermodynamic Perturbation Theory." Fluid Phase Equilibria **34**: 189-201.
- Mühlbauer, A. L. (1990). PhD Dissertation. Measurement and Thermodynamic Interpretation of High Pressure Vapour-Liquid Equilibrium Data. Department of Chemical Engineering. Durban, University of Natal.
- Mühlbauer, A. L. and J. D. Raal (1991). "Measurement and thermodynamic interpretation of

- high-pressure vapour-liquid equilibria in the toluene-CO₂ system.” Fluid Phase Equilibria **64**(1): 213-236.
- Mühlbauer, A. L. and J. D. Raal (1993). “High-Pressure Vapor-Liquid Equilibria in the Propane-1-Propanol System.” AIChE Journal **39**(4): 677-688.
- Mühlbauer, A. L. and J. D. Raal (1995). “Computation and thermodynamic interpretation of high-pressure vapour-liquid equilibria-a review.” The Chemical Engineering Journal. **60**: 1-29.
- Muirbrook, N. K. and J. M. Prausnitz (1965). “Multicomponent Vapor-Liquid Equilibria at High Pressures: Part 1. Experimental Study of the Nitrogen-Oxygen-Carbon Dioxide System at 0°C.” AIChE Journal **11**(6): 1092-1096.
- Muller, A., J. Winkelmann and J. Fischer (1996). “Backbone Family of Equations of State: 1. Nonpolar and Polar Pure Fluids.” AIChE Journal **42**: 1116-1190.
- Na, S. Y. and D. H. Kim (1996). “New Invariant Asymmetric Mixing Rules.” Journal of Chemical Engineering of Japan **29**(1): 12-19.
- Nagahama, K. (1996). “VLE measurements at elevated pressures for process development.” Fluid Phase Equilibria **116**: 361-372.
- Nagahama, K., S. Suda, T. Hakuta, and M. Hirata (1971). “Determination of Vapour-Liquid Equilibrium From Total Pressure Measurement – C₃ – Hydrocarbon – Solvent.” Sekuju Gakkai Shi **14**(4): 252-256.
- Nagarajan, N. and J. R. L. Robinson (1986). “Equilibrium Phase Compositions, Phase Densities, and Interfacial Tensions for CO₂ + Hydrocarbon Systems. 2. CO₂ + n-Decane.” J. Chem. Eng. Data **31**: 168-171.
- Nagarajan, N. and R. L. Robinson Jr. (1987). “Equilibrium Phase Compositions, Phase Densities, and Interfacial Tensions for CO₂ + Hydrocarbon Systems. 3. CO₂ + Cyclohexane. 4. CO₂ + Benzene.” J. Chem. Eng. Data **32**(3): 369-371.
- Nagarajan, N. R., A. S. Cullick and A. Griewank (1991,a). “New strategy for phase equilibrium and critical point calculations by thermodynamic energy analysis. Part II. Critical point

- calculations." Fluid Phase Equilibria **62**: 211-223.
- Nagarajan, N. R., A. S. Cullick and A. Griewank (1991,b). "New strategy for phase equilibrium and critical point calculations by thermodynamic energy analysis. Part I. Stability analysis and flash." Fluid Phase Equilibria **62**: 191-210.
- Nakayama, T., H. Sagara, K. Arai, and S. Saito (1987). "High Pressure Liquid-Liquid Equilibria for the System of Water, Ethanol and 1,1-Difluoroethane at 323.2 K." Fluid Phase Equilibria **38**(1): 109-127.
- Nasir, P., R. J. Martin and R. Kobayashi (1980/1981). "A novel apparatus for the measurement of the phase and volumetric behavior at high temperatures and pressure and its application to study VLE in the hydrogen-tetralin system." Fluid Phase Equilibria **5**(1): 279-288.
- Ng, H. -J. and D. B. Robinson (1978). "Equilibrium Phase Properties of the Toluene-Carbon Dioxide System." Journal of Chemical and Engineering Data **23**(4): 325-327.
- Ng, H. -J. and D. B. Robinson (1979). "The Equilibrium Phase Properties of Selected Naphthenic Binary Systems: Carbon Dioxide-Methylcyclohexane, Hydrogen Sulfide-Methylcyclohexane." Fluid Phase Equilibria **2**(1): 283-292.
- Nies E., L.A. Kleintjens, R. Koningsveld, R. Simha, and R.K. Jain (1983). "On Hole Theories for Liquids and Compressed Gases: Ethylene" Fluid Phase Equilibria **12**(1): 11-27
- Niesen, V., A. Palavra, A.J. Kidnay, and V.F. Yesavage (1986). "An Apparatus for Vapor-Liquid Equilibrium at Elevated Temperatures and Pressures and Selected Results for the Water-Ethanol and Methanol-Ethanol Systems." Fluid Phase Equilibria **31**(1): 283-298.
- Novenario, C. R., J. M. Caruthers and K.C. Chao (1996). "A Mixing Rule To Incorporate Solution Model into Equation of State." Industrial and Engineering Chemistry Research **35**(1): 269-277.
- Occhiogrosso, R. N., J. T. Igel, and M.A. McHugh (1986). "Phase Behaviour of Carbon Dioxide-Aromatic Hydrocarbon Mixtures." Fluid Phase Equilibria **26**: 165-179.

- Ohgaki, K. and T. Katayama (1975). "Isothermal Vapor-Liquid Equilibria for Systems Ethyl Ether-Carbon Dioxide and Methyl Acetate-Carbon Dioxide at High Pressures." Journal of Chemical and Engineering Data **20**(3): 264-267.
- Ohgaki, K. and T. Katayama (1976). "Isothermal Vapor-Liquid Equilibrium Data for Binary Systems Containing Carbon Dioxide at high-pressures: Methanol-Carbon Dioxide, n-Hexane-Carbon Dioxide, and Benzene-Carbon Dioxide Systems." Journal of Chemical and Engineering Data **21**(1): 53-55.
- Ohta, T. (1996). "On the application of G^E models to high-pressure vapor-liquid equilibrium calculations." The Chemical Engineering Journal **61**(1): 27-34.
- Orbey, H., S.I. Sandler and D.S.H. Wong (1993). "Accurate equation of state predictions at high temperatures and pressures using the existing UNIFAC model." Fluid Phase Equilibria **85**: 41-54.
- Orbey, H. and S. I. Sandler (1994). "Vapour-Liquid Equilibrium of Polymer Solutions Using a Cubic Equation of State." AIChE Journal **40**(7): 1203-1209.
- Orbey, H. and S. I. Sandler (1995, a). "Reformulation of Wong-Sandler Mixing Rule for Cubic Equations of State." AIChE Journal **41**(3): 683-689.
- Orbey, H. and S.I. Sandler (1995, b). "On the combination of equation of state and excess free energy model." Fluid Phase Equilibria **111**: 53-70.
- Orbey, H. and S. I. Sandler (1996). "A comparison of various cubic equation of state mixing rules for the simultaneous description of excess enthalpies and vapor-liquid equilibria." Fluid Phase Equilibria **121**(1-2): 67-83.
- Orbey, H. and S.I. Sandler (1997). "A comparison of Huron-Vidal type mixing rules of mixtures of compounds with large size differences, and a new mixing rule", Fluid Phase Equilibria, **132**: 1-14.
- Pak, S. C. and W. B. Kay (1972). "The Critical Properties of Binary Hydrocarbon Systems." Ind. Eng. Chem. Fund. **11**(2): 255-267.
- Pan, H. Q. and T. M. Guo (1996). "A modified Kurihara mixing rule and a comparison of

- density-independent mixing rules." The Chemical Engineering Journal **61**(1): 213-226.
- Panagiotopoulos, A. Z. and R. C. Reid (1986,b). "New mixing rules for cubic equations of state for highly polar asymmetric mixtures." in K.C. Chao and R.L. Robinson (editors), *Equations of State – Theories and Application.*, Washington, DC. ACS Symp. Ser. **300**: 571-582.
- Panayiotou, C. and J.H. Vera (1981). "Local Compositions and Local Surface Area Fractions: A Theoretical Discussion." Canadian J. Chem. Eng **59**: 501-505.
- Patel, N.C. and A.S. Teja (1982). "A new cubic equation of state for fluids and fluid mixtures." Chem. Eng. Sc. **37**: 463-473.
- Peng, D. Y. and D. B. Robinson (1976). "A new two constant equation of state." Ind. Eng. Chem. Fund. **15**: 59-64.
- Peng, D. and D. B. Robinson (1977). "A Rigorous Method for Predicting the Critical Properties of Multicomponent Systems from an Equation of State." AIChE J **23**(2): 137-145.
- Peschel, W. and H. Wenzel (1984). "Equation-of -State Predictions of Phase equilibria at Elevated Pressure in Mixtures Containing Methanol." Ber. Bunsenges. Phys. Chem. **88**(1): 807-812.
- Pfohl, O., P. Auramova, and G. Brunner (1997). "Two- and Three- Phase equilibria in systems containing benzene derivatives, carbon dioxide, and water at 373.15 K and 10-30 MPa." Personal communication.
- Pohler, H. and E. Kiran (1996). "Volumetric Properties of Carbon Dioxide + Toluene at High Pressures." Journal of Chemical and Engineering Data **41**(3): 482-486.
- Plocker, U., H. Knapp and J.M. Prausnitz (1978). "Calculation of High Pressure Vapor-Liquid Equilibria from a Corresponding States Correlation with Emphasis on Asymmetric Mixtures." Ind. Eng. Chem. Process Des. Dev. **17**: 324-332
- Pozo, M. E. and W. B. Streett (1984). "Fluid Phase Equilibria for the System Dimethyl Ether/Water from 50 to 220 °C and Pressures to 50.9 MPa." J. Chem. Eng. Data **29**(3): 324-329.

- Prausnitz, J.M., C.A. Eckert, R.V. Orge and J.P. O'Connell (1967). Computer Calculations for Multicomponent Vapor-Liquid Equilibrium. Englewood Cliffs, N.J., Prentice Hall.
- Prausnitz, J. M. and P. L. Chueh (1968). Computer Calculation of High Pressure Vapor-Liquid Equilibria. Englewood Cliffs N.J., Prentice Hall.
- Prausnitz, J. M., T. Anderson, E. Grens, C. Eckert, R. Hsieh and J. O'Connell (1980). Computer Calculations for Multicomponent Vapor-Liquid and Liquid-Liquid Equilibria. Englewood Cliffs N.J., Prentice Hall.
- Prausnitz, J. M., R. N. Lichtenthaler, and E.G. Azevedo (1986). Molecular Thermodynamics of Fluid-Phase Equilibria (2nd ed.). Englewood Cliffs N.J., Prentice Hall.
- Prausnitz, J. M. (1996). "Molecular thermodynamics: opportunities and responsibilities." Fluid Phase Equilibria 116: 12-26.
- Price, A. R. and R. Kobayashi (1959). "Low temperature Vapor-Liquid Equilibrium in Light Hydrocarbon Mixtures: Methane-Ethane Propane System." Journal of Chemical and Engineering Data 4(1): 40-52.
- Raal, J. D., R. K. Code and D.A. Best (1972). "Examination of Ethanol-n-Heptane, Methanol-n-Hexane Systems using new Vapor-Liquid Equilibrium Still." Journal of Chemical Engineering Data 17(2): 211-216.
- Raal, J. D., G. Jeffery and T.G. Tonkin (1980). Chemical Engineering Research Group Report: 331, CSIR, Pretoria.
- Raal, J. D. and P. Naidoo (1990). "Excess Enthalpy Measurements Using A Novel Highly Refined Microflow Calorimeter and the Prediction of Vapour-Liquid Equilibria from Such Data." Fluid Phase Equilibria 57(1): 147-160.
- Raal, J.D. (1992). "A New Device for the Calibration of Gas Chromatographs for Gas Mixtures." Pitcon 92, New Orleans, USA.
- Raal, J. D. and C. J. Brouckaert (1992). "Vapour-Liquid and Liquid-Liquid Equilibria in the System Methyl Butenol-Water." Fluid Phase Equilibria 74(1): 253-270.

- Raal, J. D. and A. L. Mühlbauer (1994). "The Measurement of High-Pressure Vapour-Liquid Equilibria." Developments in Chemical Engineering and Mineral Processing 2(2/3): 69-104.
- Raal, J. D. and A. L. Mühlbauer (1998). Phase Equilibria: Measurement and Computation, Taylor and Francis: Bristol, PA.
- Radosz, M. (1984). "Variable-Volume Circulation Apparatus for measuring High-Pressure Fluid-Phase Equilibria." Phys. Chem 88: 859-862.
- Radosz, M. (1986,a). "Vapor-Liquid Equilibrium for 2-Propanol and Carbon Dioxide." J. Chem. Eng. Data 31(1): 43-45.
- Radosz, M. (1986,b). "Multiphase Equilibria in High Pressure Ternary Systems Containing Secondary Alcohols and Water." Fluid Phase Equilibria 29: 515-523.
- Ramjugernath, D., M. Starzak and J.D. Raal (1997). "Mixture Critical Point Computation and High Pressure Thermodynamic Consistency Testing." Conference Proceedings: 7th National SAICChE Conference, April, Cape Town, South Africa.
- Ramjugernath D. and J.D. Raal (1999). "Modeling, Prediction and Extrapolation of High Pressure Vapour-Liquid Equilibrium Data: Direct versus Combined Methods." Proceedings of the International Conference: Progress in Computing of Physicochemical Properties. November, Warszawa, Poland.
- Redlich, O. and J. N. S. Kwong (1949). "On Thermodynamics of solutions V: An equation of state. Fugacities of gaseous solutions." Chem. Rev. 44: 233-244.
- Reid, C.R., J.M. Prausnitz, and B.E. Poling (1988). The Properties of Gases & Liquids. 4th ed. McGraw-Hill Book Co., Singapore.
- Reiff, W.-E., P. Peters-Gerth, and K. Lucas (1987). "A static equilibrium apparatus for (vapour + liquid) equilibrium measurements at high temperatures and pressures." J. Chem. Thermodynamics 19: 467-477.
- Reighard, T. S., S. T. Lee, and S.V. Olesik (1996). "Determination of methanol/CO₂ and

- acetonitrile/CO₂ vapor-liquid phase equilibria using a variable-volume view cell." Fluid Phase Equilibria 123(1-2): 215-230.
- Reklaitis, G.V. (1983). Introduction to Material and Energy Balances. John Wiley & Sons, USA.
- Renon, H. and J. M. Prausnitz (1968). "Local Compositions in Thermodynamic Excess Functions for Liquid Mixtures." AIChE J. 14(1): 135-144.
- Renon, H., S. Laugier, J. Schwartzentruber, and D. Richon (1989). "New Determinations of High Pressure Vapor-Liquid Equilibria in Binary Systems Containing n-Propylbenzene with Nitrogen or Carbon Dioxide Consistent with the Prausnitz-Keeler Test." Fluid Phase Equilibria 51(1): 285-298.
- Richon, D. (1996). "New experimental developments for phase equilibrium measurements." Fluid Phase Equilibria 116: 421-428.
- Rogers, B. L. and J. M. Prausnitz (1970). "Sample-Extrusion Apparatus for High-Pressure Vapor-Liquid Equilibria: Compositions and Densities at Pressures up to the Critical." I&EC Fund. 9(1): 174-177.
- Roof, J. G. and J. D. Baron (1967). "Critical Loci of Binary Mixtures of Propane with Methane, Carbon Dioxide, and Nitrogen." J. Chem. Eng. Data 12(3): 292-293.
- Rousseaux, P., D. Richon, and H. Renon (1983). "A Static Method for Determination of Vapour-Liquid Equilibria and Saturated Liquid Molar Volumes at High Pressures and Temperatures using a New Variable-Volume Cell." Fluid Phase Equilibria 11(1): 153-168.
- Rubio, R. G., J. A. R. Renuncio and M. Diaz Pena (1983). "Regression of Vapor-Liquid Equilibrium Data based on application of the Maximum-Likelihood Principle." Fluid Phase Equilibria 12(1): 217-234.
- Sadus, J. D. and L. Y. Colin (1987). "Critical Properties of Ternary Mixtures: Hydrocarbon, Acetone and Alkanenitrile Mixtures." Chem. Eng. Sc. 42(7): 1717-1722.
- Sadus, R. J. (1994). "Calculating Critical Transitions of Fluid Mixtures: Theory vs.

- Experiment.” AICHE Journal **40**(8): 1376-1403.
- Sadus, R.J. (1999). Molecular Simulations of Fluids: Theory, Algorithms and Object-Orientation. Elsevier Science, Amsterdam, Netherlands.
- Sagra, H., Y. Arai, and S. Saito (1972). “Vapour-Liquid Equilibria of Binary and Ternary Systems Containing Hydrogen and Light Hydrocarbons.” Journal of Chemical Engineering Japan **54**: 339-348.
- Sako, T., T. Sugeta, N. Nakazawa, K. Otake, M. Sato, K. Ishihara, and M. Kato (1995). “High pressure vapor-liquid and vapor-liquid -liquid equilibria for systems containing supercritical carbon dioxide, water and furfural.” Fluid Phase Equilibria **108**: 293-303.
- Sanchez, I.C. and R.H. Lacombe (1976). “An Elementary Molecular Theory of Classical Fluid. Pure Fluids” J. Phy. Chem. **80**(21): 2352-2362.
- Sanchez, I.C. and C.G. Panayiotou (1994). Equations of State Thermodynamics of Polymer and Related Solutions. S. I. Sandler (ed.). New York, Marcel Dekker, Inc: 187-286.
- Sandler, S. I., K.-H. Lee and H. Kim (1986). “The generalized Van der Waals partition function as a basis for eqations of state, their mixing rules and activity coefficient models.” ACS Symp. Ser. **300**: 180-200.
- Sandler, S. I. (1989). Chemical and Engineering Thermodynamics (2nd ed.). New York, John Wiley and Sons.
- Sandler, S. I., H. Orbey and B-I. Lee (1994). Equations of State. Models for Thermodynamics and Phase Equilibria Calculations. S. I. Sandler (ed.). New York, Marcel Dekker, Inc: 87-186.
- Sandler, S.I. (1994). Models for Thermodynamics and Phase Equilibria Calculations. New York, Marcel Dekker, Inc.
- Sandoval, R., C. Wilczek-Vera and J.H. Vera (1989). “Prediction of the ternary vapour-liquid equilibria with the PRSV equation of state.” Fluid Phase Equilibria **52**: 119-126.
- Schmidt, G. and H. Wenzel (1980). “A modified van der Waals equation of state.” Chem. Eng.

Sci. 35: 1503-1512.

Schneider, G. M. (1975). "Phase Equilibria of liquids and gaseous mixtures at high pressures. Part 2". Experimental Thermodynamics, Vol. II. B. Le Neindre and B. Vodar. London, Butterworths.

Schneider, G. M. (1978). "High Pressure Phase Diagrams and Critical Properties of Fluid Mixtures". A Specialist Report, Vol.2 : Chemical Thermodynamics. M. L. McGlaston. London, The Chemical Society: 105-142.

Schneider, G. M. (1991). "High-pressure investigations on fluid systems - a challenge to experiment, theory, and application." J. Chem. Thermodynamics 23: 301-326.

Schwartzentruber, J., F. Galivel-Solastiouk and H. Renon (1987). "Representation of the Vapor-Liquid Equilibrium of the Ternary System Carbon Dioxide - Propane - Methanol and its Binaries with a Cubic Equation of State : A New Mixing Rule." Fluid Phase Equilibria 38(1): 217-226.

Schwartzentruber, J. and H. Renon (1989,a). "Development of a New Cubic Equation of State for Phase Equilibria Calculations." Fluid Phase Equilibria 52(1): 127-134.

Schwartzentruber, J. and H. Renon (1989,b). "Extension of UNIFAC to high pressure and temperatures by using a cubic equation of state." Ind. Eng. Chem. Res. 28: 1049-1055.

Schwartzentruber, J. and H. Renon (1991). "Equation of state: how to reconcile flexible mixing rules, the virial coefficient constraint and the 'Michelsen-Kistenmacher" syndrome for multicomponent systems." Fluid Phase Equilibria 67(1): 99-110.

Scott, R. L. and P. H. van Konynenburg (1970). "2. Static Properties of solutions. Van der Waals and Related Models for Hydrocarbon Mixtures Disc. Faraday Soc. 49: 87-97.

Sebastian, H. M., J. J. Simnick, H.M. Lin, and K.C. Chao (1978). "Gas-Liquid equilibrium in mixtures of hydrogen and quinoline." J. Chem. Eng. Data 23(4): 305-308.

Sebastian, H. M., J. J. Simnick, H.M. Lin, and K.C. Chao (1980,a). "Vapor-Liquid Equilibrium in Binary Mixtures of Carbon Dioxide + n-Decane and Carbon Dioxide + n-Hexadecane." J. Chem. Eng. Data 25(2): 138-140.

- Sebastian, H. M., J. J. Simnick, H.M. Lin, and K.C. Chao (1980,b). "Gas-Liquid Equilibrium in Mixtures of Carbon Dioxide + Toluene and Carbon Dioxide + m-Xylene." J. Chem. Eng. Data **25**(3): 246-248.
- Segura, H., J. Wisniak, A. Aucejo, J.B. Monton and R. Munoz (1996). "Polyazeotropy in Binary Systems. 2. Association Effects." Industrial and Engineering Chemistry Research **35**(11): 4194-4202.
- Seitz, J. C., J. G. Blencoe and R.J. Bodnar (1996). "Volumetric properties for $\{(1-x)\text{CO}_2 + x\text{CH}_4\}$, $\{(1-x)\text{CO}_2 + x\text{N}_2\}$, and $\{(1-x)\text{CH}_4 + x\text{N}_2\}$ at the pressures (9.94, 19.94, 29.94, 39.94, 59.93, 79.93, and 99.93) MPa and temperatures (323.15, 373.15, 473.15, and 573.15) K." Journal of Thermodynamics **28**(5): 521-538.
- Serafimov, E. B. and S. V. Babich (1996). "New Forms of Azeotropic Relationships." Theoretical Foundations of Chemical Engineering **30**(1): 123-132.
- Shah, N. N., M. E. Pozo de Fernandez, J.A. Zollweg and W.B. Streett (1990). "Vapor-Liquid Equilibrium in the System Carbon Dioxide + 2,2-Dimethylpropane from 262 to 424 K at Pressure to 8.4 MPa." J. Chem. Eng. Data **35**(3): 278-283.
- Sheng, Y. J., Y. P. Chen, and D.S.H. Wong (1989). "A Cubic Equation of State for Predicting Vapor-Liquid Equilibria of Hydrocarbon Mixtures Using A Group Contribution Mixing Rule." Fluid Phase Equilibria **46**(1): 197-210.
- Sherman, S. R., C. A. Eckert and L.S. Scott (1996). "Modeling multicomponent equilibria from binary equilibrium data for reacting systems." Chemical Engineering and Processing **35**: 363-372.
- Shibata, S. K. and S. I. Sandler (1989,a). "High Pressure Vapor-Liquid Equilibria of Mixtures of Nitrogen, Carbon Dioxide, and Cyclohexane." J. Chem.Eng. Data **34**(4): 419-424.
- Shibata, S. K. and S. I. Sandler (1989,b). "Critical Evaluation of Equation of State Mixing Rules for the Prediction of High-Pressure Phase Equilibria." Ind. Eng. Chem. Res. **28**(12): 1893-1898.
- Shibata, S. K. and S. I. Sandler (1989,c). "High-Pressure Vapor-Liquid Equilibria Involving

- Mixtures of Nitrogen, Carbon Dioxide, and n-Butane." J. Chem. Eng. Data **34**(3): 291-298.
- Simmick, J. J., C. C. Lawson, H.M. Lin, and K.C. Chao (1977). "Vapor-Liquid Equilibrium of Hydrogen / Tetralin System at Elevated Temperatures and Pressures." AIChE Journal **23**(4): 469-476.
- Skjold-Jorgensen, S., P. Rasmussen and Aa. Fredenslund (1980). "On the Temperature Dependence of the UNIQUAC/UNIFAC Models." Chem. Eng. Sc. **35**: 2389-2403.
- Skjold-Jorgensen, S. (1984). "Gas Solubility Calculations. II. Application of a New Group-Contribution Equation of State." Fluid Phase Equilibria **16**(1): 317-351.
- Slocum, E. W. (1975). "Multipurpose High-Pressure Phase-Equilibrium Apparatus." Ind. Eng. Chem. Fund. **14**(2): 126-128.
- Smirnova, N.A. and A.I. Victorov (1987). "Thermodynamic Properties of Pure Fluids and Solutions from the Hole Group-Contribution Model." Fluid Phase Equilibria **34**: 235-263.
- Smith, J. M. and H. C. Van Ness (1987). Introduction to Chemical Engineering Thermodynamics (4th ed.), McGraw-Hill.
- Smith, J. M., H. C. Van Ness and M.M. Abbott (1996). Introduction to Chemical Engineering Thermodynamics (5th ed.), The McGraw-Hill Companies, Inc.
- Soave, G. (1972). "Equilibrium constants from a modified Redlich-Kwong equation of state." Chem. Eng. Science. **27**: 1197-1203.
- Soave, G. (1979). "Application of a cubic equation of state to vapour-liquid equilibria of systems containing polar compounds". Inst. Chem. Eng. Symp. Ser. **56**: 1.2/1-1.2/16.
- Soave, G. (1984). "Improvements of the van der Waals equation of state." Chem. Eng. Sc. **39**: 357-369.
- Soave, G. S., A. Bertucco and M. Sponchiado (1995). "Avoiding the Use of Critical Constants in Cubic Equations of State." AIChE Journal **41**(8): 1964-1971.

- Somait, F. A. and A. J. Kidnay (1978). "Liquid-Vapor Equilibria at 270.00K for Systems Containing Nitrogen, Methane, and Carbon Dioxide." Journal of Chemical Engineering Data 23(4): 301-305.
- Spear, R. R., R. L. Robinson Jr. and K.C. Chao (1969). "Critical States of Mixtures and Equation of State." I&EC Fund. 8(1): 2-8.
- Spear, R., R. L. Robinson Jr. and K.C. Chao (1971). "Critical States of Ternary Mixtures and Equations of State." Ind. Eng. Fund. 10(4): 588-592.
- Spee, M. and G. M. Schneider (1991). "Fluid Phase Equilibrium Studies on Binary and Ternary Mixtures of Carbon Dioxide with Hexadecane, 1-Dodecanol, 1,8-Octanediol and Dotriacontane at 393.2 K and at Pressures up to 100 MPa." Fluid Phase Equilibria 65: 263-274.
- Spencer, C.F. and R.P. Danner (1972). "Improved Equation for Prediction of Saturated Liquid Density." J. Chem. Eng. Data 17(2): 236-241.
- Stead, K. and J. M. Williams (1980). "Apparatus for studying phase equilibria-Phase equilibria of (carbon dioxide + 2,2-dimethylpropane) in the temperature range 220 to 300 K and at pressure up to 6.7 MPA." J. Chem. Thermodynamics 12(1): 265-275.
- Streett, W. B. and J. C. G. Calado (1978). "Liquid-vapour equilibrium for hydrogen + nitrogen at temperatures from 63 to 110 K and pressures to 57 MPa." J. Chem. Thermodynamics 10: 1089-1100.
- Streett, W. B. (1983). Phase Equilibria in Fluid and Solid Mixture at High Pressures. Chemical Engineering at Supercritical Conditions. M. E. Paulaitis, J. M. L. Penninger, R. D. Gray and P. Davison, Ann Arbor: The Butterworth Group: 3-30.
- Stryjek, R. and J. H. Vera (1986,a). "PRSV: An Improved Peng-Robinson Equation of State for Pure Compounds and Mixtures." The Canadian Journal of Chemical Engineering 64(April): 323-333.
- Stryjek, R. and J. H. Vera (1986,b). "PRSV2: A Cubic equation of state for accurate vapour-liquid equilibrium calculations." Can. J. Chem. Eng. 64: 820-826.

- Stryjek, R. and J. H. Vera (1986,c). "Vapor-Liquid Equilibrium of Hydrochloric acid Solutions with the PRSV equation of state." Fluid Phase Equilibria 25: 279-290.
- Suppes, G. J. and M. A. McHugh (1989). "Phase Behavior of the Carbon Dioxide-Styrene System." J. Chem. Eng. Data 34(3): 310-312.
- Suzuki, K., H. Sue, K. Arai, and S. Saito (1990,a). "Vapor-Liquid Equilibria for Synthetic Alcohols Process." Fluid Phase Equilibria 59(1): 115-134.
- Suzuki, K., H. Sue, M. Itou, R.L. Smith, H. Inomata, K. Arai, and S. Saito (1990,b). "Isothermal Vapor-Liquid Equilibrium Data for Binary Systems at High Pressure: Carbon Dioxide-Methanol, Carbon Dioxide-Ethanol, Carbon Dioxide-1-Propanol, Methane-Ethanol, Methane-1-Propanol, Ethane-Ethanol, and Ethane-1-Propanol Systems." J. Chem. Eng. Data 35(1): 63-66.
- Suzuki, K., H. Sue, M. Itou, R.L. Smith, H. Inomata, K. Arai, and S. Saito (1990,c). "High-Pressure Vapor-Liquid Equilibrium Data of the 10-Component System Hydrogen, Carbon Monoxide, Carbon Dioxide, Water, Methane, Ethane, Propane, Methanol, Ethanol, and 1-Propanol at 313.4 and 333.4 K." J. Chem. Eng. Data 35(1): 67-69.
- Suzuki, T., N. Tsuge and K. Nagahama (1991). "Solubilities of ethanol, 1-propanol, 2-propanol and 1-butanol in supercritical carbon dioxide at 313K and 333K." Fluid Phase Equilibria 67: 213-226.
- Swaid, I. (1983). Dissertation. University of Bochum.
- Takishima, S., K. Saiki, K. Arai, and S. Saito (1986). "Phase Equilibrium For CO₂-C₂H₅OH-H₂O System." Journal of Chemical Engineering of Japan 19(1): 48-56.
- Thies, M. C. and M. E. Paulaitis (1984). "Vapor-Liquid Equilibrium for 1-Methylnaphthalene/Methanol Mixtures at Elevated Temperatures and Pressure." J. Chem. Eng. Data 29(4): 438-440.
- Togniani, H. and D. S. Viswanath (1986). "A cubic Equation of State for Polar and Apolar fluids." Ind. Eng. Chem. Process Des. Dev. 25: 531-536.
- Toyama, A., P. S. Chappelaar, T.W. Leland and R. Kobayashi (1962). "Vapor-Liquid Equilibria

- at Low Temperatures: The Carbon Monoxide- Methane system.” Adv. in Cryogenic Engineering 7(1): 125-136.
- Treble, M.A. and P.R. Bishnoi (1986). “ Accuracy and consistency comparisons of ten cubic equations of state for polar and non-polar compounds.” Fluid Phase Equilibria 29: 465-474.
- Treble, M. A. and P. R. Bishnoi (1987). “Development of a New Four-Parameter Cubic Equation of State.” Fluid Phase Equilibria 35(1): 1-18.
- Tsang, C. Y. and W. B. Streett (1981). “Vapor-Liquid Equilibrium in the System Carbon Dioxide/Dimethyl Ether.” J. Chem. Eng. Data 26(2): 155-159.
- Tsiklis, D.S. (1968). Handbook of Techniques in High Pressure Research Engineering. New York: Plenum Press.
- Tsonopoulos, C. (1974). “An empirical correlation of second Virial coefficients.” AIChE Journal 20: 263-272.
- Tsonopoulos, C. and J.L. Heidman (1985). “From Redlich-Kwong to the present.” Fluid Phase Equilibria 24: 1-23.
- Tsonopoulos, C. and J. L. Heidman (1986). “High-Pressure Vapor-Liquid Equilibria with Cubic Equations of State.” Fluid Phase Equilibria 29(1): 391-414.
- Tsuboka, T. and T. Katayama (1975). “Modified Wilson equation for vapor-liquid and liquid-liquid equilibria.” J. Chem. Eng. Japan 8: 181-187.
- Twu, C.H., J.E. Coon and J.R. Cunningham (1995). “A new generalized alpha function for a cubic equation of state: Part 1. Peng- Robinson equation.” Fluid Phase Equilibria 105: 49-59.
- Twu, C. H. and J. E. Coon (1995). “Accurately Estimate Binary Interaction Parameters.” Chemical Engineering Progress: 46-53.
- Twu, C. H. and J. E. Coon (1996). “COES/AE Mixing Rules Constrained by VdW Mixing Rule and Second Virial Coefficient.” AIChE Journal 42: 3212-3222.

- Twu, C. H., J. E. Coon, et al. (1996). "An Approach for the Application of a Cubic Equation of State to Hydrogen-Hydrocarbon Systems." Industrial and Engineering Chemistry Research 35(3): 905-910.
- Usdin, E. and J. C. McAuliffe (1976). "A one parameter family of Equations of State." Chem. Eng. Sc. 31: 1077-1084.
- Valderrama, J. O. and E. A. Molina (1986). "Interaction Parameter for Hydrogen-Containing Mixtures in the Peng-Robinson Equation of State." Fluid Phase Equilibria 31(1): 209-219.
- Valderrama, J. O., H. de la Puente and A.A. Ibrahim (1994). "Generalization of a polar-fluid Soave-Redlich-Kwong equation of State." Fluid Phase Equilibria 93: 377-383.
- Van Konynenburg, P. H. and R. L. Scott (1980). "Critical Lines and Phase Equilibria in Binary Van Der Waals Mixtures." Philos. Trans. Roy. Soc. London, Series A 298: 495-540.
- Van Ness, H. C. (1964). Classical Thermodynamics of Nonelectrolyte Solutions. Oxford, Pergamon.
- Van Ness, H. C., S. M. Byers and R.E. Gibbs (1973). "Vapor-Liquid Equilibrium: Part I. An Appraisal of Data Reduction Methods." AIChE Journal 19(2): 238-251.
- Van Ness, H. C. and M. M. Abbott (1982). Chemical Thermodynamics of Nonelectrolyte Solutions with Applications to Phase Equilibria. New York, McGraw Hill.
- Van Ness, H.C. and M.M. Abbott (1983). "Some Practical Considerations in Reduction of Vapour-Liquid Equilibrium Data". Chemical Engineering Thermodynamics. S.A. Newman (ed.). Ann Arbor Science: 3-15.
- Verneau, P., J. Lieto, A. Boudenheim, and J. Bousquet (1994). "A Novel Technique for Rapid Liquid-Vapour Equilibrium Measurement and Modelling." Chemical Engineering Science 49(11): 1719-1727.
- Verevkin S.P. and A. Heintz (1999). "Vapour Pressure Measurements and Chemical Equilibria in Liquid and Gaseous Phases in Reacting Systems of the Type Alcohol + Iso-olefin \leftrightarrow Ether (L)." Progress in Computing of Physicochemical Properties. 18-20 November,

Warszawa, Poland.

- Verevkin, S.P. and A. Heintz (2000). "Vapour Pressure Measurements and Chemical Equilibria in liquid and gaseous phases in reacting system of the Type Alcohol + α -methyl-styrene \Leftrightarrow ether." 16th IUPAC Conference on Chemical Thermodynamics. 6-11 August, Halifax, Nova Scotia, Canada.
- Vidal, J. (1978). "Mixing rules and excess properties in cubic equations of state." Chem. Eng. Sc. **38**: 787-791.
- Vidal, J. (1984). "Phase Equilibria and Density Calculations for Mixtures in the Critical range with Simple Equation of State." Ber. Bunsenges. Phys. Chem. **88**(1): 784-791.
- Vonka, P., J. Lovland, P. Dittrich and T. Prokes (1996). "Determination of binary parameters of an equation of state from methanol + n-alkane vapor-liquid equilibrium data ensuring thermodynamic stability of the calculated liquid phase." Fluid Phase Equilibria **116**: 68-74.
- Wagner, Z. and I. Wichterle (1987). "High-Pressure Vapour-Liquid Equilibrium in Systems Containing Carbon Dioxide, 1-Hexene, and N-Hexane." Fluid Phase Equilibria **33**(1): 109-123.
- Wagner, Z. and J. Pavlicek (1993). "Vapour-liquid equilibrium in the carbon dioxide-p-cymene system at high pressure." Fluid Phase Equilibria **90**: 135-141.
- Wagner, Z. and J. Pavlicek (1994). "Vapour-liquid equilibrium in the carbon dioxide-ethyl acetate system at high pressure." Fluid Phase Equilibria **97**: 119-126.
- Wagner, Z. (1995). "Vapor-liquid equilibrium in the carbon dioxide-ethyl propanoate system at pressures from 2 to 9 MPa and temperatures from 303 to 323 K." Fluid Phase Equilibria **112**: 125-129.
- Walas, S. M. (1985). Phase Equilibria in Chemical Engineering. Stoneham, Butterworths.
- Wan, S. W. and B. F. Dodge (1940). "Solubility of Carbon Dioxide in Benzene at Elevated Pressure." Ind. Eng. Chem. **32**(1): 95-98.

- Wang, J. and V. N. Kabadi (1996). "Generalized Method for Prediction of Saturated Liquid Volumes Using Van der Waals Volumes." AICHE Journal 42: 595-600.
- Wang, W., Y. Qu, C.H. Twu and J.E. Coon (1996). "Comprehensive comparison and evaluation of the mixing rules of WS, MHV2 and Twu et al." Fluid Phase Equilibria 116: 488-494.
- Weast, R.C., M.J. Astle and W.H. Beyer (editors) (1986). CRC Handbook of Chemistry and Physics. 67th edition, Boca Raton, Fl. : CRC Press.
- Weber, W., S. Zeck and H. Knapp (1984). "Gas Solubilities in Liquid Solvents at High Pressure: Apparatus and Results for Binary and Ternary Systems of N₂, CO₂ and CH₃OH." Fluid Phase Equilibria 18(1): 253-278.
- Wei, Y.S. and R.J. Sadus (2000). "Equations of State for the Calculation of Fluid-Phase Equilibria." AICHE J. 46(1): 169-196.
- Weidlich, U. and J. Gmehling (1987). "A Modified UNIFAC Model. 1. Prediction of VLE, h^E and γ^∞ ." Ind. Eng. Chem. Res. 26: 1372-1381.
- Weng, W. L. and M. J. Lee (1992). "Phase equilibrium measurements for the binary mixtures of 1-octanol plus CO₂, C₂H₆ and C₂H₄." Fluid Phase Equilibria 73: 117-127.
- White, R. R. and G. G. Brown (1942). "Phase Equilibria at High Temperatures." Ind. Eng. Chem 34(10): 1162-1174.
- Whiting, W. B. and J. M. Prausnitz (1982). "Equations of state for strongly Nonideal fluid Mixtures: Application of local compositions toward density-dependent mixing rules." Fluid Phase Equilibria 9: 119-147.
- Wichterle, I. (1978,a). "High Pressure Vapour-Liquid Equilibrium. V." Fluid Phase Equilibria 2(1): 143-159.
- Wichterle, I. (1978,b). "High Pressure Vapour-Liquid Equilibrium. IV." Fluid Phase Equilibria 2(1): 59-78.

- Willett, J., (1987). Gas Chromatography. D. Kealey (editor) Chichester, Wiley.
- Wilner, L. B. (1960). "Variable Capacitance Liquid Level Sensors." The Review of Scientific Instruments 31(5): 501-507.
- Wilson, G.M. (1964). "Vapor-Liquid Equilibrium. XI. A New Expression for the Excess Free Energy of Mixing." J. American Chem. Soc. 86: 127-130.
- Wilson, K. S., D. D. Lindley, W.B. Kay, and H.C. Hershey (1984). "Virial coefficients of Ethanol from 373.07 to 472.15 K." J. Chem. Eng. Data 29(3): 243-245.
- Winnick, J. (1997). Chemical Engineering Thermodynamics: An introduction to Thermodynamics for Undergraduate Engineering Students, John Wiley and Sons, Inc.
- Wisniak, J. (1983). "Liquid-Liquid Phase Splitting-I : Analytical Models for Critical Mixing and Azeotropy." Chemical Engineering Science 38(6): 969-978.
- Wisniak, J. (1984). "Liquid-Liquid Phase Splitting-III: Azeotropy and Critical Solution Temperature in Ternary Systems." Chem. Eng. Sc. 39(6): 967-973.
- Wisniak, J. (1984). "Liquid-Liquid Phase Splitting-II: Ternary Systems and the Spinodal Curve." Chem. Eng. Sc. 39(1): 111-115.
- Wisniak, J., H. Segura and R. Reich (1996). "Polyazeotropy in Binary Systems." Industrial and Engineering Chemistry Research 35(10): 3742-3758.
- Wisniewska, B., J. Gregorowicz, and S. Malaowski (1993). "Development of a Vapour-Liquid Equilibrium Apparatus to work at pressure up to 3MPa." Fluid Phase Equilibria 86: 173-186.
- Won, K. W. and J. M. Prausnitz (1973). "High-Pressure Vapor-Liquid Equilibria. Calculation of Partial Pressures from Total Pressure Data. Thermodynamic Consistency." Ind. Eng. Chem. Fund. 12(4): 459-463.
- Wong, D. S. H., S. I. Sandler and A.S. Teja (1984, a). "Vapour-Liquid Equilibrium Calculations by Use of a Generalized Corresponding States Principle. 2. Comparison with Other Methods." Ind. Eng. Chem. Fund. 23(1): 45-49.

- Wong, D. S. H., S. I. Sandler and A.S. Teja (1984, b). "Vapour-Liquid Equilibrium Calculations by Use of a Generalized Corresponding States Principle. 1. New Mixing Rules." Ind. Eng. Chem. Fundam. **23**(1): 38-44.
- Wong, D. S. H. and S. I. Sandler (1984). "Calculation of Vapor-liquid-liquid equilibrium with cubic equations of state and a Corresponding States Principle." Ind. Eng. Chem. Fundamentals **23**(3): 348-354.
- Wong, D. S. H., H. Orbey, and S.I. Sandler (1992). "Equation of State Mixing Rule for Nonideal Mixtures Using available activity Coefficient Model Parameters and That allows Extrapolation Over Large Ranges of Temperature and Pressure." Ind. Eng. Chem. Res. **31**(8): 2033-2039.
- Wong, D. S. H. and S. I. Sandler (1992). "A Theoretically Correct Mixing Rule for Cubic Equations of State." AIChE Journal **38**(5): 671-680.
- Wormald, C. J., D. J. Hutchings and E.J. Lewis (1996). "The excess molar enthalpy and cross-term second virial coefficients of (nitrogen + propane) and (nitrogen + butane) from T = (241.2 to 393.4) K." Journal of Chemical Thermodynamics **28**(4): 371-378.
- Wu, G. W., N. W. Zhang, X.Y. Zheng, H. Kubota, and T. Makita (1988). "High Pressure Vapor-Liquid Equilibria of Four Binary Systems Containing Carbon Dioxide." Journal of Chemical Engineering of Japan **21**(1): 25-29.
- Wu, H. S. and S. I. Sandler (1989). "Proximity Effects on the Predictions of the UNIFAC Model: 1. Ethers." AIChE Journal **35**(1): 168-172.
- Wu, H. S. and S. I. Sandler (1991,a). "Use of ab Initio Quantum Mechanics Calculations in Group Contribution Methods. 1. Theory and the Basis for Group Identifications." Ind. Eng. Chem. Res. **30**(5): 881-889.
- Wu, H. S. and S. I. Sandler (1991,b). "Use of ab Initio Quantum Mechanics Calculations in Group Contribution Methods. 2. Test of New Groups in UNIFAC." Ind. Eng. Chem. Res. **30**(5): 889-897.
- Xu, Z. and S. I. Sandler (1987,a). "Applications to Mixtures of the Peng-Robinson Equation of State with Fluid Specific Parameters." Ind. Eng. Chem. Res. **26**(6): 1234-1238.

- Xu, Z. and S. I. Sandler (1987,b). "Temperature-Dependent Parameters and the Peng-Robinson Equation of State." Ind. Eng. Chem. Res. 26(3): 601-606.
- Xu, N., J. Yao, Y. Wang and J. Shi (1991). "Vapor-liquid equilibria of five binary systems containing R-22." Fluid Phase Equilibria 69: 261-270. •
- Yoo, S. J., K. P. Yoo, H. Kim and C.S. Lee (1996). "A new predictive quasi-lattice equation of state for high-pressure equilibria of pure fluids and mixtures." Fluid Phase Equilibria 125(1-2): 21-31.
- Yorizane, M., S. Yoshimura, H. Masuoka, Y. Mitano and Y. Kakimoto (1985). "New Procedure for Vapor-Liquid Equilibria. Nitrogen + Carbon Dioxide, Methane + Freon 22, and Methane + Freon 12." J. Chem. Eng. Data 30: 174-176.
- Young, C. L. (1978). "Experimental Methods for Studying Phase Behavior of Mixtures at High Temperatures and Pressures". A Specialist Periodical Report: Vol.2. M. L. McGlaston. London, The Chemical Society: 71-104.
- Zabaloy, M. S. and J. H. Vera (1996). "Cubic Equation of State for Pure Compound Vapor Pressures from the Triple Point to the Critical Point." Industrial and Engineering Chemistry Research 35(3): 829-836.
- Zeck, S. and H. Knapp (1986). "Vapor-Liquid and Vapor-Liquid-Liquid Phase Equilibria for Binary and Ternary Systems of Nitrogen, Ethane and Methanol: Experiment and Data Reduction." Fluid Phase Equilibria 25(1): 303-322.

APPENDIX A

A.1. Interpretation of Phase Diagrams

The phase rule:

In the construction and interpretation of phase diagrams the phase rule serves as an important guide. It imposes constraints on the geometry of the features that describe the existence or coexistence of a fixed number of phases.

For non-reacting systems the following simple relation expresses the phase rule:

$$f = c + 2 - p \quad (\text{A-1})$$

where, f - number of independent variables (sometimes called “degrees of freedom”),

c - number of component, and

p - number of phases

For a binary system, the maximum number of independent variables is three. The phase behaviour of the system can be completely described by volumes, surfaces, lines and points in three-dimensional space.

Temperature and pressure are the independent variables most convenient for the measurement and study of phase equilibria in fluid systems. In these systems changes in both temperature and pressure produce dramatic changes in phase behaviour, and a three-dimensional diagram in pressure, temperature and a third variable is required for complete description of a binary system. The most convenient choice for the third component is generally composition.

The simplest type of P - T - x diagram for a fluid system is one that describes the gas-liquid equilibria of a system in which the liquids are miscible in all proportions.

Referring to Figure A-1, lines $A_\alpha C_\alpha$ and $A_\beta C_\beta$ are the vapour pressure curves of the pure components, α and β , in the two P - T planes of the diagram ending in critical points C_α and C_β . The mixture critical line $C_\alpha C_\beta$ is continuous in P - T - X space. The two surfaces representing

saturated gas- and liquid phases extend across the diagram, and are bound in space by the lines $A_\alpha C_\alpha$, $A_\beta C_\beta$, and $C_\alpha C_\beta$. With the P-axis vertical, the lower surface represents the gas phase and the upper surface the liquid phase.

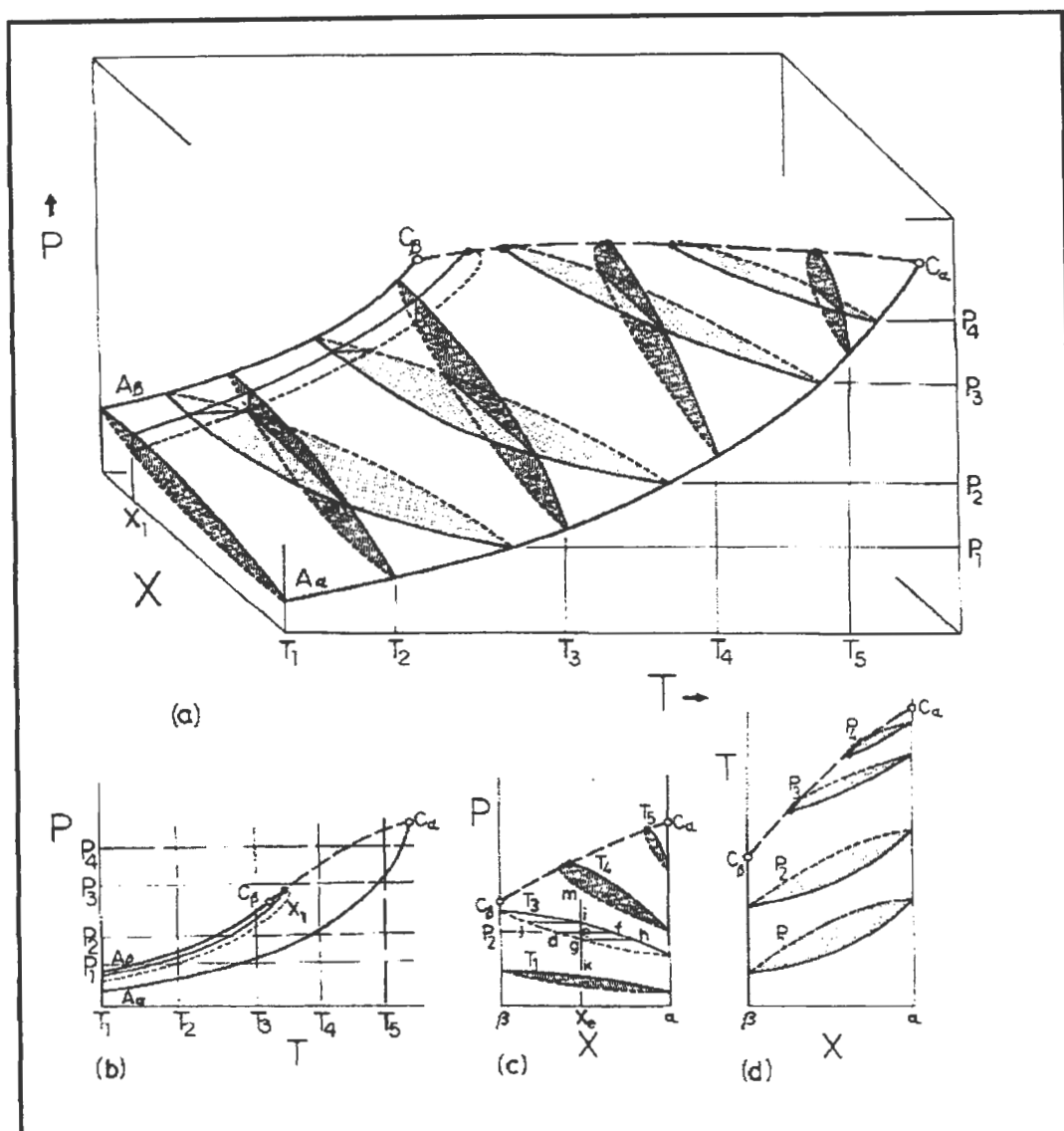


Figure A-1: Phase diagram for a simple system (extracted from Streett [1983])

As one can see sections cut by planes, within the two-phase, of constant pressure, temperature and composition produce isobars (Figure A-1(d)), isotherms (Figure A-1(c)), and isopleths (Figure A-1(b)) respectively.

Classification and description of binary fluid phase diagrams for critical properties is covered in Chapter 3 and Appendix B.

A.2. Dynamic Method: Selected examples of apparatus from literature

A.2.1. Single vapour pass

Duncan and Hiza [1970]

The equipment was designed to be multipurpose in nature, and included single vapour pass and recirculation options, temperature measurement with either a platinum or germanium resistance thermometer, and phase composition determination by chromatograph or continuous analysis. The apparatus was designed for operating temperatures of 10 to 150 K and pressure up to 200 atm.

The equilibrium cell was constructed from electrolytic tough pitch copper. Sealing of the equilibrium cell was achieved using indium-coated, copper-asbestos gaskets. To achieve the very low temperature that the apparatus is run at, refrigeration was provided by injection of refrigerant liquid through the annular space on the cell. Figure A-2 shows the phase equilibrium apparatus of Duncan and Hiza.

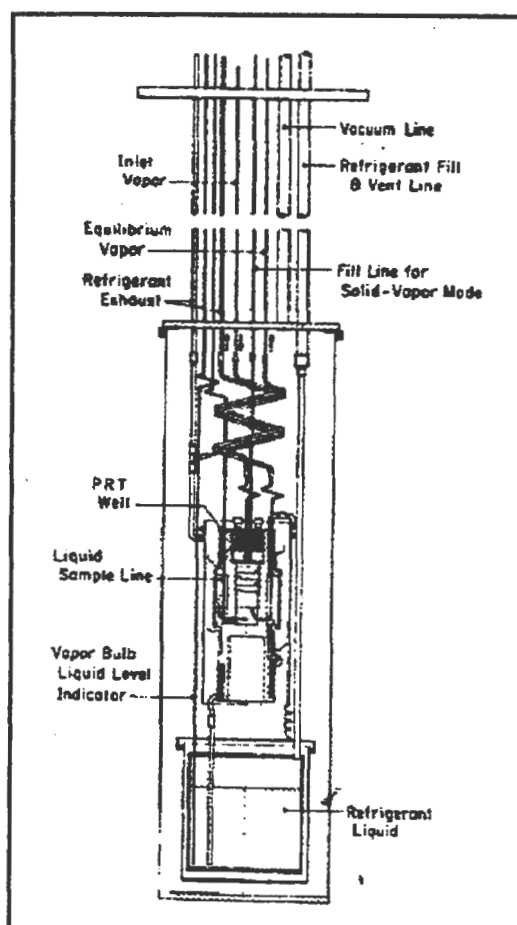


Figure A-2: Experimental apparatus of Duncan and Hiza [1970]

With this piece of equipment it is possible to study equilibrium pressure, temperature, and composition properties in the liquid-vapour and solid-vapour regions and along the three phase loci.

Table A-1 lists the details of all single vapour pass apparatus surveyed, along with the systems measured.

A.2.2. Liquid phase re-circulation

Mohamed and Holder [1987]

Figure A-3 illustrates the apparatus used by Mohamed and Holder [1987]. It consisted of primarily the following components:-

- i) two feed pumps;
- ii) a pre-heater;
- iii) an equilibrium column;
- iv) separation vessel; and
- v) a sampling system.

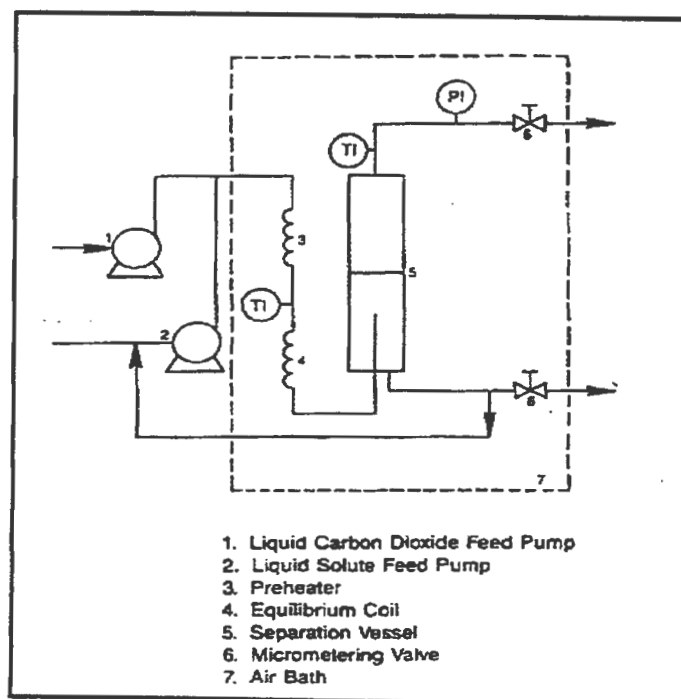


Figure A-3: Experimental apparatus of Mohamed and Holder [1987]

References	Cell volume (cm ³)	Operating Range		Equilibrium cell (1)	Measurement Device		Equilibration time (min)	Sample size (µl)		Method of sampling		Special features	Systems measured
		Temp (K)	Pressure (bar)		Temp (2)	Pressure (3)		Vapour	Liquid	Vapour	Liquid		
Wan and Dodge [1940]	-	273-573	1013	cold-rolled steel	-	B/DWP	120	-	3000	direct expansion	pressure sampler	Magnetic stirrer operated by solenoid	carbon dioxide + benzene
Duncan and Hiza [1970]	-	10-150	203	electrolytic tough pitch copper	PR	B	-	-	-	sample trap	capillary	Multipurpose - can also operate as vapour recirculation	Argon + methane
Legret et al. [1983]	-	423	200	-	TC	BM/PT	-	-	NA	sampling valve	NA	Partition coefficients at infinite dilution are measured.	Methane + ethane + n- decane; methane + propane + n- decane; methane + n-butane + n- decane; methane + n-pentane + n- decane.
Lee and Chao [1988]	300	-	345	-	TC	B	-	-	-	sample trap	sample trap	-	Carbon dioxide + 1- methylnaphthalene ; carbon dioxide + m-cresol; ethane + 1- methylnaphthalene ; ethane + m- cresol.
Weng and Lee [1992]													Carbon dioxide + 1-octanol; ethane + 1-octanol; ethylene + 1- octanol
Lee and Chen [1994]													Carbon dioxide + 2-methyl-1- pentanol; carbon

Table A-1: Single vapour pass apparatus surveyed

References	Cell volume (cm ³)	Operating Range		Equilibrium cell (1)	Measurement Device		Equilibration time (min)	Sample size (µl)		Method of sampling		Special features	Systems measured
		Temp (K)	Pressure (bar)		Temp (2)	Pressure (3)		Vapour	Liquid	Vapour	Liquid		
													dioxide + 1-octanol; carbon dioxide + 1-decanol
Di Giacomo et al. [1989]	100	473	1000	stainless steel	TC	PT	60-300	-	-	sample expansion	sample expansion	-	Carbon dioxide + limonene; carbon dioxide + citral.
Di Giacomo et al. [1994]													Carbon dioxide + m-cresol + phenol.

Table A-1 (continued): Single vapour pass apparatus surveyed

Key:

(1) Materials of construction

(2) TC - thermocouple; PR - platinum resistance thermometer

(3) B - Bourdon type pressure gauge; BM - Bourdon manometer; PT - pressure transducer; DWP - dead weight piston gauge

The feed pumps were capable of delivering both solvent and solute against pressures of up to 41.5 MPa. The pre-heater enabled the entering fluids to reach the temperature of the air-bath. The equilibrium coil was packed with glass beads so as to allow for better contact between gas and liquid.

The separation vessel was 100 cm³ in volume and the equilibrated stream that entered the vessel was allowed to disengage into the gas and liquid streams. The resultant liquid stream was then recycled to the liquid solute pump.

Temperature monitoring was performed at various locations in the apparatus. It was found that the fluid temperature downstream of the equilibrium coil was about 0.3 K lower than the temperature of the vapour exiting the separation vessel.

The sampling system consisted of a series of traps placed in a methanol-cooled bath (-25 °C) so as to condense the liquid solute. Both the gas and liquid samples were flashed across a micro-metering valve. This precipitated the liquid solute. The gas rate was measured using a wet test meter, while the liquid was collected in the trap and weighted.

Table A-2 lists the details of all liquid phase recirculation apparatus surveyed, along with the systems measured.

A.2.3. Vapour phase re-circulation

Toyama et al. [1962]

This vapour recycle VLE apparatus has the following features:-

- a mechanical vapour recycling magnetic pump which could be located in or outside the temperature bath;
- a variable-volume cell with floating piston;
- a visual glass-windowed cell allowing observation of the equilibrium cell contents at elevated pressures; and
- operability at temperatures as low as -300°F.

The variable-volume cell with the floating piston served as a reservoir for vapour and was also used for fine and precise adjustment of pressure during charging, equilibration, and sampling.

References	Cell volume (cm ³)	Operating Range		Equilibrium cell (1)	Measurement Device		Equilibration time (min)	Sample size (μl)		Method of sampling		Special features	Systems measured
		Temp (K)	Pressure (bar)		Temp (2)	Pressure (3)		Vapour	Liquid	Vapour	Liquid		
Kim et al. [1986]	100	423	137	316 stainless steel	TC	PT	10	25	0.5	sampling valves	sampling valves	Two glass windows.	Carbon dioxide + benzene; carbon dioxide + toluene; carbon dioxide + p-xylene
Mohamed and Holder [1987]	100	-	-	stainless steel	TC	PT	-	-	-	sample expansion	sample expansion	-	Carbon dioxide + p-xylene; carbon dioxide + o-xylene; carbon dioxide + p-xylene + o-xylene; carbon dioxide + butyl ether + o-xylene.

Table A-2: Single phase liquid recirculation apparatus surveyed

Key:

- (1) Materials of construction
- (2) TC - thermocouple
- (3) PT - pressure transducer

The equilibrium cell, which was transparent and had a stainless steel body, was submerged in a constant temperature bath. Temperature regulation was achieved by combining the control of evaporation of liquid nitrogen with an electric heater circuit that was connected to an electronic regulator.

Pressure measurements were made with the use of a calibrated Heise gauge, while temperature measurement was via calibrated iron-constantan thermocouples.

Fine capillary tubing (0.015" i.d.) was used for the sampling lines to minimise the hold-up in them.

Figure A-4 shows the flow diagram of the experimental apparatus of Toyama et al. [1962].

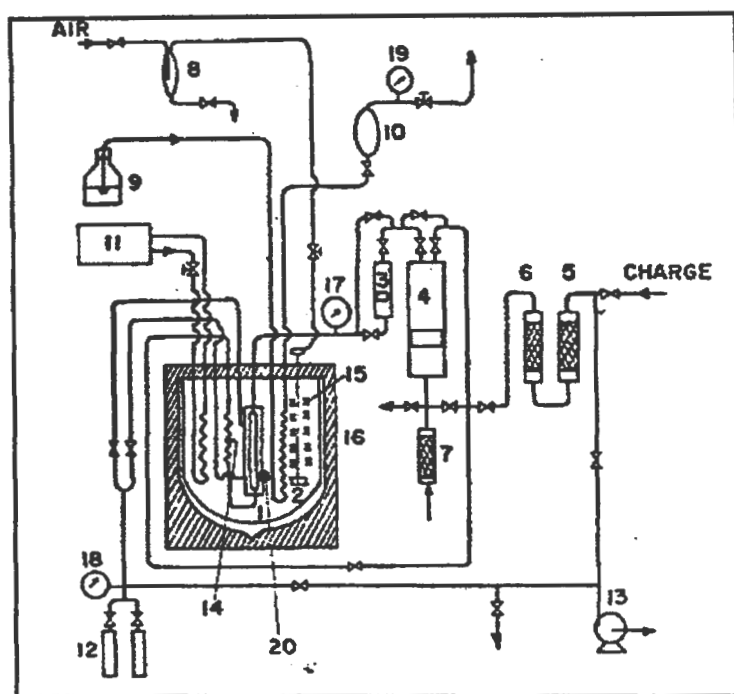


Figure A-4: Flow diagram of the experimental apparatus of Toyama et al. [1962]

1 - equilibrium cell; 2 - stirrer; 3 - magnetic pump; 4 - variable volume cell; 5 - silica gel drier; 6 - activated carbon drier; 7 - silica gel drier; 8 - knockout drum; 9 - liquid nitrogen reservoir; 10 - surge tank; 11 - Freon refrigeration unit; 12 - sample containers; 13 - vacuum pump; 14 - recirculating coil; 15 - electric heater; 16 - constant temperature bath; 17,18,19 - pressure gauges; 20 - thermocouples.

Fredenslund and Sather [1970]

The flow diagram of the experimental apparatus as used by Fredenslund and Sather [1970] is shown in Figure A-5. The equilibrium cell has built-in windows that permit visual observation of

the equilibrium cell contents. The vapour phase that is recycled enters the equilibrium cell via cooling coils. Both the equilibrium cell and the coil are immersed in a constant temperature bath. The volume of the liquid sample taken is about 0.5 cm^3 . The vapour and liquid samples are expanded into sample chambers. From the sample chambers the samples are analysed on a GC. Temperature measurement is via a quartz thermometer and pressure measurement via Bourdon pressure gauges. Fredenslund and Sather [1970] state that entrainment was minimised by using low vapour circulation rates and by keeping the liquid level in the cell low. They also state that the vapour recirculation rate does not change the vapour composition significantly.

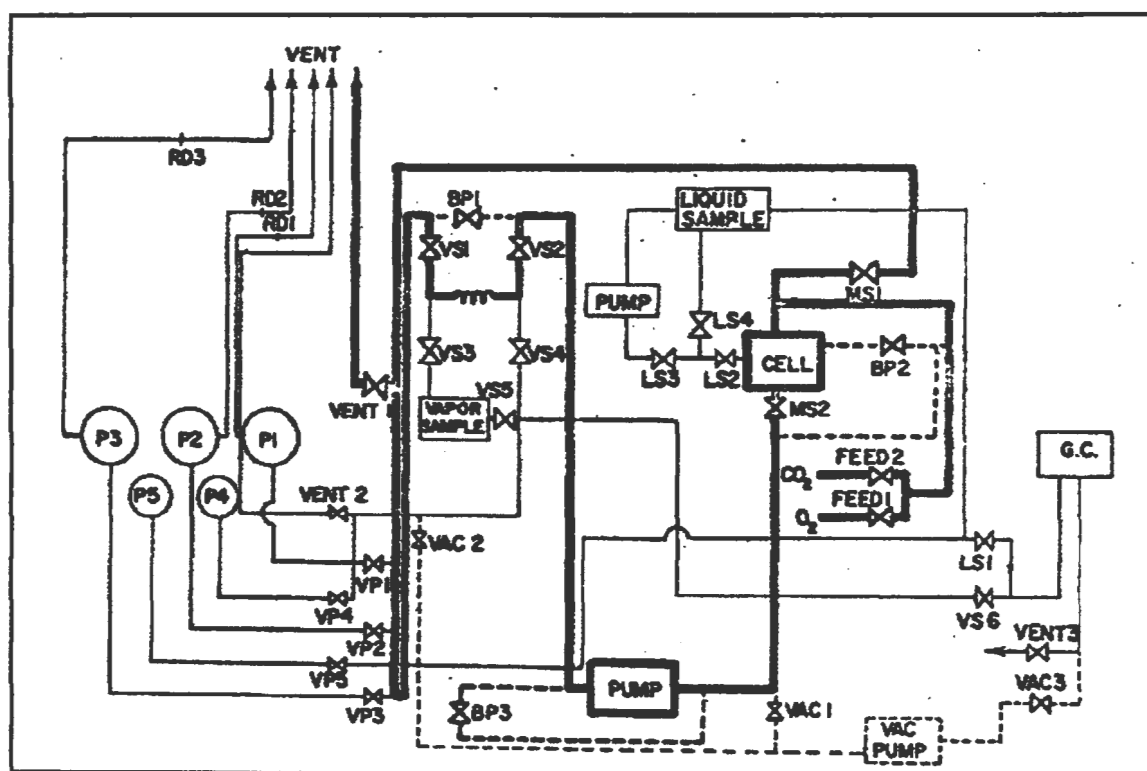


Figure A-5: Flowsheet of the experimental apparatus of Fredenslund and Sather [1970]

P - pressure gauge; RD - rupture disk; GC - gas chromatograph; MS - main system valve; VP - valve for pressure gauge; VS - vapour sampling valve; LS - liquid sampling valve; VAC - vacuum system valve; BP - bypass valve; VENT - vent valve; FEED - valve to feed.

Katayama et al. [1975]

The vapour-recirculation apparatus used by Katayama et al. [1975] is illustrated in Figure A-6. Vapour was continuously pumped (via a magnetic pump (4)) from the top of the equilibrium cell (5) and reintroduced at the bottom of the cell where it bubbled up through the liquid to establish the vapour-liquid contact needed for phase equilibrium. Sampling of the vapour is achieved by passing the recycled vapour through a vapour sampling part (7), while liquid sampling is

undertaken by operating sampling valves (6). The liquid and vapour samples were then evaporated and introduced to a sampling flask (1 and 2 respectively). From the flasks the samples were then sent to a GC for analysis of the equilibrium mixture.

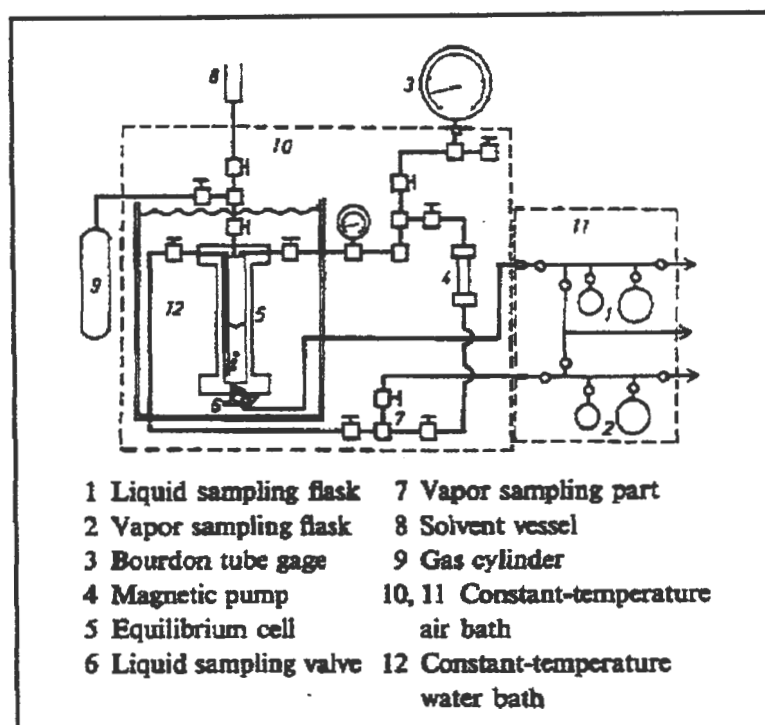


Figure A-6: Schematic of the experimental apparatus of Katayama et al. [1975]

All sampling lines were covered with ribbon heaters to avoid condensation of the sample gas. The constant temperature bath in which the sampling flasks were housed was maintained about 10°C higher than the equilibrium cell temperature.

Streett and Calado [1978]

To cope with the problem of hydrogen embrittlement, all parts of the experimental apparatus in contact with high-pressure hydrogen were made from one of two high-strength alloys:

- beryllium copper, an alloy of two mass per cent beryllium in copper; or
- stainless steel A-286, a precipitation-hardenable fully austenitic stainless steel.

Streett and Calado [1978] made use of a two-stage diaphragm compressor and an intensifier (see Figure A-7) to generate the pressures required in their studies. A compression unit was also used in our studies to achieve pressures in excess of supplied cylinder pressures (analogous to the compression device used in this project).

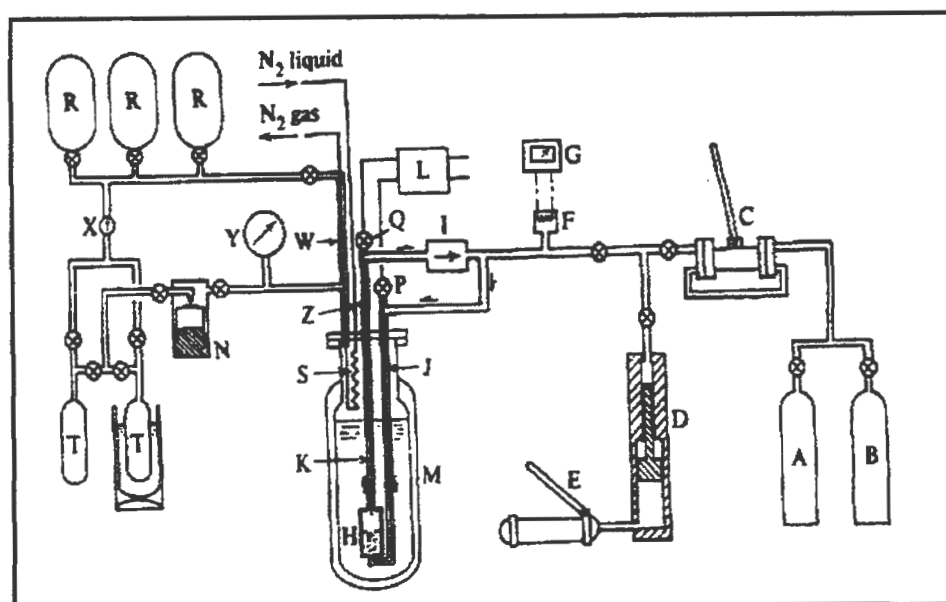


Figure A-7: Diagram of the experimental apparatus of Streett and Calado [1978]

A,B - cylinders containing the gases to be studied; C - two-stage diaphragm compressor; D - pressure intensifier; E - hydraulic pump; F - managanin pressure gauge; G - Wheatstone bridge; H - pressure vessel; I - magnetically operated pump; J,K - sampling lines; L - thermal-conductivity gas analyser; M - cryostat; N - Cartesian manometer; P,Q - sampling valves; R - gas cylinders for storing refrigerant; S - coil of copper tubing (6.35 mm O.D., 5.0 mm I.D.); T - stainless-steel cylinders; W - counterflow heat exchanger; X - check valve; Z - thermocouple junction.

Shah et al. [1990]

Shah et al. [1990] made use of two pieces of apparatus in their studies. Choice of apparatus used was dependent on the experimental temperature. The high temperature apparatus, which has a working temperature range of 325-530 K, is a modification of the apparatus used by Pozo and Streett [1984]. A schematic of the apparatus is as shown in Figure A-8.

The equilibrium cell was made from a commercial sight gauge fitted with a glass window. Pumping of the vapour phase is achieved with the use of a magnetically operated pump. The pump withdraws vapour from the top of the equilibrium cell and bubbles it through the liquid. This produces contact between the two phases, and as result equilibrium is attained in 10-15 minutes. Stainless steel rods are placed in the equilibrium cell so as to reduce the effective volume of the equilibrium cell.

Vapour and liquid samples are withdrawn from the cell for analysis through a sampling system. To overcome partial condensation during throttling, the sampling cell is placed in an insulated and separately heated chamber (J) inside an oven (H). The chamber (J) is heated to a temperature of 373 K or 20 K above the oven temperature, whichever is higher. The liquid sample is withdrawn into sampling cell (D), which is evacuated. It is allowed to stand for 10 minutes to vapourise and become well mixed. After this it is transferred into the sampling loop of the GC. The sampling valve and the lines between the sample cell and the GC are heated.

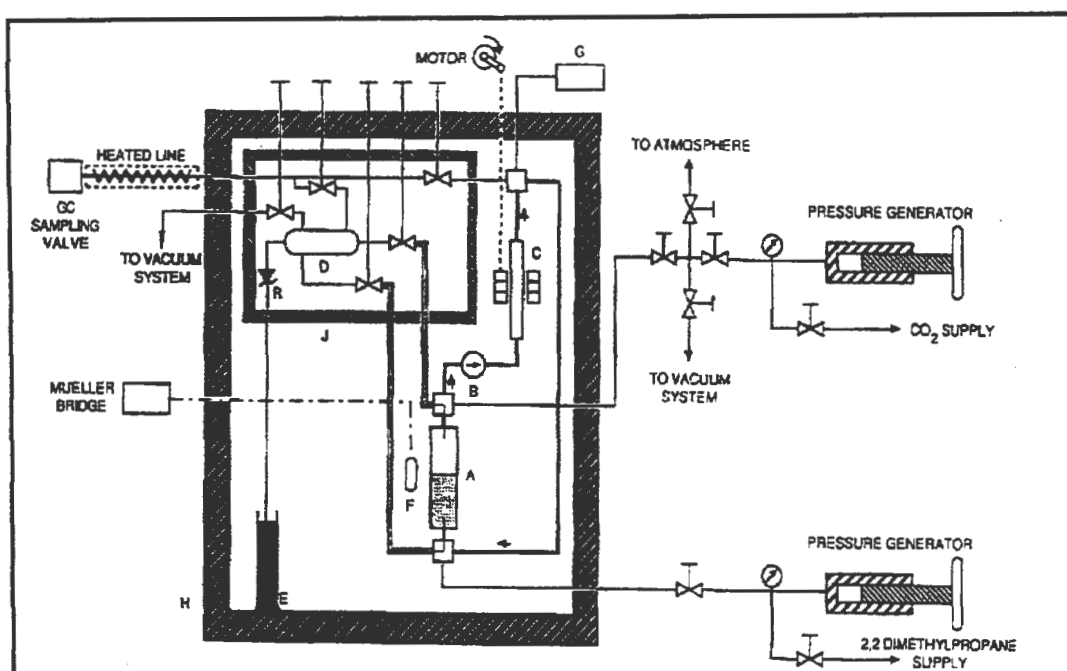


Figure A-8: Schematic diagram of the high temperature vapour-liquid equilibrium apparatus of Shah et al. [1990]

A - equilibrium cell; B - check valve; C - magnetically actuated recirculation pump; D - sampling chamber; E - beaker of oil; F - platinum resistance thermometer; G - digital pressure gauge; H - oven; J - heated chamber. Heavy line from the equilibrium cell through the check valve and the magnetic pump indicates the recirculation loop.

For the study of systems below a temperature of 325 K, a modification of the apparatus of Chang et al. [1982] was used. It is similar to the high temperature apparatus, but differs in that it uses a liquid bath for temperature control instead of an air bath. The equilibrium cell was made of a sapphire tube (see Figure A-9).

The sapphire tube is confined between steel flanges. Sealing is provided by stainless steel mushrooms, sleeves, and Teflon gaskets. Apart from the equilibrium cell, the rest of the assembly is identical to the high temperature apparatus.

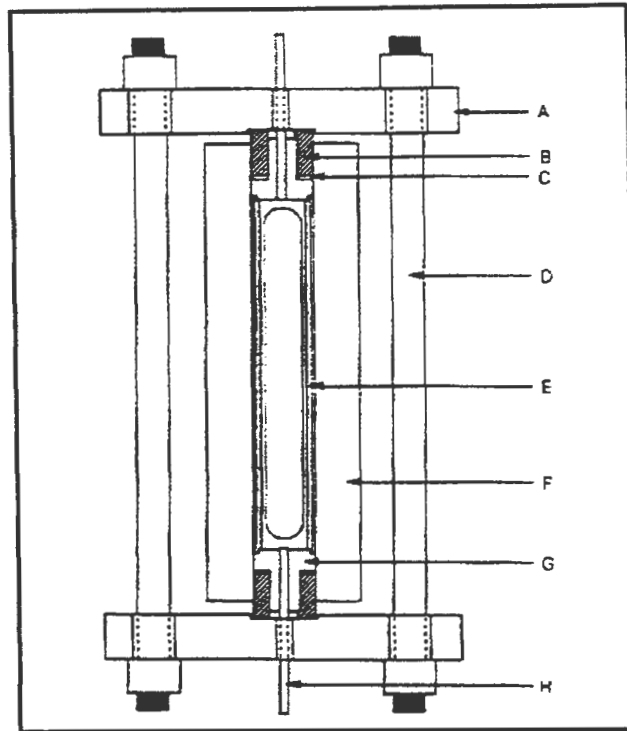


Figure A-9: Schematic illustrating details of the sapphire-tube pressure vessel of Shah et al. [1990]

A - flange; B - sleeve; C - Teflon gasket; D - threaded rod; E - spacer; F - sapphire tube; G - mushroom plug; H - stainless steel tube.

Table A-3 lists the details of all vapour phase re-circulation apparatus, along with the systems measured.

A.2.4. Two phase recirculation

Behrens and Sandler [1983]

The equilibrium cell basically was a large autoclave with a stirrer. The stirrer was driven by magnetic coupling with an external motor. Circulation of the vapour and liquid was achieved by using magnetically driven double-acting pumps.

The magnetic pumps were designed by the above authors. The pumps consisted of a barrel and heads constructed of nonmagnetic 316 stainless steel and a piston of magnetic 410 stainless steel. The piston was driven by two electromagnet coils wrapped on the barrel of the pump (Figure A-10 illustrates the pump). A solid-state timer/power supply was used to pulse the coils in partially

References	Cell volume (cm ³)	Operating Range		Equilibrium cell (1)	Measurement Device		Equilibration time (min)	Sample size (μl)		Method of sampling		Special features	Systems measured
		Temp (K)	Pressure (bar)		Temp (2)	Pressure (3)		Vapour	Liquid	Vapour	Liquid		
Price and Kobayashi [1959] Hong and Kobayashi [1988]	V.V.	115-293	138	stainless steel	TC	B	30-60	-	-	sample trap	capillary	Glass windows. Variable-volume cell.	Methane + ethylene; methane + ethane; methane + propane; methane + n-butane; ethylene + ethane; ethylene + propane; ethylene + propylene; methane + ethylene + ethane; ethylene + ethane + acetylene; natural gases. Carbon dioxide + methanol
Toyama et al. [1962]	V.V.	88-298	69	stainless steel	TC	B	-	-	-	capillary	capillary	Glass window. Variable-volume cell.	Carbon monoxide + methane
Fredenslund and Sather [1970]	-	-	-	stainless steel	QT	B	-	-	-	sampling valve	sampling valve	Visual cell.	Oxygen + carbon dioxide
Fredenslund et al. [1973]	15	93-298	350	304 stainless steel	PR	DWP	120-180	-	3.5	sampling valve	sampling rod	Fused quartz windows. Method of liquid sampling.	Carbon dioxide + oxygen; methane + argon; methane + carbon monoxide; argon + carbon monoxide

Table A-3: Vapour phase recirculation apparatus surveyed

References	Cell volume (cm ³)	Operating Range		Equilibrium cell (1)	Measurement Device		Equilibration time (min)	Sample size (μl)		Method of sampling		Special features	Systems measured
		Temp (K)	Pressure (bar)		Temp (2)	Pressure (3)		Vapour	Liquid	Vapour	Liquid		
Katayama et al. [1975]	-	-	-	stainless steel	T	B	-	-	-	sample trap	sampling valve	Housed in water bath.	Carbon dioxide + acetone; carbon dioxide + methanol.
Streett and Calado [1978]	4.2		10000	stainless steel A- 286	PR	PT	5-10	5000- 10000	5000- 10000	capillary	capillary	Special material of construction to resist hydrogen embrittlement.	Hydrogen + nitrogen.
Somait and Kidnay [1978]	-	-	138	stainless steel	PR	B	-	-	-	sample trap	capillary	Vapour passed through heat exchanger before re- entering cell.	Nitrogen + carbon dioxide; methane + carbon dioxide; nitrogen + methane + carbon dioxide.
Stead and Williams [1980]	34	>300	90	copper	PR	B	60	-	-	capillary	capillary	Visual cell	Carbon dioxide + ethane; carbon dioxide + 2,2- dimethylpropane.
Tsang and Streett [1981] Cheng et al. [1989]	10	313-523	2000	stainless steel	PR	PT	5-10	-	-	capillary	capillary	-	Carbon dioxide + dimethyl ether Carbon dioxide + n-pentane
Chang et al. [1982]	75	-	-	stainless steel	PR	PT	5-10	-	-	capillary	capillary	-	Dimethyl ether + methanol

Table A-3 (continued): Vapour phase recirculation apparatus surveyed

References	Cell volume (cm ³)	Operating Range		Equilibrium cell (1)	Measurement Device		Equilibration time (min)	Sample size (μl)		Method of sampling		Special features	Systems measured
		Temp (K)	Pressure (bar)		Temp (2)	Pressure (3)		Vapour	Liquid	Vapour	Liquid		
Pozo and Streett [1984]	-	523	290	stainless steel	PR	PT	10-15	-	-	capillary	capillary	Multiple sapphire windows. Able to measure VLLE.	Dimethyl ether + water
Pozo and Streett [1984] Cheng et al. [1989]	-	233-343	80	pyrex tubing	PR	PT	10-15	-	-	capillary	capillary	Can view entire cell content.	Dimethyl ether + water. Carbon dioxide + n-pentane.
Weber et al. [1984] Zeck and Knapp [1986]	230	223-300	3-180	chromium-nickel steel	PR	B	-	-	-	sample trap	capillary	Glass windows.	Carbon dioxide + methanol; nitrogen + methanol; nitrogen + carbon dioxide; nitrogen + carbon dioxide + methanol Ethane + methanol; nitrogen + ethane; nitrogen + ethane + methanol
Freitag and Robinson [1986]	100	256-405	280	Hastelloy C-276	TC	B	30	-	50-200	capillary	capillary	Refractive indices of phases were measured.	Hydrogen + n-pentane; hydrogen + methane + carbon dioxide; hydrogen + carbon dioxide + n-pentane.

Table A-3 (continued): Vapour phase recirculation apparatus surveyed

References	Cell volume (cm ³)	Operating Range		Equilibrium cell (1)	Measurement Device		Equilibration time (min)	Sample size (μl)		Method of sampling		Special features	Systems measured
		Temp (K)	Pressure (bar)		Temp (2)	Pressure (3)		Vapour	Liquid	Vapour	Liquid		
Jou et al. [1987]	150	-	-	316 stainless steel	TC	B	-	-	-	sample valve	sample bomb	For low pressures had windowed cell.	Triethylene glycol (TEG) + carbon dioxide; TEG + hydrogen sulphide; TEG + methane; TEG + ethane; TEG + propane.
Jou et al. [1995]													Carbon dioxide + propane + 3 M MDEA (methyldiethanol amine)
Chou et al. [1990]	100	-	-	-	TC	B	60	30	30	special sampling valve.	special sampling valve.	Special sampling valves called microcells.	Carbon dioxide + n-decane; carbon dioxide + tetralin; carbon dioxide + n- decane + tetralin.
Shah et al. [1990]	-	325-530	-	stainless steel	PR	PT	5-10	-	-	capillary	capillary	Made from a commercial sight gauge with a glass window.	Carbon dioxide + 2,2- dimethylpropane.
Shah et al. [1990]	-	>325	-	sapphire tube	PR	PT	5-10	-	-	capillary	capillary	Can view entire cell contents.	Carbon dioxide + 2,2- dimethylpropane.
Suzuki et al. [1991]	300	373	350	316 stainless steel	QT	PT	-	-	-	sample expansion	-	Glass windows.	Carbon dioxide + 1-propanol; carbon dioxide + 2-propanol; carbon dioxide + ethanol; carbon dioxide + 1- butanol.

Table A-3 (continued): Vapour phase recirculation apparatus surveyed

Key:

- (1) Material of construction of equilibrium cell
- (2) TC - thermocouple; PT - platinum resistance thermometer; TS - thermistor; QT - quartz thermometer
- (3) B - Bourdon pressure gauge; PT - pressure transducer; DWP - dead weight piston gauge

overlapping cycles so that the piston decelerated near the end of its stroke. This provided a pumping action whilst minimising the piston-pump head contact at the end of each stroke. An electronic stethoscope was used to detect the piston movement, and hence pumping, during operation.

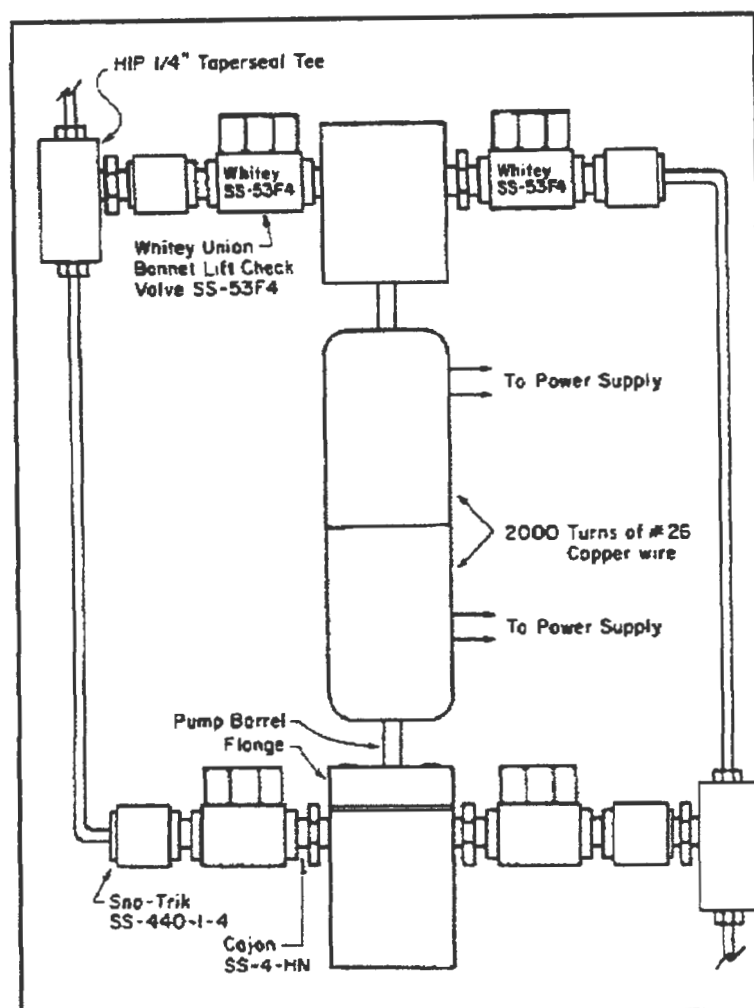


Figure A-10: Illustration of the electromagnetic pump of Behrens and Sandler [1983]

Temperature range of the equipment was 283 to 373 K. The temperature of the system was maintained by the use of a large oil bath. Propellers were used to agitate the oil bath so as to dampen changes in temperature and control it to approximately 0.02 K. Platinum resistance thermometers were used to monitor the cell temperature.

Pressure was monitored with a strain gauge type pressure transducer. It was read on a digital readout.

Sampling of the phases was achieved via the use of fine capillary tubes and analysis of the samples was undertaken on a GC.

Figure A-11 below illustrates the vapour-liquid equilibrium equipment of Behrens and Sandler [1983].

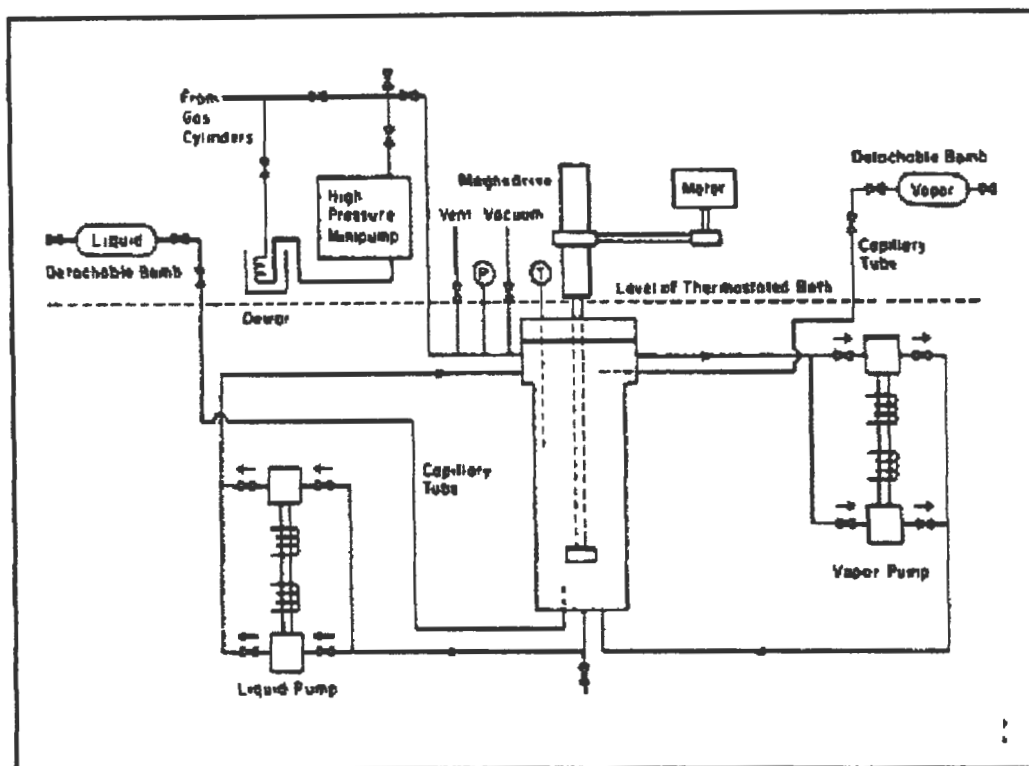


Figure A-11: Vapour-liquid equilibrium apparatus of Behrens and Sandler [1983]

Hsu et al. [1985]

The apparatus was designed so that a single charge of fluid could be employed for all property measurements (phase compositions, phase densities, and interfacial tension). The high pressure see-through windowed cell, interfacial tension cell, switching and sampling valves, and a magnetic re-circulation pump were housed in a commercial air oven.

A six-port switching valve was used to facilitate selection of either vapour or liquid circulation, or to reverse the direction of circulation in the density cell when changing from liquid to vapour circulation.

An optical/photographic system was used to photograph the pendent drops in the interfacial cell. The phase densities were measured by using a Mettler/Parr digital density meter. Measurements

were made by circulating saturated vapour and liquid, in sequence, through the vibrating U-tube of the density meter.

The sampling system for the compositional analysis of the vapour and liquid samples consisted of a combination of sampling and switching valves and was capable of delivering microliter size samples directly from the cell to the GC.

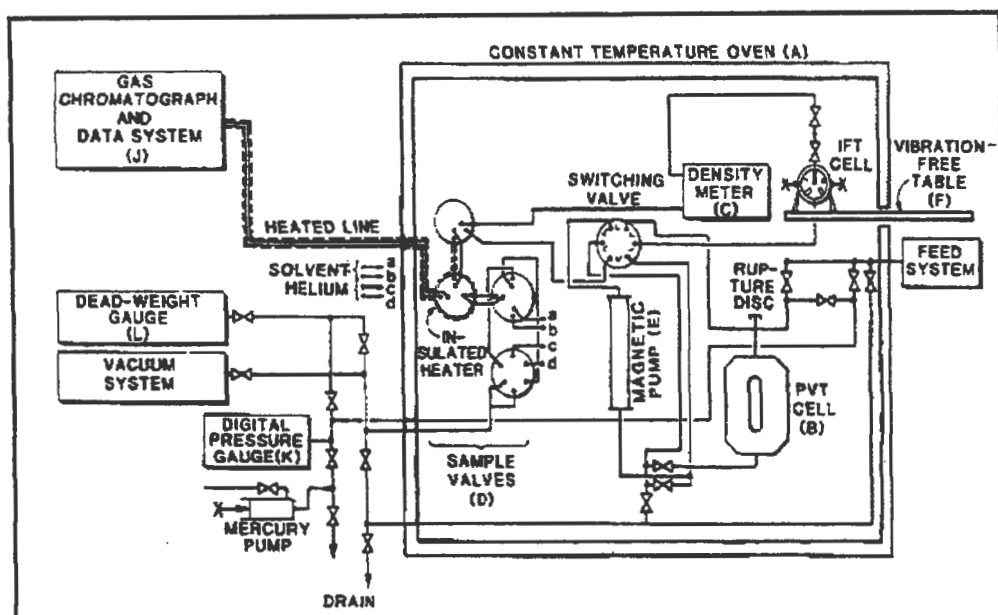


Figure A-12: Phase Equilibria measurement apparatus of Hsu et al. [1985]

Kneisl et al. [1988]

The apparatus of Kneisl et al. [1988] is claimed to be capable of measuring multiple-phase, multiple-component equilibria in the operating ranges of 310 to 425 K and 60 to 345 bar. A moveable probe permits the withdrawal of samples, from any number of phases, for analysis by GC. It also features a mercury piston, allowing easy pressure adjustment coupled with very small sample sizes, which allows numerous measurements to be made at a given feed composition over a wide pressure range.

The high-pressure cell consists of a Jerguson liquid-level gauge that is modified. The probe traverses the entire length of the cell, which is approximately 10" long. Figures A-13 and A-14 illustrate the equilibrium cell and the probe guide assembly respectively.

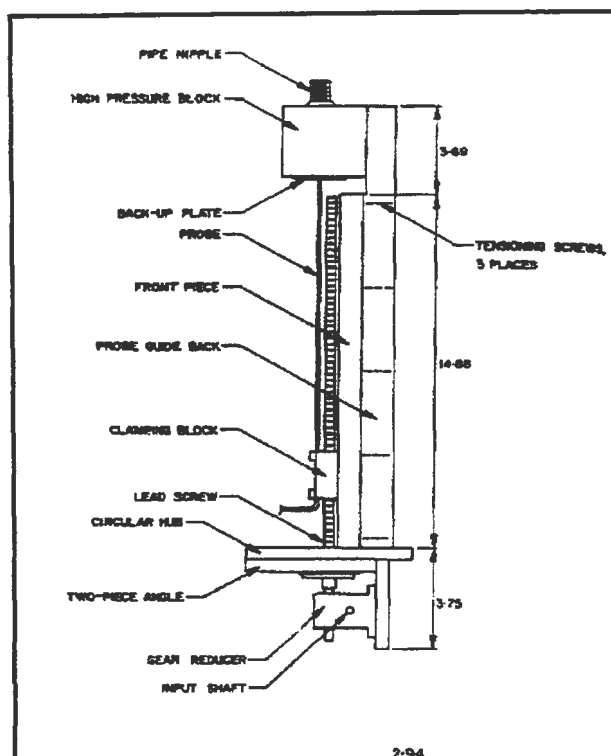


Figure A-13: Probe guide assembly of Kneisl et al. [1988]

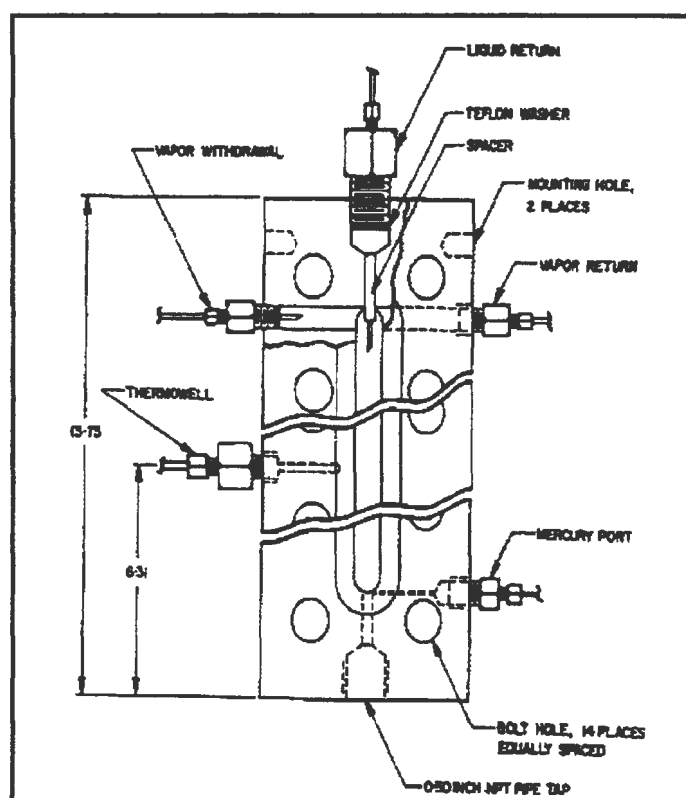


Figure A-14: Equilibrium cell assembly of Kneisl et al. [1988]

The probe guide assembly consists of three main sections:-

- the high pressure head,
- the probe guide, and
- the drive mechanism.

The high-pressure head connects the entire assembly to the equilibrium cell and houses the high-pressure seal. The probe guide supports the probe and allows smooth linear movement of the probe through the seal. The adjustability required to mount the drive motor outside the oven is provided by the drive mechanism.

Table A-4 lists the details of all two phase re-circulation apparatus, along with the systems measured.

A.2.5. Single liquid and vapour pass

Simnick et al. [1977]

The gas and liquid streams are joined at a tee and the two-phase mixture is heated initially in a tube of 2.11 mm i.d., and finally in a larger tube of 5.15 mm i.d. The larger tubing was fitted within with a notched twisted ribbon in its entire length to promote mixing of the flowing fluids.

The function of the equilibrium cell was to separate the gas and liquid phases. It was a pressure vessel approximately 90 cm³ in internal volume. Two nozzles are welded on opposite sides at mid section of the vessel. One provided the opening for the gas-liquid feed and the other for an Aminco cone compression type of electrical connection to a liquid level detector.

To avoid entrainment of gas in the liquid withdrawn from the cell, a pool of liquid is maintained in the cell. The liquid level is sensed by a capacitor in the cell. A demistor pad in the equilibrium cell prevents entrained liquid droplets from escaping overhead.

A uniform temperature is insured in the equilibrium cell by enclosing the entire cell in a copper jacket 32 mm thick.

Table A-5 lists the details of all single liquid and vapour apparatus, along with the systems measured.

References	Cell volume (cm ³)	Operating Range		Equilibrium cell (l)	Measurement Device		Equilibration time (min)	Sample size (μl)		Method of sampling		Special features	Systems measured
		Temp (K)	Pressure (bar)		Temp (2)	Pressure (3)		Vapour	Liquid	Vapour	Liquid		
Griswold et al. [1943]	600	273-553	207	steel	TC	B	300	30000	60000	sample bomb	sample bomb	Is a modified Othmer Still	benzene + toluene
Muirbrook and Prausnitz [1965]	200	233-303	103.4	403 stainless steel	TC	B	-	-	-	sample trap	sample trap	High pressure vane pumps	nitrogen + carbon dioxide; oxygen + carbon dioxide
Behrens and Sandler [1983]	1000	283-373		316 stainless steel	PR	PT	240-360	2000	2000	sample bomb	sample bomb	Electronic stethoscope to detect piston movement in pump.	Carbon dioxide + n-butane; carbon dioxide + 1-butene.
Eckert and Sandler [1986]													Carbon dioxide + cyclopentane.
Kubota et al. [1983]	106	283-353	800	304 stainless steel	T	B	120	-	-	4-port ball valve	4-port ball valve	A pair of pyrex glass windows. Sampling via ball valves.	Ethylene + propylene
Wu et al. [1988]													carbon dioxide + pentane; carbon dioxide + diethyl ether; carbon dioxide + methyl tert-butyl ether; carbon dioxide + 1-pentane
Radosz [1984]	60	283-533	350	-	PR	PT	15	100	100	Variable-volume cylinder with sampling valve	Variable-volume cylinder with sampling valve	Ability to measure V.L.L.E. Variable-volume cylinder for sampling. Windowed cell.	carbon dioxide + isopropanol; carbon dioxide + isopropanol + water

Table A-4: Two-phase recirculation apparatus surveyed

References	Cell volume (cm ³)	Operating Range		Equilibrium cell (1)	Measurement Device		Equilibration time (min)	Sample size (μl)		Method of sampling		Special features	Systems measured
		Temp (K)	Pressure (bar)		Temp (2)	Pressure (3)		Vapour	Liquid	Vapour	Liquid		
Radosz [1986(a)] Radosz [1986(b)]													2-propanol + carbon dioxide 2-propanol + water + carbon dioxide; 2- butanol + water + n-butane
Morris and Donohue [1985]	100	311 588	147 109	316 stainless steel	TC	PT	10-15	20/250	0.5	sampling valve	sampling valve	A pair of transparent glass windows	carbon dioxide + toluene; carbon dioxide + 1- methylnaphthalene ; carbon dioxide + toluene + 1- methylnaphthalene
Hsu et al. [1985] Nagarajan and Robinson [1986] Nagarajan and Robinson [1987]	-	422	690	stainless steel	PR	PT	120-360	-	-	six-port GC valve	six-port GC valve	Sampling using standard GC valves. Ability to measure densities. An optical/photogr aphic system.	Carbon dioxide + n-butane. Carbon dioxide + n-decane. Carbon dioxide + cyclohexane; carbon dioxide + benzene.
Takishima et al. [1986]	700				QT	B				sample expansion	sample expansio n	Windowed equilibrium cell.	Carbon dioxide + ethanol; carbon dioxide + water; carbon dioxide + ethanol.

Table A-4 (continued): Two-phase recirculation apparatus surveyed

References	Cell volume (cm ³)	Operating Range		Equilibrium cell (1)	Measurement Device		Equilibration time (min)	Sample size (µl)		Method of sampling		Special features	Systems measured
		Temp (K)	Pressure (bar)		Temp (2)	Pressure (3)		Vapour	Liquid	Vapour	Liquid		
Adams et al. [1988]	-	513	346	sapphire	PR	PT	5-10	455	18	six-port GC valve	six-port GC valve	Sampling using standard GC valves. Visual cell.	carbon dioxide + decane; carbon dioxide + methyl linoleate
D'Souza et al. [1988] D'Souza and Teja [1988]	100	-	-	stainless steel	PR	B	60	300/100	300/100	10-port GC valve	10-port GC valve	Sampling using standard GC valves. Glass windows.	Carbon dioxide + n-hexadecane; carbon dioxide + water glucose + fructose + water + ethanol + carbon dioxide
Kneisl et al. [1988]	-	310-425	60-345	stainless steel	PR	PT	90	1	1	sample probe	sample probe	Sampling of any phase using a sample probe. Windows viewed by mirrors. Jerguson liquid-level gauge.	Carbon dioxide + n-decane
Inomata et al. [1988]	750	-	-	316 stainless steel	TC	PT	-	-	-	sampler	sampler	Windowed cell.	Ammonia + water; ammonia + methanol + water.
Shibata and Sandler [1989(c)]	100	422	345	-	TC	PT	60	-	-	sampling valve	sampling valve	Density meters in recirculation loops. Visual cell.	Carbon dioxide + n-butane; nitrogen + n-butane; nitrogen + n-butane + carbon dioxide

Table A-4 (continued): Two-phase recirculation apparatus surveyed

References	Cell volume (cm ³)	Operating Range		Equilibrium cell (1)	Measurement Device		Equilibration time (min)	Sample size (μl)		Method of sampling		Special features	Systems measured
		Temp (K)	Pressure (bar)		Temp (2)	Pressure (3)		Vapour	Liquid	Vapour	Liquid		
Shibata and Sandler [1989(a)] Marathe and Sandler [1991]													Carbon dioxide + cyclohexane; nitrogen + cyclohexane; nitrogen + carbon dioxide + cyclohexane Cyclopentane + carbon dioxide; cyclopentane + nitrogen; cyclopentane + argon; argon + neopentane; argon + n-butane
Kim et al. [1989]	150	293-430	250	316 stainless steel	TC	PT	10	100	1	6-port GC sampling valve	6-port GC sampling valve	Glass window. Sampling using standard GC valves.	Carbon dioxide + anisole; carbon dioxide + benzaldehyde; carbon dioxide + tetralin; carbon dioxide + 1-methylnaphthalene; ethane + anisole; ethane + benzaldehyde; ethane + tetralin; ethane + 1-methylnaphthalene
Jennings and Teja [1989]	40	-	-	stainless steel	TS	B	-	1	0.2	sampling valves	sampling valves	Visual cell. Variable-volume controller similar to Radosz (1984).	Carbon dioxide + 1-hexene; carbon dioxide + 1-hexyne.

Table A-4 (continued): Two-phase recirculation apparatus surveyed

References	Cell volume (cm ³)	Operating Range		Equilibrium cell (1)	Measurement Device		Equilibration time (min)	Sample size (µl)		Method of sampling		Special features	Systems measured
		Temp (K)	Pressure (bar)		Temp (2)	Pressure (3)		Vapour	Liquid	Vapour	Liquid		
Suzuki et al. [1990(b)]	500	453	250	-	PR	B	480	1000-10000	750	sampler	sampler	Three pairs of windows.	Carbon dioxide + methanol; carbon dioxide + ethanol; carbon dioxide + 1-propanol; methane + ethanol; methane + 1-propanol; ethane + ethanol; ethane + 1-propanol.
Suzuki et al. [1990(c)]													Hydrogen + carbon monoxide + carbon dioxide + water + methane + ethane + propane + methanol + 1-propanol.
Wisniewska et al. [1993]	50	-	30	stainless steel	PR	B	-	300	300	sampling valve	sampling valve	Modified Rogalski-Malaowski ebulliometer.	Benzene + heptane; benzene + cyclohexane.

Table A-4 (continued): Two-phase recirculation apparatus surveyed

Key:

(1) Material of construction of equilibrium cell

(2) TC - thermocouple; PT - platinum resistance thermometer; TS - thermistor; QT - quartz thermometer

(3) B - Bourdon pressure gauge; PT - pressure transducer; DWP - dead weight piston gauge

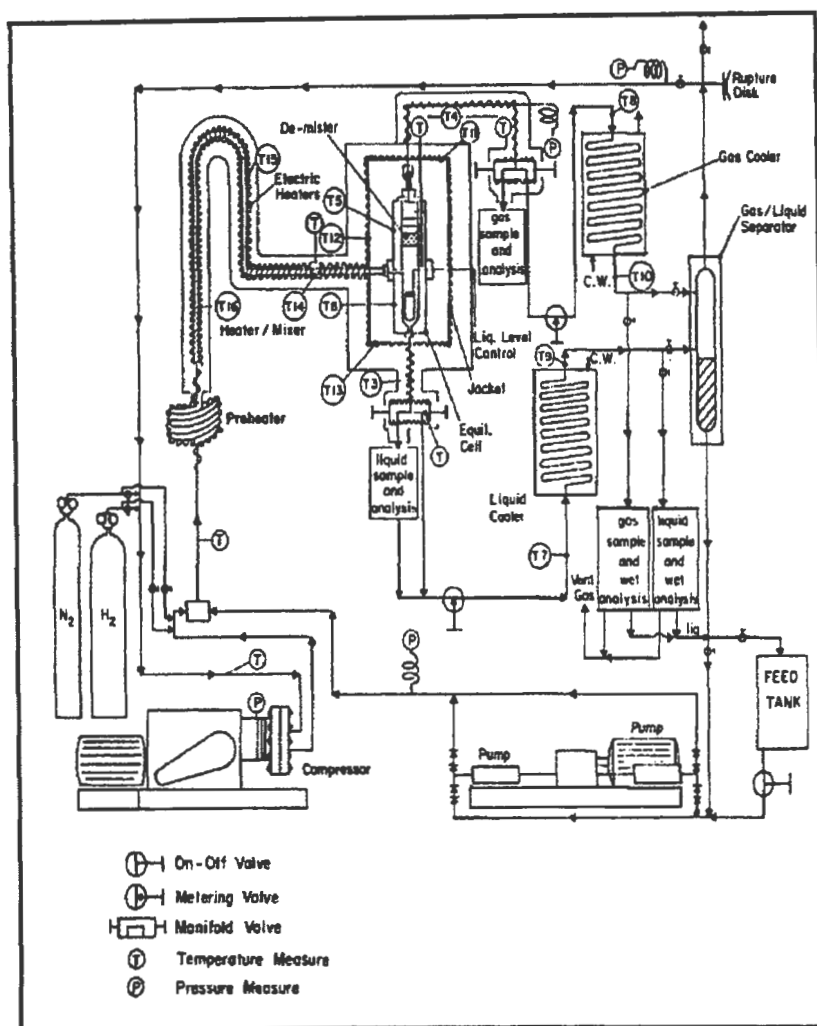


Figure A-15: Experimental apparatus of Simnick et al. [1977]

A.2.6. Static Methods

A.2.6.1. Static Analytical Methods

Ohgaki and Katayama [1975]

Sampling of the liquid phase was accomplished with a unit that comprised a tube (approximately 0.15 cm^3 in volume), a ball valve, and a needle valve (approximately 2 cm^3 in volume). The liquid phase sampler is illustrated in Figure A-16 (denoted by K). Ball valves were used with the sampling valves to avoid the flashing phenomenon. Once a sample of the gas phase had been taken, it was introduced into a container of variable volume (denoted by B in Figure A-16) and expanded to about 0.1 atm. The liquid phase sample on the other hand was vapourized and then introduced to a liquid phase container which was also maintained at about 0.1 atm. These samples were then sent to a GC for analysis. Ohgaki and Katayama [1975].

References	Cell volume (cm ³)	Operating Range		Equilibrium cell (1)	Measurement Device		Equilibration time (min)	Sample size (μl)		Method of sampling		Special features	Systems measured
		Temp (K)	Pressure (bar)		Temp (2)	Pressure (3)		Vapour	Liquid	Vapour	Liquid		
Simnick et al. [1977] Sebastian et al. [1978] Sebastian et al. [1980(a)] Sebastian et al. [1980(b)]	90	703	-	316 stainless steel	TC	B	-	-	-	Manifold valve	Manifold valve	Liquid level detector.	Hydrogen + tetralin. Hydrogen + quinoline Carbon dioxide + n-decane; carbon dioxide + n-hexadecane. Carbon dioxide + toluene; carbon dioxide + m-xylene.
Thies and Paulaitis [1984]	60	723	345	316 stainless steel	PR	B	-	-	-	sample expansion	sample expansion	High temperature aluminasilicate glass.	Methanol + 1-methylnaphthalene.
Lin et al. [1985]	10	710	250	316 stainless steel	TC	B	-	-	-	sample expansion	sample expansion	Sapphire windows. Liquid level indicator.	Carbon dioxide + toluene; propane + n-butylaldehyde; carbon dioxide + n-octadecane; carbon dioxide + phenyloctane; carbon dioxide + 1-hexadecene; carbon dioxide + n-propylcyclohexane; carbon dioxide + water + diethylamine.

Table A-5: Single liquid and vapour pass apparatus surveyed

References	Cell volume (cm ³)	Operating Range		Equilibrium cell (1)	Measurement Device		Equilibration time (min)	Sample size (μl)		Method of sampling		Special features	Systems measured
		Temp (K)	Pressure (bar)		Temp (2)	Pressure (3)		Vapour	Liquid	Vapour	Liquid		
Niesen et al. [1986]	-	625	100	316 stainless steel	PR	PT/B	-	-	-	sample expansion	sample expansion	Borosilicate glass window.	Water + ethanol; methanol + ethanol.
Inomata et al. [1986]	30	710	250	316 stainless steel	TC	B	-	-	-	sample expansion	sample expansion	Employed an overflow type self-control system.	Carbon dioxide + n-heptane; carbon dioxide + n-decane; carbon dioxide + trans- decalin; carbon dioxide + tetralin; carbon dioxide + quinoline; benzene + tetralin; benzene + quinoline.
Inomata et al. [1987]													Carbon dioxide + benzene + tetralin; carbon dioxide + n- decane + tetralin; carbon dioxide + benzene.
Jennings et al. [1991]	-	-	-	stainless steel	TS	B	20-30	-	-	sample trap	sample trap	Visual cell.	Carbon dioxide + ethanol; carbon dioxide + 1-butanol.
Chen et al. [1994]	100	700	700	Nimonic	TC	B	-	-	-	sample expansion	sample expansion	Sapphire windows.	1-propanol + p- xylene.

Table A-5 (continued): Single liquid and vapour pass apparatus surveyed

Key:

- (1) Material of construction of equilibrium cell
- (2) TC - thermocouple; PT - platinum resistance thermometer; TS - thermistor; QT - quartz thermometer
- (3) B - Bourdon pressure gauge; PT - pressure transducer; DWP - dead weight piston gauge

prepared their calibration samples at 0.1 atm as well so that the concentrations were comparable.

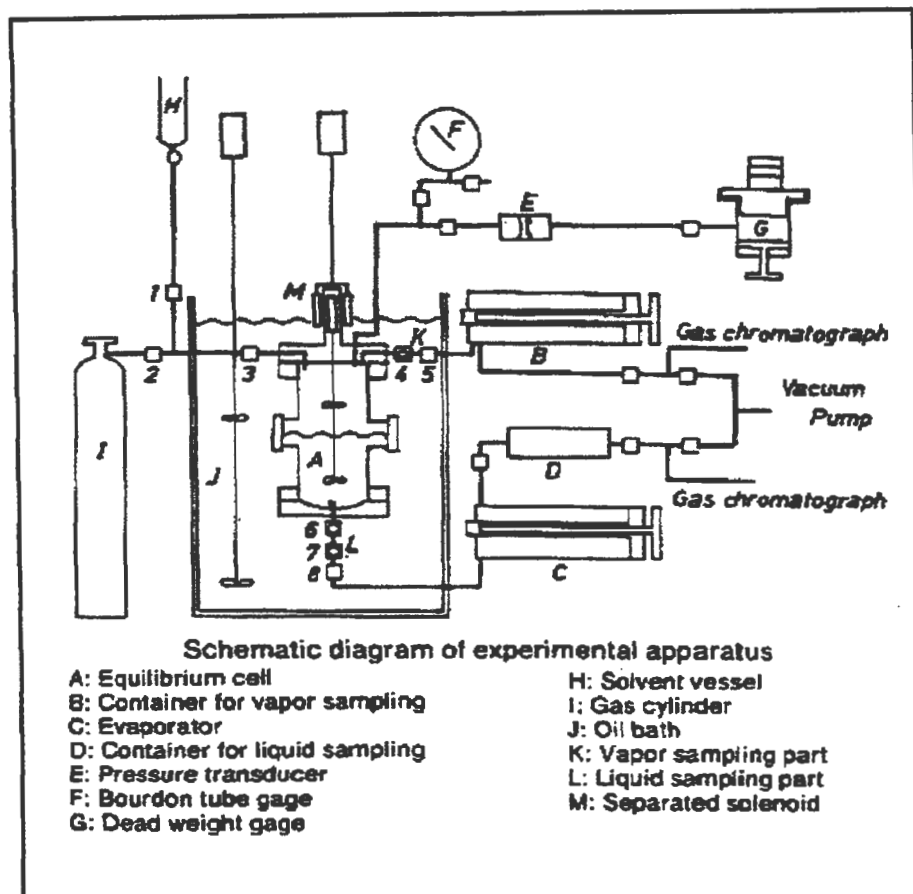


Figure A-16: Experimental apparatus of Ohgaki and Katayama [1975]

Slocum [1975]

Slocum [1975] designed a glass equilibrium cell that permitted observation of single- or multiphase systems in the temperature range of -50 to 250 °C and a pressure range of vacuum to 1000 psig. He claimed that the equipment had a wide range of applicability, and could be used in the study of reactions, densities, vapour pressures, vapour-liquid equilibria, liquid-liquid equilibria, and critical phenomena.

The cell volume was varied by mercury injection from an adjacent reservoir. Equilibrium cell volume and internal pressure was controlled by adjustment of inert-gas pressure over the mercury reservoir. The mercury height in both the equilibrium cell and reservoir was measured with a cathetometer. The variable volume capability of the equilibrium apparatus made the equipment capable of determining P-V-T data for gases or liquids.

Unfortunately Slocum [1975] did not present any experimental results, and one could not judge how reliable or accurate the apparatus was.

Reiff et al. [1987]

Sampling of the gas and liquid phases was undertaken by the use of high-pressure capillaries that had an internal diameter of 1.5 mm. The withdrawn samples were homogenised in a low-pressure sampling chamber of volume 700 cm³ with the aid of electromagnetic stirrers. To ensure that the sample was in the gaseous state, the sampling chamber was heated. Figure A-17 illustrates the sampling chamber.

A feature of the sampling chamber was a triple-loop sampling valve. At a particular time, the first loop was open to the sampling chamber and thus contained the sample; the second was open to the carrier gas; and the third was open to the vacuum system. Turning the loop valve to the second position, the loop containing the sample is open to the carrier gas and thus the sample is sent to the GC; the second evacuated; and the third took in the sample. This provided a means of sampling and conveying of sample to the GC.

The sampling chamber was also used as a mixing chamber, in which gaseous mixtures were prepared for GC calibration. Reiff et al. [1987] calculated the compositions of the gas mixtures used to calibrate the GC from the partial pressures according to Dalton's Law.

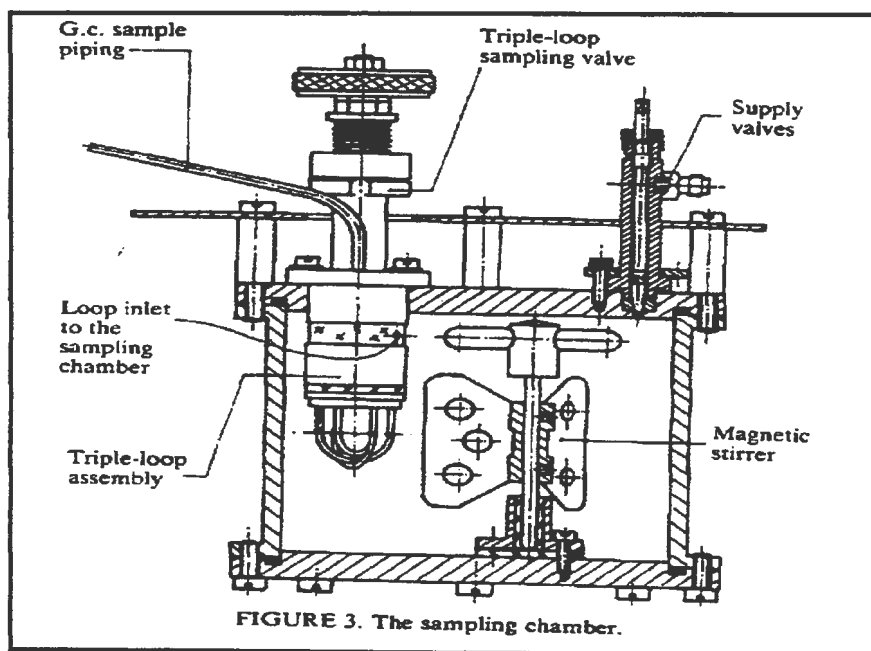


Figure A-17: The sampling chamber of Reiff et al. [1987]

A.2.6.2. Static non-analytical Methods

Laugier et. al. [1990]

The apparatus was designed for operating pressures and temperatures of up to 20 MPa and 353 K respectively. The cylindrical part of the cell was made of transparent sapphire, which allowed direct optical measurements of phase volumes. The composition of the equilibrium phases and the saturated molar volumes were calculated from material balance equations. This was achieved by measuring the phase volumes and the total number of moles for three different loadings of the equilibrium cell. Thus accurate measurement of mass and volume was critical to the success of the experimental method. A more detailed description of the experimental method is available in Laugier et al. [1990].

Table A-6 lists all the static apparatus surveyed, along with the systems measured.

A.3. Dew- and bubble point method for determination of VLE

By the variation of pressure, temperature, or composition, the dew point or bubble point of a mixture can be induced. This is as a result of the mixture entirely vapourizing or entirely liquefying. The approach of varying the pressure of a mixture of known composition is experimentally the simplest, as it can be achieved by the variation of the system volume. The dew point or bubble point is detected in such an experimental procedure by continuously monitoring the pressure-volume (P - V) profile. Dew points and bubble points are represented by sharp breaks in the P - V profile. The break in the P - V profile is particularly pronounced for the bubble point. Figure A-18 illustrates a P - V profile and the y - x equilibrium diagram corresponding to it.

With reference to Figure A-18, if a mixture of overall composition Z is decompressed from compressed liquid at A , the first vapour will form at B . This corresponds to the bubble pressure, P_B . Further vapourization will continue until the sample is entirely vapourized at the dew point, P_D . The procedure could of course have been undertaken in the opposite direction, i.e. compression from C to A . Thus B and D are two equilibrium points on a vertical line on the P - x - y diagram. Thus the breaks in the P - V profile determine the placing of the dew point and bubble point on the equilibrium curve.

To determine vapour-liquid equilibria via the dew and bubble point method as described above, it is evident that experimental apparatus must consist of a variable-volume equilibrium cell with precise volume measurement, precise pressure measurement, and an isothermal environment.

An excellent review by Malanowski [1982(a)] describes the various methods used in dew and bubble point measurement. Interestingly, earlier apparatus were visual and dew points and bubble points were detected by visually observing the appearance of condensation or the first bubble in the liquid respectively.

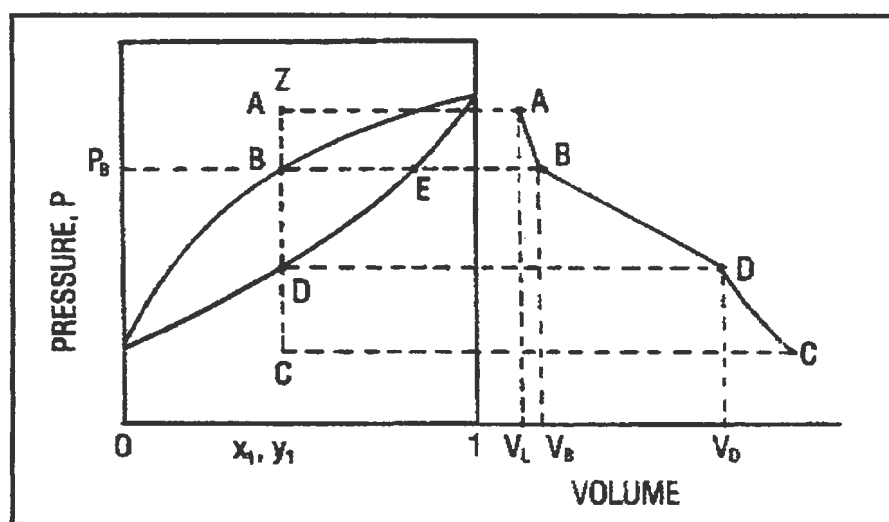


Figure A-18: Pressure-composition and pressure-volume diagrams for the method of dew and bubble point determination of VLE [extracted from Raal and Mühlbauer, 1998]

A.4. P - V - T Apparatus

Most of the equipment reviewed, that had variable-volume equilibrium cells, were capable of measuring P - V - T data. However, none of the researchers had undertaken P - V - T measurements for the determination of second virial coefficients for pure gases or gas mixtures (greater detail on virial EOS is available in Chapter 3.2.). Equipment designed to undertake P - V - T measurements and determination of second virial coefficients (Chun et al. [1981], Barber et al. [1982 (a,b,c)], and Wilson et al. [1984]) were all based on the experimental apparatus or modifications thereof by Kay [1936].

Experimental apparatus of Kay [1936]

The apparatus of Kay [1936] (Figure A-19) was used to determine the P - V - T relations of petroleum gases and vapours over a wide temperature and pressure range. The equipment was as result of modifications to the Bahlke and Kay [1932] apparatus. Equipment was later modified by Kay [1938], and Kay and Rambosek [1953] to determine P - V - T - x relations. The measurements were performed via the dew point and bubble point methods referred to in Appendix A.3.

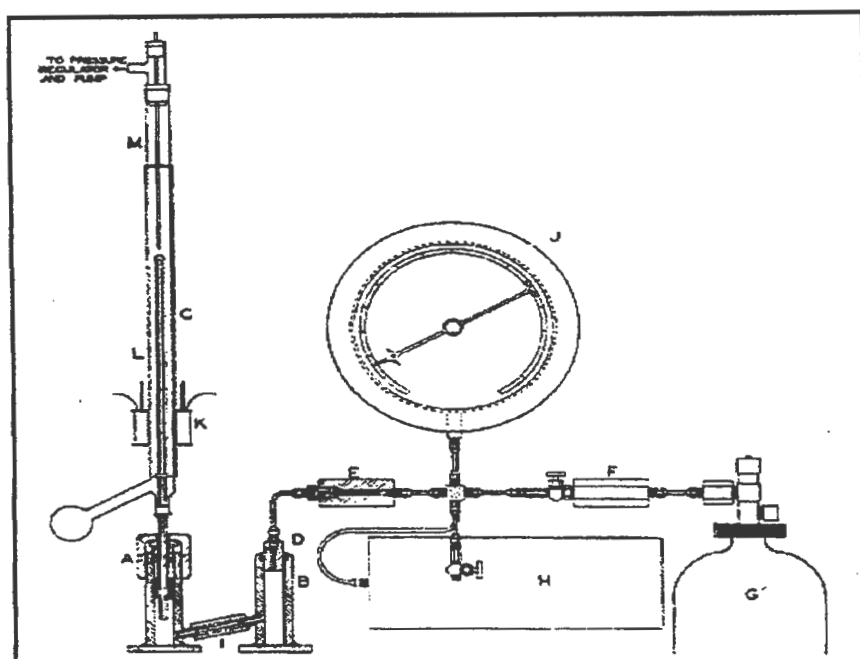


Figure A-19: P-V-T Apparatus of Kay [1936]

A,B - legs of U-tube; C - thick-walled capillary tube; D - steel plug; E,F - capillary constrictions; G - high pressure gas cylinder; H - connecting vessel; I - simple ball check valve; J - pressure gauge; K - electromagnet; L - vapour jacket; M - thermocouple.

P - V - T measurements were performed in a Pyrex capillary tube (C) of 2 mm internal diameter. It had a wall thickness of approximately 3 mm. The tube was calibrated by weighing the amount of mercury to fill it to various points, and the volume calculated from the sealed end. The volume was expressed in terms of the distance from a reference line etched around the tube near the sealed end. Pressure was measured with a precision spring gauge (J) and the pressure of the system and consequently volume was adjusted by the injection of mercury into the capillary tube. Temperature measurement was by means of a copper-constantan thermocouple (M), and the isothermal state of the tube was maintained by boiling liquid at a regulated pressure in the vapour jacket (L). The sample in the tube was stirred by means of a small steel ball which was moved by an electromagnet (K) surrounding the tube.

References	Cell volume (cm ³)	Operating Range		Equilibrium cell (1)	Measurement Device		Equilibration time (min)	Sample size (μl)		Method of sampling		Special features	Systems measured
		Temp (K)	Pressure (bar)		Temp (2)	Pressure (3)		Vapour	Liquid	Vapour	Liquid		
Kobayashi and Katz [1953]	-	367	207	-	TC	B	120	-	-	Sample expansion	Sample expansion	Glass windows.	Propane + water.
Akers et al. [1954 (a)] Akers et al. [1954 (b,c,d)]	500	-	670	stainless steel	T	B	30	-	-	Sample expansion	Sample expansion	Equilibrium cell agitated by rocking.	Methane + Propane Carbon Dioxide + Propane.
Din [1960]	-	-	-	copper	PR	DM	-	250000	-	capillary	sample bomb	Use of a differential mercury manometer to measure high pressures.	Nitrogen + oxygen.
Kohn [1961] Hottovy et al. [1981] Hottovy et al. [1982] Chen et al. [1989]	5/12	-	69/104	pyrex glass	PR	B	-	NA	NA	NA	NA	Non-analytical method to determine composition. Dew and bubble point method.	Methane + n-heptane. Methane + ethane + n-octane. Methane + propane + n-octane; methane + n-butane + n-octane; methane + carbon dioxide + n-octane. Nitrogen + methane + n-heptane.

Table A-6: Static apparatus surveyed

References	Cell volume (cm ³)	Operating Range		Equilibrium cell (1)	Measurement Device		Equilibration time (min)	Sample size (μl)		Method of sampling		Special features	Systems measured
		Temp (K)	Pressure (bar)		Temp (2)	Pressure (3)		Vapour	Liquid	Vapour	Liquid		
Rogers and Prausnitz [1970]	150	223-423	1013	stainless steel	TC	PT	-	-	-	sampling piston	sampling piston	Sampling using a piston. Thermistor to determine vapour-liquid interface.	Argon + neopentane.
Besserer and Robinson [1971]	V.V. 10-175	255-395	207	316 stainless steel	TC	PT	10	10 ⁻³ g	10 ⁻³ g	sample expansion	sample expansion	Has optical system to measure refractive index. Windowed cell. Mixing of phases by movement of pistons.	Carbon dioxide + n-butane.
Kalra et al. [1978]											four-port ball valve		Carbon dioxide + n-heptane.
Brunner et al. [1974]	1000	623	1000	316 stainless steel	TC	B	-	-	-	capillary	capillary	-	Nitrogen + n-heptane; nitrogen + methylecyclohexane; nitrogen + n-heptane + methylecyclohexane.
Ohgaki and Katayama [1975]	300	-	152	stainless steel	PR	DWP/PT	-	V.V.	150	sample expansion.	ball valve	Agitation by magnetic stirrer operated by solenoid.	Carbon dioxide + ethyl ether; carbon dioxide + methyl acetate.
Ohgaki and Katayama [1976]													Carbon dioxide + methanol; carbon dioxide + n-hexane; carbon dioxide + benzene.

Table A-6 (continued): Static apparatus surveyed

References	Cell volume (cm ³)	Operating Range		Equilibrium cell (1)	Measurement Device		Equilibration time (min)	Sample size (µl)		Method of sampling		Special features	Systems measured
		Temp (K)	Pressure (bar)		Temp (2)	Pressure (3)		Vapour	Liquid	Vapour	Liquid		
Slocum [1975]	V.V.	223-523 223-598	69 35	pyrex glass	-	-	-	-	-	-	-	Visual cell.	-
Antezana and Cheh [1975]	800	-	-	316 stainless steel	TC	DWP	300-1500	-	-	capillary	capillary	Thermistor operated liquid level probe.	Hydrogen + ammonia; hydrogen + propane; hydrogen + ammonia + propane.
Klink et al. [1975]													Hydrogen + n- butane.
Gomez-Nieto and Thodos [1978]	V.V.	325-425	56	stainless steel	TC	PT	640	50	50	magnetic agitator	magnetic agitator	Agitation by a rising and falling cylinder actuated by solenoids.	Propane + ethanol.
Ng and Robinson [1978]	150	310-589	173	316 stainless steel	TC	B	180	-	-	specially designed sampling valve	sampling rod.	Specially designed sampling techniques. Pyrex windows.	Carbon dioxide + toluene.
Ng and Robinson [1979]													Carbon dioxide + methylecyclohexa ne; hydrogen sulfide + methylecyclohexa ne.
Huang and Robinson [1984]													m-Xylene + hydrogen sulphide; mesitylene + hydrogen sulphide.

Table A-6 (continued): Static apparatus surveyed

References	Cell volume (cm ³)	Operating Range		Equilibrium cell (1)	Measurement Device		Equilibration time (min)	Sample size (μl)		Method of sampling		Special features	Systems measured
		Temp (K)	Pressure (bar)		Temp (2)	Pressure (3)		Vapour	Liquid	Vapour	Liquid		
Huang and Robinson [1985]													Methane + mesitylene; carbon dioxide + mesitylene.
Kalra and Robinson [1979]	241.1	77-298	104	stainless steel	TC	PT	-	-	-	sampling valve	sampling valve	Cathetometer used to measure liquid volume.	Six-component sour natural gas.
Figuiere et al. [1980]	50	673	400	stainless steel	TC	PT	-	1	1	sampling valve	sampling valve	Stirring via magnetic induction using solenoid coils. Sampling using valves which open for a very short time (0.01 s).	Nitrogen + n-heptane.
Laugier et al. [1980]													Hydrogen + 2,2,4-trimethylpentane; hydrogen + toluene.
Renon et al. [1989]													Carbon dioxide + n-propylbenzene; nitrogen + n-propylbenzene.
Legret et al. [1981]	100	233-433	50-1000	stainless steel	TC	PT	10	15	15	sampling microcell	sampling microcell	Stirring by magnetic induction using solenoid coils. Sampling using detachable microcells.	Nitrogen + n-heptane.

Table A-6 (continued): Static apparatus surveyed

References	Cell volume (cm ³)	Operating Range		Equilibrium cell (1)	Measurement Device		Equilibration time (min)	Sample size (μl)		Method of sampling		Special features	Systems measured
		Temp (K)	Pressure (bar)		Temp (2)	Pressure (3)		Vapour	Liquid	Vapour	Liquid		
Renon et al. [1989]													Carbon dioxide + n-propylbenzene; nitrogen + n- propylbenzene.
Bae et al. [1981]	300	223-323	100	304 stainless steel	PR	PT	120	-	8	sample expansion	sampling rod.	Large glass window. Sampling of liquid using a sampling rod.	Ethylene + 1- butene; ethylene + propylene.
Meskel-Lesavre et al. [1981]	V.V.	373	50	titanium	TC	PT	60	NA	NA	NA	NA	Entire cell sits on a mass balance. Movable piston.	Ethane + n- dodecane.
Konrad et al. [1983]	100	293-473	2000	stainless steel Nimonic 90	TC	B	-	50 mg	50 mg	capillary	capillary	Two pairs of sapphire windows. Agitation by magnetic induction produced by solenoid coils.	Carbon dioxide + tridecane + hexadecane; carbon dioxide + tridecane + 1- hexadecanol.
Spee and Schneider [1991]													Carbon dioxide + hexadecane; carbon dioxide + 1-dodecanol; carbon dioxide + 1,8-octanediol; carbon dioxide + dotriacontane; hexadecane + 1,8-octanediol.

Table A-6 (continued): Static apparatus surveyed

References	Cell volume (cm ³)	Operating Range		Equilibrium cell (1)	Measurement Device		Equilibration time (min)	Sample size (μl)		Method of sampling		Special features	Systems measured
		Temp (K)	Pressure (bar)		Temp (2)	Pressure (3)		Vapour	Liquid	Vapour	Liquid		
Kordikowski and Schneider [1995]													Carbon dioxide + 1-dodecanol + dodecanoic acid + (quinoxaline or 1,8-octanediol); carbon dioxide + 1-dodecanol + dodecanoic acid; carbon dioxide + 1-dodecanol + quinoxaline; carbon dioxide + dodecanoic acid + quinoxaline.
Konrad et al. [1983]	100	300-450	2000	stainless steel Nimonic 90	TC	B	-	NA	NA	NA	NA	Spectroscopic methods to determine composition. Sapphire windows.	Carbon dioxide + decane.
Rousseaux et al. [1983]	V.V.	573	600	stainless steel	TC	PT	300	NA	NA	NA	NA	Entire cell sits on a mass balance.	Methane + n-nonane
Guillevic et al. [1983]	V.V.	558	70	316 stainless steel	TC	PT	-	-	-	capillary	capillary	Stirring by magnetic induction using solenoid coils.	Propane + n-octane.
Galivel-Solastionk et al. [1986]													Propane + methanol; propane + methanol + carbon dioxide

Table A-6 (continued): Static apparatus surveyed

References	Cell volume (cm ³)	Operating Range		Equilibrium cell (1)	Measurement Device		Equilibration time (min)	Sample size (μl)		Method of sampling		Special features	Systems measured
		Temp (K)	Pressure (bar)		Temp (2)	Pressure (3)		Vapour	Liquid	Vapour	Liquid		
Asheroft et al. [1983]	885	333	690	manganese steel	TS	PT	180	60	60	sampling rod	sampling rod	Sampling of phases using a retractable rod. Windows. Agitation via rocking of cell.	Methane + n- hexane.
de Loos et al. [1984]	-	-	-	stainless steel	PR	DWP	-	-	-	-	-	Windowed autoclave.	Ethylene + n- eicosane; ethylene + hexacosane; ethylene + n- tetracontane.
Fontalba et al. [1984]	V.V. 60 (max)	433	450	titanium alloy	TC	PT	-	NA	NA	NA	NA	Thermistor probe to measure vapour-liquid interface. Piston activated by magnetic field induced by solenoid coils. Micrometer to measure piston level.	Carbon dioxide + isopentane.
Galivel-Solastiouk et al. [1986]													Propane + methanol; propane + methanol + carbon dioxide.
Renon et al. [1989]													Carbon dioxide + n-propylbenzene; nitrogen + n- propylbenzene.

Table A-6 (continued): Static apparatus surveyed

References	Cell volume (cm ³)	Operating Range		Equilibrium cell (1)	Measurement Device		Equilibration time (min)	Sample size (μl)		Method of sampling		Special features	Systems measured
		Temp (K)	Pressure (bar)		Temp (2)	Pressure (3)		Vapour	Liquid	Vapour	Liquid		
Fall and Luks [1984]	7-8	398	104	pyrex glass	PR	PT	-	NA	NA	NA	NA	Phase volumes measured using a cathetometer.	Carbon dioxide + n-dotriacontane; carbon dioxide + n-docosane.
Fall and Luks [1985]													Carbon dioxide + n-tridecane; carbon dioxide + n-paraffin.
Huang et al. [1985]	V.V. (45 max)	523	345	sapphire and stainless steel	TC	PT	-	-	-	sample expansion	sample expansion	Agitation by rocking. Entire cell visual.	Methane + carbon dioxide + hydrogen sulphide + water
Leu and Robinson [1988]													Carbon dioxide + neopentane.
Japas and Franck [1985]	-	673	2900	nickel-base corrosion-resistant high strength alloy	TC	PT	-	-	-	capillary	capillary	Can be run in synthetic or analytical mode. Sapphire windows.	Nitrogen + water
Laugier and Richon [1986]	50	423	100	316 stainless steel	TC	PT	-	-	-	special capillary	special capillary	Kalrez is used a gasket. Unique sampling method using capillaries.	Ethane + cyclohexane.
Galivel-Solastiouk et al. [1986]													Propane + methanol; propane + methanol + carbon dioxide.

Table A-6 (continued): Static apparatus surveyed

References	Cell volume (cm ³)	Operating Range		Equilibrium cell (1)	Measurement Device		Equilibration time (min)	Sample size (μl)		Method of sampling		Special features	Systems measured
		Temp (K)	Pressure (bar)		Temp (2)	Pressure (3)		Vapour	Liquid	Vapour	Liquid		
Renon et al. [1989]													Carbon dioxide + n-propylbenzene; nitrogen + n-propylbenzene.
Occhiogrosso et al. [1986]	V.V. (45 max)	535	700	316 stainless steel	PR	PT	-	NA	NA	NA	NA	Movable piston sealed with Viton o-rings. Visual cell. Isopleth measurements.	Carbon dioxide + cumene
Suppes and McHugh [1989]													Carbon dioxide + styrene.
Wagner and Wichterle [1987]	65	-	100	stainless steel	QT	B	-	-	-	capillary	capillary	Pyrex glass windows.	Carbon dioxide + 1-hexane; carbon dioxide + n-hexane; carbon dioxide + 1-hexene + n-hexane.
Wagner and Pavlicek [1993]													Carbon dioxide + p-cymene.
Wagner and Pavlicek [1994]													Carbon dioxide + ethyl acetate.
Wagner [1995]													Carbon dioxide + ethyl propanoate.
Nakayama et al. [1987]	270	450	200	316 stainless steel	TC	PT	720	100 250	100 250	sampling rod capillary	sampling rod capillary	Sampling via sliding rod and capillary compared.	Water + 1,1-difluoroethane; water + ethanol + 1,1-difluoroethane; water + carbon dioxide.

Table A-6 (continued): Static apparatus surveyed

References	Cell volume (cm ³)	Operating Range		Equilibrium cell (I)	Measurement Device		Equilibration time (min)	Sample size (μl)		Method of sampling		Special features	Systems measured
		Temp (K)	Pressure (bar)		Temp (2)	Pressure (3)		Vapour	Liquid	Vapour	Liquid		
Kalra et al. [1987]	V.V.	-	200	316 stainless steel	TC	B	720-900	-	-	sample expansion	sample expansion	Windowed cell. Agitation by rocking. Liquid level using cathetometer. Mercury in cell.	Limonene + citral + carbon dioxide.
Kalra et al. [1987]	V.V.	-	240	316 stainless steel	TC	PT	1440	-	-	capillary sample bomb	capillary sample bomb	Agitation via turbine impeller. Pressure drop across capillary used to measure viscosity.	Palm oil + carbon dioxide.
Reiff et al. [1987]	2000	273-473	300	chromium + nickel + molybdenum steel	PR	B/PT	-	-	-	capillary	capillary	-	Methane + n-pentane.
Laugier et al. [1990]	V.V. (10 max)	353	200	Sapphire	TC	PT	-	NA	NA	NA	NA	Entire cell visual. Cathetometer to indicate liquid level. Piston sealed with o-ring.	Carbon dioxide + tetradecane; carbon dioxide + acetic acid; carbon dioxide + water + acetic acid.
Muhlbauer [1990]	350	453	200	stainless steel	PR	PT/B	-	900	8.8	sample expansion	sampling rod	Use of jet-mixers to homogenise samples.	Carbon dioxide + toluene; propane + water; propane + 1-propanol
Muhlbauer and Raal [1991]													Carbon dioxide + toluene.
Muhlbauer and Raal [1993]													Propane + 1-propanol.

Table A-6 (continued): Static apparatus surveyed

References	Cell volume (cm ³)	Operating Range		Equilibrium cell (1)	Measurement Device		Equilibration time (min)	Sample size (μl)		Method of sampling		Special features	Systems measured
		Temp (K)	Pressure (bar)		Temp (2)	Pressure (3)		Vapour	Liquid	Vapour	Liquid		
Xu et al. [1991] Bian et al. [1993]	500	-	500	Stainless steel	PR	PT	-	600	300	capillary	capillary	Reinforced glass windows.	Carbon dioxide + 1-pentane; R-22 + ethanol; R-22 + 2-propanol; R-22 + 1-hexane; R-22 + cyclohexane; R-22 + tetrachloromethane. Carbon dioxide + 2-methylbutane; carbon dioxide + methane.
Brunner et al. [1994]	1000	773	350	-	TC	PT	-	-	-	capillary	capillary	Equilibrium cell is an autoclave.	Carbon dioxide + n-hexadecane; water + n-hexadecane + carbon dioxide; benzene + n-hexadecane + carbon dioxide; benzene + n-hexadecane + hydrogen.
Verneau et al. [1994]	500	273-423	1-20	-	PR	PT	-	-	-	sample expansion	sample expansion	Automated ebulliometer.	Acetone + methanol; isopropanol + methanol.
Sako et al. [1995]	500	480	300	-	PR	B	240-300	-	3000	metering valve	magnetic circulating pump	Sampling of liquid using a pump. Glass windows.	Carbon dioxide + furfural; carbon dioxide + water + furfural.

Table A-6 (continued): Static apparatus surveyed

References	Cell volume (cm ³)	Operating Range		Equilibrium cell (1)	Measurement Device		Equilibration time (min)	Sample size (µl)		Method of sampling		Special features	Systems measured
		Temp (K)	Pressure (bar)		Temp (2)	Pressure (3)		Vapour	Liquid	Vapour	Liquid		
Pfohl et al. [1997]	1100	-	520	stainless steel	TC	PT	720	-	-	capillary	capillary	Can sample three phases.	Carbon dioxide + o-cresol + p-cresol; water + benzene derivative; carbon dioxide + benzene derivative; carbon dioxide + water + benzene derivative.

Table A-6 (continued): Static apparatus surveyed

Key:

(1) Material of construction of equilibrium cell

(2) TC - thermocouple; PT - platinum resistance thermometer; TS - thermistor; QT - quartz thermometer

(3) B - Bourdon pressure gauge; PT - pressure transducer; DWP - dead weight piston gauge

APPENDIX B

B.1. DEVELOPMENT OF THE CRITERION FOR PHASE EQUILIBRIUM

For a closed system the fundamental property relation relating Gibbs energy, temperature and pressure is given by :

$$d(nG) = (nV)dP - (nS)dT \quad (\text{B-1})$$

If one applies this equation to a single-phase fluid that does not undergo chemical reaction, the system is then of constant composition, and one can write that :

$$\left[\frac{d(nG)}{dP} \right]_{T,n} = nV \quad (\text{B-2})$$

and

$$\left[\frac{d(nG)}{dT} \right]_{P,n} = -nS \quad (\text{B-3})$$

In Equations (B-2) and (B-3) the subscript n indicates that the number of moles of all the chemical species are held constant.

For the more general case of a single-phase, open system, the total Gibbs energy is still a function of temperature and pressure, but now it is also related to number of moles of each chemical species present. The total differential of nG is :

$$d(nG) = \left[\frac{d(nG)}{dP} \right]_{T,n} dP + \left[\frac{d(nG)}{dT} \right]_{P,n} dT + \sum_i \left[\frac{d(nG)}{dn_i} \right]_{P,T,n_j} dn_i \quad (\text{B-4})$$

where summation is over all species present and subscript n_j indicates that all mole numbers except the i th are held constant.

Replacing the first two partial derivatives by (nV) and $-(nS)$ and defining the chemical potential of species i in the mixture as:

$$\mu_i = \left[\frac{d(nG)}{dn_i} \right]_{P,T,n_j} \quad (\text{B-5})$$

one obtains the fundamental property relation for single-phase open systems :

$$d(nG) = (nV)dP + (nS)dT + \sum \mu_i dn_i \quad (\text{B-6})$$

Consider now a closed system consisting of two phases in equilibrium. Within this closed system, each of the individual phases is an open system, free to transfer mass to the other. Equation (B-6) may therefore be written for each phase:

$$d(nG)^\alpha = (nV)^\alpha dP + (nS)^\alpha dT + \sum \mu_i^\alpha dn_i^\alpha \quad (\text{B-7})$$

$$d(nG)^\beta = (nV)^\beta dP + (nS)^\beta dT + \sum \mu_i^\beta dn_i^\beta \quad (\text{B-8})$$

where superscripts α and β identify the phases.

If at equilibrium temperature and pressure are uniform throughout the entire system, then the total change in the Gibbs energy of the system is the sum of these equations, (B-7) and (B-8).

$$d(nG) = (nV)dP - (nS)dT + \sum \mu_i^\alpha dn_i^\alpha + \sum \mu_i^\beta dn_i^\beta \quad (\text{B-9})$$

Since the two-phase system is closed, Equation (B-1) must be valid. Comparing (B-1) and (B-9) one has that:

$$\sum \mu_i^\alpha dn_i^\alpha + \sum \mu_i^\beta dn_i^\beta = 0 \quad (\text{B-10})$$

The changes dn_i^α and dn_i^β , however, result from mass transfer between the phases, and mass conservation requires that:

$$dn_i^\alpha = -dn_i^\beta \quad (\text{B-11})$$

Therefore,

$$\sum (\mu_i^\alpha - \mu_i^\beta) dn_i^\alpha = 0 \quad (\text{B-12})$$

Hence,

$$\mu_i^\alpha = \mu_i^\beta \quad i = (1, 2, \dots, N) \quad (\text{B-13})$$

where, N is the number of species present in the system.

By successively considering pairs of phases, one may readily generalise to more than two phases.

For π phases,

$$\mu_i^\alpha = \mu_i^\beta = \dots = \mu_i^\pi \quad i = (1, 2, \dots, N) \quad (\text{B-14})$$

For a species i in a real solution, we have the defining equation,

$$d\bar{G}_i = RT d \ln \hat{f}_i \quad (\text{const. T}) \quad (\text{B-15})$$

where \hat{f}_i is the fugacity of species i in solution.

Since by Equation (B-5), $\mu_i = \bar{G}_i$, one may write

$$d\mu_i = RT d \ln \hat{f}_i \quad (\text{const. T}) \quad (\text{B-16})$$

Integration at constant temperature gives :

$$\mu_i = RT \ln \hat{f}_i + \theta_i(T) \quad (\text{B-17})$$

where the integration constant depends on temperature only.

Since all phases are in equilibrium at the same temperature, substitution for the μ_i 's in Equation (B-14) leads to :

$$\hat{f}_i^\alpha = \hat{f}_i^\beta = \dots = \hat{f}_i^\pi \quad i = (1,2,\dots,N) \quad (\text{B-18})$$

B.2. STANDARD STATES: SYMMETRIC/UNSYMMETRIC NORMALISATION OF ACTIVITY COEFFICIENTS

For condensable components ($T_{\text{system}} < T_{\text{ci}}$) it is customary to normalise the activity coefficient such that,

$$\lim_{x_i \rightarrow 1} \gamma_i = 1 \quad (\text{B-19})$$

This means that as the composition of the solution approaches that of the pure liquid, the component's liquid fugacity becomes equal to the mole fraction multiplied by the standard-state fugacity, f_i° . This is referred to as the symmetric convention for normalisation of activity coefficients.

For non-condensable components ($T_{\text{system}} > T_{\text{ci}}$) normalisation is as follows:

$$\lim_{x_i \rightarrow 0} \gamma_i^* = 1 \quad (\text{B-20})$$

Equation (B-20) implies that the component's liquid fugacity equals the mole fraction multiplied by the standard-state fugacity in the limit as the component mole fraction becomes very small. This concentration region where γ_i is essentially unity is called the ideal dilute solution or Henry's-Law region.

Henry's constant (H), defined by:

$$H = \lim_{x_i \rightarrow 0} \frac{\hat{f}_i}{x_i} = f_i^\circ \quad (\text{B-21})$$

is the standard-state fugacity for any component i whose activity coefficient is normalised by Equation (B-20). As a result the standard-states for these components depend on solvent properties.

For a binary liquid solution containing a condensable and a non-condensable component, normalisation of the solvent and solute are via Equations (B-19) and (B-20) respectively. As a result of the components being normalised differently, they are said to follow the unsymmetric convention.

B.3. CONDENSABLE AND NON-CONDENSABLE COMPONENT ACTIVITY COEFFICIENTS

Condensable components

For a component where $T_{\text{critical}} > T_{\text{system}}$ the constant pressure activity coefficient at constant temperature and composition can be determined by:

$$\gamma_i^{(p')} = \gamma_i^{(p)} \exp \int_p^{p'} \left(\frac{\bar{V}_i}{RT} \right) dP \quad (3-21)$$

where $\gamma_i^{(p')}$ is the activity coefficient at the arbitrary reference pressure p' .

The liquid phase fugacity \hat{f}_i^L is then described by:

$$\hat{f}_i^L = x_i f_i^{OL} \gamma_i^{(p')} \exp \int_{p'}^p \frac{\bar{V}_i^L}{RT} dP \quad (3-22)$$

In order that $\gamma_i^{(p')} \rightarrow 1$ as $x_i \rightarrow 1$ the standard-state reference fugacity must be that of pure liquid component i at the system temperature and chosen reference pressure.

$$f_i^{OL} = f_i^L \quad (B-22)$$

At equilibrium conditions, the fugacity of a pure liquid component equals the fugacity of the pure gaseous component, and the latter is a readily available quantity. Therefore f_i^L is expressed by means of the fugacity at the saturated vapour pressure, P_i^s .

$$f_i^{L(P_i^r)} = f_i^{V(P_i^r)} = \phi_i^{(P_i^r)} P_i^s \quad (\text{B-23})$$

If the reference pressure is set equal to zero, then the integrated form of Equation (3-23) yields the following standard-state fugacity:

$$f_i^{OL} = \phi_i^s P_i^s \exp\left(-\frac{V_i^L P_i^s}{RT}\right) \quad (\text{B-24})$$

Non-condensable components

For a non-condensable component the liquid phase fugacity may be described analogously to that for a condensable component.

$$\hat{f}_i^L = x_i f_i^{OL} \gamma_i^{*(P^r)} \exp\int_{P^r}^P \frac{\bar{V}_i^L}{RT} dP \quad (\text{3-24})$$

The hypothetical standard-state for the non-condensable component is avoided by using the normalisation:

$$\gamma_i^{*(P^r)} \rightarrow 1 \text{ as } x_{\text{non-condensable},j} \rightarrow 0 \text{ and } x_{\text{condensable},i} \rightarrow 1 \quad (\text{B-25})$$

As a result the standard-state fugacity (f_i^{OL}) of the non-condensable component (i) in the condensable component (j) at the temperature of the mixture and the reference pressure (P^r) is just Henry's constant.

The pressure dependence of Henry's constant is expressed by:

$$H_{ij}^{(P_2)} = H_{ij}^{(P_1)} \exp \int_{P_1}^{P_2} \left(\frac{\bar{V}_{ij}^\infty}{RT} \right) dP \quad (\text{B-26})$$

Now, Henry's constant is usually measured at the saturated vapour pressure (P_i^s) of the condensable component i . Thus, assuming \bar{V}_{ij}^∞ to be independent of pressure, the pressure-correction (given by the equation below) converts Henry's constant from the experimental pressure to the desired reference pressure.

$$H_{ij}^{(P')} = H_{ij}^{(P_i^s)} \exp \int_{P_i^s}^{P'} \left(\frac{\bar{V}_{ij}^\infty}{RT} \right) dP \quad (\text{B-27})$$

Setting the reference pressure to zero, Equation (B-27) reduces to:

$$H_{ij} = H_{ij}^{(P_i^s)} \exp \left(- \frac{\bar{V}_{ij}^\infty P_i^s}{RT} \right) \quad (\text{B-28})$$

B.4. COMBINED METHODS IN LITERATURE

Wichterle [1978(b)] gives an excellent review on the combined methods in literature. Here is a summary of his review.

Chao-Seader Method

It represented the first easy analytical description of high-pressure vapour-liquid equilibrium. Since it does not require adjustable parameters, the method is predictive rather than correlative. The method originated during the time that the direct method based on the Benedict-Webb-Rubin (BWR) EOS existed. The BWR had a complicated numerical solution and was non-generalised.

The equilibrium condition in terms of the combined method of Chao-Seader is given by :

$$x_i \gamma_i \phi_i = y_i \hat{\phi}_i \quad (\text{B-29})$$

where ϕ_i^L is the standard-state fugacity in Equation (3-15) being replaced by the fugacity coefficient of component i as a pure liquid at the system temperature and pressure.

$$\phi_i^L = \frac{f_i^o}{P} = \frac{f_i^L}{P} \quad (\text{B-30})$$

The fugacity coefficient ϕ_i^L was obtained from the three parameter corresponding states principle proposed by Pitzer,

$$\log \phi_i^L = \log \phi_i^{(0)} + \omega_i \log \phi_i^{(1)} \quad (\text{B-31})$$

where $\phi_i^{(0)}$ and $\phi_i^{(1)}$ are analytical functions of reduced temperature and pressure.

The liquid phase activity coefficients γ_i were calculated from the Scatchard-Hildebrand regular solution theory,

$$\ln \gamma_i = \frac{V_i}{RT} (S_i - \bar{S})^2 \quad (\text{B-32})$$

where S is the solubility parameter which is a function of pressure.

The vapour phase fugacity coefficients $\hat{\phi}_i$ were based on the Redlich-Kwong EOS.

Fictitious values of ϕ_i , S_i , and V_i have to be used for supercritical components. These values are determined for components by trial so as to produce results in agreement with data. This was an unsatisfactory solution and Prausnitz and Chueh [1968] and Prausnitz et al. [1980] dealt with supercritical components more rigorously.

Prausnitz-Chueh Method

The more complicated Prausnitz-Chueh method was elaborated as a counterpart of the simple Chao-Seader model because it was obvious that a more exact approach would yield better results. The Prausnitz-Chueh method is distinguished by the selection of a standard-state and by the correlation of the activity coefficient. The method is based on the symmetric-unsymmetric

convention for normalisation of activity coefficients using standard-states 3 and 8 (Table 3-1) for the condensable and non-condensable liquid components respectively.

The equilibrium condition for component i is expressed by Equation (3-15)

$$y_i \hat{\phi}_i^V P = x_i \gamma_i f_i^o \quad (3-15)$$

The standard-state fugacity f_i^o for a condensable component using standard-state 3 (Table 3-1) is then written as:

$$f_i^o = f_i^{OL} = f_i^{L(P)} \exp \int_0^P \left(-\frac{V_i^L}{RT} \right) dP \quad (B-33)$$

A similar expression could be written in terms of Henry's constant for the non-condensable component using standard-state 8 (Table 3-1). The standard-state fugacities are evaluated from polynomial expansions of temperature. Each component requires 5 or 6 parameters. The activity coefficients γ_i are derived from the following equation:

$$\gamma_i^{(P_1)} = \gamma_i^{(P_2)} \exp \int_{P_1}^{P_2} \left(\frac{\bar{V}_i^L}{RT} \right) dP \quad (B-34)$$

which yields:

$$\gamma_i^{(P)} = \gamma_i^{(o)} \exp \int_0^P \left(\frac{\bar{V}_i^L}{RT} \right) dP \quad (B-35)$$

The unsymmetrically normalised activity coefficient at zero pressure $\gamma_i^{(o)}$ were expressed by means of a modified van Laar equation.

For a binary mixture the temperature dependence of $\gamma_i^{(o)}$ required 7 interaction parameters and one parameter for the pure component. The partial molar volume \bar{V}_i was generalised by means of an 18 parameter relation. The vapour-phase fugacity coefficient was described by the Redlich-Kwong EOS. Two pure component parameters and three interaction parameters were required.

The complexity of the Prausnitz-Chueh method is reflected in the number of parameters required. A survey undertaken by Wichterle (1978,b) yielded the data in Table B-1.

Other Methods

The origins of the other combined methods were in an attempt to improve the simple Chao-Seader method or simplify the complicated Prausnitz-Chueh method. For an excellent review on these methods refer to Wichterle [1978(b)].

Components	Pure Component Data	Adjustable Parameters		Total
		Pure	Binary	
2	10	20	34	64
3	15	30	51	96
4	20	40	102	162

Table B-1: Number of parameters required for the Prausnitz-Chueh Method [Wichterle, 1978(b)]

B.5. RATING OF THE COMPUTATIONAL METHODS FOR HPVLE

Raal and Mühlbauer [1998] have drawn up the following table as a comparison of the capabilities of the combined and direct methods. They also rate the capabilities of the various classes of equations of state.

Method	System				Phase Density	Method Complexity	Predictive capabilities
	Polarity Hi	Structural Complexity Hi	Pressure Hi	Temperature Hi			
Combined	Fair/good ¹	Fair/good ¹	Fair/good ¹	Fair/good ¹	Fair/good	Medium	No ⁴
Direct	Poor/fair ²	Poor/fair ²	Poor/fair ²	Poor/fair ²	Poor/fair	Low/medium	No ⁴
Modern Direct	Fair/good ³	Fair/good ³	Fair/good ³	Fair/good ³	Fair/good	Medium/high	Yes ⁵

1 - Depends on the liquid phase model and the EOS being used.

2 - Depends on the EOS being used.

3 - Depends on the mixing rule dependency and the liquid phase model and EOS being used.

4 - Possibilities exist at low pressure and medium temperature.

5- Possible if low pressure and medium temperature VLE data are available

Table B-2: Rating of the computational methods for HPVLE [Raal and Mühlbauer, 1998]

In Table B-2 Raal and Mühlbauer [1998] refer to the Modern direct method. This refers to predictive methods using a linear programming method in the EOS mixing rule, e.g. the Wong and Sandler [1992] mixing rule. Refer to Raal and Mühlbauer [1998] for greater detail. Raal and Mühlbauer also summarised the capabilities of the various classes of EOS's in Table B-3.

EOS	System				Phase Density	Method Complexity	Predictive capability
	Polarity Hi	Structural complexity Hi	Pressure Hi	Temperature Hi			
Complex virial	Fair/good	Fair/good	Poor/fair	Fair/good	Poor/fair	High	No
Perturbation theory	Fair/good	Fair/good	Fair/good	Fair/good	Fair/good	Medium/high	No ¹
Traditional cubic	Poor/fair	Poor/fair	Fair	Fair	Fair	Low	No
Virial	Fair/good	Fair/good	Poor/Fair ²	Fair/good	Fair/good ²	Low	No
Novel mixing rules ³	Fair/good	Fair/good	Fair	Fair	Fair	Low/medium	No
Modern direct method	Fair/good	Fair/good	Fair/good	Fair/good	Fair/good	Medium/high	Yes

1 - Neglecting the interaction parameter can sometimes yield accurate data.

2 - Depends if the two parameter or three parameter form is being used.

3 - Depends on which novel mixing rule dependency is being used and capabilities can vary.

Table B-3: Capabilities of the various classes of equations of state [Raal and Mühlbauer, 1998]

Criterion	Direct Method	Combined Method
Accuracy of the calculation: depends on the particular method, number of parameter etc.	Good, including the critical region.	Excellent, except for the critical region.
Range of conditions	Up to the critical region.	Limited.
Type of components	Complex hydrocarbon mixtures without large deviations from ideal behaviour, but small content of non-hydrocarbons is acceptable.	Less complicated mixtures with medium or greater deviations from ideality.
Calculation within critical region	Good	Poor
Execution time	Generally slow, depending on number of roots in EOS.	Fast
Input parameters	It depends on the degree of generalisation.	Usually generalised better, but more parameters are required.
Sensitivity to initial guess	Very sensitive.	Not important.
Correlation abilities	Only binary interaction parameters can be adjusted.	Number of adjusting parameters unlimited.
Consistency of computation	Good	Reliable results cannot be expected at higher pressures.

Table B-4: Comparison of the Direct and Combined Methods [Wichterle, 1978(b)]

B.6. CORRELATIONS FOR THE VIRIAL COEFFICIENTS

The virial coefficients are determined as follows:

$$B = \lim_{V \rightarrow \infty} (Z - 1)V \quad (\text{B-36})$$

Similarly,

$$C = \lim_{V \rightarrow \infty} [(Z - 1)V - B]V \quad (\text{B-37})$$

and

$$D = \lim_{V \rightarrow \infty} [(Z - 1)V - BV - C]V \quad (\text{B-38})$$

Now, as V approaches infinity, P approaches zero at constant T , therefore equation (B-36) may be transformed into the following expression:

$$B = \lim_{V \rightarrow \infty} (Z - 1)V = RT \lim_{P \rightarrow 0} \left(\frac{Z - 1}{P} \right) = RT \lim_{P \rightarrow 0} \left(\frac{\partial Z}{\partial P} \right)_T \quad (\text{B-39})$$

Then, the second virial coefficient can be obtained from PVT data by plotting Z versus P at constant T and taking the slope at $P = 0$. Much of this type of data has been obtained for various fluids at various isotherms, and has been used to develop correlations for the second virial coefficient. The most widely used correlations are those of Tsonopoulos [1974] and Hayden and O'Connell [1975].

The Tsonopoulos correlation is:

$$\frac{BP}{RT} = B^{(0)} + \omega B^{(1)} \quad (\text{B-40})$$

where:

$$B^{(0)} = 0,1445 - \frac{0,33}{T_r} - \frac{0,1385}{T_r^2} - \frac{0,0121}{T_r^3} - \frac{0,000607}{T_r^8} \quad (\text{B-41})$$

$$B^{(1)} = 0,0637 + \frac{0,331}{T_r} - \frac{0,424}{T_r^2} - \frac{0,008}{T_r^8} \quad (\text{B.41})$$

The Hayden-O'Connell [1975] correlation is more complex and it includes the dipole moments and radii of gyration. It is used by Prausnitz et. al. [1980] and us in computation of VLE. For completeness here is the generalised method of Hayden and O'Connell [1975].

Hayden-O'Connell

The pure-component and cross second virial coefficients B_{ij} are given by the sum of two contributions:

$$B_{ij} = B_{ij}^F + B_{ij}^D \quad (\text{B.42})$$

where

$$B_{ij}^F = \left(B_{nonplar}^F \right)_{ij} + \left(B_{polar}^F \right)_{ij} \quad (\text{B.43})$$

and

$$B_{ij}^D = \left(B_{metastable} \right)_{ij} + \left(B_{bond} \right)_{ij} + \left(B_{chemical} \right)_{ij} \quad (\text{B.44})$$

The superscripts F and D denote relatively "free" molecules (weak physical forces), and relatively "bound" or "dimerized" molecules ("chemical" forces) respectively.

The individual contributions to the second virial coefficient are calculated from temperature-dependent correlations:

$$\left(B_{nonplar}^F \right)_{ij} = b_{0ij} \left(0,94 - \frac{1,47}{T_{ij}^{*r}} - \frac{0,85}{T_{ij}^{*r2}} - \frac{1,015}{T_{ij}^{*r3}} \right) \quad (\text{B.45})$$

$$\left(B_{polar}^F \right)_{ij} = -b_{0ij} \mu_{ij}^{*r} \left(0,74 - \frac{3,0}{T_{ij}^{*r}} + \frac{2,1}{T_{ij}^{*r2}} + \frac{2,1}{T_{ij}^{*r3}} \right) \quad (\text{B.46})$$

$$(B_{metastable})_{ij} + (B_{bound})_{ij} = b_{0ij} A_{ij} \exp\left(\frac{\Delta h_{ij}}{T_{ij}^*}\right) \quad (\text{B-48})$$

$$(B_{chemical})_{ij} = b_{0ij} E_{ij} \left[1 - \exp\left(\frac{1500\eta_{ij}}{T}\right) \right] \quad (\text{B-49})$$

$$\frac{1}{T_{ij}^*} = \frac{1}{T_{ij}^*} - 1,6\omega_{ij} \quad (\text{B-50})$$

$$T_{ij}^* = \frac{T}{\left(\frac{\varepsilon_{ij}}{k}\right)} \quad (\text{B-51})$$

The temperature-independent parameters used in equations (B-45) to (B-51) are:

$$b_{0ij} = 1,26184\sigma_{ij}^3 \quad (\text{B-52})$$

$$\begin{aligned} \mu_{ij}^* &= \mu_{ij}^* & \mu_{ij}^* < 0,04 \\ &= 0 & 0,04 \leq \mu_{ij}^* < 0,25 \\ &= \mu_{ij}^* - 0,25 & \mu_{ij}^* \geq 0,25 \end{aligned} \quad (\text{B-53})$$

$$A_{ij} = -0,3 - 0,05\mu_{ij}^* \quad (\text{B-54})$$

$$\Delta h_{ij} = 1,99 + 0,2\mu_{ij}^{*2} \quad (\text{B-55})$$

$$\mu_{ij}^* = \frac{7243,8\mu_i\mu_j}{\left(\frac{\varepsilon_{ij}}{k}\right)\sigma_{ij}^3} \quad (\text{B-56})$$

$$E_{ij} = \exp\left\{ \eta_{ij} \left[\frac{650}{\left(\frac{\varepsilon_{ij}}{k}\right) + 300} - 4,27 \right] \right\} \quad \text{for } \eta_{ij} < 4,5 \quad (\text{B-57a})$$

or

$$E_{ij} = \exp \left\{ \eta_{ij} \left[\frac{42800}{\left(\frac{\varepsilon_{ij}}{k} \right) + 22400} - 4,27 \right] \right\} \quad \text{for } \eta_{ij} \geq 4,5 \quad (\text{B-57b})$$

where

- T - temperature (K)
 (ε_{ij}/k) - characteristic energy for the i - j interaction (K)
 σ_{ij} - molecular size (angstroms)
 μ_i - dipole moment of component i (Debye)
 η_{ij} - association parameter ($i = j$); solvation parameter ($i \neq j$)
 ω_{ij} - nonpolar acentric factor

For $i = j$, parameters (ε_{ii}/k) , σ_{ii} , and ω_{ii} are predicted from the pure component properties.

$$\omega_{ii} = 0,006026R_{D_i} + 0,02096R_{D_i}^2 - 0,001366R_{D_i}^3 \quad (\text{B-58})$$

$$\left(\frac{\varepsilon_{ii}}{k} \right)' = \left(\frac{\varepsilon_{ii}}{k} \right)' \left\{ 1 - \xi c_1 \left[1 - \frac{\xi(1+c_1)}{2} \right] \right\} \quad (\text{B-59})$$

$$\sigma_{ii} = \sigma_{ii}' (1 + \xi c_2)^{1/3} \quad (\text{B-60})$$

$$\left(\frac{\varepsilon_{ii}}{k} \right)' = T_{C_i} \left[0,748 + 0,91\omega_{ii} - \frac{0,4\eta_{ii}}{2 + 20\omega_{ii}} \right] \quad (\text{B-61})$$

$$\sigma_{ii}' = (2,44 - \omega_{ii}) \left(1,0133 \frac{T_{C_i}}{P_{C_i}} \right)^{1/3} \quad (\text{B-62})$$

$$\xi = 0 \quad \text{for } \mu_i < 1,45 \quad (\text{B-63a})$$

$$\xi = \frac{1,7941 \times 10^7 \mu_i^4}{\left[\left(2,882 - \frac{1,882\omega_{ii}}{0,03 + \omega_{ii}} \right) T_{C_i} \sigma_{ii}' \left(\frac{\varepsilon_{ii}}{k} \right)' \right]} \quad \text{for } \mu_i \geq 1,45 \quad (\text{B-63b})$$

$$c_1 = \frac{16 + 400\omega_{ii}}{10 + 400\omega_{ii}} \quad (\text{B-64})$$

$$c_2 = \frac{3}{10 + 400\omega_{ii}} \quad (\text{B-65})$$

Pure component parameters that are required in equations (B-58) to (B-65) are:

- T_{C_i} - critical temperature of component i (K)
- P_{C_i} - critical pressure of component i (bar)
- R_{D_i} - mean radius of gyration of component i (angstroms)

Cross parameters (ε_{ij}/k) , σ_{ij} , and ω_{ij} ($i \neq j$) are calculated using suitable mixing rules and pure component parameters given by equations (B-58) to (B-65).

$$\omega_{ij} = \frac{1}{2}(\omega_{ii} + \omega_{jj}) \quad (\text{B-66})$$

$$\left(\frac{\varepsilon_{ij}}{k} \right) = \left(\frac{\varepsilon_{ij}}{k} \right)' (1 + \xi c_1') \quad (\text{B-67})$$

$$\sigma_{ij} = \sigma_{ij}' (1 - \xi c_2') \quad (\text{B-68})$$

where

$$\left(\frac{\varepsilon_{ij}}{k} \right)' = 0,7 \left[\left(\frac{\varepsilon_{ii}}{k} \right) \left(\frac{\varepsilon_{jj}}{k} \right) \right]^{1/2} + \frac{0,6}{\left[\left(\frac{\varepsilon_{ii}}{k} \right) + \left(\frac{\varepsilon_{jj}}{k} \right) \right]} \quad (\text{B-69})$$

$$\sigma'_{ij} = (\sigma_{ii}\sigma_{jj})^{1/2} \quad (\text{B-70})$$

$$\xi' = \frac{\mu_i^2 \left(\frac{\varepsilon_{jj}}{k}\right)^{2/3} \sigma_{ij}^4}{\left(\frac{\varepsilon_{ij}}{k}\right)' \sigma_{ij}'^6} \quad \text{for } \mu_i \geq 2 \text{ and } \mu_j = 0 \quad (\text{B-71a})$$

or

$$\xi' = \frac{\mu_j^2 \left(\frac{\varepsilon_{kk}}{k}\right)^{2/3} \sigma_{ij}^4}{\left(\frac{\varepsilon_{ij}}{k}\right)' \sigma_{ij}'^6} \quad \text{for } \mu_j \geq 2 \text{ and } \mu_i = 0 \quad (\text{B-71b})$$

or

$$\xi' = 0,0 \text{ for all other values of } \mu_i \text{ and } \mu_j \quad (\text{B-71c})$$

$$c_1' = \frac{16 + 400\omega_{ij}}{10 + 400\omega_{ij}} \quad (\text{B-72})$$

$$c_2' = \frac{3}{10 + 400\omega_{ij}} \quad (\text{B-73})$$

Variations of the virial EOS are either truncated forms of the virial equation or curve fitting forms e.g. Beattie-Bridgeman and Benedict-Webb-Rubin EOS's. The variations of the virial EOS's are excellently covered by Sandler [1994].

B.7. DETERMINATION OF PARAMETERS (*A* AND *B*) FOR CUBIC EOS

There are two ways to determine the parameters (*a* and *b*) in the EOS's. The first is to change the parameters to fit experimental data, usually the vapor pressure and liquid or vapor density. In the van der Waals equation, the parameters are constants and this can only be done at one temperature. For EOS's with parameters which are functions of temperature, the fitting is performed over a range of temperatures.

The second way is to fit parameters to the critical point using the EOS concerned and the following critical-point conditions.

$$\left(\frac{dP}{dV}\right)_{T_c} = \left(\frac{d^2P}{d^2V}\right)_{T_c} = 0 \quad (\text{B-74})$$

Applying the criteria of equation (B-74) to the van der Waals equation we obtain:

$$a = \frac{27R^2T_c^2}{64P_c} \quad (\text{B-75})$$

$$b = \frac{RT_c}{8P_c} \quad (\text{B-76})$$

where subscript *c* denotes a property at the critical point.

For cubic EOS in which the parameters are dependent on temperature, the critical point condition, equation (B-74) is used to obtain values of the parameters at the critical point i.e. a_c and b_c . Then a multiplicate temperature dependent correction term is introduced [equation (B-77)], which is unity at the critical point and adjusted to produce better predictions over the whole temperature range.

$$a(T) = a_c \alpha(T) \quad (\text{B-77})$$

For more detail on parameter determination refer to Walas [1985].

B.8. METHODS FOR APPLICATION OF CUBIC EOS TO MIXTURES

There are essentially two basic methods of applying a cubic EOS to a mixture. The first involves the formulation of effective combining rules for mixture pseudo-critical properties and the second involves the derivation of mixture parameters from those of the individual components.

In the first method, a mixture's critical properties (T_{cm} , P_{cm} , etc.) are determined via suitable combining rules. These are then used to calculate the EOS a_m and b_m parameters. The simplest of these combining rules are mole-fraction-weighted sums of the corresponding property parameter for the components of the mixture. Refer to Walas [1985] for various combining rules proposed for this method.

In the second method, pure component a_i and b_i parameters are calculated using pure component properties (T_{ci} , P_{ci} , etc.). Mixing rules are then used to express the EOS a_m and b_m parameters as some function of the composition and pure component a_i and b_i parameters. This method was used in this project and is discussed in detail in Chapter 3.

B.9. FORMULATION OF THE WONG-SANDLER MIXING RULE

The following is the full formulation of the Wong-Sandler mixing rules for the Peng-Robinson EOS with the NRTL Gibbs excess model, as it appears in Wong and Sandler [1992].

The Peng-Robinson EOS is:

$$P = \frac{RT}{(\bar{V} - b)} - \frac{a(T)}{\bar{V}^2 + 2b\bar{V} - b^2} \quad (\text{B-78})$$

The Helmholtz free energy departure function for the Peng-Robinson EOS at a given temperature, pressure and composition is:

$$\frac{(\bar{A} - \bar{A}^{IGM})}{RT} = -\ln \left[\frac{P(\bar{V} - b)}{RT} \right] + \frac{a}{2\sqrt{2}RT} \ln \left[\frac{\bar{V} + (1 - \sqrt{2})b}{\bar{V} + (1 + \sqrt{2})b} \right] \quad (\text{B-79})$$

Taking the limit as pressure approaches infinity, one obtains:

$$\lim_{P \rightarrow \infty} \frac{(\bar{A} - \bar{A}^{IGM})}{RT} = \frac{a}{bRT} C \quad (\text{B-80})$$

with the constant C being:

$$C = \frac{1}{\sqrt{2}} \ln(\sqrt{2} - 1) \quad (\text{B-81})$$

The excess Helmholtz free energy at infinite pressure is then:

$$\frac{\bar{A}_{\infty}^E}{CRT} = \frac{a_m}{b_m RT} - \sum_i x_i \frac{a_i}{b_i RT} \quad (\text{B-82})$$

The expressions for the EOS parameters a_m and b_m :

$$b_m = \frac{Q}{(1-D)} \quad (\text{B-83})$$

and

$$\frac{a_m}{RT} = Q \frac{D}{(1-D)} \quad (\text{B-84})$$

with Q and D defined as:

$$Q = \sum_i \sum_j x_i x_j \left(b - \frac{a}{RT} \right)_{ij} \quad (\text{B-85})$$

and

$$D = \sum_i x_i \frac{a_i}{b_i RT} + \frac{\bar{A}_{\infty}^E}{CRT} \quad (\text{B-86})$$

The fugacity coefficient is computed from:

$$\ln \phi_i = \int_{\bar{V}}^{\infty} \left[\frac{1}{RT} \left(\frac{\partial P}{\partial n_i} \right)_{T, V, n_j} - \frac{1}{\bar{V}} \right] d\bar{V} - \ln \left(\frac{P\bar{V}}{RT} \right) \quad (\text{B-87})$$

For the Peng-Robinson EOS and an arbitrary set of mixing rules for a_m and b_m , one obtains:

$$\begin{aligned} \ln \phi_i = & -\ln \left[\frac{P(\bar{V} - b_m)}{RT} \right] + \frac{1}{b_m} \left(\frac{\partial n b_m}{\partial n_i} \right) \left(\frac{P\bar{V}}{RT} - 1 \right) + \\ & \frac{1}{2\sqrt{2}} \left(\frac{a_m}{b_m RT} \right) \left[\frac{1}{a_m} \left(\frac{1}{n} \frac{\partial n^2 a_m}{\partial n_i} \right) - \frac{1}{b_m} \left(\frac{\partial n b_m}{\partial n_i} \right) \right] \ln \left[\frac{\bar{V} + b_m(1 - \sqrt{2})}{\bar{V} + b_m(1 + \sqrt{2})} \right] \end{aligned} \quad (\text{B-88})$$

The partial derivatives of a_m and b_m are:

$$\frac{\partial n b_m}{\partial n_i} = \frac{1}{(1-D)} \left(\frac{1}{n} \frac{\partial n^2 Q}{\partial n_i} \right) - \frac{Q}{(1-D)^2} \left(1 - \frac{\partial n D}{\partial n_i} \right) \quad (\text{B-89})$$

and

$$\frac{1}{RT} \left(\frac{1}{n} \frac{\partial n^2 a_m}{\partial n_i} \right) = D \frac{\partial n b_m}{\partial n_i} + b_m \frac{\partial n D}{\partial n_i} \quad (\text{B-90})$$

with the partial derivatives of Q and D given by:

$$\left(\frac{1}{n} \frac{\partial n^2 Q}{\partial n_i} \right) = 2 \sum_j x_j \left(b - \frac{a}{RT} \right)_{ij} \quad (\text{B-91})$$

and

$$\frac{\partial n D}{\partial n_i} = \frac{a_i}{b_i RT} + \frac{\ln \gamma_{\infty i}}{C} \quad (\text{B-92})$$

with

$$\ln \gamma_{\infty i} = \frac{1}{RT} \frac{\partial \bar{A}_{\infty}^E}{\partial n_i} \quad (\text{B-93})$$

Using the NRTL model for Helmholtz energy at infinite pressure:

$$\frac{\bar{A}_{\infty}^E}{RT} = \sum_i x_i \left(\frac{\sum_j x_j \tau_{ji} g_{ji}}{\sum_k x_k g_{ki}} \right) \quad (\text{B-94})$$

with

$$g_{ij} = \exp(-\alpha_{ij} \tau_{ij}) \quad (\alpha_{ij} = \alpha_{ji}) \quad (\text{B-95})$$

Applying equation (B-93) to the NRTL model one obtains:

$$\ln \gamma_{\infty i} = \frac{\sum_j x_j \tau_{ji} g_{ji}}{\sum_k x_k g_{ki}} + \sum_j \frac{x_j g_{ij}}{\sum_k x_k g_{kj}} \left(\tau_{ij} - \frac{\sum_l x_l \tau_{lj} g_{lj}}{\sum_k x_k g_{kj}} \right) \quad (\text{B-96})$$

B.10. TWO PARAMETER VAN DER WAALS ONE-FLUID MODEL (2PVDW)

Referring to Table 3-4 the binary interaction parameter (k_{ij}) is now a composition-dependent two-parameter term. All combining rules in table 3-4 reduce to equation (B-97) for a binary system.

$$k_{ij} = K_{ij} x_i + K_{ji} x_j \quad (\text{B-97})$$

For the Peng-Robinson EOS the fugacity expression is then given by:

$$\ln \phi_i = \frac{b_i}{b_m} (Z-1) - \ln(Z-B) - \frac{A}{2\sqrt{2}B} \left[\frac{\left(\frac{\partial n a_m}{\partial n_i} \right)_{T,n_j}}{a_m} + 1 - \frac{b_i}{b_m} \right] \ln \left(\frac{Z + (1+\sqrt{2})B}{Z + (1-\sqrt{2})B} \right) \quad (\text{B-98})$$

with

$$\left(\frac{\partial n a_m}{\partial n_i} \right)_{T,n_j} = 2 \left\{ \sum_k x_k a_{ik} + \sum_{j \neq i} x_j x_j (a_i a_j)^{0.5} [x_j K_{ji} - (1-x_i) K_{ij}] \right\} - a_m \quad (\text{B-99})$$

for binary mixtures.

The other equations remain the same as for the Peng-Robinson EOS with the classical van der Waals mixing rules.

B.11. HURON-VIDAL MIXING RULE (HVO) (Huron and Vidal [1979])

The b_m parameter is identical to the mixing rule for the classical van der Waal's. The a_m mixing rule is now:

$$a_m = b_m \left[\sum_i x_i \frac{a_i}{b_i} + \frac{\overline{G}_\infty^E}{C^*} \right] \quad (\text{B-100})$$

where, $C^* = \ln 2$.

The fugacity coefficient for Peng-Robinson EOS is then given by:

$$\ln \phi_i = \frac{b_i}{b_m} (Z-1) - \ln(Z-B) - \frac{1}{2\sqrt{2}} \left[\frac{a_i}{b_i RT} + \frac{\ln \gamma_i}{C^*} \right] \ln \left\{ \frac{Z + (1+\sqrt{2})B}{Z + (1-\sqrt{2})B} \right\} \quad (\text{B-101})$$

B.12. MODIFIED HURON –VIDAL FIRST ORDER MIXING RULE (MHV1) (Michelsen [1990(b)])

The b_m parameter is unchanged from the classical van der Waals mixing rule. The a_m parameter is now defined as:

$$\frac{a_m}{b_m RT} = \left\{ \sum_i x_i \frac{a_i}{b_i RT} + \frac{1}{q_1} \left[\frac{\bar{G}_\infty^E}{RT} + \sum_i x_i \ln \left(\frac{b_m}{b_i} \right) \right] \right\} \quad (\text{B-102})$$

where, q_1 is an empirical parameter obtained by fitting pure component information.

The fugacity coefficient for the Peng-Robinson EOS is given by:

$$\ln \phi_i = \frac{b_i}{b_m} (Z - 1) - \ln(Z - B) - \frac{1}{2\sqrt{2}} \left[\frac{a_i}{b_i RT} + \frac{\ln \gamma_i}{q_1} + \frac{1}{q_1} \ln \left(\frac{b_m}{b_i} \right) + \frac{1}{q_1} \left(\frac{b_i}{b_m} - 1 \right) \right] \\ \ln \left\{ \frac{Z + (1 + \sqrt{2})B}{Z + (1 - \sqrt{2})B} \right\} \quad (\text{B-103})$$

$\ln \gamma_i$ is determined from an appropriate Gibbs free-excess model.

B.13. MODIFIED HURON-VIDAL SECOND ORDER MIXING RULE (MHV2) (Dahl and Michelsen [1990])

The b_m parameter is unchanged from the classical van der Waals mixing rule. The a_m parameter is now obtained by solving the following quadratic expression for ε :

$$q_2 \varepsilon^2 + q_1 \varepsilon + \left[-q_1 \sum_i x_i \varepsilon_i - q_2 \sum_i x_i \varepsilon_i^2 - \frac{\bar{G}_\infty^E}{RT} - \sum_i x_i \ln \left(\frac{b_m}{b_i} \right) \right] = 0 \quad (\text{B-104})$$

where,

$$\varepsilon = \frac{a}{bRT} \quad (\text{B-105})$$

When solving for ε the larger of the two real roots is chosen to obtain a_m . q_1 and q_2 are empirical constants obtained by fitting pure component properties.

The fugacity coefficient for the Peng-Robinson EOS is then given by:

$$\ln \phi_i = \frac{b_i}{b_m} (Z - 1) - \ln(Z - B) - \frac{1}{2\sqrt{2}} \left(\frac{\partial n\varepsilon}{\partial n_i} \right) \ln \left\{ \frac{Z + (1 + \sqrt{2})B}{Z + (1 - \sqrt{2})B} \right\} \quad (\text{B-106})$$

where,

$$\frac{\partial n\varepsilon}{\partial n_i} = \frac{q_1 \varepsilon_i + q_2 (\varepsilon^2 + \varepsilon_i^2) + \ln \gamma_i + \ln \left(\frac{b_m}{b_i} \right) + \left(\frac{b_i}{b_m} \right) - 1}{q_1 + 2q_2 \varepsilon} \quad (\text{B-107})$$

$\ln \gamma_i$ is determined from an appropriate Gibbs free-excess model.

B.14. LINEAR COMBINATION OF HURON-VIDAL AND MICHELSEN MODELS (LCVM) (Boukouvalas et al. [1994])

The b_m parameter is unchanged from the classical van der Waals mixing rule. The a_m parameter is now obtained from:

$$\frac{a_m}{b_m RT} = \left[\left(\frac{\lambda}{C^*} + \frac{1 - \lambda}{q_1} \right) \frac{\overline{G}_\infty^E}{RT} + \frac{1 - \lambda}{q_1} \sum_i x_i \ln \left(\frac{b_m}{b_i} \right) + \sum_i x_i \frac{a_i}{b_i RT} \right] \quad (\text{B-108})$$

where, λ is an arbitrary parameter that has been selected to give the best results for the particular system under consideration once the excess free energy model is chosen. Note that $\lambda = 1$ gives the HVO model, while $\lambda = 0$ gives the MHV1 model. The fugacity coefficient is then given by:

$$\ln \phi_i = \frac{b_i}{b_m}(Z-1) - \ln(Z-B) - \frac{1}{2\sqrt{2}} \left[\frac{a_i}{b_i RT} + \left(\frac{\lambda}{C^*} + \frac{1-\lambda}{q_1} \right) \ln \gamma_i + \frac{1-\lambda}{q_1} \left\{ \ln \left(\frac{b_m}{b_i} \right) + \frac{b_i}{b_m} - 1 \right\} \right] \ln \left\{ \frac{Z + (1+\sqrt{2})B}{Z + (1-\sqrt{2})B} \right\} \quad (\text{B-109})$$

B.15. ORBEY-SANDLER MODIFICATION OF HURON-VIDAL MIXING RULE (HVOS) (Orbey and Sandler [1995(b)])

The b_m parameter is unchanged from the classical van der Waals mixing rule. The a_m parameter is now obtained from:

$$\frac{a_m}{b_m RT} = \left\{ \sum_i x_i \frac{a_i}{b_i RT} + \frac{1}{C^*} \left[\frac{\bar{G}_\infty^E}{RT} + \sum_i x_i \ln \left(\frac{b_m}{b_i} \right) \right] \right\} \quad (\text{B-110})$$

The fugacity coefficient is then given by:

$$\ln \phi_i = \frac{b_i}{b_m}(Z-1) - \ln(Z-1) - \frac{1}{2\sqrt{2}} \left[\frac{a_i}{b_i RT} + \frac{\ln \gamma_i}{C^*} + \frac{1}{C^*} \ln \left(\frac{b_m}{b_i} \right) + \frac{1}{C^*} \left(\frac{b_i}{b_m} - 1 \right) \right] \ln \left\{ \frac{Z + (1+\sqrt{2})B}{Z + (1-\sqrt{2})B} \right\} \quad (\text{B-111})$$

B.16. THE CORRESPONDING STATES PRINCIPLE

Van der Waal first proposed the law of corresponding states in 1873. He expressed the generalization that equilibrium properties depend on intermolecular forces and can therefore be related to critical properties in a universal way. This led to Wichterle [1978(b)] stating that principal feature of corresponding states principle (CSP) is the “advantageous combination of generality, accuracy, and simplicity”.

Pitzer’s three-parameter corresponding states theory states that all fluids having the same accentric factor (ω) must have the same reduced configurational properties at identical reduced

pressures and temperatures. This enables the fugacity coefficient of a component in a mixture to be obtain from:

$$\ln \phi_i = \ln \phi_m + \sum_j y_j \left(\frac{\partial \ln \phi_m}{\partial y_j} \right)_{y_k} \quad (\text{B-112})$$

Equation (B-112) can be expressed as differentials of critical pressure (P_c), temperature (T_c) and accentric factor with respect to composition (y_i) as follows:

$$\ln \phi_i = \ln \phi_m - \frac{1}{T} \left(\frac{\Delta H_m}{RT_c} \right) \sum_j \left(\frac{dT_c}{dy_j} \right)_{y_k} + \frac{Z_m - 1}{P_c} \sum_j \left(\frac{dP_c}{dy_j} \right)_{y_k} - \left(\frac{\partial \ln \phi_m}{\partial \omega} \right)_{T, P_c} \sum_i \left(\frac{d\omega}{dy_i} \right)_{y_k} \quad (\text{B-113})$$

All the differentials in equation (B-113) are functions of T_c , P_c and ω and can be obtained from generalised pure-component properties. Some form of combining rule will have to be used however to express the critical temperature, pressure and accentric factor as a function of composition, as explained in Appendix B.8. Prausnitz et al. [1986] details how the fugacity coefficients are calculated and phase equilibrium determined. The main limitation of the CSP lies in applying it to mixtures, due to the inaccuracy of the combining rules.

Examples of the use of the CSP to calculate HPVLE in literature surveyed are Mollerup [1980] (used for mixtures of natural gas), Plocker et al. [1978] (used for asymmetric mixtures), Arai et al. [1982], Wong and Sandler [1984], Wong et al. [1984 (a,b)] and Gani et al. [1989].

B.17. MODIFIED CUBIC EQUATIONS OF STATE

The Peng-Robinson and Soave EOS's are widely used in industry. The main reasons for this are because they require little input information (only the critical properties and accentric factor for the generalized parameters) and little computer time. These EOS's predict the phase equilibria reasonably well for hydrocarbon systems. They have shortcomings however when it comes to prediction of liquid densities and prediction of phase equilibria for polar, associating and long-chain molecules.

The main objective of proposed modifications to the “traditional” cubic EOS’s and their mixing rules has been mainly to provide for better representation of the liquid phase and for polar, associating and long-chain molecules.

Abbott [1979] points out that the most general form of a cubic EOS contains five parameters and is of the form:

$$P = \frac{RT}{V-b} - \frac{\theta(V-\eta)}{(V-b)(V^2 + \delta V + \varepsilon)} \quad (\text{B-114})$$

Modifications to the cubic EOS to improve their predictions have generally involved the introduction of additional parameters e.g. Schmidt and Wenzel [1980], Harmens and Knapp [1980], Heyen [1980], Patel and Teja [1982] and Trebble and Bishnoi [1987]. Each of the above modified EOS’s reduces to the Soave or Peng-Robinson EOS forms when special values are given to their parameters. Tsonopoulos and Heidman [1985], Georgeton et al. [1986] and Anderko [1990] have made comparisons of the abilities of each of these equations. Trebble and Bishnoi [1986] state that among these modifications, the Patel-Teja equation is the most popular.

Table B-5 shows some modifications that have been made to the attractive pressure term (equation (3-35)) as reproduced from Mühlbauer and Raal [1995].

Reference	Volume function, $g(V)$
Clausius [1880]	$V^2 + 2cV + c^2$
Usdin-McAuliffe [1976]	$V^2 + cV$
Heyen [1980]	$V^2 + cV + bV - bc$
Harmens-Knapp [1980]	$V^2 + cbV - cb^2 + b^2$
Toghiani and Viswanath [1986]	$V^2 + cbV + bV - cb^2$

Table B-5: Modifications to the attractive term (equation (3-35)) as reproduced from Mühlbauer and Raal [1995].

Another type of modification has been to leave the volume dependence of the Peng-Robinson and Soave EOS’s unchanged and introduce additional parameters into the temperature dependence

function of the a term. The most widely used modification of this type has been that of Stryjek and Vera [1986 (a,b)]. Table 3-3 lists other modifications of this type.

Modifications have also been made to the hard core parameter, b , in order to improve the poor density predictions of cubic EOS's. Xu and Sandler [1987(b)] made this modification to the original Peng-Robinson EOS. Other researchers have introduced various temperature dependencies into three-parameter cubic equations (Heyen [1981] and Fuller [1976], or even added a fourth parameter to their cubic EOS e.g. Adachi et al. [1983] and Lin et al. [1983]. Trebble and Bishnoi [1986] have shown however, that if the temperature dependencies for the a and b parameters are not chosen carefully, the isotherms may cross over in certain regions of the PVT and PHT space leading to negative heat capacities.

B.18. MODIFICATIONS TO THE CUBIC EOS CLASSICAL MIXING RULES

Modifications to the commonly used van der Waals one-fluid classical mixing rules (discussed in Chapter 3) have been developed to enable more accurate modelling of complex, highly non-ideal mixtures. Mühlbauer and Raal [1995] have classified the present mixing rules into five main categories (see Figure 3-4). They have also included local composition theory into three of the categories, in the process expanding the number of categories to eight. Each of the categories will be briefly discussed.

B.18.1. van der Waals one-fluid classical mixing rule

The van der Waals classical mixing rules have been discussed in Chapter 3. Developments will be discussed here. Shibata and Sandler [1989(b)] pointed out two shortcomings of the classical (CMR) mixing rules when applied with the direct method. The predicted liquid densities are generally in error by 5% or more for pure fluid and/or mixtures, and secondly, for the high-density phase of mixtures containing molecules dissimilar in size and/or chemical nature, agreement between experimental and correlated phase behaviour is poor.

HcHugh and Krukoni [1986] and Tsonopoulos and Heidman [1986] incorporated an interaction parameter (η_{ij}) in the van der Waals covolume (b_m):

$$b_m = \sum \sum y_i y_j (1 - \eta_{ij}) \left(\frac{b_i + b_j}{2} \right) \quad (\text{B-115})$$

The fugacity coefficient for the Peng-Robinson EOS is then given by:

$$\ln \phi_i = \frac{(bN)}{b_m} (Z - 1) - \ln(Z - B) - \frac{A}{2.83B} \left[\left(\frac{2 \sum x_j a_{ji}}{a_m} \right) - \frac{(bN)}{b_m} \right] \ln \left[\frac{Z + 2.4B}{Z - 0.4B} \right] \quad (\text{B-116})$$

where,

$$bN = 2 \sum_k y_k b_{ik} - \sum_j y_j b_{jj} - 2 \sum_i \sum_j y_i y_{i-j} b_{ij} \quad (\text{B-117})$$

When the additional interaction parameter (η_{ij}) is set to zero, equation B-116 reduces to the expression for the Peng-Robinson EOS with CMR.

Deiters and Schneider [1986(b)] also applied an interaction parameter in b_m . This was done to permit more accurate modelling near the critical point using the Redlich-Kwong EOS. They achieved reasonable agreement between correlated and experimental data for binary systems differing in structure, molecular size and/or polarity.

To overcome the shortcomings pointed out by Shibata and Sandler [1989(b)], Xu and Sandler [1987 (a,b)] proposed polynomial expressions for both the a_i and b_i parameters which are fluid specific. The a_i and b_i parameters are fluid specific as they are derived from experimental vapour pressure and density data.

To overcome the second shortcoming, complex mixing rules have to be incorporated into the EOS's. The very first complex mixing rules were local composition mixing rules (LCMR).

B.18.2. Local Composition Mixing Rules (LCMR)

Huron and Vidal [1979] were the first to develop the concept of local composition mixing rules. Their proposal related the excess Gibbs energy (G^E) to the pure component (ϕ_i) and mixture (ϕ) fugacity coefficients as follows:

$$\frac{G^E}{RT} = \ln \phi - \sum_i x_i \ln \phi_i \quad (\text{B-118})$$

Equation (B-118) enables one to relate an EOS through the fugacity coefficient to activity coefficient models through the excess Gibbs free energy. The pure and mixture fugacity coefficients in equation (B-118) can both be calculated from the same EOS. For more detail on the approach of local-composition theory, refer to Danner and Gupte [1986].

Huron and Vidal then related the a and b parameter to the excess Gibbs energy at infinite pressure as follows:

$$G_\infty^E = - \left[\frac{a_m(T)}{b_m} - \sum_i x_i \frac{a_i(T)}{b_i} \right] \Delta \quad (\text{B-119})$$

where G_∞^E is the excess Gibbs free energy in the limit of infinite pressure and Δ is a numerical constant which is dependent on the cubic EOS chosen.

The Huron-Vidal mixing rules have serious limitation, as have been pointed out by Shibata and Sandler [1989(b)] and Wong and Sandler [1992] (discussed in Chapter 3). Tsonopoulos and Heidman [1986] also pointed out another disadvantage, which was the computational time.

Huron and Vidal [1979] introduced the local composition concept into the EOS in an indirect manner. Heyen [1981] empirically introduced local composition directly into the cubic EOS a_m parameter as follows:

$$a_m = \sum_i \sum_j x_i x_j a_{ij} \left[\frac{x_j \tau_{ij}}{\sum_k x_k \tau_{ik}} \right] \quad (\text{B-120})$$

Heyen [1981] proposed this mixing rule to correlate phase equilibria of complex systems including those exhibiting miscibility gaps.

B.18.3. Density-dependent mixing rules (DDMR)

These mixing rules resulted as a consequence of a major shortcoming of the local composition (LC) and composition-dependent (CD) mixing rules. The shortcoming was the non-quadratic composition dependence of the second virial coefficient in the low density limit. Mollerup [1981] and Whiting and Prausnitz [1982] introduced the concept of density-dependence. The DDMR have a form that reduces to that of the CMR at low density and still have higher order composition dependence at high densities. Wong and Sandler [1992] have however stated that the DDMR is an ad-hoc approach, which does not preserve the cubic nature of EOS's when applied to mixtures.

Shibata and Sandler [1989(b)] proposed a DDMR that was an adaptation of the DDMR suggested by Luedecke and Prausnitz [1985] for the Helmholtz free energy. The Peng-Robinson energy mixture parameter was then given by:

$$\alpha_m^H = \sum_i \sum_j x_i x_j (a_i a_j)^{0.5} (1 - k_{ij}) + \left[\frac{\rho}{RT} \sum_i \sum_j x_i x_j (x_i \bar{c}_j \alpha_{ij}^2(T_c)) \right] \quad (\text{B-121})$$

The mixing rule satisfies the low-density statistical-mechanical requirement that the second virial coefficient be a quadratic function of composition. The cubic nature of the EOS was not preserved as is indicated by equation (B-122). The EOS of Shibata and Sandler [1989(b)] was as follows:

$$P = \frac{RT}{V - b_m} - \frac{a_m}{V(V + b_m) + b_m(V - b_m)} - \frac{1}{2\sqrt{2}RTV^2 b_m} \sum_{i \neq j} \sum_{i \neq j} x_i x_j [x_i \alpha_i^2(T_{ci}) \bar{c}_{ij} + x_j \alpha_j^2(T_{cj}) \bar{c}_{ji}] \ln \left(\frac{V + \alpha b_m}{V + \beta b_m} \right) - \frac{\sum_{i \neq j} \sum_{i \neq j} x_i x_j [x_i \alpha_i^2(T_{ci}) \bar{c}_{ij} + x_j \alpha_j^2(T_{cj}) \bar{c}_{ji}]}{VRT(V(V + b_m) + b_m(V - b_m))} \quad (\text{B-122})$$

Equation (B-122) is clearly non-polynomic.

Lee and Sandler [1987] developed a simpler mixing rule. They found that their DDMR did not yield significant improvements over the van der Waals one-fluid mixing rule for P , T , x , y data

correlation. However the interaction parameter calculated was extremely small and could thus be taken as zero. This made the EOS with the DDMR completely predictive. The results obtained with the interaction parameter set to zero were more accurate than for similarly setting the interaction parameter for CMR to zero.

Mohamed and Holder [1987] proposed a DDMR that incorporated an adjustable density-dependent interaction parameter (k_{ij}) in the Peng-Robinson EOS cross parameter (a_{ij}). k_{ij} was allowed to vary linearly with the phase density of the mixture:

$$k_{ij} = \alpha_{ij} + \rho\beta_{ij} \quad (\text{B-123})$$

They also incorporated correction factors into the Peng-Robinson mixture parameter a_i and b_i . Significant improvements were achieved with their DDMR and density-dependent EOS for correlations in the critical region. Systems modelled by Mohamed and Holder [1987] were limited to carbon dioxide + aromatic binaries however.

B.18.4. Density-dependent local composition mixing rules

Traditional EOS's require experimental data input in order to determine an interaction parameter/s. These parameters are also system dependent. This makes them incapable of being predictive in nature, as the interaction parameter is always needed. Neglecting the interaction parameter leads to inaccurate results except for highly ideal system. The contribution of the interaction parameter to the accuracy can be made less important through changing the form of the EOS e.g. the mixing rules of Lee and Sandler [1987].

In order to develop truly predictive methods for VLE modelling, recent approaches have been towards the introduction of local-composition theory either directly into the EOS, i.e. the Group contribution (GC) EOS (Skjold-Jorgensen [1984] and Skjold-Jorgensen [1988]), or into the EOS mixing rules, i.e. the UNIWAALS method (Gupte et al. [1986(a,b)]).

B.18.4.1. The GC EOS

The GC EOS was developed by Skjold-Jorgensen to describe polar and non-polar components in the temperature range 100-700 K and at pressures up to 30 MPa. The GC EOS makes predictive VLE computation possible for both the direct and combined methods. The only information required is the pure-component data such as critical temperature and pressure and molecular

structure parameters. The method does not require binary interaction parameters. The error in the predicted K values is claimed to be usually less than 5%.

The GC principle in conjunction with the statistical thermodynamic van der Waals partition function is applied in the derivation of the GC EOS. The full derivation of the GC EOS is given in Skjold-Jorgensen [1984]. For a brief summary of the underlying equations in the GC EOS refer to Mühlbauer and Raal [1995].

Application of the GC EOS requires breaking down the components of the binary system into relevant groups. Tables of the relevant groups are given in Skjold-Jorgensen [1984] and Skjold-Jorgensen [1988]. The computational procedure for the GC EOS is discussed in Mühlbauer [1990] and Mühlbauer and Raal [1995].

B.18.4.2. The UNIWAALS EOS

The UNIWAALS EOS was developed by Gupte et al. [1986 (a,b)] by combining modified expressions for the UNIFAC GC method with the van der Waals EOS using Huron –Vidal mixing rule principles. The UNIWAALS EOS was developed from the outset to be completely predictive. It requires only UNIFAC group interaction parameters and pure component data for the computation of VLE. The formulation of the UNIWAALS EOS is described in detail in Gupte et al. [1986 (a,b)].

Some of the limitations of the UNIWAALS EOS (as pointed out by Schwartzenruber and Renon [1989 (a,b)]) are:-

- The UNIFAC equation was introduced into the van der Waals equation without using the infinite pressure limit. This leads to a volume-dependent mixing rule from volume-independent van der Waals EOS mixing rules.
- The modified UNIFAC equation was assumed to be accurate over a range of temperatures (which is only valid if the temperature dependence of the parameter is known).
- UNIWAALS uses the UNIFAC expression for both liquid and vapour calculations.
- Supercritical components cannot be handled by the normal calculation procedure. Gani et al. [1989] developed a procedure to handle supercritical components.

B.18.5. Composition-dependent mixing rules (CDMR)

Panagiotopoulos and Reid [1986(b)] proposed a simple modification to the classical mixing rule which incorporated composition. This resulted in the first CDMR. The proposed non-quadratic mixing rule, which was written as a linear function of mole fraction is:

$$a_{ij} = (a_i a_j)^{0.5} [1 - k_{ij} + (k_{ij} - k_{ji})x_i] \quad (\text{B-124})$$

Table 3-4 lists some of the CDMR surveyed. They are also discussed briefly in Chapter 3.

B.18.6. Composition and density-dependent mixing rules

Michelsen and Kistenmacher [1990] pointed out the limitations of the CDMR (as discussed in Chapter 3). This led to Schwartzentruber and Renon [1991] developing a new formulation of their original mixing rules (Schwartzentruber and Renon [1989 (a,b)]) to overcome the inconsistencies pointed out by Michelsen and Kistenmacher [1990]. Their revised mixing rule still kept the efficiency and flexibility of the CDMR originally proposed. They now expressed a_m as the sum of a quadratic and non-quadratic term as follows:

$$a_m = \sum \sum (a_i a_j)^{0.5} [1 - k_{ij}] (x_i x_j) (x_i - x_j) + \sum \sum \sum X_{ijk} x_i x_j x_k \quad (\text{B-125})$$

The X_{ijk} in the non-quadratic term of equation (B-125) is defined as an expansion of Kronecker deltas (δ_{ij}) which allows for the Michelsen-Kistenmacher Syndrome to be avoided. This did not overcome the dilution effect though. To overcome the dilution effect the Kronecker deltas were treated as binary parameters which are correlated to the distance between molecules i and j as follows:

$$\delta_{ij} = (1 - D_{ij}) \quad (\text{B-126})$$

where D_{ij} is the normalized distance between two molecules and is a function of the critical values of a_i and b_i parameters for pure component i and pure-component acentric factor and dipole moment.

In order that the new mixing rule be consistent with the constraint on the second virial coefficient and still remain flexible, a five-parameter EOS that remains cubic in volume was proposed:

$$Z = \frac{1}{1-b\rho} - \frac{a\rho/RT}{1+c\rho+d\rho} + \left(\frac{bX}{RT}\right) \frac{\rho^2}{(1-b\rho)(1+c\rho+d\rho^2)} \quad (\text{B-127})$$

where

$$X_m = \sum_i \sum_j \sum_k X_{ijk} x_i x_j x_k \quad (\text{B-128})$$

and

$$a_m = \sum_i \sum_j (a_i a_j)^{0.5} (1 - k_{ij}) x_i x_j \quad (\text{B-129})$$

$$b_m = \sum_i b_i x_i \quad (\text{B-130})$$

$$c_m = \sum_i c_i x_i \quad (\text{B-131})$$

$$d_m = \sum_i d_i x_i \quad (\text{B-132})$$

The a_m parameter introduces density-dependence, which results in a loss of correlation efficiency for strongly non-ideal systems. The flexibility loss was avoided by Schwartzentruber and Renon by writing the volume-dependent factor as $b/(V-b)$ which is less dependent on composition.

This however results in the third virial coefficient now being fourth degree in mole fraction, i.e. the virial coefficient requirement is violated at higher order. Application of the new mixing rule showed that although it solved the inconsistencies of the their original mixing rule, it did not yield significant improvement in modelling capabilities.

B.18.7. Density-independent mixing rules (DIMR)

The mixing rules of Wong and Sandler [1992] are discussed in detail in Chapter 3. A modification of this mixing rule proposed by Twu and Coon [1996] which is claimed to be more flexible and avoids the problems associated with the Wong and Sandler mixing rules is also discussed in Chapter 3.

B.19. EQUATIONS OF STATE FROM THEORY AND COMPUTER SIMULATION

Thermodynamics has its basis in statistical mechanics. Much of the EOS's discussed in this thesis however have their origins in classical thermodynamics as opposed to statistical thermodynamics. The field of statistical mechanics is complex and numerous publications have been produced in recent years. Sadus [1999] has an excellent book detailing molecular simulations for fluids. Sandler et al. [1994] also gives a very good summary of equations of state from statistical mechanics. The field of statistical thermodynamics is extremely voluminous and so only a very brief introduction will be presented here. Reference should be made to the above-mentioned authors for greater detail. Prausnitz [1996] in a recent paper discusses the opportunities in molecular thermodynamics.

Different aspects of statistical mechanical theory have resulted in developments of EOS's e.g. renormalisation group theory has shown the universality of critical phenomena (Sandler [1994]) and lattice theory of dense fluids has been the basis for many activity coefficient models (Abbott and Prausnitz [1994]) and for models of polymer solutions (Sanchez and Panayiotou [1994]).

B.19.1. Integral Equation Theory

By making various assumptions, equations are derived for the spatial correlation function between molecules in a fluid. These equations can be derived from graph theory, from functional analysis, by deriving a hierarchy of equations which is then truncated, and by postulate. The equations derived can be solved numerically only for the spatial correlation function at each temperature and density and the pressure and other thermodynamic properties can be computed from them. Thus one obtains the pressure at chosen values of volume and temperature for a given potential function between a pair of molecules, rather than an analytical expression for the EOS.

B.19.2. Perturbation Theory

Perturbation theory involves performing a Taylor series expansion of properties (e.g. the Helmholtz free energy) of a system about the known properties of a reference system. The dimensionless difference between the intermolecular potential functions of the system of interest and the reference system is known as the perturbation parameter. The usual choice of a reference system is the hard-sphere fluid. The perturbed theory is comprehensively explained in Sandler et

al. [1994] and Mühlbauer and Raal [1995]. Mühlbauer and Raal [1995] have a comprehensive table that shows the different perturbed hard chain theory EOS's.

B.19.3. Computer Simulations

Computer simulations are computationally intensive and are becoming ever more popular as the speed of computer processors increases. They have an advantage in that they do not require any information on theory or reference systems. They also have the added advantage that much more complicated molecular systems can be studied by simulation, than is possible from theory. The behaviour of a collection of molecules can be simulated directly, either by determining average values of properties over likely states (Monte Carlo simulation) or by solving the dynamical equations of motion and following the time evolution of the system (Molecular dynamics). Sadus [1999] comprehensively details both computational methods in his text.

For greater detail on EOS's and mixing rules refer to Sandler [1994] and Mühlbauer and Raal [1995].

B.20. APPLICATION OF THE DEITERS AND SCHNEIDER METHOD [1976] TO THE PENG-ROBINSON EOS

Deiters and Schneider state that the total Helmholtz energy for a binary system is given by:

$$A(T, V) = A^+(T, V^+) + RT(n_1 \ln x_1 + n_2 \ln x_2) - \int_{V^+}^V p dV \quad (\text{B-133})$$

where the "+" properties refer to perfect gases or a perfect gas state.

For the Redlich-Kwong EOS they then obtained:

$$A(T, V) = A^+(T, V^+) - nRT \ln \frac{V - \hat{b}}{V^+} - \frac{\hat{a}}{\hat{b}\sqrt{T}} \ln \left(1 + \frac{\hat{b}}{V} \right) + RT(n_1 \ln x_1 + n_2 \ln x_2) \quad (\text{B-134})$$

where $\hat{a} = an^2$ and $\hat{b} = bn$.

Applying equation (B-133) to the Peng-Robinson EOS, the following expression was obtained for the Helmholtz energy:

$$\frac{A}{RT} = \frac{A^+}{RT} - \ln(1-h) - \frac{a}{RT} \frac{1}{2.828b} \ln\left(\frac{1+2.414h}{V-0.414h}\right) + n_1 \ln x_1 + n_2 \ln x_2 \quad (\text{B-135})$$

where $h = b/V$.

Equation (B-135) was then used in equations (3-129) and (3-130). Application of equation (B-135) in equations (3-129) and (3-130) merely involves tedious differentiation.

B.21. HPVLE CONSISTENCY TESTS

B.21.1 Chueh et al. [1965] Area Test

The Chueh et al. [1965] equal area test is developed, like all others, from the Gibbs-Duhem equation. One form of this equation, in terms of the fugacity of component i , \hat{f}_i , is as follows for constant temperature:

$$\frac{V^L}{RT} dP = \sum x_i d \ln \frac{\hat{f}_i}{x_i} \quad (\text{B-136})$$

To obtain the form used by Chueh et al. [1965] equation (B-136) is written for a binary mixture as follows:

$$d \ln \frac{\hat{f}_1}{x_1} + x_2 d \ln \frac{\hat{f}_2/x_2}{\hat{f}_1/x_1} = \frac{V^L}{RT} dP \quad (\text{B-137})$$

The second term may be written in terms of the differential $d\left(x_2 \ln\left[\left(\hat{f}_2/x_2\right)/\left(\hat{f}_1/x_1\right)\right]\right)$ and becomes:

$$\frac{V^L}{RT} dP + \ln \left(\frac{\hat{f}_2 / x_2}{\hat{f}_1 / x_1} \right) dx_2 = d \left\{ \ln \frac{\hat{f}_1}{x_1} + x_2 \ln \left(\frac{\hat{f}_2 / x_2}{\hat{f}_1 / x_1} \right) \right\} \quad (\text{B-138})$$

Introducing the fugacity coefficients $\hat{\phi}_i = \frac{\hat{f}_i}{y_i P}$ and the equilibrium ratio $K_i = y_i / x_i$ gives:

$$\begin{aligned} \frac{V^L}{RT} dP + \left(\ln \frac{\hat{\phi}_2}{\hat{\phi}_1} + \ln \left(\frac{K_2}{K_1} \right) \right) dx_2 = \\ d \left\{ \ln K_1 + \ln \hat{\phi}_1 P + x_2 \left(\ln \frac{\hat{\phi}_2}{\hat{\phi}_1} + \ln \left(\frac{K_2}{K_1} \right) \right) \right\} \end{aligned} \quad (\text{B-139})$$

Equation (B-139) is integrated from $x_2 = 0$ (where subscript 2 refers to the more volatile component) to some arbitrary upper limit x_2 to give:

$$\int_{x_2=0}^{x_2} \ln \left(\frac{K_2}{K_1} \right) dx_2 + \int_{x_2=0}^{x_2} \ln \left(\frac{\hat{\phi}_2}{\hat{\phi}_1} \right) dx_2 + \frac{1}{RT} \int_{x_2=0}^{x_2} V^L dP = \text{LHS} \quad (\text{B-140})$$

where,

$$\text{RHS} = \left[\ln K_1 + \ln \left(\frac{\hat{\phi}_1 P}{\hat{\phi}_1^{\text{sat}} P_1^{\text{sat}}} \right) + x_2 \left(\ln \frac{\hat{\phi}_2}{\hat{\phi}_1} + \ln \frac{K_2}{K_1} \right) \right]_{x_2=0}^{x_2} \quad (\text{B-141})$$

(At $x_2 = 0$, $\hat{\phi}_1 = \hat{\phi}_1^{\text{sat}}$, $P = P_1^{\text{sat}}$ and $K_1 = 1$.)

The thermodynamic consistency test is therefore:

$$\text{Area I} + \text{Area II} + \text{Area III} = \text{RHS}$$

The areas are found by graphical integration and the RHS is evaluated at several x_2 values over the relevant composition range. The fugacity coefficients $\hat{\phi}_i$ are evaluated from an appropriate equation of state.

B.21.2 Won and Prausnitz [1973] Consistency Test

The comparison of the calculated and measured vapour compositions over the full composition range constitutes a test for thermodynamic consistency.

For a binary mixture, the total system pressure is the sum of the two partial pressures.

$$P = y_1 P + y_2 P \quad (\text{B-142})$$

The partial pressures are related to the liquid phase activity coefficients by:

$$y_i P = \frac{x_i \gamma_i f_i^o}{\hat{\phi}_i} \quad (\text{B-143})$$

The standard state fugacities f_i^o for the condensable(1) and non-condensable(2) components were defined as that of the saturated liquid at system pressure, and Henry's constant for solute 2 in solvent 1 at system temperature and at saturation pressure P_1^{sat} respectively. With this convention,

$$\begin{aligned} \gamma_1 &\rightarrow 1 \text{ as } x_1 \rightarrow 1 \\ \gamma_2^* &\rightarrow 1 \text{ as } x_2 \rightarrow 0 \end{aligned}$$

Henry's law constant $H_{2,1}$ (for component 2 in solvent 1) is pressure dependent. The relationship between its value at pressure P and saturation pressure P_1^{sat} for example is given by (Prausnitz et al. [1986]):

$$H_{2,1}(P) = H_{2,1}(P_1^{sat}) \exp\left(\int_{P_1^{sat}}^P \frac{\bar{V}_2^\infty}{RT} dP\right) \quad (\text{B-144})$$

where \bar{V}_2^∞ is the partial molar volume of solute 2 at infinite dilution.

In the Won and Prausnitz [1973] consistency procedure an arbitrary function $F_2(x_2)$ is used to represent the variation of γ_2^* along the saturation line and its coefficients are determined from total pressure data:

$$\ln \gamma_2^* = F_2(x_2) \quad (\text{B-145})$$

An arbitrary function of pressure $G(P)$ is used to represent the liquid molar volume of the mixture, which is assumed to be known.

The working equation for P was developed from the Gibbs-Duhem equation:

$$(1-x_2) \frac{d \ln \gamma_1}{dx_2} + x_2 \frac{d \ln \gamma_2^*}{dx_2} = \frac{V^L}{RT} \frac{dP}{dx_2} \quad (\text{B-146})$$

Rearrangement and integration of equation (B-146) one obtains:

$$\ln \gamma_1 = F_1(x_2) \quad (\text{B-147})$$

and substitution into equation (B-142) gives the following working equation :

$$P = \frac{x_1 f_1^o}{\hat{\phi}_1} \exp(F_1) + \frac{x_2 f_2^o}{\hat{\phi}_2} \exp(F_2) \quad (\text{B-148})$$

Equation (B-148) is then used in the method outlined below:

- (1) For the first iteration the $\hat{\phi}_1$ are set equal to 1 and F_2 to zero for all x_2 . The first estimates of y_1 (the desired quantity) were obtained from :

$$y_1 = \frac{x_1 f_1^o}{P} \exp(F_1)$$

$$y_2 = 1 - y_1$$

- (2) f_2^o was obtained from experimental P - x data where x_2 is small e.g. ~ 0.01 ,

$$f_2^o = \left[P - \frac{x_1 P_1^{sat} \phi_1^{sat}}{\hat{\phi}_1} \exp \frac{V_1^L (P - P_1^{sat})}{RT} \right] \times \frac{\hat{\phi}_2}{x_2}$$

- (3) The constants in F_2 are adjusted to give the best fit of the P - x data to equation (B-148).

(4) The next set of y_i are calculated from :

$$y_1 = \frac{x_1 f_1^o}{\hat{\phi}_1 P} \exp(F_1)$$

The y_i 's were summed and if the sum did not equal unity, the y_i 's were normalized by

$$y_{i(\text{normalised})} = \frac{y_i}{y_1 + y_2}$$

(5) A new f_2^o was found from :

$$f_2^o = \lim_{x_2 \rightarrow 0} \frac{\hat{\phi}_2 y_2 P}{x_2} (H_{2,1})$$

(6) The iteration procedure was continued until the continuously generated constants for γ_2^* in equation (B-145) no longer changed.

B.21.3. Christiansen and Fredenslund [1975] Consistency Test

Christiansen and Fredenslund [1975] developed a thermodynamic consistency test applicable to either isothermal high pressure (P - x) or isobaric (T - x) data. As in the Won and Prausnitz [1973] test, vapour phase compositions are calculated and can then be compared with measured values where a full P - T - x - y data set is available. It differs from the Won and Prausnitz [1973] approach in that no analytical expression for G^E is required, i.e., it may be classed as a *model free* method. It thus serves as a procedure to predict or extend high pressure P - x or T - X data, producing both the vapour phase composition (if not measured) and the Henry's law constant if the unsymmetric standard state convention for fugacities is used for a system with a supercritical component.

The data reduction procedure was based on three equations for $\ln \gamma_1$, $\ln \gamma_2$ and the total pressure, P . The non-isothermal non-isobaric, Gibbs-Duhem equation, as derived by Van Ness [1964] was used together with:

$$G^E / RT = \sum x_i \ln \gamma_i \quad (\text{B-149})$$

to obtain expressions for the activity coefficients :

$$\begin{aligned} \ln \gamma_l &= \frac{G^E}{RT} + x_k \left(\frac{d(G^E / RT)}{dx_i} \right) - \\ &\frac{x_k}{RT} \left[V \left(\frac{dP}{dx_i} \right)_\sigma - \sum x_j V_j^o \left(\frac{dP_j^o}{dx_i} \right) \right] + \\ &x_k \frac{H^E}{RT^2} \left(\frac{dT}{dx_i} \right)_\sigma \end{aligned} \quad (\text{B-150 a,b})$$

which could be written for $l = 1, k = 2$ and $l = 2, k = 1$. Also,

$$P = \sum \frac{x_i y_i f_i^o}{\hat{\phi}_i} \quad (\text{B-151})$$

where f_i^o = standard state liquid fugacity of component i .

Subscript σ denotes values along the saturation line. The three equations (B-150 a,b) and (B-151) contain three unknowns, viz. γ_1, γ_2 and G^E and can in principle be solved for the unknowns. Since the system is highly non-linear and difficult to solve, Christiansen and Fredenslund used the method of *orthogonal collocation* to obtain solutions. For isothermal data, the term involving H^E vanishes whereas for isobaric data the bracketed term involving pressure derivatives vanishes.

The essential steps in the data reduction and consistency test procedure are as follows :

- (1) T, P and x are known. f_i^o, V_i^o, V, H^E , and the slope of the equilibrium curve were assumed known or available by calculation. Initially $\hat{\phi}_i = 1$ for $i = 1, 2$
- (2) Equations (B-150 a,b) and (B-151) were solved for γ_1, γ_2 and G^E for the value of x_i .
- (3) Vapour mole fractions were calculated using :

$$y_i = \frac{x_i \gamma_i f_i^o}{\hat{\phi}_i P}$$

- (4) New values of $\hat{\phi}_i$ were calculated using y_i from step 3 and steps 2 and 4 were repeated until the successive calculated values of y_i agreed to within a predetermined tolerance, i.e. 10^{-4} .
- (5) The value of y_i was calculated at each point by interpolation among the values of y_i last obtained under step 3.
- (6) The experimentally obtained values of y_i were compared with the calculated values. If

$$|y_i^c - y_i^e| \leq \Delta x_i + \Delta y_i$$

where Δx_i and Δy_i are the uncertainties in the liquid and vapour mole fraction measurements, the data point was deemed thermodynamically consistent in the limit of the methods used to calculate f_i , V and H^E . If however

$$|y_i^c - y_i^e| > \Delta x_i + \Delta y_i$$

Two possibilities existed :

- (1) The data were inconsistent, or
- (2) The methods used to calculate f_i , V and H^E were erroneous.

B.21.4. Muhlbauer Consistency Test Based on Vapour Compositions

Muhlbauer [1990] developed a thermodynamic consistency test based on vapour-phase compositions. The equations that constitute the test are as follows:

$$\int_{y_2=0}^{y_2} \ln(\hat{\phi}_2 / \hat{\phi}_2^0) dy_2 + \int_{P=P^{\text{sat}}}^P \frac{V^V}{RT} dP = \text{RHS} \quad (\text{B-152})$$

$$\left[\ln \hat{\phi}_1 P + y_2 \ln(\hat{\phi}_2 / \hat{\phi}_1) \right]_{y_2=0}^{y_2} = \text{LHS} \quad (\text{B-153})$$

The fugacity coefficients $\hat{\phi}_i$ refers to the vapour phase. For thermodynamic consistency, LHS = RHS. The test can be applied if only P - T - y data are available. As one can see the beauty of this test is its simplicity, and the fact that one does not have to calculate the liquid molar volume,

which as mentioned before is difficult to undertake at high pressures. A disadvantage of the test though is that measured liquid phase compositions are not utilized.

B.22. SOME INTERESTING PUBLICATIONS NOT DIRECTLY REFERENCED

The following are some rather interesting papers that we not referenced directly. For convenience they will be listed under appropriate sections:

Van der Waals Theory

1. Abbott and Praunitz [1987] – discussion of generalized van der Waals theory
2. David and Bossoutrot [1996] – properties of ternary fluid mixture.

Equations of state and mixing rules

1. Vidal [1984] – simple EOS's for calculations in critical range.
2. Kim et al. [1986] – Cubic chain-of-rotators EOS.
3. Lee and Chao [1986] – cubic chain-of-rotators EOS with DDLICMR.
4. Leet et al. [1986] – cubic chain-of-rotators EOS.
5. Cisternas [1987] – technique to obtain component parameters for three-parameter EOS.
6. Donohue and Vimalchand [1988] – Perturbed hard chain theory.
7. Iwai et al. [1988] – new three-parameter cubic EOS.
8. Adachi et al. [1990] – discussion of available EOS's.
9. Chen and Chen [1993] – hard convex body expansion.
10. Cha et al. [1996] – new mixing rule using two fluid corresponding states model.
11. Cuadros and Okrasinski [1996] – comparison of EOS for predicting vapour pressure.
12. Fotouh and Shukla [1996(a)] – Perturbation theory – ternary mixtures.
13. Fotouh and Shukla [1996(b)] – numerical methods.
14. Fu et al. [1996] – prediction of VLE in polymer systems.
15. Gregorowicz et al. [1996] – pure fluid characteristic that challenge EOS models.
16. Hanif et al. [1996] – Maxwell areas for pure-component phase equilibria.
17. Heideman [1996] – excess free energy mixing rules.
18. Inomata et al. [1996] – local composition model based on Lennard-Jones potential.
19. Kakhu and Homer [1996] – prediction of VLE.
20. Kontogeorgis et al. [1996] – EOS for associating fluids.
21. Kraska and Gubbins [1996 (a,b)] – modified SAFT EOS.
22. Lin et al. [1996] – generalized quartic EOS.
23. Muller et al. [1996] – backbone family of EOS's.
24. Na and Kim [1996] – new invariant asymmetric mixing rules.
25. Novenario et al. [1996] – mixing rule.
26. Orbey and Sandler [1994] – cubic EOS for polymers.
27. Zabaloy and Vera [1996] – cubic EOS for pure compound vapour pressures.

Activity coefficient models

1. Dunnebeil et al. [1996] – comparison of two predictive models.
2. Huang and Lee [1996] – modified Wilson model.
3. Ohta [1996] – application of excess Gibbs energy to HPVLE.
4. Wu and Sandler [1989] – UNIFAC predictions –proximity effects.

Azeotropy

1. Aucejo et al. [1996] – double azeotropy.
2. Burguet et al. [1996] - polyazeotropy.
3. Garcia-Sanchez et al. [1996] – prediction of azeotropic behaviour.
4. Segura et al. [1996] – polyazeotropy.
5. Serafimov and Babich [1996] – azeotropic relationships.
6. Wisniak et al. [1996] – polyazeotropy.

VLE data

1. Chun et al. [1971] – triethylamine + water and methyldiethylamine + water.
2. Elliot et al. [1974] – methane + n-butane.
3. Eng and Sandler [1984] – Aldehyde + hydrocarbon.
4. Bennett et al. [1993] – hydrocarbons and fuel oxygenates.
5. Laugier and Richon [1996] – ethylene + 4-methyl-pentene and butene + 1-hexane.
6. Nagahama [1996] – discussion of VLE measurements at high pressure.

VLLE

1. Engelezos et al. [1990] – simultaneous regressions of binary VLE and VLLE.

Supercritical Extraction

1. Braun and Schmidt [1984] – crude montan wax.
2. Brignole et al. [1987] – alcohols from water.
3. Campanella et al. [1987] – equilibrium properties.
4. Chrisochoou and Schaber [1996] – design of process.

Molecular Thermodynamics

1. Chen [1996] – Gibbs energy of mixing.
2. Wu and Sandler [1991 (a,b)] – ab Initio Quantum mechanical calculations.

Gas solubility

1. Chialvo et al. [1996] – at sub and near-critical conditions

LLE

1. de Pablo and Prausnitz [1988] – discussion of LLE including the critical region.
2. de Pablo and Prausnitz [1990] – discussion of LLE including the critical region.

HPVLE Apparatus

1. Kragas et al. [1984] – chromatographic apparatus.

2. Nasir et al. [1980/1981] – novel apparatus for measurement of phase and volumetric behaviour.

APPENDIX C

C.1. DESCRIPTION OF ANCILLARY EQUIPMENT

C.1.1. The degassing apparatus

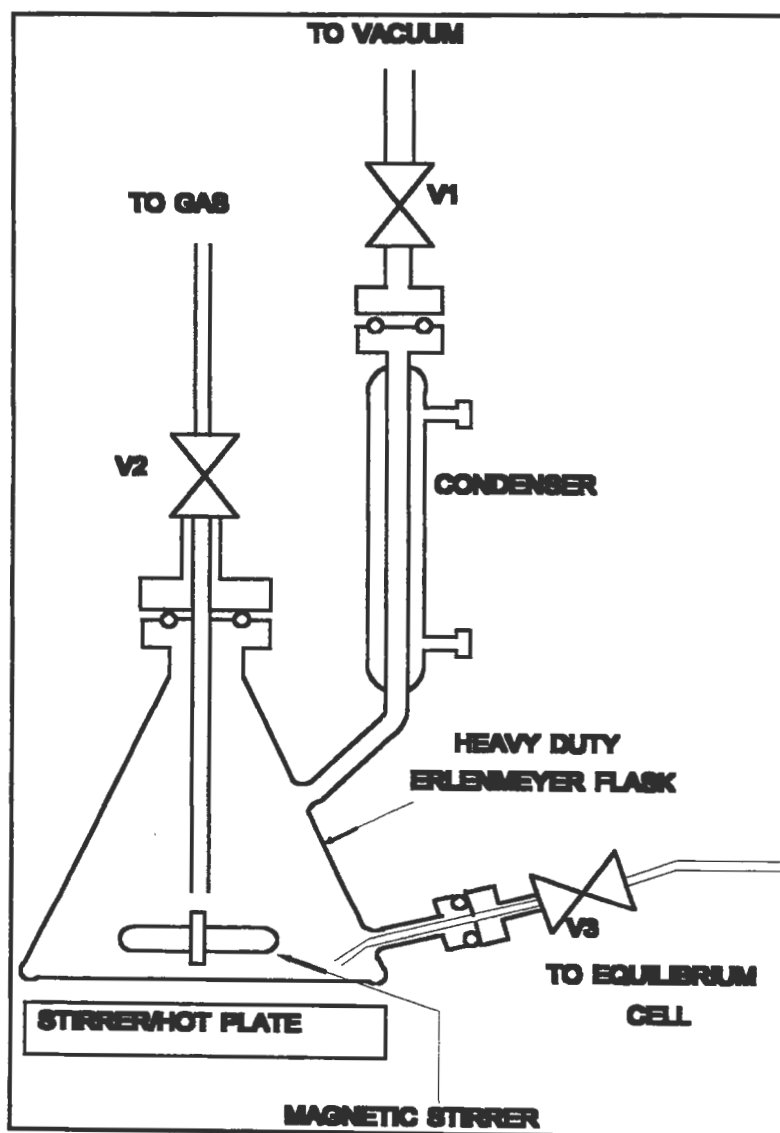


Figure C-1: Schematic of the degassing apparatus

The degassing equipment consisted of a heavy-duty graduated Erlenmeyer flask and a flat heater/stirrer mantle. The Erlenmeyer flask which can withstand high vacuums was modified to incorporate a condenser (single walled). All the valves on the apparatus were stainless steel and

of the needle type. Sealing between the stainless steel valves and the glassware was achieved via Viton “o”-rings. As denoted in Figure C-1 valves V1, V2, and V3 link the degassing apparatus to vacuum, gas cylinder (gaseous component of interest), and the equilibrium cell respectively.

The operating procedure for the degassing apparatus is outlined in Appendix D.

C.1.2. The propane compression device

Figure C-2 illustrates the construction details for the propane compression device. The apparatus consists of two chambers viz., the compressed air and propane chambers. Both chambers were constructed from stainless steel type 316 billets. The two chambers are attached by 12 high tensile 8 mm steel caphead screws and aligned by a spigot.

Heating of the propane chamber was achieved by the insertion of three 150 W electric cartridge heaters into the wall of the chamber. They were positioned longitudinally and equi-spaced around the circumference. The heater cartridges outputs were controlled by a Variac voltage regulator. A type J thermocouple was placed in a well in the propane chamber body so as to measure the temperature of the chamber.

The compressed air chamber was linked to a compressed air cylinder that delivered air at approximately 200 bar. The pressure created in this chamber was transferred to the propane chamber by a double-ended, stainless steel type 316, piston. Sealing on both ends of the piston was achieved with Viton “o”-rings.

The compression device was designed for propane, but any gas whose vapour pressure is very low at room temperature can be compressed to a suitable pressure with the use of this apparatus.

The operating procedure for the propane compression device is outlined in Appendix D.

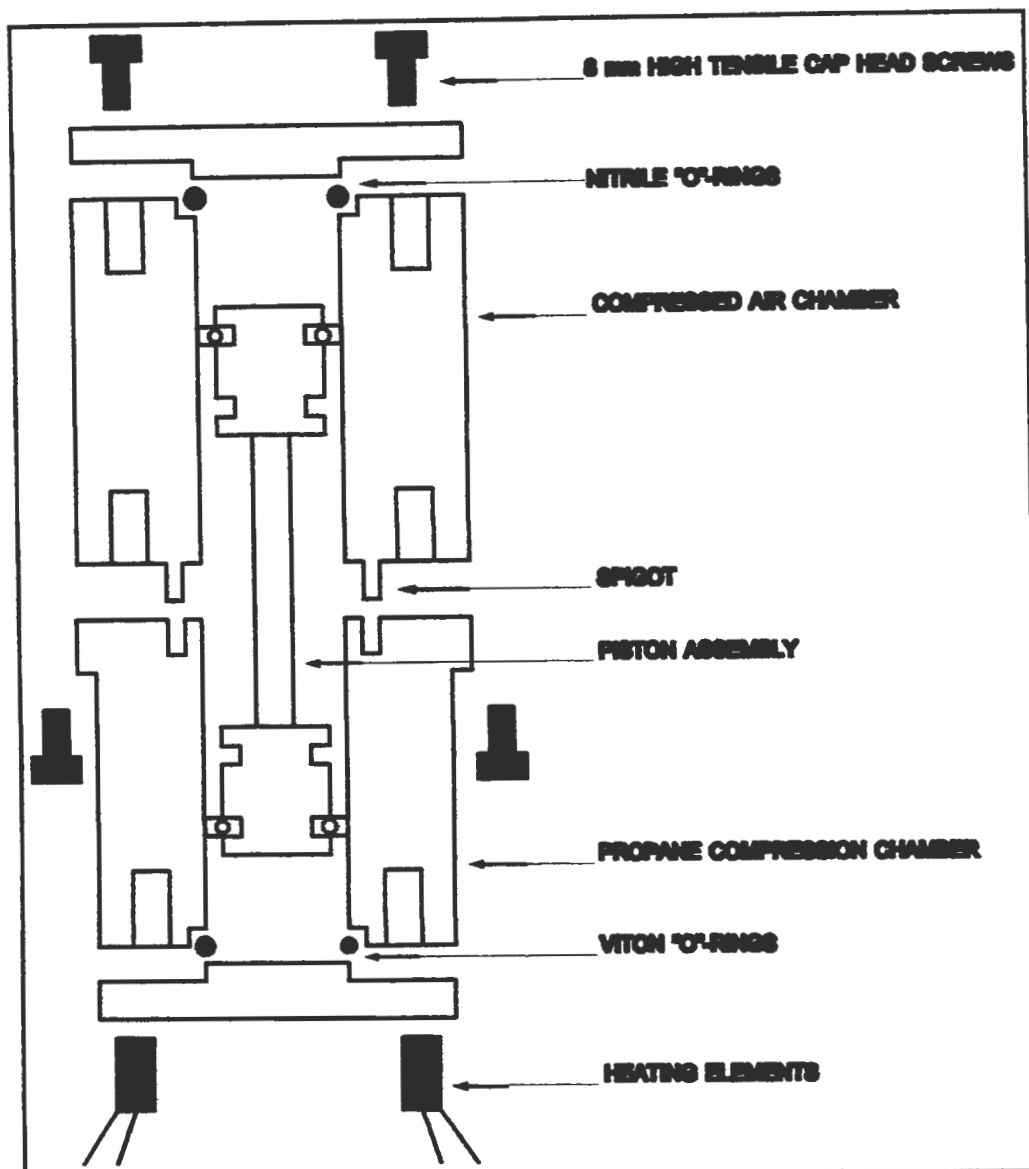


Figure C-2: The propane compression device

C.2. DETAILS FOR THE STEPPER MOTOR

The stepper motor (ORM 296E) and stepper motor drive (IB106) were supplied by Eagle Electronics. CyberResearch manufactured both the stepper motor and stepper motor drive. The stepper motor had a maximum torque of 1.75 Nm. This torque gave it the capability to drive against a pressure differential of approximately 10 bar.

A simple circuit was designed by the Electronics workshop in the School to permit stepwise movement of the motor and consequently the piston. The circuit enabled the motor to perform single or double steps in both a clockwise and anti-clockwise direction. This allowed the piston to

be moved either up or down in the equilibrium cell. By stepwise movement of the stepper motor and by utilization of the micrometer attached to the stepper motor, the exact distance that the piston had moved could be calculated. This information was used in the P-V-T studies.

C.3. LIQUID-LEVEL DETERMINATION DEVICES

The liquid-level can be determined by direct or indirect methods. Direct methods include viewing windows and fibre optics whereas indirect methods rely on capacitors, solid-state sensors and floats.

C.3.1. Direct Methods

C.3.1.1. Viewing windows

This requires extensive machining of the equilibrium cell and a relatively complex mechanical design if the windows are to be fitted into a compact arrangement. Most researchers resort to viewing windows for the observation of the cell contents. Some equilibrium cells are constructed entirely out of pyrex or sapphire making the entire contents visible. Chapter 3 details a number of apparatus with viewing windows.

C.3.1.2. Fibre Optics

Fibre optics is a very elegant method by which to determine liquid-level or view the cell contents. The problems though with fibre optics is that of sealing (the point at which the cable enters the equilibrium cell contents). Also, extreme conditions of high pressure and high temperature are not conducive to fibre optics.

C.3.2. Indirect Methods

C.3.2.1. Capacitance Measurement

A number of researchers have made use of capacitance measurement as a means of determining the liquid-level (refer to Chapter 2). White and Brown [1942] describe a typical capacitance system. Wilner [1960] gives a good review and also makes some suggestions on the use of variable capacitance liquid-level sensors for both conductive and non-conductive liquids. Limitations of this method are as follows:-

- Certain materials are unresponsive to capacitance measurement (Lin et al. [1985]).

- At conditions close to the critical point where differences between the physical properties of the phases diminish, accurate determination of the liquid-level will be a problem.
- Capacitance measurement can only be undertaken for the time the stirrers are switched off. This results in discontinuous information on liquid-level.

C.3.2.2. Solid-state sensors

Sensors of this nature are produced by a number of manufactures, e.g. Honeywell. These sensors can accurately detect liquid-level and also produce a milliampere or voltage output signal that can be linked to a computer. The sensors have no mechanical parts and are available in a range of sizes. Sensors that are able to cope with the extremely demanding conditions of 175 °C and 175 bar were sourced. They were, however, not available in miniature versions and were extremely costly.

C.3.2.3. Float sensors

Another means of determining the liquid-level is by measurement of the position of a magnetic float extension. The method does have inherent problems associated with it:-

- Installation of the float mechanism vastly complicates equilibrium cell design, especially when one is constructing a compact and relatively small equilibrium cell.
- The float extension creates stagnant areas, which is undesirable from an equilibrium point of view.
- Vigorous stirring of the equilibrium cell contents and resultant vortex formation would be detrimental to the float and its extension.

C.4. PRESSURE EQUALIZATION CIRCUIT

A simple electronic circuit and valving arrangement was designed so as to maintain a pressure differential across the piston of approximately one bar. Figure C-3 illustrates the valving arrangement for the pressure equalization mechanism.

The valving arrangement consisted of two high pressure solenoid valves, which were connected to the nitrogen compartment. By opening the solenoid valves (supplied by General Valve Company) the nitrogen compartment could be either pressurized or vented. By controlling the pressurizing

and venting of the nitrogen compartment, its pressure could be maintained within a bar of the equilibrium cell.

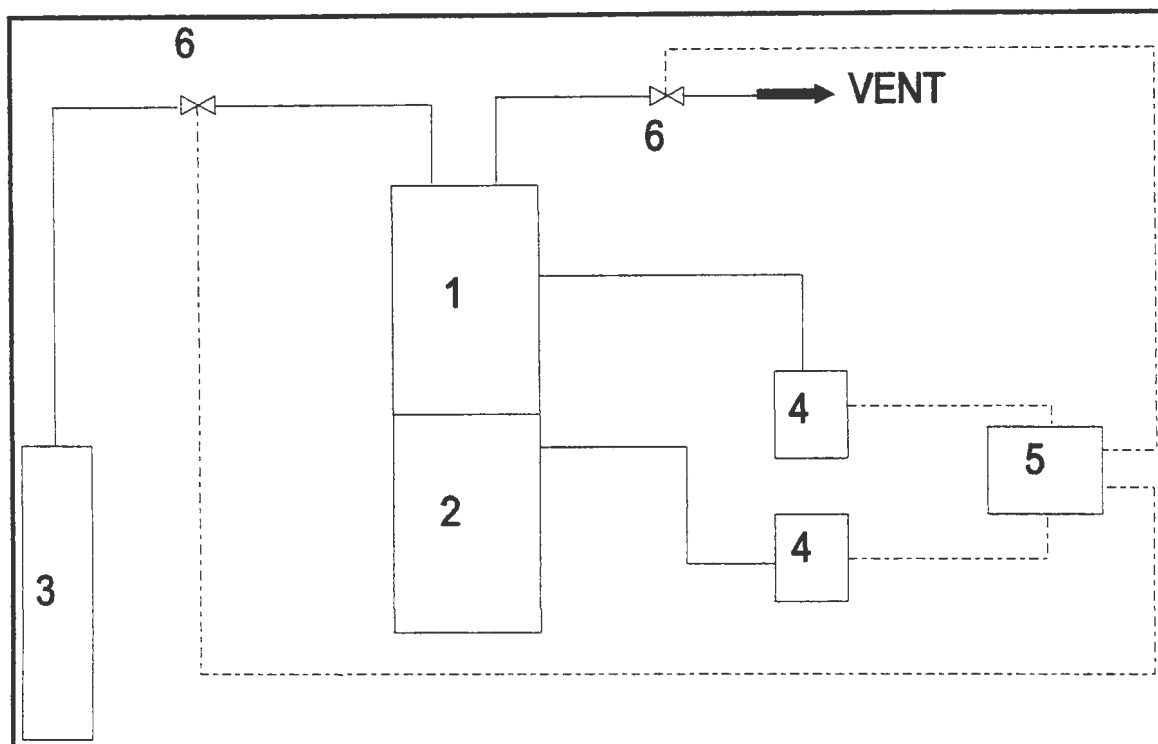


Figure C-3: Schematic of the valving arrangement for the pressure equalization mechanism
 1 – Nitrogen compartment; 2 – Equilibrium cell; 3 – Nitrogen storage cylinder (high pressure); 4 – Pressure transducer with output signal; 5 – Pressure equalization circuit; 6 – Solenoid valve (high pressure)

The electronic circuit basically consisted of a simple comparator. mV signals from the pressure transducers reading the pressures in the nitrogen compartment and the equilibrium cell were compared. If the difference was greater than a certain tolerance (mV), then either solenoid valve would be actuated depending on whether the nitrogen compartment pressure was higher or lower than the equilibrium cell pressure.

The solenoid valves tended to overheat when they were actuated. To prevent overheating of the valves and probably destroying them, a simple power supply circuit was designed. The circuit pulsed the power to the solenoid valves. They were thus actuated for short periods rapidly, mimicking full actuation for the specified period. This considerably reduced heating of the solenoid valves.

C.5. UPPER STIRRER DESIGN

The circuitry for the stirring mechanism was designed with the assistance of Dr M. Hippner of the School of Electrical and Electronic Engineering at the University of Natal. The design was based on that of a stepper motor. There were four solenoid coils. The orientation of the solenoid coils was such that the angle between two adjacent coils was either 60 or 90 degrees. The reason that they were not symmetrically spaced 90 degrees apart was because they were inserted at a much later stage and they therefore had to be designed around what had already been constructed. Figure C-4 illustrates a cross-section through the equilibrium cell body showing the arrangement of the solenoid coils and the rare-earth magnets in the upper stirrer.

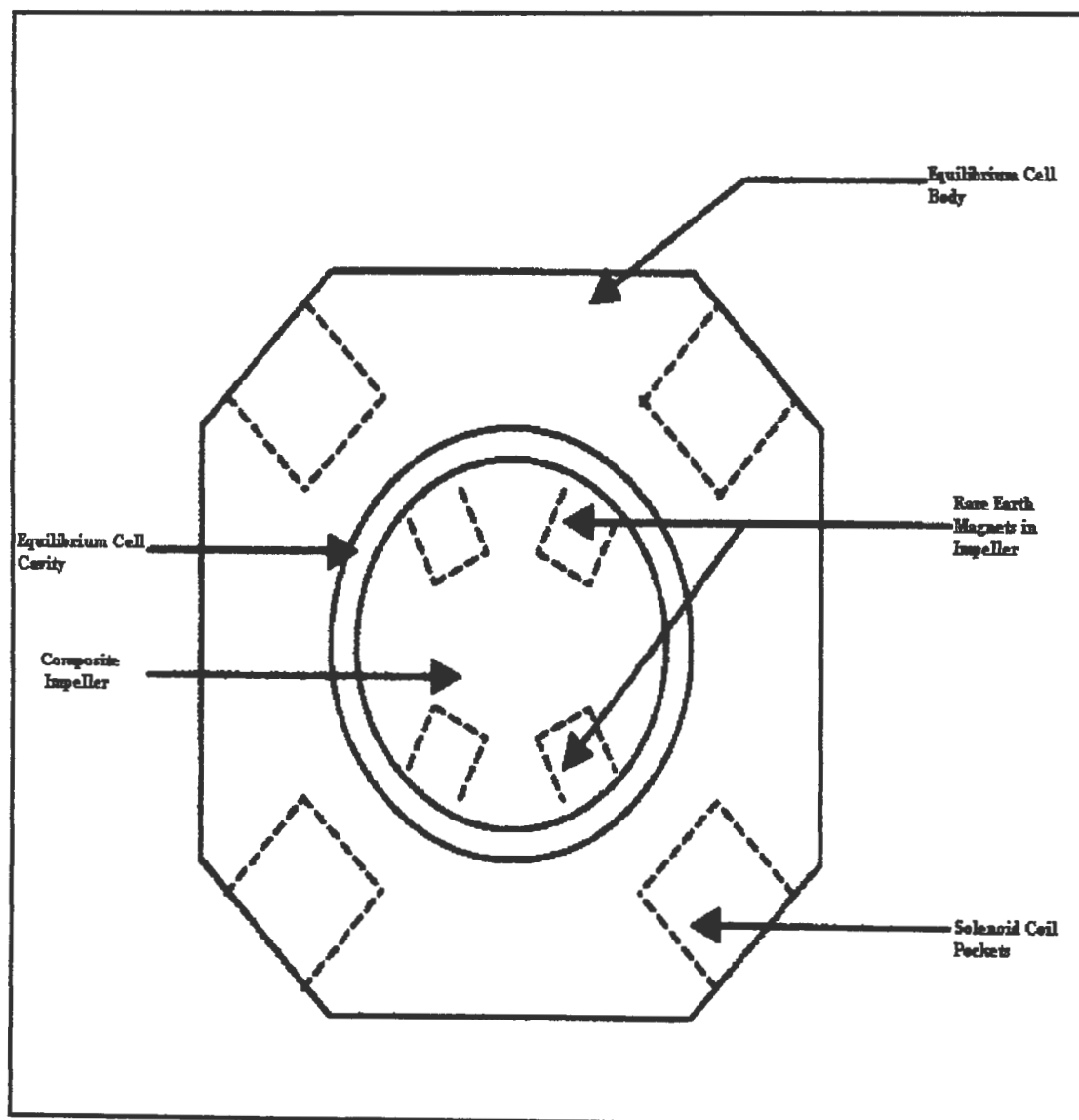


Figure C-4: Cross-section through the equilibrium cell body and the upper stirrer

The solenoid coils had a soft metal core and the windings were made with thin nickrome wire. There were approximately 3000 turns in each coil. Each coil had a resistance of approximately 200 ohms. Foreseeing that the coils would generate heat when they were energized, heat exchanger fins were designed into the coils so as to dissipate the heat that would be generated. This would prevent hot spots from being formed on the equilibrium cell body. The solenoid coils were held in place in the wells that housed them with the use of "o"-rings. The "o"-rings gave the coils a very snug fit in the wells and produced an insulating air layer between the solenoid body and the cell wall. Figure C-5 illustrates the solenoid coil designed.

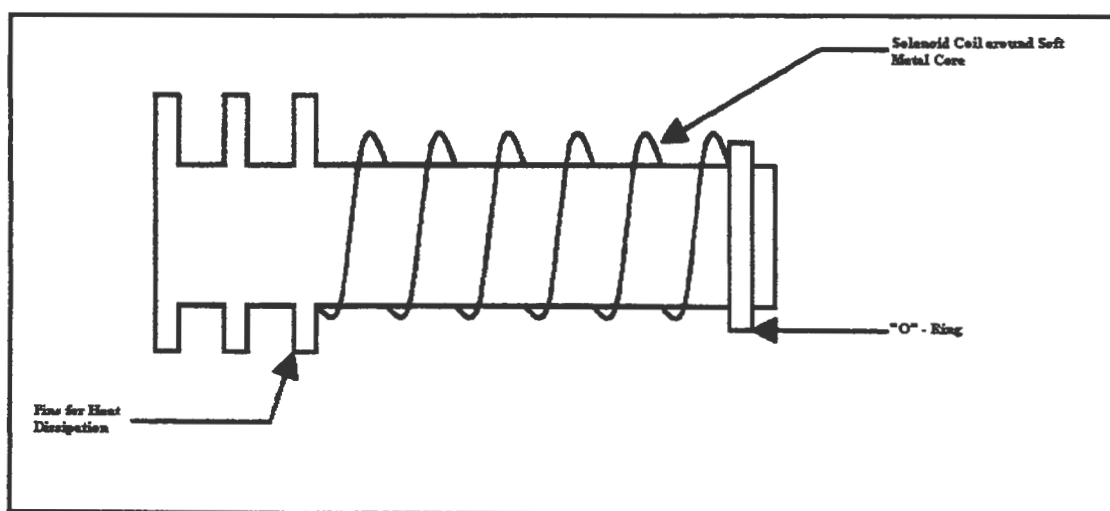


Figure C-5: Illustration of the solenoid coil designed

C.6. JET-MIXER DESIGN

The design of the jet-mixer was reproduced from the work of Mühlbauer [1990]. Prof. Raal originally came up with the design concept. The major difference in the design of jet-mixers is design for effective internal free volume. The desired effective internal free volume can be achieved with various combinations of length to diameter of the internal and external cylinders (see Figure 4-8). The researcher can design according to his limitations.

The volume (effective) that the jet-mixer needs to be designed to is determined by:-

1. The size of the sample loop on the GC sampling valve (number of moles of component). The pressure of the equilibrium sample can be estimated using the ideal gas law. This means that

the number of moles of component, which is determined from the sample loop volume, determines the pressure.

2. Temperatures that the air-bath is to be operated at, and consequently the jet-mixer. The jet-mixer temperatures should ideally be maintained at between five to ten degrees Celsius higher than the air-bath temperature. If their temperatures are far greater than that of the air-bath, then they create temperature gradients as a result of their radiation. These gradients may adversely affect the uniformity of the equilibrium cell temperature resulting in not a true representative equilibrium sample, even with substantial thermal insulation around the jet-mixer.
3. Sensitivity of the GC detector. The sensitivity of the GC detector gives a lower limit of concentration for the sample that is analysed. The jet-mixer volume and the pressurization (dilution of the components) of the jet-mixer with carrier gas determines the concentration to the GC.

Points one to three have to be taken into consideration when sizing the jet-mixers. The process can be trial and error, as there can be various combinations for a particular size.

C.7. PROPERTIES OF INSULATION MATERIAL

The material was Fibrefrax Duraback. It was chosen as an insulation because it has the following properties:-

1. Excellent cold handling strength
2. Excellent hot strength
3. Low thermal conductivity
4. Low heat storage
5. Light weight
6. Resiliency
7. Thermal shock resistance
8. Excellent thermal stability
9. High heat reflectance
10. Good sound absorption
11. Excellent corrosion resistance

Typical physical properties were as follows:-

Continuous Use Limit	927 °C
Melting Point	Above 1648 °C
Specific Heat at 1093 °C	1130 Jkg ⁻¹ K ⁻¹
Thermal Conductivity at 200 °C	0.072 Wm ⁻¹ K ⁻¹

Table C-1: Typical physical properties of Fibrefrax Duraback [Carborundum Company Catalogue, 1995]

C.8. CALIBRATION OF TEMPERATURE SENSORS AND TUNING OF TEMPERATURE CONTROLLERS

C.8.1. Calibration of temperature sensors

A Hewlett Packard Quartz Thermometer was used to calibrate the Pt-100 Ω resistors. The temperature controllers and displays had an adjustment for deviation that was set to correct the readout on the temperature display to the readout on the Quartz Thermometer. The Pt-100 Ω resistors were very linear over the temperature range of calibration. Once corrected for a few temperatures, the temperature readings between the Pt-100 Ω resistors and the Quartz Thermometer were within 0.3% of each other for a wide range of temperatures (30 to 250 °C).

C.8.2. Tuning of temperature controllers

The temperature controllers (Eurotherm 808 and 818) could be tuned both manually and automatically (Eurotherm [1995]). Manual tuning entailed setting variables for proportional, differential and integral times. These values can be calculated using fundamental process control technology (Luyben [1990]). Tuning of the temperature controllers is also possible using the *autotuning* function that is available. In this project all the temperature controllers were tuned using this *autotuning* function.

Autotuning was very simple. The set-point required was set on the temperature controller and the *autotune* function was then pressed. The controller automatically calculated the variables for PID control. With the autotune facility the temperature controller was able to maintain the

temperature to within 0.1 °C of the set-point (which was in fact the uncertainty in the readout from the temperature display).

C.9. CALIBRATION OF PRESSURE TRANSDUCERS

The pressure transducers were calibrated against the Bourdon type Heisse gauges. The Heisse gauges had calibration results traceable to the National Bureau of Standards. The 0-5000 psi Heisse gauge was used to calibrate the 0-175 bar absolute pressure transducers and the 0-500 psi Heisse gauge to calibrate the 0-5 bar absolute pressure transducer.

The calibration procedure involved connecting the Heisse gauge and the pressure transducer in parallel to a pressure source (nitrogen cylinder). The cylinder regulator was then used to set a “rough” pressure. The pressure was read on the Heisse gauge and was then adjusted on the pressure display for the pressure transducer. The display for the pressure transducer had the facility for coarse and fine adjustment of the *zero* and *span*. Using the *zero* and *span* screws the pressure on the display was set to the readout on the Heisse gauge. This procedure was performed for a number of different pressures over the range. For each pressure calibration the procedure was iterative. Calibration for each pressure was usually accomplished in three to four iterations.

APPENDIX D

D.1. EXPERIMENTAL PROCEDURE FOR AUXILIARY EQUIPMENT

D.1.1. Degassing Apparatus

Reference must be made to Figure D-1 when following the experimental procedure.

1. The apparatus was charged by removing valve V1 from the "o"-ring attachment above the condenser and pouring the liquid component through the top of the condenser. The apparatus was usually charged with about 130 ml of liquid. Once filled, valve V1 was replaced.
2. The cooling water tap was opened and an adequate flowrate set so as to condense all of the liquid component. Generally tapped water was adequate for use as a coolant.
3. The stirrer/heater was then switched on. The stirrer was generally set to 600-800 rpm. This provided vigorous stirring of the boiling liquid. The heater was set to a temperature greater than the boiling point temperature of the liquid component at the vacuum pressure (approximately 5 mbar).
4. Valve V1 was opened, and the vacuum pump switched on.
5. Valve V2 was opened, and a slow flowrate (approximately 5 l/min) of the gas component bubbled through the liquid in the degassing apparatus. This allowed for saturation of the liquid component with the gas component and enhanced degassing of the volatile impurities from the liquid component.
6. The degassing procedure was generally undertaken for a period of 25 to 30 minutes.
7. Once degassed, the vacuum and the gas flow were turned off by closing valves V1 and V2 respectively. Great care must be taken that the gas flow is turned off before the vacuum. If this is not adhered to there will be a build up of pressure in the degassing apparatus and hence an explosion. The glass degassing apparatus can not withstand pressures much in excess of atmospheric pressure.
8. The liquid component is then transferred from the degassing apparatus to the equilibrium cell by opening valve V3. The procedure is explained in Chapter 5.2. It basically works on the principle of pressure as a driving force.

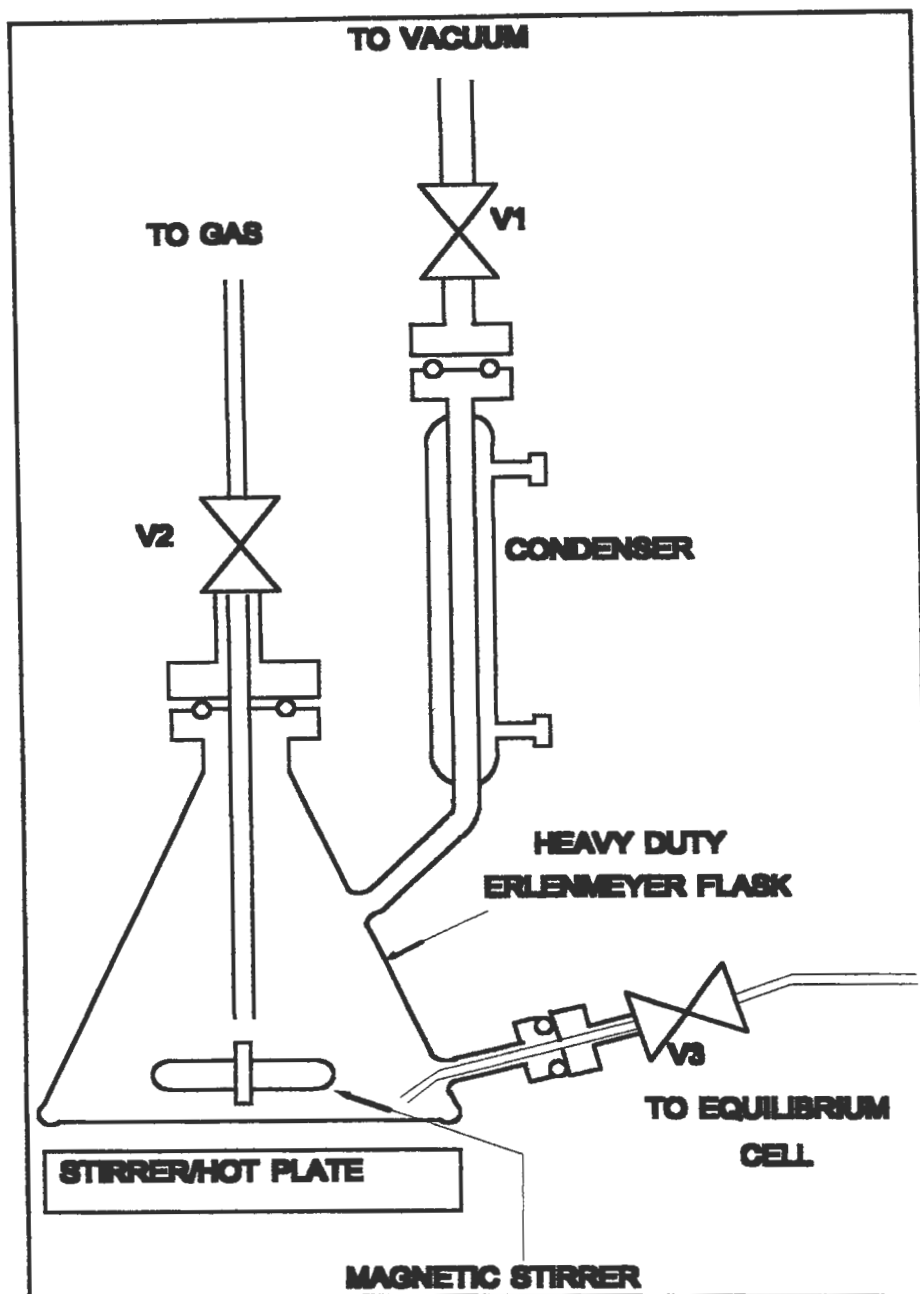


Figure D-1: Schematic of the degassing apparatus

D.1.2. Propane Compressor

Reference must be made to Figure D-2 when following the experimental procedure.

1. Both chambers were vented. In addition the propane chamber (chamber 1) was evacuated so as to remove any residual air that may have got into the chamber. The propane chamber was then flushed with propane about 4 or 5 times. Venting of the air chamber (chamber 2) was

achieved by opening valves V3 and V2. Venting and evacuation of the propane chamber was achieved by opening valves V6 and V7.

2. The heater cartridges were switched on, and the temperature was set to a value greater than the critical temperature for propane. The heaters were generally switched on a few hours before the compressor was to be used. This was to ensure that the chamber was at the proper uniform temperature when the propane chamber was being filled.
3. Filling of the propane chamber was accomplished by having valve V7 closed whilst having valves V5 and V6 open. At the same time valves V3 and V2 had to remain open, so as to allow the piston to move to the end of its travel as the propane filled its chamber.
4. Valve V6 was then closed and the propane was left in the chamber for about 20 minutes so as to achieve the temperature of the propane chamber. Since the temperature is greater than the critical temperature, condensation of any propane is avoided.
5. Valve V2 was then closed and V1 opened. The flowrate of air into the air chamber was controlled by adjusting the opening of valve V3. The air chamber was pressurised and the piston allowed to move to the end of its travel in the propane chamber. A pressure gauge on the propane chamber indicated the propane pressure.
6. To fill the equilibrium cell, valves V6, V7, and V4 were opened.
7. The procedure was repeated until the desired pressure was attained in the equilibrium cell.

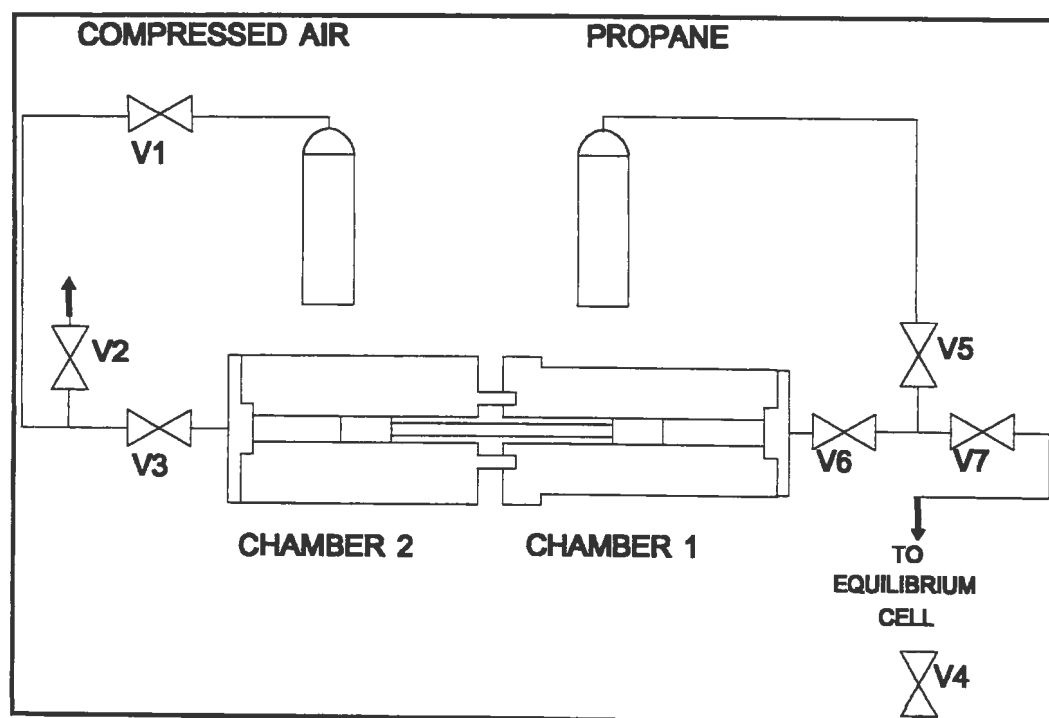


Figure D-2: Schematic of the propane compression device arrangement

D.2. GC CALIBRATION

The different methods of GC detector calibration and the aspects of calibration are briefly dealt with in this section. For greater detail into gas chromatography there are a number of available references e.g. Littlewood [1970], Willett [1987], Fowles [1995], and Grob [1995]. Raal and Mühlbauer [1998] also contains details on GC calibration, especially for VLE measurement.

D.2.1. Calibration Methods

There are basically two methods of detector calibration i.e. the internal standardisation and direct injection methods.

D.2.1.1. Internal Standardisation

As the name suggests this method makes use of an internal standard, not present in the samples to be analysed, as a reference. Samples of known concentration, with an internal standard not present in the sample are injected into the GC. Response factors (f_i) are then assigned to each of the components present. The response factor for the internal standard (f_r) is assigned a value of unity. The relationship between the measured peak areas (A_i), concentration (C_i), and response factor (f_i) are related by the following direct proportionality:

$$C_i = f_i A_i \quad (D-1)$$

$$C_r = f_r A_r \quad (D-2)$$

The response factors of the components can therefore be calculated from the following relation:

$$f_i = \left(\frac{A_r}{A_i} \right) \left(\frac{C_i}{C_r} \right) f_r \quad (D-3)$$

When the concentration of a sample has to be determined, a known quantity of internal standard is added directly to the sample, and the unknown concentration is calculated by the following relation:

$$C_i = \left(\frac{A_i}{A_r} \right) C_r f_i \quad (\text{D-4})$$

D.2.1.2. Direct Injection

This method involves the injection of known volumes of standard solution into the GC. A calibration curve of component peak area (A_i) versus quantity injected is then generated. The slope of the calibration curve (f_i) can then be determined by linear regression, if the response is linear (as is the case normally). An unknown component quantity can then be calculated from the peak area and the calibration slope.

$$n_i = f_i A_i \quad (\text{D-5})$$

D.2.2. Quantitative and qualitative aspects

The qualitative and quantitative aspects of gas chromatography are well explained in a review by Debbrecht [1985].

Qualitative aspects basically refer to the peak shape and separation. This aspect is mainly determined by the type of column used and the operating method or conditions used. Well separated sharp peaks ensure the most accurate quantitative analysis. Experimentation with different types of columns, oven temperatures, carrier gas flowrates etc. usually ensure good separation.

Quantitative analysis can only be undertaken once the detector has been calibrated, as discussed above. This is as a result of the peak area being representative of the quantity of component present in the sample analysed.

The details of the GC method used in this project are available in Chapter 7.4.

D.2.3. GC Calibration method utilised in this project

The GC method applied in this project was the direct injection method. Since the binary systems studied consisted of a liquid and gas component at room temperature, separate calibration curves had to be generated for the gas and liquid components.

D.2.3.1. Liquid component calibration

The liquid component was calibrated by injecting known volumes of the pure liquid component into the GC. Conversion of the known volumes into moles then generated a calibration curve of *peak area versus number of moles*. The liquid component was injected with either a 1 μl or 10 μl liquid syringes manufactured by Dynatech and Hamilton. Two different types of syringes were used to check the consistency of injected volumes. Each volume was injected at least 10 times and only the results that correlated to within 1.0 % were used to generate the calibration curve.

The conversion from volumes to number of moles is as follows:-

$$n = \frac{\rho V}{MW} \quad (\text{D-6})$$

where: ρ - density of component;
 V - volume injected; and
 MW - molecular weight of component.

D.2.3.2. Gas component calibration

The gas components were also calibrated by injecting known volumes into the GC, and obtaining a calibration curve of *peak area versus number of moles*. As with the liquid component calibration two different types of gas syringe were used. The pure gas components were injected into the GC with either a 100 μl or 1 cm^3 syringe. Each volume was also injected at least 10 times and only the results that correlated to within 1.0 % were used to generate the calibration curve.

The volumes injected were converted into number of moles by using the truncated two-parameter virial EOS:

$$n = \frac{V}{\left(\frac{RT}{P} + B\right)} \quad (\text{D-7})$$

where: V - volume in cm^3 ;

T - temperature in K;

P - pressure in kPa;

R - universal gas constant; and

B - second virial coefficient (Dymond and Smith [1980]).

D.2.3.3. Precautions taken during calibration

The following precautions were taken during calibration to ensure reproducibility and accuracy of injected volumes:-

1. Always use good quality syringes and maintain in good working condition. All syringe needles were regularly checked during calibration for needle blockages due to septa coring. The tightness of the piston plunger seal for gas and liquid syringes, and the needle seal for the liquid syringes were regularly checked.
2. The GC septa were replaced after every 30 injections during calibration. This was so as to avoid potential error due to leakage pass the septum. Leakage pass the septum can be detected by a drop in the column head pressure.
3. The GC carrier gas and reference flowrates were checked at regular intervals.
4. To negate any errors due to the extra syringe needle volume, for gas injections, only volumes greater than 50 % of the total syringe volume were injected during calibration. Only when it was unavoidable were volumes less than 50 % of the total syringe volume injected.

D.3. DETERMINATION OF JET-MIXER OPERATING TEMPERATURE

The purpose of the jet-mixer is to homogenise the equilibrium phase sample before conveying it to the GC for analysis. Thus the sample in the jet-mixer has to be homogeneous vapour. Any partial condensation in the jet-mixer will result in the jet-mixer behaving as an equilibrium cell. Thus the sample conveyed to the GC will not be a representation of the true equilibrium phase. To ensure that the sample is vapourised, the jet-mixer operating temperature has to be sufficiently high so that condensation of the equilibrium sample does not occur.

One can determine the operating temperature of the jet-mixer by performing a calculation for the vapour pressure in the jet-mixer versus the saturation pressure of the mixture in the jet-mixer for a range of operating pressures.

The vapour pressure in the jet-mixer can be simply calculated by making the following assumptions:-

1. The jet-mixer contains only the non-volatile component; and
2. the component obeys the Ideal gas law.

The vapour pressure is then calculated via the Ideal gas law equation:-

$$P = \frac{nRT}{V} \quad (\text{D-8})$$

where, P - vapour pressure;

n - number of moles (calculated from volume of sample loop);

T - temperature of jet-mixer;

R - Universal gas constant;

V - volume of jet-mixer.

The saturation pressure of the mixture in the jet-mixer can be calculated by using the Antoine equations. For simplification one can assume that the jet-mixer contains only the non-volatile component. One thus obtains the extreme operating conditions for the jet-mixer.

A plot as illustrated in Figure D-3 was then constructed. The operating temperature was chosen so that the jet-mixer pressure was 10% of the saturation pressure. This ensured that there would be no partial condensation possible.

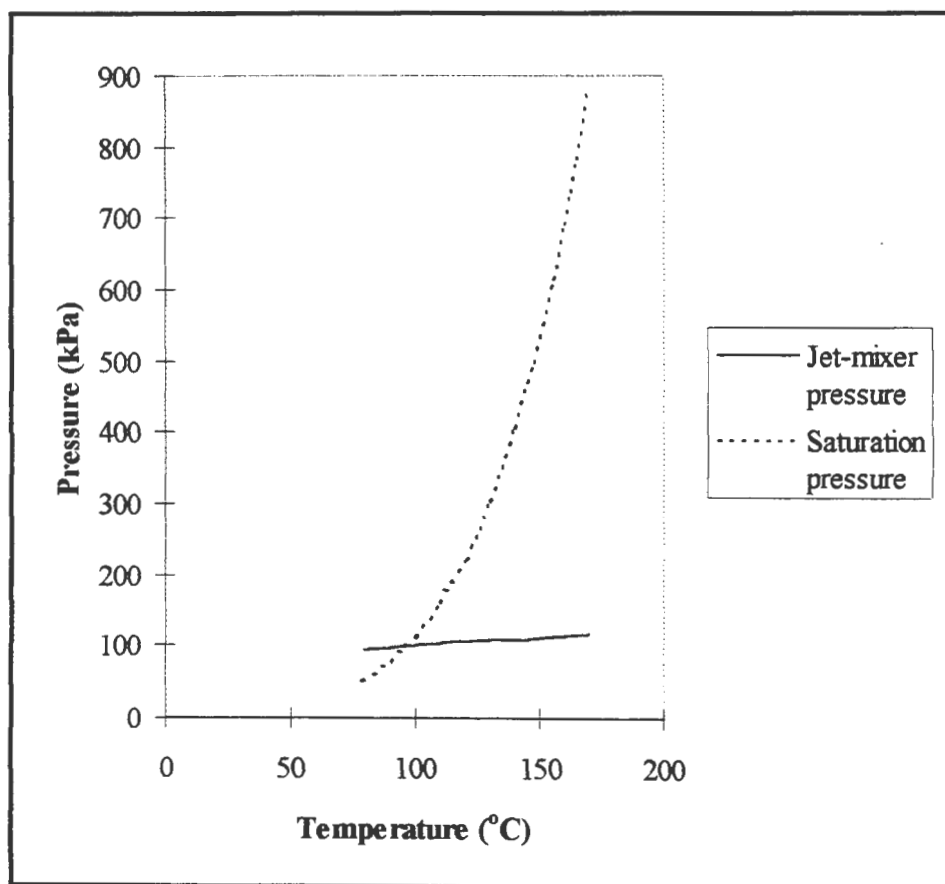


Figure D-3: Plot of jet-mixer pressure versus saturation pressure to determine the operating temperature for the jet-mixer

APPENDIX E

E.1. LITERATURE DATA FOR SYSTEMS STUDIED

Listed in the following tables are literature data for the systems studied in this project for the conditions of investigation.

E.1.1. Carbon dioxide + Toluene

E.1.1.1. Data at approximately 311.15 K

Absolute Pressure (bar)	Liquid composition (X_{CO_2})	Vapour composition (Y_{CO_2})
3.34	0.030	0.978
14.89	0.133	0.993
28.54	0.264	0.997
40.68	0.406	0.996
55.78	0.603	0.994
69.36	0.869	0.992
73.36	0.931	0.993
77.43	0.971	0.993

Table E-1: Experimental VLE data of Ng and Robinson [1978] for the system Carbon Dioxide + Toluene at 311.26 K

Absolute Pressure (bar)	Liquid composition (X_{CO_2})	Vapour composition (Y_{CO_2})
8.04	0.0627	0.9889
14.75	0.1229	0.9918
22.01	0.1886	0.9892
23.67	0.2110	0.9949
29.93	0.2745	0.9923
32.00	0.2990	0.9956
38.43	0.3732	0.9944
48.43	0.4923	0.9925
48.95	0.5118	0.9947
53.15	0.5724	0.9919
55.91	0.6288	0.9950
59.17	0.6896	0.9936
63.21	0.7962	0.9945
66.38	0.8502	0.9951
69.21	0.9082	0.9948

Table E-2: Experimental VLE data of Fink and Hershey [1990] for the system Carbon Dioxide + Toluene at 308.16 K

E.1.1.2. Data at approximately 353.15 K

Absolute Pressure (bar)	Liquid composition (X_{CO_2})	Vapour composition (Y_{CO_2})
3.76	0.0206	0.886
13.99	0.0765	0.963
30.75	0.172	0.978
57.23	0.328	0.981
83.63	0.491	0.978
95.56	0.588	0.973
112.11	0.720	0.961
116.04	0.749	0.954
119.21	0.787	0.946
123.07	0.843	0.931

Table E-3: Experimental VLE data of Ng and Robinson [1978] for the system Carbon Dioxide + Toluene at 352.59 K

Absolute Pressure (bar)	Liquid composition (X_{CO_2})	Vapour composition (Y_{CO_2})
2.59	0.0102	0.856
5.79	0.0287	0.926
9.05	0.0463	0.952
19.50	0.105	0.968
31.25	0.170	0.978
42.90	0.239	0.980
53.50	0.300	0.981
64.75	0.366	0.980
80.40	0.468	0.975
94.95	0.546	0.974
103.35	0.613	0.971
119.30	0.783	0.939

Table E-4: Experimental VLE data of Morris and Donohue [1985] for the system Carbon Dioxide + Toluene at 353.15 K

Absolute Pressure (bar)	Liquid composition (X_{CO_2})	Vapour composition (Y_{CO_2})
6.72	0.033	0.887
13.33	0.073	0.932
22.22	0.125	0.958
28.84	0.166	0.969
36.28	0.210	0.979
44.24	0.258	0.979
52.70	0.308	0.969
61.77	0.361	0.980

Table E-5: Experimental VLE data of Kim et al. [1986] for the system Carbon Dioxide + Toluene at 353.4 K

Absolute Pressure (bar)	Liquid composition (X_{CO_2})	Vapour composition (Y_{CO_2})
5.18	0.0232	0.8810
7.65	0.0375	0.9237
7.77	0.0376	0.9197
10.88	0.0567	0.9424
14.82	0.0784	0.9534
22.80	0.1235	0.9711
29.54	0.1631	0.9753
37.31	0.2093	0.9790
47.65	0.2683	0.9826
55.87	0.3137	0.9824
64.39	0.3645	0.9811
74.63	0.4191	0.9815
83.55	0.4769	0.9804
92.95	0.5352	0.9768
98.85	0.5885	0.9744
110.89	0.6750	0.9626
115.16	0.7194	0.9592
116.81	0.7385	0.9546
123.50	0.8301	0.9324

Table E-6: Experimental VLE data of Fink and Hershey [1990] for the system Carbon Dioxide + Toluene at 353.18 K

Absolute Pressure (bar)	Liquid composition (X_{CO_2})	Vapour composition (Y_{CO_2})
8.76	0.0495	0.9300
17.58	0.1100	0.9675
31.37	0.1731	0.9775
54.81	0.3000	0.9820
55.50	0.3100	0.9820
86.53	0.5000	0.9820
103.08	0.6490	0.9725
105.83	0.6693	0.9720
109.97	0.7080	0.9650

Table E-7: Experimental VLE data of Mühlbauer and Raal [1990] for the system Carbon Dioxide + Toluene at 352.15 K

E.1.1.3. Data at approximately 391.45 K

Absolute Pressure (bar)	Liquid composition (X_{CO_2})	Vapour composition (Y_{CO_2})
4.03	0.0172	0.660
9.89	0.0396	0.847
24.41	0.106	0.926
52.26	0.231	0.953
84.25	0.368	0.953
112.73	0.495	0.943
138.17	0.621	0.921
152.93	0.715	0.879

Table E-8: Experimental VLE data of Ng and Robinson [1978] for the system Carbon Dioxide + Toluene at 393.71 K

Absolute Pressure (bar)	Liquid composition (X_{CO_2})	Vapour composition (Y_{CO_2})
9.76	0.0385	0.8558
24.18	0.1032	0.9258
40.17	0.1742	0.9392
51.98	0.2261	0.9485

Table E-9: Experimental VLE data of Sebastian et al. [1980] for the system Carbon Dioxide + Toluene at 393.25 K

Absolute Pressure (bar)	Liquid composition (X_{CO_2})	Vapour composition (Y_{CO_2})
13.13	0.046	0.839
18.09	0.069	0.877
26.77	0.110	0.922
34.92	0.148	0.936
43.41	0.180	0.945
52.72	0.227	0.949
64.50	0.276	0.952

Table E-10: Experimental VLE data of Kim et al. [1986] for the system Carbon Dioxide + Toluene at 393.2 K

E.1.2. Carbon dioxide + Methanol

E.1.2.1. Data at approximately 313.15 K

Absolute Pressure (bar)	Liquid composition (X_{CO_2})	Vapour composition (Y_{CO_2})
5.772	0.0285	0.9363
17.701	0.1023	0.9774
30.047	0.1641	0.9847
40.871	0.2339	0.9868
57.059	0.3655	0.9882
62.723	0.4201	0.9880
70.934	0.5429	0.9866
77.028	0.6892	0.9840
80.584	0.8970	0.9748

Table E-11: Experimental VLE data of Ohgaki and Katayama [1976] for the system
Carbon Dioxide + Methanol at 313.15 K

Absolute Pressure (bar)	Liquid composition (X_{CO_2})	Vapour composition (Y_{CO_2})
6.83	0.031	0.944
11.26	0.055	0.965
21.45	0.111	0.980
29.86	0.163	0.983
49.10	0.283	0.986
69.54	0.482	0.984
74.00	0.552	0.983
77.13	0.616	0.981

Table E-12: Experimental VLE data of Suzuki et al. [1990] for the system Carbon Dioxide
+ Methanol at 313.4 K

Absolute Pressure (bar)	Liquid composition (X_{CO_2})	Vapour composition (Y_{CO_2})
13.2	0.0682	0.9646
16.7	0.0911	0.9727
20.3	0.1159	0.9815
24.7	0.1372	0.9843
31.3	0.1773	0.9849
36.1	0.2006	0.9857
39.6	0.2318	0.9867
45.6	0.2733	0.9876
55.0	0.3464	0.9881
59.1	0.3838	0.9879
62.0	0.4128	0.9882
66.0	0.4658	0.9871
69.0	0.5138	0.9865
70.6	0.5467	0.9867
73.9	0.5907	0.9864
76.9	0.6816	0.9842
80.3	0.8783	0.9677

Table E-13: Experimental VLE data of Chang et al. [1997] for the system Carbon Dioxide + Methanol at 313.14 K

E.1.2.2. Data at approximately 373.15 K

Absolute Pressure (bar)	Liquid composition (X_{CO_2})	Vapour composition (Y_{CO_2})
20.1	0.0392	
38.1	0.0880	
48.4	0.1185	
58.4	0.1445	
83.7	0.2262	
90.7	0.2456	
117.4	0.3429	
127.1	0.3968	
147.5	0.5185	
154.1	0.6197	
154.2	0.6664	
154.2	0.6735	0.6735
154.2		0.6805
154.2		0.6959
153.2		0.7577
153.1		0.7695
140.6		0.8500
134.4		0.8727
129.5		0.8870
110.5		0.9048
103.1		0.9076
80.6		0.9109
66.2		0.9111
39.7		0.8820
28.3		0.8523

Table E-14: Experimental VLE data of Brunner et al. [1987] for the system Carbon Dioxide + Methanol at 373.15 K

E.1.3. Propane + 1-Propanol

E.1.3.1. Data at approximately 378.25 K

Absolute Pressure (bar)	Liquid composition (X_{propane})	Vapour composition (Y_{propane})
35.49	0.5886	
35.49	0.5864	
34.45	0.5758	
34.45	0.5746	
30.32	0.4588	
30.14	0.4584	
27.21	0.3874	
23.08	0.3071	
20.25	0.2552	
17.49	0.2139	
15.56	0.1877	
12.80	0.1484	
11.05	0.1220	
10.80	0.1219	
8.46	0.0887	
6.11	0.0610	
5.00	0.0601	
29.97		0.9161
27.21		0.9296
27.14		0.9294
23.08		0.9230
23.08		0.9204
23.08		0.9159
20.18		0.9067
17.49		0.8935
15.49		0.9014
11.15		0.8864
11.15		0.8871
10.80		0.8779
8.46		0.8513
8.46		0.8489
6.05		0.7924
4.58		0.7209

Table E-15: Experimental VLE data of Mühlbauer and Raal [1993] for the system Propane + 1-Propanol at 378.15 K

E.1.3.2. Data at approximately 393.15 K

Absolute Pressure (bar)	Liquid composition (X_{propane})	Vapour composition (Y_{propane})
40.45	0.5613	
40.31	0.5652	
40.31	0.5627	
36.73	0.4782	
34.97	0.4448	
31.21	0.3689	
31.21	0.3674	
26.52	0.2999	
22.46	0.2424	
22.46	0.2402	
19.97	0.2045	
15.84	0.1585	
13.29	0.1288	
10.05	0.0904	
9.22	0.0787	
6.39	0.0493	
6.39	0.0485	
4.53	0.0297	
40.31		0.9355
40.11		0.9327
36.73		0.9273
34.80		0.9304
30.66		0.9199
30.66		0.9350
26.52		0.9100
26.18		0.9149
22.32		0.9036
22.32		0.8969
19.63		0.8900
16.11		0.8681
13.22		0.8701
10.05		0.8356
9.22		0.8144
6.32		0.7364
6.32		0.7122
4.53		0.5890
4.46		0.5762

Table E-16: Experimental VLE data of Mühlbauer and Raal [1993] for the system Propane + 1-Propanol at 393.15 K

E.2. REFERENCES TO SYSTEMS REVIEWED WHICH CONTAINED COMPONENTS INVESTIGATED IN THIS PROJECT

Below are references to systems that have been reviewed which contain one of the components investigated in this project. These references exclude those given in Table A-1 to A-6.

E.2.1. Systems containing Carbon Dioxide

Vapour-liquid equilibrium has been studied for the following components with carbon dioxide:-

1. Cyclohexane - Chen and Lee [1996];
2. Ethanol - Day et al. [1996];
3. 1-Butanol - Ishihara et al. [1996];
4. Limonene - Iwai et al. [1996];
5. Nonane and C₉ alkylbenzenes - Jennings and Schucker [1996];
6. Aqueous solutions of triethanolamine - Jou et al. [1996], and Li and Mather [1996];
7. Aqueous solutions of N-methyldiethanolamine - Kuranov et al. [1996];
8. Nitrogen - Yorizane et al. [1985]; and
9. Anthracene - Hampson [1996].

In addition volumetric properties are available for the following components with carbon dioxide:-

1. Pentane at high pressure - Kiran et al. [1996];
2. Methane and nitrogen - Seitz et al. [1996].

E.2.2. Systems containing Toluene

Landwehr et al. [1958] determined VLE with ethyl alcohol.

E.2.3. Systems containing Methanol

Vapour-liquid equilibrium has been studied for the following components with methanol:-

1. Water - Kato et al. [1970];
2. n-Hexane - Raal et al. [1972];
3. 2,3-Dimethylbutane – Hiaki et al. [1994(a)]; and
4. n-Alkane - Vonka et al. [1996].

EOS predictions of HPVLE in mixtures containing methanol is available in Peschel and Wenzel [1984].

E.2.4. Systems containing Propane

Vapour-liquid equilibrium has been studied for the following components with propane:-

1. 2-Butanol and 2-propanol - Gros et al. [1996]; and
2. Nonane and C₉ alkylbenzenes - Jennings and Schucker [1996].

Cotterman et al. [1984] studied the extraction of high boiling petroleum fractions using propane.

E.2.5. Systems containing 1-Propanol

Vapour-liquid equilibrium has been studied for the following components with 1-propanol:-

1. 2,2,4-Trimethylpentane – Hiaki et al. [1994(b)], and
2. Octane – Hiaki et al. [1995].

E.3. LITERATURE DATA FOR SECOND VIRIAL COEFFICIENTS

E.3.1. Second Virial coefficients for Nitrogen

The following tables are literature values for the second virial coefficient for nitrogen as extracted from Dymond and Smith [1980].

E.3.1.1. Second virial coefficients at 323.15 K

Investigator/s	B (cm ³ /gmol)
Holburn and Otto [1925]	-0.26
Otto et al. [1934]	-0.50
Michels et al. [1934]	-0.28
Michels et al. [1951]	-0.25
Gunn [1958]	-0.52

Table E-17: Second Virial coefficients for Nitrogen at 323.15 K (Dymond and Smith [1980])

E.3.1.2. Second virial coefficients at 348.15 K

Investigator/s	B (cm ³ /gmol)
Otto et al. [1934]	3.25
Michels et al. [1934]	3.20
Michels et al. [1951]	3.38
Gunn [1958]	3.31

Table E-18: Second Virial coefficients for Nitrogen at 348.15 K (Dymond and Smith [1980])

E.3.1.3. Second virial coefficients at 373.15 K

Investigator/s	B (cm ³ /gmol)
Holburn and Otto [1925]	6.14
Otto et al. [1934]	6.23
Michels et al. [1934]	6.56
Michels et al. [1951]	6.50
Gunn [1958]	6.19

Table E-19: Second Virial coefficients for Nitrogen at 373.15 K (Dymond and Smith [1980])

E.3.2. Second Virial coefficients for Propane

The following tables are literature values for the second virial coefficient for Propane as extracted from Dymond and Smith [1980].

E.3.2.1. Second virial coefficients at 323.15 K

Investigator/s	B (cm ³ /gmol)
Jessen and Lightfoot [1938]	-325 ± 10
Lichtenthaler and Schafer [1969]*	-338.2

*Measurement at 322.8 K

Table E-20: Second Virial coefficients for Propane at 323.15 K (Dymond and Smith [1980])

E.3.2.2. Second virial coefficients at 348.15 K

Investigator/s	B (cm ³ /gmol)
Deschner and Brown [1940]	-293

Table E-21: Second Virial coefficients for Propane at 348.15 K (Dymond and Smith [1980])

E.3.2.3. Second virial coefficients at 373.15 K

Investigator/s	B (cm ³ /gmol)
Beattie et al. [1937]	-247
Deschner and Brown [1940]	-256
Strein et al. [1971]	-242.1

Table E-22: Second Virial coefficients for Propane at 373.15 K (Dymond and Smith [1980])

E.3.3. Second Virial coefficients for Propane + Nitrogen binary system

Table E-23 below lists the measured cross-term second virial coefficients for the system propane + nitrogen, as undertaken by Wormald et al. [1996].

Temperature (K)	B ₁₂ (cm ³ /gmol)
241.1	-126
253.6	-109
262.9	-100
273.5	-87
283.2	-81
293.2	-73
303.4	-67
323.1	-64
343.2	-49
363.2	-37
383.2	-37
393.4	-33

Table E-23: Cross-term second virial coefficients for the system propane + nitrogen as measured by Wormald et al. [1996]

Data are also available in Dymond and Smith [1980], but it is rather sparse.

APPENDIX F

F.1. PROPERTIES FOR COMPONENTS INVESTIGATED

Table's F-1 to F-6 summarize the properties for the components studied. These were the values entered into the parameter optimization and bubble pressure computations. All properties were referenced from Prausnitz et al. [1980], Reid et al. [1988], Reklaitis [1983] or computed.

Component	Properties						
	T_c (K)	P_c (bar)	ω	ZRA	DM (D)	RD (Å)	K_I
Carbon Dioxide	304.1	73.8	0.239	0.2000	0.18	0.992	0.1021
Propane	369.8	42.5	0.153	0.2763	0.00	2.426	0.0264
Methanol	512.6	80.9	0.556	0.2318	1.71	1.536	-0.1104
1-Propanol	536.8	51.7	0.623	0.2485	1.68	2.736	0.2701
Toluene	591.8	41	0.263	0.2646	0.36	3.443	-0.0125

Table F-1: Properties for components studied

The K_I parameter for the Peng-Robinson-Stryjek-Vera EOS was obtained by regressing vapour pressure data for the component as explained in Chapter Eight. Vapour pressures were computed from the Antoine equation (Reklaitis [1983]) and vapour pressure correlations (Reid et al. [1988]). Antoine constants are given in Table F-2 and constants for vapour pressure correlation of Reid et al. [1988] in Table F-3.

Components	Antoine Constants		
	A	B	C
Carbon Dioxide	15.3768	1956.25	-2.1117
Propane	13.7097	1872.82	-25.1011
Methanol	16.4948	3593.39	-35.2249
1-Propanol	15.2175	3008.31	-86.4909
Toluene	14.2515	3242.38	-47.1806

Table F-2: Antoine constants for the components studied

Component	Correlation Constants			
	A	B	C	D
Carbon Dioxide	-6.95626	1.19695	-3.12614	2.99448
Methanol	-8.54796	0.76982	-3.10850	1.54481
Propane	-6.72219	1.33236	-2.13868	-1.38551
1-Propanol	-8.05594	4.25183E-2	-7.51296	6.89004
Toluene	-7.28607	1.38091	-2.83433	-2.79168

Table F-3: Correlation constants for vapour pressure

$$\ln\left(\frac{P}{P_c}\right) = (1-x)^{-1} [Ax + Bx^{1.5} + Cx^3 + Dx^6]$$

$$x = 1 - \frac{T}{T_c}$$

UNIQUAC parameters for the components investigated are given in Table F-4.

Component	UNIQUAC parameters		
	R	Q	Q'
Carbon Dioxide	1.32	1.28	1.28
Propane	2.48	2.24	2.24
Methanol	1.43	1.43	0.96
1-Propanol	2.78	2.51	0.89
Toluene	3.92	2.97	2.97

Table F-4: UNIQUAC parameters for the components investigated

Component	Standard-state fugacity correlation constants				
	C ₁	C ₂	C ₃	C ₄	C ₅
Methanol	3.3387E+2	-1.2679E+4	1.3761E-1	-5.7722E+1	-5.9496E-5
Carbon Dioxide	6.3208	-2.6426E+3	-3.9322E-2	2.7347	2.6718E-5
Propane	1.0491E+1	-2.8237E+3	-1.9487E-2	1.0303	1.1171E-5
1-Propanol	-1.0789E+3	1.8583E+4	-5.3858E-1	2.025E+2	2.2251E-4
Toluene	2.0899E+1	-5.7902E+3	-2.0741E-2	7.144E-2	1.1510E-5

Table F-5: Constants for the standard-state zero pressure fugacity as given by Equation

(8-6)

The constants for the standard-state zero pressure fugacity (Prausnitz et al. [1980]) as given by Equation (8-6) are listed in Table F-5.

The association and solvation parameters (Prausnitz et al. [1980]) used in the computation of the second virial coefficients via the Hayden and O'Connell method are given in Table F-6.

Association and Solvation parameters					
Component	Methanol	Carbon Dioxide	Propane	1-Propanol	Toluene
Methanol	1.63	0.30	-	-	-
Carbon Dioxide	0.30	0.16	-	-	0.00
Propane	-	-	0.00	0.00	-
1-Propanol	-	-	0.00	1.40	-
Toluene	-	0.00	-	-	0.00

Table F-6: Association and solvation parameters for the systems investigated

F.2. ACTIVITY COEFFICIENT PLOTS

F.2.1. The Carbon Dioxide + Toluene System

Activity coefficient plots were undertaken for the carbon dioxide + toluene system for each of the isotherms measured. Figures F-1 to F-3 illustrate the activity coefficients plots. The activity coefficients were computed using the NRTL activity coefficient model and NRTL activity coefficient parameters fitted using the PRSVWS-NRTL + NRTL model.

F.2.2. The Carbon Dioxide + Methanol System

Figures F-4 to F-6 illustrate the activity coefficients plots for the carbon dioxide + methanol system. The activity coefficients were computed using the NRTL activity coefficient model and NRTL activity coefficient parameters fitted using the PRSVWS-NRTL + NRTL model.

F.2.3. The Propane + 1-Propanol System

Figures F-7 to F-8 illustrate the activity coefficients plots for the propane + 1-propanol system. The activity coefficients were computed using the NRTL activity coefficient model and NRTL activity coefficient parameters fitted using the PRSVWS-NRTL + NRTL model.

Figure F-1: Plot of activity coefficient versus liquid mole fraction for the Carbon Dioxide (1) + Toluene (2) System for the 38 °C isotherm

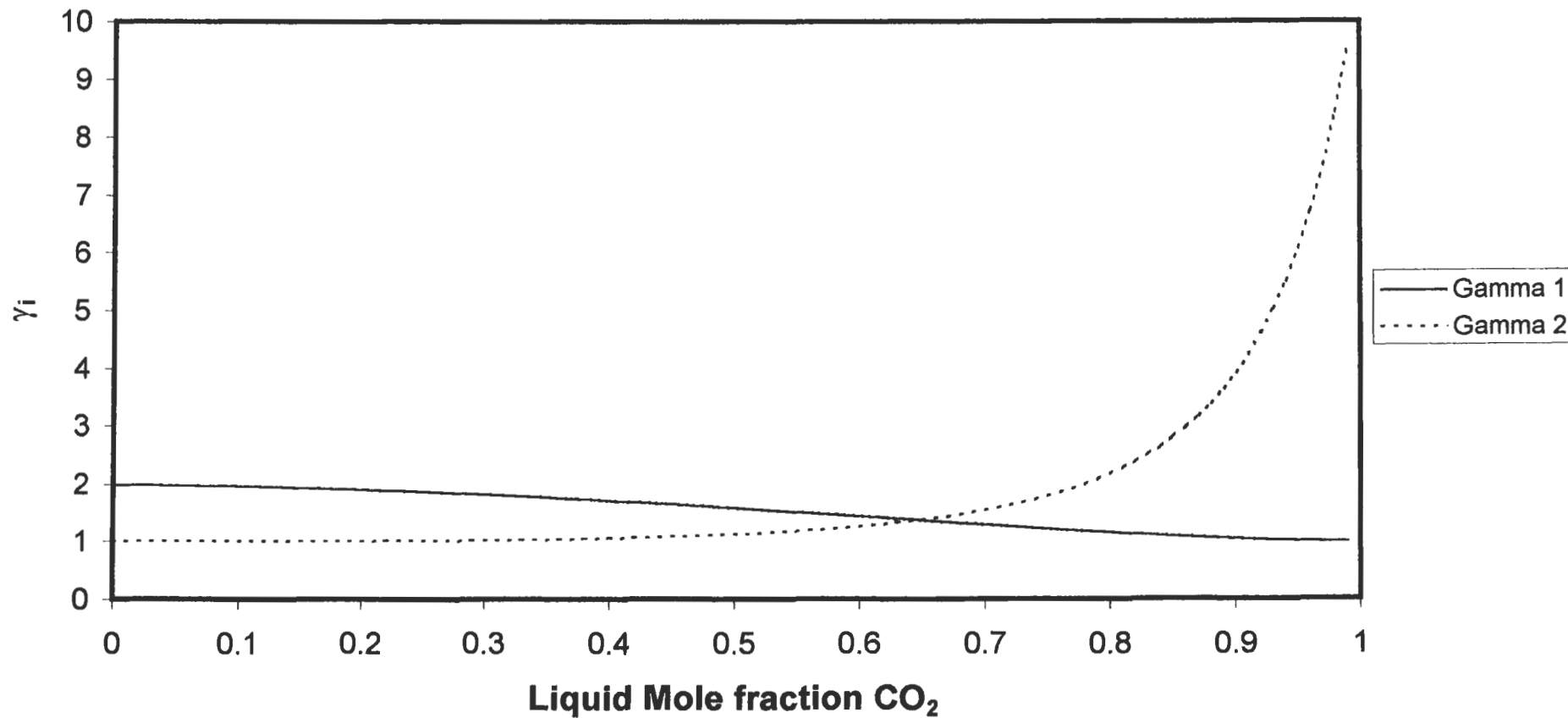


Figure F-2: Plot of activity coefficient versus liquid mole fraction for the Carbon Dioxide (1) + Toluene (2) System for the 80 °C isotherm

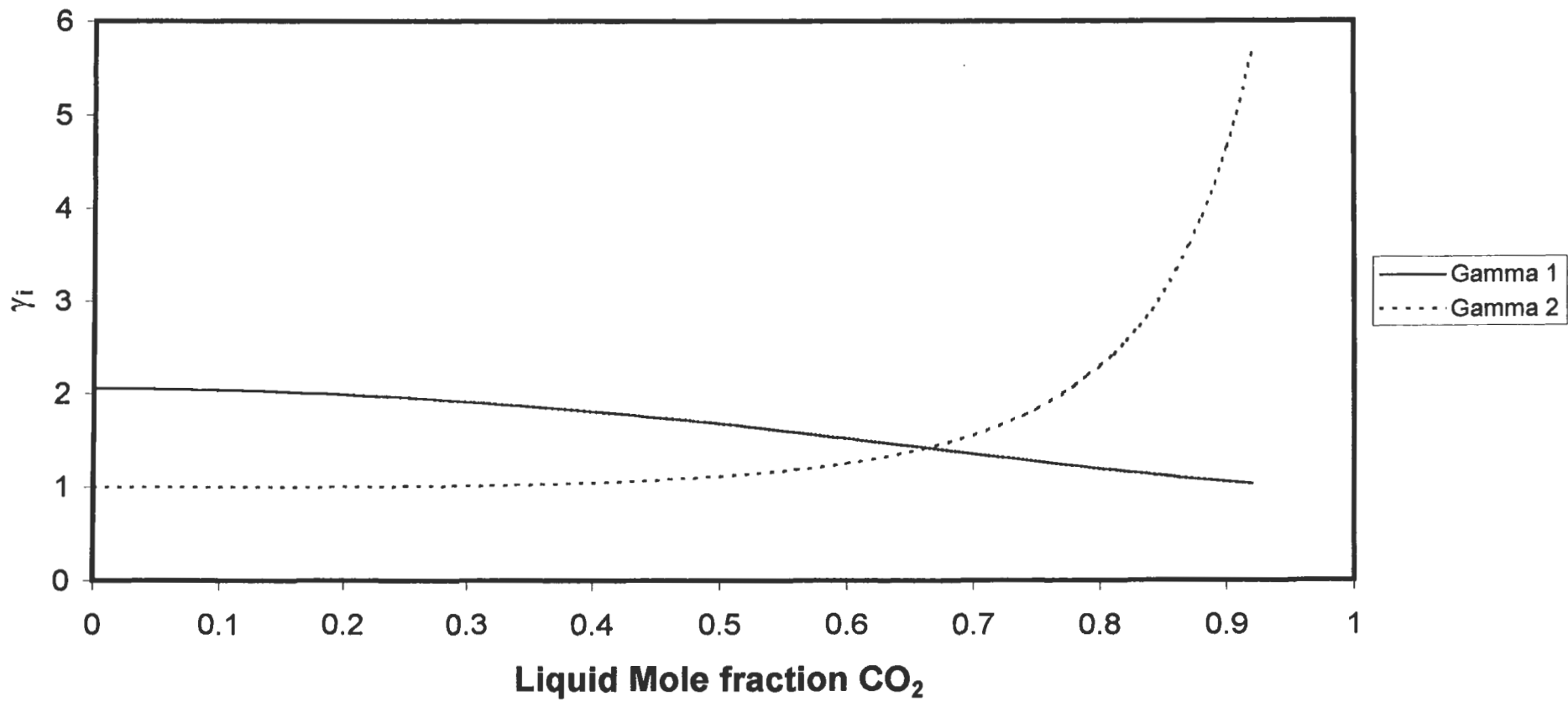


Figure F-3: Plot of activity coefficient versus liquid mole fraction for the Carbon Dioxide (1) + Toluene (2) System for the 118.3 °C isotherm

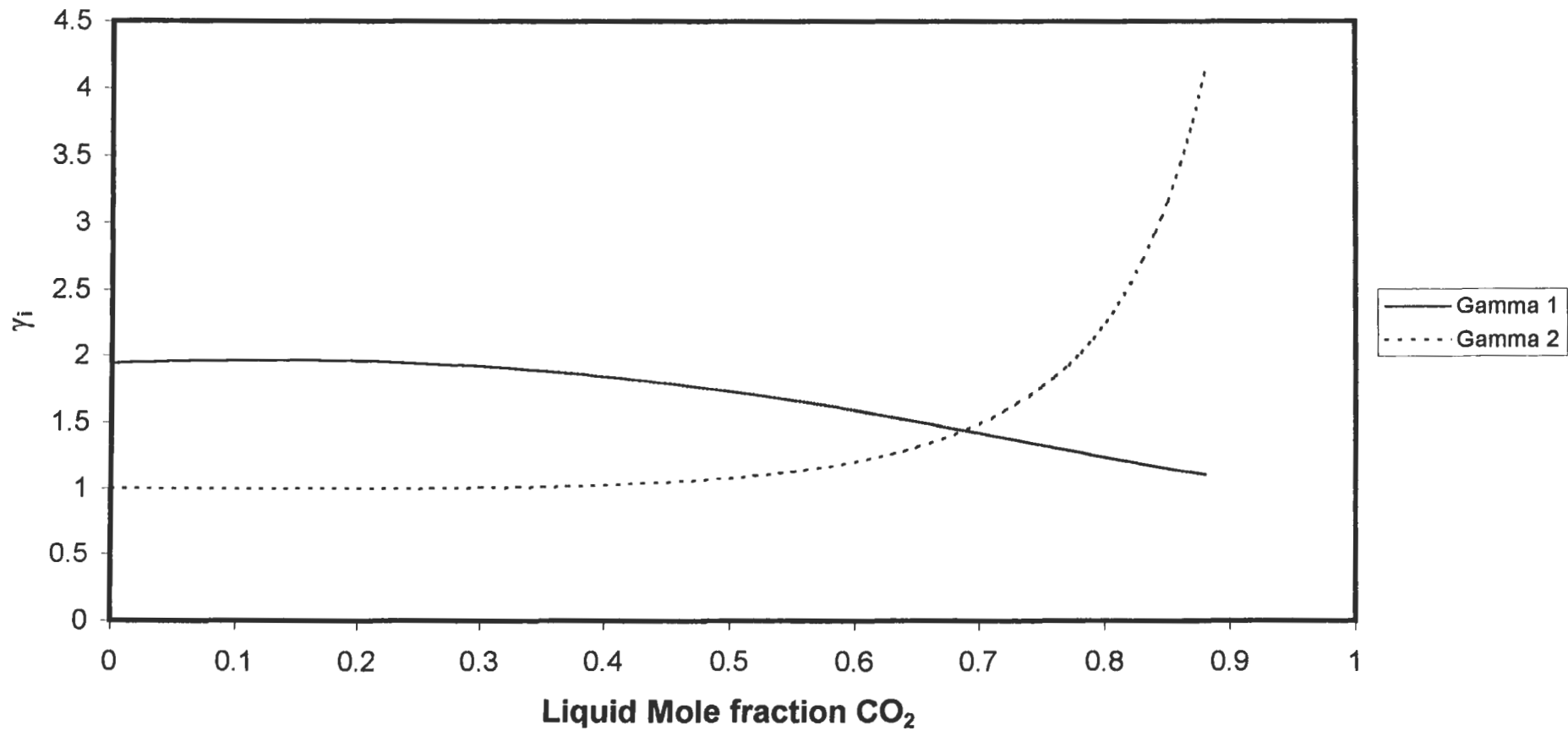


Figure F-4: Plot of activity coefficient versus liquid mole fraction for the Carbon Dioxide (1) + Methanol (2) System for the 40 °C isotherm

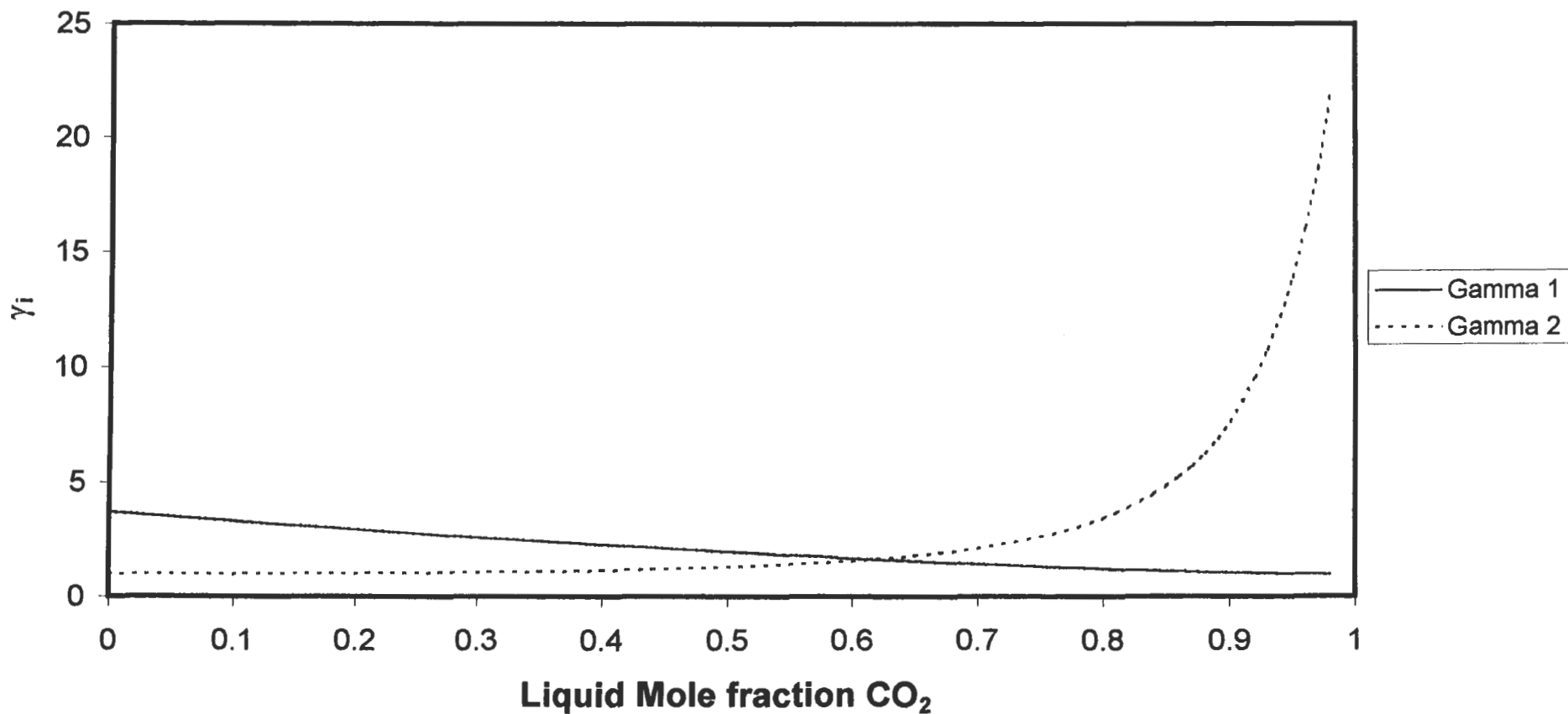


Figure F-5: Plot of activity coefficient versus liquid mole fraction for the Carbon Dioxide (1) + Methanol (2) System for the 90 °C isotherm

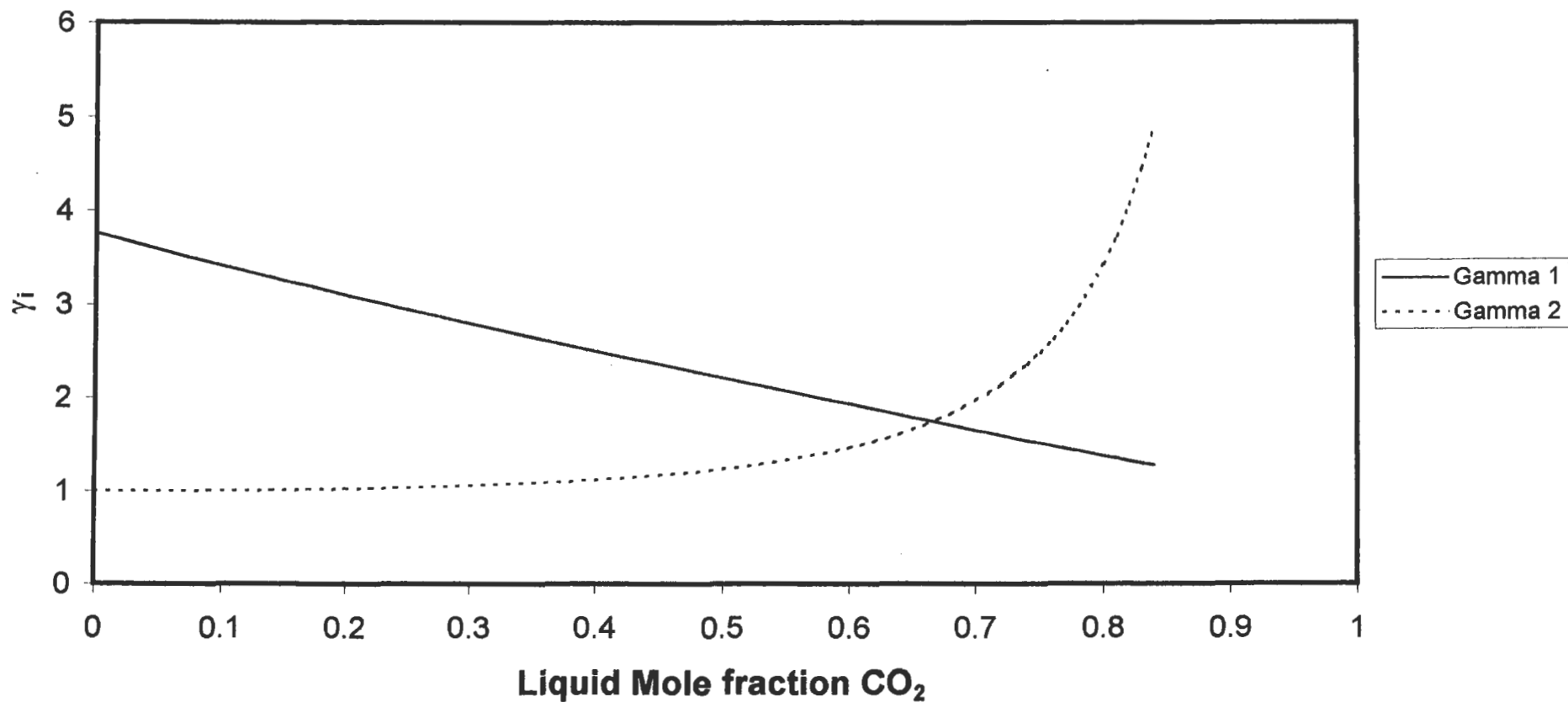


Figure F-6: Plot of activity coefficient versus liquid mole fraction for the Carbon Dioxide (1) + Methanol (2) System for the 100 °C isotherm

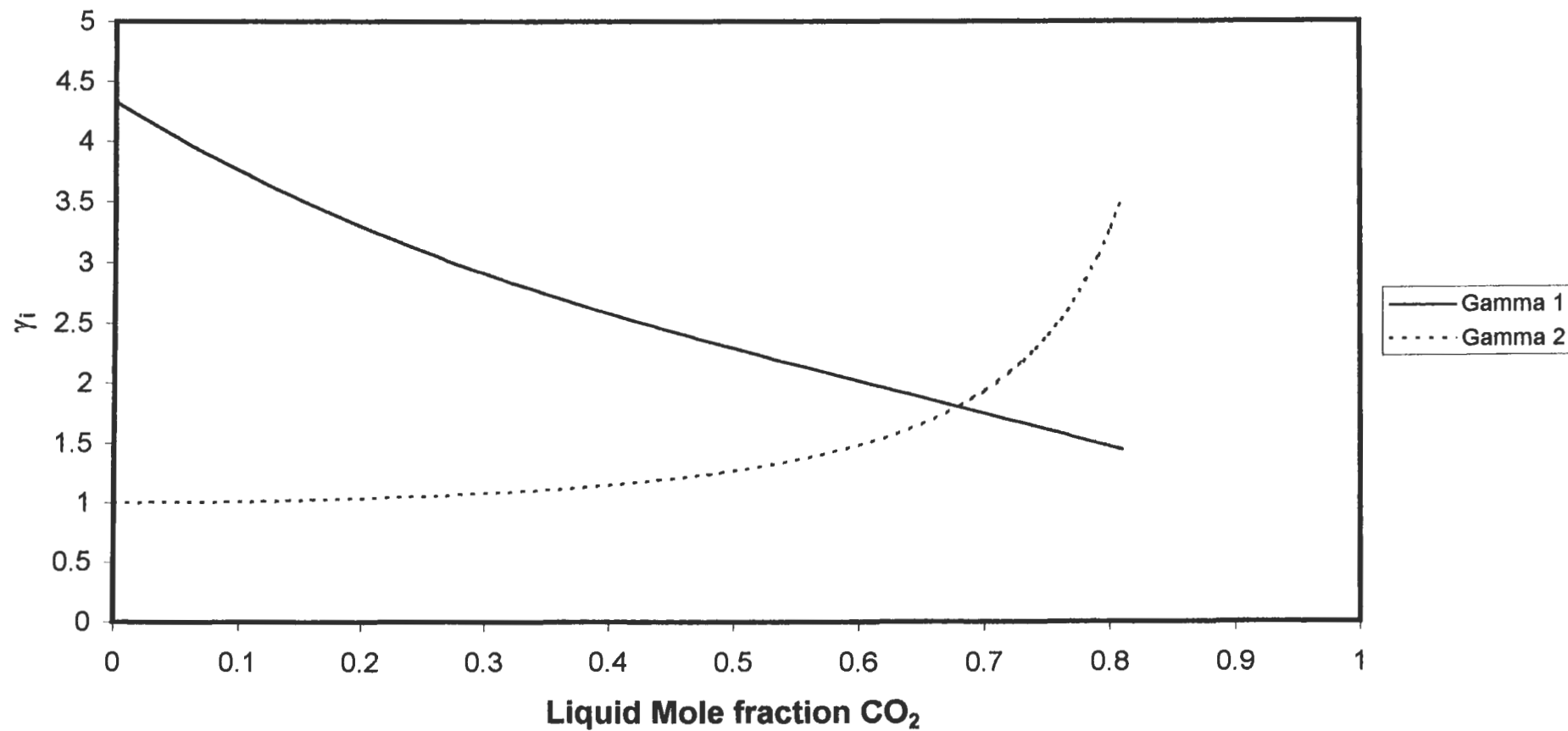


Figure F-7: Plot of activity coefficient versus liquid mole fraction for the Propane (1) + 1-Propanol (2) System for the 105.1 °C isotherm

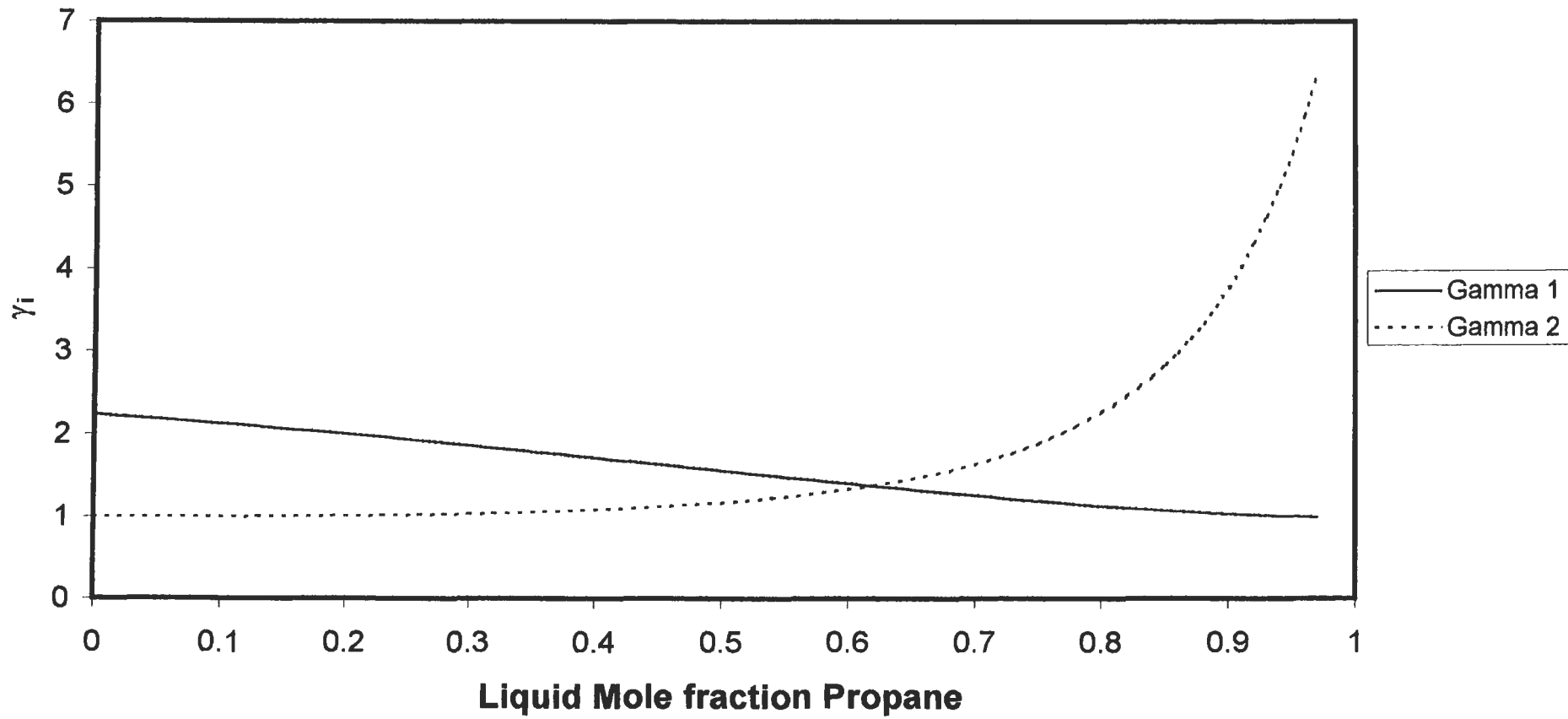
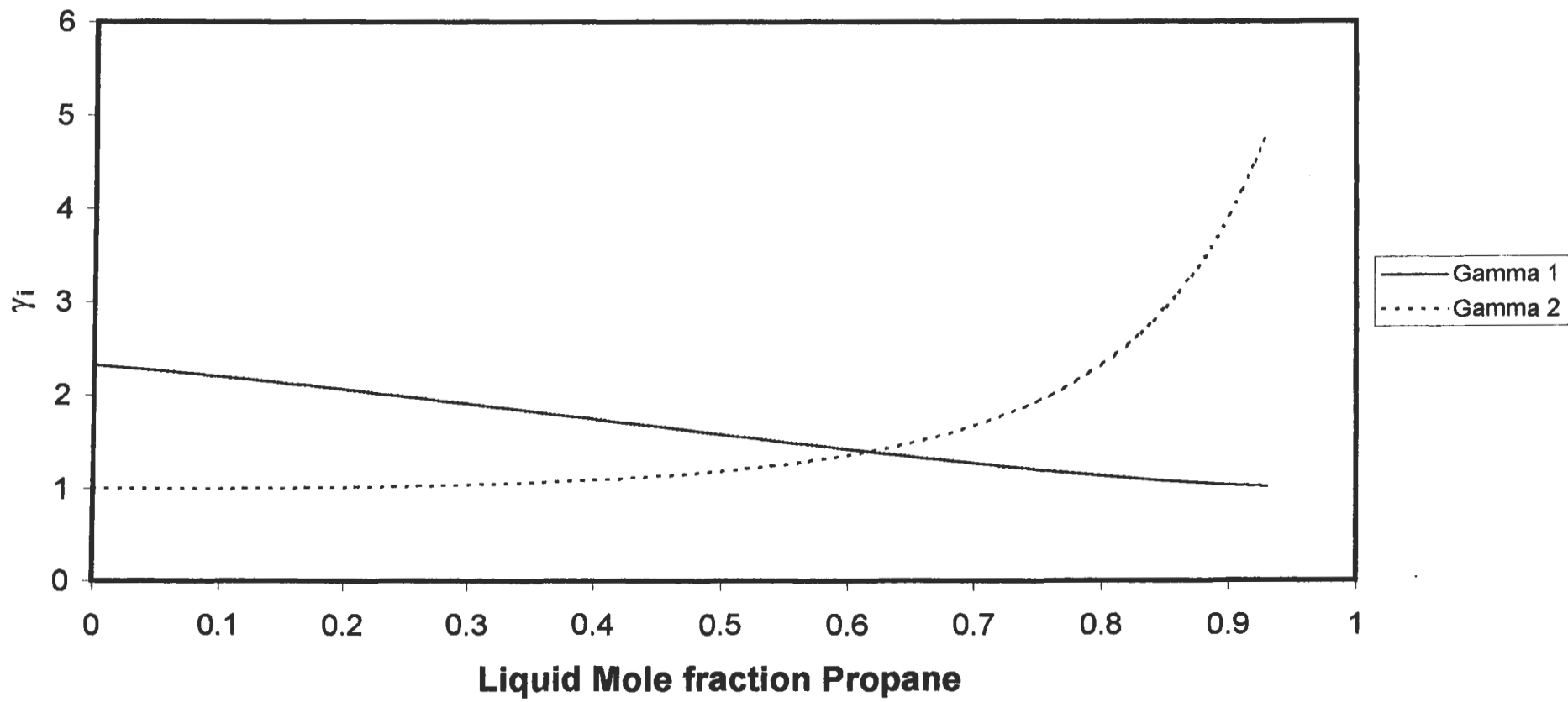


Figure F-8: Plot of activity coefficient versus liquid mole fraction for the Propane (1) + 1-Propanol (2) System for the 120 °C isotherm



F.3. CRITICAL PROPERTIES

Critical property computations were undertaken using the SRK, PR and PRSV EOS's. For each of the systems investigated, plots were undertaken of critical temperature, critical pressure, critical volume and critical compressibility factor against mole fraction for the volatile components.

F.3.1. The Carbon Dioxide + Toluene System.

Figures F-9 to F-12 represent graphically the computed critical temperature, critical pressure, critical volume and critical compressibility factor for the carbon dioxide + toluene system respectively.

F.3.2. The Carbon Dioxide + Methanol System.

Figures F-13 to F-16 represent graphically the computed critical temperature, critical pressure, critical volume and critical compressibility factor for the carbon dioxide + methanol system respectively.

F.3.3. The Propane + 1-Propanol System.

Figures F-17 to F-20 represent graphically the computed critical temperature, critical pressure, critical volume and critical compressibility factor for the propane + 1-propanol system respectively.

Figure F-9: Plot of critical temperature versus composition for the carbon dioxide + toluene binary system

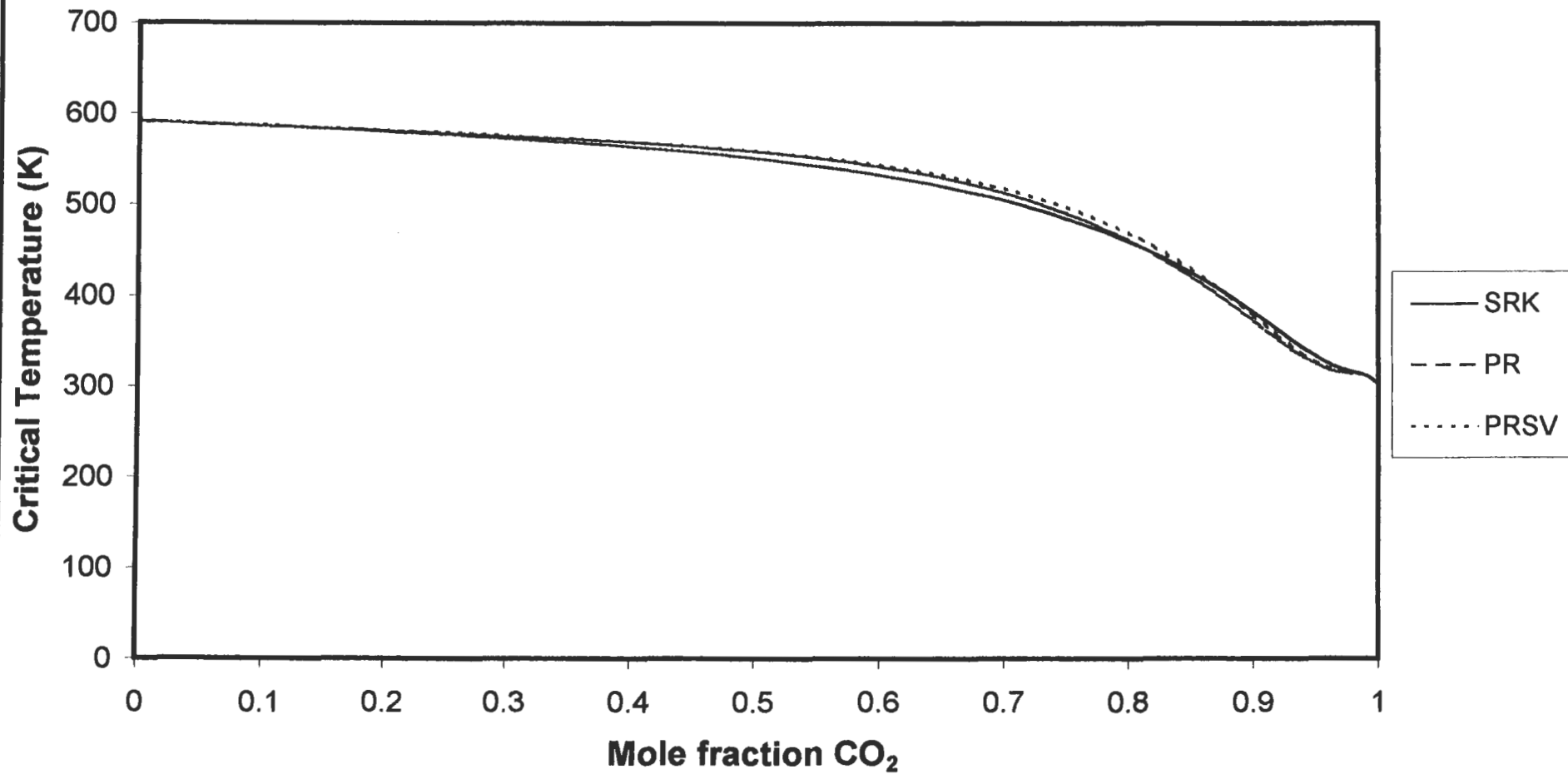


Figure F-10: Plot of critical pressure versus composition for the carbon dioxide + toluene binary system

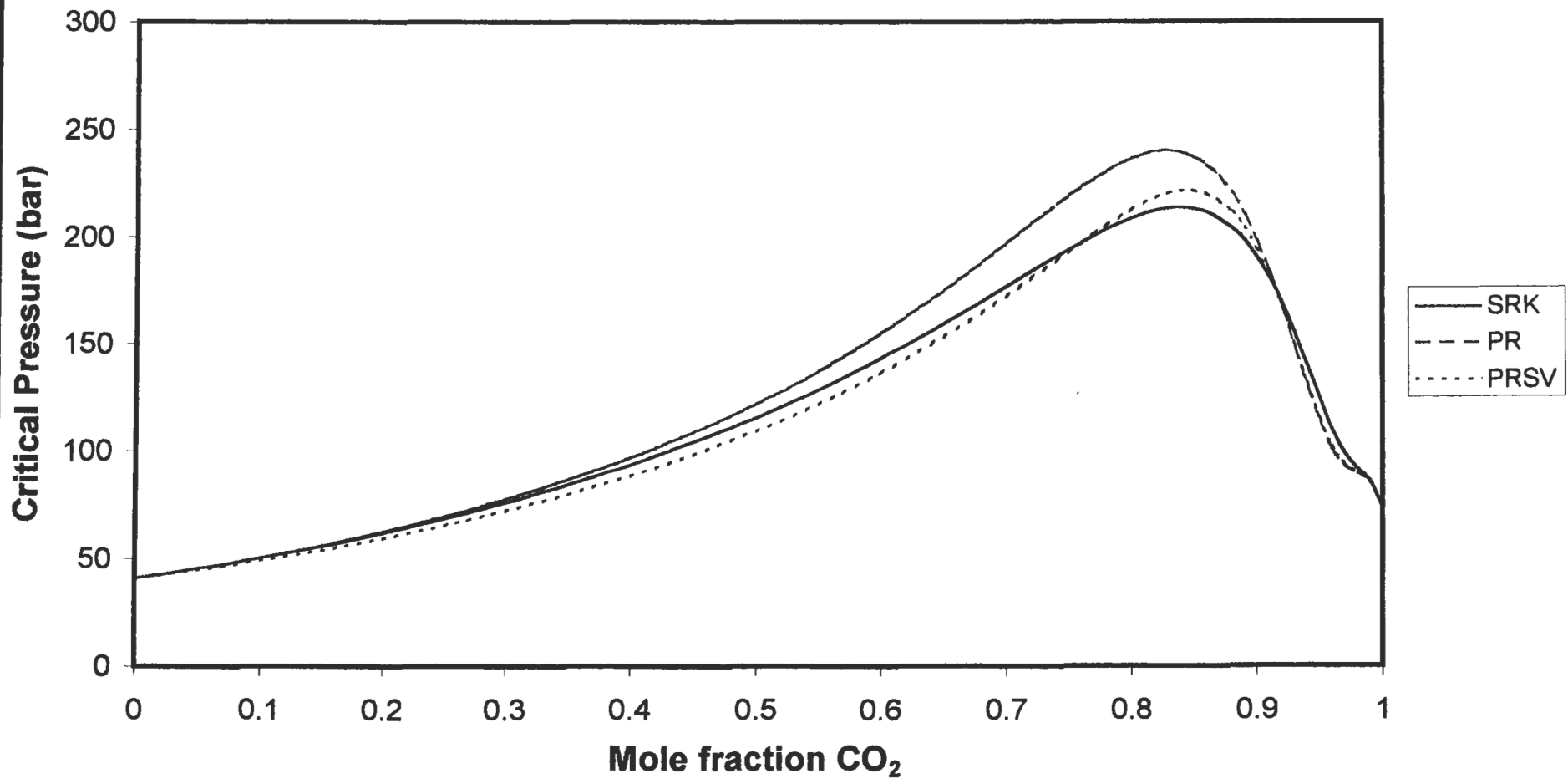


Figure F-11: Plot of critical volume versus composition for the carbon dioxide + toluene binary system

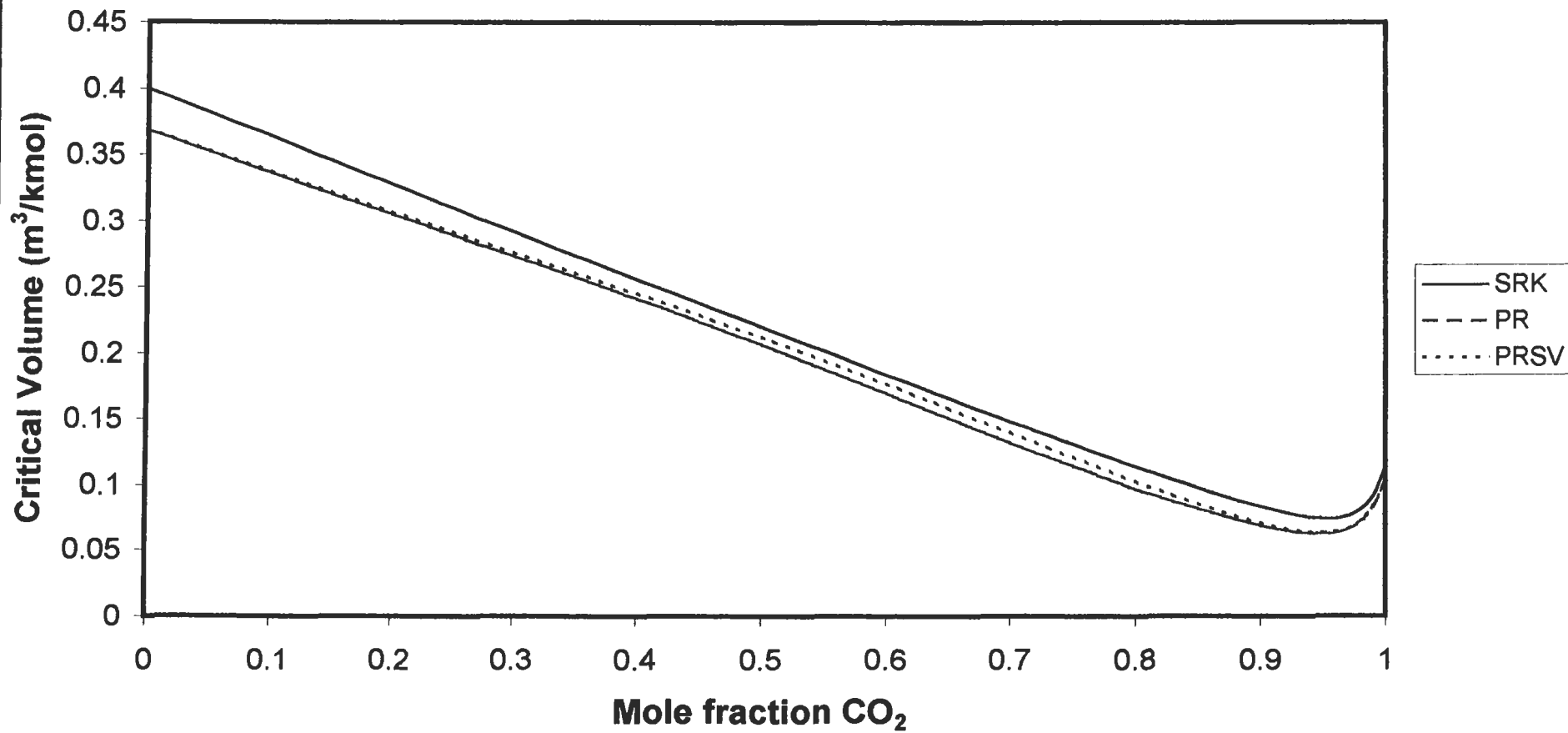


Figure F-12: Plot of critical compressibility factor versus composition for the carbon dioxide + toluene binary system

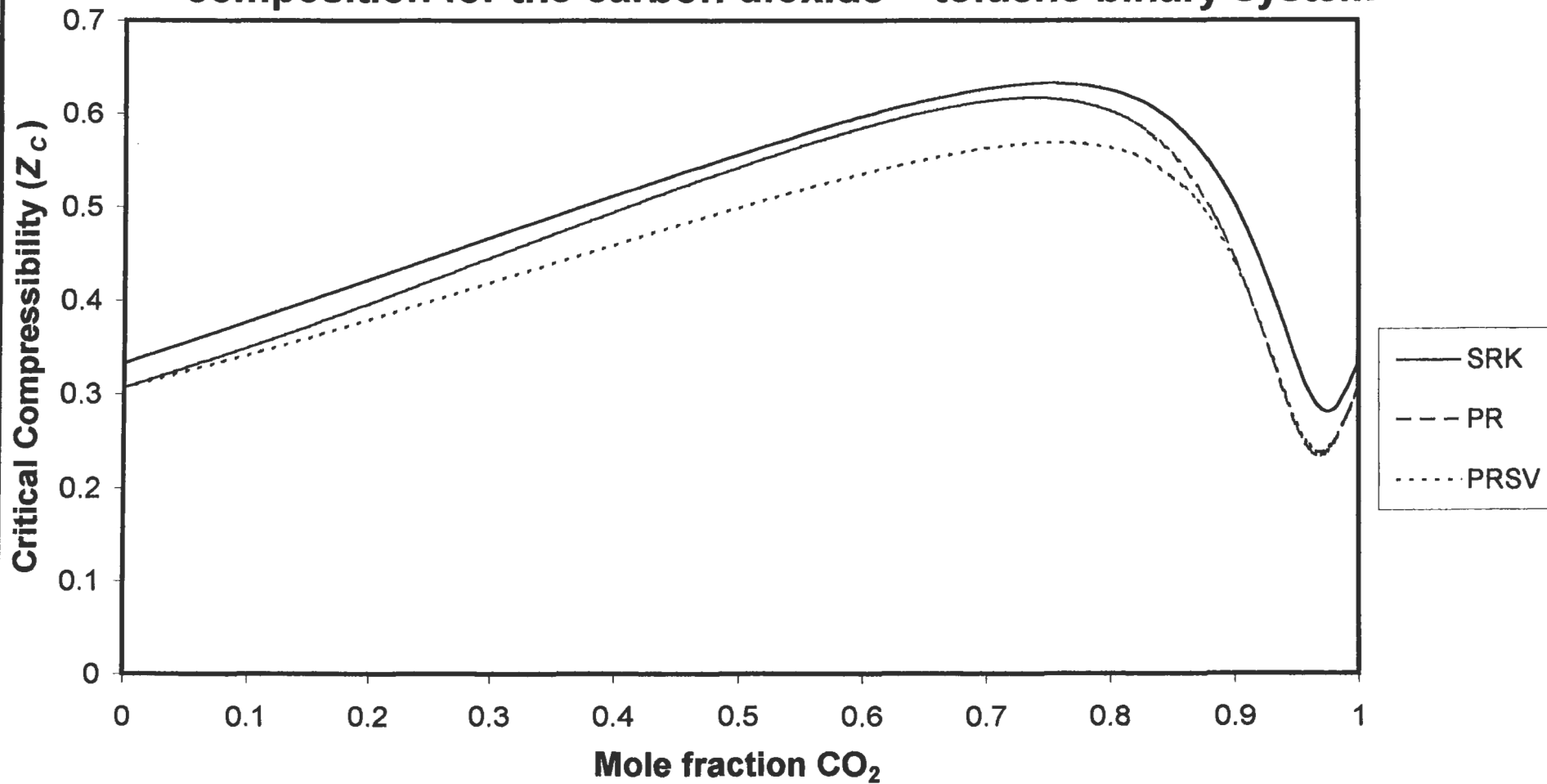


Figure F-13: Plot of critical temperature versus composition for the carbon dioxide + methanol binary system

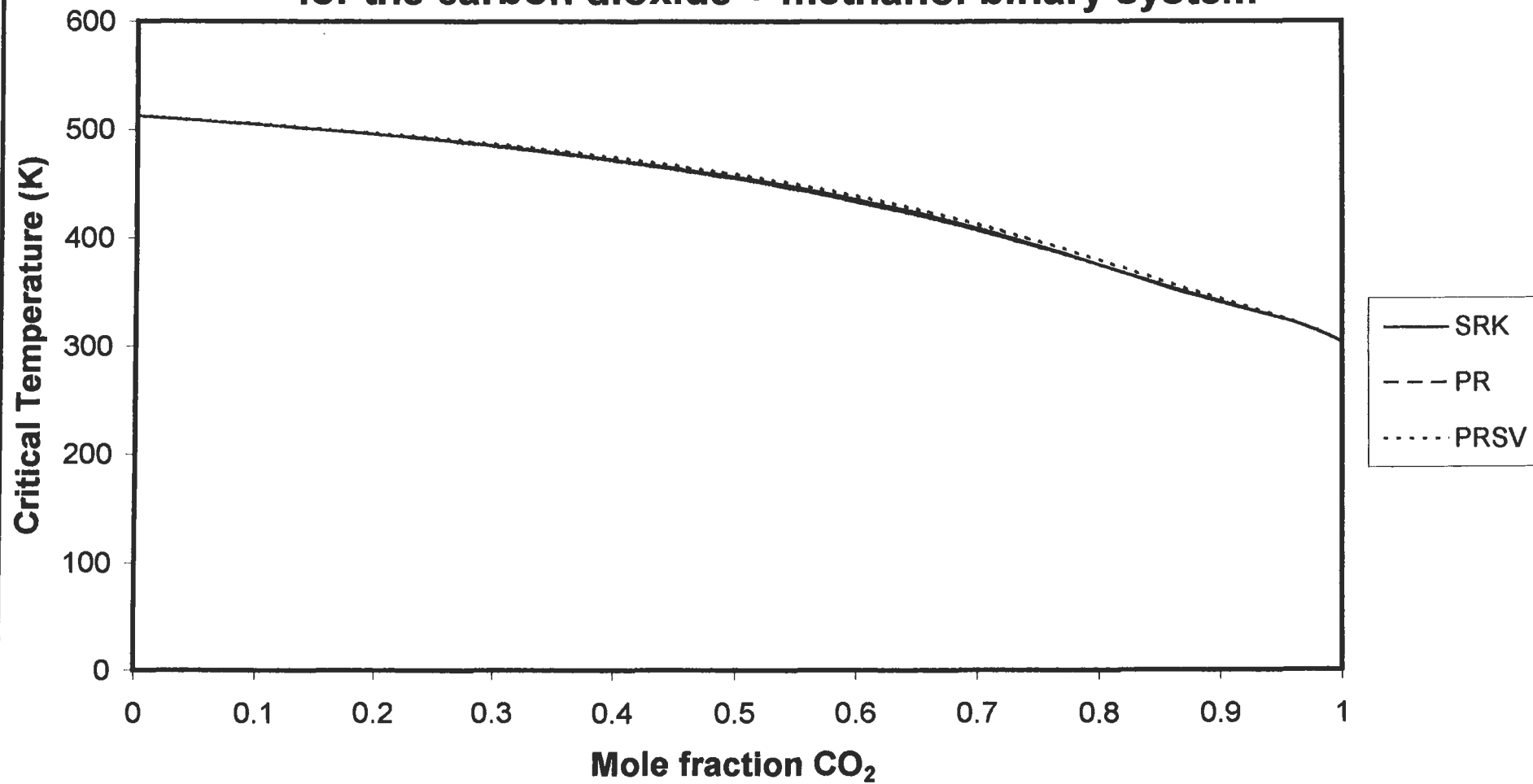


Figure F-14: Plot of critical pressure versus composition for the carbon dioxide + methanol binary system

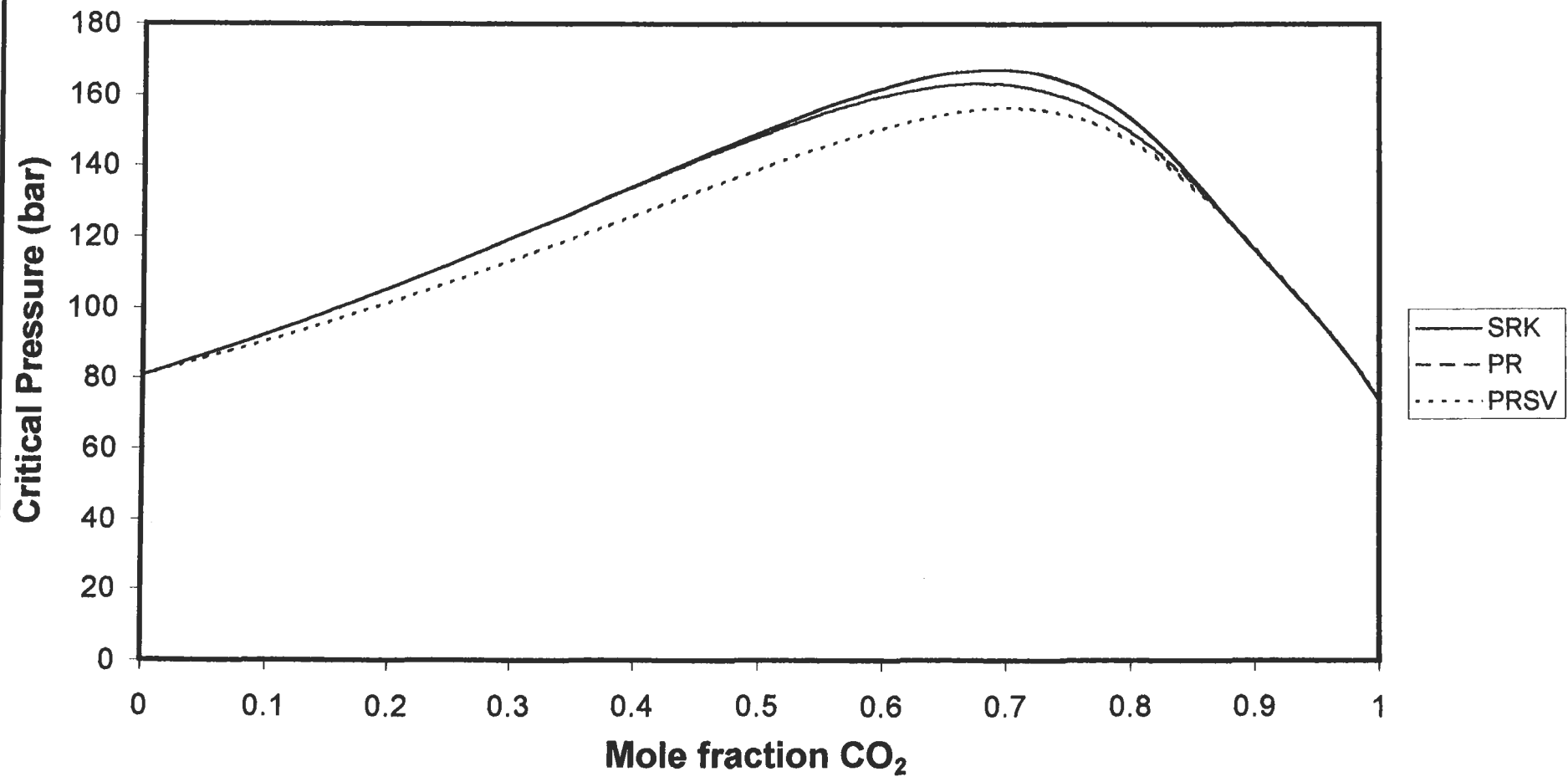


Figure F-15: Plot of critical volume versus composition for the carbon dioxide + methanol system

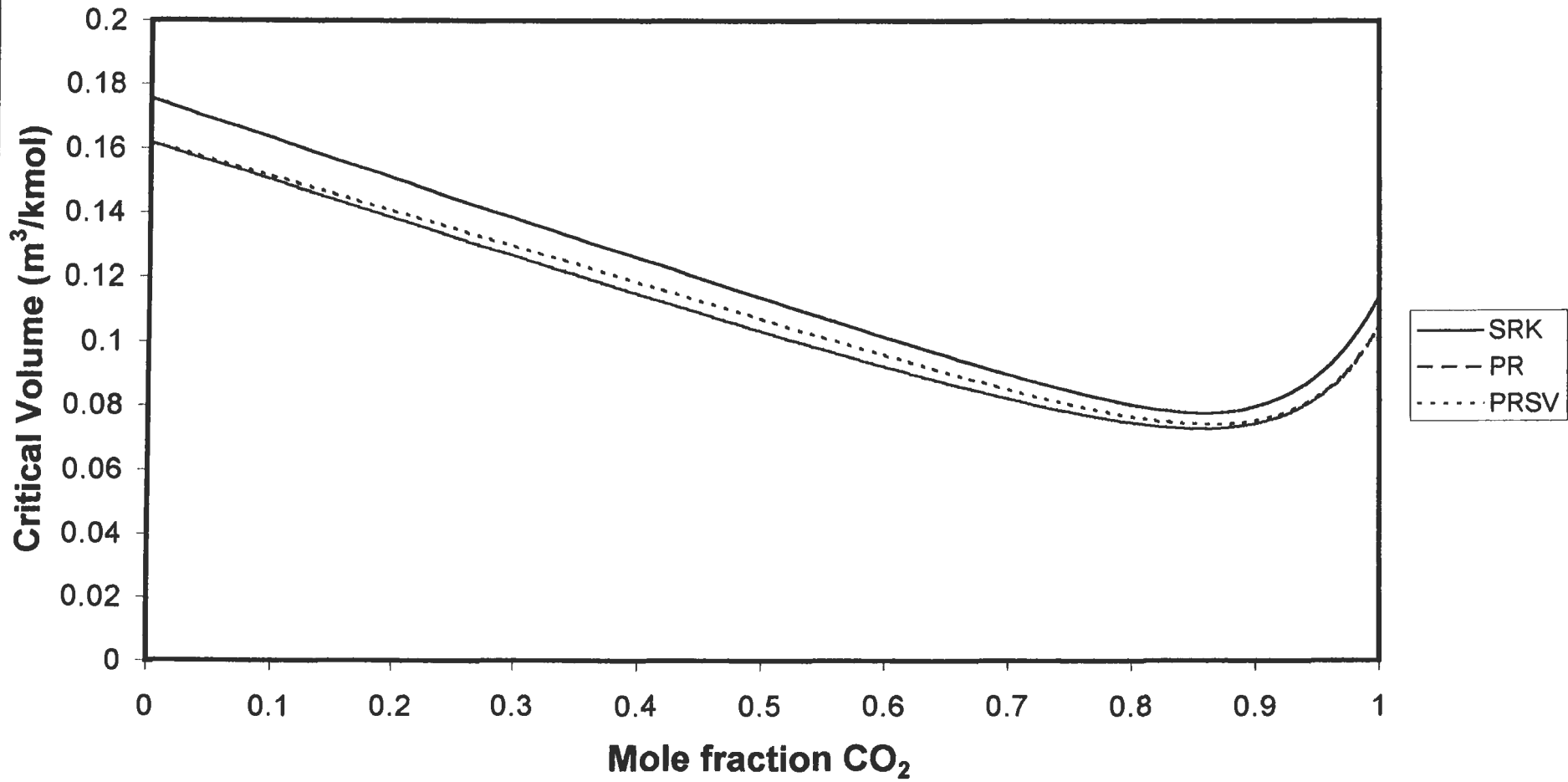


Figure F-16: Plot of critical compressibility versus composition for the carbon dioxide + methanol binary system

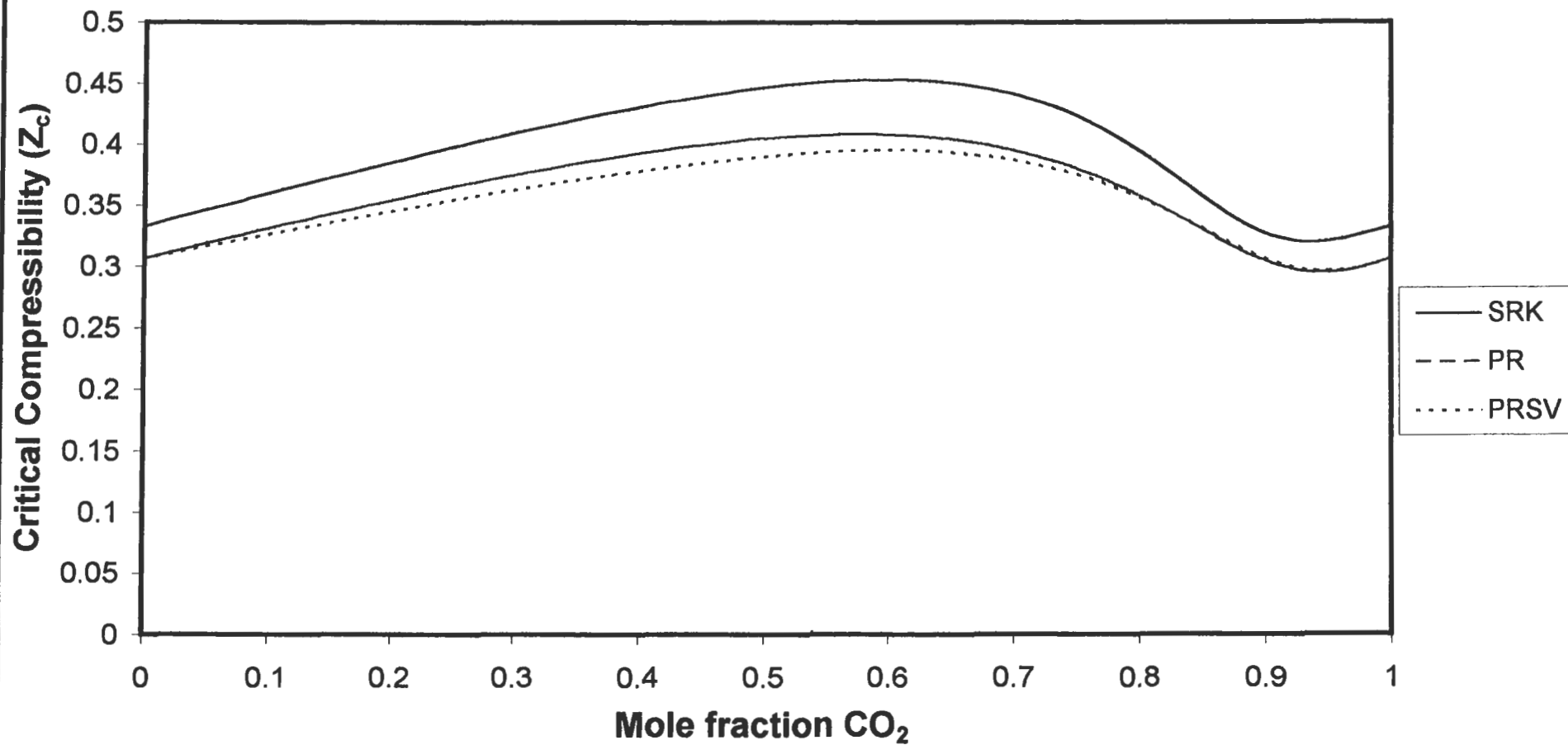


Figure F-17: Plot of critical temperature versus composition for the propane + 1-propanol binary system

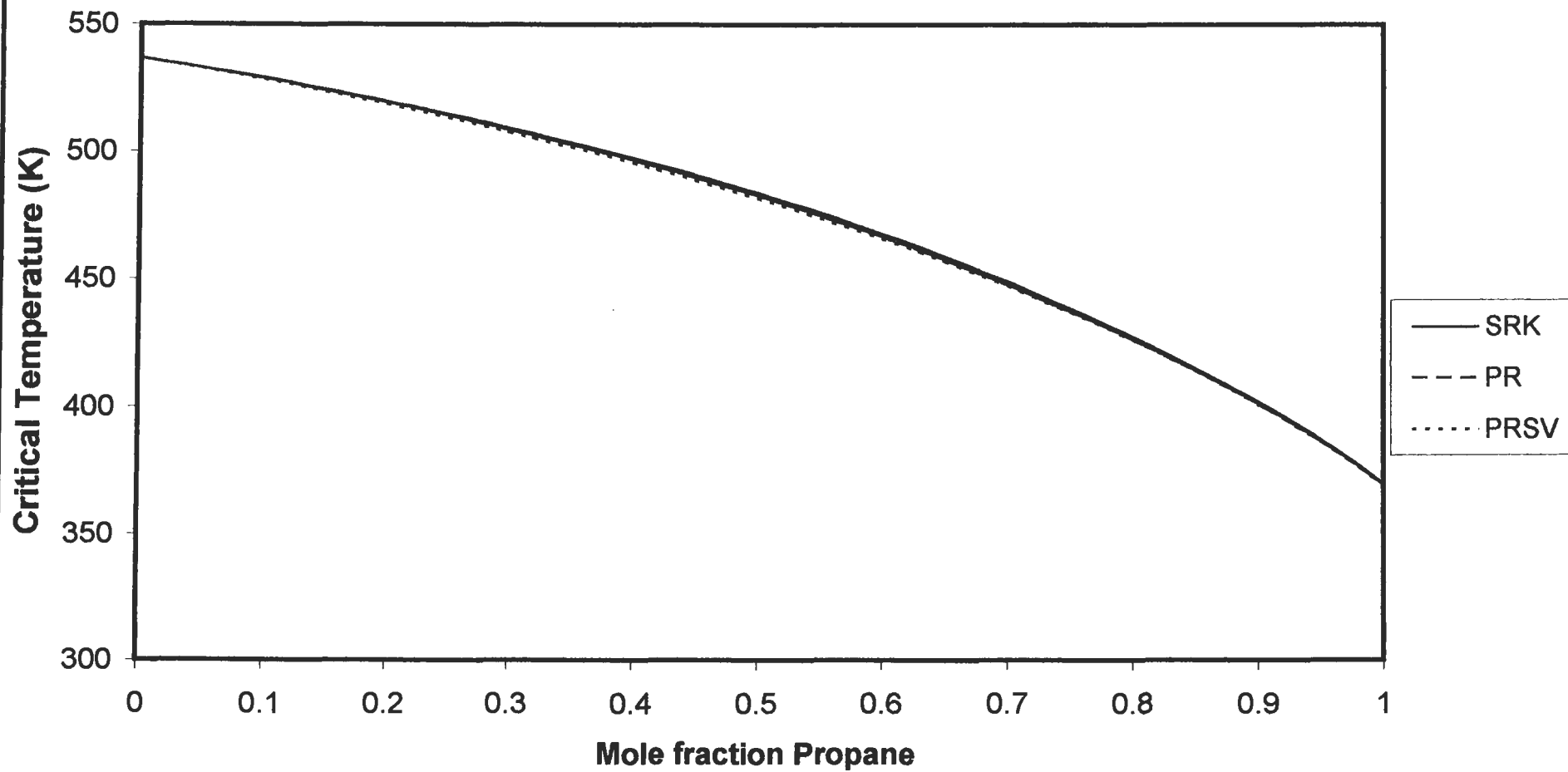


Figure F-18: Plot of critical pressure versus composition for the propane + 1-propanol binary system

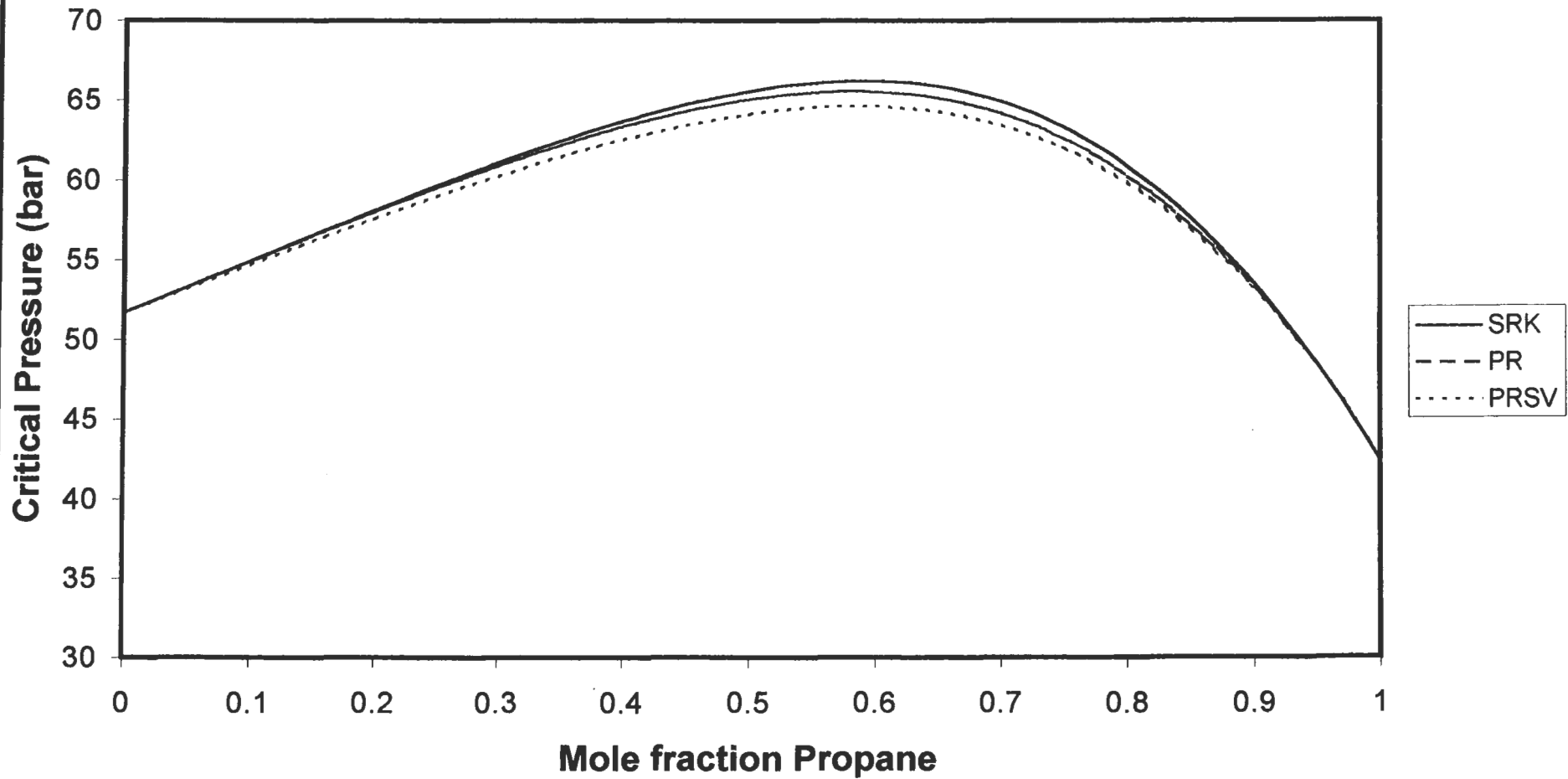


Figure F-19: Plot of critical volume versus composition for the propane + 1-propanol binary system

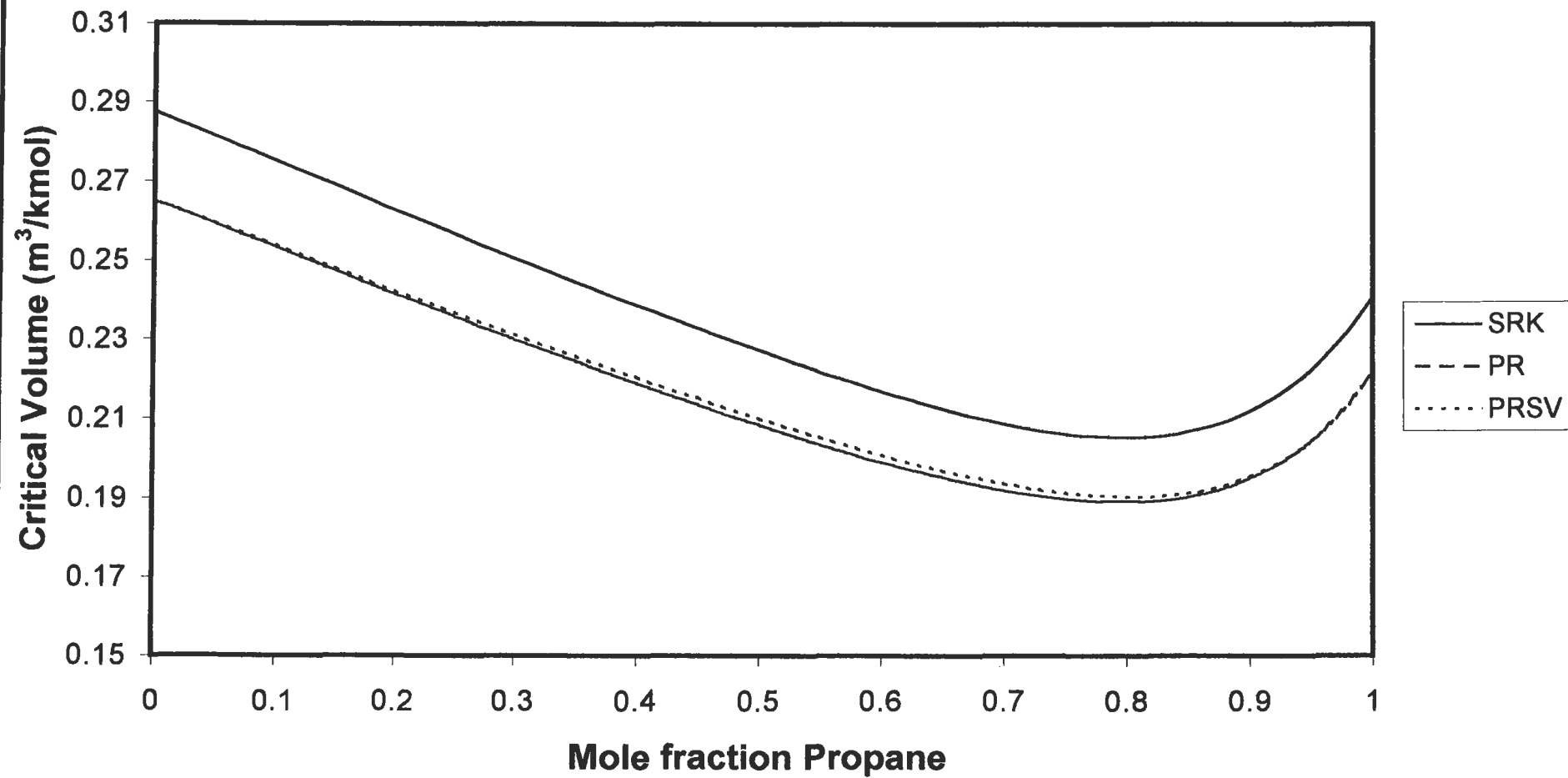
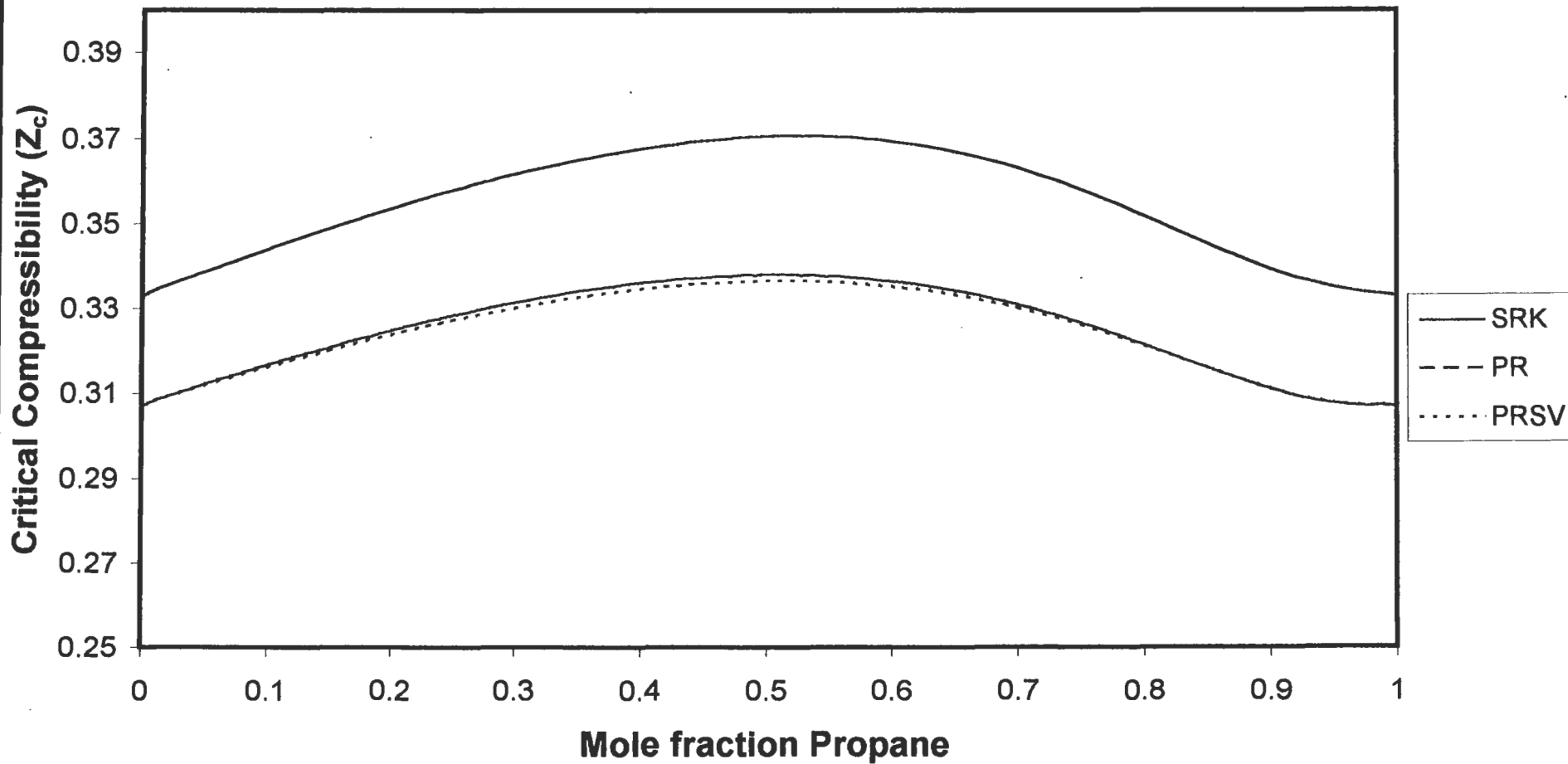


Figure F-20: Plot of critical compressibility factor versus composition for the propane + 1-propanol binary system



F.4. THERMODYNAMIC CONSISTENCY

The Chueh et al. [1965] consistency test along with residual plots were used to judge the thermodynamic consistency of the systems measured. The Chueh et al. test entailed the computation of areas under appropriate curves as explained in Appendix B and Chapter 8.

Figures F-21 to F-44 illustrate the plots of $\ln(K_2/K_1)$ and $\ln\left(\frac{\hat{\phi}_2}{\hat{\phi}_1}\right)$ versus liquid mole fraction of component 2 (x_2), as well as the plots of liquid molar volume versus pressure for the carbon dioxide + toluene, carbon dioxide + methanol and propane + 1-propanol at the various isotherms measured.

All computations were undertaken using the PRSVWS-NRTL + NRTL model. In some cases the computations were not stable over the entire composition range up to the critical point, and therefore for these computations, the plots are only over the composition range that the computation was stable.

Figures F-45 to F-52 illustrate the plots of residual pressure versus liquid mole fraction of the volatile components for the carbon dioxide + toluene, carbon dioxide + methanol and propane + 1-propanol system.

Computations of the residuals were undertaken using a number of models as are indicated in Figures F-45 to F-52.

In judging the thermodynamic consistency of a system, one of the criteria for thermodynamic consistency is that there is even scatter of the residuals about the zero x-axis. Plots of residual vapour composition, pressure and the Chueh et al. [1965] test were together used to judge the thermodynamic consistency of the system measured.

Figure F-21: Plot of $\ln(K_2/K_1)$ versus liquid mole fraction CO_2 for the carbon dioxide (2) + toluene (1) system at 38 °C

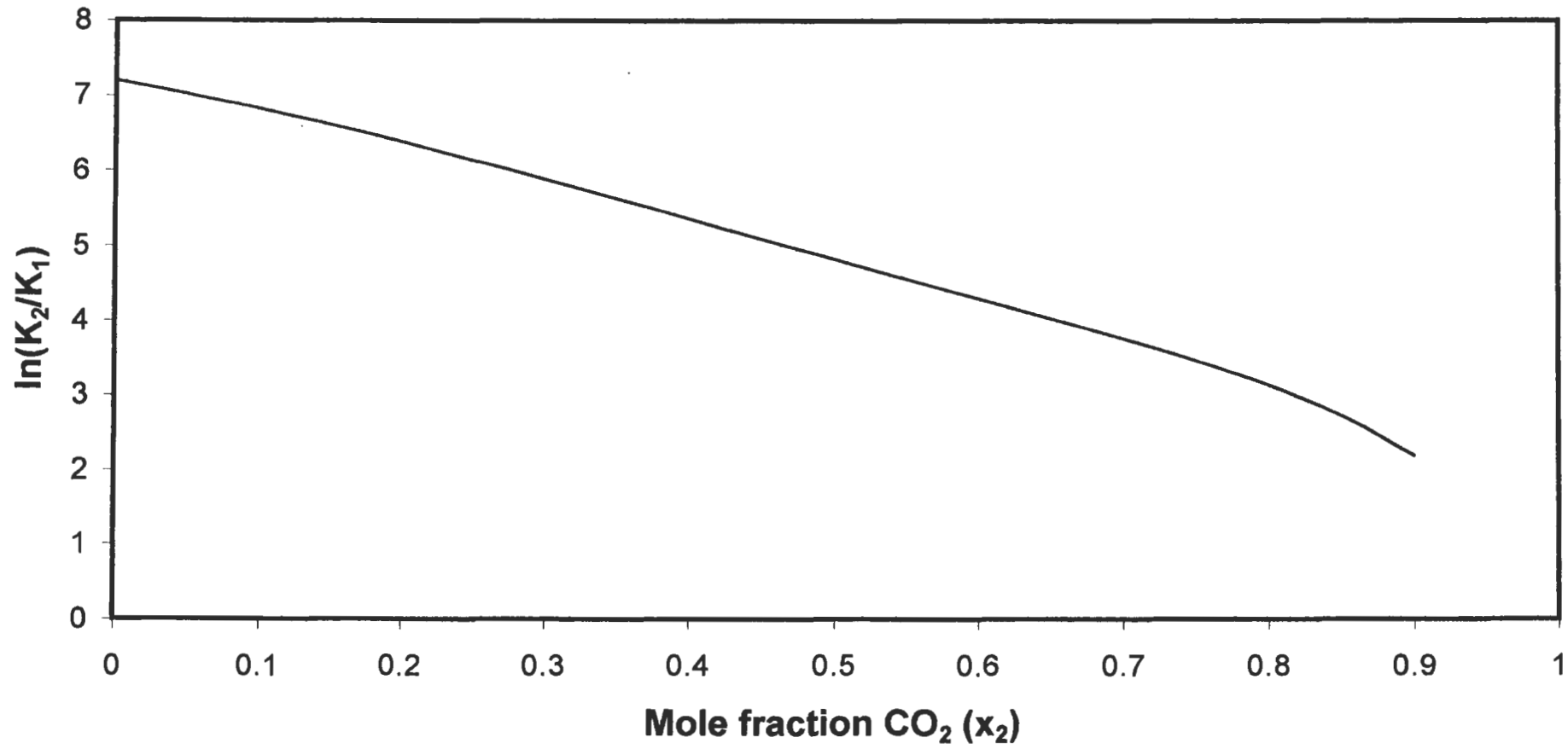


Figure F-22: Plot of $\ln(\phi_2/\phi_1)$ versus liquid mole fraction CO_2 for the carbon dioxide (2) + toluene (1) system at 38 °C

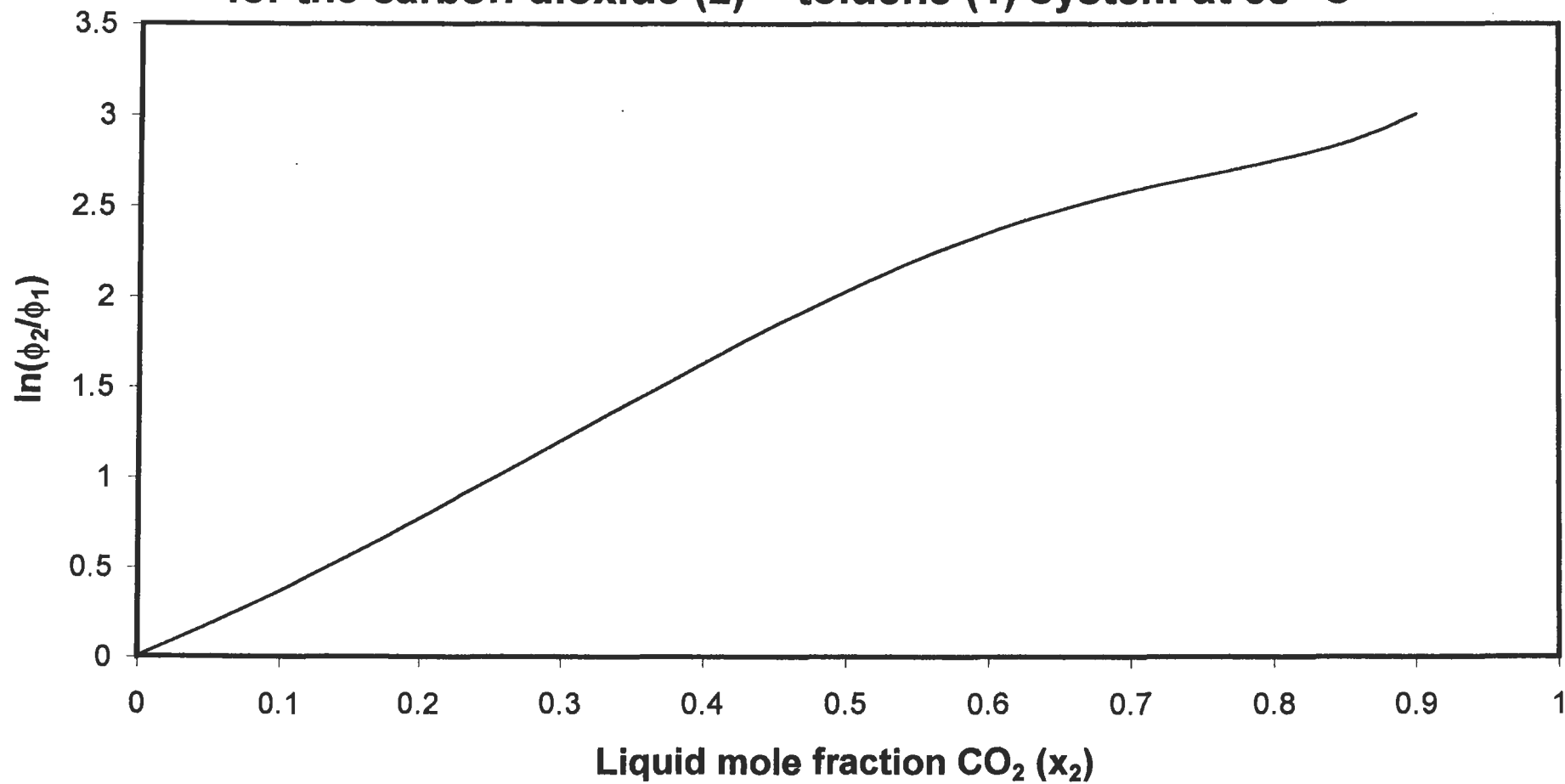


Figure F-23: Plot of liquid molar volume versus pressure for the carbon dioxide + toluene system at 38 °C

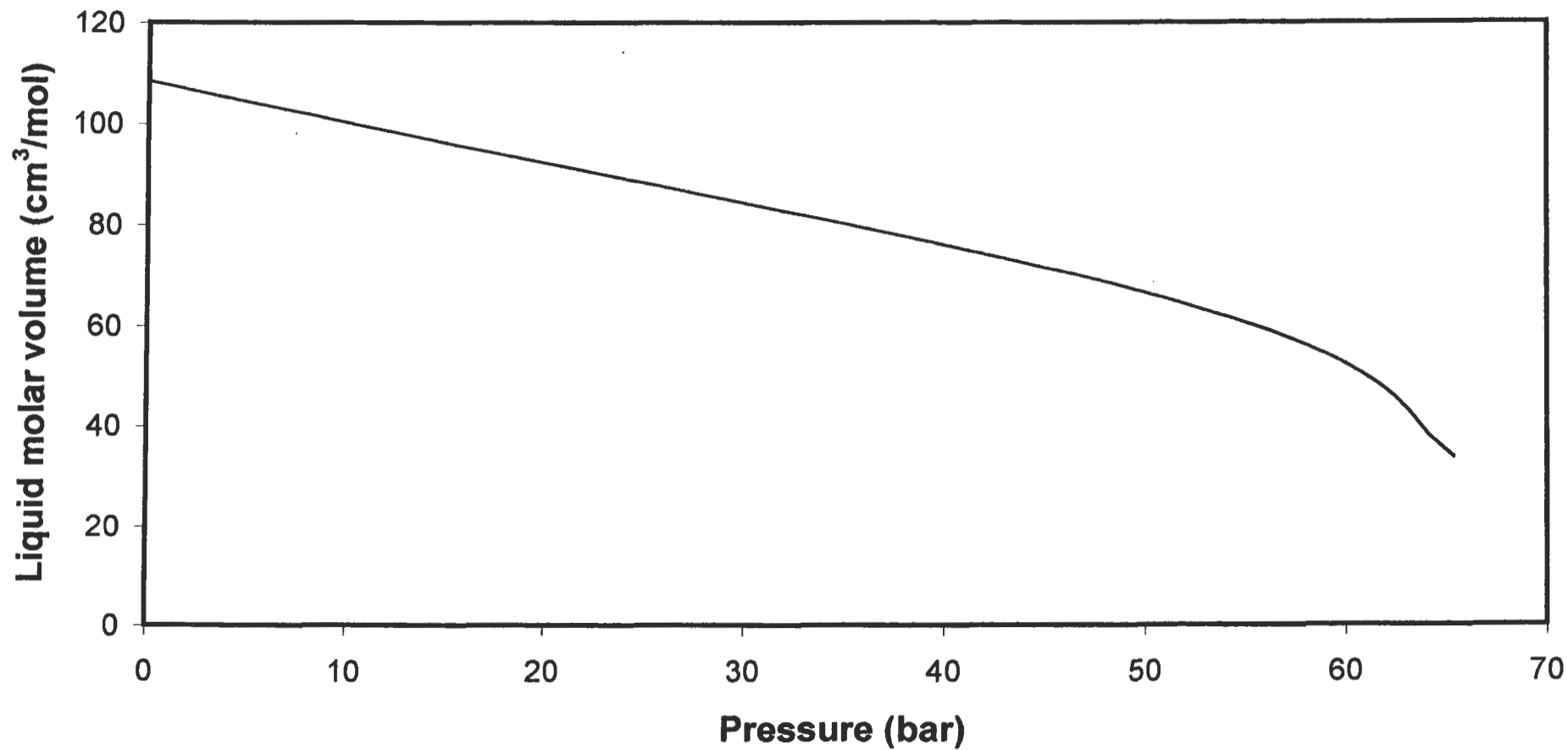


Figure F-24: Plot of $\ln(K_2/K_1)$ versus liquid mole fraction CO_2 for the carbon dioxide (2) + toluene (1) system at 80°C

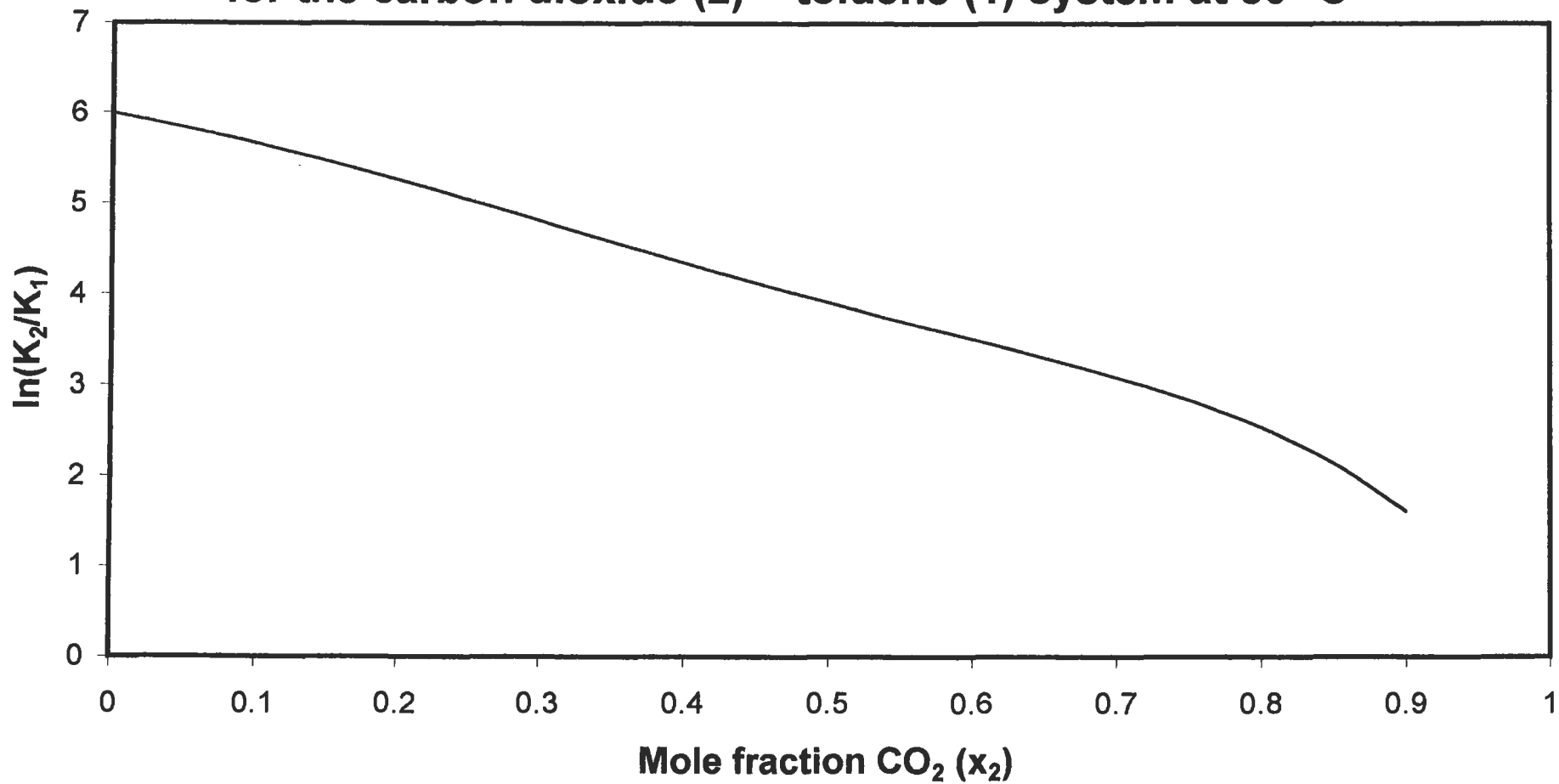


Figure F-25: Plot of $\ln(\phi_2/\phi_1)$ versus liquid mole fraction CO_2 for the carbon dioxide (2) + toluene (1) system at 80 °C

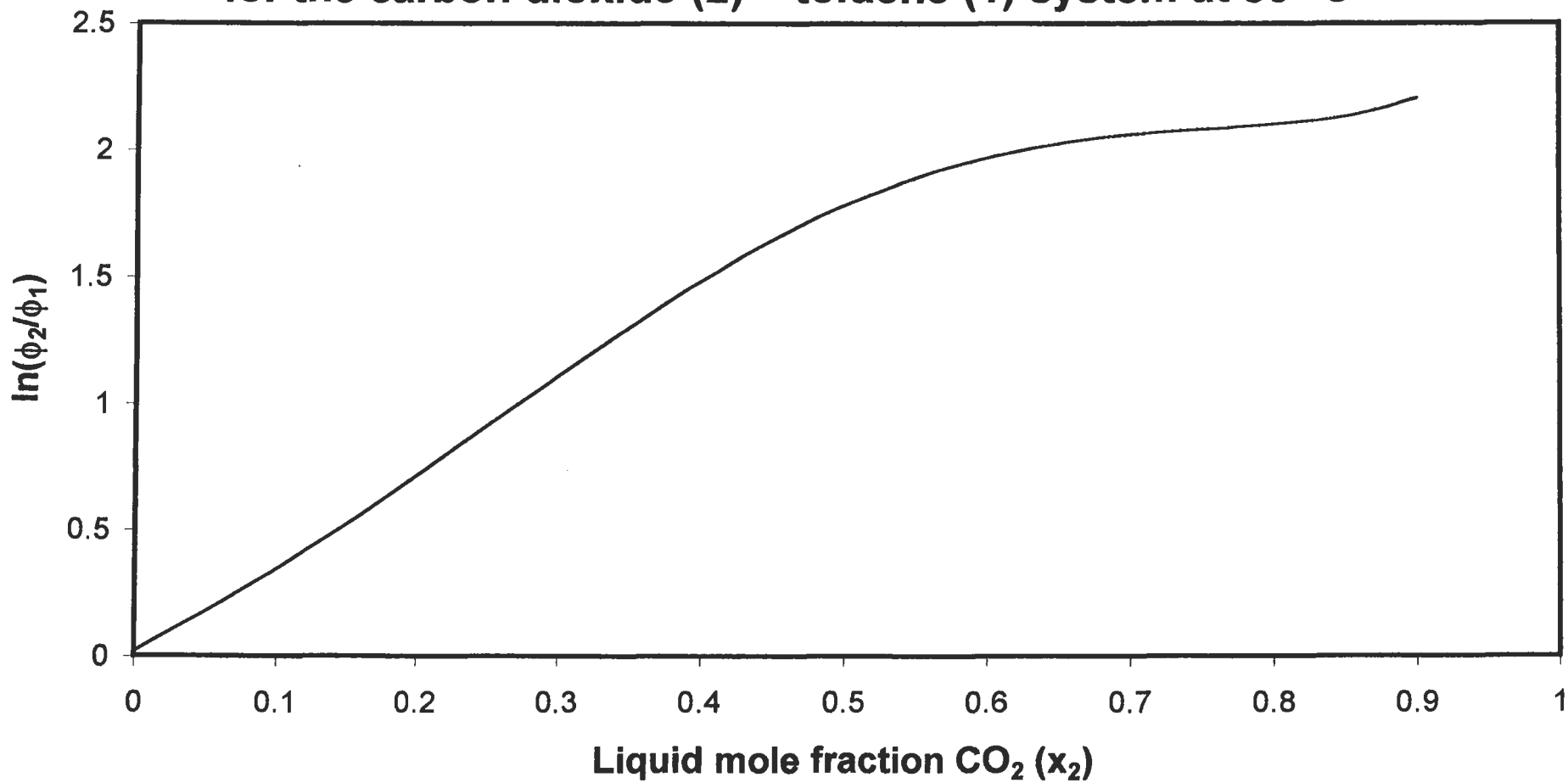


Figure F-26: Plot of liquid molar volume versus pressure for the carbon dioxide + toluene system at 80 °C

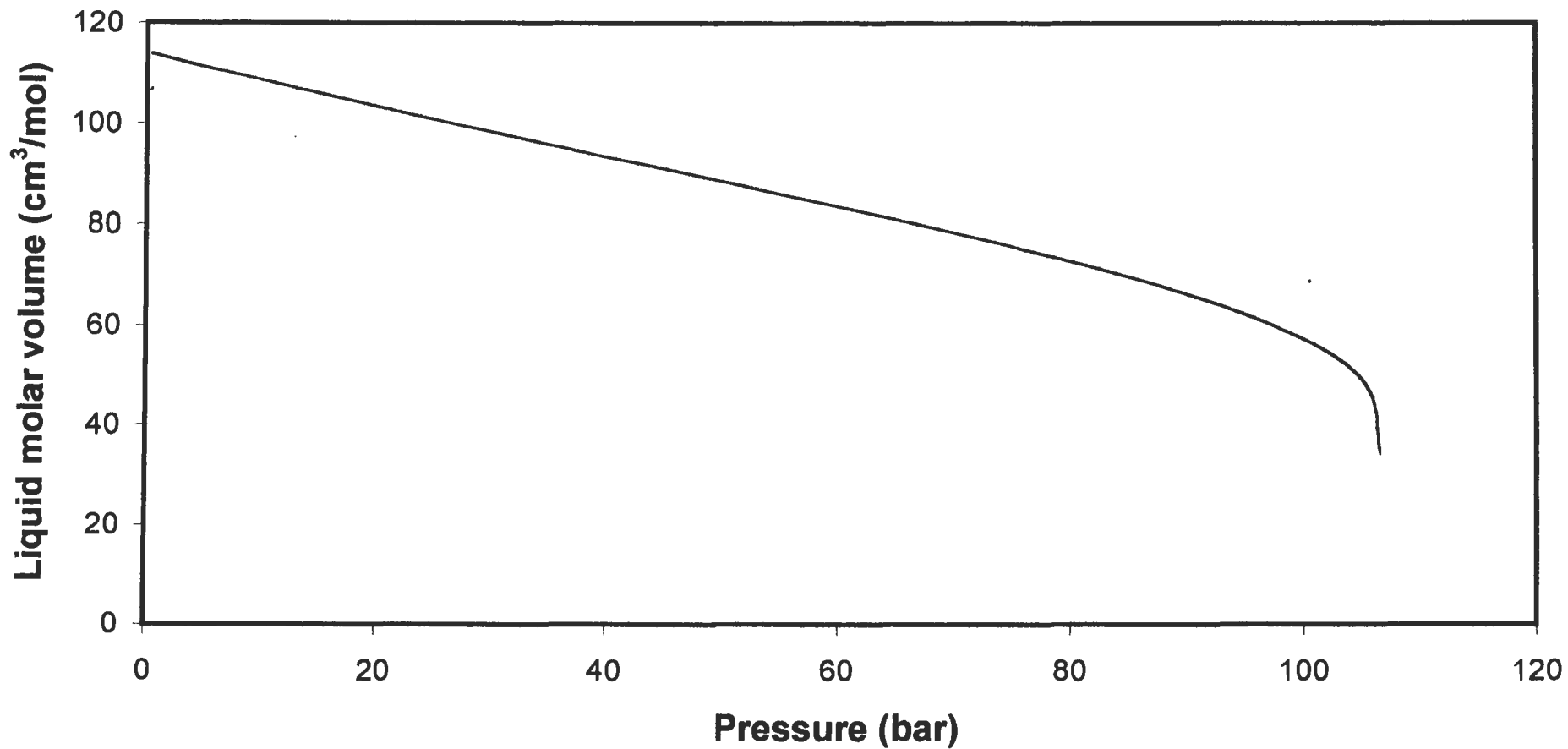


Figure F-27: Plot of $\ln(K_2/K_1)$ versus liquid mole fraction CO_2 for the carbon dioxide (2) + toluene (1) system at 118.3°C

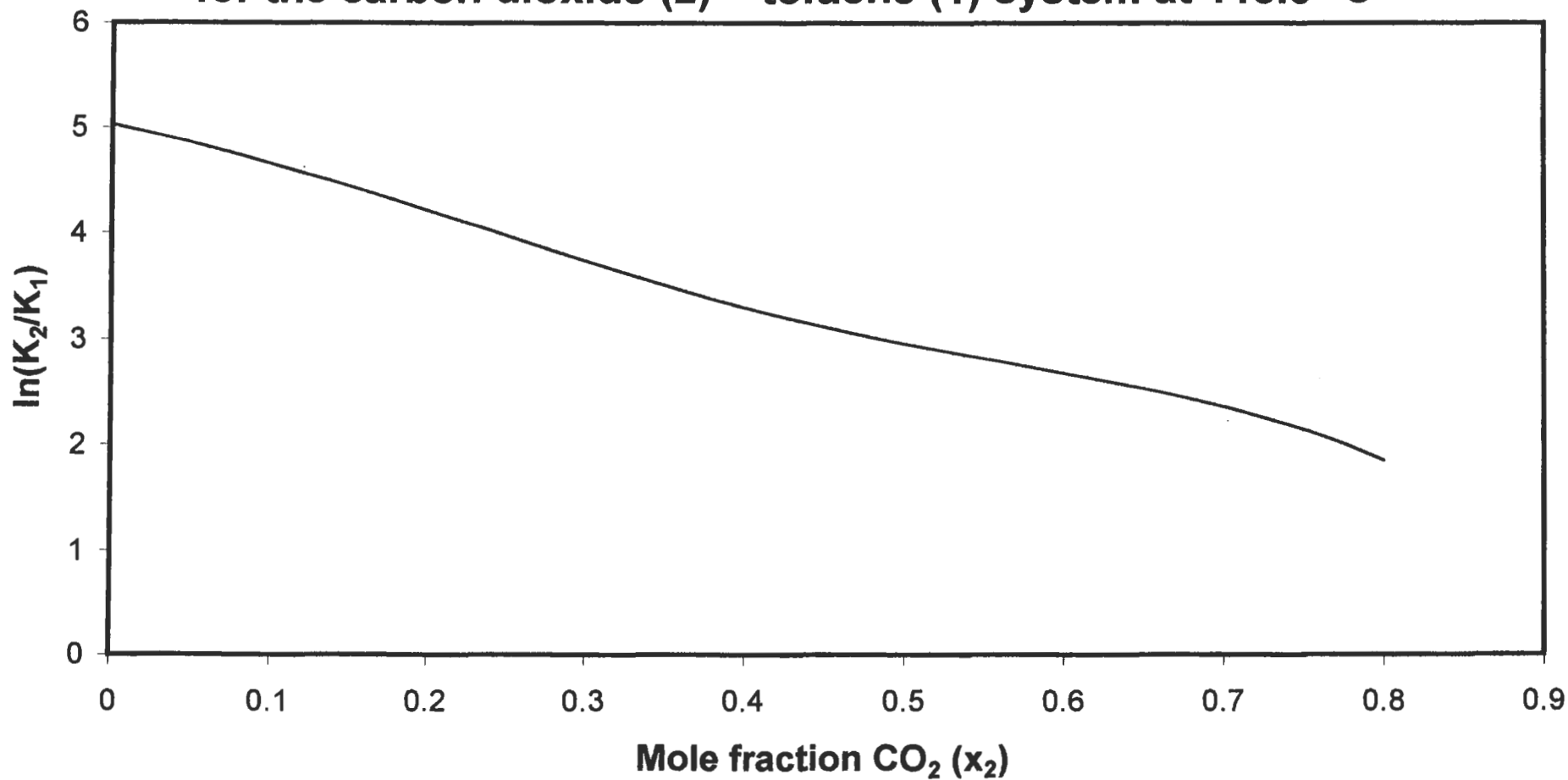


Figure F-28: Plot of $\ln(\phi_2/\phi_1)$ versus liquid mole fraction CO_2 for the carbon dioxide (2) + toluene (1) system at 118.3 °C

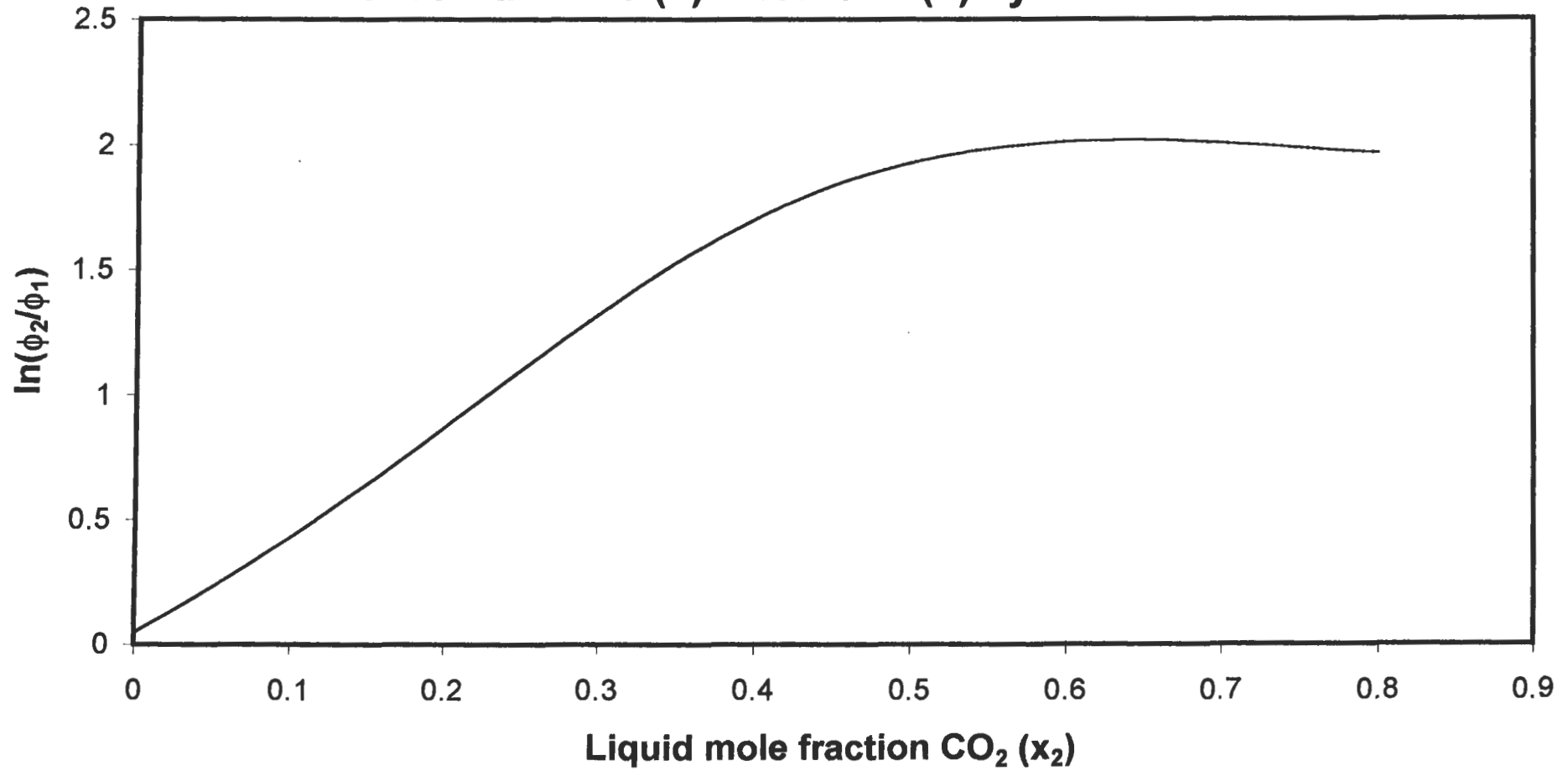


Figure F-29: Plot of liquid molar volume versus pressure for the carbon dioxide + toluene system at 118.3 °C

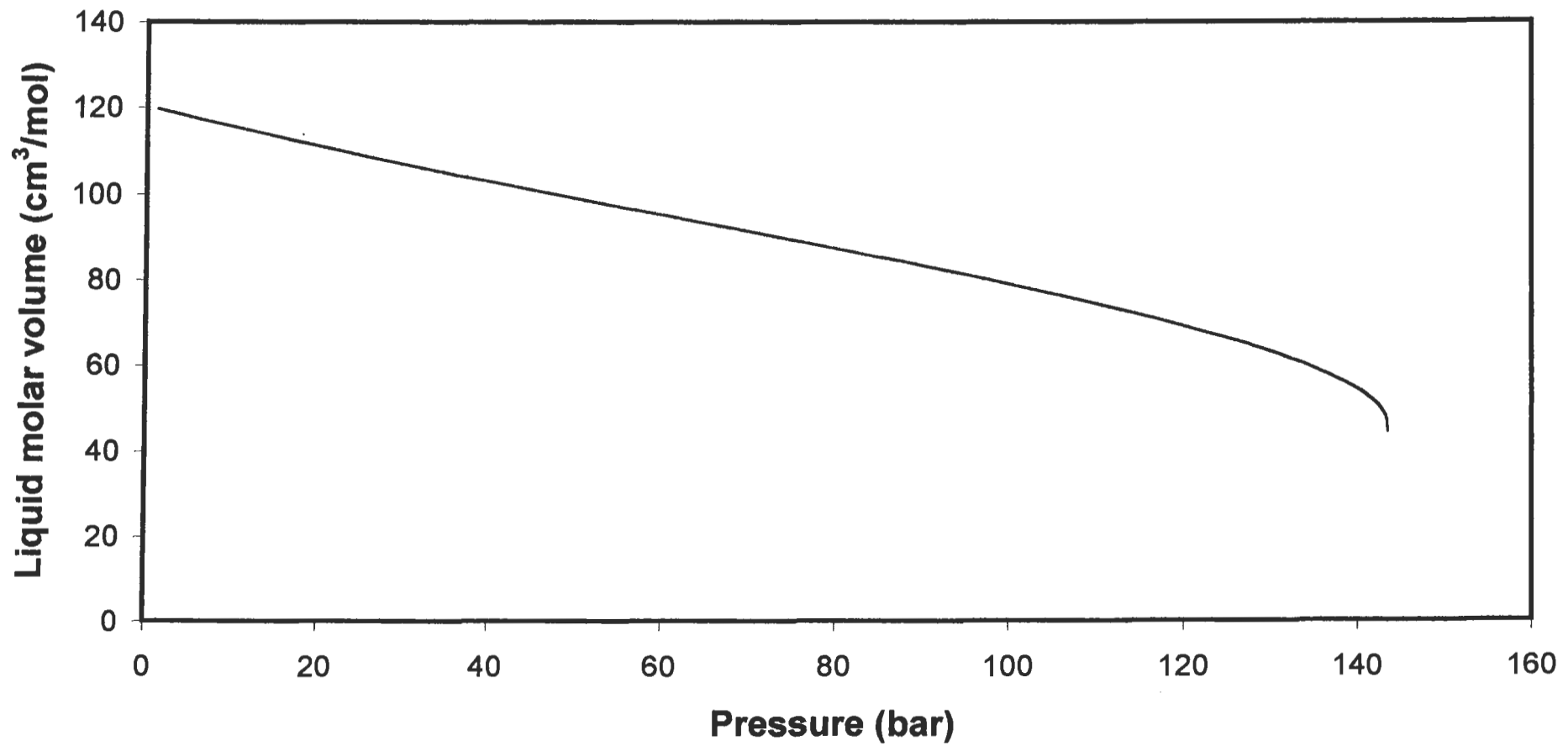


Figure F-30: Plot of $\ln(K_2/K_1)$ versus liquid mole fraction CO_2 for the carbon dioxide (2) + methanol (1) system at 40 °C

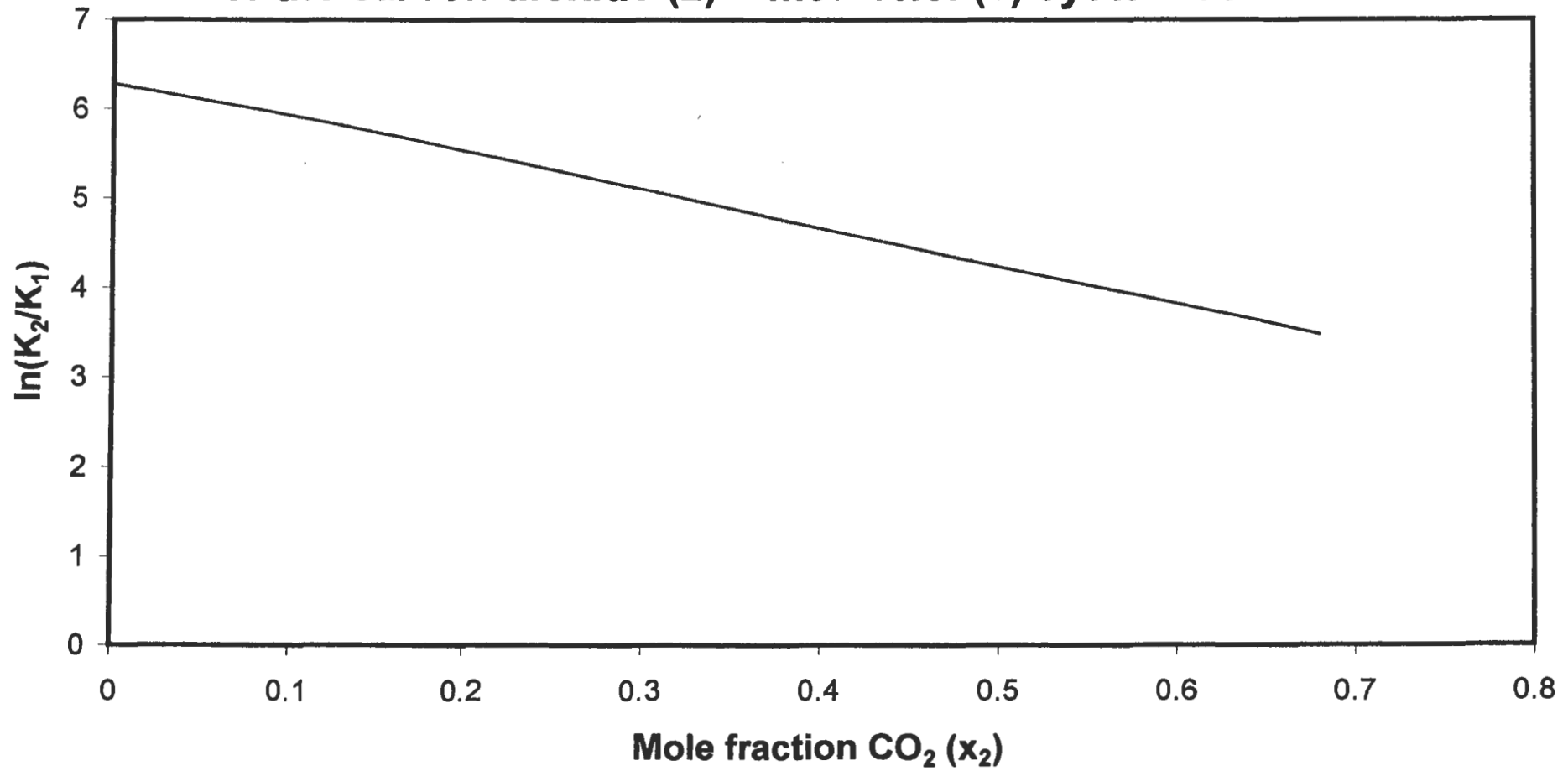


Figure F-31: Plot of $\ln(\phi_2/\phi_1)$ versus liquid mole fraction CO_2 for the carbon dioxide (2) + methanol (1) system at 40 °C

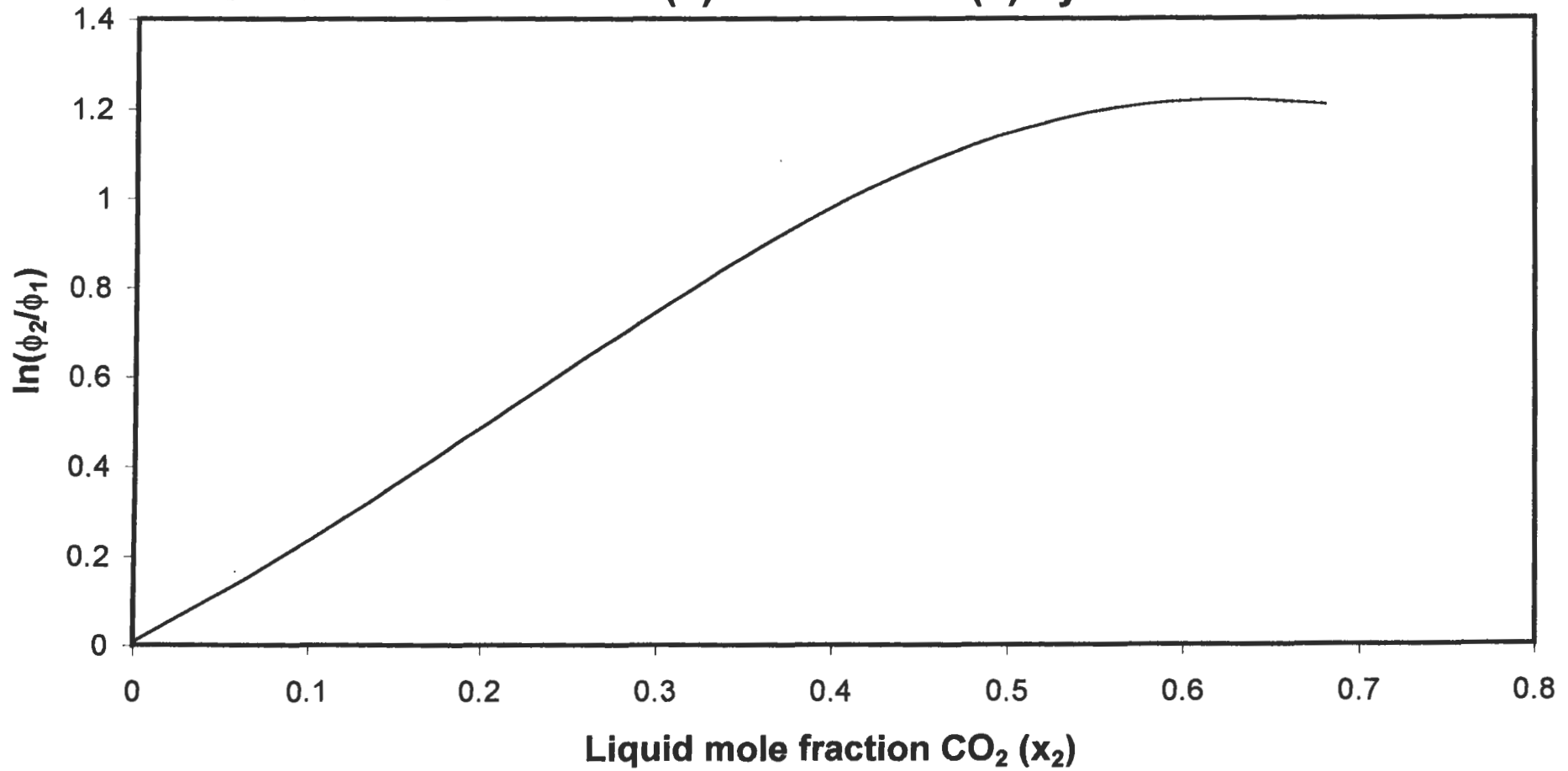


Figure F-32: Plot of liquid molar volume versus pressure for the carbon dioxide + methanol system at 40 °C

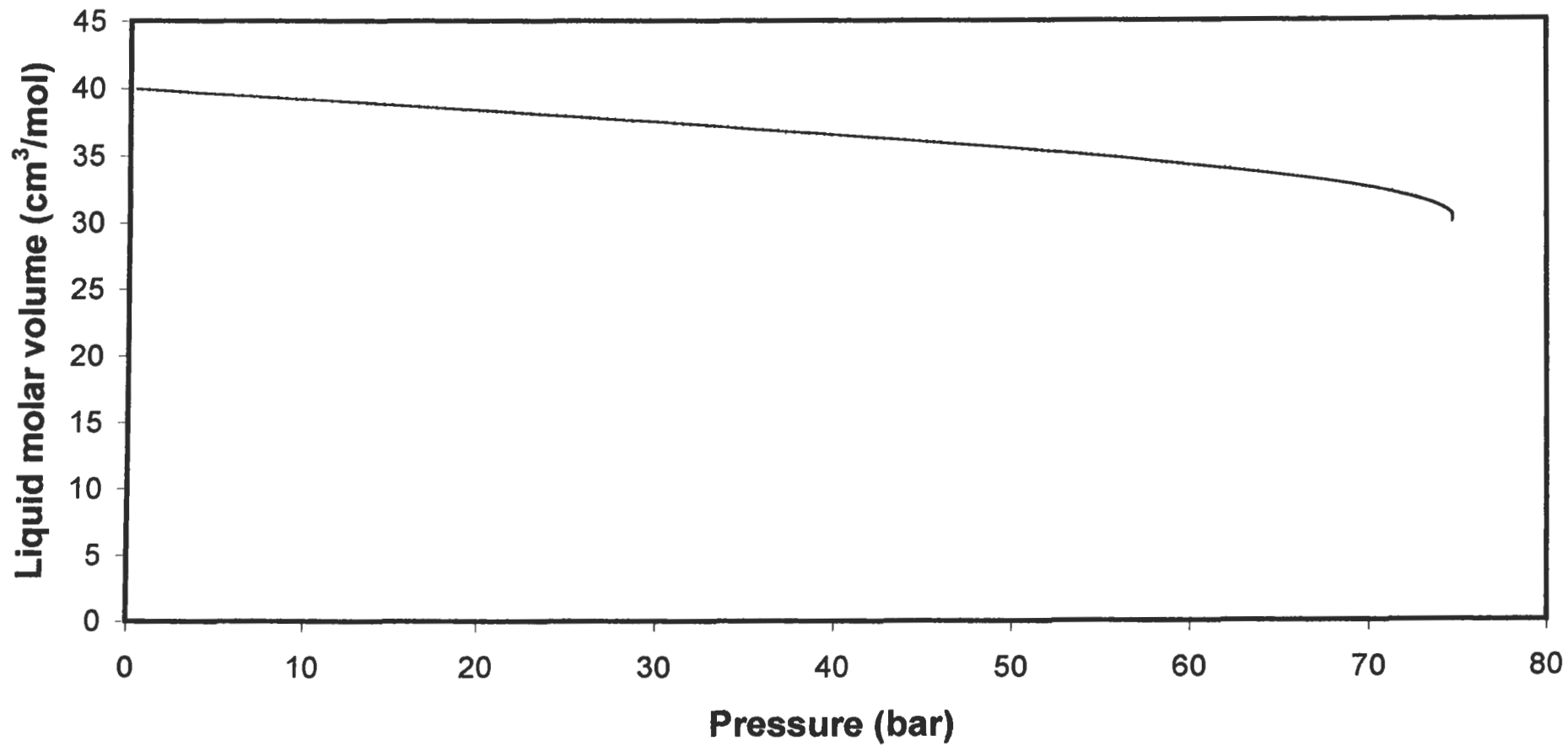


Figure F-33: Plot of $\ln(K_2/K_1)$ versus liquid mole fraction CO_2 for the carbon dioxide (2) + methanol (1) system at 90 °C

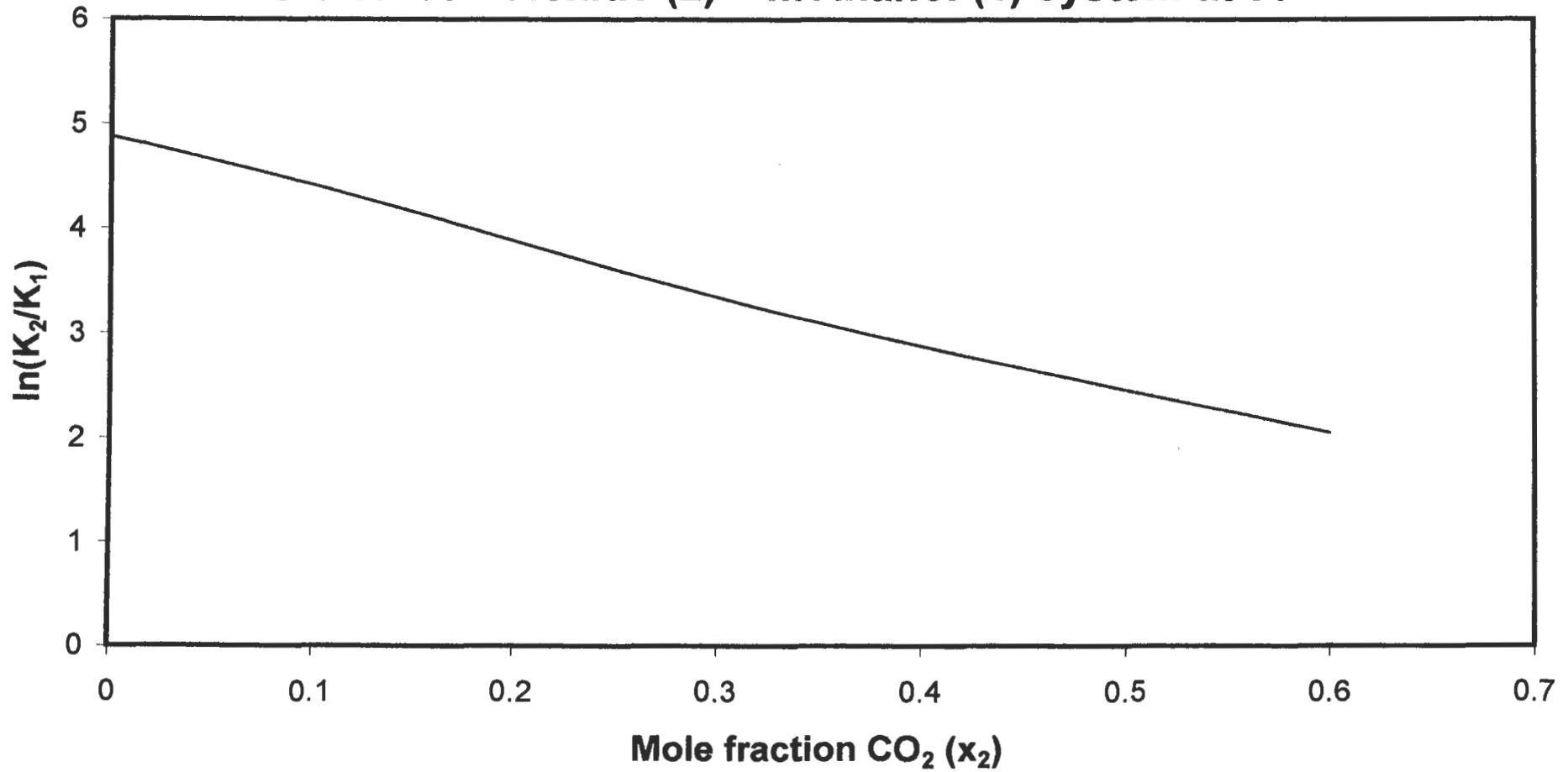


Figure F-34: Plot of $\ln(\phi_2/\phi_1)$ versus liquid mole fraction CO_2 for the carbon dioxide (2) + methanol (1) system at 90 °C

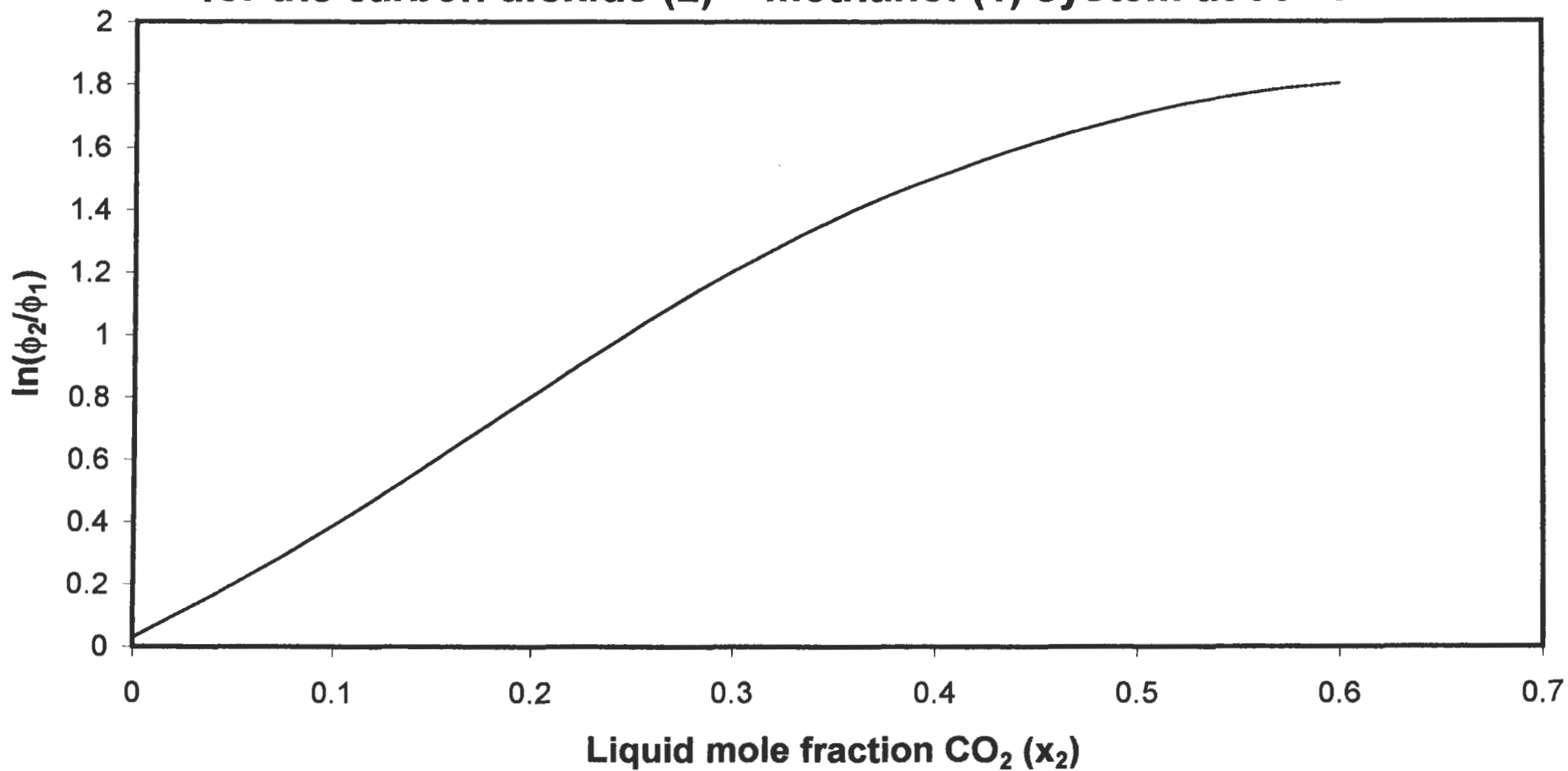


Figure F-35: Plot of liquid molar volume versus pressure for the carbon dioxide + methanol system at 90 °C

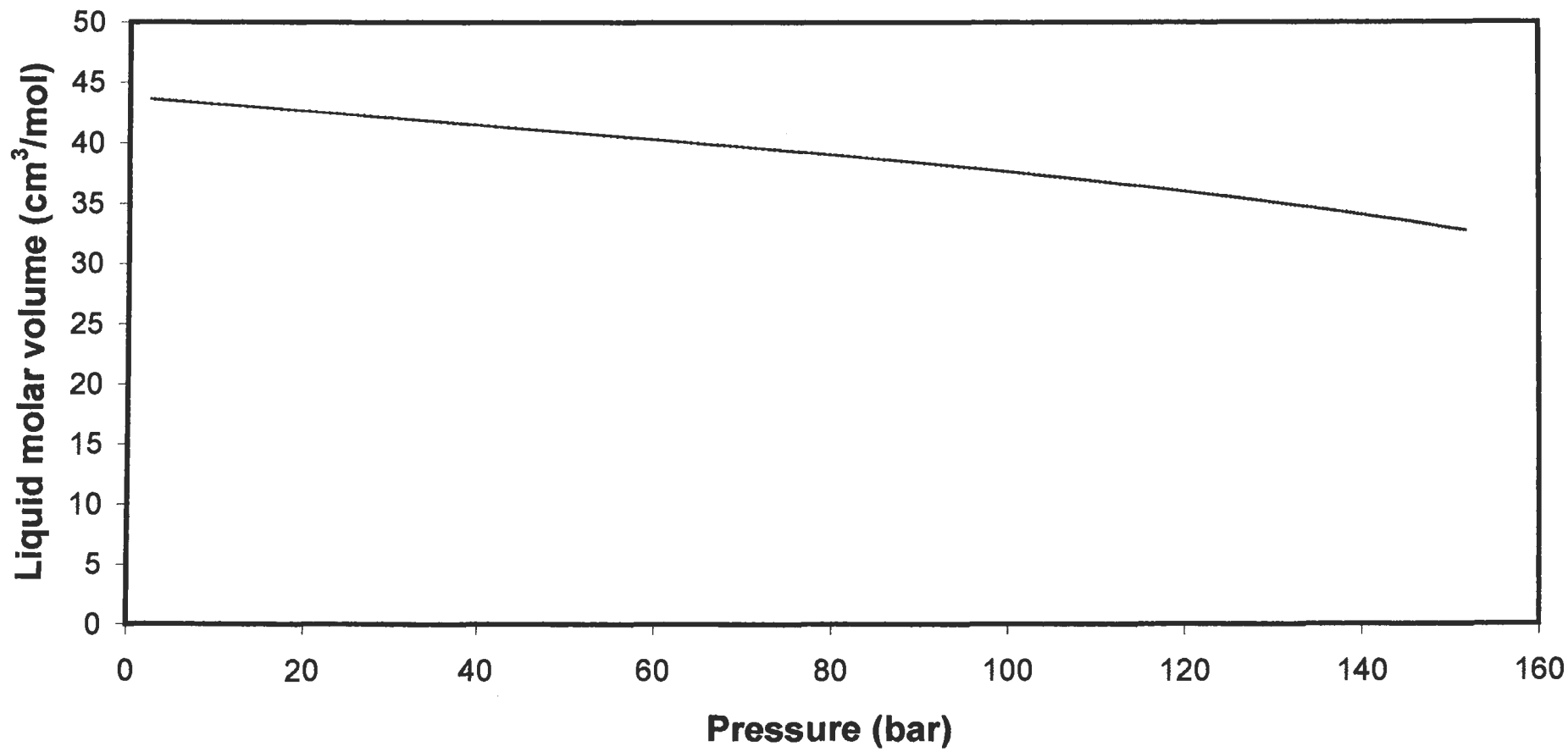


Figure F-36: Plot of $\ln(K_2/K_1)$ versus liquid mole fraction CO_2 for the carbon dioxide (2) + methanol (1) system at 100 °C

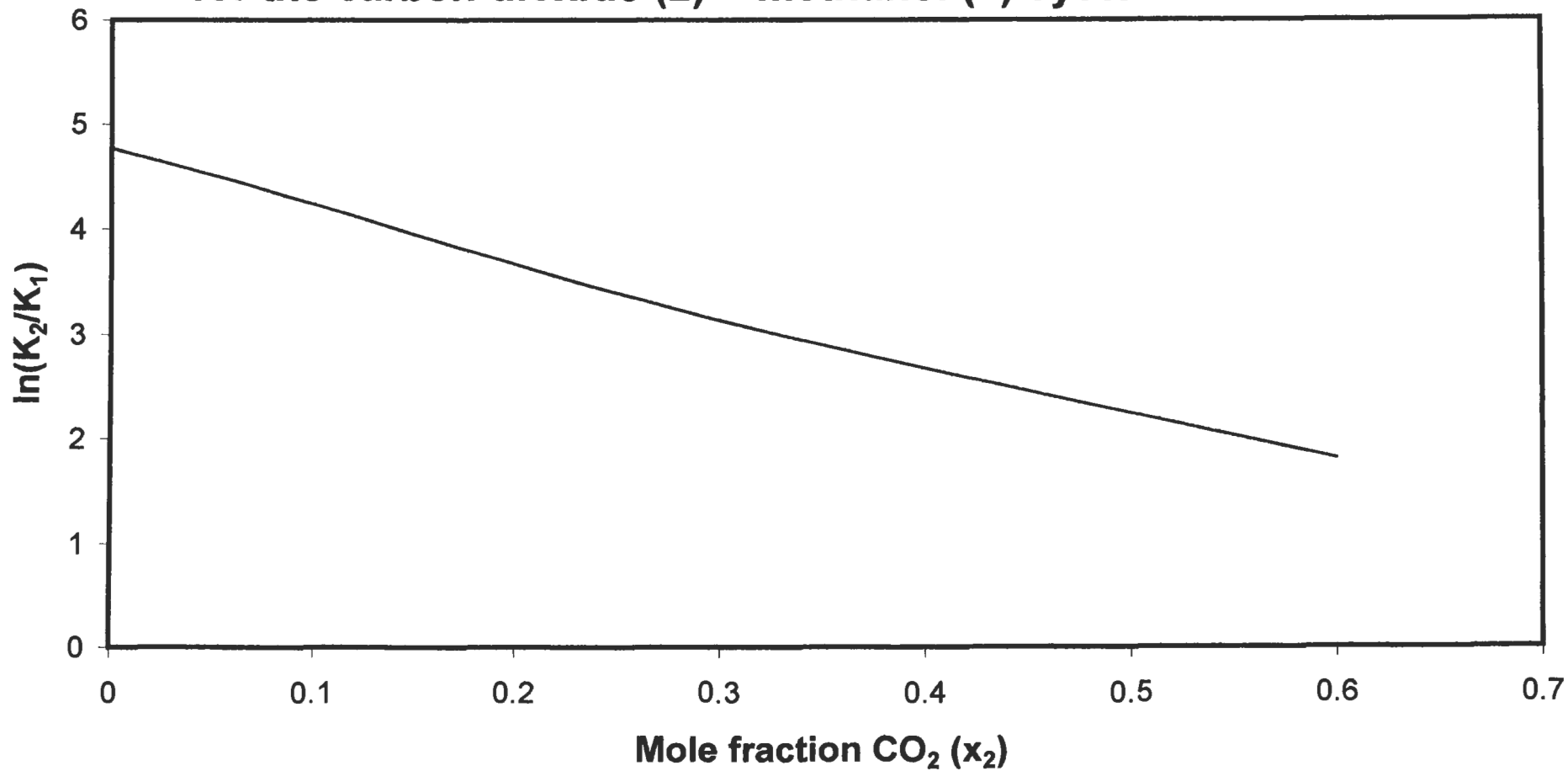


Figure F-37: Plot of $\ln(\phi_2/\phi_1)$ versus liquid mole fraction CO_2 for the carbon dioxide (2) + methanol (1) system at 100 °C

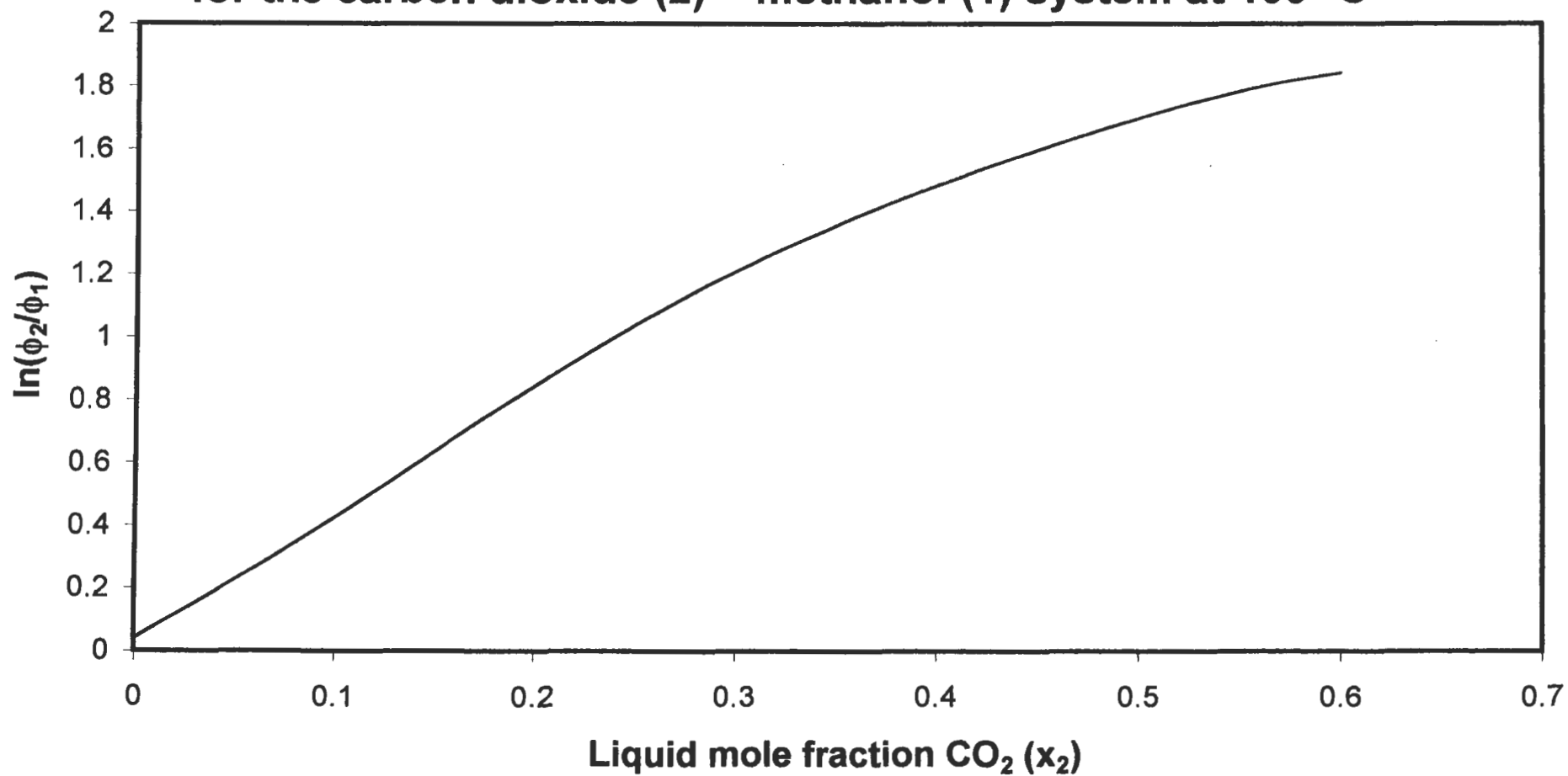


Figure F-38: Plot of liquid molar volume versus pressure for the carbon dioxide + methanol system at 100 °C

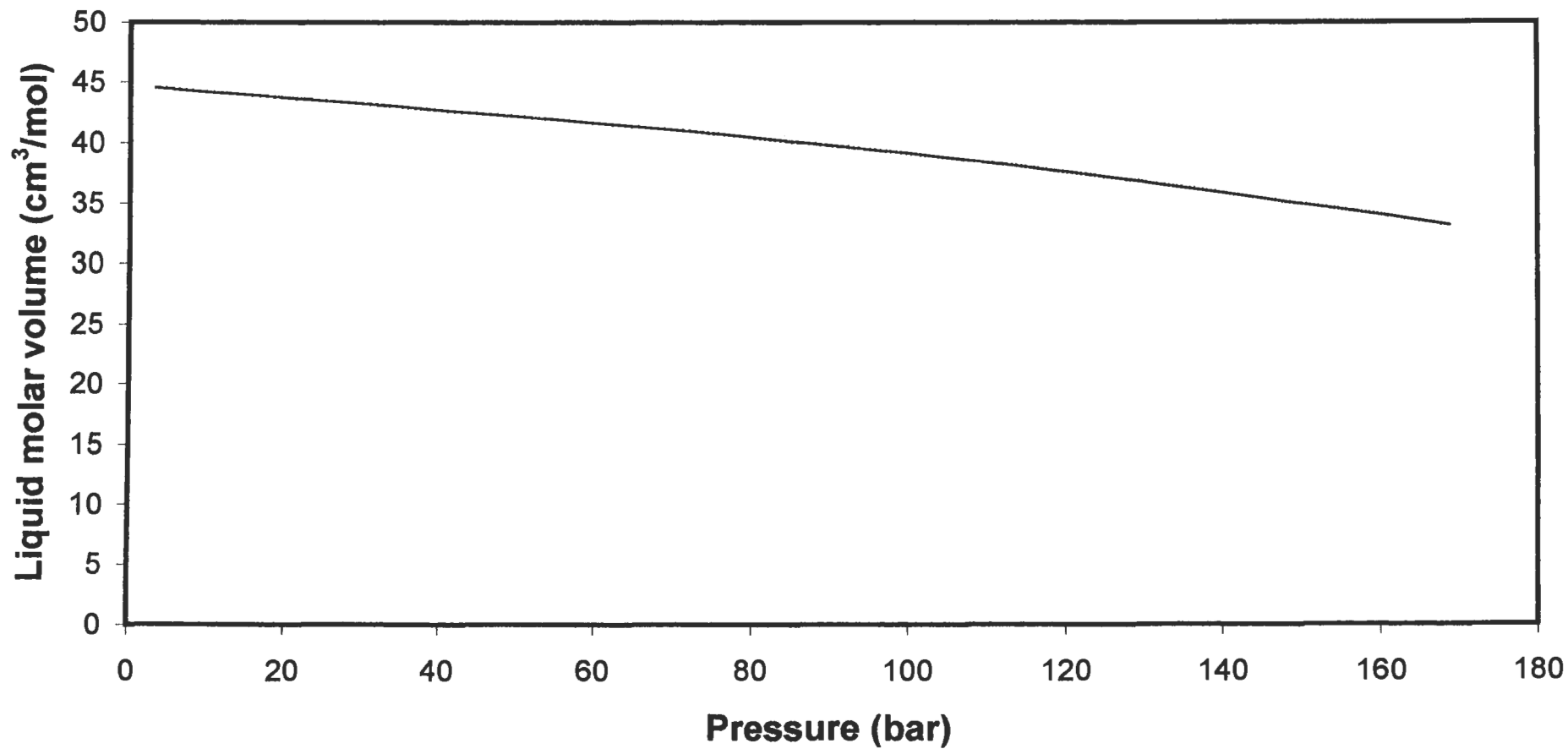


Figure F-39: Plot of $\ln(K_2/K_1)$ versus liquid mole fraction propane for the propane (2) + 1-propanol (1) system at 105.1 °C

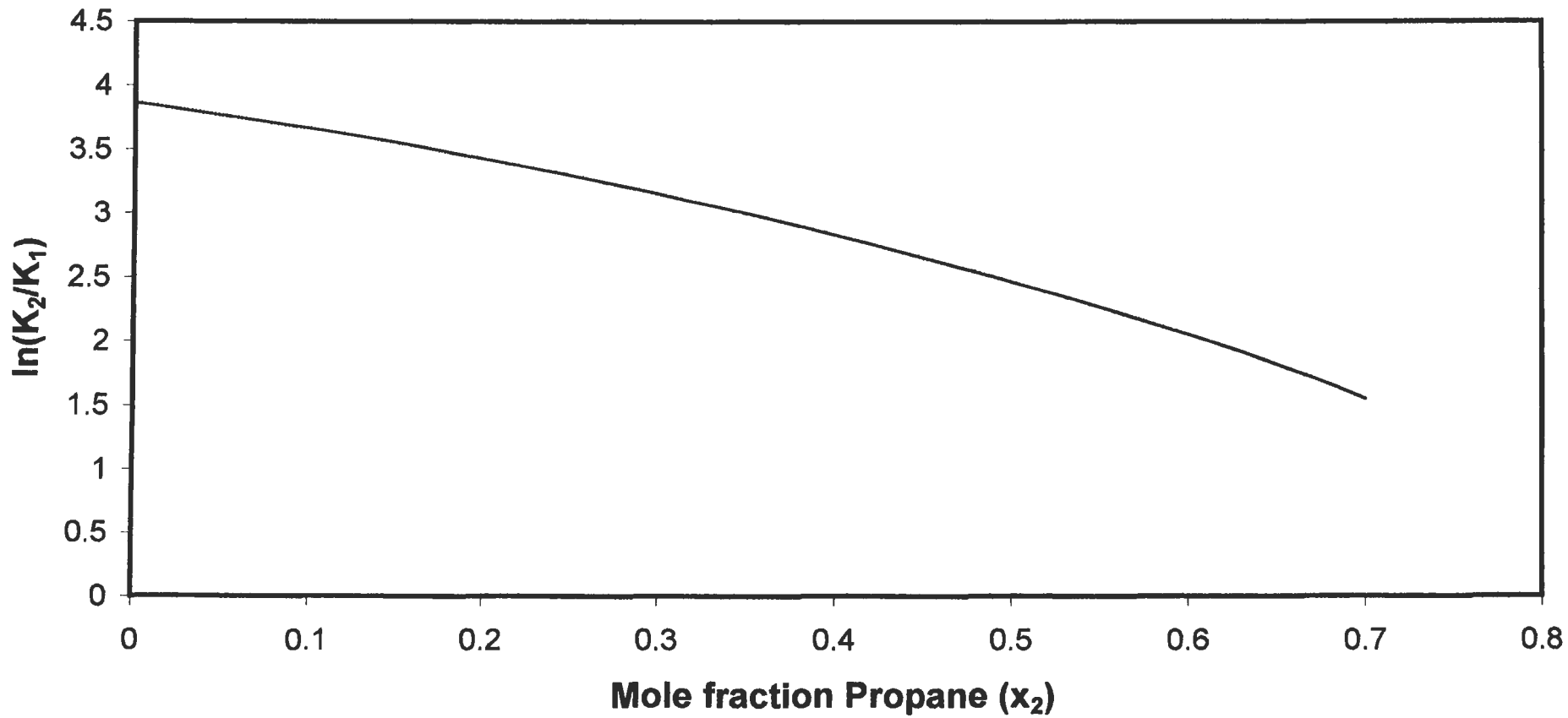


Figure F-40: Plot of $\ln(\phi_2/\phi_1)$ versus liquid mole fraction propane for the propane (2) + 1-propanol (1) system at 105.1 °C

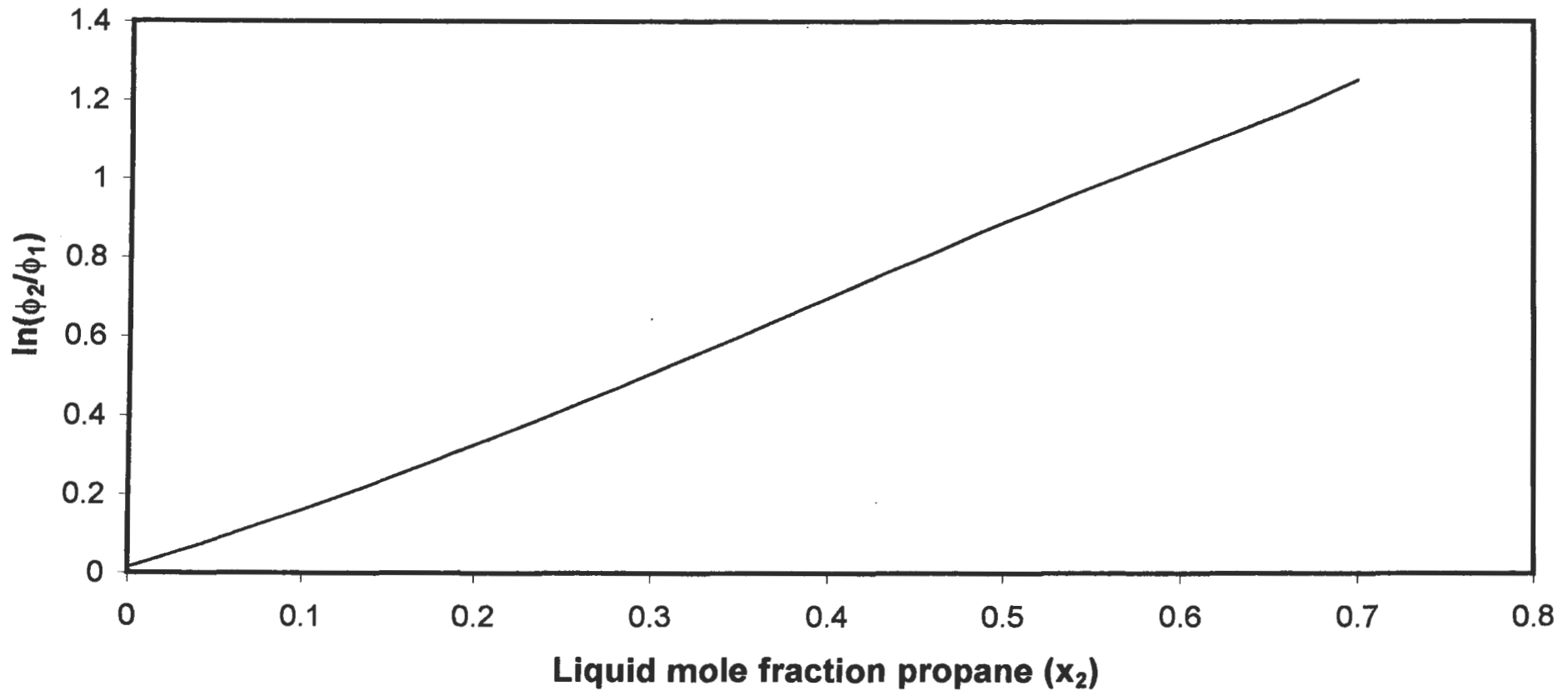


Figure F-41: Plot of liquid molar volume versus pressure for the propane + 1-propanol system at 105.1 °C

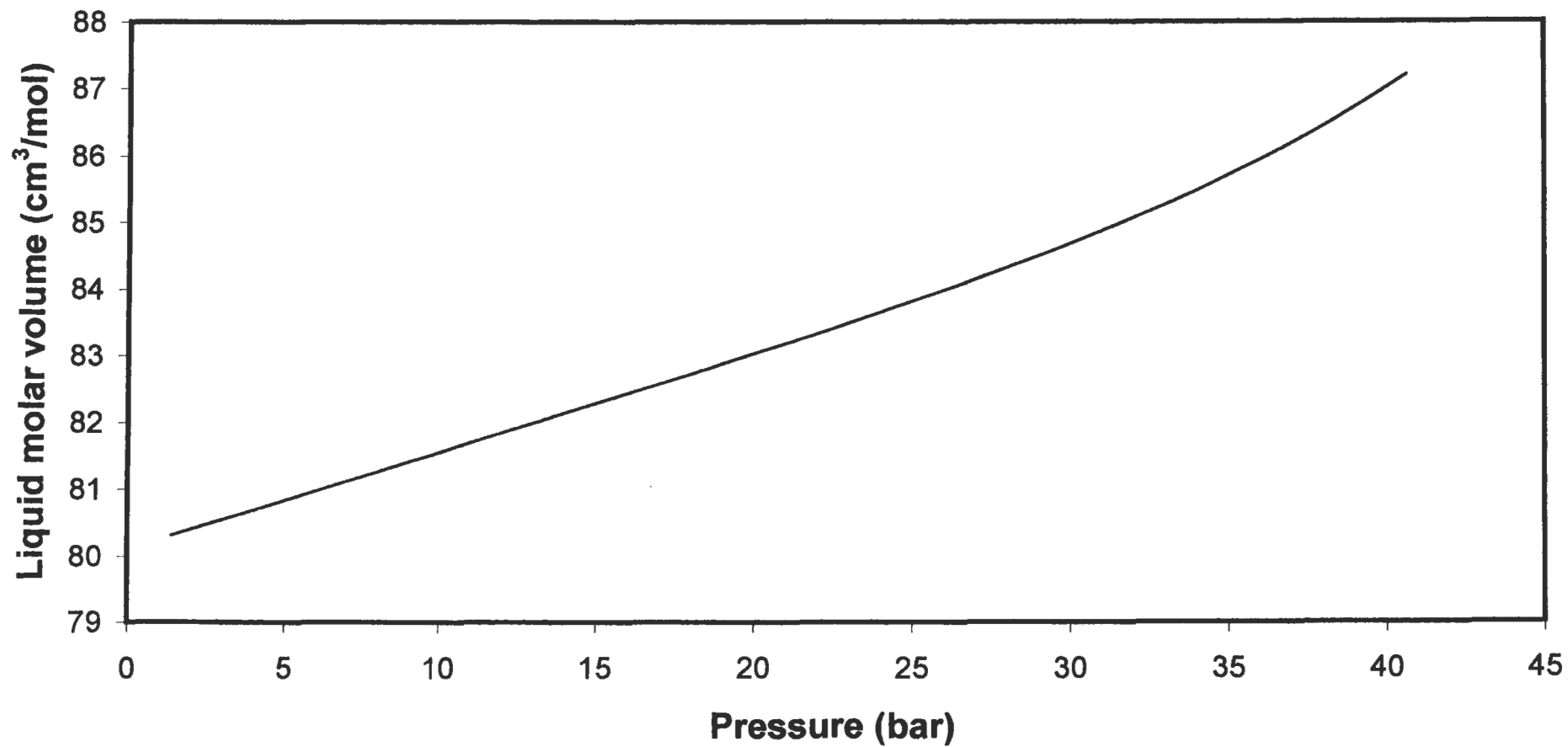


Figure F-42: Plot of $\ln(K_2/K_1)$ versus liquid mole fraction propane for the propane (2) + 1-propanol (1) system at 120 °C

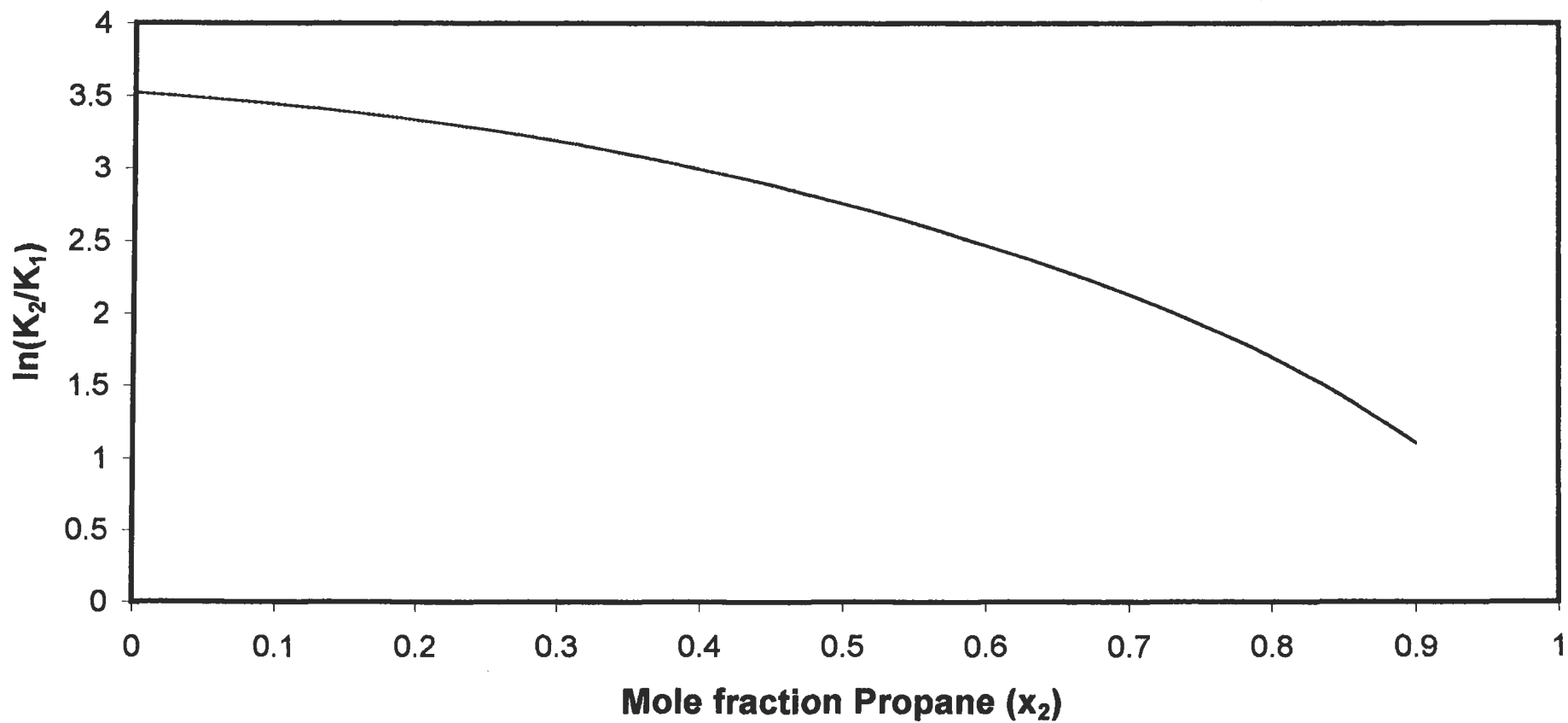


Figure F-43: Plot of $\ln(\phi_2/\phi_1)$ versus liquid mole fraction propane for the propane (2) + 1-propanol (1) system at 120 °C

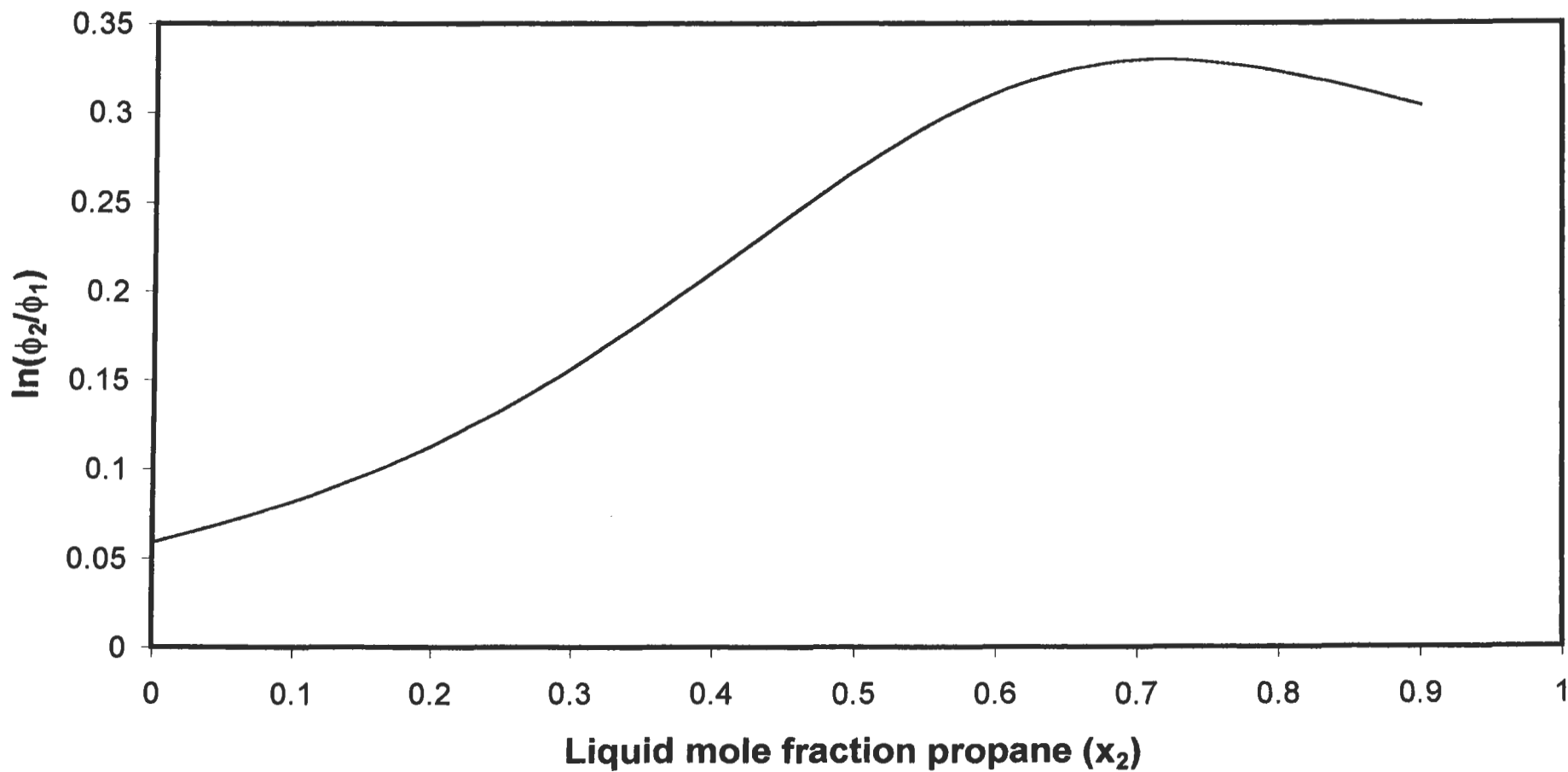


Figure F-44: Plot of liquid molar volume versus pressure for the propane + 1-propanol system at 120 °C

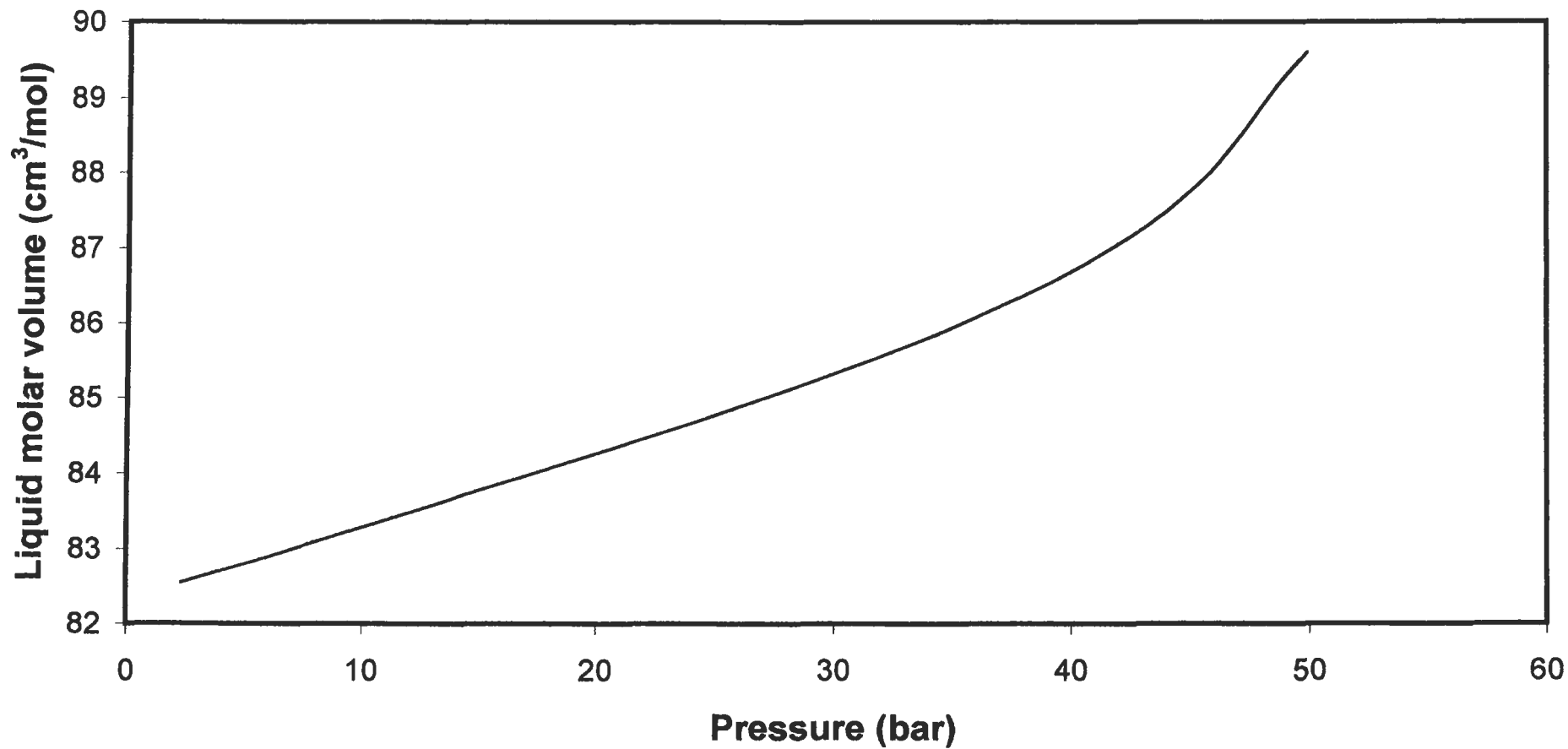


Figure F-45: Residual plot of Pressure for the Carbon Dioxide + Toluene System at 38 °C isotherm

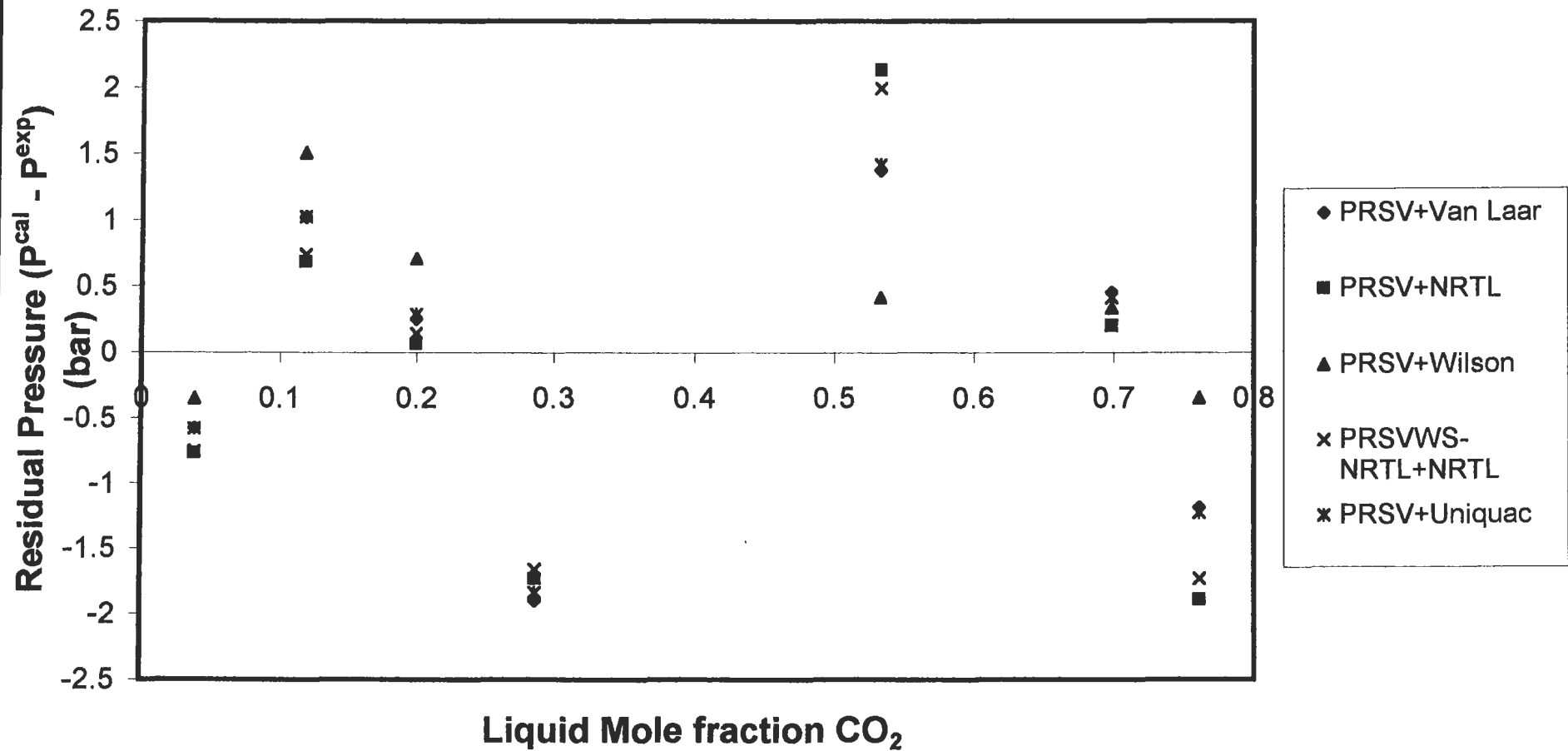


Figure F-46: Residual plot of Pressure for the Carbon Dioxide + Toluene System at 80 °C

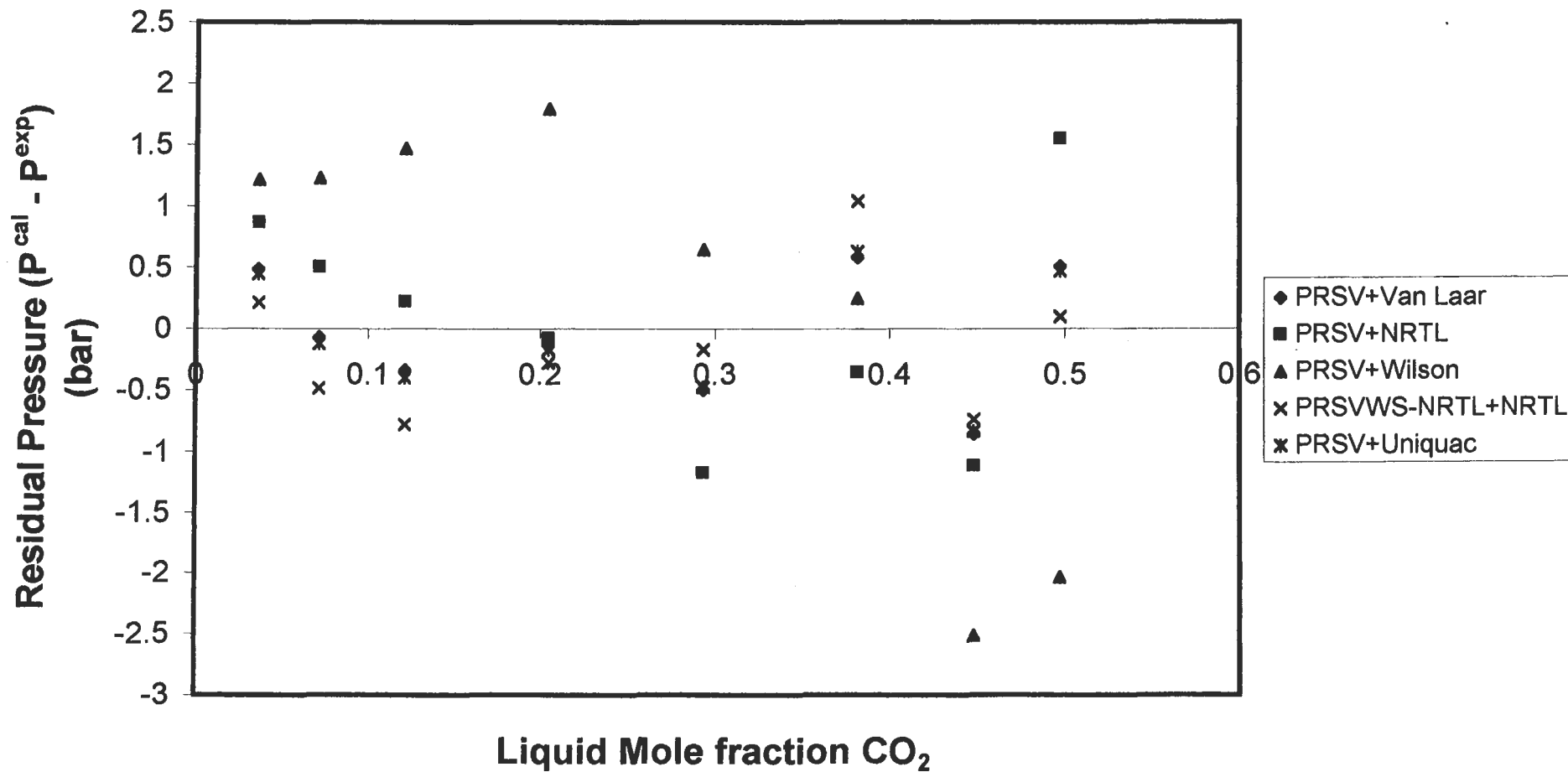


Figure F-47: Residual plot of Pressure for the Carbon Dioxide + Toluene System at 118.3 °C

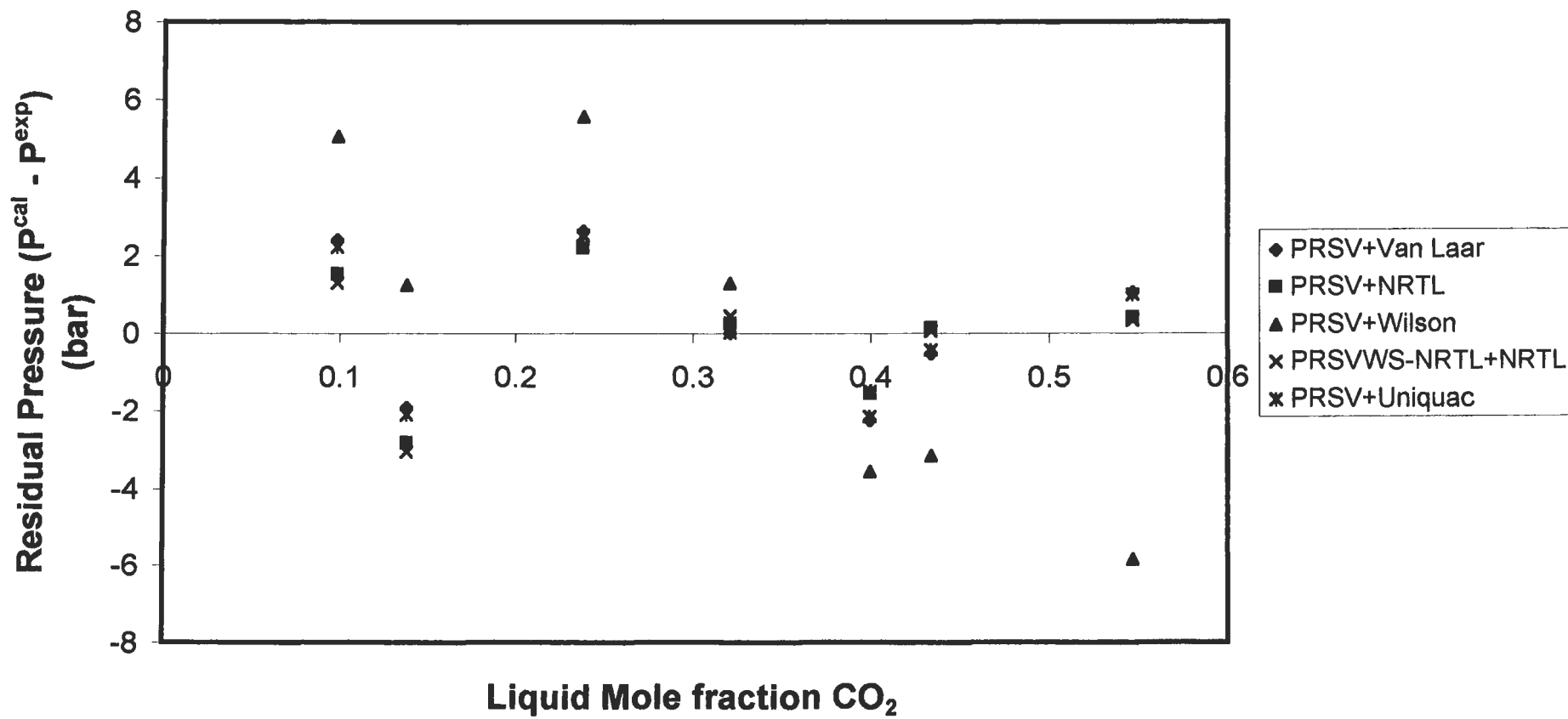


Figure F-48: Residual plot of Pressure for the Carbon Dioxide + Methanol System at 40 °C

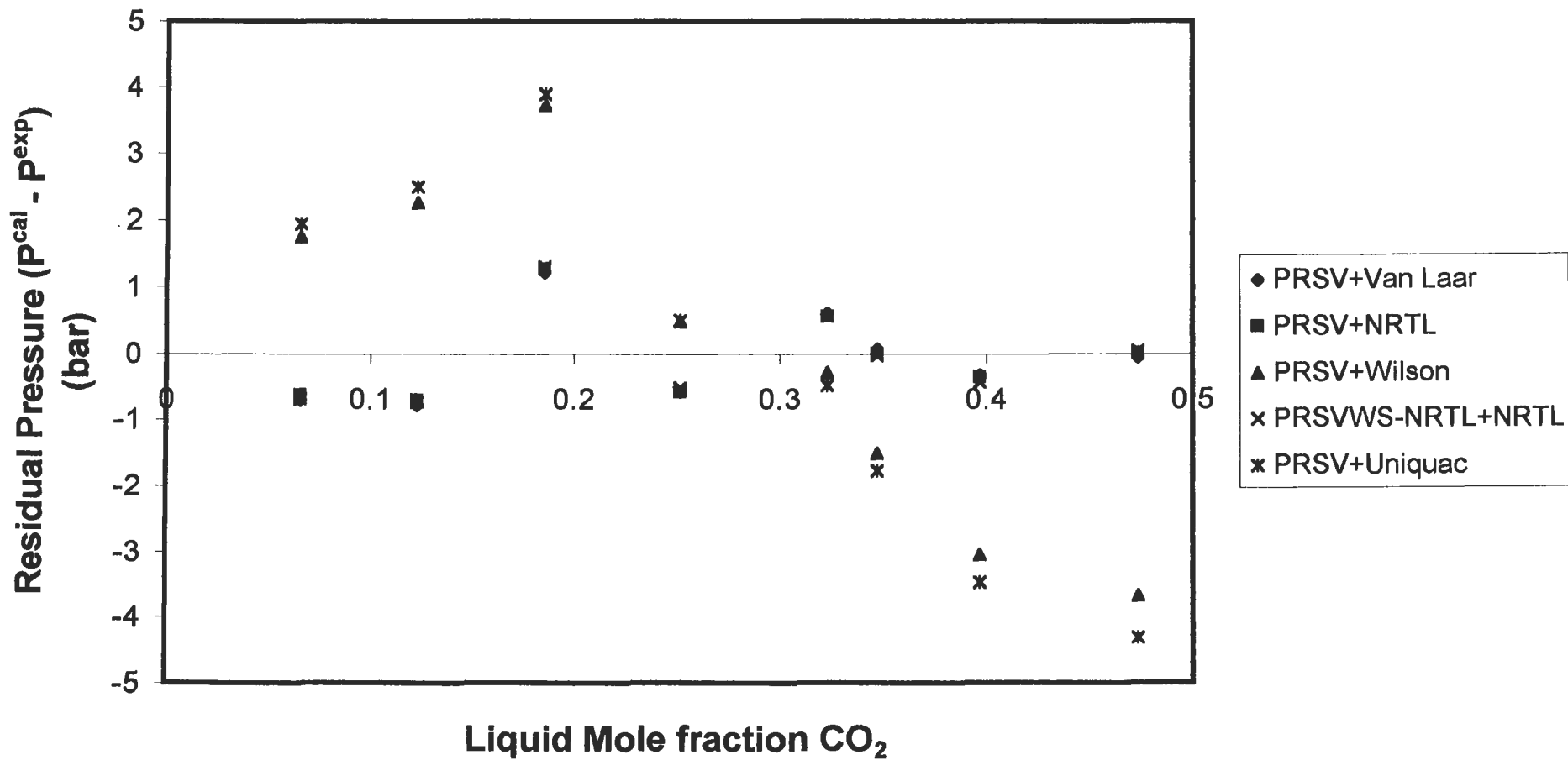


Figure F-49: Residual plot of Pressure for the Carbon Dioxide + Methanol System at 90 °C

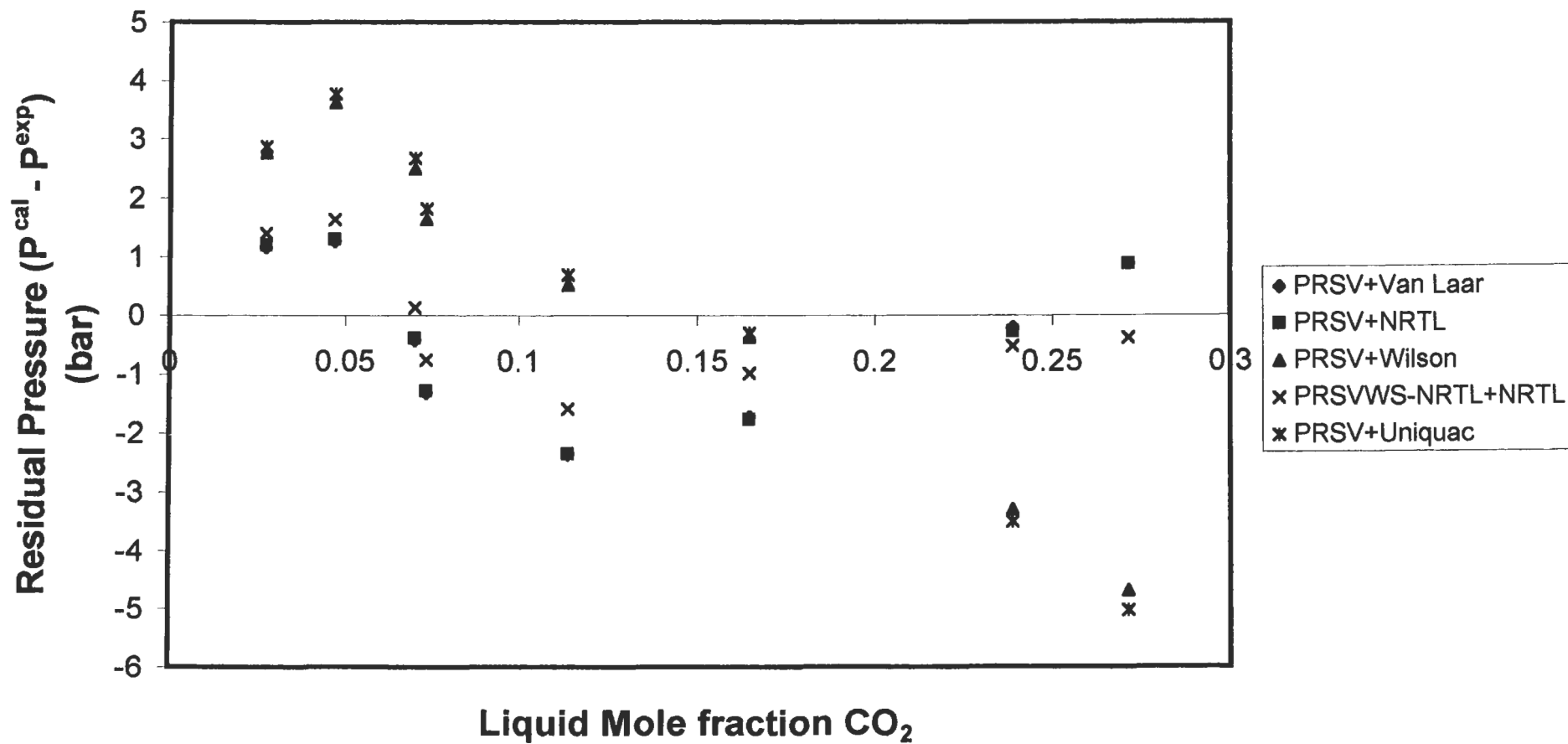


Figure F-50: Residual plot of pressure for the Carbon Dioxide + Methanol System at 100 °C

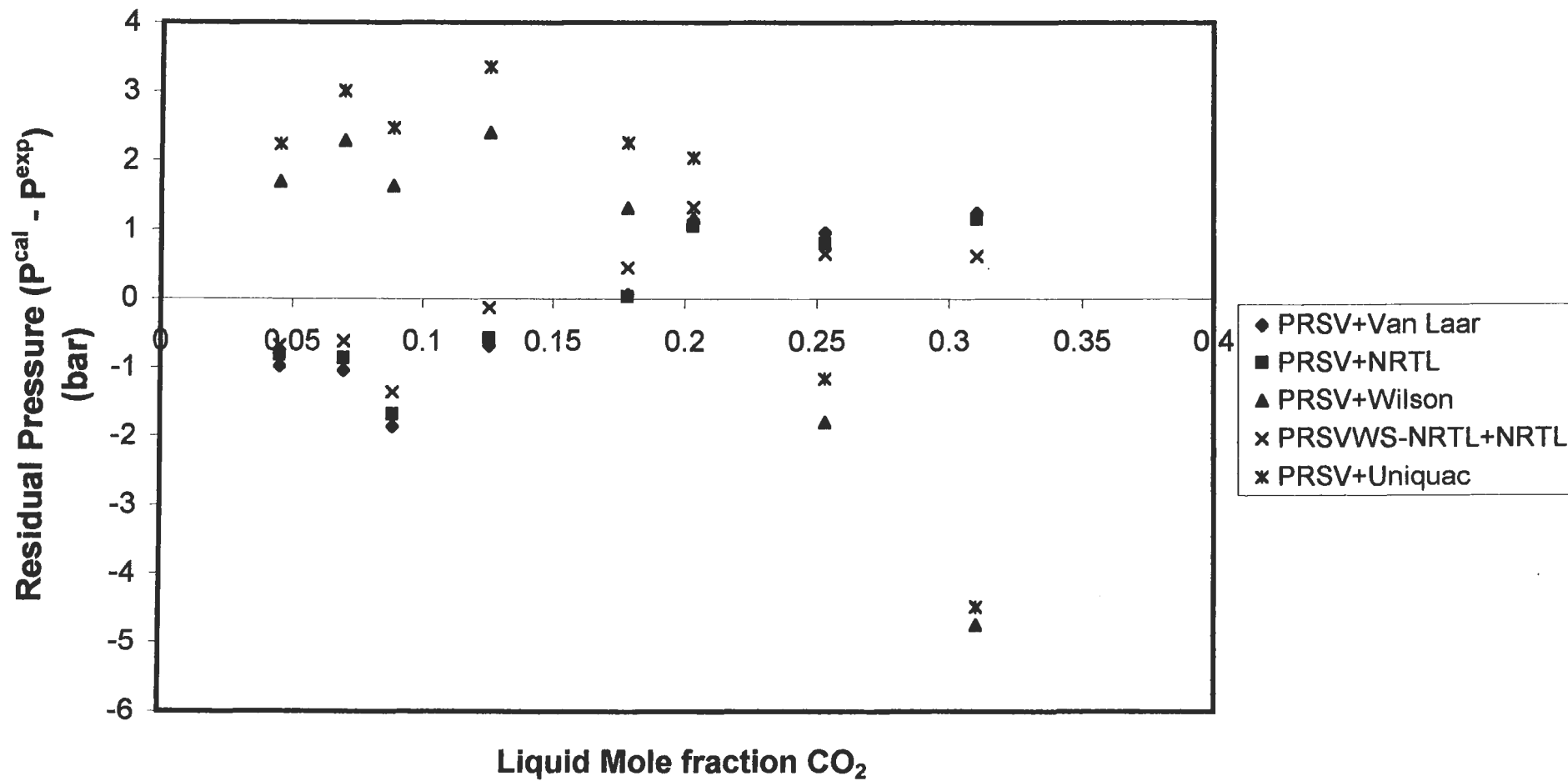


Figure F-51: Residual plot of Pressure for the Propane + 1-Propanol System at 105.1 °C isotherm

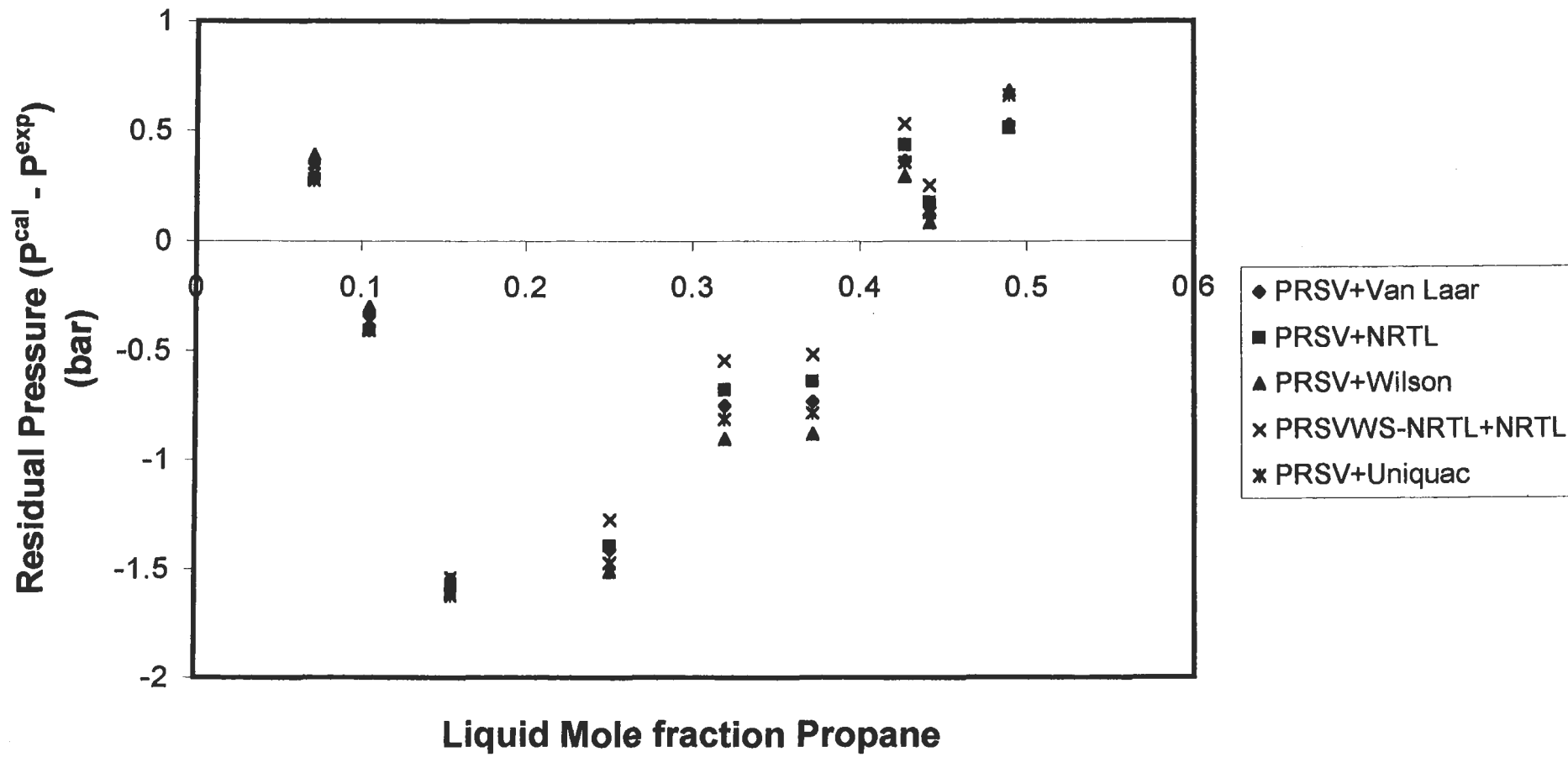
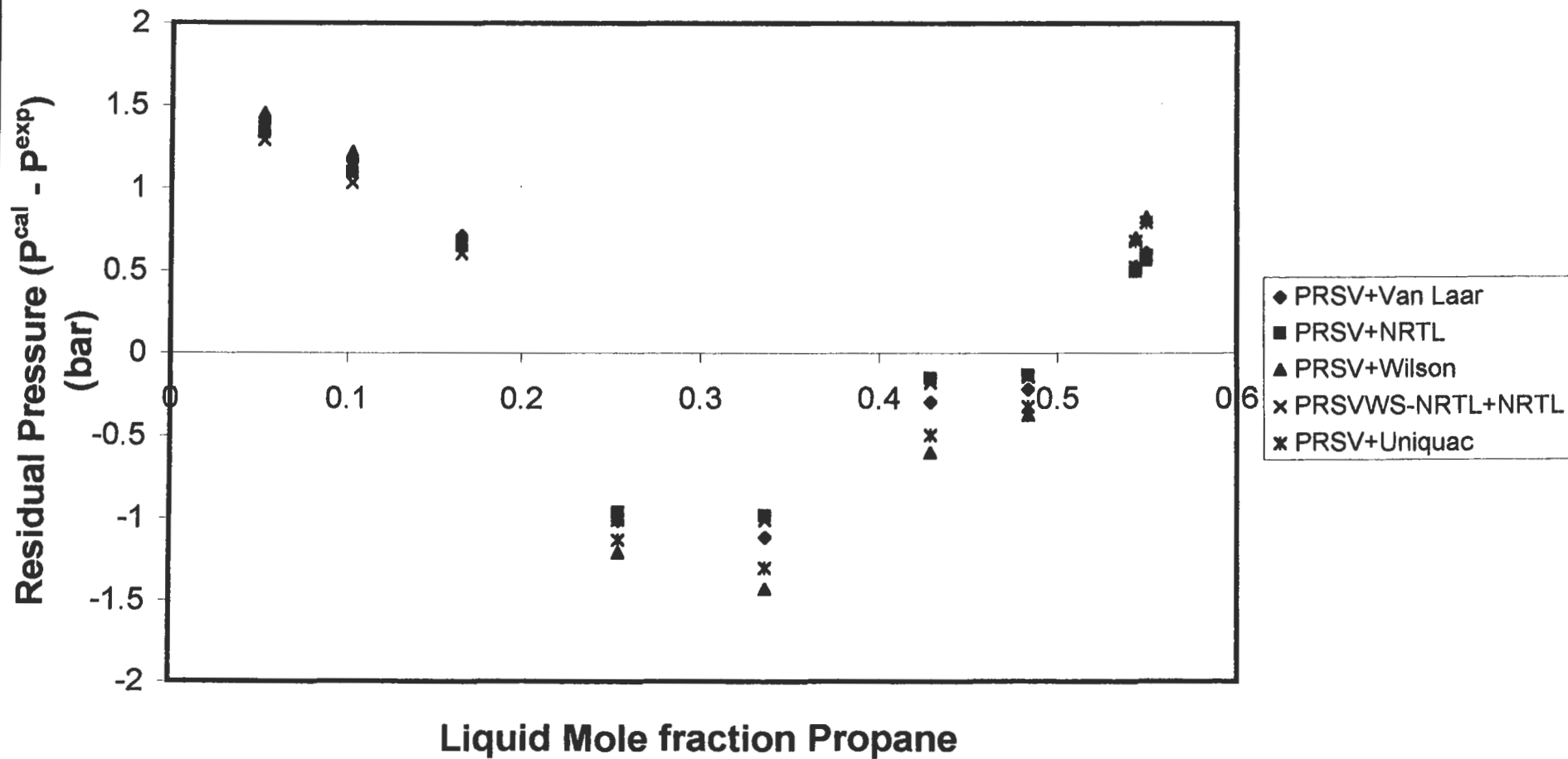


Figure F-52: Residual plot of Pressure for the Propane + 1-Propanol System at 120 °C isotherm



F.5. P-V-T COMPUTATIONS – DETERMINATION OF VOLUME

The new equilibrium cell can also be used to obtain P-V-T information and to measure dew or bubble points. For this purpose the equilibrium cell volume at any piston position has to be known exactly. The effective equilibrium cell interior volume at any piston position can be found from an equation of state (EOS). If the number of moles of gas contained in the equilibrium space, n , is known the volume, V_o , can be calculated using e.g. the truncated Virial EOS, $Z = 1 + (BP/RT)$, as follows:

$$V_o = \frac{nRT_o}{P_o} \left\{ 1 + \frac{B_o P_o}{RT_o} \right\} \quad (\text{F-1})$$

where B_o is the second virial coefficient

P_o, T_o are the measured pressure and temperature at an initial piston position

The number of moles of gas can be found by moving the piston upwards or downwards to expand or compress the gas and re-measuring the pressure. Temperature remains constant because the equilibrium cell is isothermal.

The new volume is given by:

$$V_1 = \frac{nRT_o}{P_1} \left\{ 1 + \frac{B_o P_1}{RT_o} \right\} \quad (\text{F-2})$$

The difference in volumes, $V_1 - V_o = \Delta V$ is given by:

$$\Delta V = nR \left\{ T_o \left(\frac{1}{P_1} - \frac{1}{P_o} \right) \right\} \quad (\text{F-3})$$

and also by:

$$\Delta V = \frac{\pi}{4} D^2 \Delta L \quad (\text{F-4})$$

where: D is the cell interior diameter

ΔL is the piston travel

The number of moles, n , in the equilibrium space is found from Equations (F-3) and (F-4):

$$n = \frac{\frac{\pi}{4} D^2 \Delta L}{RT_o \left(\frac{1}{P_1} - \frac{1}{P_o} \right)} \quad (\text{F-5})$$

Substitution of Equation (F-5) into Equation (F-1) gives the effective interior equilibrium cell volume at the zero displacement position:

$$V_o = \frac{\left(\frac{T_o}{P_o} + \frac{B_o}{R} \right) \left[\frac{\pi}{4} D^2 \Delta L \right]}{T_o \left(\frac{1}{P_1} - \frac{1}{P_o} \right)} \quad (\text{F-6})$$

The volume at any piston position after the movement ΔL from the initial zero position, is found from Equation (F-4). The micrometer dial on the stepper motor drive is very convenient for accurate measurement of ΔL .

The equations developed above thus enable the equilibrium cell to be used to furnish P-V-T data and dew and bubble points if the total mass or moles of a binary system introduced into the equilibrium cell is known. The components will have to be thoroughly degassed before introduction into the equilibrium cell.